

# Oceanologia

Official Journal of the Polish Academy of Sciences



## EDITOR-IN-CHIEF

Prof. Jacek Piskozub  
Institute of Oceanology, Polish Academy of Sciences, Sopot, Poland

## MANAGING EDITOR

Agata Bielecka – abielecka@iopan.pl

## Editorial Office Address

Institute of Oceanology, Polish Academy of Sciences (IO PAN)  
Powstańców Warszawy 55  
81–712 Sopot, Poland  
Mail: editor@iopan.pl

## THEMATIC EDITORS

Dr. Katarzyna Błachowiak-Samołyk – Institute of Oceanology, Polish Academy of Sciences, Sopot, Poland

Dr. Artur Burzyński – Institute of Oceanology, Polish Academy of Sciences, Sopot, Poland

Prof. Piotr Kowalczyk – Institute of Oceanology, Polish Academy of Sciences, Sopot, Poland

Prof. Krzysztof Opaliński – Institute of Ecology and Bioethics, Warsaw, Poland

Prof. Żaneta Polkowska – Gdańsk University of Technology, Gdańsk, Poland

Dr. hab. Krzysztof Rychert – Pomeranian University in Słupsk, Poland

Prof. Marek Zajęczkowski – Institute of Oceanology, Polish Academy of Sciences, Sopot, Poland

## ADVISORY BOARD

**Prof. Xosé Antón Álvarez Salgado**  
Marine Research Institute, Spanish Research Council (CSIC), Vigo, Spain

**Dr. Boris Chubarenko**  
P.P. Shirshov Institute of Oceanology, Russian Academy of Sciences, Kaliningrad, Russia

**Dr. Mirosław Darecki**  
Institute of Oceanology, Polish Academy of Sciences, Sopot, Poland

**Prof. Jerzy Dera**  
Institute of Oceanology, Polish Academy of Sciences, Sopot, Poland

**Prof. Agnieszka Herman**  
Institute of Oceanography, University of Gdańsk, Gdynia, Poland

**Prof. Genrik Sergey Karabashev**  
P.P. Shirshov Institute of Oceanology, Russian Academy of Sciences, Moscow, Russia

**Prof. Alicja Kosakowska**  
Institute of Oceanology, Polish Academy of Sciences, Sopot, Poland

**Prof. Zygmunt Kowalik**  
Institute of Marine Science, University of Alaska Fairbanks (UAF), USA

**Prof. Matti Leppäranta**  
Institute of Atmospheric and Earth Sciences, University of Helsinki, Finland

**Prof. Ewa Łupikasza**  
Faculty of Earth Sciences, University of Silesia, Sosnowiec, Poland

**Prof. Hanna Mazur-Marzec**  
Institute of Oceanography, University of Gdańsk, Gdynia, Poland

**Prof. Dag Myrhaug**  
Norwegian University of Science and Technology (NTNU), Trondheim, Norway

**Prof. Sergej Olenin**  
Coastal Research and Planning Institute, Klaipeda University CORPI, Klaipeda, Lithuania

**Prof. Tarmo Soomere**  
Tallinn University of Technology, Estonia

**Prof. Hans von Storch**  
Institute of Coastal Research, Helmholtz Center Geesthacht, Germany

**Prof. Dariusz Stramski**  
Scripps Institution of Oceanography, University of California, San Diego, USA

**Prof. Piotr Szefer**  
Department of Food Sciences, Medical University of Gdańsk, Poland

**Prof. Antoni Śliwiński**  
Institute of Experimental Physics, University of Gdańsk, Poland

**Prof. Muhammet Türkoğlu**  
Çanakkale Onsekiz Mart University, Turkey

**Prof. Jan Marcin Węśławski**  
Institute of Oceanology, Polish Academy of Sciences, Sopot, Poland

This journal is supported by the Ministry of Science and Higher Education, Warsaw, Poland

Indexed in: ISI Journal Master List, Science Citation Index Expanded, Scopus, Current Contents, Zoological Record, Thomson Scientific SSCI, Aquatic Sciences and Fisheries Abstracts, DOAJ

IMPACT FACTOR ANNOUNCED FOR 2020 IN THE 'JOURNAL CITATION REPORTS' IS 2.427; 5-year IF is 2.671. CITESCORE ANNOUNCED FOR 2020 IS 4.3

**Publisher**  
Elsevier B.V.  
Radarweg 29  
1043 NX Amsterdam  
The Netherlands

**Senior Publisher**  
Tobias Wesselius  
+31 6 5370 3539

ISSN 0078-3234



## ORIGINAL RESEARCH ARTICLE

# Long term variation of sardine *Sardina pilchardus* spawning along the Atlantic coast of northwest Africa (21–26°N): characterization and spatiotemporal variability in spawning habitat

Hinde Abdelouahab<sup>a,\*</sup>, Amina Berraho<sup>a</sup>, Tarik Baibai<sup>a</sup>, Jamila Larissi<sup>a</sup>, Said Charib<sup>a</sup>, Aziz Agouzouk<sup>a</sup>, Ahmed Makaoui<sup>a</sup>, Omar Ettahiri<sup>a</sup>, Ahmed Errhif<sup>b</sup>

<sup>a</sup>Institut National de Recherche Halieutique, Casablanca, Morocco

<sup>b</sup>University Hassan II of Casablanca, Faculty of Sciences, Ain Chock, Casablanca, Morocco

Received 3 February 2020; accepted 25 August 2020

Available online 3 September 2020

## KEYWORDS

Sardine;  
Spawning habitat;  
Environment;  
Time series;  
Sea surface  
temperature

**Abstract** Small pelagic fish such as sardine show strong recruitment variability often associated with environmental changes influencing the spawning process and ultimately, affecting population dynamics. Sardine (*Sardina pilchardus*, Walbaum 1792) is one of the most exploited pelagic species along the northwest African coast. The main spawning occurs during the cold season (autumn–winter). A time-series autumn–winter surveys extending from 1994 to 2015 sampled sardine eggs, along the southern area of the Moroccan Atlantic coast (26°N–21°N) were analyzed. The present work focuses on examining the inter-annual variability of the spawning habitat by analyzing the spatial-temporal variability of sardine egg distribution and density extracted from the data collected over the period 1994–2015. Generalized additive models (GAM) were used to detect the relationships between the sardine distribution, expressed as

\* Corresponding author at: Institut National de Recherche Halieutique, 2 Bd Sidi Abderrahmane, Casablanca, Morocco.

E-mail addresses: [hind.abdelouahab@gmail.com](mailto:hind.abdelouahab@gmail.com) (H. Abdelouahab), [aminaberraho@gmail.com](mailto:aminaberraho@gmail.com) (A. Berraho), [baibaitarik@gmail.com](mailto:baibaitarik@gmail.com) (T. Baibai), [larissijamila@gmail.com](mailto:larissijamila@gmail.com) (J. Larissi), [saidcharib@gmail.com](mailto:saidcharib@gmail.com) (S. Charib), [oceanosaad@gmail.com](mailto:oceanosaad@gmail.com) (A. Agouzouk), [oceanomakaoui@gmail.com](mailto:oceanomakaoui@gmail.com) (A. Makaoui), [omarettahiriomar@gmail.com](mailto:omarettahiriomar@gmail.com) (O. Ettahiri), [aerrhif@gmail.com](mailto:aerrhif@gmail.com) (A. Errhif).

Peer review under the responsibility of the Institute of Oceanology of the Polish Academy of Sciences.



Production and hosting by Elsevier

<https://doi.org/10.1016/j.oceano.2020.08.006>

0078-3234/© 2020 Institute of Oceanology of the Polish Academy of Sciences. Production and hosting by Elsevier B.V. This is an open access article under the CC BY-NC-ND license (<http://creativecommons.org/licenses/by-nc-nd/4.0/>).

egg density and the presence or absence data and relevant hydrobiological environmental variables, such as salinity, temperature and zooplankton biomass. The generalized additive models showed significant relationships between the environment variables (SST, SSS and Zooplankton biomass) and sardine density, but not with sardine presence. Given that the study area is characterized by high mesoscale features and significant upwelling activities, the variability of upwelling processes could explain the changes of spawning ground position and thermal window.

© 2020 Institute of Oceanology of the Polish Academy of Sciences. Production and hosting by Elsevier B.V. This is an open access article under the CC BY-NC-ND license (<http://creativecommons.org/licenses/by-nc-nd/4.0/>).

## 1. Introduction

The Moroccan Atlantic coast (36°N–21°N), located in the central canary current system, is characterized by the presence of one of the four world's major coastal upwelling systems with year-round activity (Aristegui et al., 2009; Benazzouz et al., 2015; Makaoui, 2008). In fact, the Moroccan coastal upwelling is evidenced at the surface by cold waters near the coast in response to the intensification of northeasterly winds and Ekman transport along the Moroccan continental shelf. The upwelling process promotes high primary productivity by dispersing nutrients elements and organisms over the surface layer, favoring the blooming of phytoplankton concentration and the decrease in sea surface temperatures in onshore direction. Moreover, the Moroccan upwelling region supports the highest fish abundance, because of high year-round productivity and favorable environmental conditions for larval survival and recruitment (Abdelouahab et al., 2017; Berraho, 2007; Brochier et al., 2009; Ettahiri et al., 2012), the majority of catches are composed of small coastal pelagic similar to those encountered in other coastal upwelling systems, with a domination of the European sardine (*Sardina pilchardus*).

The European pilchard *Sardina pilchardus* (Walbaum, 1792) is an important, commercial pelagic fish species in the north-west coast of Africa and especially in Morocco, with a wide distribution area in the Mediterranean Sea, and the northeastern Atlantic Ocean from the North Sea to Senegal (Parrish et al., 1989). Northern and southern limits seem to be related to the average water temperature, being located within 10 and 20°C isotherm (Furnestin, 1945). Spawning occurs in open waters and larvae remain in plankton for long periods (Olivar et al., 2001). In the Moroccan area, the exploitation of the southern stock started in the late 1950s. Thus, the long-term catch of sardine shows a gradual increase with peaks of landings of sardine in the 1970s followed by a decrease in the 1980s and an increase again in the 1990s to ≈1 million tons per year (Kifani, 1998). The constant exploitation of this resource (for several decades) makes Morocco the leader among the sardine-producer countries (where the total sardine catch represents approximately 80% of the total Moroccan catch in 2017, particularly in the southern region of Morocco, between Cape Blanc (21°N) and Cape Boujador (26°N)). In this area, sardine main spawning season occurs during the cold season from autumn to winter (Abdelouahab, 2018; Berraho, 2007; Ettahiri et al., 2012), and is characterized

by high productivity due to the permanent upwelling activity in the area which promotes food availability for larval feeding.

Worldwide, small pelagic fish species stocks, exhibit strong inter-annual fluctuations and instabilities, especially in the upwelling areas (Aristegui et al., 2009; Brochier et al., 2009; Giannoulaki et al., 2013). Many hypotheses have been reported to explain biomass fluctuations. Regardless overfishing, fluctuations may be the effect of climate changes (Alheit et al., 2012; Bonanno et al., 2016; Malta et al., 2016), or other environmental conditions (hydrodynamic circulations, water temperature, nutrient availability), or the location of the spawning habitat which can be a limiting factor for the survival of the eggs. The latter can also impact the juvenile stage and dispersing across different habitats while minimizing predation and maximizing food intake (Ciannelli et al., 2015; Drinkwater et al., 2010; Fréon et al., 2009). However, stock variability of small pelagic appears to be the result of a successful combination of processes enhancing eggs and larval development (Bakun, 2010).

In Morocco, the large fluctuation in the abundance of *Sardina pilchardus* species is one of the current problems of the global fishery management. This research provides information over large spatial and temporal scales, from data collected of sardine egg distribution, over the period 1994–2015, in the southern part of the Moroccan coast (21°N–26°N), which allows the tracking of the influence of the environmental conditions on the distribution of the European pilchard by defining their potential spawning habitat in the Northwest African coastal area.

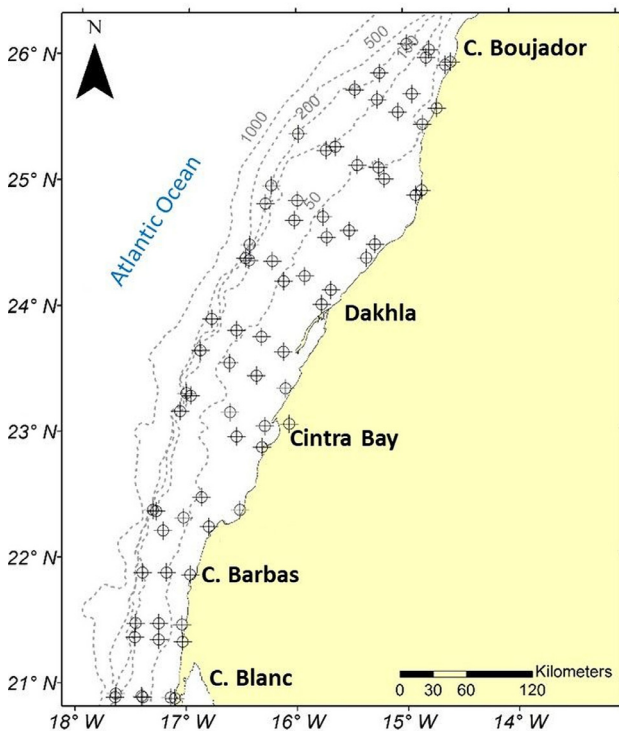
## 2. Material and methods

### 2.1. Study area

In Ichthyoplankton surveys sardine egg sampling was carried out in the southern area of the Moroccan Atlantic coast, along the region Cape Blanc–Cape Boujador (21–26°N) (12 surveys: 1994–2015) (Table 1). Sampling stations were positioned to cover all the region between the coast and the isobaths 1000 m and varying slightly from year to year (Figure 1). The surveys focused mainly on the peak spawning period of sardine in this region (cold season). Ichthyoplankton samples were collected by a small 20 cm diameter bongo net geared with a 417 µm mesh. Plankton oblique

**Table 1** Survey period conducted in the study area.

Years	Survey period			
	Season	Beginning of the survey	End of the survey	Code
1994	Winter	17-jan	26-jan	W94
1995	Winter	25-jan	04-feb	W95
1997	Winter	20-jan	03-feb	W97
1998	Winter	06-mar	23-mar	W98
1999	Spring	12-apr	01-may	S99
2003	Autumn	26-oct	11-nov	A03
2005	Autumn	05-dec	16-dec	A05
2007	Autumn	21-nov	02-dec	A07
2009	Winter	19-dec	10-jan	W09
2011	Winter	06-jan	31-jan	W11
2013	Autumn	28-nov	25-dec	A13
2015	Autumn	20-nov	15-dec	A15

**Figure 1** Example of a fish egg sampling plan network in the study area during the autumn–winter periods 1994–2015.

tows were carried out to a maximum depth of 200 m leaving 5 m over the bottom when in shallower depths. The samples were immediately preserved in 5% borax-buffered formalin. The water volume filtered was measured by a flowmeter attached to the opening of the bongo net. In the laboratory, sardine eggs were sorted from the ichthyoplankton samples and counted. The depth and water volume filtered were used to standardize abundance into egg  $10\text{ m}^{-2}$ .

Sea Surface Temperature (SST) and Sea Surface Salinity (SSS) were recorded at each station with a SBE-911+ CTD. Zooplankton biomass (ZP) was calculated as wet

weight from 5% buffered formaldehyde preserved samples (Wiebe et al., 1975) and expressed into  $\text{mg m}^{-3}$ .

## 2.2. Data analysis

For the long-term variation of spawning location, the centre of gravity was calculated. The centre of gravity is the mean location of the population, in our case, of the sardine eggs in the period of the 2000s. Using the following formula (Jenness, 2004), centres of gravity has been calculated:

$$\bar{X} = \frac{\sum_i f_i x_i}{\sum_i f_i} \quad \bar{Y} = \frac{\sum_i f_i y_i}{\sum_i f_i}$$

$\bar{X}$  and  $\bar{Y}$ : mean longitude and latitude respectively;  $f_i$ : sardine egg abundance at station  $i$ ;  $x_i$  and  $y_i$ : the longitude and latitude coordinates respectively of station  $i$ .

The spawning habitat preference of sardine was modelled based on the egg data using Generalized Additive Model (GAM) (Wood, 2006) to detect the relationships between sardine eggs and the environmental variables SST, SSS and ZP.

The relationship between the presence/absence of sardine eggs data and density data against the environmental variables were tested by the generalized additive model (GAM). GAMs with a binomial error distribution and a logit-link function were fitted to sardine binary data, while the Gaussian distribution was used to model the density data (only on given presence density) and where depths were not beyond 500 m (where the majority of the eggs were found). This analysis was performed using R 3.0.2 (R Development Core Team 2014) and ‘mgcv’ package (Wood, 2001).

## 3. Results

### 3.1. Inter-annual variability of spawning distribution and location

The distribution of sardine eggs abundances varied considerably from year to year and from decade to decade showing a large degree of inter-annual variability of sardine egg distribution during the 2000s (Figure 2). Generally, the observed egg distributions were restricted to near-shore waters except for few stations whose depth exceeded 500 m.

In the period of 1990s, high abundances were reported during 1994, 1995 and 1999 (maximum abundance: 23529 egg  $10\text{ m}^{-2}$  in 1995), whereas the lowest abundances were recorded in 1997 (maximum abundance: 216 egg  $10\text{ m}^{-2}$ ). In terms of spatial distribution, sardine eggs were concentrated between Dakhla and Cape Boujador during 1994, 1995 and 1997, whilst eggs were recorded more in the south, between Cintra bay and Dakhla in 1998–1999.

In the 2000s, high to medium sardine eggs abundances were found in 2003–2009, particularly between Cape Barbas and the northern part of Dakhla, except for the 2005, where the spatial distribution is patchy and spreads over the most shelf of the region of Cape Blanc. Besides, in 2011–2015, sardine egg abundance tends to decrease despite the high values recorded in only one station in 2013 (68539 egg  $10\text{ m}^{-2}$ ). Spatially, sardine eggs were distributed between Cintra Bay and Dakhla during 2002–2007, while eggs were

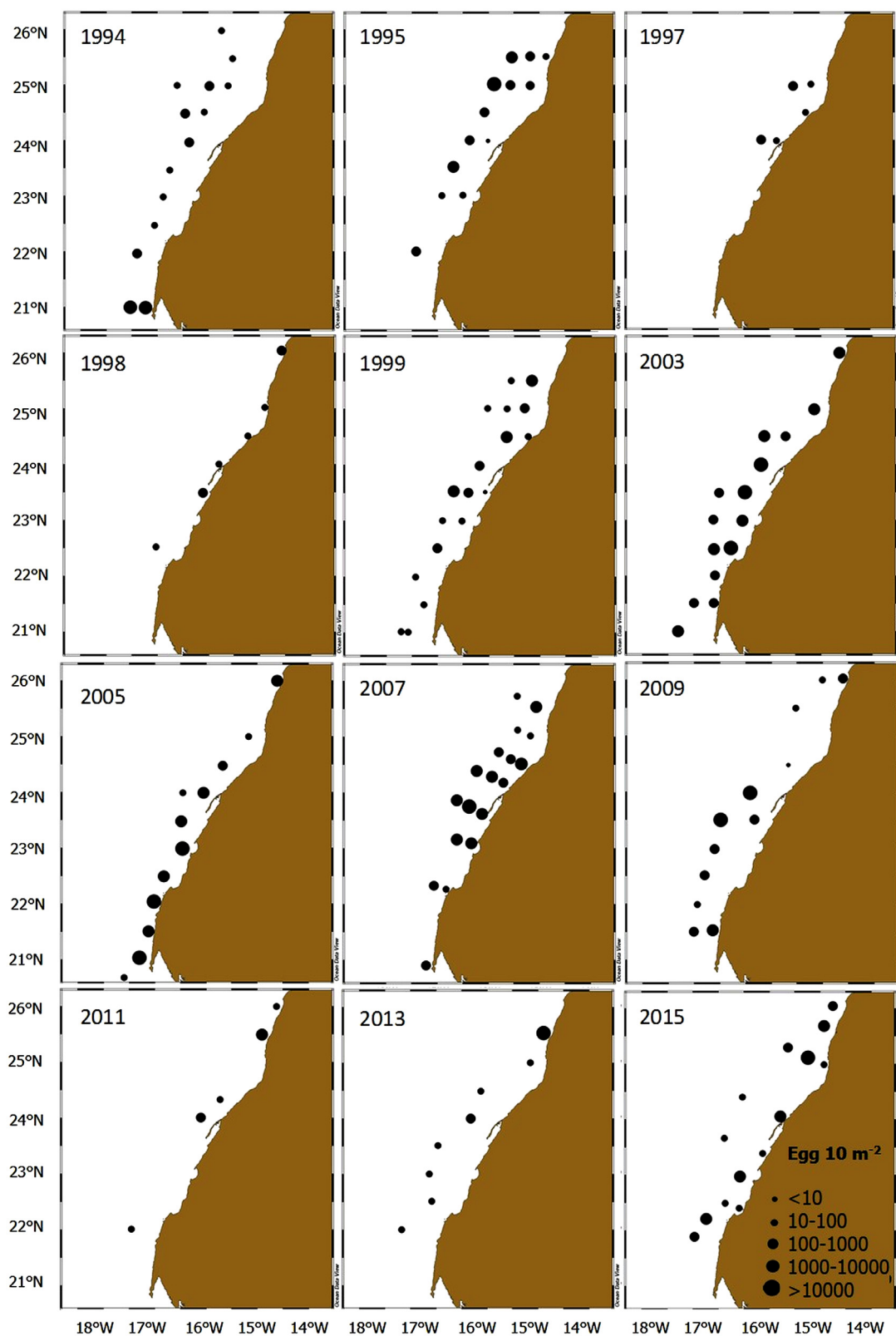


**Figure 2** Distribution of sardine egg abundance ( $\text{egg m}^{-2}$ ) in the study area during the autumn-winter periods 1994–2015.

**Table 2** Results of Generalized Additive Models (GAMs) for sardine eggs.

	Presence/absence				
	Estimate	SE	Z	p-value	p
Intercept	-0.3064	0.1042	-2.94	0.00328	**
Term	edf	Ref.df	X <sup>2</sup>	p-value	p
SST	1.000	1.001	1.195	0.274	n.s
SSS	1.656	2.030	1.850	0.402	n.s
ZP	1.492	1.830	2.765	0.216	n.s
Given presence data					
Term	Estimate	SE	Z	p-value	p
Intercept	56.927	0.1617	35.22	<2e-16	***
Term	edf	Ref.df	F	p-value	p
SST	1	1	9.585	0.00231	**
SSS	1	1	5.855	0.01663	**
ZP	1	1	7.480	0.00693	*

Code of significance: \*\*\* 0.001; \*\* 0.01; \* n.s.

found further north (southern part of Cape Boujador) in 2011–2015.

### 3.2. Long term variation of spawning location

To show the long-term variation, centers of gravity of spawning location were calculated based on the location of each grid weighted by the number of eggs for each year. Generally, all sardine spawning areas were coastal areas where maximum depths were not over 50 meters' depth.

During the period of 1990s, the main spawning area of sardine was observed between Dakhla (24°N) and the south of Boujador (25°N). Throughout the 2000s, the mean centres spawning gravity location showed changes between 2003–2009 and 2011–2015 (Figure 3). The spawning position was found concretely around Dakhla. Thus, in the early 2000s, the spawning location was observed between Cintra Bay and Dakhla, with the exception of 2005, where the main spawning occurred further down south, particularly near Cape Barbas. Contrarily, during the period from 2011–2015, a shift of the spawning location of sardine was observed towards the north of Dakhla.

### 3.3. Sardine spawning relationship with SST, SSS and ZP

GAM modeling was used to explore the relationship of sardine spawning with SST, SSS and ZP by using the density data and the presence/absence data of sardine eggs acquired from the time series data of surveys from 1994–2015. The results of the model are shown in Table 2. No significant relationship was detected between the presence/absence of sardine eggs with SST, SSS and ZP. However, a highly significant linear relationship between egg abundance and SST, SSS and ZP was observed. To confirm this linear relationship, a multiple regression analysis was applied verifying its statistical significance (Table 3). Figure 4 shows the GAM plot depicting the potential relationships of sardine egg abundance and SST, SSS and ZP. The results of the GAMs analysis revealed that eggs are likely to be found at surface

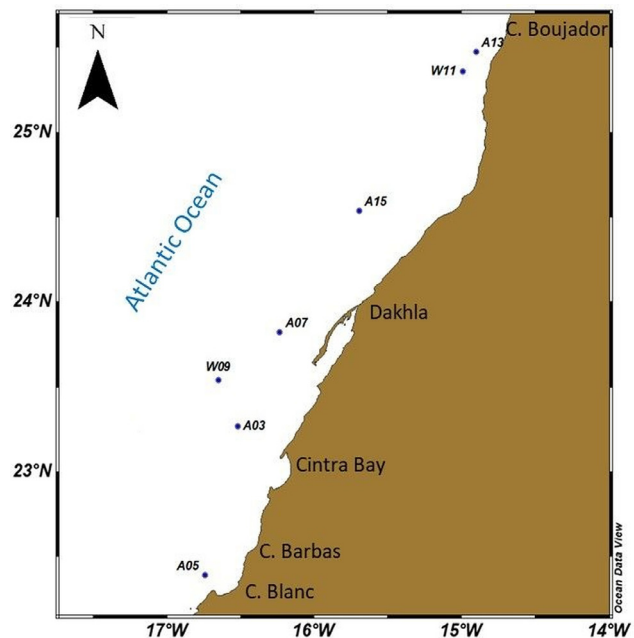


**Figure 3** Centres of gravity of spawning location of sardine in the study area.

temperatures between 18.5 and 22.5°C. Sardine eggs were associated with lower values of salinities (< 36.4 psu). Furthermore, eggs were more abundant in areas of high biomass of mesozooplankton.

### 3.4. Spatial-temporal dynamics of the sardine spawning habitat

The modelled potential spawning habitat of sardine covers larger areas and is patchier during the period of the 2000s (Figure 5b) than during the 1990s (Figure 5a). During the 1990s, the area with a probability of more than 50% egg presence may be considered as a favorable area for sardine

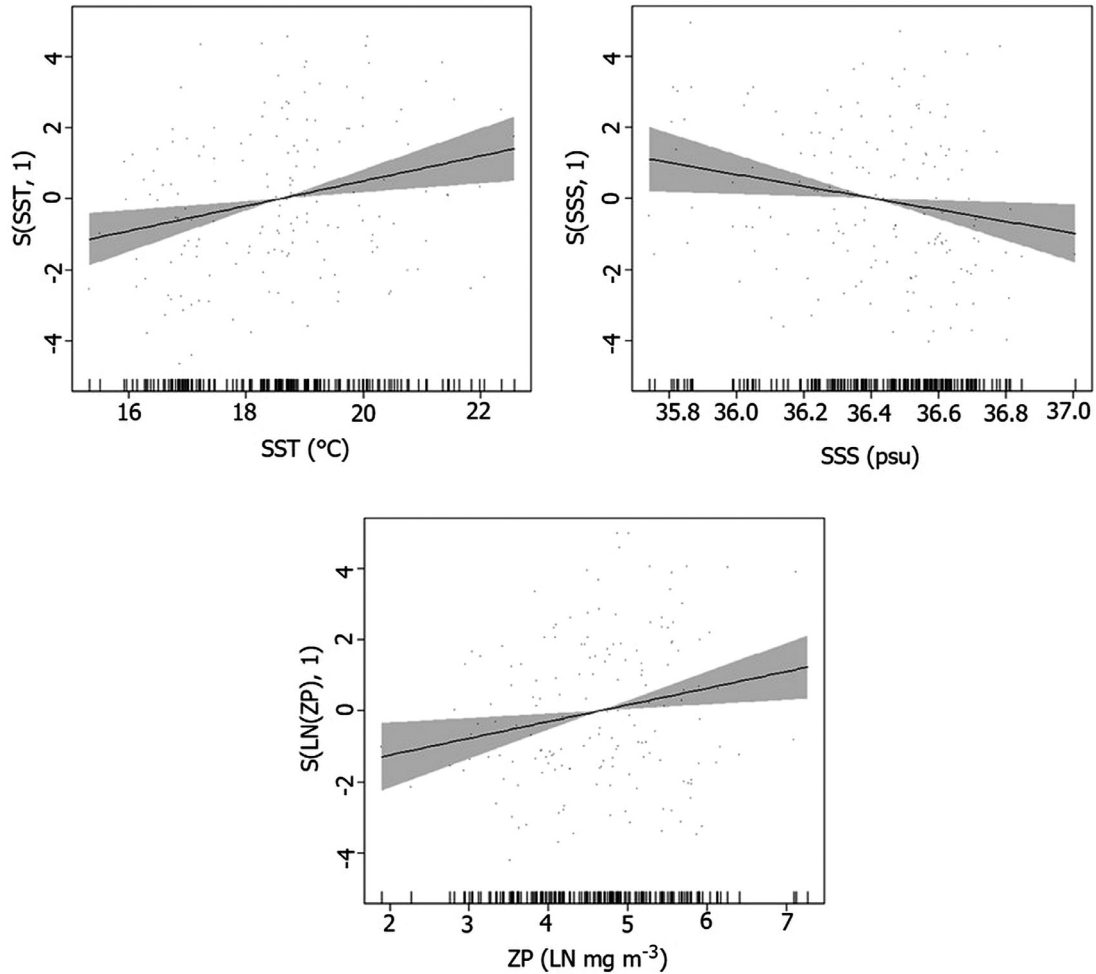


**Figure 4** Results of Generalized Additive Models (GAM). The panels show the effect of SST: Sea surface temperature, SSS: Sea surface salinity and ZP: Zooplankton biomass, on the distribution of sardine eggs.

**Table 3** Result of multiple linear regression between egg densities (positive stations) and environmental parameters (SST, SSS and ZP).

	Estimate	SE	t value	Pr(>  t )	p
SST	0.318	0.114	2.785	0.006	**
SSS	-1.638	0.687	2.385	0.018	*
ZP	0.002	0.001	-2.877	0.005	**

Code of significance: \*\*\* 0.001; \*\* 0.01; \* 0.05.

spawning. This area constricted to the coastal area between Dakhla and the southern part of Cape Boujador (Figure 5a).

During the 2000s, the potential spawning area of this species is more dispersed, from Cape Boujador to Cape Barbas (Figure 5b). However, three areas of high egg probabilities (> 75%) were identified: (1) between Cape Boujador and 25°N, (2) in the Dakhla region and (3) between Cintra Bay and Cape Barbas.

The offshore region between Cape Barbas and Cape Blanc showed a low probability of sardine egg presence in both periods of the 1990s and the 2000s. The analysis of the average

and variability maps of egg presence of both periods allowed the identification of a recurrent spawning area of high egg probability (> 75%) located between Dakhla and Cape Boujador. An occasional spawning area is located between the northern area of Cape Barbas and Cintra Bay where the average probability of egg presence is high but showing high variability. Offshore areas show low average probability of sardine spawning according to data on egg presence and likewise showing low variability (Figure 5c).

#### 4. Discussion

Our samples were collected in the cold season coinciding with the peak spawning period of sardine in this area. During the study period, sardine eggs abundances varied from year to year. The distribution maps of sardine eggs revealed high abundances in the period of 2003–2009 compared to the 1990s, particularly in the coastal areas. In the winter of 1997/1998, a decrease of the sardine eggs abundances was observed. Indeed, the Moroccan stock of sardine has experienced dramatic changes in terms of abundance, especially during the 1997/1998 spawning season. This period corresponds to an El Niño warming trend that increased

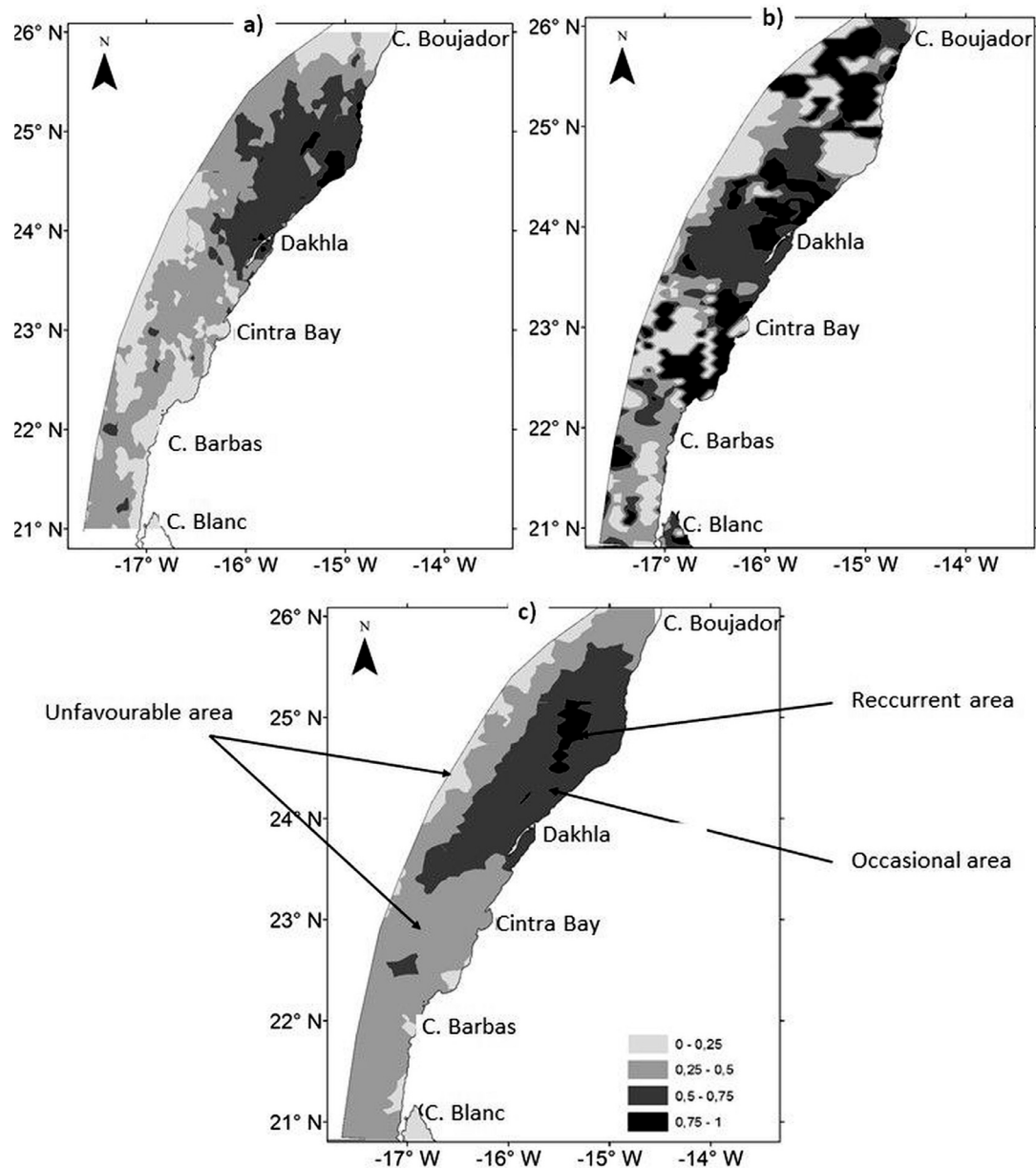


**Figure 5** Spatial location of recurrent, occasional and unfavourable sardine spawning area (Grey scale is proportional to the probability of presence of eggs). Top left (a): average map of sardine spawning area for the period of 1990's. Top right (b): variability map of sardine spawning area for the period of 2000's. Bottom (c): average map of the probability of presence of eggs for the period of 1994–2015.

temperatures in the study area (INRH, 2002) which may have affected the optimal temperature regime for sardine spawning.

The period 2011–2013 showed low sardine egg abundances which only increased slightly in 2015. Considering the sampling periods of each decade (in winter of 1990s and in late autumn of 2000s), spawning variability between the two decades can be attributed to seasonal variations, jointly with the inter-annual variability of the environmental conditions. Petitgas et al. (2013) found strong sardine spawning variability in the Bay of Biscay, which corresponded to inter-annual differences in temperature.

In the 1994–1999 period, the spawning ground of the southern population of sardine was found between Dakhla (24°N) and the south of Cape Boujador (26°N) (Berraho, 2007; Ettahiri et al., 2012). During the period of autumn-winter of the 2000s, sardine spawning grounds were located in the south, particularly between Dakhla (24°N) and Cintra Bay (23°N), except for the year 2005 and the period between 2011–2015. The high variability in the distribution of eggs between the spawning years and within the same area is probably driven by environmental conditions. Indeed, the inter-annual variability of the spawning ground of sardine is related to the variability of the environmen-

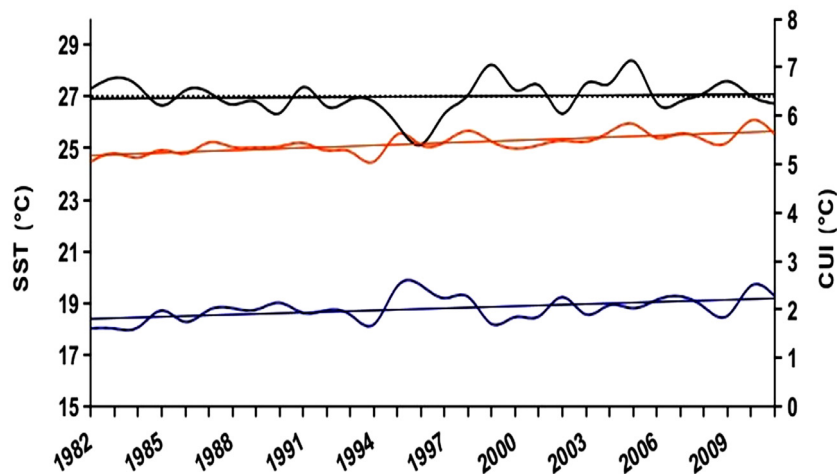


**Figure 6** The annual-mean SST (Sea surface temperature) during 1982–2011 for SST<sub>max</sub> (red line), SST<sub>min</sub> (blue line) and CUI (Coastal upwelling index; thick black line) (Benazzouz et al., 2015).

tal parameters (Berraho et al., 2005; Ettahiri et al., 2012) which are influenced by the global environmental changes. During the last decade, fish populations have decreased, particularly regarding small pelagic fish stocks (INRH, 2014). Bakun and Cury (1999) have noted that changes in the wind intensity and the onset of the upwelling season can also be related to changes in the main atmospheric circulation patterns such as the North Atlantic Oscillation (NOA) and the Pacific Decadal Oscillation (PDO) (Guisande et al., 2004; Lindegren et al., 2013) and may cause fluctuations in the abundance of the small pelagic year per year. In general, the spawning habitat of small pelagic must conform to having suitable hydrophysical conditions (e.g., temperature, salinity and availability of food), the necessary trophic resources, and the coexistence of relatively few predators (Weber et al., 2015). In the Moroccan coast off Northwest Africa, sardine spawning is observed within an optimal temperature range of 16–18.5°C (Ettahiri et al., 2003; Furnestin and Furnestin, 1959).

Generally, a preferential spawning habitat must comply with favorable conditions for spawning of a given species, particularly defined by its hydroclimatic features and the necessary trophic resources, as well as, being surrounded by few numbers of the predator spectrum (Weber et al., 2015). The optimum spawning habitat of sardine off NW Africa has been defined by assessing the link between sardine egg densities and their presence/absence data with the implementation of a Generalized Additive Model (GAM). The relative presence/absence egg data did not show any significant relationship with SST, SSS and ZP. However, the results of the Generalized Additive Model indicate a significant linear relationship ( $p < 0.05$ ) between the referred environmental variables and the egg density data. The predicted model showed that sardine was mostly to be found at sea surface temperatures between 18 and 22°C. However, the results of the quotient analysis carried out in the 1990s showed that the preferred temperature ranges from 15.5 to 17.5°C (Berraho, 2007; Ettahiri et al., 2012). The results of the GAMs imply that the preferred temperature range for the sardine spawning has shifted to a higher temperatures regime possibly consequent with the global

warming trend in this region (Benazzouz, 2014). Changes in the preferred environmental conditions may also be due to a direct consequence of changes in the location of sardine spawning grounds through time, as reported in previous studies (van der Lingen et al., 2001, 2006). In the southern Benguela region, sea surface temperature experienced a warming trend during the 2000s period which accounted for the changes in the spawning distribution patterns as suggested by Roulaut et al. (2010) and which was confirmed by a gradual eastward shift of spawning habitat of sardine as a response to this warming (Mhlongo et al., 2015). In this climatic context, Peck et al. (2013) argued that sardine is an excellent bio-indicator of the climate-driven changes in marine systems. Indeed, these authors suggested a dependence of preferred SST ranges for the European sardine spawning in the function of their geographical location. Thus, at decadal scales, these thermal preference variations for spawning can be attributed to significant sea surface temperature variability, as supported by Benazzouz et al. (2014; 2015) that found significant changes in temperature between the 1990s and the warming trend beyond the 2000s. This warming trend is observed in the coastal and oceanic parts of the Canary Current region, as observed from the thermal field trends from 1998 to 2014, also visible in the southern part of the Moroccan Atlantic (Figure 6). Similarly, thermal conditions in the Benguela current ecosystem have recently evolved towards a warming period (Rouault et al., 2010), and correspondingly, sardine and anchovy spawning distribution patterns seem to have followed accordingly to these changes (Mhlongo et al., 2015). Both species are considered climate change bio-indicators of marine ecosystems (Peck et al., 2013), due to their capacity to respond to climatic changes (Mhlongo et al., 2015). In the Benguela ecosystem, single parameter quotient applied yearly from 1988 to 2009 highlighted a wide range of the preferential temperature from 16–22°C for the Benguela sardine spawning (*Sardinops sagax*) (Mhlongo et al., 2015). The salinity range in which sardine eggs were found was wide (35.7–36.4) and within the same range described previously (Berraho et al., 2005; Ettahiri et al., 2003). The GAM's results suggest that the

availability of food is one of the biotic factors involved in selecting a suitable habitat for spawning.

According to the results observed in 2004, there is a synchrony between the abundance of ichthyoplankton and zooplankton, which showed an overlap of zooplankton and fish egg distributions, promoting a favorable habitat for the future larvae. In fact, Chicharo et al. (2003) studying the nutritional conditions of sardine larvae found a significant correlation between zooplankton biomass and specifically on the microzooplankton fraction with the RNA/DNA ratio. Similarly, seasonal and annual variability of the potential spawning habitat of sardinella (*Sardinella aurita*) has been observed associated with planktonic biomass, thus providing favorable feeding conditions for larval survival after spawning (Mbaye et al., 2015).

The GAMs analysis revealed a significant relationship between sardine eggs and zooplankton biomass, where egg abundance is related to higher zooplankton biomass. Sardine regulates trophic links between zooplankton and the upper trophic level of fish constituting a midtrophic level in highly productive ecosystems (Cury et al., 2000). In fact, most eggs are found in similar sites presenting similar environmental conditions to those in which the spawning occurred (Weber and McClatchie, 2010). These results suggest that food availability is among the biological factors contributing to the selection of suitable spawning habitat.

The temporal variability of environmental conditions not only influences spawning habitats but also impacts the spatial dynamics in terms of spawning ground's distribution of different sardine populations (Bellier et al., 2006; Gigliotti et al., 2010; Mhlongo et al., 2015; Planque et al., 2007; van der Lingen et al., 2001).

The location of suitable spawning areas was assessed based on the analysis of the probability of occurrence of eggs during two decades, the 1990s and the 2000s. As a result of this study, a strong inter-decadal variability in the spatial positioning of spawning grounds was determined. In the 1990s, a restricted area of a high probability of egg occurrence was identified near the coast at a latitude of 25°N where sardines spawned regularly every year. This was a large area characterized by its inter-annual variability of sardine egg production. In the 2000s, areas of high spawning probability were more spatially spread out. In addition, over the entire period from 1994–2015, three categories of spawning habitats were identified by Bellier et al. (2006): a) a persistent spawning area where the spawning is observed every year being delimited by 24°30'–25°30'N; b) an occasional spawning area where sardines spawned variably from year to year in the spatial extension from southern Cape Boujador to Cintra Bay and c) unfavorable spawning areas where quasi-absence of sardine eggs in this area is observed which is likely due to hydrographic features causes rather than spawning.

## Acknowledgements

This work was carried out in the context of the oceanographic program of the Moroccan coastal sites undertaken by the National Institute of Fisheries Research. The authors thank all the team that took part in the surveys. The au-

thors would also like to thank the editor and the reviewers for their useful comments.

## References

- Abdelouahab, H., 2018. Assemblages des larves de poissons et variabilité temporelle de la phase planctonique de la sardine (Atlantique marocain), Ph.D. thesis. Hassan II Univ., Casablanca, Morocco, 194 pp.
- Abdelouahab, H., Berraho, A., Baibai, T., Agouzouk, A., Makaoui, A., Errhif, A., 2017. Autumn larval fish assemblages in the northwest African Atlantic coastal zone. *Chin. J. Oceanol. Limnol.* 35 (3), 515–527. <http://dx.doi.org/10.1007/s00343-017-5302-7>
- Alheit, J., Pohlmann, T., Casini, M., Greve, W., Hinrichs, A., Mathis, M., O'Driscoll, K., 2012. Climate variability drives anchovies and sardines into North and Baltic Sea. *Prog. Oceanogr.* 96 (1), 128–139. <https://doi.org/10.1016/j.pocean.2011.11.015>
- Arístegui, J., Barton, E.D., Álvarez-Salgado, X.A., Santos, A.M.P., Figueiras, F.G., Kifani, S., Hernández-León, S., Mason, E., Machu, E., Demarcq, H., 2009. Sub-regional ecosystem variability in the Canary current upwelling. *Prog. Oceanogr.* 83 (1–4), 33–48. <https://doi.org/10.1016/j.pocean.2009.07.031>
- Bakun, A., 2010. Linking climate to population variability in marine ecosystems characterized by non-simple dynamics: Conceptual templates and schematic constructs. *J. Mar. Syst.* 79, 361–373. <https://doi.org/10.1016/j.jmarsys.2008.12.008>
- Bakun, A., Cury, P., 1999. The “school trap”: a mechanism promoting large-amplitude out-of-phase population oscillations of small pelagic fish species. *Ecol. Lett.* 2 (6), 349–351.
- Bellier, E., Planque, B., Petitgas, P., 2006. Historical fluctuations in spawning locations of anchovy (*Engraulis encrasicolus*) and sardine (*Sardina pilchardus*) in the Bay of Biscay during 1967–73 and 2000–2004. *Fish. Oceanogr.* 16 (1), 1–15. <https://doi.org/10.1111/j.1365-2419.2006.00410.x>
- Benazzouz, A., 2014. Upwelling côtier et effet de la dynamique océanique à méso-échelle sur la variabilité planctonique dans le système du Courant des Canaries, Ph.D. thesis. Hassan II Univ., Casablanca, Morocco, 261 pp.
- Benazzouz, A., Demarcq, H., González-Nuevo, G., 2015. Changes and trends of the upwelling intensity in the Canary Current Large Marine Ecosystem. In: Valdés, L., Déniz-González, I. (Eds.), *Oceanographic and Biological Features in the Canary Current Large Marine Ecosystem*. IOC-UNESCO, IOC Tech. Series 115, Paris, 321–330.
- Benazzouz, A., Mordane, S., Orbi, A., Chagdali, M., Hilmi, K., Atilah, A., Pegri, J.L., Demarcq, H., 2014. An improved coastal upwelling index from sea surface temperature using satellite-based approach – the case of the Canary Current upwelling system. *Cont. Shelf Res.* 81, 38–54. <http://dx.doi.org/10.1016/j.csr.2014.03.012>
- Berraho, A., 2007. Relations spatialisées entre milieu et ichtyoplancton des petits pélagiques de la côte Atlantique Marocaine (Zones central et sud), Ph.D. thesis. Mohammed V Univ., Rabat, Morocco, 261 pp.
- Berraho, A., Ettahiri, O., Letourneur, Y., Orbi, A., Yahyaoui, A., 2005. Importance des paramètres hydrologiques dans la distribution des oeufs et larves des petits pélagiques du sud de l'Atlantique marocain. *Cybiu* 29 (1), 21–31.
- Bonanno, A., Barra, M., Basilone, G., Genovese, S., Rumolo, P., Goncharov, S., Popov, S., Buongiorno Nardelli, B., Iudicone, D., Procaccini, G., Aronica, S., Patti, B., Giacalone, G., Ferreri, R., Fontana, I., Tranchida, G., Mangano, S., Pulizzi, M., Gargano, A., Di Maria, A., Mazzola, S., 2016. Environmental processes driving anchovy and sardine distribution in a highly vari-

- able environment: the role of the coastal structure and riverine input. *Fish. Oceanogr.* 25 (5), 471–490. <http://dx.doi.org/10.1111/fog.12166>
- Brochier, T., Colas, F., Lett, C., Echevin, V., Cubillos, L.A., Tamf, J., Chlaida, M., Mullon, C., Fréon, P., 2009. Small pelagic fish reproductive strategies in upwelling systems: A natal homing evolutionary model to study environmental constraints. *Prog. Oceanogr.* 83 (1–4), 261–269. <https://doi.org/10.1016/j.pocean.2009.07.044>
- Chicharo, M.A., Esteves, E., Santos, M.A., dos Santos, A., Peliz, A., Ré, P., 2003. Are sardine larvae caught off northern Portugal in winter starving? An approach examining nutritional conditions. *Mar. Ecol. Prog. Ser.* 257, 303–309. <https://doi.org/10.3354/meps257303>
- Ciannelli, L., Bailey, K., Olsen, E.M., 2015. Evolutionary and ecological constraints of fish spawning habitats. *ICES J. Mar. Sci.* 72 (2), 285–296. <https://doi.org/10.1093/icesjms/fsu145>
- Cury, P., Bakun, A., Crawford, R.J.M., Jarre, A., Quiñones, R.A., Shannon, L.J., Verheye, H.M., 2000. Small pelagics in upwelling systems: patterns of interaction and structural changes in “wasp-waist” ecosystems. *ICES J. Mar. Sci.* 57, 603–618. <https://doi.org/10.1006/jmsc.2000.0712>
- Drinkwater, K.F., Beaugrand, G., Kaeriyama, M., Kim, S., Ottersen, G., Perry, R.I., Pörtner, H.O., Plovina, J.J., Takasuka, A., 2010. On the processes linking climate to ecosystem changes. *J. Mar. Syst.* 79 (3–4), 374–388. <https://doi.org/10.1016/j.jmarsys.2008.12.014>
- Ettahiri, O., Berraho, A., Houssa, R., Ramzi, A., Somoue, L., Zizah, S., Machu, E., 2012. Characteristics of the spawning habitats of sardine, *Sardina pilchardus*, off the Moroccan Atlantic coast (21°N–26°N). *FAO, Pêch. Aquac.* 18, 157–186.
- Ettahiri, O., Berraho, A., Vidy, G., Ramdani, M., Do chi, T., 2003. Observation on the spawning of *Sardina* and *Sardinella* off the south Moroccan Atlantic coast (21–26°N). *Fish. Oceanogr.* 60 (2–3), 207–222. [https://doi.org/10.1016/S0165-7836\(02\)00172-8](https://doi.org/10.1016/S0165-7836(02)00172-8)
- Fréon, P., Werner, F., Francisco, P., Chavez, F.P., 2009. Conjectures on future climate effects on marine ecosystems dominated by small pelagic fish. In: Checkley, D., Alheit, J., Oozeki, Y., Roy, C. (Eds.), *Climate Change and Small Pelagic Fish*. Cambridge Univ. Press, 312–343.
- Furnestin, J., 1945. Note préliminaire sur l’Anchois (*Engraulis encrasicolus*) du Golfe de Gascogne. *Rev. Trav. Off. Sci. Tech. Pêches Marit* 13 (1–4), 197–209
- Furnestin, J., Furnestin, M.L., 1959. La reproduction de la sardine et de l’anchois des côtes Atlantiques du Maroc (saisons et aires de ponte). *Rev. Trav. Ins. Pêches Marit.* 23 (1), 79–104.
- Giannoulaki, M., Iglesias, M., Tugores, M.P., Bonanno, A., Patti, B., De Felice, A., Leonori, I., Bigot, J.L., Tičina, V., Pyrrounaki, M.M., Tsagarakis, K., Machias, A., Somarakis, S., Schismenou, E., Quinci, E., Basilone, G., Cuttitta, A., Campanella, F., Miquel, J., Onate, D., Roos, D., Valavanis, V., 2013. Characterizing the potential habitat of European anchovy *Engraulis encrasicolus* in the Mediterranean Sea, at different life stages. *Fish. Oceanogr.* 22 (2), 69–89. <https://doi.org/10.1111/fog.12005>
- Gigliotti, E.S., Gherardi, D.F.M., Paes, E.T., Souza, R.B., Katsuragawa, M., 2010. Spatial analysis of egg distribution and geographic changes in the spawning habitat of the Brazilian sardine *Sardinella brasiliensis*. *J. Fish Biol.* 77 (10), 2248–2267. <https://doi.org/10.1111/j.1095-8649.2010.02802.x>
- Guisande, C., Vergara, A., Riveiro, I., Cabanas, J., 2004. Climate Change and Abundance of the Atlantic-Iberian Sardine (*Sardina pilchardus*). *Fish. Oceanogr.* 13, 91–101. <https://doi.org/10.1046/j.1365-2419.2003.00276.x>
- INRH, 2002. Les ressources halieutiques marocaines: situation et niveaux d’exploitation. *Doc. Tech. INRH*, 167 pp.
- INRH, 2014. *Etat des Stocks et des Pêcheries Marocaines*. Doc. Tech. INRH, 305 pp
- Jenness, J., 2004. Weighted mean extension for Arc View3. x, v. 1.2c. Jenness enterprises
- Kifani, S., 1998. Climate dependent fluctuations of the Moroccan sardine and their impact on fisheries. In: ORSTOM (Ed.), *Global Versus Local Changes in Upwelling Systems*. Colloq. Inst. Fr. Rech. Sci.Dev. Coop., Paris, 235–247.
- Lindegren, M., Checkley, D., Rouyer, T., Maccall, A., Stenseth, N., 2013. Climate, fishing, and fluctuations of sardine and anchovy in the California Current. *Proc. Natl. Acad. Sci. USA.* 110 (33), 13577–13677. <http://dx.doi.org/10.1073/pnas.1305733110>
- Makaoui, A., 2008. Etude de l’upwelling côtier de la côte atlantique marocaine et sa contribution à la sédimentologie du plateau continental, Ph.D. thesis. Hassan II Univ., Casablanca, Morocco, 163 pp.
- Malta, T., Santos, P.T., Santos, A.M.P., Rufino, M., Silva, A., 2016. Long-term variations in Ibero-Atlantic sardine (*Sardina pilchardus*) population dynamics: Relation to environmental conditions and exploitation history. *Fish. Res.* 179, 47–56. <http://dx.doi.org/10.1016/j.fishres.2016.02.009>
- Mbaye, B.C., Brochier, T., Echevin, V., Lazar, A., Lévy, M., Masson, E., Gaye, A.T., Machu, E., 2015. Do *Sardinella aurita* spawning seasons match local retention patterns in the Senegalese-Mauritanian upwelling region? *Fish. Oceanogr.* 24 (1), 69–89. <http://dx.doi.org/10.1111/fog.12094>
- Mhlongo, N., Yemane, D., Hendricks, M., Van Der Lingen, C.D., 2015. Have the spawning habitat preferences of anchovy (*Engraulis encrasicolus*) and sardine (*Sardinops sagax*) in the southern Benguela changed in recent years? *Fish. Oceanogr.* 24 (Suppl. 1), 1–14. <https://doi.org/10.1111/fog.12061>
- Olivar, M.P., Salat, J., Palomera, I., 2001. Comparative study of spatial distribution patterns of the early stages of anchovy and pilchard in the NW Mediterranean Sea. *Mar. Ecol. Prog. Ser.* 217, 111–120.
- Parrish, R.H., Serra, R., Grant, W.S., 1989. The Monotypic Sardines, *Sardina* and *Sardinops*: Their Taxonomy, Distribution, Stock Structure, and Zoogeography. *Can. J. Fish. Aquat. Sci.* 46 (11), 2019–2036.
- Peck, M.A., Reglero, P., Takahashi, M., Catalan, I.A., 2013. Life cycle ecophysiology of small pelagic fish and climate-driven changes in populations. *Prog. Oceanogr.* 116, 220–245. <http://dx.doi.org/10.1016/j.pocean.2013.05.012>
- Petitgas, P., Rijnsdorp, A.D., Dickey-Collas, M., Engelhard, G.H., Peck, M.A., Pinnegar, J.K., Drinkwater, K., Huret, M., Nash, R.D.M., 2013. Impacts of climate change on the complex life cycles of fish. *Fish. Oceanogr.* 22 (2), 121–139. <https://doi.org/10.1111/fog.12010>
- Planque, B., Bellier, E., Lazure, P., 2007. Modelling potential spawning habitat of sardine (*sardina pilchardus*) and anchovy (*engraulis encrasicolus*) in the Bay of Biscay. *Fish. Oceanogr.* 16, 16–30. <https://doi.org/10.1111/j.1365-2419.2006.00411.x>
- Rouault, M., Pohl, B., Penven, P., 2010. Coastal oceanic climate change and variability from 1982 to 2009 around South Africa. *Afr. J. Mar. Sci.* 32 (2), 237–246. <https://doi.org/10.2989/1814232X.2010.501563>
- van der Lingen, C.D., Hutchings, L., Merkle, D., van der Westhuizen, J.J., Nelson, J., 2001. Comparative spawning habitats of anchovy (*Engraulis capensis*) and sardine (*Sardinops sagax*) in the southern Benguela upwelling ecosystem. In: Kruse, G.H., Bez, N., Booth, T., Dorn, M., Hills, S., Lipcius, R.N., Pelletier, D., Roy, C., Smith, S.J., Witherell, D. (Eds.), *Spatial Processes and Management of Marine Populations*. Alaska Sea Grant Univ., Fairbanks, 185–209.
- van der Lingen, C.D., Shannon, L.J., Cury, P., Kreiner, A., Moloney, C.L., Roux, J-P., Vaz- Velho, F., 2006. Resource and

- Ecosystem Variability, Including Regime Shifts, in the Benguela Current System. *Large Mar. Ecosyst.* 147–184. [https://doi.org/10.1016/S1570-0461\(06\)80013-3](https://doi.org/10.1016/S1570-0461(06)80013-3)
- Weber, E.D., Chao, Y., Chai, F., McClatchie, S., 2015. Transport patterns of Pacific sardine *Sardinops sagax* eggs and larvae in the California Current System. *Deep-Sea Res. I.* 100, 127139. <https://doi.org/10.1016/j.dsr.2015.02.012>
- Weber, E.D., McClatchie, S., 2010. Predictive models of northern anchovy *Engraulis mordax* and Pacific sardine *Sardinops sagax* spawning habitat in the California current. *Mar. Ecol. Prog. Ser.* 406, 251–263.
- Wiebe, W.J., Johannes, R.E., Webb, K.L., 1975. Nitrogen fixation in a coral reef community. *Science* 188 (4185), 257–259. <https://doi.org/10.1126/science.188.4185.257>
- Wood, S.N., 2001. mgcv: GAMs and Generalized Ridge Regression for R. *R News* 1 (2), 20–25
- Wood, S.N., 2006. *Generalized Additive Models: An Introduction with R*. J. Stat. Softw. Chapman et Hall/CRC, Boca Raton, 410 pp.



Available online at [www.sciencedirect.com](http://www.sciencedirect.com)

ScienceDirect

journal homepage: [www.journals.elsevier.com/oceanologia](http://www.journals.elsevier.com/oceanologia)



ORIGINAL RESEARCH ARTICLE

# Assessment of a sheltered euhaline area of the southeastern Bay of Biscay to sustain bivalve production in terms of phytoplankton community composition

Jone Bilbao<sup>a,b,\*</sup>, Oihane Muñiz<sup>c</sup>, José Germán Rodríguez<sup>c</sup>, Marta Revilla<sup>c</sup>, Aitor Laza-Martínez<sup>a,b</sup>, Sergio Seoane<sup>a,b</sup>

<sup>a</sup> Department of Plant Biology and Ecology, Faculty of Science and Technology, University of the Basque Country, UPV/EHU, Leioa, Spain

<sup>b</sup> Research Centre for Experimental Marine Biology and Biotechnology (Plentzia Marine Station, PiE – UPV/EHU), University of the Basque Country, Plentzia, Spain

<sup>c</sup> AZTI, Marine Research Division, Pasaia, Spain

Received 28 April 2020; accepted 27 August 2020

Available online 6 September 2020

## KEYWORDS

Phytoplankton community composition;  
Biomass;  
Physico-chemical variables;  
Aquaculture;  
Mussels;  
Bay of Biscay

**Abstract** This study describes the phytoplankton community in sheltered euhaline waters of the Basque coast (southeastern Bay of Biscay). Phytoplankton composition, cell size, abundance, biomass and the presence of potentially toxic taxa, together with chlorophyll *a*, nutrients and hydrographic and optical conditions were measured, from August 2016 to August 2017, in the Mutriku port, with the main aim of assessing the suitability of the phytoplankton community as a food resource for bivalves. The water column in Mutriku showed the typical environmental conditions of Basque marine waters, with no significant nutrient enrichment caused by anthropogenic pressures. Haptophytes represented the greatest contribution to cell abundance (31–47%), and diatoms were the dominant group in terms of biomass (52–79%), which could favour mussel growth due to their high fatty acid content. In addition, the size

\* Corresponding author at: Department of Plant Biology and Ecology, Faculty of Science and Technology, University of the Basque Country, UPV/EHU, Leioa 48940, Spain. Tel.: +34 946012694.

E-mail address: [jone.bilbao@ehu.eus](mailto:jone.bilbao@ehu.eus) (J. Bilbao).

Peer review under the responsibility of the Institute of Oceanology of the Polish Academy of Sciences.



Production and hosting by Elsevier

<https://doi.org/10.1016/j.oceano.2020.08.007>

0078-3234/© 2020 Institute of Oceanology of the Polish Academy of Sciences. Production and hosting by Elsevier B.V. This is an open access article under the CC BY-NC-ND license (<http://creativecommons.org/licenses/by-nc-nd/4.0/>).

structure of the phytoplankton community was suitable for mussel ingestion, since the predominant cell size was 2–20  $\mu\text{m}$ . Regarding toxic phytoplankton, the genera that pose a risk for human health and those that affect negatively mussel physiology and survival were considered. Altogether, ten toxic phytoplankton taxa were identified, contributing in less than 5% to the total cell abundance of Mutriku. However, median chlorophyll *a* concentration was low (0.5  $\mu\text{g L}^{-1}$ ), reflecting the oligotrophic conditions of the area. Therefore, even if the composition of the phytoplankton community could be favourable for bivalve aquaculture, biomass values are low compared to other zones of bivalve production.

© 2020 Institute of Oceanology of the Polish Academy of Sciences. Production and hosting by Elsevier B.V. This is an open access article under the CC BY-NC-ND license (<http://creativecommons.org/licenses/by-nc-nd/4.0/>).

## 1. Introduction

Phytoplankton, as major primary producers in marine coastal systems, play an indispensable role in sustaining the pelagic food webs (e.g., Reynolds, 2006) and maintaining the ecosystem's healthy structure and functioning (e.g., Malone et al., 2016). In addition, phytoplankton communities exhibit large variations, mainly as a response to changes in abiotic factors driven by meteorological and hydrographic processes, but also because of biotic factors like grazing, competition, parasitism and microbial attack (Granéli and Turner, 2006).

Phytoplankton composition and dynamics are very important for shellfish aquaculture, being these organisms the main source of energy for filter-feeder bivalves like mussels (e.g., Petersen et al., 2008). However, not all phytoplankton species have either an appropriate cell size for ingestion or a good nutrient composition for the growth of bivalves (e.g., Brown, 2002; Marshall et al., 2010). The ingestion and retention efficiency of mussels depends on the cell size of the phytoplankton species, and although there is controversy about the most appropriate particle-size, most of the studies agree that a size range of 4–45  $\mu\text{m}$  is the most suitable for high food depletion (Cranford et al., 2014). Moreover, several studies observed low retention of picophytoplankton (0.2–3.0  $\mu\text{m}$ ) in mussel rafts (Petersen et al., 2008) and long-line culture systems (Cranford et al., 2008). When it comes to nutrient composition, since lipids are the principal source of energy for bivalve larvae, the nutritional value of phytoplankton species principally belongs to their lipid content, especially essential fatty acids (EFA), which varies depending on the species or group (Marshall et al., 2010; Pettersen et al., 2010). In addition, several studies recognise that the nutritional value of a multispecies algal diet (at least one species of flagellate and one type of diatom) is higher than that of a monoculture, having synergistic effects on mussel growth (Pettersen et al., 2010; Stromgren and Cary, 1984).

On the other hand, phytoplankton can be problematic for shellfish aquaculture due to the potential for synthesising toxins that some phytoplankton species or strains have. When bivalves filter toxic phytoplankton, toxins are actively accumulated and concentrated in the hepatopancreas and get transferred to higher trophic levels, becoming a serious risk to humans and other consumers such as marine mammals or sea birds (e.g., Anderson, 2009; Davidson and

Bresnan, 2009; Lawrence et al., 2011). Amnesic, paralytic and diarrhetic shellfish poisonings (ASP, PSP and DSP, respectively) are some of the most common syndromes caused by phytotoxins in humans. In order to avoid the intoxication of consumers, closures of shellfish harvesting areas occur regularly all over the world, which leads to economic losses. In addition, there is evidence that toxic phytoplankton may affect filtration, feeding, growth, valve closure, byssus production, oxygen consumption, cardiac activity and survival in marine bivalves (Cao et al., 2018), which also affects the aquaculture industry negatively.

Globally, shellfish aquaculture production has undergone a major increase in recent years. In Spain, the overall aquaculture production was 293,000 t in 2015 and 77% of it (225,000 t) corresponded to mussel (*Mytilus galloprovincialis*) aquaculture (De la Figuera, 2017). More than a 95% of Spanish mussel production is carried out in Galicia (north-western Spain), where mussels are cultivated in the coastal inlets (Rías) by means of floating rafts (Eurofish, 2016). The interaction between the coastal upwelling and the circulation patterns in the Rías leads to a massive response in the productivity of phytoplankton populations inside these inlets, even during weak upwelling events along the coast. This response of the phytoplankton provides the filter-feeding organisms with food of a high quality that determines high absorption efficiency, while the characteristics of the Rías maintain the seston concentrations at levels below the threshold of pseudo-faeces production (Figueiras et al., 2002). These favourable conditions make Galicia one of the largest mussel producers worldwide (Romalde et al., 2018).

Recently, in the Basque Country (north of Spain, south-eastern Bay of Biscay), where hydrographic and physico-chemical conditions differ from Galicia, there is an increasing interest in shellfish aquaculture, and several studies have been conducted in order to establish this activity in offshore waters (Azpeitia et al., 2016, 2017). Thus, the commercial production of mussels began in 2019 with longlines in open marine waters (approximately 2 km offshore) in the area called “Mendexa”. So far, bivalve production has not started in inshore areas, which are scarce, and most of them sustain activities incompatible with aquaculture. However, in 2016, a raft was installed in a sheltered area within a small port (“Mutriku”) for the experimental culture of bivalves.

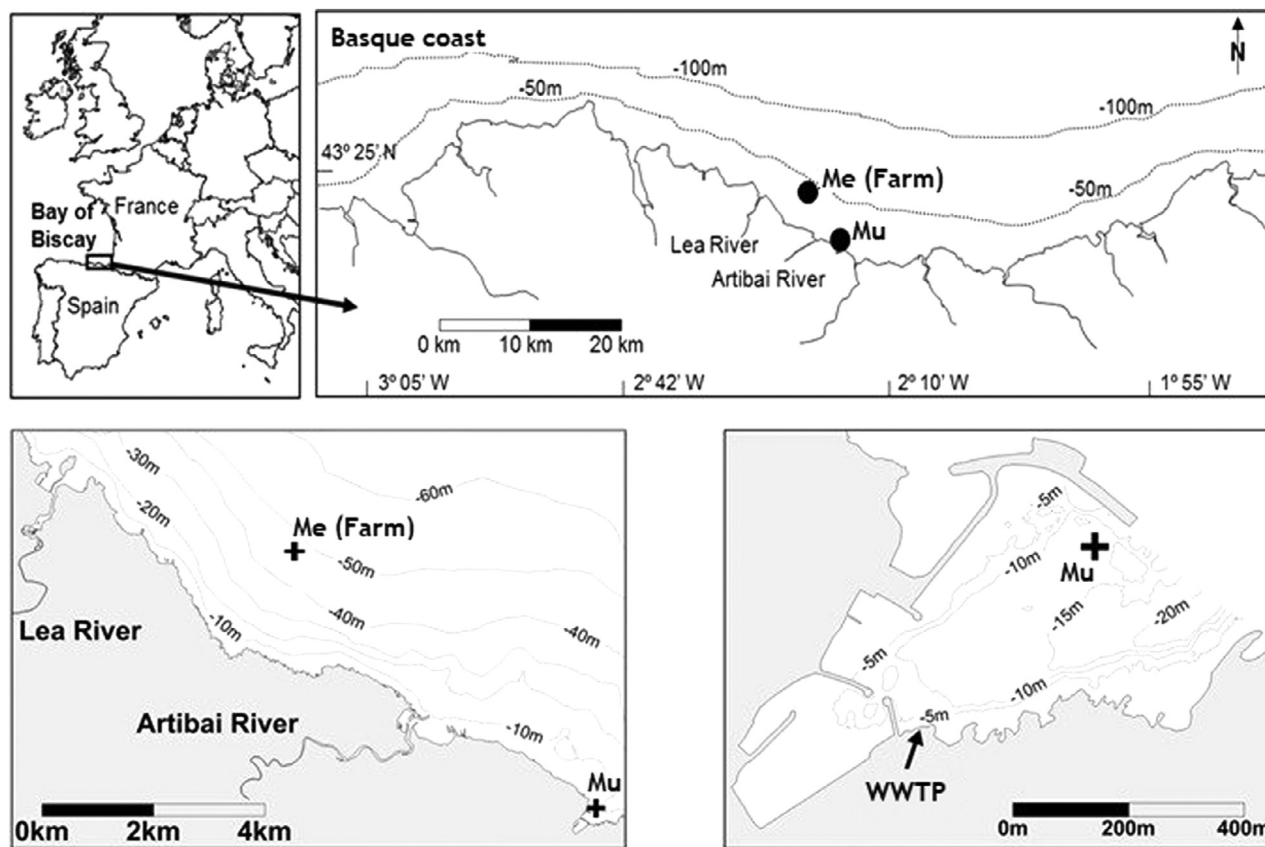


**Figure 1** Study area and sampling station. On the top: the Basque coast, the location of the bivalve farm of “Mendexa” (Me) and “Mutriku” (Mu) station, within the context of the Bay of Biscay. Lower panels: the location of “Mendexa” (Me) and the station “Mutriku” (Mu); on the right, the Mutriku port is depicted with the sampling station and the discharge point of a Wastewater Treatment Plant (WWTP).

Several studies have been carried out that address phytoplankton communities in the southeastern Bay of Biscay. Most of these studies were focused on describing the phytoplankton communities' taxonomic composition and dynamics in estuaries and open marine waters (e.g., Batifoulier et al., 2013; Garmendia et al., 2011; Orive et al., 2010; Seoane et al., 2005; Seoane and Orive, 2012; Trigueros and Orive, 2000). However, when it comes to the study of phytoplankton in relation with bivalve aquaculture, just a few studies have been carried out, all of them in open marine waters (Muñiz et al., 2017, 2018, 2019) and just one that included an inshore area (Bilbao et al., 2020). Recently, Azpeitia et al. (2019) assessed the annual settlement and recruitment patterns of *Mytilus galloprovincialis* in several inshore areas on the Basque coast, concluding that they could be suitable for future seed gathering for the mussel aquaculture industry. This research addresses the phytoplankton community as a food resource for bivalves and as phytotoxins producers in an inshore area, the Mutriku port (Spanish Basque coast). This is relevant for the potential development of aquaculture in the southeastern Bay of Biscay, since the previous studies on this topic were mainly limited to open marine waters whose environmental conditions, such as light and nutrient availability for phytoplankton, could be different.

In this context, we have examined the composition, cell size, abundance and biomass of the phytoplankton commu-

nity and the presence of potentially toxic taxa, from August 2016 to August 2017, in the Mutriku port, with the aim of analysing, in detail, the suitability of this area to sustain shellfish aquaculture. In addition, we have compared the results with the studies conducted in open waters in this region, in terms of phytoplankton community composition. These results could contribute to a better knowledge of the phytoplankton community composition and dynamics in this type of systems (i.e., sheltered euhaline waters of the southeastern Bay of Biscay).

## 2. Material and methods

### 2.1. Study area

The Spanish Basque coast is placed in the southeastern Bay of Biscay and has an extension of ca. 100 km (Figure 1). The area is described as an exposed littoral coast of high energy, mainly erosional, with large cliffs (Cearreta et al., 2004). The climate is rainy, temperate and oceanic, with moderate winters and warm summers (Fontán et al., 2009). Consequently, the seasonal pattern of major climatic and hydrographic conditions corresponds to that of temperate sea areas: winters characterised by water column mixing, which leads to nutrient input from deep waters to the surface; springs with increases in surface water temperature

and relative stabilisation due to solar irradiance; summers with stratification resulting from greater solar irradiance; and autumn mixing processes induced by the cooling of surface waters and southerly and westerly winds (Fontán et al., 2008; Valencia et al., 2004).

Along the Basque coast, the tide is semi-diurnal, the mean tidal range is approximately 1.5 m at neap tides and 4 m at springs tides. The region is defined as ‘low meso-tidal’ during neaps and ‘high meso-tidal’ during spring tides (González et al., 2004). In addition, this coast is influenced by 12 rivers, which are torrential in character (Ferrer et al., 2009) and annually provide ca.  $150 \text{ m}^3 \text{ s}^{-1}$  of fresh water to the coastal water bodies. This freshwater supply leads to alterations in the physico-chemical composition of the shallow waters and often an increase in nutrient concentration in inner shelf waters (Ferrer et al., 2009; Valencia et al., 2004).

This study was carried out at an experimental bivalve culture platform located in the port of Mutriku, on the Basque coast (Figure 1). The station is located in the outer part of a marina ( $43^\circ 18.7' \text{N}$ ,  $2^\circ 22.6' \text{W}$ ), and it is protected from the wave action by a jetty. Its depth is 15 m, approximately, and although rivers do not discharge into this harbour, the station receives the effluents from a Wastewater Treatment Plant (WWTP) that serves the surrounding population (ca. 5,300 inhabitants).

## 2.2. Sampling/laboratory strategy and data acquisition

Samplings were carried out over 13 months (from August 2016 to August 2017), and samples were collected on a monthly basis at two depths (3 m and 10 m) (supplementary material Table A1).

Information on tidal conditions and water height is also presented in Table A1. Although the samplings were not conducted exactly at the same phase of the tide, this factor was controlled to some extent and it only caused a slight variation in the water height. Most of the samplings (10 out of 13) took place at neap or medium tides. Furthermore, 10 samplings were closer to low water time than to high water time.

The water height was measured using a GPS sounder (Garmin Ltd.) on boat. The high and low water times, as well as the tidal coefficient, were those provided by AZTI for Pasaia, a standard port located at about 40 km from Mutriku. The tidal coefficient was used to distinguish spring tides ( $> 0.85$ ) from neap tides ( $< 0.55$ ), following a criterion previously used for the Basque coast (González et al., 2004). This coefficient was calculated by dividing the tidal semi-amplitude by 1.967, which is the constant value of the Pasaia Port (Instituto Hidrográfico de la Marina, 1992).

Several measurements were undertaken *in situ* for the characterisation of the physico-chemical conditions. Secchi disk depth was measured in order to estimate water transparency, and a Seabird25 CTD was used for the measurement of temperature, salinity, density (Sigma Theta), Light Transmission (LT), Photosynthetically Active Radiation (PAR), chlorophyll *a*, oxygen concentration, oxygen saturation and pH at the studied depths. The CTD was calibrated, regularly, with water samples filtered through What-

man GF/F filters and analysed by spectrophotometry, after pigment extraction in acetone.

Water samples were collected with Niskin bottles at the two depths. These samples were employed for the analysis of Suspended Solids (SS), turbidity, Total Organic Carbon (TOC), dissolved inorganic nutrients and phytoplankton identification and counting.

In the laboratory, the concentration of SS was measured following the indications of Clesceri et al. (1989), after filtration of the water through Whatman GF/C filters. Turbidity of seawater was measured using a turbidimeter (2100 Turbidimeter, HACH; Loveland, Colorado, USA). For TOC, an analyser (TOC-V CSH/CSN, Shimadzu Corporation, Kyoto, Japan) was employed in non-purgeable organic carbon (NPOC) mode, as Grasshoff et al. (1983) described. When it came to nutrients (ammonium, nitrite, nitrate, silicate and phosphate), the measurements were carried out using a Continuous-Flow Autoanalyser (Bran + Luebbe Autoanalyser 3, Norderstedt, Germany), following the colourimetric methods described by Grasshoff et al. (1983). The quantification limit for ammonium, nitrate and silicate was  $1.6 \mu\text{mol L}^{-1}$ , for nitrite, it was  $0.4 \mu\text{mol L}^{-1}$  and for phosphate, it was  $0.16 \mu\text{mol L}^{-1}$ . In order to calculate average concentrations, a quantity equal to 50% of the limit was assumed for the measurements that did not reach the quantification limit.

Moreover, in order to describe hydrographic conditions, two variables were estimated: the light extinction coefficient and the depth of the photic zone. The light extinction coefficient (*k*) was calculated graphically based on the general equation of the vertical extinction coefficient (see below), and that was obtained with the representation of the PAR measured by the CTD at every meter of the water column.

$$I_z = I_0 \cdot e^{-kz}$$

where  $I_z$  [ $\text{E m}^{-2} \text{ d}^{-1}$ ] is the radiation received at a specific depth,  $I_0$  is the radiation at a surface and  $z$  is the specific depth [m].

The *k* was then applied to estimate the depth of the photic layer using the following equation: photic zone [m] =  $4.605/k$ .

The phytoplankton community was analysed according to cell concentration [ $\text{cell L}^{-1}$ ] and biomass [ $\mu\text{g C L}^{-1}$ ]. Water samples used for phytoplankton identification were fixed with acidic Lugol's solution (0.4% v/v), immediately after collection, and stored in 125 ml topaz borosilicate, in a dark and cool ( $4^\circ\text{C}$ ) place, until analysis. For taxonomic identification and cell counting, subsamples of 50 ml were analysed following the Utermöhl sedimentation method (Edler and Elbrächter, 2010) under a Nikon diaphot TMD inverted microscope. The whole chamber was analysed at low magnifications ( $100\times$ ) to count the larger and less abundant taxa. For more abundant cells, transects at different magnifications ( $100\times$ ,  $200\times$  or  $400\times$ ) were analysed depending on the organism's abundance and size. For chain-forming taxa, cells were counted, not chains. Most of the diatoms and dinoflagellates were identified until genus level, and the nomenclature of the identified taxa was standardised according to AlgaeBase (Guiry and Guiry, 2018). However, some of them could not be identified to that level and were classified in the following groups: pennate diatoms, cen-

tric diatoms, thecated dinoflagellates, athecated dinoflagellates and flagellates.

In order to calculate the phytoplankton biomass, the biovolume was determined by assigning each taxon a mean equivalent spherical diameter (ESD), mostly based on Olenina et al. (2006), taking into account cells shape and size. The biovolume of the taxa that could not be accurately calculated from Olenina et al. (2006) was determined based on Muñiz et al. (2019). Then, the biomass was calculated using the equation reported for marine phytoplankton by Montagnes et al. (1994):  $\text{Biomass} = 0.109 \times \text{Volume}^{0.991}$ , where biomass is expressed in  $\mu\text{g C cell}^{-1}$  and volume is expressed in  $\mu\text{m}^3$ .

In addition, in order to determine which taxa had to be considered potentially toxic, the Taxonomic Reference List of Harmful Micro Algae from the Intergovernmental Oceanographic Commission of the UNESCO was used as a checklist (Moestrup et al., 2009; <http://www.marinespecies.org/hab/>, accessed on 30 June 2018). As a measure of precaution, when a genus contained both toxic and non-toxic species, the whole genus was considered as potentially toxic if the identification could not reach the species level. Moreover, risk of shellfish poisoning was determined by applying alert levels of cell concentration to the genera causing the three main syndromes of concern in this study area (ASP, DSP and PSP): *Pseudo-nitzschia* spp., *Dinophysis* spp. and *Alexandrium* spp., respectively. The threshold levels employed were (Swan and Davidson, 2012) 50,000 cells  $\text{L}^{-1}$  for *Pseudo-nitzschia* spp., 100 cells  $\text{L}^{-1}$  for *Dinophysis* spp. and “presence” for *Alexandrium* spp.

### 2.3. Statistical analyses

Main statistical parameters (range, median and arithmetic mean) were calculated for physico-chemical and hydrographic variables and phytoplankton cell abundance and biomass, for the whole year and for each studied depth. The comparison between the studied depths was done in a descriptive way rather than statistically.

## 3. Results

### 3.1. Hydrographic and physico-chemical conditions

In order to describe the environmental conditions of the water that could most be related to phytoplankton communities, Figure 2 shows the intra-annual variability of some of the variables measured in Mutriku. The range (minimum–maximum) and the medians for the whole year can be consulted in Table B1 and the variability of additional variables in Figure B1 (supplementary material, Appendix B).

There were no parameters among the several hydrographic and physico-chemical conditions measured that showed consistent and remarkable differences between 3 m and 10 m (Figure 2 and Figure B1).

When it comes to the variations among samplings, water column depth varied in a range of 3 m (from 13 m to 16 m), with a median value of 14 m (Table B1). Salinity variations were small, it ranged from 34.28 to 35.47 at 3 m, and

from 34.36 to 35.52 at 10 m; therefore, Mutriku presented euhaline conditions throughout the study period.

Median seawater temperature was 15°C. This parameter showed a marked seasonal variability, with the highest temperatures being recorded in summer and the lowest in winter. Optical conditions also showed notable changes throughout the study period. Secchi disk depth, light transmission and the photic layer depth registered the highest values in spring and the lowest in winter. This was in accordance with the patterns of the light extinction coefficient ( $k$ ) and turbidity, which, in contrast to the parameters named above, registered their maxima in winter.

Chlorophyll  $a$  concentration was low, with an average concentration of  $0.5 \pm 0.3 \mu\text{g L}^{-1}$  and  $0.6 \pm 0.3 \mu\text{g L}^{-1}$  at 3 m and 10 m respectively, and a median of  $0.5 \mu\text{g L}^{-1}$  at both depths. Values ranged between  $0.1 \mu\text{g L}^{-1}$  (in autumn, at 3 m) and  $1.4 \mu\text{g L}^{-1}$  (in winter, at 10 m).

With regard to inorganic nutrients, although sporadic peaks could be observed, generally they did not show very high concentrations. Nitrate and silicate registered their maxima in winter (at 3 m), being  $6.3 \mu\text{mol L}^{-1}$  and  $3.1 \mu\text{mol L}^{-1}$ , respectively. Ammonium, on the contrary, registered its maximum in spring (at 10 m) with  $6.4 \mu\text{mol L}^{-1}$ . Phosphate did not exceed  $0.5 \mu\text{mol L}^{-1}$ , and nitrite was recorded above the quantification limit just twice (December and January) during the study period.

### 3.2. Phytoplankton composition, abundance and biomass

Concerning phytoplankton diversity, a total of 87 taxa were identified, 81 of them until genus level at least. Dinoflagellates represented the group with the highest number of taxa, with 46% of the total taxa identified, followed by diatoms, with 36%. The list of these taxa, their appearance frequency and their abundance range (minimum–maximum) can be consulted in the supplementary material (supplementary material Appendix C).

Phytoplankton total cell abundance ranged from  $1.9 \times 10^4$  to  $7.1 \times 10^5$  cells  $\text{L}^{-1}$ . Both cell abundance and biomass presented several peaks throughout the year, which, in general, were associated. At 3 m, the maximum cell abundance, which was also the absolute maximum, was observed in July, when the community was characterised by a large proportion of haptophytes and cryptophytes (Figure 3). However, at this depth, the maximum biomass ( $85.4 \mu\text{g C L}^{-1}$ ) was recorded in October, coinciding with the dinoflagellate maximum abundance. At 10 m, on the contrary, the maximum phytoplankton abundance ( $6.2 \times 10^5$  cells  $\text{L}^{-1}$ ) and biomass ( $94.4 \mu\text{g C L}^{-1}$ ) were registered in the same month, February, with a community dominated by diatoms, *Thalassiosira* spp. concretely.

Regarding phytoplankton community composition (Figure 3), similar results were obtained for both depths. At 3 m, the groups that contributed the most to the total cell abundance were haptophytes and cryptophytes, with an average contribution of 37% and 36%, respectively. At 10 m, haptophytes were also the most contributing group (41%) in terms of abundance; however, the average contribution of diatoms was higher than at 3 m (24%), the same as cryptophytes. Nevertheless, the contribution of these groups

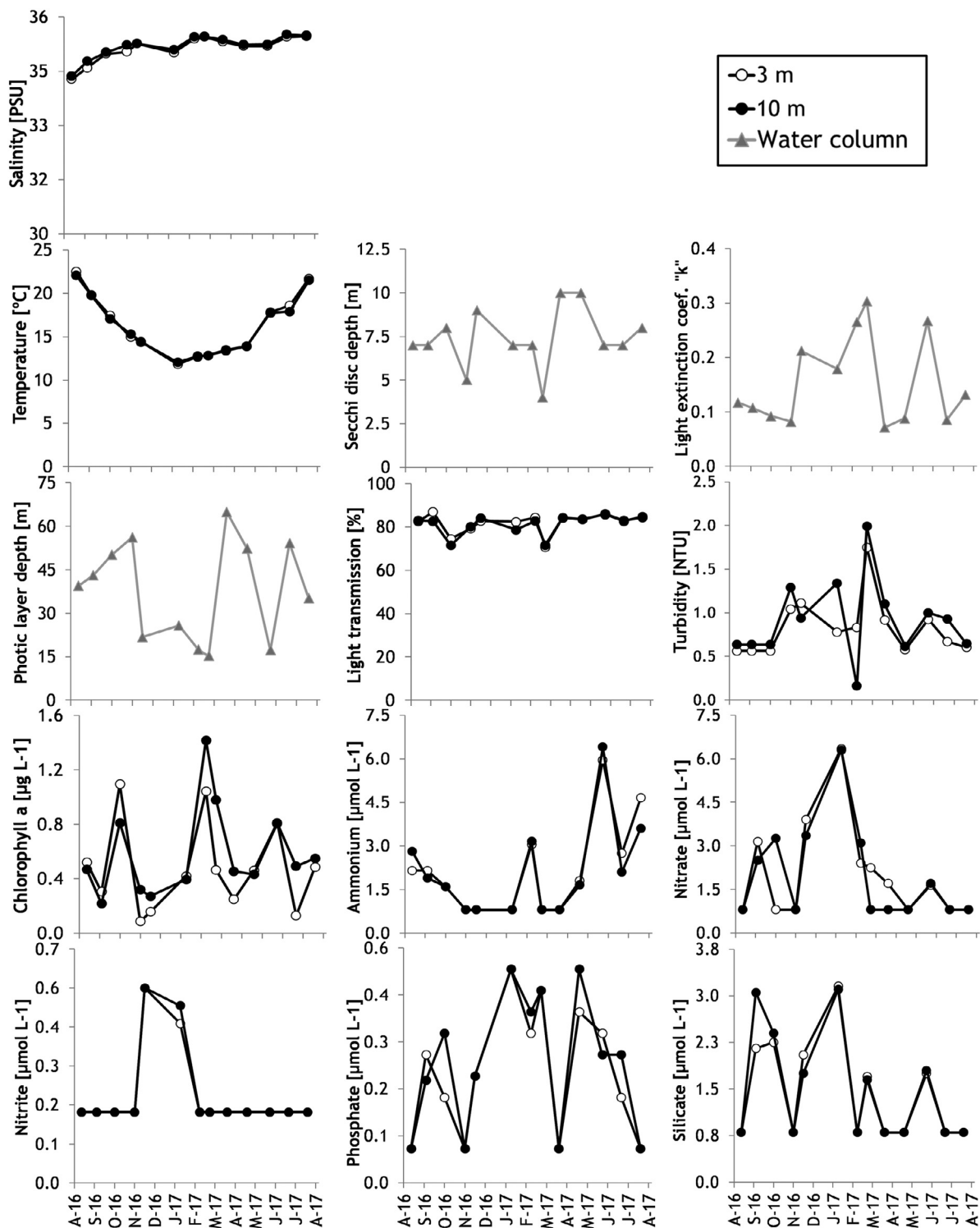


**Figure 2** Intra-annual variability of the main hydrographic and physico-chemical conditions in Mutriku. In the case of nutrients, for values below the quantification limit, the value of half of the limit is represented. Some additional variables (suspended solids, total organic carbon and oxygen) are shown in supplementary material (supplementary material Appendix B).

to the total phytoplankton abundance differed from their contribution to the total biomass. Diatoms were, by far, the most contributing group in Mutriku terms of biomass (52% at 3 m and 79% at 10 m), followed by dinoflagellates (23% and 8%, at 3 m and 10 m, respectively). On the other

hand, haptophytes and cryptophytes, two of the most abundant groups, only reached 7–8% of the contribution to the total phytoplankton biomass. Diatoms recorded their highest contribution values in winter, dinoflagellates in autumn and haptophytes and green algae in summer. The

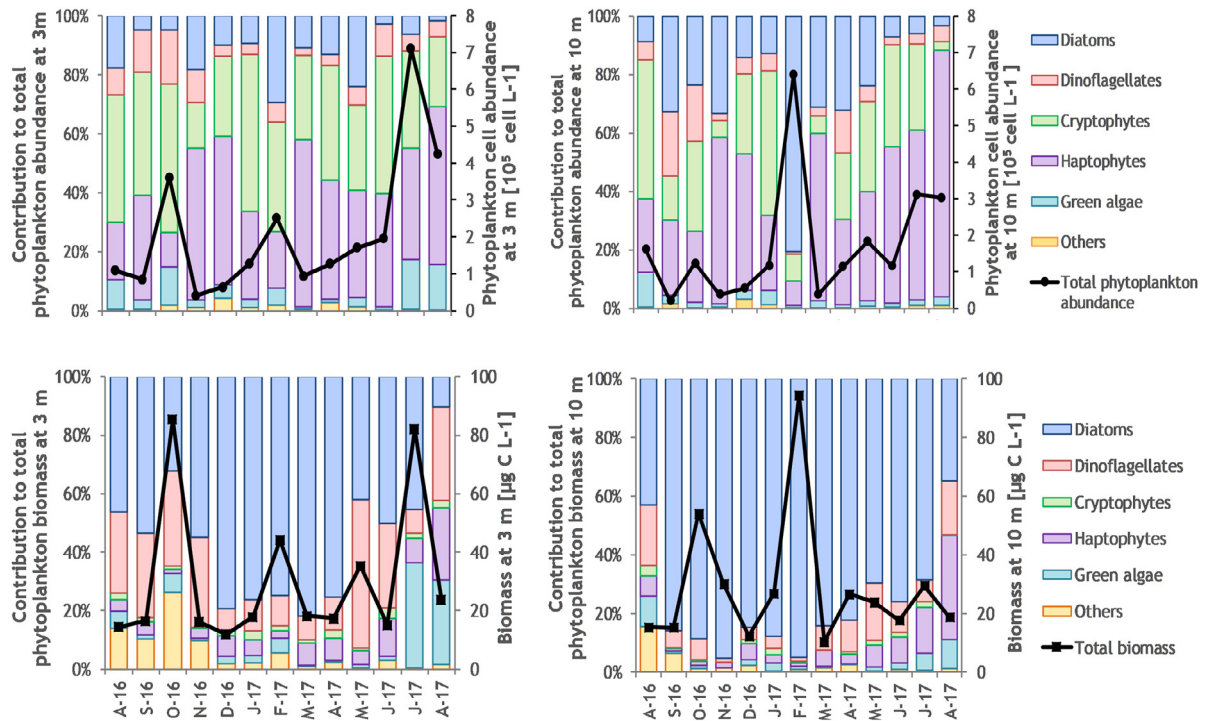


**Figure 3** Contribution to total phytoplankton abundance (upper panels) and biomass (lower panels) of the main phytoplankton groups at both 3 m (left) and 10 m (right) depths.

**Table 1** List of the most abundant taxa in each phytoplankton group at the two sampled depths, together with their appearance frequency throughout the year, maximum abundance and date when the maximum was registered.

Group	Depth [m]	Most abundant taxon	Appearance frequency [%]	Maximum abundance [cells L <sup>-1</sup> ]	Date of maximum abundance
Haptophytes	3	Prymnesiales	100	$2.7 \times 10^5$	Jul. 2017
	10	Prymnesiales	100	$2.5 \times 10^5$	Aug. 2017
Cryptophytes	3	<i>Plagioselmis</i> sp.	100	$2.3 \times 10^5$	Jul. 2017
	10	<i>Plagioselmis</i> sp.	100	$9.1 \times 10^4$	Jul. 2017
Diatoms	3	<i>Pseudo-nitzschia</i> spp. < 3 µm	77	$2.3 \times 10^4$	Feb. 2017
	10	<i>Thalassiosira</i> spp. < 20 µm	8	$4.2 \times 10^5$	Feb. 2017
Dinoflagellates	3	Atheated dinoflagellates < 20 µm	100	$3.8 \times 10^4$	Oct. 2016
	10	Atheated dinoflagellates < 20 µm	92	$1.5 \times 10^4$	Apr. 2017
Green algae	3	<i>Tetraselmis</i> sp.	100	$5.1 \times 10^4$	Jul. 2017
	10	<i>Tetraselmis</i> sp.	100	$1.9 \times 10^4$	Aug. 2016

only difference was recorded for cryptophytes, which, at 3 m, reached the maximum contribution in autumn and, at 10 m, in spring.

The most abundant haptophyte and cryptophyte taxa were Prymnesiales and *Plagioselmis* sp., respectively, regardless of the depth and season, and they registered their maximum abundances in the summer months of 2017 (Table 1). In addition, both of these taxa appeared in every

water sample analysed during this study. Among dinoflagellates, atheated cells (< 20 µm) were the most abundant taxon at both depths and were observed in most of the samples. The maximum atheated cell abundance was registered at different months depending on the depth, in October at 3 m and in April at 10 m. Diatoms were the group showing the greatest variability in the dominant taxon, since while at 3 m, *Pseudo-nitzschia* spp. (< 3 µm) was

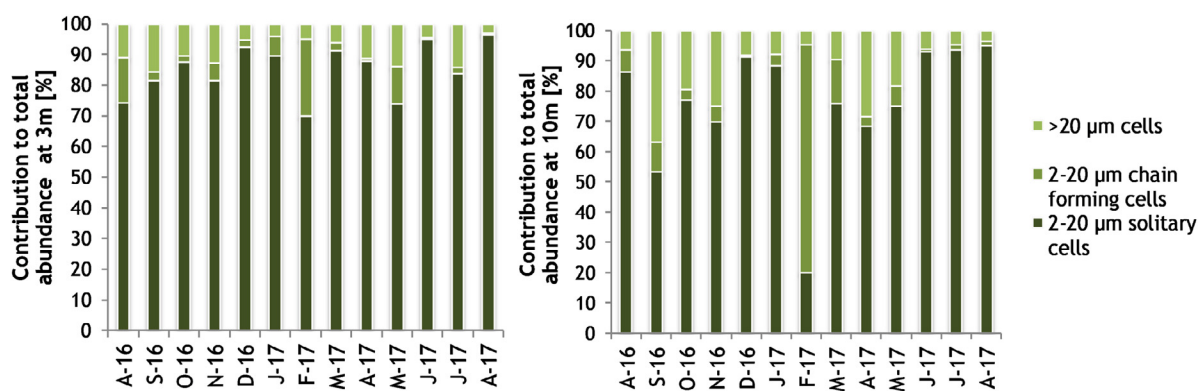


**Figure 4** Contribution percentage of the two size-fractions considering the 2–20  $\mu\text{m}$  at both the 3 m (left) and 10 m (right) depths during the study period and highlighting the 2–20  $\mu\text{m}$  size-fraction's chain forming diatoms. Note: when referring to chain forming cells, the 2–20  $\mu\text{m}$  size refers to each cell size, not the whole chain.

the most abundant diatom group, *Thalassiosira* spp. (< 20  $\mu\text{m}$ ) dominated at 10 m. When it comes to green algae, *Tetraselmis* sp. was the most abundant taxon, appearing in every analysed sample and registering its maximum values in summer.

When analysing the quality of the phytoplankton as a food resource for mussels, the observed community was assessed by considering cell size and toxicity. It was found that the community was dominated by cells ranging 2–20  $\mu\text{m}$  (ESD) (Figure 4). The average contribution to the total phytoplankton cell abundance of this group along the study period was 90.9% at 3 m and 86.2% at 10 m. Nevertheless, part of this contribution corresponded to chain-forming diatoms, specifically 6.6% and 11.7% of the 2–20  $\mu\text{m}$  size cells at 3 m and 10 m, respectively.

Regarding potentially toxic phytoplankton, ten taxa were registered. Among them, *Pseudo-nitzschia* spp. was the only potentially toxic diatom, whereas eight taxa belonged to the dinoflagellates group: *Alexandrium* spp., cf. *Azadinium* spp., *Dinophysis* spp., *Dinophysis acuminata*, *Goniaulax* cf. *spinifera*, *Ostreopsis* cf. *siamensis*, *Phalacroma* spp. and *Takayama* sp. From other groups, only one haptophyte (*Phaeocystis globosa*) was identified as a potentially toxic taxon. The average contribution of the potentially toxic taxa found in Mutriku to the total phytoplankton abundance was 3.6% at 3 m and 4.5% at 10 m.

Regarding the taxa responsible for producing the most concerning poisoning syndromes (*Pseudo-nitzschia* spp. of ASP; *Alexandrium* spp. of PSP; *Dinophysis* spp. and *Phalacroma* spp. of DSP), several differences were found between their appearance frequencies. While *Pseudo-nitzschia* spp. was the only taxon identified in every sample analysed, *Dinophysis* spp. appeared in 23% of the samples and *Alexandrium* spp. and *Phalacroma* spp. in 7.7% of them. In addition, these last two genera were only present at 3 m. When it comes to the exceedance of the abundance thresholds that determine risk for shellfish toxicity, alert limits for shellfish poisoning were registered in four of the 13 sampling days carried out in Mutriku, twice by *Alexandrium* spp. (at 3 m) and once by *Pseudo-nitzschia* spp. and *Dinophysis* spp. (at 10 m and 3 m respectively). Among the rest of the toxic taxa found in Mutriku, *Ostreopsis* cf. *siamensis* was the most frequent, appearing in 23% of the samples at 3 m

and in 31% at 10 m. *Goniaulax* cf. *spinifera*, *Takayama* sp., cf. *Azadinium* spp. and *Phaeocystis globosa* appeared in less than 16% of the samples, being cf. *Azadinium* spp. the most frequent (identified in 15.4% of the samples).

#### 4. Discussion

Waters in Mutriku showed some of the classical environmental conditions and seasonal cycles of temperate coastal areas, which have previously been described for Basque marine waters (Valencia et al., 2004). Temperature, for example, showed a seasonal warming and cooling pattern, which is thought to be highly related to air temperature in the Basque shelf waters (Valencia et al., 2003) and has previously been recorded in several studies (e.g., Muñiz et al., 2019). Optical conditions in the area also varied a lot, and even if they did not show a clear seasonal pattern, turbidity registered its maximum values in winter. In this period, there is more water turbulence and, consequently, a higher chance for sediment resuspension, which is a common phenomenon in shallow waters and increases turbidity (González et al., 2004).

When it comes to the seasonal variation of dissolved nutrients, the effects of the thermal cycle and the succession of mixing and stratification conditions could be detected, as in other zones of the SE Bay of Biscay (Valencia and Franco, 2004). In Mutriku, nitrate and silicate registered their maximum values in winter, similarly to the patterns seen in Arcachon Bay, a shallow mesotrophic estuary (Glé et al., 2008), which can be attributed to the turbulent mixing processes and the subsequent input of nutrients to the surface waters from the deeper layer (Valencia and Franco, 2004). Ammonium, on the contrary, registered its maximum in spring and, together with nitrate, is one of the most abundant nutrients in Mutriku. It is known that sewage discharges are rich in ammonium and phosphate; nevertheless, the WWTP that discharges its waters to Mutriku performs the biological treatment, which targets residual organic matter and suspended solids present in wastewater after the primary treatment stage and includes the removal of dissolved nutrients (Carey and Migliaccio, 2009). In addition, according to the data available in the Basque

Water Agency (URA, <https://www.uragentzia.euskadi.eus/u81-0002/es/>, accessed on 2 April 2020), the nutrient concentrations registered in Mutriku were within the range of concentrations observed in nearby areas that are not subject to direct discharges from WWTPs, like the open marine waters of Sopelana (“L-N20” station) or Orío (“L-O10” station). Moreover, the annual average of ammonium, nitrate and phosphate concentrations in Mutriku were below the ones recorded by Revilla et al. (2009) along the Basque coast in a six-year-long survey for 13 different nearshore sites. Therefore, this might indicate that, in Mutriku, the effects of the WWTP were not significant when it comes to nutrient enrichment, as previously concluded by Bilbao et al. (2020).

Regarding the phytoplankton attributes studied here, the median value of chlorophyll *a* (chl *a*) concentration was 0.5  $\mu\text{g L}^{-1}$ , with a maximum of 1.4  $\mu\text{g L}^{-1}$ , reflecting the oligotrophic conditions of the area. Orive et al. (2004) indicated that the chl *a* sub-surface maximum in the Basque shelf waters was usually between 2  $\mu\text{g L}^{-1}$  and 4  $\mu\text{g L}^{-1}$ . Recent studies in the inner Bay of Biscay (Fanjul et al., 2017) registered similar chl *a* concentrations to Mutriku in Urdaibai estuary, where the annual mean concentration ranged from around 0.5  $\mu\text{g L}^{-1}$  to 1  $\mu\text{g L}^{-1}$  in most of the studied years (1998–2013). On the contrary, in Bilbao estuary, the annual mean of chl *a* concentration was above 1  $\mu\text{g L}^{-1}$  in all the years of the study period (Fanjul et al., 2017). This might be mostly explained by the trophic conditions of these sites, since the Mutriku port presents oligotrophic conditions similar to those of Urdaibai and many other sites of the Basque coast, differing from the mesotrophic conditions reported for Bilbao estuary. In addition, the results obtained in Mutriku are also similar to those observed in the farm of Mendexa (located in an oligotrophic area as well), where the mean annual chl *a* value was  $0.6 \pm 0.4 \mu\text{g L}^{-1}$  (Muñiz et al., 2019). Moreover, chl *a* concentration in surface waters of Mendexa was below 0.6  $\mu\text{g L}^{-1}$  for most of the studied year, only registering higher values from February to May, and Mutriku only registered values above 0.6  $\mu\text{g L}^{-1}$  in 4 of the 13 sampled months (although these were detected at any season except summer). This makes both zones similar in terms of chl *a*, a proxy for phytoplankton biomass, for sustaining aquaculture production. Despite that, chl *a* in Mutriku was very small during the entire survey in comparison with other European aquaculture sites. Studies conducted in Galician Rías, where most of the Spanish mussel production is carried out, recorded mean values of chl *a* between 0.7  $\mu\text{g L}^{-1}$  (winter) and 13.6  $\mu\text{g L}^{-1}$  (spring) (Varela et al. 2005). In addition, Spyrales et al. (2011) also found higher mean chl *a* concentrations in Rías Baixas than in Mutriku, with values lower than 1  $\mu\text{g L}^{-1}$  in winter, close to 5  $\mu\text{g L}^{-1}$  in summer and up to 8  $\mu\text{g L}^{-1}$  during spring and autumn. Studies in the Eastern English Channel (France), where shellfish farming was one of the most important aquaculture industries of Europe, also showed higher chl *a* concentrations than in Mutriku, in the range of 1–25  $\mu\text{g L}^{-1}$  according to Jouenne et al. (2007) and between 0.9 and 18.9  $\mu\text{g L}^{-1}$  according to Klein et al. (2010). However, knowing that the total biomass is an important factor for the growth of bivalves, in field studies, Wall et al. (2013) observed that the growth rates of bivalves were more related to the community composition, especially the density of certain cellular types, than to the total phytoplankton biomass.

The total phytoplankton cell-abundance range registered in Mutriku was within the values previously found at nearshore stations along the Basque coast (Muñiz et al., 2017). In Mutriku the phytoplankton community was dominated by haptophytes and cryptophytes, in terms of cell concentrations, during most of the year. Haptophytes, concretely, were especially dominant from March to August. However, these groups are mainly composed of small nanoplankton, meaning that their contribution to total biomass was small. Haptophytes are known to be one of the main components of marine phytoplankton (Latasa et al., 2005; Not et al., 2005; Rodríguez et al., 2003), especially in oceanic waters, but they can also be abundant in coastal and estuarine waters (Dahl et al., 1998). Seoane et al. (2005, 2006, 2009) described the relative importance of haptophytes in terms of abundance in the Nervión River estuary (Bilbao estuary), concluding that this group was not among the most abundant since the estuary was mainly dominated by diatoms, chlorophytes and cryptophytes. Nevertheless, Muñiz et al. (2019) reported a high abundance of haptophytes, especially in spring and summer, in the neighbouring marine waters of Mendexa, where this group was 46% of the total cell abundance, exceeding the dominance of haptophytes in Mutriku (37–41%). This dominance of haptophytes in oligotrophic waters like Mutriku or Mendexa might be explained by their small cell size and mixotrophic ability (Hansen and Hjorth 2002; Jones et al., 1993; Lessard et al., 2005). In addition, nanophytoplankton also dominates the phytoplankton community in terms of abundance in other Atlantic areas, for example, the Western English Channel (Widdicombe et al., 2010). Besides that, a study of the phytoplankton distribution between 62 and 37°N in the northeastern Atlantic showed that, in surface waters between 62 and 50°N, haptophytes were the most abundant group (Gibb et al., 2001).

Diatoms were the most important group in Mutriku in terms of biomass during the whole year. This group was especially abundant at 10 m, becoming the second most abundant group after haptophytes, and reached their maximum values in winter at both depths. Diatoms are organisms that prefer turbulent and nutrient-rich conditions, and therefore, strong vertical mixing favours their dominance (Glibert, 2016; Margalef, 1978), conditions that typically appear in winter. In addition, diatoms are generally adapted to low light levels (Brahim et al., 2015), which favours their survival in turbid conditions (Lionard et al., 2005), and tend to have significantly higher maximum uptake rates of nutrients than any other group (Litchman et al., 2006), which might explain their predominance in late winter light and nutrient conditions. Moreover, since diatom cells are non-motile (Ross and Sharples, 2007), the higher water turbulence that is usually found in winter enables them to keep re-suspending into the surface, where growth conditions are more favourable (Ross, 2006). Previous studies in the southern Bay of Biscay also described these late winter diatom peaks (Guillaud et al., 2008; Labry et al., 2001; Muñiz et al., 2019). Muñiz et al. (2019), in particular, described for Mendexa a diatom peak in March, when diatoms made up 50% of the total cell abundance; however, during the rest of the year, diatoms contributed in 13% of the total cell abundance, which is less than in Mutriku. Regarding the contribution to total biomass, diatoms only dominated the

community in Mendexa during winter, representing between 54% and 78% of the total biomass, being less important than in Mutriku as well.

The dominance of diatoms in biomass found in Mutriku suggests favourable phytoplankton nutritional quality for mussels. Several studies have reported a direct correlation between diatoms and bivalve growth (Pernet et al., 2012; Wall et al., 2013; Weiss et al., 2007). On the other hand, haptophytes dominate in terms of cell concentration, although their small size makes their contribution to total phytoplankton biomass smaller. While diatoms are known to be rich in eicosapentaenoic acid (EPA), some haptophytes are a rich source of docosahexaenoic acid (DHA) (Catarina and Xavier, 2012). EPA and DHA are two important essential fatty acids (EFA) for bivalves; the first one has an energetic function (Martínez-Pita et al., 2012; Sánchez-Lazo and Martínez-Pita, 2012), and the second one is known for promoting growth (Parrish, 2013). Due to this, diatoms and haptophytes (especially *Isochrysis galbana* and *Pavlova lutheri*) are frequently used as feed for shellfish worldwide (Catarina and Xavier, 2012; Eikrem et al., 2017; Volkman et al., 1989, 1991). Mixed microalgal diets of these two groups are common in bivalve hatcheries and considered highly nutritious in terms of polyunsaturated fatty acids (PUFAs) (Catarina and Xavier, 2012; Knuckey et al., 2002).

Apart from that, the presence of dinoflagellates in Mutriku has to be mentioned as well. Although it is not among the most abundant groups, the contribution of dinoflagellates to the total biomass (especially at 3 m) is notable. The presence of this group is beneficial to shellfish aquaculture since dinoflagellates also contain DHA (e.g., Azpeitia et al., 2016). Moreover, Trotter et al. (2008) found that dinoflagellates, together with diatoms, show some of the highest retentions in mussels compared to other phytoplankton groups.

When it comes to the suitability of cell size for efficient ingestion and retention, the composition of the phytoplankton community in Mutriku seems favourable for the correct growth of bivalves. While some researchers concluded that the most adequate cell size is 35–45  $\mu\text{m}$  (Cranford et al., 2014; Strohmeier et al., 2012), some others set the size range at 15–20  $\mu\text{m}$  (Lucas et al., 1987; Stenton-Dozey and Brown, 1992). However, as it has been mentioned before, most studies agree that the size range of 4–45  $\mu\text{m}$  is the most suitable for high food depletion (Cranford et al., 2014). Therefore, taking into account that the predominant cell size in Mutriku was 2–20  $\mu\text{m}$ , the size structure of the phytoplankton community was suitable for mussel ingestion. Similar results were obtained in a previous study of the Basque coastal waters (Muñiz et al., 2017).

The counterpoint to the benefits of phytoplankton growth lies in the presence of species that can be toxic and pose one of the main risks to shellfish aquaculture. Some potentially toxic phytoplankton taxa were found in Mutriku, all of them were previously described in the SE Bay of Biscay (e.g., David et al., 2012, 2013; Laza-Martínez et al., 2011; Muñiz et al., 2017; Orive et al., 2008, 2010; Revilla et al., 2009; Seoane et al., 2012). Mutriku registered abundances above the alert limits for shellfish poisoning four times during the study period, once for *Pseudonitzschia* spp. and *Dinophysis* spp. and twice for *Alexan-*

*drium* spp., which in general coincided with the frequencies found within open coastal waters of the Basque Country (Muñiz et al., 2017). However, when directly comparing the presence of toxic phytoplankton taxa and biotoxins in Mutriku and Mendexa, Bilbao et al. (2020) found that mussels that grew in Mendexa, where the offshore farm is located, presented a statistically higher amount of okadaic acid and a higher cell abundance of *Dinophysis* spp. than in Mutriku. Among the potentially toxic species found, special attention should be paid to *Dinophysis acuminata*, which is likely the species most responsible for the high concentrations of okadaic acid (OA) in oysters and mussels in the neighbouring West French coast (Batifoulouier et al., 2013; Maurer et al., 2010). Although this genus generally appears in very low concentrations (< 100 cells  $\text{L}^{-1}$ ) on the Basque coast (Muñiz et al., 2017), high concentrations of *D. acuminata* (maxima of  $5 \times 10^3$  cells  $\text{L}^{-1}$ ) have been previously registered in euhaline waters of this region (Bilbao et al., 2020; Seoane and Orive, 2012). Indeed, OA concentrations above the banning threshold have been recently reported for mussels growing in these waters (Bilbao et al., 2020).

Besides the potential shellfish poisoning risk, the presence of toxic taxa might also threaten the development of the aquaculture industry in Mutriku due to the negative effects of toxins in mussel physiology and survival. In several studies, negative effects on energy metabolism and neural function, combined with behavioural functions such as valve closure, feeding, cardiac activity and respiration, have been observed in different bivalve species exposed to harmful marine algae and their toxins (Basti et al., 2016; Estrada et al., 2007; Haberkorn et al., 2011; Moroño et al., 2001; Ramos and Vasconcelos, 2010). In addition, some types of toxins can lead to declined reproduction and growth rates in marine bivalves, which could be a major cause of mortality in natural populations (Blanco et al., 2006; Samson et al., 2008). Some of the toxic genera found in Mutriku and their toxins are among these threatening types. Nielsen et al. (2020) proved that DST (Diarrhetic Shellfish Poisoning toxins) contained by *D. acuta* had a severe negative effect on the clearance rates of mussels (*Mytilus edulis*), reduced their feeding and, therefore, may cause low-quality mussels. The effects of PST (Paralytic Shellfish Poisoning toxins) produced by *Alexandrium catanella* have also been tested in seven different bivalve species (Shumway and Cucci, 1987). In this case, the responses included shell-valve closure, siphon retraction and mucus production in *M. edulis*, while the rest of bivalves showed different reactions. In addition, saxitoxins (produced by *Alexandrium* and *Gymnodinium*) may reduce growth, reproduction and survival rates of marine bivalves like green mussels (*Perna vidiris*) according to Shumway et al. (2006).

Finally, it has to be mentioned that phytoplankton abundance and community composition can vary in a very short timescale, even within the same day (e.g., Abreu et al., 2009; Li et al., 2009). Therefore, sampling on a monthly basis could impose constraints on the efficiency at which variability can be resolved and provides data of monthly variability that might have potential errors (Jassby et al., 2005). Considering this limitation, the present study is only intended to acquire a general knowledge of the phytoplankton community on an annual scale (e.g., Muñiz et al., 2019). If the results obtained were to be extrapolated to other

areas with similar hydrographic characteristics, it would be necessary to carry out additional studies to characterize the community more accurately. This could be done by increasing the sampling frequency with short-term studies (e.g., Madariaga 1995, 2002) or by maintaining a monthly frequency but with long-term studies (e.g., O'Brien et al., 2012).

## 5. Conclusion

The water column in the experimental bivalve culture platform located in Mutriku showed the typical environmental conditions previously described for Basque marine waters, with no remarkable anthropogenic pressures caused by the WWTP. The composition of the phytoplankton community of the area could be described as favourable for bivalve growth from the perspective of its composition due to the dominance of diatoms, the predominant adequate phytoplankton cell size for ingestion and retention and the relatively low presence of toxic phytoplankton. However, even if bivalve farms are now working in zones with similar phytoplankton community composition and biomass values (i.e., on the Basque coast, the open marine area of Mendexa), these values are low compared with classical zones of bivalve production (e.g., Galician Rías).

## Acknowledgements

This study was partially supported by the project EGRECOST CALIDAD – Control de Calidad de Aguas Cultivos Marinos (Departamento de Desarrollo Económico e Infraestructuras del Gobierno Vasco) and the project PPG17/67 funded by the University of the Basque Country (UPV/EHU). J. Bilbao was funded by a grant from the University of the Basque Country (UPV/EHU – PIF 18/306). This paper is contribution number 991 from AZTI (Marine Research Division).

## Supplementary materials

Supplementary material associated with this article can be found, in the online version, at <https://doi.org/10.1016/j.oceano.2020.08.007>

## References

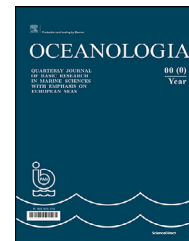
- Abreu, P., Bergesch, M., Proença, L., Garcia, C., Odebrecht, C., 2009. Short- and long-term chlorophyll a variability in the shallow microtidal Patos Lagoon estuary, southern Brazil. *Estuar. Coast.* 33 (2), 554–569. <https://doi.org/10.1007/s12237-009-9181-9>
- Anderson, D.M., 2009. Approaches to monitoring, control and management of harmful algal blooms (HABs). *Ocean. Coast. Manag.* 52, 342–347. <https://doi.org/10.1016/j.ocecoaman.2009.04.006>
- Azpeitia, K., Ferrer, L., Revilla, M., Pagaldai, J., Mendiola, D., 2016. Growth, biochemical profile, and fatty acid composition of mussel (*Mytilus galloprovincialis* Lmk.) cultured in the open ocean of the Bay of Biscay (northern Spain). *Aquaculture* 454, 95–108. <https://doi.org/10.1016/j.aquaculture.2015.12.022>
- Azpeitia, K., Rios, Y., Garcia, I., Pagaldai, J., Mendiola, D., 2017. A sensory and nutritional validation of open ocean mussels (*Mytilus galloprovincialis* Lmk.) cultured in SE Bay of Biscay (Basque Country) compared to their commercial counterparts from Galician Rías (Spain). *Int. Aquatic Res.* 9 (5), 1–18. <https://doi.org/10.1007/s40071-017-0159-0>
- Azpeitia, K., Rodríguez-Ezpeleta, N., Mendiola, D., 2019. Settlement and recruitment pattern variability of the mussel *Mytilus galloprovincialis* Lmk. from SE Bay of Biscay (Basque Country). *Reg. Stud. Mar. Sci.* 27, art. no. 100523. <https://doi.org/10.1016/j.rsma.2019.100523>
- Basti, L., Nagai, S., Watanabe, S., Oda, T., Tanaka, Y., 2016. Neuroenzymatic activity and physiological energetics in Manila clam, *Ruditapes philippinarum*, during short-term sublethal exposure to harmful alga, *Heterocapsa circularisquama*. *Aquat. Toxicol.* 176, 76–87. <https://doi.org/10.1016/j.aquatox.2016.04.011>
- Batifoulter, F., Lazure, P., Velo-Suarez, L., Maurer, D., Bonneton, P., Charria, G., Dupuy, C., Gentien, P., 2013. Distribution of *Dinophysis* species in the Bay of Biscay and possible transport pathways to Arcachon Bay. *J. Mar. Syst.* 109–110, 273–283. <https://doi.org/10.1016/j.jmarsys.2011.12.007>
- Bilbao, J., Muñoz, O., Revilla, M., Rodríguez, J.G., Laza-Martínez, A., Seoane, S., 2020. Suitability of two areas of the Basque coast to sustain shellfish aquaculture according to both the presence of potentially toxic phytoplankton and the biotoxins regulated by the European Union. *Reg. Stud. Mar. Sci.* 36, art. no. 101279. <https://doi.org/10.1016/j.rsma.2020.101279>
- Blanco, J., Cano, J., Mariño, M., Campos, M.J., 2006. Effect of phytoplankton containing paralytic shellfish and amnesic shellfish toxins on the culture of the king scallop *Pecten maximus* in Málaga (SE Spain). *Aquat. Living Resour.* 19, 267–273. <https://doi.org/10.1051/alr:2006027>
- Brahim, M.B., Feki-Sahnouna, W., Feki, M., Mahfoudi, M., Hamza, A., 2015. Seasonal and daily fluctuation of diatoms during spring tide periods in Kerkennah Islands. *J. Coast. Life Med.* 3 (6), 446–452. <https://doi.org/10.12980/JCLM.3.2015JCLM-2015-0016>
- Brown, M.R., 2002. Nutritional value and use of microalgae in aquaculture. In: Cruz Suárez, L.E., Ricque Marie, D., Tapia Salazar, M., Gaxiola Cortés, M.G., Simoes, N. (Eds.). In: *Avances en Nutrición Acuícola VI. Memorias del VI Simposium Internacional de Nutrición Acuícola. 3 al 6 de Septiembre de 2002. Cancún, Quintana Roo, México, 3.* Universidad Autónoma de Nuevo León, Monterrey, 281–292.
- Cao, R., Wang, D., Wei, Q., Wang, Q., Yang, D., Liu, H., 2018. Integrative Biomarker Assessment of the Influence of Saxitoxin on Marine Bivalves: A Comparative Study of the Two Bivalve Species Oysters, *Crassostrea gigas*, and Scallops, *Chlamys farreri*. *Front. Physiol.* 9, art. no. 1173. <https://doi.org/10.3389/fphys.2018.01173>
- Carey, R.O., Migliaccio, K.W., 2009. Contribution of wastewater treatment plant effluents to nutrient dynamics in aquatic systems. *Environ. Manage.* 44 (2), 205–217. <https://doi.org/10.1007/s00267-009-9309-5>
- Catarina, A., Xavier, F., 2012. Nutritional Value and Uses of Microalgae in Aquaculture. *Aquaculture* 10 (1516), 59–78. <https://doi.org/10.5772/30576>
- Cearreta, A., Irabien, M.J., Pascual, A., 2004. Chapter 2 Human activities along the Basque coast during the last two centuries: geological perspective of recent anthropogenic impact on the coast and its environmental consequences. In: Borja, A., Collins, M. (Eds.). In: *Oceanography and Marine Environment of the Basque Country.* Elsevier Oceanography Ser, 70, 27–50. [https://doi.org/10.1016/S0422-9894\(04\)80040-0](https://doi.org/10.1016/S0422-9894(04)80040-0)

- Clesceri, L., Greenberg, A., Trussell, R., 1989. Standard methods for the examination of water and wastewater. American Public Health Assoc., Washington DC, 133 pp.
- Cranford, P., Duarte, P., Robinson, S., Fernández-Reiriz, M., Labarta, U., 2014. Suspended particulate matter depletion and flow modification inside mussel (*Mytilus galloprovincialis*) culture rafts in the Ria de Betanzos, Spain. *J. Exp. Mar. Biol. Ecol.* 452, 70–81. <https://doi.org/10.1016/j.jembe.2013.12.005>
- Cranford, P., Li, W., Strand, Ø., Strohmeier, T., 2008. Phytoplankton depletion by mussel aquaculture: high resolution mapping, ecosystem modeling and potential indicators of ecological carrying capacity. ICES CM 2008/H:12. International Council for the Exploration of the Sea. [www.ices.dk/products/CMdocs/CM-2008/H/H1208.pdf](http://www.ices.dk/products/CMdocs/CM-2008/H/H1208.pdf)
- Dahl, E., Edvardsen, B., Eikrem, W., 1998. *Chrysochromulina* blooms in the Skagerrak after 1988. In: Reguera, B., Blanco, J., Fernandez, M.L., Wyatt, T. (Eds.), *Harmful algae*. Xunta de Galicia and Intergovernment. Oceanogr. UNESCO, Santiago de Compostela, 104–105.
- David, H., Ganzedo, U., Laza-Martínez, A., Orive, E., 2012. Relationships between the presence of *Ostreopsis* (Dinophyceae) in the Atlantic coast of the Iberian. *Cryptogamie Algol.* 33, 199–207. <https://doi.org/10.7872/crya.v33.iss2.2011.199>
- David, H., Laza-Martínez, A., Miguel, I., Orive, E., 2013. *Ostreopsis* cf. *siamensis* and *Ostreopsis* cf. *ovata* from the Atlantic Iberian Peninsula: Morphological and phylogenetic characterization. *Harmful Algae* 30, 44–55. <https://doi.org/10.1016/j.hal.2013.08.006>
- Davidson, K., Bresnan, E., 2009. Shellfish toxicity in UK waters: a threat to human health? *Environ. Health* 8, art. no. S12. <https://doi.org/10.1186/1476-069X-8-S1-S12>
- De la Figuera, R., 2017. Visión general del sector acuícola nacional – España. National Aquaculture Sector Overview Fact Sheets 2005–2018. Departamento de Pesca y Acuicultura de la FAO, Roma Updated 12 May 2017. [http://www.fao.org/fishery/countrysector/naso\\_spain/es](http://www.fao.org/fishery/countrysector/naso_spain/es)
- Eidler, L., Elbrächter, M., 2010. Chapter 2: The Utermöhl method for quantitative phytoplankton analysis. In: Karlson, B., Cusak, C., Bresnan, E. (Eds.), *In: Microscopic and molecular methods for quantitative phytoplankton analysis*, 55. UNESCO Publ., Paris, 13–20.
- Eikrem, W., Medlin, L.K., Henderiks, J., Rokitta, S., Rost, B., Robert, I., Thronsen, J., Edvardsen, B., 2017. Haptophyta. In: Archibald, J., Simpson, A., Slamovits, C. (Eds.), *Handbook of the Protists*. Springer, Cham, 893–953. [https://doi.org/10.1007/978-3-319-28149-0\\_38](https://doi.org/10.1007/978-3-319-28149-0_38)
- Eurofish, 2016. Overview of the Spanish fisheries and aquaculture sector. Retrieved from: <https://www.eurofish.dk/spain> (accessed on 17 February 2018).
- Estrada, N., de Jesús Romero, M., Campa-Córdova, A., Luna, A., Ascencio, F., 2007. Effects of the toxic dinoflagellate, *Gymnodinium catenatum* on hydrolytic and antioxidant enzymes, in tissues of the giant lions-paw scallop *Nodipecten subnodosus*. *Comp. Biochem. Physiol. C Toxicol. Pharmacol.* 146, 502–510. <https://doi.org/10.1016/j.cbpc.2007.06.003>
- Fanjul, A., Villate, F., Uriarte, I., Iriarte, A., Atkinson, A., Cook, K., 2017. Zooplankton variability at four monitoring sites of the Northeast Atlantic Shelves differing in latitude and trophic status. *J. Plankton Res.* 39 (6), 891–909. <https://doi.org/10.1093/plankt/fbx054>
- Ferrer, L., Fontán, A., Mader, J., Chust, G., González, M., Valencia, V., Uriarte, A., Collins, M.B., 2009. Low-salinity plumes in the oceanic region of the Basque Country. *Cont. Shelf Res.* 29 (8), 970–984. <https://doi.org/10.1016/j.csr.2008.12.014>
- Figueiras, F., Labarta, U., Reiriz, M.F., 2002. Coastal upwelling, primary production and mussel growth in the Rías Baixas of Galicia. *Hydrobiologia* 484, 121–131. <https://doi.org/10.1023/A:1021309222459>
- Fontán, A., González, M., Wells, N., Collins, M., Mader, J., Ferrer, L., Esnaola, G., Uriarte, A., 2009. Tidal and wind-induced circulation within the Southeastern limit of the Bay of Biscay: Pasaia Bay. *Basque Coast. Cont. Shelf Res.* 29 (8), 998–1007. <https://doi.org/10.1016/j.csr.2008.12.013>
- Fontán, A., Valencia, V., Borja, Á., Goikoetxea, N., 2008. Oceanometeorological conditions and coupling in the southeastern Bay of Biscay, for the period 2001–2005: a comparison with the past two decades. *J. Marine Syst.* 72 (1–4), 167–177. <http://dx.doi.org/10.1016/j.jmarsys.2007.08.003>
- Garmendia, M., Revilla, M., Bald, J., Franco, J., Laza-Martínez, A., Orive, E., Seoane, S., Valencia, V., Borja, Á., 2011. Phytoplankton communities and biomass size structure (fractionated chlorophyll “a”), along trophic gradients of the Basque coast (northern Spain). *Biogeochemistry* 106, 243–263. <https://doi.org/10.1007/s10533-010-9445-2>
- Gibb, S.W., Cummings, D.G., Irigoien, X., Barlow, R.G., Fauzi, R., Mantoura, C., 2001. Phytoplankton pigment chemotaxonomy of the northeastern Atlantic. *Deep Sea Research Pt. II* 48 (4–5), 795–823. [https://doi.org/10.1016/S0967-0645\(00\)00098-9](https://doi.org/10.1016/S0967-0645(00)00098-9)
- Glé, C., Del Amo, Y., Sautour, B., Laborde, P., Chardy, P., 2008. Variability of nutrients and phytoplankton primary production in a shallow macrotidal coastal ecosystem (Arcachon Bay, France). *Estuar. Coast. Shelf Sci.* 76, 642–656. <https://doi.org/10.1016/j.ecss.2007.07.043>
- Glibert, P.M., 2016. Margalef revisited: A new phytoplankton mandala incorporating twelve dimensions, including nutritional physiology. *Harmful Algae* 55, 25–30. <https://doi.org/10.1016/j.hal.2016.01.008>
- González, M., Uriarte, Ad., Fontán, A., Mader, J., Gyssels, P., 2004. Marine dynamics. In: Borja, A., Collins, M. (Eds.), *In: Oceanography and Marine Environment of the Basque Country*. Elsevier Oceanogr. Ser, 70. Elsevier, Amsterdam, 133–157. [https://doi.org/10.1016/S0422-9894\(04\)80044-8](https://doi.org/10.1016/S0422-9894(04)80044-8)
- Granéli, E., Turner, J., 2006. Ecology of harmful algae. In: *Ecological Studies* 189. Springer-Verlag, Berlin and Heidelberg, 413 pp.
- Grasshoff, K., Ehrhardt, M., Kremling, K., 1983. *Methods of seawater analyses*. Verlag Chemie, Weinheim, Germany, 342–355.
- Guillaud, J.F., Aminot, A., Delmas, D., Gohin, F., Lunven, M., Labry, C., Herbland, A., 2008. Seasonal variation of riverine nutrient inputs in the northern Bay of Biscay (France), and patterns of marine phytoplankton response. *J. Marine Syst.* 72, 309–319. <https://doi.org/10.1016/j.jmarsys.2007.03.010>
- Guiry, M.D., Guiry, G.M., 2018. *AlgaeBase*. World-wide electronic publication, National University of Ireland, Galway. <http://www.algaebase.org>
- Haberkorn, H., Tran, D., Massabuau, J.C., Ciret, P., Savar, V., Soudant, P., 2011. Relationship between valve activity, microalgae concentration in the water and toxin accumulation in the digestive gland of the Pacific oyster *Crassostrea gigas* exposed to *Alexandrium minutum*. *Mar. Pollut. Bull.* 62, 1191–1197. <https://doi.org/10.1016/j.marpolbul.2011.03.034>
- Hansen, P.J., Hjorth, M., 2002. Growth and grazing responses of *Chrysochromulina ericina* (Prymnesiophyceae): the role of irradiance, prey concentration and pH. *Mar. Biol.* 141, 975–983. <https://doi.org/10.1007/s00227-002-0879-5>
- Instituto Hidrográfico de la Marina, 1992. *Anuario de Mareas*. Servicio de Publicaciones de la Armada. Talleres del Instituto Hidrográfico de la Marina, Cádiz.
- Jassby, A., Müller-Solger, A., Vayssières, M., 2005. Short-term variability of chlorophyll and implications for sampling frequency in the San Joaquin River. *IEP News* 18 (1), 28. [http://www.iep.ca.gov/report/newsletter/2004\\_newsletters/IEPNewsletter\\_fall\\_2004\\_winter\\_2005.pdf](http://www.iep.ca.gov/report/newsletter/2004_newsletters/IEPNewsletter_fall_2004_winter_2005.pdf)
- Jones, H.L.J., Leadbeater, B.S.C., Green, J.C., 1993. Mixotrophy in marine species of *Chrysochromulina* (Prymnesiophyceae): ingestion and digestion of a small green flagellate. *J. Mar.*

- Biol. Assoc. U.K. 73 (2), 283–296. <https://doi.org/10.1017/S0025315400032859>
- Jouenne, F., Lefebvre, S., Véron, B., Lagadeuc, Y., 2007. Phytoplankton community structure and primary production in small intertidal estuarine-bay ecosystem (eastern English Channel, France). *Mar. Biol.* 151 (3), 805–825. <https://doi.org/10.1007/s00227-006-0440-z>
- Klein, C., Claquin, P., Bouchart, V., Le Roy, B., Véron, B., 2010. Dynamics of *Pseudo-nitzschia* spp. and domoic acid production in a macrotidal ecosystem of the Eastern English Channel (Normandy, France). *Harmful Algae* 9 (2), 218–226. <https://doi.org/10.1016/j.hal.2009.10.004>
- Knuckey, R.M., Brown, M.R., Barrett, S.M., Hallegraeff, G.M., 2002. Isolation of new nanoplanktonic diatom strains and their evaluation as diets for juvenile Pacific oysters (*Crassostrea gigas*). *Aquaculture* 211, 253–274. [https://doi.org/10.1016/S0044-8486\(02\)00010-8](https://doi.org/10.1016/S0044-8486(02)00010-8)
- Labry, C., Herbland, A., Delmas, D., Laborde, P., Lazure, P., Froidefond, J., Jegou, A.M., Sautour, B., 2001. Initiation of winter phytoplankton blooms within the Gironde plume waters in the Bay of Biscay. *Mar. Ecol. Prog. Ser.* 212, 117–130. <https://doi.org/10.3354/meps212117>
- Latasa, M., Moran, X.A.G., Scharek, R., Estrada, M., 2005. Estimating the carbon flux through main phytoplankton groups in the northwestern Mediterranean. *Limnol. Oceanogr.* 50, 1447–1458. <https://doi.org/10.4319/lo.2005.50.5.1447>
- Lawrence, J., Loreal, H., Toyofuku, H., Hess, P., Karunasagar, I., Ababouch, L., 2011. Assessment and management of biotoxin risks in bivalve molluscs. *FAO Fisheries and Aquaculture Tech. Pap. No. 551*. FAO, Rome, 337 pp.
- Laza-Martínez, A., Orive, E., Miguel, I., 2011. Morphological and genetic characterization of benthic dinoflagellates of the genera *Coolia*, *Ostreopsis* and *Prorocentrum* from the south-eastern Bay of Biscay. *Eur. J. Phycol.* 46, 45–65. <https://doi.org/10.1080/09670262.2010.550387>
- Lessard, E., Merico, A., Tyrrell, T., 2005. Nitrate:phosphate ratios and *Emiliania huxleyi* blooms. *Limnol. Oceanogr.* 50, 1020–1024. <https://doi.org/10.4319/lo.2005.50.3.1020>
- Li, W., Lewis, M., Harrison, W., 2009. Multiscalarity of the nutrient–chlorophyll relationship in coastal phytoplankton. *Estuar. Coast.* 33, 440–447. <https://doi.org/10.1007/s12237-008-9119-7>
- Lionard, M., Muylaert, K., Gansbeke, D.V., Vyverman, W., 2005. Influence of changes in salinity and light intensity on growth of phytoplankton communities from the Schelde river and estuary (Belgium/The Netherlands). *Hydrobiologia* 540, 105–115. <https://doi.org/10.1007/s10750-004-7123-x>
- Litchman, E., Klausmeier, C.A., Miller, J.R., Schofield, O.M., Falkowski, P.G., 2006. Multi-nutrient, multi-group model of present and future oceanic phytoplankton communities. *Biogeosciences* 3, 585–606. <https://doi.org/10.5194/bg-3-585-2006>
- Lucas, M., Newell, R., Shumway, S., Seiderer, L., Bally, R., 1987. Particle clearance and yield in relation to bacterioplankton and suspended particulate availability in estuarine and open coast populations of the mussel *Mytilus edulis*. *Mar. Ecol. Prog. Ser.* 36, 215–224. <https://doi.org/10.3354/meps036215>
- Madariaga, I., 1995. Photosynthetic characteristics of phytoplankton during the development of a summer bloom in the Urdaibai Estuary, Bay of Biscay. *Estuar. Coast. Shelf Sci.* 40 (5), 559–575. <https://doi.org/10.1006/ecss.1995.0038>
- Madariaga, I., 2002. Short-term variations in the physiological state of phytoplankton in a shallow temperate estuary. In: Orive, E., Elliott, M., de Jorge, V. (Eds.), *Nutrients and Eutrophication in Estuaries and Coastal Waters*. Developments in Hydrobiology. Springer, Dordrecht, 345–358. [https://doi.org/10.1007/978-94-017-2464-7\\_25](https://doi.org/10.1007/978-94-017-2464-7_25)
- Margalef, R., 1978. Life-forms of phytoplankton as survival alternatives in an unstable environment. *Oceanol. Acta* 1 (4), 493–509.
- Malone, T., Azzaro, M., Bode, A., Brown, E., Duce, R., Kamykowski, D., Kang, S., Kedong, Y., Thorndyke, M., Wang, J., Park, C., Calumpang, H., Eghtesadi, P., 2016. Chapter 6. Primary production, cycling of nutrients, surface layer and plankton. The first global integrated marine assessment World Ocean. Oceans and Law of the Sea, United Nations. [http://www.un.org/depts/los/global\\_reporting/WOA\\_RegProcess.htm](http://www.un.org/depts/los/global_reporting/WOA_RegProcess.htm)
- Marshall, R., McKinley, S., Pearce, C., 2010. Effects of nutrition on larval growth and survival in bivalves. *Aquaculture* 2 (1), 33–55. <http://dx.doi.org/10.1111/j.1753-5131.2010.01022.x>
- Martínez-Pita, I., Sánchez-Lazo, C., Ruíz-Jarabo, I., Herrera, M., Mancera, J.M., 2012. Biochemical composition, lipid classes, fatty acids and sexual hormones in the mussel *Mytilus galloprovincialis* from cultivated populations in south Spain. *Aquaculture* 358–359, 274–283. <https://doi.org/10.1016/j.aquaculture.2012.06.003>
- Maurer, D., Bec, B., Neaud-Masson, N., Rumebe, M., Auby, I., Grémare, A., 2010. Etude des relations entre le phytoplancton et les phénomènes de toxicité d'origine inconnue dans le Bassin d'Arcachon. IFREMER Internal Rep., RST/INER/AR/10.004. <https://archimer.ifremer.fr/doc/00031/14245/>
- Moestrup, Ø., Akselmann, R., Fraga, S., Hoppenrath, M., Iwataki, M., Komárek, J., Larsen, J., Lundholm, N., Zingone, A., 2009 onwards. IOC-UNESCO Taxonomic Reference List of Harmful Micro Algae. <http://www.marinespecies.org/hab> (accessed on 30 June 2018).
- Montagnes, D.J.S., Berges, J.A., Harrison, P.J., Taylor, F.J.R.L., 1994. Estimating carbon, nitrogen, protein, and chlorophyll a from volume in marine phytoplankton. *Limnol. Oceanogr.* 39 (5), 1044–1060. <http://dx.doi.org/10.4319/lo.1994.39.5.1044>
- Moroño, A., Franco, J., Miranda, M., Reyero, M.I., Blanco, J., 2001. The effect of mussel size, temperature, seston volume, food quality and volume-specific toxin concentration on the uptake rate of PSP toxins by mussels (*Mytilus galloprovincialis* Lmk). *J. Exp. Mar. Biol. Ecol.* 257, 117–132. [https://doi.org/10.1016/S0022-0981\(00\)00336-1](https://doi.org/10.1016/S0022-0981(00)00336-1)
- Muñiz, O., Revilla, M., Rodríguez, J.G., Laza-Martínez, A., Fontán, A., 2019. Annual cycle of phytoplankton community through the water column: Study applied to the implementation of bivalve offshore aquaculture in the southeastern Bay of Biscay. *Oceanologia* 61 (1), 114–130. <https://doi.org/10.1016/j.oceano.2018.08.001>
- Muñiz, O., Revilla, M., Rodríguez, J.G., Laza-Martínez, A., Seoane, S., Franco, J., Orive, E., 2017. Evaluation of phytoplankton quality and toxicity risk based on a long-term time series previous to the implementation of a bivalve farm (Basque coast as a case study). *Reg. Stud. Mar. Sci.* 10, 10–19. <https://doi.org/10.1016/j.rsma.2016.12.012>
- Muñiz, O., Rodríguez, J.G., Revilla, M., Laza-Martínez, A., Seoane, S., Franco, J., 2018. Seasonal variations of phytoplankton community in relation to environmental factors in an oligotrophic area of the European Atlantic coast (southeastern Bay of Biscay). *Reg. Stud. Mar. Sci.* 17, 59–72. <https://doi.org/10.1016/j.rsma.2017.11.011>
- Nielsen, P., Krock, B., Hansen, P.J., Vismann, B., 2020. Effects of the DSP-toxic dinoflagellate *Dinophysis acuta* on clearance and respiration rate of the blue mussel, *Mytilus edulis*. *PLoS one* 15 (3), art. no. e0230176. <https://doi.org/10.1371/journal.pone.0230176>
- Not, F., Massana, R., Latasa, M., Marie, D., Colson, C., Eikrem, W., Pedrós-Alió, C., Vaulot, D., Simon, N., 2005. Late summer community composition and abundance of photosynthetic picoeukaryotes in Norwegian and Barents Seas. *Limnol. Oceanogr.* 50 (5), 1677–1686. <https://doi.org/10.4319/lo.2005.50.5.1677>
- O'Brien, T., Li, W., Morán, X. (Eds.), 2012. *ICES Phytoplankton and Microbial Plankton Status Report 2009/2010*. ICES Cooperative Res. Rep. No. 313, 196 pp.
- Olenina, I., Hajdu, S., Edler, L., Andersson, A., Wasmund, N., Busch, S., Göbel, J., Gromisz, S., Huseby, S., Huttunen, M.,

- Jaanus, A., Kokkonen, P., Ledaine, I., Niemkiewicz, E., 2006. In: Biovolumes and size-classes of phytoplankton in the Baltic Sea, 106. Helsinki Commission. Baltic Marine Environ. Prot. Comm., 144.
- Orive, E., Franco, J., Madariaga, I., Revilla, M., 2004. Bacterioplankton and phytoplankton communities. In: Borja, Á., Collins, M. (Eds.). In: Oceanography and Marine Environment of the Basque Country. Elsevier Oceanogr. Ser. 70. Elsevier, Amsterdam, 367–393.
- Orive, E., Laza-Martinez, A., Seoane, S., 2008. Seguimiento del fitoplancton en el estuario del río Nervión: identificación de especies potencialmente tóxicas. In: Avances y tendencias en fitoplancton tóxico y biotoxinas, Actas de la IX Reunión Ibérica sobre Fitoplancton Tóxico y Biotoxinas, Cartagena 7–10 May 2007. Universidad Politécnica de Cartagena, 99–102.
- Orive, E., Laza-Martinez, A., Seoane, S., Alonso, A., Andrade, R., Miguel, I., 2010. Diversity of *Pseudo-nitzschia* in the southeastern Bay of Biscay. Diatom Res. 25, 125–145. <https://doi.org/10.1080/0269249X.2010.9705834>
- Parrish, C., 2013. Lipids in Marine Ecosystems. ISRN Oceanogr. 2013, 1–16. <https://doi.org/10.5402/2013/604045>
- Pernet, F., Malet, N., Pastoureaud, A., Vaquer, A., Quéré, C., Dubroca, L., 2012. Marine diatoms sustain growth of bivalves in a Mediterranean lagoon. J. Sea Res. 68, 20–32. <https://doi.org/10.1016/j.seares.2011.11.004>
- Petersen, J.K., Nielsen, T.G., Van Duren, L., Maar, M., 2008. Depletion of plankton in a raft culture of *Mytilus galloprovincialis* in Ría de Vigo. NW Spain. I. Phytoplankton. Aquat. Biol. 4, 113–125. <https://doi.org/10.3354/ab00124>
- Pettersen, A.K., Turchini, G.M., Jahangard, S., Ingram, B.A., Sherman, C.D., 2010. Effects of different dietary microalgae on survival, growth, settlement and fatty acid composition of blue mussel (*Mytilus galloprovincialis*) larvae. Aquaculture 309 (1), 115–124. <http://dx.doi.org/10.1016/j.aquaculture.2010.09.024>
- Ramos, V., Vasconcelos, V., 2010. Palytoxin and analogs: biological and ecological effects. Mar. Drugs 8, 2021–2037. <https://doi.org/10.3390/md8072021>
- Revilla, M., Franco, J., Bald, J., Borja, Á., Laza, A., Seoane, S., Valencia, V., 2009. Assessment of the phytoplankton ecological status in the Basque coast (northern Spain) according to the European Water Framework Directive. J. Sea Res. 61, 60–67. <https://doi.org/10.1016/j.seares.2008.05.009>
- Reynolds, C.S., 2006. Ecology of Phytoplankton. Cambridge University Press, Cambridge, 535 pp.
- Rodríguez, F., Pazos, Y., Maneiro, J., Zapata, M., 2003. Temporal variation in phytoplankton assemblages and pigment composition at a fixed station of the Ria of Pontevedra (NW Spain). Estuar. Coast. Shelf Sci. 58, 499–515. [https://doi.org/10.1016/S0272-7714\(03\)00130-6](https://doi.org/10.1016/S0272-7714(03)00130-6)
- Romalde, J.L., Rivadulla, E., Varela, M.F., Barja, J.L., 2018. An overview of 20 years of studies on the prevalence of human enteric viruses in shellfish from Galicia, Spain. J. Appl. Microbiol. 124 (4), 943–957. <https://doi.org/10.1111/jam.13614>
- Ross, O.N., 2006. Particles in motion: how turbulence affects plankton sedimentation from an oceanic mixed layer. Geophys. Res. Lett. 33 (10) art. no. L10609. <https://doi.org/10.1029/2006gl026352>
- Ross, O.N., Sharples, J., 2007. Swimming for survival: a role of phytoplankton motility in a stratified turbulent environment. J. Marine Syst. 70, 248–262. <https://doi.org/10.1016/j.jmarsys.2006.07.008>
- Samson, J.C., Shumway, S.E., Weis, J.S., 2008. Effects of the toxic dinoflagellate, *Alexandrium fundyense* on three species of larval fish: a foodchain approach. J. Fish Biol. 72, 168–188. <https://doi.org/10.1111/j.1095-8649.2007.01698.x>
- Sánchez-Lazo, C., Martínez-Pita, I., 2012. Biochemical and energy dynamics during larval development of the mussel *Mytilus galloprovincialis* (Lamarck, 1819). Aquaculture 358–359, 71–78. <https://doi.org/10.1016/j.aquaculture.2012.06.021>
- Seoane, S., Eikrem, W., Arluzea, J., Orive, E., 2009. Haptophytes of the Nervión River estuary, northern Spain. Bot. Mar. 52 (1), 47–59. <https://doi.org/10.1515/bot.2009.027>
- Seoane, S., Laza, A., Orive, E., 2006. Monitoring phytoplankton assemblages in estuarine waters: the application of pigment analysis and microscopy to size-fractionated samples. Estuar. Coast. Shelf Sci. 67, 343–354. <https://doi.org/10.1016/j.eccs.2005.10.020>
- Seoane, S., Laza, A., Urrutxurtu, I., Orive, E., 2005. Phytoplankton assemblages and their dominant pigments in the Nervión River Estuary. Hydrobiologia 549, 1–13. <https://doi.org/10.1007/s10750-005-1736-6>
- Seoane, S., Orive, E., 2012. First report of *Dinophysis acuminata* bloom in Basque waters. Northern Spain. Harmful Algae News no. 46, 9 pp.
- Seoane, S., Puente, A., Guinda, X., Juanes, J.A., 2012. Bloom forming and toxic phytoplankton in transitional and coastal waters of Cantabria region coast (Southeastern Bay of Biscay, Spain). Mar. Pollut. Bull. 64, 2860–2866. <https://doi.org/10.1016/j.marpolbul.2012.08.023>
- Shumway, S.E., Burkholder, J.M., Springer, J., 2006. Effects of the estuarine dinoflagellate *Pfiesteria shumwayae* (Dinophyceae) on survival and grazing activity of several shellfish species. Harmful Algae 5, 442–458. <https://doi.org/10.1016/j.hal.2006.04.013>
- Shumway, S.E., Cucci, T.L., 1987. The effects of the toxic dinoflagellate *Protogonyaulax tamarensis* on the feeding and behaviour of bivalve molluscs. Aquat. Toxicol. 10 (1), 9–27. [https://doi.org/10.1016/0166-445X\(87\)90024-5](https://doi.org/10.1016/0166-445X(87)90024-5)
- Spyrakos, E., Vilas, L.G., Palenzuela, J.M.T., Barton, E.D., 2011. Remote sensing chlorophyll a of optically complex waters (rias Baixas, NW Spain): Application of a regionally specific chlorophyll a algorithm for MERIS full resolution data during an upwelling cycle. Remote Sens. Environ. 115 (10), 2471–2485. <https://doi.org/10.1016/j.rse.2011.05.008>
- Stenton-Dozey, J., Brown, A., 1992. Clearance and retention efficiency of natural suspended particles by the rock-pool bivalve *Venerupis corrugatus* in relation to tidal availability. Mar. Ecol. Prog. Ser. 82, 175–186. <https://doi.org/10.3354/meps082175>
- Strohmeier, T., Strand, Ø., Alunno-Bruscia, M., Duinker, A., Cranford, P.J., 2012. Variability in particle retention efficiency by the mussel *Mytilus edulis*. J. Exp. Mar. Biol. Ecol. 412, 96–102. <https://doi.org/10.1016/j.jembe.2011.11.006>
- Stromgren, T., Cary, C., 1984. Growth in length of *Mytilus edulis* fed on different algal diets. J. Exp. Mar. Biol. Ecol. 76, 23–34. [https://doi.org/10.1016/0022-0981\(84\)90014-5](https://doi.org/10.1016/0022-0981(84)90014-5)
- Swan, S., Davidson, K., 2012. Monitoring programme for the presence of toxin producing plankton in shellfish production areas in Scotland. Ann. Rep. Food Standards Agency, Scotland. [www.food.gov.uk](http://www.food.gov.uk)
- Trigueros, J.M., Orive, E., 2000. Tidally driven distribution of phytoplankton blooms in a shallow, macrotidal estuary. J. Plankton Res. 22 (5), 969–986. <https://doi.org/10.1093/plankt/22.5.969>
- Trottet, A., Roy, S., Tamigneaux, E., Lovejoy, C., Tremblay, R., 2008. Impact of suspended mussels (*Mytilus edulis* L.) on plankton communities in a Magdalen Islands lagoon (Québec, Canada): A mesocosm approach. J. Exp. Mar. Biol. Ecol. 365 (2), 103–115. <https://doi.org/10.1016/j.jembe.2008.08.001>
- Valencia, V., Borja, Á., Fontán, A., Pérez, F.F., Ríos, A.F., 2003. Temperature and salinity fluctuations along the Basque Coast (southeastern Bay of Biscay), from 1986 to 2000, related to climatic factors. ICES J. Mar. Sci. 219, 340–342.
- Valencia, V., Franco, J., 2004. Chapter 8 – Main characteristics of the water masses. In: Borja, Á., Collins, M. (Eds.). In: Oceanography and Marine Environment of the Basque Country, 70. Elsevier Oceanogr. Ser. Elsevier, Amsterdam, 197–232.

- Valencia, V., Franco, J., Borja, Á., Fontán, A., 2004. Hydrography of the southeastern Bay of Biscay. In: Borja, A., Collins, M. (Eds.), *Oceanography and Marine Environment of the Basque Country*. Elsevier Oceanogr. Ser. Vol. 70. Elsevier, Amsterdam, 159–194.
- Varela, M., Prego, R., Pazos, Y., Morono, Á., 2005. Influence of upwelling and river runoff interaction on phytoplankton assemblages in a Middle Galician Ria and Comparison with northern and southern rias (NW Iberian Peninsula). *Estuar. Coast. Shelf Sci.* 64 (4), 721–737. <https://doi.org/10.1016/j.ecss.2005.03.023>
- Volkman, J.K., Dunstan, G.A., Jeffrey, S.W., Kearney, P.S., 1991. Fatty acids from microalgae of the genus *Pavlova*. *Phytochemistry* 30, 1855–1859. [https://doi.org/10.1016/0031-9422\(91\)85028-X](https://doi.org/10.1016/0031-9422(91)85028-X)
- Volkman, J.K., Jeffrey, S.W., Nichols, P.D., Rogers, G.I., Garland, C.D., 1989. Fatty acid and lipid composition of 10 species of microalgae used in mariculture. *J. Exp. Mar. Biol. Ecol.* 128, 219–240. [https://doi.org/10.1016/0022-0981\(89\)90029-4](https://doi.org/10.1016/0022-0981(89)90029-4)
- Wall, C.C., Gobler, C.J., Peterson, B.J., Ward, J.E., 2013. Contrasting growth patterns of suspension-feeding molluscs (*Mercenaria mercenaria*, *Crassostrea virginica*, *Argopecten irradians*, and *Crepidula fornicata*) across a eutrophication gradient in the Peconic Estuary, NY, USA. *Estuar. Coast.* 36 (6), 1274–1291. <https://doi.org/10.1007/s12237-013-9632-1>
- Weiss, M.B., Curran, P.B., Peterson, B.J., Gobler, C.J., 2007. The influence of plankton composition and water quality on hard clam (*Mercenaria mercenaria* L.) populations across Long Island's south shore lagoon estuaries (New York, USA). *J. Exp. Mar. Biol. Ecol.* 345, 12–25. <https://doi.org/10.1016/j.jembe.2006.12.025>
- Widdicombe, C.E., Eloire, D., Harbour, D., Harris, R.P., Somerfield, P.J., 2010. Long-term phytoplankton community dynamics in the Western English Channel. *J. Plankton Res.* 32 (5), 643–655. <https://doi.org/10.1093/plankt/fbp127>



## ORIGINAL RESEARCH ARTICLE

# Assessment of wave energy in the Persian Gulf: An evaluation of the impacts of climate change

Hamid Goharnejad<sup>a,b,\*</sup>, Ehsan Nikaein<sup>a</sup>, Will Perrie<sup>b</sup>

<sup>a</sup> Department of Civil Engineering, Environmental Sciences Research Center, IslamShahr Branch, Islamic Azad University, IslamShahr, Iran

<sup>b</sup> Fisheries and Oceans Canada, Bedford Institute of Oceanography, Dartmouth, Nova Scotia, Canada

Received 31 January 2020; accepted 9 September 2020

Available online 28 September 2020

## KEYWORDS

Wave energy potential;  
RCP8.5;  
RCP4.5;  
Persian gulf;  
Mike SW

**Abstract** We are motivated to study the exploitation of marine energy as a renewable resource because of society's ever-increasing energy demands, and a concomitant need to reduce greenhouse gas emissions. Additionally, climate-related variations in wave energy should be investigated in order to ensure the stability of its long-term availability. Here, we investigate the potential for wave energy in the Persian Gulf along the southern coasts of Iran. To do so, we have applied the Mike SW numerical model and ECMWF wind field data for a 30-year study, from 1988 to 2017. For this purpose, wave energy was evaluated at six points in the western, northern, southern, and eastern parts of the Persian Gulf. To assess the impacts of climate change, we also consider the wave regime from 2070 to 2099 (for 30 years) following IPCC RCP4.5 and RCP8.5 climate change scenarios. Our findings suggest that in the present climate, seasonal variations in the mean wave parameters (i.e. wave energy, wave period, and significant wave height) correspond to the lowest wave energy in the summers, and highest in the winters. In the future climate change scenarios, energy level variations generally have similar patterns, with slight modulations in some local areas.

© 2020 Institute of Oceanology of the Polish Academy of Sciences. Production and hosting by Elsevier B.V. This is an open access article under the CC BY-NC-ND license (<http://creativecommons.org/licenses/by-nc-nd/4.0/>).

\* Corresponding author at: Department of Civil Engineering, Environmental Sciences Research Center, IslamShahr Branch, Islamic Azad University, IslamShahr, Iran.

E-mail addresses: [hgn1982@gmail.com](mailto:hgn1982@gmail.com) (H. Goharnejad), [nikaein\\_e@yahoo.com](mailto:nikaein_e@yahoo.com) (E. Nikaein), [william.perrie@dfo-mpo.gc.ca](mailto:william.perrie@dfo-mpo.gc.ca) (W. Perrie). Peer review under the responsibility of the Institute of Oceanology of the Polish Academy of Sciences.



Production and hosting by Elsevier

<https://doi.org/10.1016/j.oceano.2020.09.004>

0078-3234/© 2020 Institute of Oceanology of the Polish Academy of Sciences. Production and hosting by Elsevier B.V. This is an open access article under the CC BY-NC-ND license (<http://creativecommons.org/licenses/by-nc-nd/4.0/>).

## 1. Introduction

According to the [Implementation Agreement on Ocean Energy Systems \(2007\)](#), the global ocean wave energy is estimated at approximately 93100 TWh/yr. Therefore, in recent years extensive studies have been completed on wind-wave energies in the global ocean and coastal seas, and the potential for wave energy extraction ([Besio et al., 2016](#); [Kumar and Anoop 2015](#); [Neil and Hashemi, 2013](#)). A lot of studies have been completed to assess the wave energy potential around the world ([Alonso et al., 2015](#); [Appendini et al. 2015](#); [Gallagher et al., 2016](#); [Jadidoleslam et al., 2016](#); [Liang et al., 2016](#); [López et al., 2015](#); [Morim al., 2014](#); [Neill et al., 2014](#); [Ponce de León et al., 2016](#); [Rusu and Onea, 2013](#); [Wang et al., 2016](#), [Zhou et al. 2015a,b](#)). All of these indicate that the use of high precision data is indispensable for assessing the local parameters of wave energy. Therefore, our study is focused on a high accuracy evaluation of the temporal and spatial parameters of waves in coastal areas of the Persian Gulf. In addition, the present and future wind climate must be considered as the main source of wave energy production. Recent research has shown that in the twentieth century, the mean sea level and the average wind speed have increased by 30 cm and 1 m/s, respectively ([WCRP, 2018](#)).

Meanwhile, several studies have considered climate change and winds in areas such as the Red Sea ([Aboobacker et al., 2017](#); [Langodan et al., 2016](#); [Shanas et al., 2017](#)), the Mediterranean Sea ([Kapelonis et al., 2015](#)), and the Caspian Sea ([Amirinia et al., 2017](#)), the Persian Gulf and Oman sea ([Armanfar et al., 2019](#); [Goharnejad et al., 2013](#)) for a variety of purposes, including wave energy assessment and climate change impacts. Also, the IPCC climate change scenarios, specifically RCP8.5 emissions scenarios for the end-of-century period (2081–2100), suggest that mean wind speeds will decrease in the North Atlantic, but increase in the Southern Hemisphere, and thus that the wave climate may experience higher wave heights in these areas. These changes will increase the peak periods of the waves, for example in the eastern South Pacific Ocean and the Indian Ocean, causing the mean wave direction to tend to experience counterclockwise rotation in southern oceans ([Casas-Prat et al., 2018](#)).

[Vieira et al. \(2020\)](#) studied wave climate-energy patterns for different seasons for the Persian Gulf and found that waves during winter and springtime are more energetic, and become milder in the autumn. [Alizadeh et al. \(2020\)](#) showed a decreasing trend for the overall Persian Gulf, which is relatively severe in northern areas and has an impact on the potential for future wave energy. In the Persian Gulf, the mean significant wave height has greater variability than that of wind speed, although the dominant wave direction has greater stability than that of wind direction ([Kamranzad, 2018](#)). [Kamranzad et al. \(2017\)](#) compared two stations in the northern Persian Gulf, at Asalouyeh and Boushehr, and found that the sustainability for wave energy and harvesting is higher at the former, compared to the latter. Moreover, [Kamranzad et al. \(2015\)](#) suggest that the annual wave energy will decrease at both stations for A2, B1, and A1B climate change scenarios. In terms of the present climate, for the period from 1984 to 2008, [Kamranzad et al. \(2013\)](#) investigated the wave energy characteristics at three

locations in the Persian Gulf (western, central and eastern) and report that both seasonal and decadal variations can be seen in the wave energy trends, on account of present climate variability.

The focus of this study is the wave climate in the Persian Gulf, motivated by the potential for exploitation of renewable wave energy. An assessment of wave climate in this area suggests that the most significant wave heights should occur in the central part of the Persian Gulf in January and February ([Kamranzad and Chegini, 2014](#)).

In this paper, we assessed the potential wave energy for the Persian Gulf area. Although, a wide range of research has been completed in this study area, consideration has not been given to climate change impacts according to the latest scenarios, RCP8.5 and RCP4.5. Moreover, in this research, we almost tried to assign a 'Wave Energy Development Index' as an indicator of potential energy development. Finally, we provide a 'bivariate probability distribution of occurrence' and wave energy matrices.

## 2. Study area

The Persian Gulf is formed as an extension of the Indian Ocean, with an area of 237,473 square kilometers, and following the Gulf of Mexico and the Hudson Bay, is the third largest bay in the world. The Persian Gulf runs from the waters east of the Strait of Hormuz and the Oman Sea to the Indian Ocean and the Arabian Sea. According to a previous sensitivity analysis completed in this study area by [Liao and Kaihatu \(2016\)](#), the impacts of the boundary waves at the Oman Sea on wind-waves in the Persian Gulf are negligible; therefore no wave spectral are specified as outer boundary conditions. The Gulf's geographic coordinates are from 24° to 30°30'N and from 48° to 56°25'E of the Greenwich meridian. The length of the Persian Gulf from the Strait of Hormuz to its most western location is about 805 kilometers. At its widest, the Gulf is 290 kilometers. The maximum depth of the Persian Gulf is 93 meters and the shallowest waters are about 10–30 meters in the western part. There are several islands in the Gulf. In terms of topography ([Figure 1](#)), the Persian Gulf is asymmetrical and the slopes of its southern coasts are milder than the slopes of its northern shores ([Pous et al., 2015](#)).

## 3. Material and methods

### 3.1. Spectral wave model setup and wave data

In order to study the wave regimes in the Persian Gulf, it is necessary to specify bathymetry data, wind speeds and directions, buoy wave data, and sea level pressure data. In this study, the Spectral Wave (SW) model component of the MIKE modeling system ([DHI, 2005](#)) is used in order to hind-cast the wave characteristics, driven by wind climate data. Waves are numerically modeled using the SW model, a dynamic modeling system based on the SWAN spectral wave model, which is implemented on an irregular unstructured grid. For more details about the unstructured grid mesh, see [Korn \(2017\)](#). The SW model solves the energy transfer

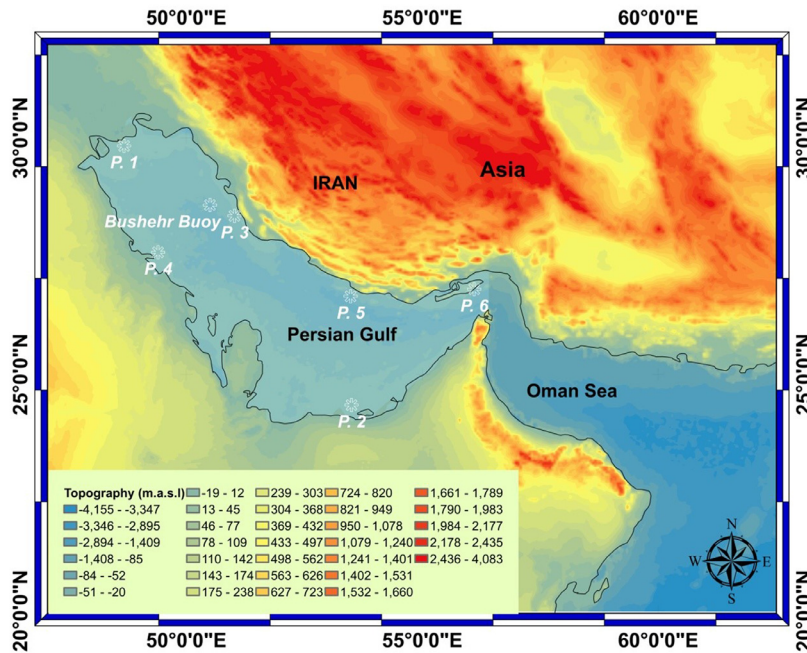


Figure 1 Location of selected points in the Persian Gulf.

equation including source and sink terms to predict the de-veloping wave field.

The SW governing wave model equation is the spectral action balance equation, which in Cartesian coordinates is:

$$\frac{\partial}{\partial t} N + \frac{\partial}{\partial x} C_{g,x} N + \frac{\partial}{\partial y} C_{g,y} N + \frac{\partial}{\partial \sigma} C_{g,\sigma} N + \frac{\partial}{\partial \theta} C_{g,\theta} N = \frac{S}{\sigma}, \quad (1)$$

where  $\sigma$  is the relative frequency,  $\theta$  is wave direction,  $N$  is wave action density, which is equal to the energy density divided by the relative frequency ( $N(\sigma, \theta) = E(\sigma, \theta) / \sigma$ ), and  $C_g$  is the propagation velocity of wave action in  $(x, y, \sigma, \theta)$  space. The last term on the left side of Eq. (1) represents the effects of refraction and shoaling. The source term on the right side is defined as:

$$S = S_{in} + S_{nl} + S_{dis} + S_{ot} + S_{surf}, \quad (2)$$

where  $S_{in}$  represents energy transfer from the wind to the waves,  $S_{nl}$  is the energy transferred from one frequency to other frequencies by nonlinear wave-wave interactions,  $S_{dis}$  is wave dissipation due to the effects of white-capping,  $S_{ot}$  is the wave dissipation due to bottom friction, and  $S_{surf}$  represents wave dissipation resulting from the wave breaking in a shallow area.

### 3.2. Model implementation

Bathymetry must be specified in order to use the SW model to simulate waves. This is achieved by implementing grid- ded bathymetric data at 30 arc-second intervals in the north/south latitudinal direction and also the east/west longitudinal direction, as provided by the British Oceanographic Data Center (BODC), as extracted from gebco.net. The bathymetric chart and unstructured mesh of the study area, including 17000 meshes and 8670 nodes, are presented in Figure 2 (A and B, respectively).

Table 1 Specifications for Boushehr buoy in the Persian Gulf.

Station Name	Latitude (°N)	Longitude (°E)	Water depth (m)
Boushehr	28.58	50.5	28

One of the important inputs for this model is the wind field data. For this purpose, data from the European Center for Medium-Range Weather Forecasts (ECMWF) was used in this study. The ECMWF ERA-interim wind field data was extracted from <http://apps.ecmwf.int> with  $0.125 \times 0.125$  degrees spatial resolution in the study zone and 6-hourly time interval.

A sensitivity analysis of dissipation parameters due to white capping, bottom friction, and depth induced wave breaking was carried out, which suggests that the white capping factor is effectively the dominating factor.

### 3.3. Spectral wave model performance

In order to evaluate the model performance, the model is implemented using available data for particular case studies. After analyzing the sensitivity of its' parameters to observed field data (calibration), the model is implemented for additional conditions and the results are compared with more field data to estimate model accuracy (validation). In the present study, the model is implemented for two 6-month periods while varying the effective parameters. Table 1 presents the specifications of the Boushehr buoy in the study area.

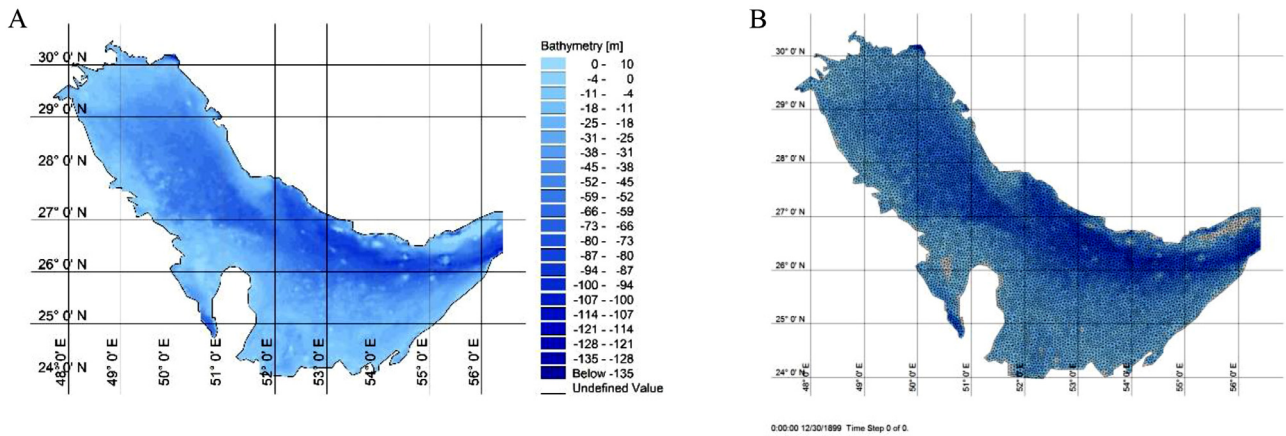


Figure 2 A) Bathymetry data, and B) triangular meshes including 17000 meshes and 8670 nodes in the study area.

Table 2 Model performance indices for the Boushehr buoy.

Parameter	Normal Range	Ideal Range	Calibration	Validation
Bias (m)	0.2–0.5	<0.3	0.22	0.20
CC	0.75–0.90	>0.8	0.79	0.82
RMSE(m)	0.1–0.7	<0.5	0.40	0.35
SI	0.15–0.35	<0.3	0.23	0.16

Statistical parameters between observed and modeled data are calculated:

$$\text{Bias} = \bar{S} - \bar{O}, \quad (3)$$

$$\text{Root mean squared errors} \quad \text{RMSE} = \sqrt{\frac{1}{N} \sum (S_i - O_i)^2}, \quad (4)$$

$$\text{Correlation coefficient} \quad \text{CC} = \frac{\sum (S_i - \bar{S})(O_i - \bar{O})}{\sqrt{\sum (S_i - \bar{S})^2 \sum (O_i - \bar{O})^2}}, \quad (5)$$

$$\text{Dispersion coefficient} \quad \text{SI} = \frac{\sqrt{\frac{1}{n} \sum ((S_i - \bar{S}) - (O_i - \bar{O}))^2}}{\bar{O}}, \quad (6)$$

where  $O_i$  is the observed value at the  $i^{\text{th}}$  time step,  $S_i$  is a forecast value at the same time,  $N$  is the number of time steps and  $\bar{O}$  and  $\bar{S}$  is the mean value of the observed data. Table 2 presents results for the model performance, with columns 2 and 3 giving the normal and ideal ranges for each performance index. These results suggest that the SW model is sufficiently accurate to use for wave climate estimates in this study. Associated values for modeled and observed significant wave heights ( $H_s$ ) are presented in Figure 3 and 4 as a calibration and validation periods.

For calibration and validation, two 6-month periods are selected from March 7, 2015 to September 7, 2015 and from September 8, 2015 to March 7, 2016, respectively. These periods are chosen because they contain the best performance times of the buoy with minimal data gaps.

### 3.4. Evaluation of wave energy

The wave estimates obtained from the SW model are used to estimate wave power potential in the study area. Several methods are presented by Ertekin and Yingfan (1994) to estimate wave power using  $H_s$  and wave period,  $T$ . The mean wave energy density per unit horizontal area ( $J/m^2$ ) is calculated as:

$$E = \frac{1}{16} \rho g H_s^2 \quad (7)$$

in which  $\rho$  is the seawater density ( $kg/m^3$ ),  $g$  is the gravity ( $m/s^2$ ) and  $H_s$  is the significant wave height (m). The wave power is expressed as:

$$P = ECn, \quad (8)$$

where  $C$  is the wave speed (m/s) and  $n$  is the ratio of the wave group speed and wave speed.  $C$  is equal to the wavelength divided by the wave period ( $T$ ) and is equal to  $\frac{gT}{2\pi}$ . The approximate value of  $n$  is 0.5 in deep water. Therefore, the wave power is calculated as:

$$P = \frac{1}{16} \rho g H_s^2 \times \frac{gT}{2\pi} \times 0.5 \approx 0.49 H_s^2 T. \quad (9)$$

### 3.5. Impact of climate change

In their Fifth Assessment Report (AR5), the Intergovernmental Panel on Climate Change (IPCC) has adopted several Representative Concentration Pathways (RCP) scenarios as possible greenhouse gas concentration pathways that might dominate the future climate. Four pathways have been labeled as RCP2.6, RCP4.5, RCP6, and RCP8.5, which indicate the possible radiative forcing values by the end-of-century, 2100 (Allen et al., 2014).

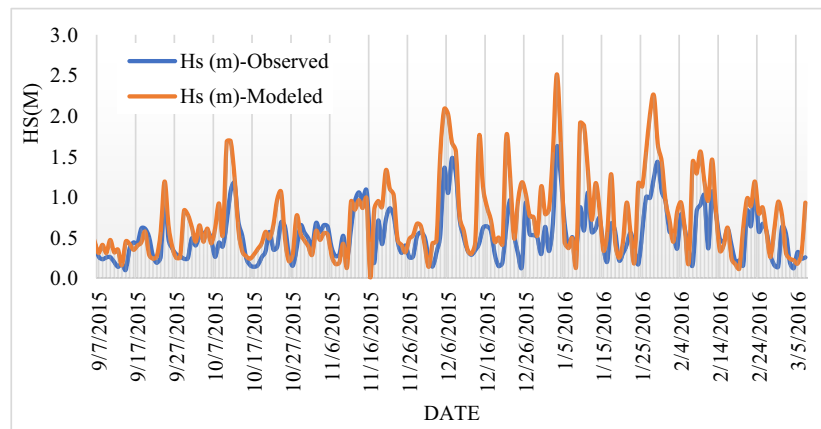


**Figure 3** Comparison of modeled and buoy-observed significant wave heights ( $H_s$ ) time series during the calibration period (8 March 2015 to 7 September 2015).

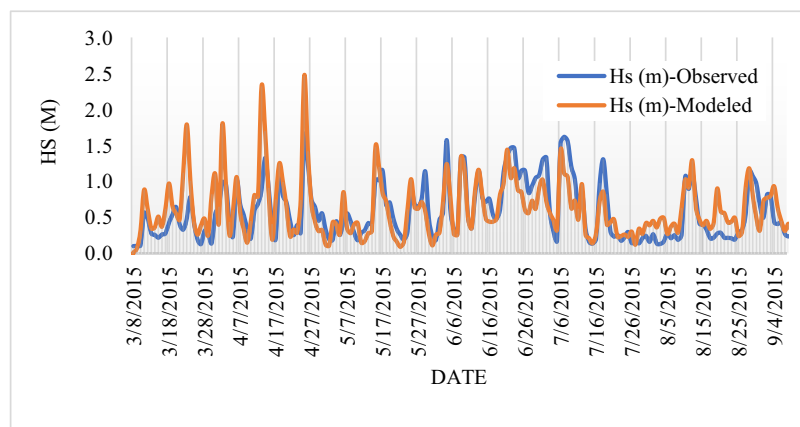


**Figure 4** As in Figure 3, comparison of modeled and buoy-observed  $H_s$  time series during the validation period (7 September 2015 to 7 March 2016).

RCP8.5 assumes a comparatively high greenhouse gas emissions pathway, associated with the implementation of no effective global climate change mitigation policies or measures, leading to a radiative forcing of  $8.5 \text{ W/m}^2$  by the end-of-century. At that time, carbon dioxide concentrations can be expected to reach 1000 ppm and continue increasing (Riahi et al., 2011). RCP4.5 scenario assumes a stabilizing of the radiative forcing at  $4.5 \text{ W/m}^2$  by 2100 (Thomson et al., 2011).

In this study, climate change data are extracted from HadGEM2-AO\_r1i1p1 (<http://apdrc.soest.hawaii.edu/data/data.php>). HadGEM2 is a coupled Earth System Model that was used by the Met Office Hadley Centre for the CMIP5 centennial simulations. On account of the large spatial and temporal scales of climate change data, downscaling should be implemented to translate the coarse-resolution HadGEM2 outputs to finer resolution climate information. In particular, the data resolution for HadGEM2 is not appropriate for modeling wave regimes in the Persian Gulf; for example, monthly time steps in climate change model outputs need to be downscaled to hourly data. In this research, a combination of dynamical and statistical approaches is applied, namely the so-called ‘change factor method’ which was used by Kamranzad et al. (2015) for the Persian Gulf

to evaluate wind/wave power, and by Breslow and Sailor (2002) in USA applications for wind power estimates.

The approach of hybrid dynamical-statistical downscaling can be considered as a challenge to use the potential of dynamical downscaling to prepare fine-scale climate changes along with the advantages of statistical downscaling. In this study, we used a dynamical-statistical downscaling technique used by Kamranzad et al. (2015).

In order to assess the dependability of outputs of the climate models, observed data and climate model data are compared over the entire study area. Thus, control periods are specified and selected locations are tested. Underestimates in wind data for climate change scenarios can be identified by comparisons between ECMWF and HadGEM2 data. Biases in climate change wind data are corrected by application of modification coefficients introduced by Kamranzad et al. (2015) for CGCM3.1 using a hybrid method, defined in terms of the monthly averages of absolute wind components, estimated as:

$$\beta_u = \frac{|U|_{\text{ECMWF(monthly average)}}}{|U|_{\text{HadGEM2(monthly average)}}}, \quad (10)$$

$$\beta_v = \frac{|V|_{\text{ECMWF(monthly average)}}}{|V|_{\text{HadGEM2(monthly average)}}}, \quad (11)$$

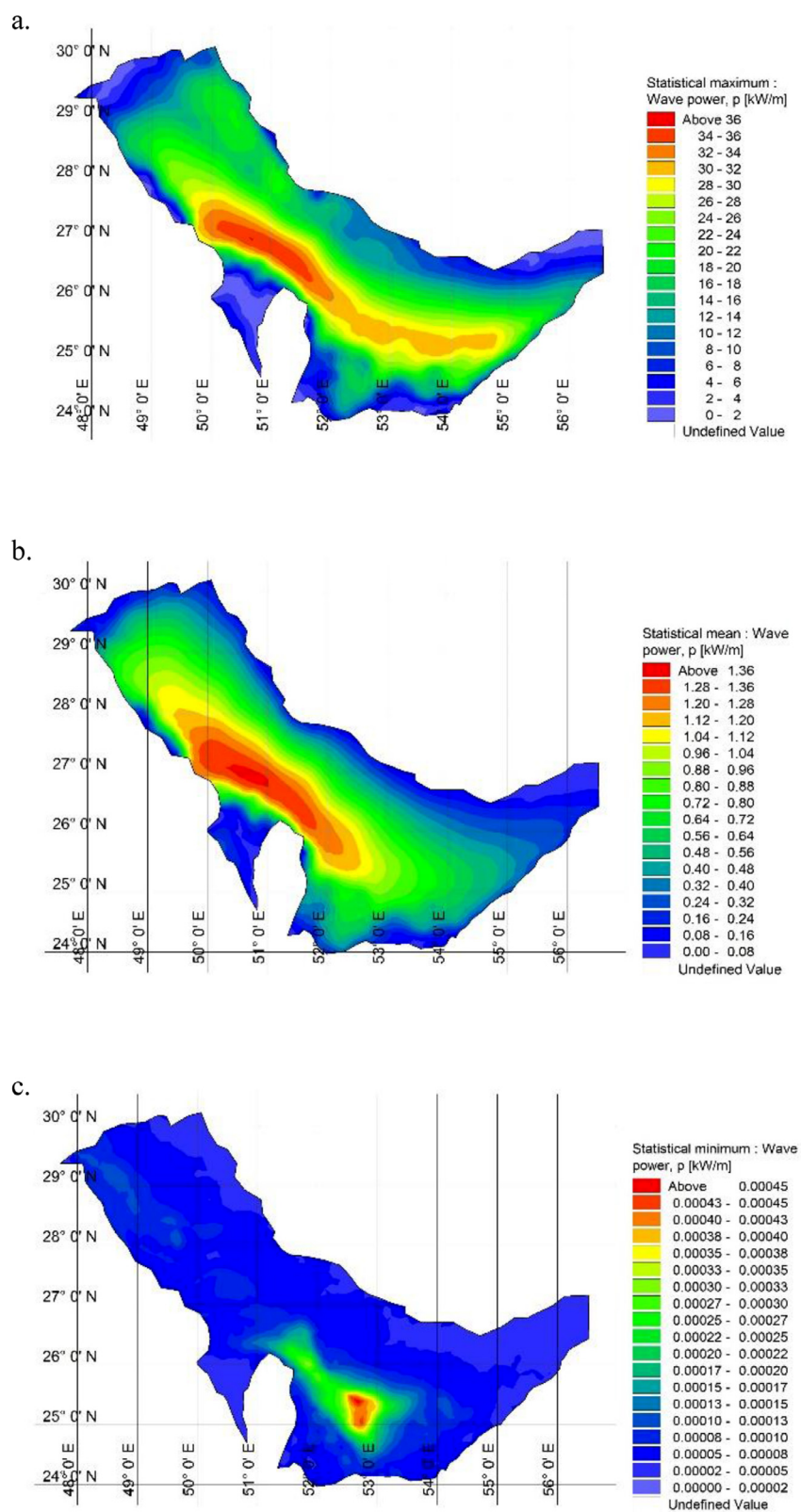


Figure 5 (a) Maximum, (b) mean, and (c) minimum wave energy for 30 years (1988–2017).

where  $\beta_u$  and  $\beta_v$  represent the modification factors for u and v components of the wind speed, respectively.

Thus, the ratios of directional wind speed data between ECMWF and HadGEM2, for scenarios RCP4.5 and RCP8.5, can be shown to vary between 1.15 to 2.15, and 1.25 to 2.30, respectively. Once climate change wind speed data were downscaled and corrected, the spectral wave model was run for 30-year periods of future scenarios (2070–2099).

### 3.6. Wave Energy Development Index

Extreme Value Analysis (EVA) and a corresponding Wave Energy Development Index (WEDI) can be used to assess the level of severity at a given spatial location. WEDI can estimate the potential hazards that may occur in terms of extreme events at Wave Energy Converters (WECs) and offshore structures:

$$WEDI = \frac{P_{wave}}{J_{wave}}, \tag{12}$$

which is the ratio of annual average wave power ( $P_{wave}$ ) to the maximum storm wave power ( $J_{wave}$ ). Wave Energy Converters are usually placed at specific locations based on estimates for mean power potential. An additional consideration is the maximum power potential, as well as estimates for the severity of extreme events, penalizing locations with high WEDI index values, as considered by Hagerman (2001).

## 4. Results and discussion

The time series of  $H_s$  and  $T_p$  are obtained from the SW model and wave energy is calculated for a period of 30 years (1988–2017) in the present climate, and a 30 years (2070–2099) in the future. Figure 5A–C gives the maximum, average and minimum values for wave energy as simulated for the current period.

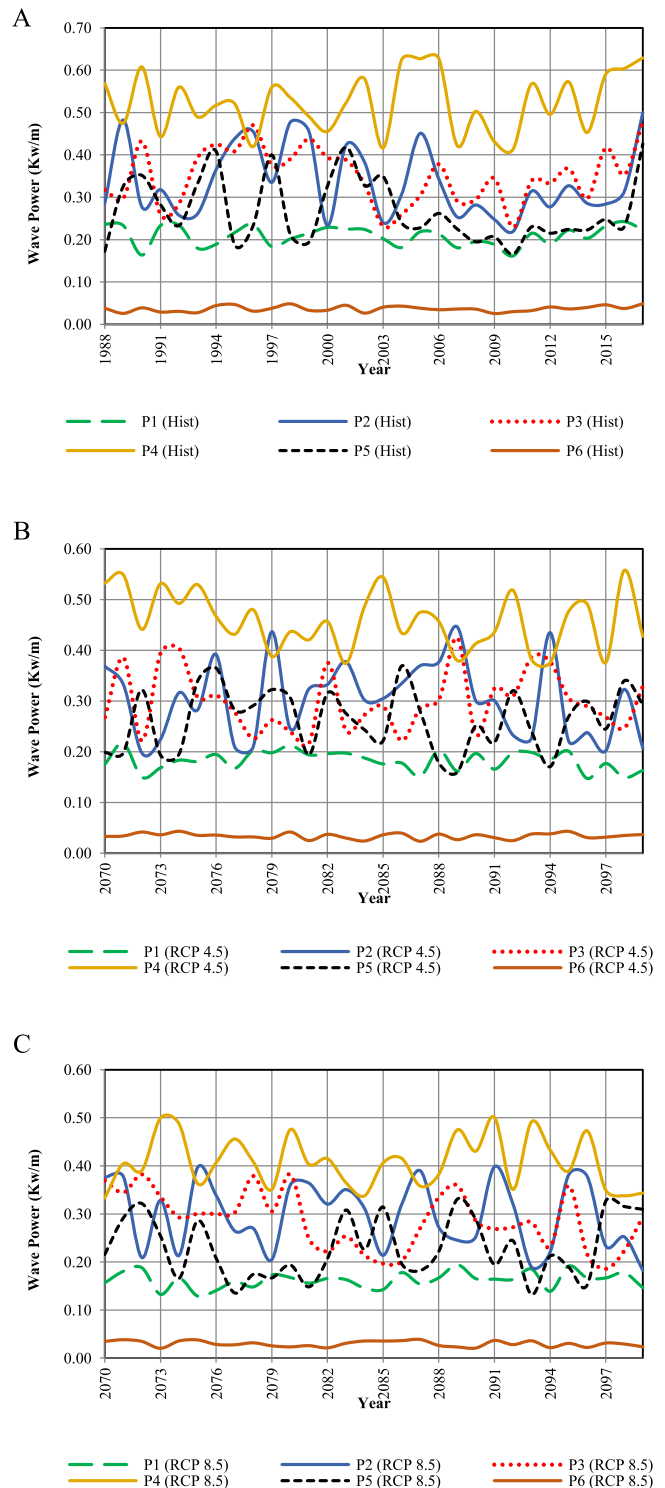
In Figure 6, mean yearly wave power changes for historical and future climate time-periods are shown. Calculations of the trends demonstrate that there is an ascending trend for the historical period, while both climate change scenarios have descending trends and the trend for RCP4.5 is milder.

### 4.1. Seasonal variations of wave energy

As shown in Figure 5, there are variations in wave energy in the western, northern, eastern and southern parts of the Persian Gulf. To assess potential wave energy in this study area, six points are selected, with regard to spatial distribution, depth and distance to the coastline, labeled 1 to 6 as shown in Figure 1. The characteristics of these locations are given in Table 3.

As shown by Figure 7, the average wave energy level in the present climate increases from the northern part of the Gulf to the southern part. The maximum energy is estimated at point 4, located in the southern Gulf, estimated at approximately 0.33 kW/m. The lowest energy is estimated in the eastern Gulf within the Strait of Hormuz, at approximately 0.08 kW/m.

With respect to RCP4.5 and RCP8.5 climate change scenarios, estimated values for energy follow similar patterns

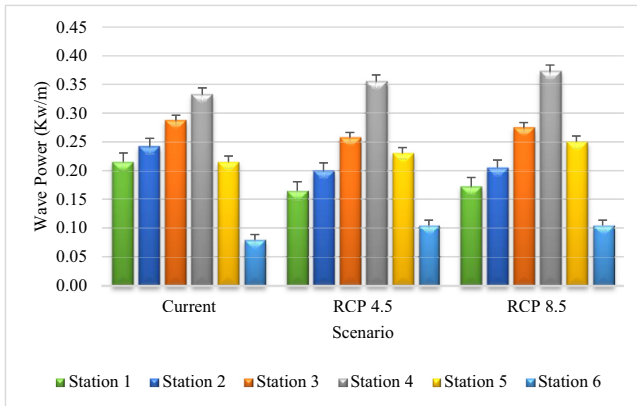
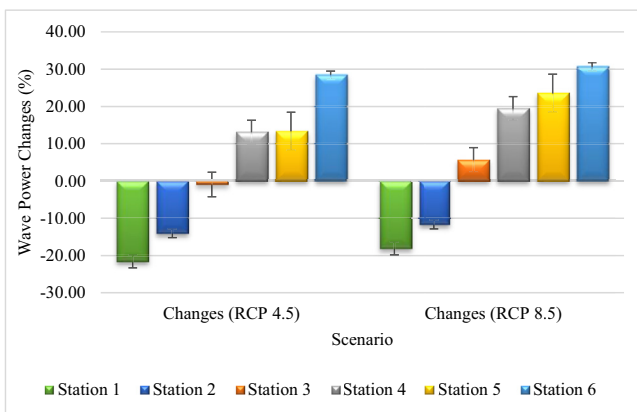


**Figure 6** Mean yearly wave energy for 30-year periods: (A) historical period, 1988–2017, (B) climate change scenario RCP4.5, and (C) climate change scenario RCP8.5, 2070–2099.

as for the present climate, implying that although the overall wave energy pattern will not change, in fact, there are significant changes in the amount of generated wave power. Competing effects occur. The extractable energy will increase by about 13–30% at locations 4, 5 and 6, in both RCP4.5 and RCP8.5 climate change scenarios, as shown

**Table 3** Characteristics and location of six selected locations.

Point ID	Latitude ( $^{\circ}$ N)	Longitude ( $^{\circ}$ E)	Depth (m)	Position in the Persian Gulf	Maximum Distance from coastline (km)	$J_{\text{mean}}$ (kW/m)
1	29.83	48.68	27	North-West	2	0.81
2	24.35	53.50	19	South	2	1.80
3	28.35	51.02	24	North	2	2.00
4	27.58	49.40	19	South	2	2.93
5	26.65	53.48	76	North	2	0.92
6	26.80	56.10	71	North-East	2	0.10

**Figure 7** Annual average wave energy at selected stations during 30 years (1988–2017) for RCP8.5 and RCP4.5 climate change scenarios for 30 years (2070–2099).**Figure 8** Annual average wave energy changes at selected stations during 30 years (1988–2017) relative to RCP8.5 and RCP4.5 climate change scenarios for 30 years (2070–2099).

in Figure 8. By comparison, at location 3, there will be about 1% reduction in energy in the RCP4.5 scenario, and about 6% more energy, in the RCP8.5 scenario. At stations 1 and 2, there is about 11–21% reduction in energy in both RCP4.5 and RCP8.5 climate change scenarios. Moreover, results have shown that the average wave energy production in the study area is about 0.23 kW/m in the present climate, which compares to 0.22 kW/m and 0.23 kW/m according to the RCP4.5 and RCP8.5 climate change scenarios, respectively. Thus, it is apparent that the negative and positive

components in the future climate scenarios may largely cancel each other out.

For the present climate conditions, the directional variations of wave energy are given for the 6 selected locations in Figure 9. Thus it is shown that the dominant wave directions at locations 1, 2, 3, 4, and 5 are from the north and northeast. Also, at location 6 the prevailing energy comes from the northwest, indicating that the Oman Sea has a direct effect on this locality.

#### 4.2. Seasonal wave energy

The average seasonal wave energy is also investigated in this study. As shown in Figure 10, the average wave energy values in winter, spring, autumn and summer are 0.33, 0.24, 0.19, and 0.16 kW/m, respectively. Thus, winter and summer have the highest and lowest wave energy values, respectively. In the RCP4.5 scenario, the maximum amount of energy is expected to be produced in winter, whereas the minimum amount occurs in autumn. In the RCP 8.5 scenario, the wave energy patterns are expected to have the highest variation i.e. the average wave energy in spring, winter, autumn and summer are 0.26, 0.24, 0.22 and 21.0 kW/m, respectively. As Figure 11 shows, the wave energy has a decreasing average in winter, whereas this average value is ascending in the other seasons. The maximum ascending average seasonal wave energy occurs in summer at 26.83 and 28.01 kW/m for the RCP4.5 and RCP8.5 climate change scenarios, respectively.

Therefore, it can be suggested that the mean values in projected changes are more severe in the RCP8.5 scenario than those in the RCP4.5 scenario.

We have also compared wave energies in each season using the 30 years (1988–2017) model results, at selected locations. At location 1 on the western side of the Persian Gulf, the amount of wave energy varies from 0.25 kW/m in winter to 0.18 kW/m in the summer. At location 2 in the southern part of the Persian Gulf, the amount of wave energy varies from 0.33 kW/m to 0.17 kW/m in winter and summer, respectively. Also, in the northwestern Gulf at location 3, the amount of wave energy changes from 0.45 kW/m to 0.20 kW/m in winter and summer, respectively. At location 4 in the southwestern part of the Gulf, the maximum amount of wave energy is observed, changing from 0.48 kW/m in the winter to 0.21 kW/m in the summer. In the northern part of the Gulf at location 5, the amount of wave energy changes from 0.31 to 0.16 kW/m in winter and summer, respectively. Finally, on the eastern side of the Gulf

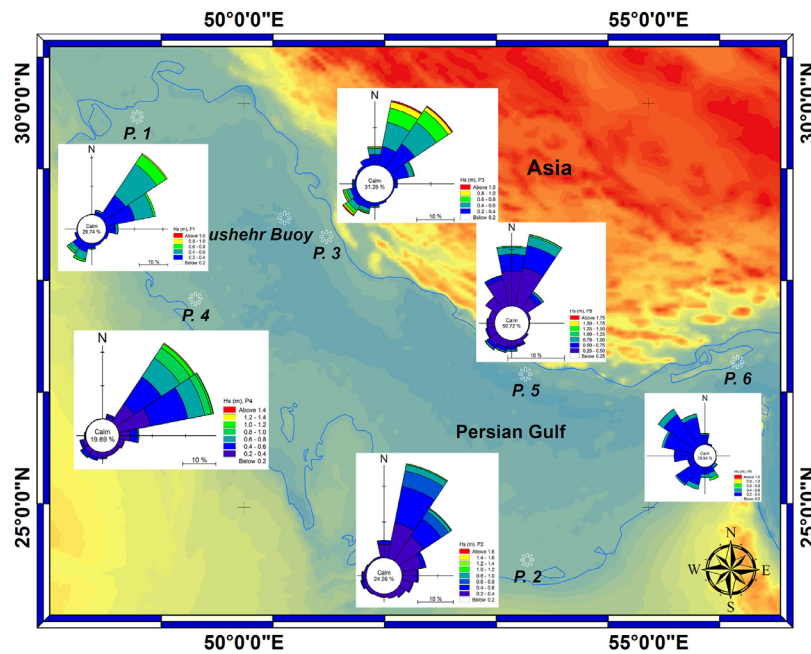


Figure 9 Directional distributions for wave energy at selected locations for the present climate.

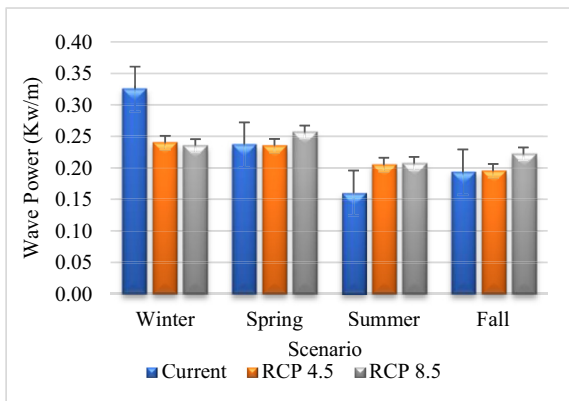


Figure 10 Seasonal mean wave energy at selected locations during 30 years (1988–2017) for the present climate, and for RCP8.5 and RCP4.5 climate change scenarios.

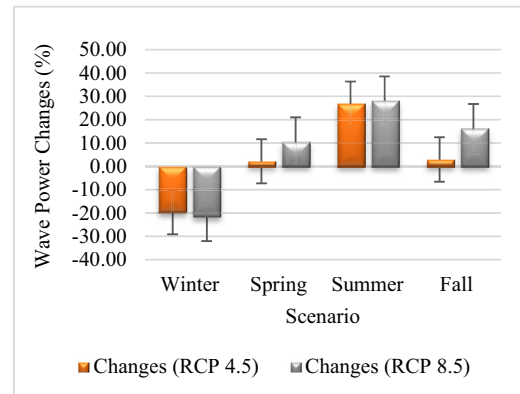


Figure 11 Seasonal mean wave energy changes (%) at selected locations for RCP8.5 and RCP4.5 climate change scenarios relative to the present climate, represented by 30 years (1988–2017).

in the Strait of Hormuz, near the Oman Sea, the minimum amount of wave energy is estimated for location 6, changing from 0.13 in winter to 0.04 kW/m in summer. The reason for this considerable reduction in the wave energy is due to the relatively short fetch in this area. Meanwhile, according to Figure 12(A–D) the amount of wave energy in the spring is higher than in autumn and summer.

According to both RCP4.5 and RCP8.5 climate change scenarios, the prevailing wave energy patterns in the locations that we considered are consistent with the present climate. However, according to Figure 13, these changes do not follow the same averages at all locations. For example at locations 1 and 2, during the winter, spring and autumn, the mean value in wave energy variations shows a downward mean amount and has an increasing average only in summer. At location 3, the mean value in wave energy variations in the winter is descending, for both scenarios of

climate change. This downward mean value is also apparent in the fall season, according to the RCP4.5 scenario. However, there is an increasing mean value in other seasons. At locations 4 and 5, in winter, both RCP4.5 and RCP8.5 climate change scenarios suggest downward mean values, whereas in the other three seasons and for both climate change scenarios, there is an upward mean value. At location 6, the wave energy variation in all seasons and in both the RCP4.5 and RCP8.5 climate change scenarios is always increasing.

### 4.3. The bivariate probability distribution of occurrence and wave energy

In order to make accurate decisions regarding the appropriate locations for wave energy converter devices (WECs), it is necessary to consider probabilistic distributions for  $H_s$  and

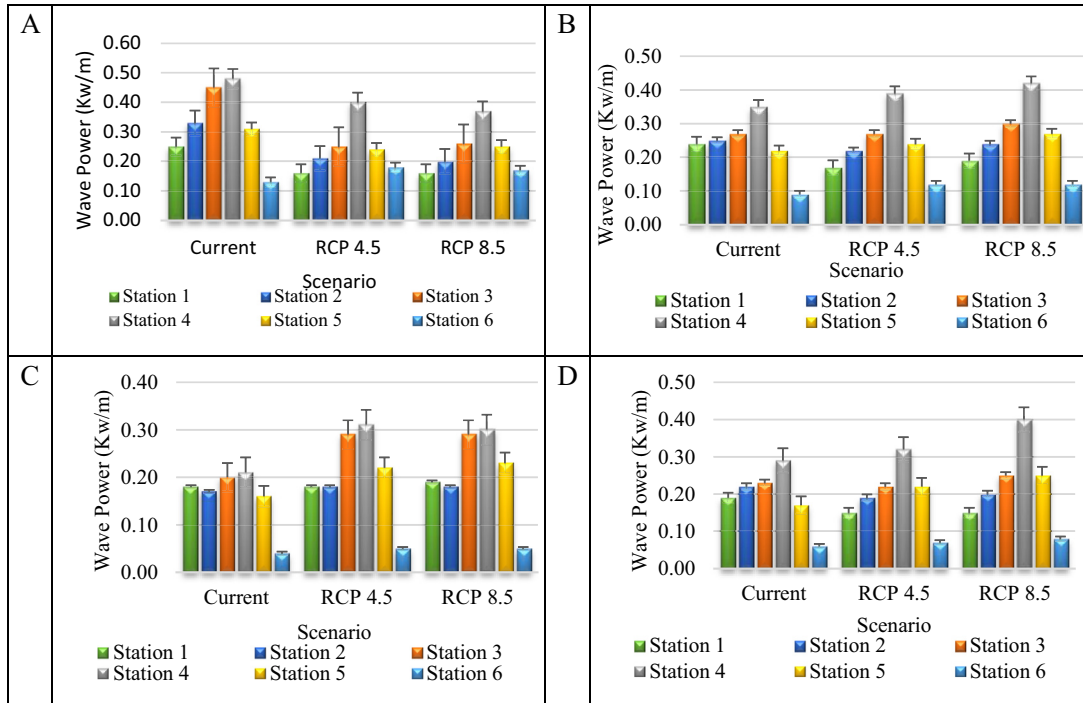


Figure 12 Mean values in wave energy changes at selected locations during winter for present climate conditions, as well as RCP8.5, and RCP4.5 climate change scenarios for 30 years (2070–2099); A) Winter, B) Spring, C) Summer, D) Fall.

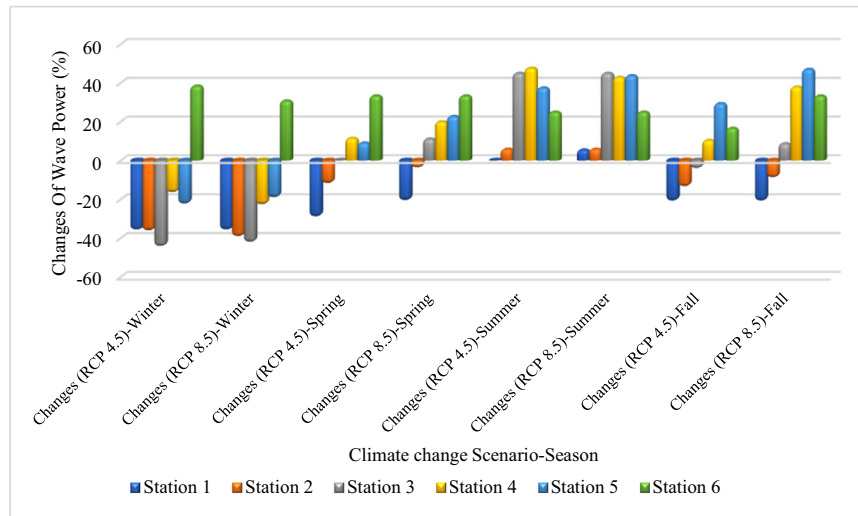


Figure 13 Changes of wave energy (%) for each season at selected station locations according to RCP8.5 and RCP4.5 climate change scenarios for 30 years (2070–2099).

$T_e$ , which are used in most energy matrices in WEC calculations. The frequency of occurrence of each value for  $H_s$  and  $T_e$  in bivariate form is an expression of the prevailing wave characteristics at the associated point location. Figure 14 A–F describes the sea state conditions at the selected point locations, and the respective matrices are plotted for each of these locations.

As shown in Figure 14A, at location 1, the results are that for 41.5 and 38.1% of occasions, the wave periods are 2.5 s and significant wave heights are 0.2 and 0.4 m; thus the wave energy will be in the range of 0.12–0.33 kW/m.

The occurrence of other wave periods and significant wave heights have occurrences that are less than 10%.

At point location 2 shown in Figure 14B, the wave periods are in the range of 1.5 to 3.5 s and significant wave heights, in the range of 0.2 to 0.6 m, with a higher probability of occurrence. The wave energy variation in these conditions is in the range of 0.1 to 0.96 kW/m.

At point location 3 shown in Figure 14C, the dominant results are wave periods of 2.5 s and significant wave heights in the range of 0.2–0.4 m. The amount of wave energy varies in the range of 0.11–0.31 kW/m.

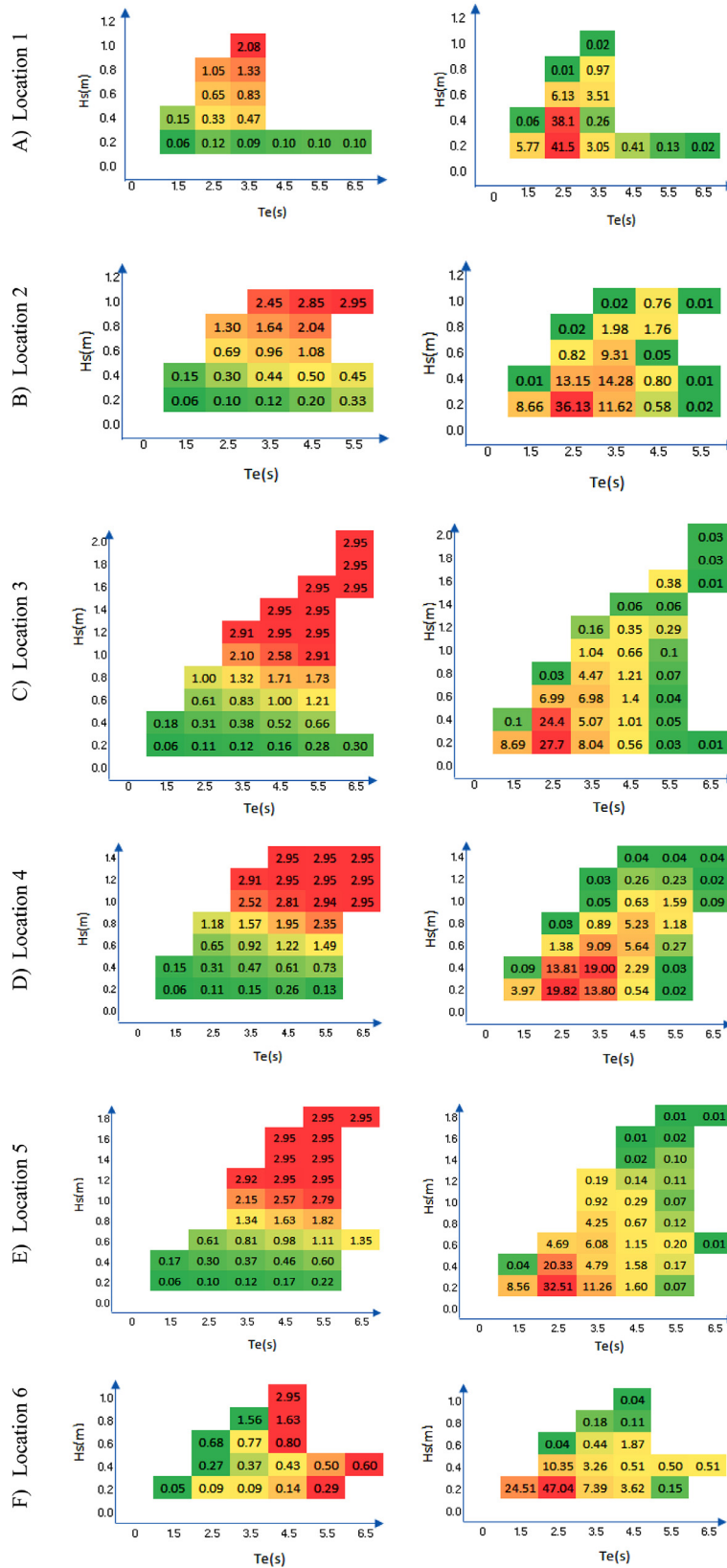
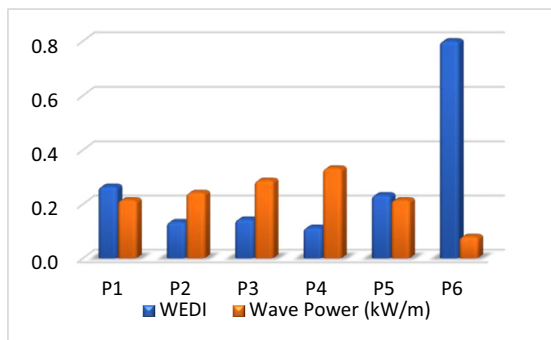


Figure 14 A, B, C, D, E and F: Bivariate distributions for the sea states  $H_s$  and  $T_e$ . The right panel represents the total of the occurrences and the left panel shows the average sea state wave energy for 30 years.



**Figure 15** The comparison of WEDI and wave power at selected point locations.

At point location 4 shown in Figure 14D, the wave periods maximum occurrence is the range of 2.5–3.5 s and the significant wave heights in the range of 0.2–0.4 m. The change in wave energy in these conditions varies from 0.11 to 0.47 kW/m.

At the point location 5, based on Figure 14E, the maximum occurrence for wave periods is 2.5 s and significant wave heights are in the range of 0.2–0.4 m. The change in wave energy values in these conditions is from 0.1 to 0.3 kW/m.

Finally, at point location 6, as shown in Figure 14F, the maximum occurrence for wave periods is 2.5 s and significant wave heights are in the range 0.2–0.4 m. The change in wave energy in these conditions is between 0.09 to 0.27 kW/m.

#### Wave Energy Development Index

A significant parameter at the beginning of a wave energy development project is the wave energy development index (WEDI) value for a specific site. This index is obtained by dividing the average annual wave energy changes by the storm wave energy changes. It is dimensionless. The WEDI index distribution for the simulated 30 years is shown in Figure 15. This figure compares the WEDI index for selected locations. The highest WEDI index is suggested for location 6, and the lowest is for location 4. Our findings suggest that location 4 in the southern part of the Gulf is the most appropriate place to install wave energy converters.

## 5. Conclusions

The aim of this study is to investigate the characteristics of ocean wave parameters and wave energy potential, and the possible influence of climate change in the Persian Gulf region. Due to the high potential for energy extraction from wind-waves and advances in wave energy converter devices, waves are nowadays considered as an appropriate source for renewable energy. This is a new perspective compared to previous times. Iran has a huge potential source for this energy with approximately 2700 km of coastline along the northern and southern borders. The harnessing of this energy, in combination with other types of renewable energies such as solar energy, in which southern Iran abounds, can potentially turn the country from a dominant dependence on fossil fuels. Moreover, although some parts of the world ocean, such as the North Atlantic, and North and South

Pacific, have a quite high wave energy values, more than 50 kW/m (Alcorn, 2013), in fact, many coastal areas like Italy (Vannucchi, and Cappietti, 2016), the Black Sea (Akpınar and Kömürçü, 2013), and North Coast of Australia (Hemer et al., 2017, 2018), have wave energy values that are less than 2 kW/m which is similar to our results. In the Persian Gulf similar study was conducted using present and future climates (A2, B1, and A1B scenarios), and the output maps showed that wave energy in coastal areas is less than 0.5 kW/m (Kamranzad, et al. 2015). The average wave power (kW/m) distribution in the Persian Gulf for a 25-year modeling period, 1984–2008, studied by Kamranzad et al. (2013), shows that done in the Persian Gulf shows the highest and lowest values of wave power were taken place in the central part and eastern part of the study area, respectively.

Computer model simulations for waves and climate change scenarios were performed. We compared present climate conditions in the Persian Gulf to future climate estimates.

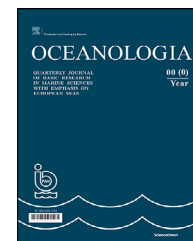
We also estimated that most of the significant wave heights are less than one-meter high with wave periods that are less than 4.5 seconds. The results show that for location 1, 80%, of time  $T_e$ ,  $H_s$ , and  $P_w$  vary between 2–3 s, 0.1–0.5 m, and 0.12–0.33 kW/m, respectively. For location 2, more than 50% of wave parameters including,  $T_e$ ,  $H_s$ , and  $P_w$ , vary between 2–3 s, 0.1–0.5 m, 0.1–0.3 kW/m, respectively. In location 3, some 50 percent of wave parameters,  $T_e$ ,  $H_s$ ,  $P_w$ , vary 2–3 s, 0.1–0.5 m, and 0.11–0.31 kW/m, respectively. For location 4, more than 70% of  $T_e$ ,  $H_s$ , and  $P_w$  change between 2–4 s, 0.1–0.5 m, 0.11–0.47 kW/m, respectively. For location 5,  $T_e$ ,  $H_s$ , and  $P_w$ , in more than 50 percent of the time, vary between 2–3, 0.1–0.5, and 0.1–0.3 kW/m, respectively. In location 6, for more than 60% of the time,  $T_e$ ,  $H_s$ , and  $P_w$  change between 2–3 s, 0.1–0.5 m, and 0.09–0.27 kW/m, respectively. For locations 1, 2, 3, 4, 5, and 6 the value of WEDI are 0.27, 0.13, 0.14, 0.11, 0.23, and 0.80, as well as mean wave power (kW/m) for locations 1, 2, 3, 4, 5, and 6 are 0.22, 0.24, 0.29, 0.33, 0.22, and 0.08 kW/m, respectively.

According to these results, it appears that the potential energy level for waves in the southern part of the Persian Gulf is higher than in other areas. Based on our assessments, the locality around location 4 has emerged as having the most favorable conditions for wave energy extraction. There are no significant differences among locations 2, 3, and 5.

## References

- Aboobacker, V.M., Shanass, P.R., Alsaafani, M.A., Albarakati, A.M., 2017. Wave energy resource assessment for Red Sea. *Renew. Eng. 114*, 46–58.
- Akpınar, A., Kömürçü, M.İ., 2013. Assessment of wave energy resource of the Black Sea based on 15-year numerical hindcast data. *Appl. Eng. 101*, 502–512.
- Alcorn, R., 2013. Wave Energy. *Future Energy: Improved, Sustainable and Clean Options for our Planet*, 357–382.
- Alizadeh, M.J., Alinejad-Tabrizi, T., Kavianpour, M.R., Shamshirband, S., 2020. Projection of spatiotemporal variability of wave power in the Persian Gulf by the end of 21st century: GCM and CORDEX ensemble. *J. Cleaner Prod. 256*, 120400. <https://doi.org/10.1016/j.jclepro.2020.120400>

- Allen, M.R., Barros, V.R., Broome, J., Cramer, W., Christ, R., Church, J.A., Clarke, L., Dahe, Q., Dasgupta, P., Dubash, N.K., Edenhofer, O., 2014. IPCC fifth assessment synthesis report-climate change synthesis report. In: WMO, UNEP, IPCC, Geneva, Switzerland, 151 pp.
- Alonso, R., Solari, S., Teixeira, L., 2015. Wave Energy resource assessment in Uruguay. *Energy* 93, 683–696.
- Amirinia, G., Mafi, S., Mazaheri, S., 2017. Offshore wind resource assessment of Persian Gulf using uncertainty analysis and GIS. *Renew. Energ.* 113, 915–929.
- Appendini, C.M., Urbano-Latorre, C.P., Figueroa, B., Dagua-Paz, C.J., Torres-Freyermuth, A., Salles, P., 2015. Wave Energy potential assessment in the Caribbean Low Level Jet using wave hindcast information. *Appl. Energy* 137, 375–384.
- Armanfar, M., Goharnejad, H., Niri, M.Z., Perrie, W., 2019. Assessment of coastal vulnerability in Chabahar Bay due to climate change scenarios. *Oceanologia* 61 (4), 412–426. <https://doi.org/10.1016/j.oceano.2019.03.001>
- Besio, G., Mentaschi, L., Mazzino, A., 2016. Wave Energy resource assessment in the Mediterranean Sea on the basis of a 35-year hindcast. *Energy* 94, 50–63.
- Breslow, P.B., Sailor, D.J., 2002. Vulnerability of wind power resources to climate change in the continental United States. *Renew. Energ.* 27 (4), 585–598.
- Casas-Prat, M., Wang, X.L., Swart, N., 2018. CMIP5-based global wave climate projections including the entire Arctic Ocean. *Ocean Model* 123, 66–85.
- DHI, M., 2005. spectral wave module—scientific documentation. Danish Hydraulic Institute.
- Ertekin, R.C., Yingfan, X., 1994. Preliminary assessment of the wave-energy resource using observed wave and wind data. *Energy* 19 (7), 729–738.
- Gallagher, S., Tiron, R., Whelan, E., Gleeson, E., Dias, F., McGrath, R., 2016. The nearshore wind and wave energy potential of Ireland: a high resolution assessment of availability and accessibility. *Renew. Energ.* 88, 494–516.
- Goharnejad, H., Shamsai, A., Hosseini, S.A., 2013. Vulnerability assessment of southern coastal areas of Iran to sea level rise: evaluation of climate change impact. *Oceanologia* 55 (3), 611–637. <https://doi.org/10.5697/oc.55-3.611>
- Hagerman, G., 2001. Southern New England Wave Energy Resource Potential. In: Proc. Building Energy Conf. 21 – 24 2001 March. Boston, USA.
- Hemer, M.A., Manasseh, R., McInnes, K.L., Penesis, I., Pitman, T., 2018. Perspectives on a way forward for ocean renewable energy in Australia. *Renew. Energ.* 127, 733–745.
- Hemer, M.A., Zieger, S., Durrant, T., O’Grady, J., Hoeke, R.K., McInnes, K.L., Rosebrock, U., 2017. A revised assessment of Australia’s national wave energy resource. *Renew. Energ.* 114, 85–107.
- Implementation Agreement on Ocean Energy Systems, 2007. Implementing agreement on ocean Energy systems (IEA-OES). Annual Rep. Internat. Energy Agency.
- Jadidolestam, N., Ozger, M., Agralioglu, N., 2016. Wave power potential assessment of Aegean Sea with an integrated 15-year data. *Renew. Energ.* 86, 104–159.
- Kamranzad, B., 2018. Persian Gulf zone classification based on the wind and wave climate variability. *Ocean Eng* 169, 604–635.
- Kamranzad, B., Chegini, V., 2014. Study of wave energy resources in Persian Gulf: seasonal and monthly distributions. In: 11th Int. Conf. ‘Coasts, Ports and Marine Structures’. Tehran, Iran.
- Kamranzad, B., Etemad-Shahidi, A., Chegini, V., 2013. Assessment of wave energy variation in the Persian Gulf. *Ocean Eng* 70, 72–80.
- Kamranzad, B., Etemad-Shahidi, A., Chegini, V., 2017. Developing an optimum hotspot identifier for wave energy extracting in the northern Persian Gulf. *Renew. Energ.* 14, 59–71.
- Kamranzad, B., Etemad-Shahidi, A., Chegini, V., Yeganeh-Bakhtiary, A., 2015. Climate change impact on wave energy in the Persian Gulf. *Ocean Dynam* 65 (6), 777–794.
- Kapelonis, Z.G., Gavriladis, N., N, P., Athanassoulis, G.A., 2015. Extreme value analysis of dynamical wave climate projections in the Mediterranean Sea. *Procedia Comput. Sci.* 66, 210–219.
- Korn, P., 2017. Formulation of an unstructured grid model for global ocean dynamics. *J. Comput. Phys.* 339, 525–552.
- Kumar, V.S., Anoop, T.R., 2015. Wave energy resource assessment for the Indian shelf seas. *Renew. Energ.* 76, 212–219.
- Langodan, S., Viswanadhapalli, Y., Dasari, H.P., Knio, O., Hoteit, I., 2016. A high-resolution assessment of wind and wave energy potentials in the Red Sea. *Appl. Energy* 181, 244–255.
- Liang, B., Fan, F., Yin, Z., Shi, H., Lee, D., 2016. Numerical modelling of the nearshore wave Energy resources of Shandong peninsula. *China. Renew. Energ.* 57, 330–338.
- Liao, Y.P., Kaihatu, J.M., 2016. Numerical investigation of wind waves in the Persian Gulf: bathymetry effects. *J. Atmos. Ocean. Technol.* 33 (1), 17–31.
- López, M., Veigas, M., Iglesias, G., 2015. On the wave Energy resource of Peru. *Energy. Convers Manage.* 90, 34–40.
- Morim, J., Cartwright, N., Etemad-Shahidi, A., Strauss, D., Hemmer, M., 2014. A review of wave Energy estimates for nearshore shelf waters off Australia. *Int. J. Marine Eng.* 7, 57–70.
- Neill, S.P., Hashemi, M.R., 2013. Wave power variability over the northwest European shelf seas. *Appl. Energy* 106, 31–46.
- Neill, S.P., Lewis, M.J., Hashemi, M.R., Slater, E., Lawrence, J., Spall, S.A., 2014. Inter-annual and inter-seasonal variability of the Orkney wave power resource. *Appl. Energy* 132, 339–348.
- Ponce de León, S., Orfila, A., Simarro, G., 2016. Wave energy in the Balearic Sea. Evolution from a 29 year spectral wave hindcast. *Renew. Energ.* 85 (C), 1192–1200. <https://doi.org/10.1016/j.renene.2015.07.076>
- Pous, S., Lazure, P., Carton, X., 2015. A model of the general circulation in the Persian Gulf and in the Strait of Hormuz: Intraseasonal to interannual variability. *Cont. Shelf Res.* 94, 55–70.
- Riahi, K., Rao, S., Krey, V., Cho, C., Chirkov, V., Fischer, G., Kindermann, G., Nakicenovic, N., Rafaj, P., 2011. RCP 8.5—A scenario of comparatively high greenhouse gas emissions. *Climat. Change* 109 (1–2), art no. 33. <https://doi.org/10.1007/s10584-011-0149-y>
- Rusu, E., Onea, F., 2013. Evaluation of the wind and wave energy along the Caspian Sea. *Energy* 50, 1–14.
- Shanas, P.R., Aboobacker, V.M., Albarakati, A.M., Zubier, K.M., 2017. Climate driven variability of wind-waves in the Red Sea. *Ocean Model* 119, 105–117.
- Thomson, A.M., Calvin, K.V., Smith, S.J., Kyle, G.P., Volke, A., Patel, P., Delgado-Arias, S., Bond-Lamberty, B., Wise, M.A., Clarke, L.E., Edmonds, J.A., 2011. RCP4. 5: a pathway for stabilization of radiative forcing by 2100. *Climat. Change* 109 (1–2), art. no 77. <https://doi.org/10.1007/s10584-011-0151-4>
- Vannucchi, V., Cappiotti, L., 2016. Wave energy assessment and performance estimation of state of the art wave energy converters in Italian hotspots. *Sustainability* 8 (12), 1300. <https://doi.org/10.3390/su8121300>
- Vieira, F., Cavalcante, G., Campos, E., 2020. Analysis of wave climate and trends in a semi-enclosed basin (Persian Gulf) using a validated SWAN model. *Ocean Eng* 196, 106821. <https://doi.org/10.1016/j.oceaneng.2019.106821>
- Wang, Z., Dong, S., Li, X., Guedes-Soares, C., 2016. Assessments of wave energy in the Bohai Sea, China. *Renew. Energ.* 90, 145–156.
- WCRP Global Sea Level Budget Group, 2018. Global sea-level budget 1993–present. *Earth Sys. Sci. Data* 10, 1551–1590. <http://dx.doi.org/10.5194/essd-10-1551-2018>
- Zhou, G., Huang, J., Yue, T., Luo, Q., Zhang, G., 2015a. Temporal-Spatial distribution of wave Energy: A case study of Beibu Gulf, China. *Renew. Energ.* 74, 344–356.
- Zhou, G., Huang, J., Zhang, G., 2015b. Evaluation of the wave Energy conditions along the coastal waters of Beibu Gulf, China. *Energy* 85, 449–457. <https://doi.org/10.1016/j.energy.2015.03.094>



## ORIGINAL RESEARCH ARTICLE

# Satellite estimates of the long-term trend in phytoplankton size classes in the coastal waters of north-western Bay of Bengal

Joereen Miranda<sup>a,\*</sup>, Aneesh Anandrao Lotliker<sup>b</sup>,  
Sanjiba Kumar Baliarsingh<sup>b</sup>, Amit Kumar Jena<sup>a</sup>, Alakes Samanta<sup>b</sup>,  
Kali Charan Sahu<sup>a</sup>, Tummala Srinivasa Kumar<sup>b</sup>

<sup>a</sup>Department of Marine Sciences, Berhampur University, Bhanjabihar-760007, India

<sup>b</sup>Indian National Centre for Ocean Information Services, Ministry of Earth Sciences, Govt. of India, Hyderabad-500090, India

Received 25 May 2020; accepted 11 September 2020

Available online 25 September 2020

## KEYWORDS

MODISA;  
Algorithm;  
Coastal;  
Monsoon;  
Phytoplankton Size  
Classes

**Abstract** The study presents long-term variability in satellite retrieved phytoplankton size classes (PSC) at two coastal sites, off Gopalpur and Visakhapatnam, in the north-western Bay of Bengal. The abundance-based models by Brewin et al. (2010) (B10) and Sahay et al. (2017) (S17), for retrieval of PSC (micro, nano, and picophytoplankton), from satellite data, were validated. Both the models performed well in the retrieval of nano and microphytoplankton. However, B10 performed poorly in retrieving picophytoplankton. The statistical analysis indicated better performance of the S17 model and hence was applied to Moderate Resolution Imaging Spectroradiometer onboard Aqua satellite (MODISA) data to understand the temporal (at monthly climatology) and spatial variability (from nearshore to offshore). The spatial distribution indicated nearshore dominance of micro and offshore dominance of picophytoplankton. In nearshore waters off Gopalpur, microphytoplankton dominated throughout the year except for months of south-west monsoon (June and July) where the dominance of picophytoplankton was observed. All PSC exhibited similar distribution at an annual scale with a primary peak during pre-monsoon (March and April) and a secondary peak during post-monsoon (September–November). However, microphytoplankton concentration during post-monsoon was higher off Gopalpur in comparison to Visakhapatnam. The higher microphytoplankton concentration

\* Corresponding author at: Department of Marine Sciences, Berhampur University, Bhanjabihar-760007, India.

E-mail address: [joereen@gmail.com](mailto:joereen@gmail.com) (J. Miranda).

Peer review under the responsibility of the Institute of Oceanology of the Polish Academy of Sciences.



Production and hosting by Elsevier

<https://doi.org/10.1016/j.oceano.2020.09.003>

0078-3234/© 2020 Institute of Oceanology of the Polish Academy of Sciences. Production and hosting by Elsevier B.V. This is an open access article under the CC BY-NC-ND license (<http://creativecommons.org/licenses/by-nc-nd/4.0/>).

during pre-monsoon was attributed to recurrent phytoplankton blooms. Whereas, post-monsoon increment could be attributed to enhanced phytoplankton growth by availing nutrients sourced from monsoonal precipitation induced terrigenous influx. The outcome of the present study recommends the use of the S17 model for satellite retrieval of PSC from the north-western Bay of Bengal.

© 2020 Institute of Oceanology of the Polish Academy of Sciences. Production and hosting by Elsevier B.V. This is an open access article under the CC BY-NC-ND license (<http://creativecommons.org/licenses/by-nc-nd/4.0/>).

## 1. Introduction

Phytoplankton are microscopic free-floating and/or drifting autotrophs present within the photic zone of the ocean and are major contributors to oceanic primary production (Uitz et al., 2010). Marine phytoplankton play a key character in the global carbon cycle and maintain the energy flow in the oceanic food web (Basu and Mackey, 2018). Apart from different taxonomic groups, phytoplankton, on the other hand, represent a range of size classes categorized as microphytoplankton ( $>20 \mu\text{m}$ ), nanophytoplankton ( $<20 \mu\text{m}$  and  $>2 \mu\text{m}$ ), and picophytoplankton ( $<2 \mu\text{m}$  and  $>0.2 \mu\text{m}$ ) (Ariñ et al., 2002). The phytoplankton size classes (PSC) dwell in specific physico-chemical environments attributed to their nutrient uptake efficiency and cellular metabolism. In general, PSC play important role in marine biogeochemistry. Microphytoplankton (MP) are the particular size class photosynthetic group responsible for the substantial quantum of carbon export to the deep ocean and play an important role in sustaining fisheries (Murty et al., 2017). The transitional size class member, nanophytoplankton (NP) are represented by small flagellates belonging to several phytoplankton groups attributable to a higher amount of carbon fixation in oscillating environmental conditions (Hannah and Boney, 1983; Ribeiro et al., 2016). On the other hand, picophytoplankton (PP) are mostly comprised of cyanobacteria and prochlorophytes that prevail in oligotrophic waters due to high surface to volume ratio. Therefore, in the lower abundance condition of MP in oligotrophic offshore waters, PP carries out carbon recycling (Campbell and Vaulot, 1993; Campbell et al., 1994). The size distribution of the phytoplankton community has a significant influence on water quality (Baliarsingh et al., 2016, 2018). In turn, the variability pattern of physico-chemical parameters of the ecosystem also regulates the PSC distribution (Jyothibabu et al., 2015; Madhu et al., 2010).

The PSC distribution is generally depicted in terms of chlorophyll-*a* (chl-*a*) (Sahay et al., 2017). It is important to mention here that chl-*a*, the principal pigment of phytoplankton is broadly used as an index of phytoplankton biomass (Huot et al., 2007). Chl-*a* exhibits a specific spectral signature that enables its remote estimation using ocean colour remote sensing (IOCCG, 2000; Neil et al., 2019; O'Reilly et al., 1998). In the past decade, ocean colour remote sensing has been widely used for retrieval of chl-*a* from remote sensors. With the advancement in technology and novel bio-optical algorithms, PSC can be also retrieved from satellite data (Brewin et al., 2012, 2014). The discrete sampling of PSC lacks in providing information over a larger spatial area. This limitation can be overcome with satellite

data having the capability to provide information at a synoptic scale with a high temporal resolution that can be used to study intra- and inter-annual variability of individual PSC (Sahay et al., 2017; Varunan and Shanmugam, 2015).

The north Indian Ocean comprises two essential components, the Arabian Sea and the Bay of Bengal (BoB). Although located at the same latitude, the processes controlling water quality largely differ in both the seas. The water quality variability in the BoB is largely controlled by the seasonally reversing monsoon currents, effluents discharge from perennial rivers and coastal industrial setups in addition to natural extreme events such as tropical cyclones. Several pockets of the north-western BoB experience recurrent algal blooms, eutrophication, and pollution. Studies on PSC distribution through *in situ*, as well as ocean colour sensors, are meagre in the coastal waters of the BoB.

The PSC forms an essential component of Phytoplankton Functional Types (PFT) in addition to taxonomy and pigment composition. The PFTs are of great interest to the biogeochemical community, especially in the coastal BoB, where the biological ecosystem is largely controlled by local and remote physical forcing (Lotliker et al., 2020; Miranda et al., 2020). The variability in PFTs can be directly linked to the phytoplankton efficiency in carbon sequestration and may be a function of climate change. On this backdrop, the present study aims to bridge the knowledge gap of PFT, in terms of PSC, with the objectives, (i) to evaluate two “abundance” based models for satellite estimation of PSC, and (ii) to understand the long-term trend of PSC at two ecologically important coastal sites, off Gopalpur and off Visakhapatnam, along the north-western BoB.

## 2. Material and methods

### 2.1. Study area

The BoB experiences various dynamic oceanographic processes such as seasonal reversal of wind, and current pattern along with immense freshwater discharge through rivers resulting in excess precipitation over evaporation (Varkey et al., 1996). The present study was carried out in the coastal waters off Gopalpur and off Visakhapatnam, north-western BoB (Figure 1). In general, waters along the coast of the eastern seaboard of India on north and south of  $15^\circ\text{N}$  are considered as north-western and south-western BoB, respectively (Lotliker et al., 2016). Both the study regions experience annual precipitation during the tropical south-west monsoon period from July to October bringing in adequate rainfall. However, the maximum rainfall is re-

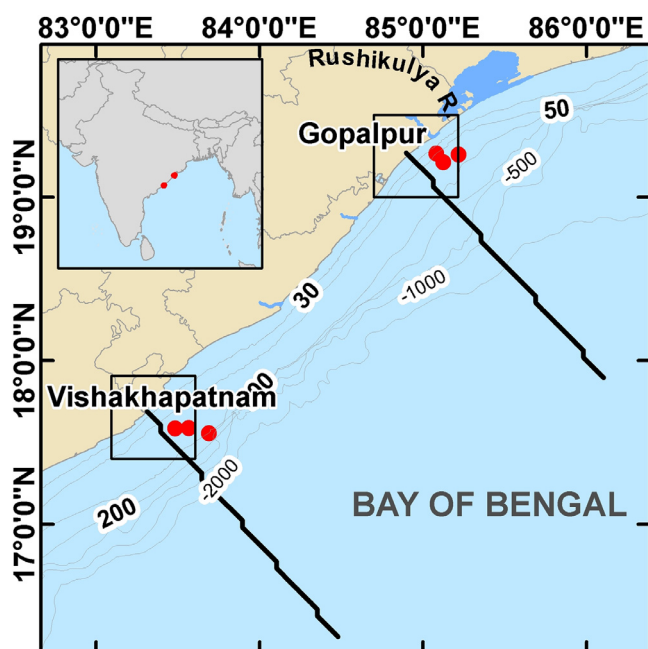


**Figure 1** Map of the study area. The dots indicate *in situ* sampling locations. The boxes represent areas of which time-series of satellite-derived size-fractionated chlorophyll-*a* (chl-*a*) were presented. The solid lines represent transects along which time-series of size-fractionated chl-*a* from satellite data is presented.

ceived from July to September during the active phase of the south-west monsoon season. The south-west monsoon gets totally withdrawn by October–November. During the north-east monsoon season, the BoB often experiences low pressure resulting in tropical cyclones. A significant amount of rainfall also occurs during this period. The north-east monsoon becomes inactive by end of November with the start of the winter season. The winter condition continues until February, after which the hot pre-monsoon conditions prevail spreading from March to May/June.

The circulation pattern of both regions is governed by more than one factor such as the effects of seasonally reversing East India Coastal Current (EICC) (Shetye et al., 1991), monsoonal wind-driven surface current (Vinayachandran and Mathew, 2003), cyclonic circulation (Vinayachandran and Yamagata, 1998) and river discharges flowing into the bay (Rao et al., 2007). The two major currents prevailing along this coast in a year are a north-easterly current that flows during January–July and a south-westerly current during August–December (Shankar et al., 2002). In addition, there are noticeable differences at both the locations on the local scale. The coastal waters off Gopalpur are well known for the periodic stay of migratory sea turtles, recurring high-biomass phytoplankton blooms and jellyfish swarming (Baliarsingh et al., 2016). The formation of two local water types on both sides of 30 m bathymetry makes coastal waters off Gopalpur ecologically distinct (Baliarsingh et al., 2015). The freshwater influx from the Rushikulya River estuary significantly influences the coastal water quality off Gopalpur. Additionally, upwelling along the coast, discharge from anthro-

pogenic sources and sea-port activities also largely control biogeochemistry of the coastal waters off Gopalpur.

Visakhapatnam, (260 km south of Gopalpur), is a port city and receive no direct major river discharge into its coastal domain. However, a major river estuary (Godavari) is located ~200 km south of Visakhapatnam. The influx of Godavari estuary may have an impact on the coastal waters off Visakhapatnam during the south-west monsoon season due to high-flow condition (Shankar et al., 1996). The other minor rivers such as Gosthani and the Sarada-Varaha which are towards the north (15 km) and south (40 km), respectively of Visakhapatnam city have a meager impact on the coastal waters off Visakhapatnam during the non-monsoon season. However, coastal upwelling along with anthropogenic activities due to sea-port influences the biogeochemistry of Visakhapatnam coastal waters.

## 2.2. Methodology

### 2.2.1. In situ sampling and analysis

Seawater samples were collected onboard ORV *Sagar Manjusha* in four expeditions in the BoB during 2017 (May and October) and 2018 (July and November). During these expeditions, a total number of 18 samples for each PSC were collected within a distance of ~10 km from the coast. The water samples were collected using Niskin sampling bottles and a known volume was sequentially filtered through 20  $\mu\text{m}$  (for MP), 2  $\mu\text{m}$  (for NP) and 0.2  $\mu\text{m}$  (for PP) pore size filter papers (Brewin et al., 2014). The filtration was carried out using a flow-through vacuum pump (make: Sartorius, model: Microstart Jet) under subdued light conditions. Subsequently, each filter was transferred to a sterilized cryotube and stored in liquid nitrogen until further analysis.

The chl-*a* concentration of individual PSC was estimated spectrophotometrically following the method prescribed by Parsons et al. (1984). The extraction of the pigment within the residue retained on the filter paper was carried out using 90% acetone. The extraction was carried out overnight with no light, under low temperature (in a refrigerator), and thereafter centrifuged for 20 minutes at 4000 rpm. The supernatant solution was then transferred to a 1 cm path length cuvette for analysis in a Double Beam UV-Visible Spectrophotometer (Make: Shimadzu, Model: UV-2600). The extinction coefficients of the sample were measured at specific wavelengths using acetone as blank. The chl-*a* concentration (in  $\text{mg m}^{-3}$ ) was then calculated as follows (Strickland and Parsons., 1965).

$$\text{Chl-}a(\text{mg m}^{-3}) = \frac{[(11.6 \times OD_{665}) - (1.31 \times OD_{645}) - (0.14 \times OD_{630})] \times v}{V \times l}$$

where OD is the optical density at discrete wavelengths after correction by the cell-to-cell blank and subtraction of the absorbance at 750 nm, *v* is volume of acetone in ml, *V* is the volume of filtered water in liter, and *l* is the path length in cm.

### 2.2.2. Satellite retrieval of size-fractionated chlorophyll-*a*

The daily Level-3 chl-*a* concentration from Moderate Resolution Imaging Spectroradiometer onboard Aqua satellite (MODISA) at 4 km resolution was acquired from National Aeronautics and Space Administration (NASA)'s Ocean Color Web supported by the Ocean Biology Processing

**Table 1** Model parameterization to calculate chlorophyll-*a* concentration in different size classes (pico, nano and microphytoplankton), using satellite data, provided by Brewin et al. (2010) and Sahay et al. (2017). The notations in the equations are chlorophyll-*a* concentration (*C*) which is the sum from pico (*C<sub>p</sub>*), nano (*C<sub>N</sub>*) and microphytoplankton (*C<sub>M</sub>*). *C<sub>PN</sub><sup>m</sup>* and *C<sub>p</sub><sup>m</sup>* are the asymptotic maximum values that can be attained by the combination of pico- and nanophytoplankton (*C<sub>PN</sub>*) and picophytoplankton (*C<sub>p</sub>*), respectively. *S<sub>PN</sub>* and *S<sub>p</sub>* are the corresponding initial slopes.

	$C = C_p + C_N + C_M$ $C_{PN} = C_{PN}^m [1 - \exp(-S_{PN}C)]$ $C_M = C - C_{PN}$ $C_p = C_p^m [1 - \exp(-S_pC)]$ $C_N = C_{PN} - C_p$	
Parameter	Brewin et al. (2010)	Sahay et al. (2017)
<i>C<sub>PN</sub><sup>m</sup></i>	0.977	1.2330
<i>C<sub>p</sub><sup>m</sup></i>	0.095	0.7243
<i>S<sub>PN</sub></i>	0.910	0.6792
<i>S<sub>p</sub></i>	7.822	0.6645

Group (OBPG) (<https://oceancolor.gsfc.nasa.gov/l3/>). The abundance-based model of Brewin et al. (2010) (hereafter B10) and Sahay et al. (2017) (hereafter S17) were used to calculate chl-*a* concentration of each PSC. The B10 model is the extension of the approach of Satyendranath et al. (2001), whereas the S17 model is basically the B10 model tuned for the Arabian Sea. The mathematical formulations including the model parameters are provided in Table 1. These abundance-based models assume that the concentration of total chl-*a* (*C*) is the sum of the individual PSC fractions from PP (*C<sub>p</sub>*), NP (*C<sub>N</sub>*) and MP (*C<sub>M</sub>*) (Brewin et al., 2010, 2012; Sahay et al., 2017).

$$C = C_p + C_N + C_M \tag{1}$$

The chl-*a* concentration of PP and the combined PP + NP fractions was parameterized as follows:

$$C_p = C_p^m [1 - \exp(-S_pC)] \tag{2}$$

$$C_{PN} = C_{PN}^m [1 - \exp(-S_{PN}C)] \tag{3}$$

where *C<sub>p</sub><sup>m</sup>* and *C<sub>PN</sub><sup>m</sup>* are the asymptotic values of maximum chl-*a* concentration attained by the combination of pico and nanophytoplankton (*C<sub>PN</sub>*) and picophytoplankton (*C<sub>p</sub>*). *S<sub>PN</sub>* and *S<sub>p</sub>* are the corresponding slopes. The chl-*a* concentration of MP and NP were subsequently calculated as follows:

$$C_M = C - C_{PN} \tag{4}$$

$$C_N = C_{PN} - C_p \tag{5}$$

The sensor-default atmospheric correction scheme was applied while generating chl-*a* from MODISA. The default, ocean chl-*a* with 3-band maximum ratio (OC3M) bio-optical algorithm was used for estimation of chl-*a* from MODISA. The functional form of the algorithm is expressed below.

$$\log_{10}(\text{chl-}a) = a_0 + \sum_{i=1}^{i=4} a_i \left\{ \log_{10} \left[ \frac{R_{rs}(\lambda_{blue})}{R_{rs}(\lambda_{green})} \right] \right\}^i \tag{6}$$

$$a = [0.2424, -2.7423, 1.8017, 0.0015, -1.2280] \tag{7}$$

For MODISA, *R<sub>rs</sub>(λ<sub>blue</sub>)* is the maximum of remote sensing reflectance (*R<sub>rs</sub>*) at wavelengths (*λ*) 443 and 488 nm. *λ<sub>green</sub>* is 547 nm.

In addition, the monthly climatology of PSC was constructed for the period from 2002–2018. The monthly climatology was then averaged over a region of 0.5° × 0.5° off Gopalpur (19.0–19.5°N and 84.7–85.2°E), and off Visakhapatnam (17.4–17.9°N and 83.1–83.6°E) for subsequent assessment. In addition, the fractions of chl-*a* concentration of PP, NP and MP to total chl-*a* concentration were computed along the transect off Gopalpur and off Visakhapatnam from nearshore to 200 km offshore.

### 3. Results and discussion

#### 3.1. Model performance in satellite retrieval of PSC

The satellite estimates of PSC have an advantage over conventional *in situ* data as they provide information over large spatial domains. Such information is necessary to discern ecosystem dynamics at the basin scale. However, the assessment of model accuracy in the retrieval of PSC from satellite data is also very important. Therefore, two "abundance" models B10 and S17 were applied to MODISA data and validated with *in situ* data generated within the study area. The satellite data were extracted within a box of 3 × 3 pixels, corresponding to *in situ* observations and the matchup points were selected containing more than 50% of the valid data (Bailey and Werdell, 2006). In addition to the concentration of chl-*a*, the fraction of individual PSC to total chl-*a* was also validated. The fraction depicts the contribution of individual PSC to the total concentration to represent and to understand the spatio-temporal trend (Brewin et al., 2015; Devred et al., 2011; Sahay et al., 2017). In the present study, fractions of individual PSC to total chl-*a* were used to understand the long-term trend from nearshore to offshore waters. Therefore, the fractions were also validated along with the concentrations of individual PSC.

**Table 2** Performance of statistical indices for the relative errors between *in situ* measured and satellite estimated chlorophyll-*a* (chl-*a*) concentration ( $\text{mg m}^{-3}$ ) in various size classes (P: Pico, N: Nano and M: Microphytoplankton) and their fractions (%) to total chl-*a* concentration (F\_P: Pico, F\_N: Nano and F\_M: Micro-phytoplankton) using Brewin et al. (2010) and Sahay et al. (2017) algorithms. Statistical indices include slope (S), intercept (I), regression coefficient ( $R^2$ ), the average ratio of *in situ* measured to satellite estimated value ( $r$ ), root mean squared error (RMSE) and the relative percentage difference between *in situ* measured and satellite estimated value (RPD). A total of 13 data points were used for validation.

		S	I	$R^2$	$r$	RMSE	RPD
Brewin et al. (2010) B10	P	25.08	-1.99	0.51	0.32	0.28	-262
	N	0.45	0.05	0.72	1.81	0.23	40.2
	M	0.96	0.02	0.93	1.01	0.13	-12.6
	F_P	0.65	26.35	0.60	0.36	22.28	-235
	F_N	0.52	1.19	0.50	1.87	21.88	45.7
	F_M	0.77	8.81	0.83	1.00	5.21	-1.6
Sahay et al. (2017) S17	P	0.82	0.07	0.77	0.98	0.07	-7.8
	N	0.90	0.03	0.74	0.99	0.05	-7.7
	M	1.05	0.01	0.93	0.98	0.14	-15.5
	F_P	0.97	0.28	0.72	1.03	3.60	2.0
	F_N	0.89	2.24	0.78	1.03	2.28	2.6
	F_M	0.93	3.95	0.83	0.97	4.63	-4.4

The coastal areas of the north-western BoB often remain cloudy and a total of 13 match-up points were available. The *in situ* chl-*a* concentration of PP, NP and MP varied from 0.1 to 0.76, 0.07 to 0.87 and 0.05 to 2.88  $\text{mg m}^{-3}$ , respectively which covers the entire dynamic range in the north Indian Ocean (Jyothibabu et al., 2013; Sarma et al., 2016; Sahay et al., 2017). Therefore, the *in situ* data was presented along with the dynamic range of the satellite estimates, using B10 (Figure 2a–c) and S17 (Figure 3a–c) model, for the corresponding months. The MODISA estimates of PSC are represented as minimum and maximum values over a month covering *in situ* sampling date. In addition, the relationship between *in situ* measured and satellite estimates of chl-*a* concentration in various size classes along with their fractions were also validated using B10 (Figure 2d–f) and S17 (Figure 3d–f) model. The statistical indices for the relative errors between *in situ* measured and MODISA estimates of PSC and their fractions (%) to total chl-*a* concentration are provided in Table 2.

The validation analysis showed underestimation and overestimation of the B10 model in retrieving PP (Figure 2a) and NP (Figure 2b), respectively. The statistical indicators also showed a high slope (25) and intercept (-1.99) for PP. The poor performance of the B10 model in capturing the *in situ* trend for PP is clearly evident with a low correlation coefficient ( $R^2=0.51$ ). The statistical indicators for NP retrieval, using the B10 model showed low slope (0.45), low intercept (0.05) and good correlation ( $R^2=0.72$ ). The B10 model performed well in estimating MP with all the *in situ* data falling within the dynamic range of MODISA (Figure 2c) with better slope (0.96), lower intercept (0.02), and good correlation ( $R^2=0.93$ ). The estimated relative error in the retrieval of PSC from MODISA satellite data, using B10 model, was 262% for PP, 40.2% for NP and 12.6% for MP.

The S17 model performed relatively better, in comparison to B10. The *in situ* data falls well within the dynamic range of MODISA retrieved PP (Figure 3a), NP (Figure 3b) and MP (Figure 3c). The statistical indices for S17 showed better

slope (0.82 to 1.05), lower intercept ( $\leq 0.01$ ), a good correlation coefficient ( $R^2 \geq 0.74$ ) and lower root mean squared error (RMSE) ( $\leq 0.14$ ). In addition, the estimated error in the retrieval of PSC from MODISA satellite data, using the S17 model, was 7.8% for PP, 7.7% for NP, and 15.5% for MP.

The fraction of PSC to total chl-*a* concentration was also statistically evaluated. The statistical performance indicators are provided in Table 2. The B10 model was found to be underestimating fractions of PSC with a slope value of  $\leq 0.77$ . In addition, the fraction of PP and NP showed higher RMSE ( $\geq 21.88$ ), lower correlation coefficient ( $R^2 \leq 0.6$ ) and estimated error was 235 and 45.7%, respectively. However, the fraction of MP from the B10 model showed good performance with a slope value of 0.77, lower intercept (8.81), lower RMSE (5.21) and a high correlation coefficient ( $R^2=0.83$ ). The estimated error was also lower (1.6%).

The S17 model performed much better in the retrieval of PSC fractions with a slope close to unity ( $\geq 0.89$ ), low intercept ( $\leq 3.95$ ), low RMSE ( $\leq 4.63$ ), high correlation ( $R^2 \geq 0.72$ ) and lower estimated error ( $\leq 4.4\%$ ). The overall statistical results of PSC fraction was similar to that of absolute concentration where the poor performance of the B10 was observed to estimate the fraction of PP and NP. Considering the better performance, the subsequent analysis was carried out using the S17 model.

The estimation of PSC was carried out by using a three-component abundance model that calculates the fractional contribution from three PSC (PP, NP, and MP) to total chl-*a* concentration. The B10 model was the extension of the approach of Satyendranath et al. (2001), which was based on the assumption that the smaller cells dominate at lower chl-*a* concentrations and large cells at higher chl-*a* concentrations. In addition, the parameterization of the B10 model was carried out using *in situ* data from the Atlantic Ocean during the Atlantic Meridional Transect (AMT) campaign (Brewin et al., 2010). The B10 model performed well at a global scale when applied to Sea-Viewing Wide Field-of-View Sensor (SeaWiFS) data. Although the model was de-

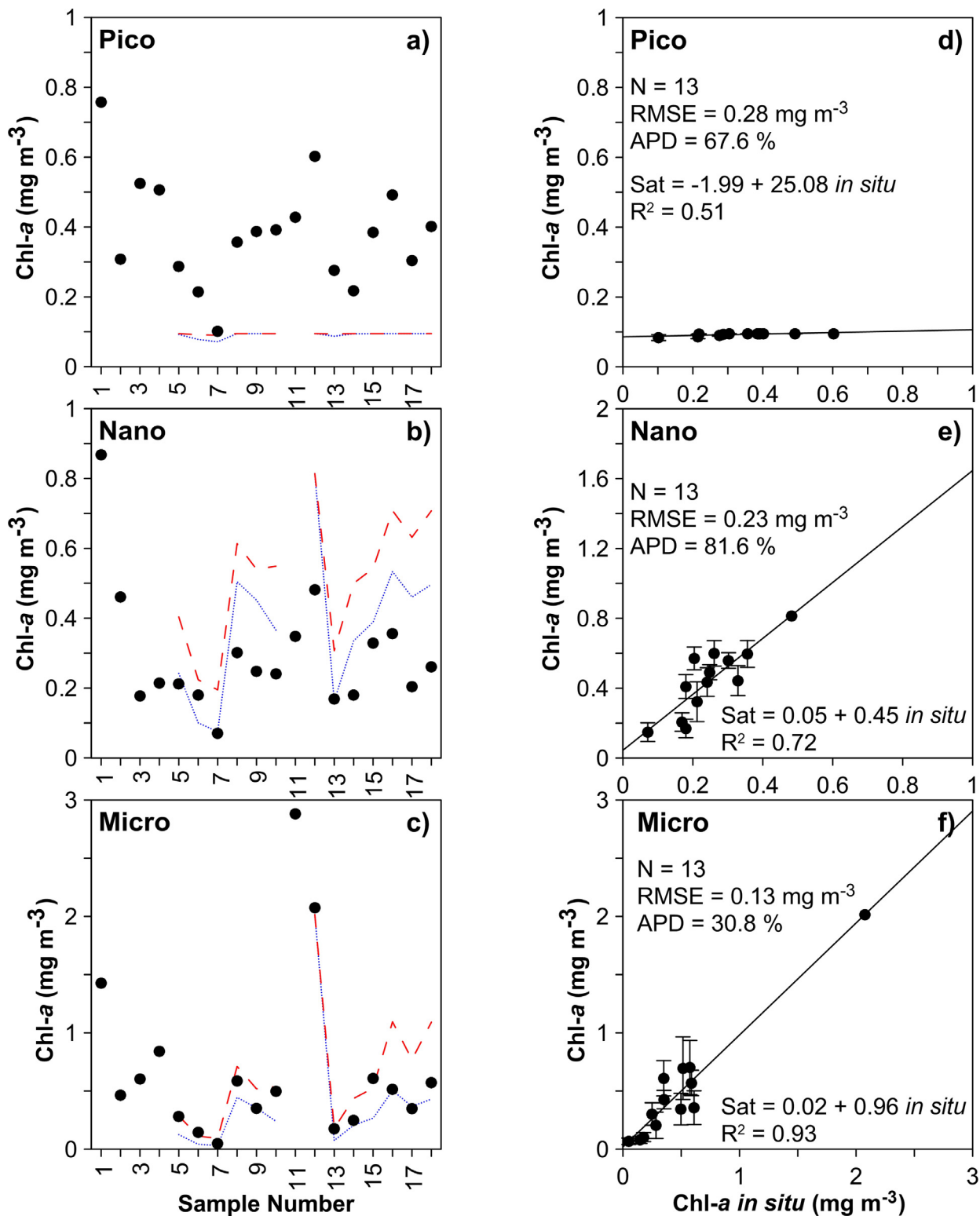


**Figure 2** The left panel represents variability between *in situ* measured (black dots) and satellite estimated (Brewin et al. 2010) chlorophyll-*a* (chl-*a*) concentration of a) pico, b) nano and c) microphytoplankton. The dotted (blue) line represents the minimum and dashed (red) line represents maximum value from satellite data over a month covering *in situ* sampling date. The right panel represents scatter plot showing relationship between *in situ* measured and satellite estimated (Brewin et al. 2010) chl-*a* concentration of d) pico, e) nano and f) microphytoplankton. The vertical bars indicate the standard deviation within *in situ* data.

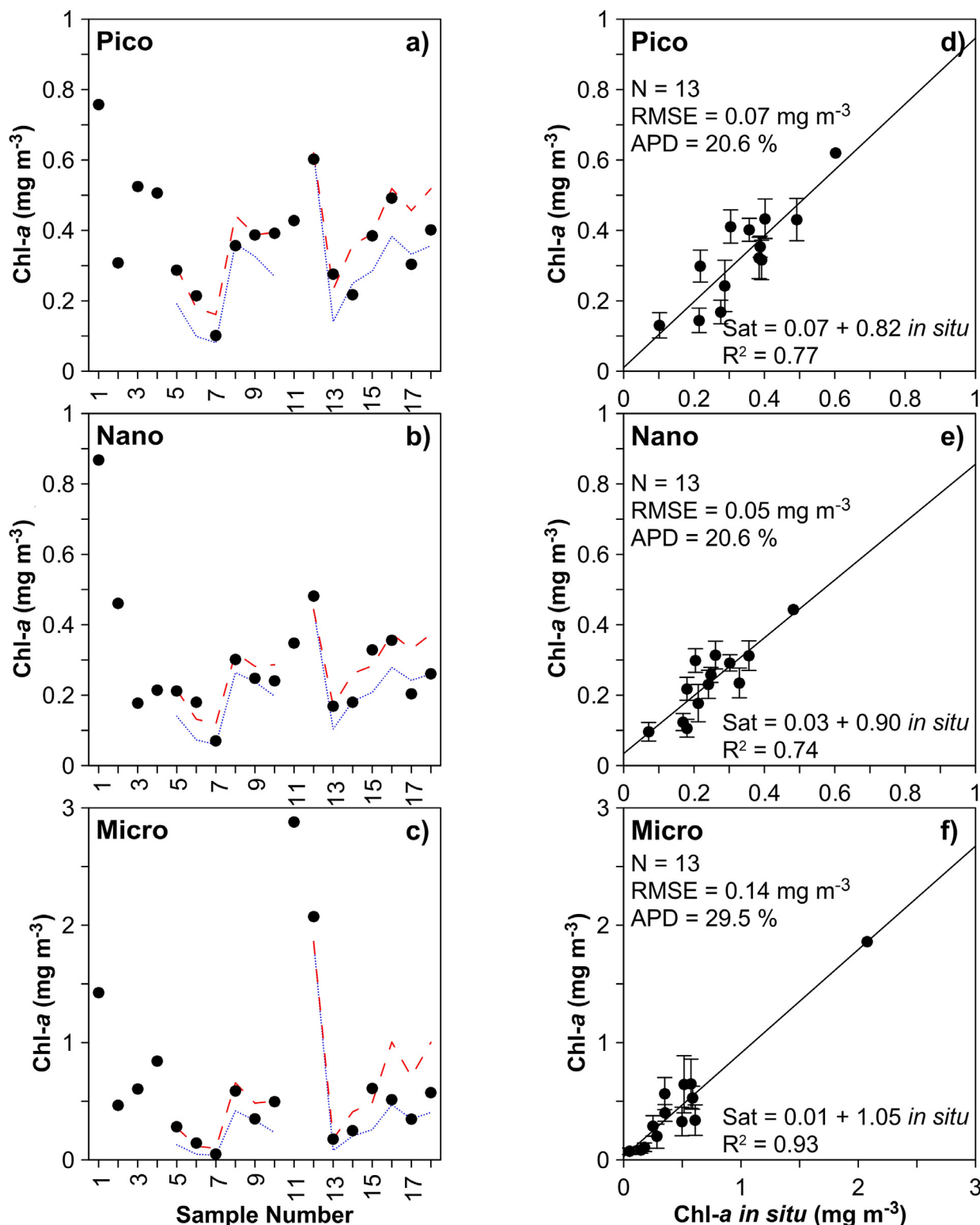


**Figure 3** The left panel represents variability between *in situ* measured (black dots) and satellite estimated (Sahay et al. 2017) chlorophyll-*a* (chl-*a*) concentration of a) pico, b) nano and c) microphytoplankton. The dotted (blue) line represents the minimum and dashed (red) line represents maximum value estimated from satellite data over a month covering *in situ* sampling date. The right panel represents scatter plot showing relationship between *in situ* measured and satellite estimated (Sahay et al. 2017) chl-*a* concentration of d) pico, e) nano and f) microphytoplankton. The vertical bars indicate the standard deviation within *in situ* data.

veloped for global application, the parameterization may vary with different biogeochemical provinces (Devred et al., 2009). In contrast, the S17 model is the regionally tuned version of Brewin et al. (2010) for the north Indian Ocean. The S17 model was tuned utilizing the *in situ* data from various Indian expeditions in the Arabian Sea including TARA Ocean Expedition dataset available in SeaWiFS Bio-optical Archive and Storage System (SeaBASS) maintained by the NASA – OBPG. The better performance of the S17 model could be attributed very well to its regional parameterization.

### 3.2. Long-term spatio-temporal distribution of PSC

The PSC are closely linked with several biogeochemical processes that have significant forcing on the marine carbon cycle, nutrient recycling and food web dynamics (Irwin et al., 2006). Therefore, the dynamics of PSC within the study area were analyzed through its spatial and temporal variability. The monthly climatology of PSC concentration and fractions was generated from MODISA data using S17 model. The monthly time-series of PSC averaged over  $0.5^\circ \times 0.5^\circ$  region off Gopalpur and Visakhapatnam is illustrated in Figure 4. The overall variability showed a similar trend with a peak during the pre-south-west monsoon (March–April) and the post-south-west monsoon (October) period. However, there was a marked difference in terms of the magnitude of individual PSC, especially during south-west monsoon and post south-west monsoon period. The distribution of PSC showed the dominance of MP throughout the year off Visakhapatnam (Figure 4b). However, PP dominated during south-west monsoon (June–July) and MP during rest of the year in coastal waters off Gopalpur. The cloudy condition and enhanced water column turbidity retards growth of large-sized phytoplankton in coastal waters and favours proliferation of small-sized phytoplankton during the monsoon season (Madhu et al., 2010). Further, the magnitude of all PSC was higher off Gopalpur during the post-south-west monsoon period (Figure 4a). The higher concentration during pre-monsoon could be attributed to the recurrent phytoplankton bloom events (Baliarsingh et al., 2016; Miranda et al.,

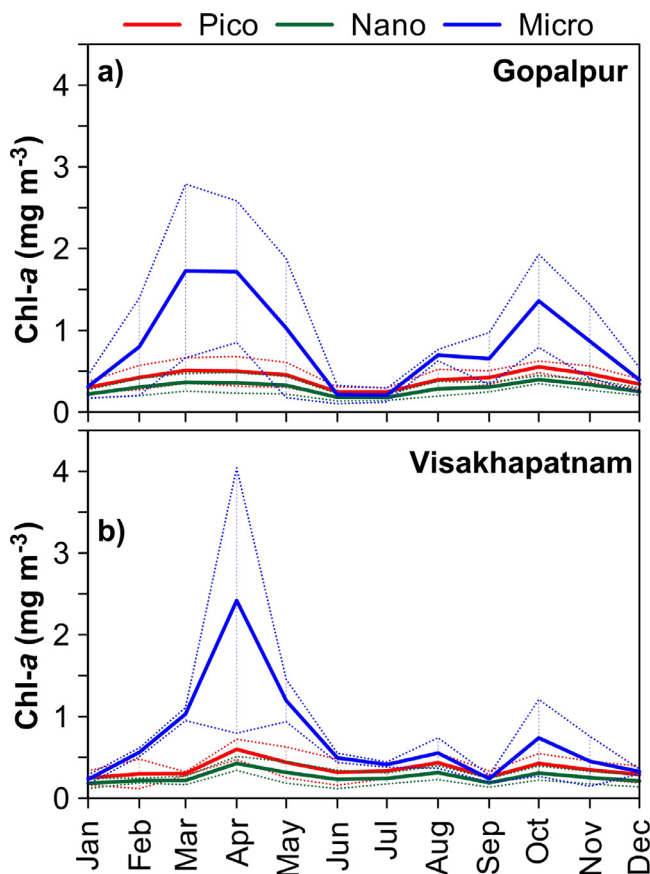


Figure 4 Area averaged monthly climatological variability (2002–2018) of satellite estimated (Sahay et al., 2017) chlorophyll-*a* (chl-*a*) concentration of pico, nano and microphytoplankton in coastal waters of a) Gopalpur and b) Visakhapatnam. The area over which the average is taken is defined in Figure 1. The solid lines represent mean and dotted lines represent standard deviation.

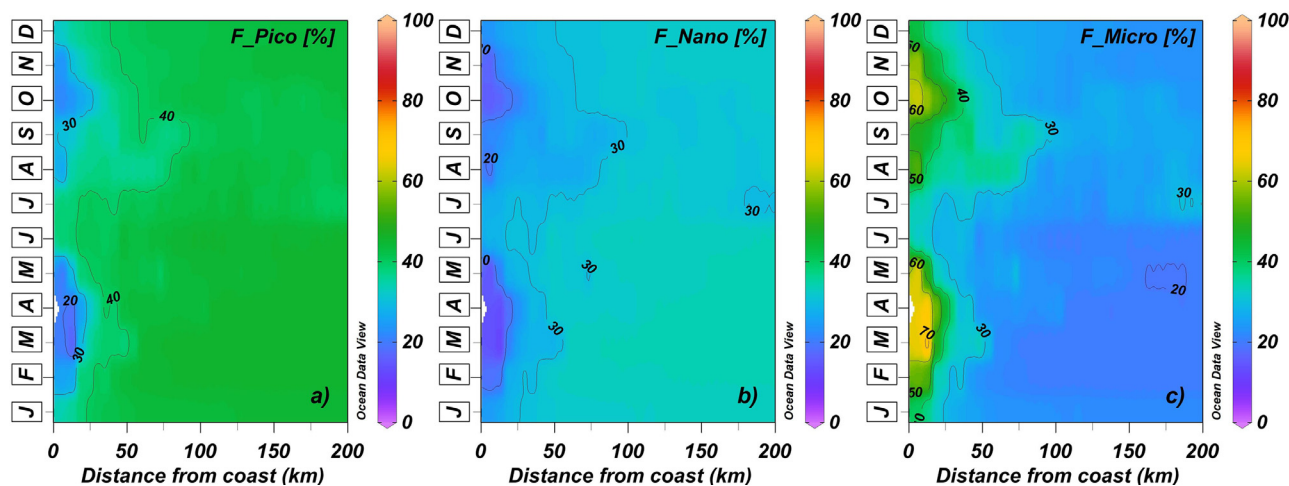
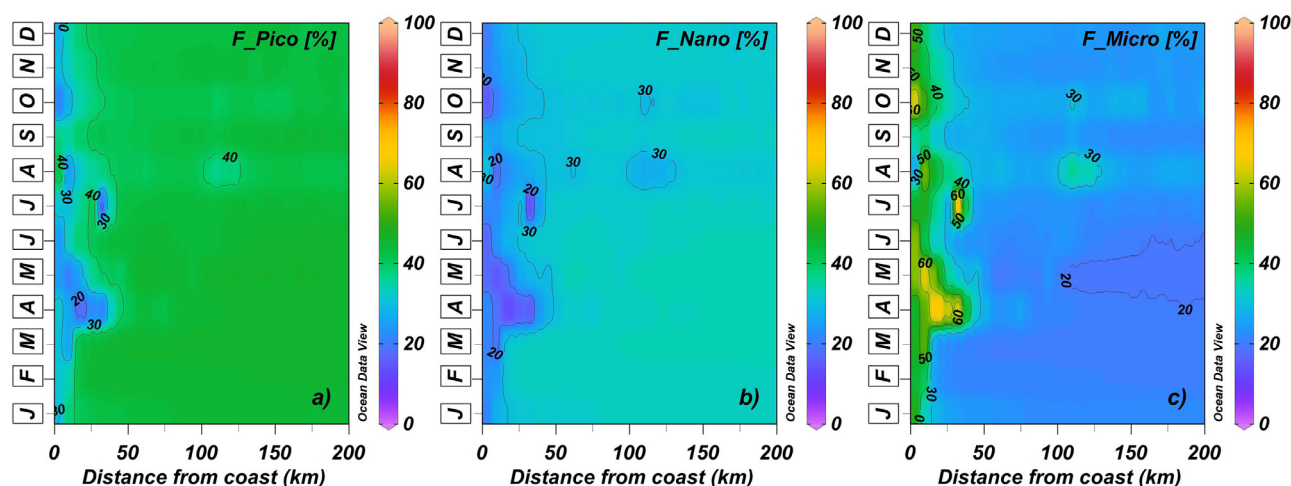


Figure 5 Hovmöller diagram showing monthly climatological variability (2002–2018) in satellite estimated (Sahay et al., 2017) fractions of a) pico, b) nano and c) microphytoplankton concentration to total chlorophyll-*a* (chl-*a*) concentration along the transect (described in Figure 1) off Gopalpur.



**Figure 6** Hovmöller diagram showing monthly climatological variability (2002–2018) in satellite estimated (Sahay et al., 2017) fractions of a) pico, b) nano and c) microphytoplankton concentration to total chlorophyll-*a* (chl-*a*) concentration along the transect (described in Figure 1) off Visakhapatnam.

2020). In general, the larger PSC prevails at higher concentrations of chl-*a*, whereas, both small, as well as large phytoplankton play an important role in the variability of chl-*a* at lower concentrations (Arin et al., 2005). The post-south-west monsoon increment could be attributed to enhanced phytoplankton growth by availing nutrients sourced from monsoonal precipitation induced terrigenous influx. The possible upwelling events enriching nutrients in the euphotic zone along the western BoB during the south-west monsoon season could also have played a pivotal role in elevating chl-*a* concentration (Rao et al., 1986; Shankar et al., 2002).

In subsequent analysis, nearshore to offshore variability in the fraction of PSC, off Gopalpur and Visakhapatnam, was analyzed through Hovmöller diagram (Figures 5 and 6). The nearshore dominance of MP and offshore dominance of PP were evident in both the areas. In nearshore region (up to 25 km from the coast), MP composition was nearly 70% that gradually decreased offshore in both the areas during the pre-south-west monsoon. During the post-south-west monsoon, up to 40% dominance of MP was observed off Gopalpur at a distance of ~4 km from the coast (Figure 5). However, the Visakhapatnam region showed less than 20% MP at a distance of ~40 km from the coast (Figure 6). In addition, during the south-west monsoon, nearshore waters off Gopalpur were observed with 40% of PP, 25% of NP and 35% of MP, whereas in off Visakhapatnam, PP, NP, and MP was 30%, 30% and 40%, respectively.

In corroboration to the present study, Mitbavkar and Anil (2011) have observed a higher abundance of PP in the offshore region of the BoB. In the open ocean region of the BoB, the PSCs percentage contribution to total chl-*a* have been reported in the order of PP > NP > MP. The higher contribution of PP was attributed to the low nutrient levels and a deeper nitracline (Sarma et al., 2016). The offshore higher abundance of PP in the BoB was comparatively higher than in the western counterpart, the Arabian Sea. Previous studies have reported ~30% and 70–80% contribution of PP to the total phytoplankton biomass in the Arabian Sea and the BoB, respectively (Baliarsingh et al., 2018; Mitbavkar and Anil, 2011; Roy et al., 2006). As a function of size, PP is ca-

pable of maintaining high uptake rates at low nutrient conditions, which gives a better competitive advantage over other PSCs in oligotrophic regions (Donald et al., 1997). In addition, PP also confers a greater efficiency to absorb and use solar radiation compared to larger PSC (Agusti et al., 1994).

#### 4. Conclusions

Marine phytoplankton play a critical role in modulating the earth's climate and responsible for half of the planetary primary production. The phytoplankton biochemical functions such as nutrient uptake and growth rate are largely controlled by its size characteristics. In addition, absorption of light, photosynthetic rate, export production and the structure of the marine food chain depend upon phytoplankton size structure. The present study investigated the performance of two “abundance” based models for satellite estimation of PSC and to understand the long-term trend of PSC, using the best-suited model, at two ecologically important coastal sites, off Gopalpur and off Visakhapatnam, along the north-western BoB. This is the first attempt to study the long-term distribution of PSC using satellite data. The significant conclusions drawn from the present study are (i) better performance of three-component abundance-based S17 model in the estimation of PSC from the north-western BoB using MODISA satellite data, (ii) nearshore dominance of MP that gradually reduces offshore, (iii) dominance of MP throughout the year off Visakhapatnam, (iv) dominance of PP during south-west monsoon and MP rest of the year, respectively off Gopalpur, (v) possible source of higher MP concentration during pre-monsoon attributed to recurrent phytoplankton bloom, (vi) possible fuelling the post-south-west monsoon increment in MP concentration from monsoonal precipitation induced terrigenous influx enhancing phytoplankton growth. The present study recommends the use of S17 model for satellite retrieval of phytoplankton size classes from coastal waters of the north-western BoB. The satellite-based detection of PSC has provided a new avenue to study the spatio-temporal distribution that can be further linked to ocean climate dynamics. In addition, the

present study bridged the knowledge gap on PSC distribution in coastal waters of the north-western BoB.

## Acknowledgements

The authors wish to acknowledge NASA – GSFC for making available MODIS – Aqua data through OBPG project. The authors also thank the development team of SeaDAS, using which the satellite data was processed. The authors also acknowledge “Coastal Monitoring” programme of Indian National Centre for Ocean Information Services (INCOIS) for *in situ* data. The authors wish to acknowledge the encouragement and support extended by competent authorities of Berhampur University and INCOIS. This paper is part of the doctoral work of the first author (Joereen Miranda).

## References

- Agusti, S., Enríquez, S., Frost-Christensen, H., Sand-Jensen, K., Duarte, C.M., 1994. Light harvesting among photosynthetic organisms. *Funct. Ecol.* 8, 273–279. <https://doi.org/10.2307/2389911>
- Arin, L., Estrada, M., Salat, J., Cruzado, A., 2005. Spatio-temporal variability of size fractionated phytoplankton on the shelf adjacent to the Ebro river (NW Mediterranean). *Cont. Shelf Res.* 25 (9), 1081–1095. <https://doi.org/10.1016/j.csr.2004.12.011>
- Arin, L., Morán, X.A.G., Estrada, M., 2002. Phytoplankton size distribution and growth rates in the Alboran Sea (SW Mediterranean): short term variability related to mesoscale hydrodynamics. *J. Plankton Res.* 24 (10), 1019–1033. <https://doi.org/10.1093/plankt/24.10.1019>
- Bailey, S.W., Werdell, P.J., 2006. A multi-sensor approach for the on-orbit validation of ocean color satellite data products. *Remote Sens. Environ.* 102 (1–2), 12–23. <https://doi.org/10.1016/j.rse.2006.01.015>
- Baliarsingh, S.K., Lotliker, A.A., Sahu, K.C., Kumar, T.S., 2015. Spatio-temporal distribution of chlorophyll-*a* in relation to physico-chemical parameters in coastal waters of the north-western Bay of Bengal. *Environ. Monit. Assess.* 187, art. no. 481. <https://doi.org/10.1007/s10661-015-4660-x>
- Baliarsingh, S.K., Lotliker, A.A., Sudheesh, V., Samanta, A., Das, S., Vijayan, A.K., 2018. Response of phytoplankton community and size classes to green *Noctiluca* bloom in the northern Arabian Sea. *Mar. Pollut. Bull.* 129 (1), 222–230. <https://doi.org/10.1016/j.marpolbul.2018.02.031>
- Baliarsingh, S.K., Lotliker, A.A., Trainer, V.L., Wells, M.L., Parida, C., Sahu, B.K., Srichandan, S., Sahoo, S., Sahu, K.C., Kumar, T.S., 2016. Environmental dynamics of red *Noctiluca scintillans* bloom in tropical coastal waters. *Mar. Pollut. Bull.* 111 (1–2), 277–286. <https://doi.org/10.1016/j.marpolbul.2016.06.103>
- Basu, S., Mackey, K.R.M., 2018. Phytoplankton as key mediators of the biological carbon pump: Their responses to a changing climate. *Sustainability* 10 (3), 869. <https://doi.org/10.3390/su10030869>
- Brewin, R.J.W., Sathyendranath, S., Jackson, T., Barlow, R., Brotas, V., Aïrs, R., Lamont, T., 2015. Influence of light in the mixed-layer on the parameters of a three-component model of phytoplankton size class. *Remote Sens. Environ.* 168, 437–450. <https://doi.org/10.1016/j.rse.2015.07.004>
- Brewin, R.J.W., Hirata, T., Hardman-Mountford, N.J., Lavender, S.J., Sathyendranath, S., Barlow, R., 2012. The influence of the Indian Ocean Dipole on interannual variations in phytoplankton size structure as revealed by Earth Observation. *Deep Sea Res. Pt. II* 77–80, 117–127. <https://doi.org/10.1016/j.dsr2.2012.04.009>
- Brewin, R.J.W., Sathyendranath, S., Hirata, T., Lavender, S.J., Barciela, R.M., Hardman-Mountford, N.J., 2010. A three-component model of phytoplankton size class for the Atlantic Ocean. *Ecol. Model.* 221 (11), 1472–1483. <https://doi.org/10.1016/j.ecolmodel.2010.02.014>
- Brewin, R.J.W., Sathyendranath, S., Lange, P.K., Tilstone, G., 2014. Comparison of two methods to derive the size-structure of natural populations of phytoplankton. *Deep Sea Res. Pt. I* 85, 72–79. <https://doi.org/10.1016/j.dsr.2013.11.007>
- Campbell, L., Nolla, H.A., Vaultot, D., 1994. The importance of *Prochlorococcus* to community structure in the central North Pacific Ocean. *Limnol. Oceanogr.* 39 (4), 954–961. <https://doi.org/10.4319/lo.1994.39.4.0954>
- Campbell, L., Vaultot, D., 1993. Photosynthetic picoplankton community structure in the subtropical North Pacific Ocean near Hawaii (station ALOHA). *Deep Sea Res. Pt. I* 40 (10), 2043–2060. <https://doi.org/10.1016/0967-0637>
- Devred, E., Sathyendranath, E., Stuart, V., Platt, T., 2011. A three component classification of phytoplankton absorption spectra: Application to ocean-color data. *Remote Sens. Environ.* 115 (9), 2255–2266. <https://doi.org/10.1016/j.rse.2011.04.025>
- Devred, E., Sathyendranath, S., Platt, T., 2009. Decadal changes in ecological provinces of the Northwest Atlantic Ocean revealed by satellite observations. *Geophys. Res. Lett.* 36 (19), art. no. L19607, <https://doi.org/10.1029/2009GL039896>
- Donald, K.M., Scanlan, D.J., Carr, N.G., Mann, N.H., Joint, I., 1997. Comparative phosphorus nutrition of the marine cyanobacterium *Synechococcus* WH7803 and the marine diatom *Thalassiosira weissflogii*. *J. Plankton Res.* 19 (12), 1793–1813. <https://doi.org/10.1093/plankt/19.12.1793>
- Hannah, F.J., Boney, A.D., 1983. Nanophytoplankton in the Firth of Clyde, Scotland: seasonal abundance, carbon fixation and species composition. *J. Exp. Mar. Biol. Ecol.* 67 (2), 105–147. [https://doi.org/10.1016/0022-0981\(83\)90085-0](https://doi.org/10.1016/0022-0981(83)90085-0)
- Huot, Y., Babin, M., Bruyant, F., Grob, C., Twardowski, M.S., Claustre, H., 2007. Does chlorophyll-*a* provide the best index of phytoplankton biomass for primary productivity studies? *Biogeosciences Discuss.* 4 (2), 707–745.
- IOCCG, 2000. Remote sensing of ocean colour in coastal, and other optically-complex, waters. In: Sathyendranath, S. (Ed.), *Reports of the International Ocean-Colour Coordinating Group, No. 3*. IOCCG, Dartmouth, 1–140.
- Irwin, A.J., Finkel, Z.V., Schofield, O.M.E., Falkowski, P.G., 2006. Scaling-up from nutrient physiology to the size-structure of phytoplankton communities. *J. Plankton Res.* 28 (5), 459–471. <https://doi.org/10.1093/plankt/fbi148>
- Jyothibabu, R., Mohan, A.P., Jagadeesan, L., Anjusha, A., Muraliedharan, K.R., Lallu, K.R., Kiran, K., Ullas, N., 2013. Ecology and trophic preference of picoplankton and nanoplankton in the Gulf of Mannar and the Palk Bay, southeast coast of India. *J. Marine Syst.* 111–112, 29–44. <https://doi.org/10.1016/j.jmarsys.2012.09.006>
- Jyothibabu, R., Vinayachandran, P.N., Madhu, N.V., Robin, R.S., Karnan, C., Jagadeesan, L., Anjusha, A., 2015. Phytoplankton size structure in the southern Bay of Bengal modified by the Summer Monsoon Current and associated eddies: Implications on the vertical biogenic flux. *J. Marine Syst.* 143, 98–119. <https://doi.org/10.1016/j.jmarsys.2014.10.018>
- Lotliker, A.A., Baliarsingh, S.K., Sahu, K.C., Kumar, T.S., 2020. Long-term chlorophyll-*a* dynamics in tropical coastal waters of the western Bay of Bengal. *Environ. Sci. Pollut. Res.* 27, 6411–6419. <https://doi.org/10.1007/s11356-019-07403-0>
- Lotliker, A.A., Omand, M.M., Lucas, A.J., Laney, S.R., Mahadevan, A., Ravichandran, M., 2016. Penetrative radiative flux in the Bay of Bengal. *Oceanography* 29 (2), 214–221. <https://doi.org/10.5670/oceanog.2016.53>

- Madhu, N.V., Jyothibabu, R., Balachandran, K.K., 2010. Monsoon-induced changes in the size-fractionated phytoplankton biomass and production rate in the estuarine and coastal waters of southwest coast of India. *Environ. Monit. Assess.* 166, 521–528. <https://doi.org/10.1007/s10661-009-1020-8>
- Miranda, J., Baliarsingh, S.K., Lotliker, A.A., Sahoo, S., Sahu, K.C., Kumar, T.S., 2020. Long-term trend and environmental determinants of phytoplankton biomass in coastal waters of northwestern Bay of Bengal. *Environ. Monit. Assess.* 192, 55. <https://doi.org/10.1007/s10661-019-8033-8>
- Mitbavkar, S., Anil, A.C., 2011. Tiniest primary producers in the marine environment: an appraisal from the context of waters around India. *Curr. Sci.* 100 (7), 986–988.
- Murty, K.N., Sarma, N.S., Pandi, S.R., Chiranjeevulu, G., Kiran, R., Muralikrishna, R., 2017. Hydrodynamic control of microphytoplankton bloom in a coastal sea. *J. Earth Syst. Sci.* 126, 82. <https://doi.org/10.1007/s12040-017-0867-2>
- Neil, C., Spyrakos, E., Hunter, P.D., Tyler, A.N., 2019. A global approach for chlorophyll-*a* retrieval across optically complex inland waters based on optical water types. *Remote Sens. Environ.* 229, 159–178. <https://doi.org/10.1016/j.rse.2019.04.027>
- O'Reilly, J.E., Maritorena, S., Mitchell, B.G., Siegel, D.A., Carder, K.L., Garver, S.A., Kahru, M., McClain, C., 1998. Ocean color chlorophyll algorithms for SeaWiFS. *J. Geophys. Res.-Oceans* 103 (C11), 24937–24953. <https://doi.org/10.1029/98JC02160>
- Parsons, T.R., Maita, Y., Lalli, C.M., 1984. *A Manual of Chemical and Biological Methods for Seawater Analysis*. Pergamon Press, New York, 173 pp.
- Rao, A.D., Dash, S., Jain, I., Dube, S.K., 2007. Effect of estuarine flow on ocean circulation using a coupled coastal-bay estuarine model: an application to the 1999 Orissa cyclone. *Nat. Hazards* 41, 549–562. <https://doi.org/10.1007/s11069-006-9049-2>
- Rao, T.V.N., Rao, D.P., Rao, B.P., Raju, V.S.R., 1986. Upwelling and sinking along Visakhapatnam coast. *Indian J. Mar. Sci.* 15, 84–87.
- Ribeiro, C.G., Santos, A.L., Marie, D., Pellizari, V.H., Brandini, F.P., Vaulot, D., 2016. Pico and nanoplankton abundance and carbon stocks along the Brazilian Bight. *PeerJ.* 4, art. no. e2587, <https://doi.org/10.7717/peerj.2587>
- Roy, R., Pratihary, A., Mangesh, G., Naqvi, S.W.A., 2006. Spatial variation of phytoplankton pigments along the southwest coast of India. *Estuar. Coast Shelf Sci.* 69 (1–2), 189–195. <https://doi.org/10.1016/j.ecss.2006.04.006>
- Sahay, A., Ali, S.M., Gupta, A., Goes, J.I., 2017. Ocean color satellite determinations of phytoplankton size class in the Arabian Sea during the winter monsoon. *Remote Sens. Environ.* 198, 286–296. <https://doi.org/10.1016/j.rse.2017.06.017>
- Sarma, V.V.S.S., Rao, G.D., Viswanadham, R., Sherin, C.K., Salisbury, J., Omand, M.M., Mahadevan, A., Murty, V.S.N., Shroyer, E.L., Baumgartner, M., Stafford, K.M., 2016. Effects of freshwater stratification on nutrients, dissolved oxygen, and phytoplankton in the Bay of Bengal. *Oceanography* 29 (2), 222–231. <https://doi.org/10.5670/oceanog.2016.54>
- Sathyendranath, S., Cota, G., Stuart, V., Maass, H., Platt, T., 2001. Remote sensing of phytoplankton pigments: a comparison of empirical and theoretical approaches. *Int. J. Remote Sens.* 22 (2–3), 249–273. <https://doi.org/10.1080/014311601449925>
- Shankar, D., McCreary, J.P., Han, W., Shetye, S.R., 1996. Dynamics of the East India Coastal Current: 1. Analytic solutions forced by interior Ekman pumping and local alongshore winds. *J. Geophys. Res.-Oceans* 101 (C6), 13975–13991. <https://doi.org/10.1029/96JC00559>
- Shankar, D., Vinayachandran, P.N., Unnikrishnan, A.S., 2002. The monsoon currents in the north Indian Ocean. *Prog. Oceanogr.* 52 (1), 63–120. [https://doi.org/10.1016/S0079-6611\(02\)00024-1](https://doi.org/10.1016/S0079-6611(02)00024-1)
- Shetye, S.R., Shenoi, S.S.C., Gouveia, A.D., Michael, G.S., Sundar, D., Nampoothiri, G., 1991. Wind-driven coastal upwelling along the western boundary of the Bay of Bengal during the southwest monsoon. *Cont. Shelf Res.* 11 (11), 1397–1408. [https://doi.org/10.1016/0278-4343\(91\)90042-5](https://doi.org/10.1016/0278-4343(91)90042-5)
- Strickland, J.D.H., Parsons, T.R., 1965. *A manual of seawater analysis*. Bull. 125. Fisher. Res. Board Can., Ottawa, 203 pp.
- Uitz, J., Claustre, H., Gentili, B., Stramski, D., 2010. Phytoplankton class-specific primary production in the world's oceans: seasonal and interannual variability from satellite observations. *Global Biogeochem. Cy.* 24 (3). art. no. GB3016, <https://doi.org/10.1029/2009GB003680>
- Varkey, M.J., Murthy, V.S.N., Suryanarayana, A., 1996. *Physical oceanography of the Bay of Bengal and Andaman Sea*. *Oceanogr. Mar. Biol. Ann. Rev.* 34, 1–70.
- Varunan, T., Shanmugam, P., 2015. A model for estimating size-fractionated phytoplankton absorption coefficients in coastal and oceanic waters from satellite data. *Remote Sens. Environ.* 158, 235–254. <https://doi.org/10.1016/j.rse.2014.11.008>
- Vinayachandran, P.N., Mathew, S., 2003. Phytoplankton bloom in the Bay of Bengal during the northeast monsoon and its intensification by cyclones. *Geophys. Res. Lett.* 30 (11). art. no. 1572, <https://doi.org/10.1029/2002GL016717>
- Vinayachandran, P.N., Yamagata, T., 1998. Monsoon response of the sea around Sri Lanka: generation of thermal domes and anticyclonic vortices. *J. Phys. Oceanogr.* 28 (10), 1946–1960 [https://doi.org/10.1175/1520-0485\(1998\)028<1946:MR0TSA>2.0.CO;2](https://doi.org/10.1175/1520-0485(1998)028<1946:MR0TSA>2.0.CO;2)



ORIGINAL RESEARCH ARTICLE

# Historical occurrences of marine microalgal blooms in Indian peninsula: Probable causes and implications

Oyeshina Gideon Oyeku<sup>a,b,c</sup>, Subir Kumar Mandal<sup>a,b,\*</sup>

<sup>a</sup> CSIR-Central Salt & Marine Chemicals Research Institute, Gujarat, India

<sup>b</sup> Academy of Scientific and Innovative Research (AcSIR), Ghaziabad, India

<sup>c</sup> Bowen University, Iwo, Osun State, Nigeria

Received 31 March 2020; accepted 31 August 2020

Available online 11 September 2020

## KEYWORDS

Arabian Sea;  
Bay of Bengal;  
Harmful algal  
blooms;  
Indian peninsula;  
Microalgal blooms;  
Surface Seawater  
Temperature

**Abstract** The Indian marine environment supports employment for over 200 million people, including revenue of nearly \$7 billion per annum. However, ecological goods and services of the shallow coast and the marine environment of the Indian peninsula are being affected by recurrent blooms of microalgae. One hundred and six published literature, starting from the first report in 1908 to 2017, were reviewed to investigate the historical occurrences of marine microalgal blooms (MMBs) around the Indian peninsula. 154 MMBs comprising 24 genera and 7 classes were reported during the study period. *Noctiluca* (dinophyceae) and *Trichodesmium* (cyanophyceae) bloom contributed 34.4% and 31.8% of total blooms. PCA revealed that high sea surface temperature (SST) and salinity were significant driving forces for *Trichodesmium* blooms formation, while high nutrients (NO<sub>3</sub>-N, PO<sub>4</sub>-P, and SiO<sub>4</sub>-Si) and low salinity triggered prymnesiophyceae, raphidophyceae, bacillariophyceae and most of the dinophyceae blooms. *Noctiluca* blooms were linked with both eutrophication and the abundance of prey organisms. HABs were generally dinophyceae dominated and were associated with mass mortality of aquatic fauna, human intoxication, paralytic, and ciguatera shellfish poisoning and even death. Increasing SST and anthropogenic influences around the Indian peninsula could increase the occurrences of MMBs (including HABs) and the number of causative taxa. Proper safety measures such as rou-

\* Corresponding author at: CSIR-Central Salt & Marine Chemicals Research Institute, Gijubhai Badheka Marg, Bhavnagar-364002, Gujarat, India. Phone: +91 (278) 2567760 Ex. 6130, fax: +91 (278) 2567562/6970.

E-mail address: [skmandal@csmcri.res.in](mailto:skmandal@csmcri.res.in) (S.K. Mandal).

Peer review under the responsibility of the Institute of Oceanology of the Polish Academy of Sciences.



Production and hosting by Elsevier

<https://doi.org/10.1016/j.oceano.2020.08.008>

0078-3234/© 2020 Institute of Oceanology of the Polish Academy of Sciences. Production and hosting by Elsevier B.V. This is an open access article under the CC BY-NC-ND license (<http://creativecommons.org/licenses/by-nc-nd/4.0/>).

tine monitoring of phycotoxin levels in the environment and local seafood are required to be put in place in order to protect the health of the public.

© 2020 Institute of Oceanology of the Polish Academy of Sciences. Production and hosting by Elsevier B.V. This is an open access article under the CC BY-NC-ND license (<http://creativecommons.org/licenses/by-nc-nd/4.0/>).

## 1. Introduction

Marine ecosystems are the major backbone of life on earth and constitute the largest source of habitat and biodiversity (Anderson et al., 2012). They are primarily supported by the microalgae, which provide the basic food in the food web/chain and play an important role in nutrient recycling and gaseous exchange (Chassot et al., 2010; Passow and Carlson, 2012). Microalgae are unicellular microscopic photosynthetic creatures which exist in different forms (single, filamentous or colonial), shapes (ovoid, cylindrical, spherical) and size (nano: 2–20  $\mu\text{m}$ , micro: 2–200  $\mu\text{m}$ , macro: > 200  $\mu\text{m}$ ). They may be free-floating or moving in the water column (i.e., pelagic microalgae), settled on the sediment (benthic microalgae), macrophytes, or other substrates (epiphytic microalgae). They contain pigments for harvesting light/solar radiation and utilize sunlight, nutrients, and carbon dioxide for productivity, growth, and reproduction (Gireesh et al., 2015; Ignatiades, 2016). Marine microalgae are taxonomically diverse and comprise various groups, including diatoms, coccolithophores, chlorophytes, flagellate protists (dinoflagellates, raphidophytes) and cyanobacteria (Brierley, 2017). In total, it consists of about 5000 extant species as a whole.

Generally, microalgae respond rapidly to variations in environmental conditions. Such response includes a change in growth that differs among different taxa or groups (Sharma et al., 2012). Hence, certain changes in physicochemical conditions, e.g., temperature, salinity, nutrients, etc. can stimulate the proliferation of opportunistic micro-algae into large biomass or otherwise cell numbers capable of causing harm, a phenomenon referred to as “bloom” (Anderson et al., 2012). Typically, the cell, biomass, or chlorophyll-*a* concentration, which defines a bloom has not been delineated in the global scientific community. Though a few authors have proposed cell densities (Kim et al., 1993) and chlorophyll-*a* concentration (Binding et al., 2018) defining a bloom, none is yet unanimously accepted. Smayda (1997), in his opinion, discussed that defining this benchmark will vary according to species nature (i.e., whether toxic or non-toxic) and size, location, or habitat type (i.e., whether oligotrophic, mesotrophic or eutrophic) and season. Hence, the term “bloom” has been conventionally used in literature to describe the rapid increase or growth of one or more species of microalgae resulting into visible water discoloration, e.g., red tide, foam production and harm to aquatic biota, ecosystem and human health (Aleynik et al., 2016; Smayda, 1997).

The dominance of either single or multiple species of marine microalgae is called marine microalgal bloom (MMB), and this forms part of the natural cycle of photosynthetic organisms in marine ecosystems, and play a key role in maintaining their community structure and dynamics as well as

ensuring sustained services/benefits to humans (Berdalet et al., 2015). However, harmful algal blooms (HABs) may bring severe health and socio-economic consequences to humans, organisms, and the environment (Willis et al., 2018). Six human syndromes namely; paralytic shellfish poisoning (PSP), neurotoxic shellfish poisoning (NSP), amnesic shellfish poisoning (ASP), diarrhetic shellfish poisoning (DSP), ciguatera fish poisoning (CFP) and azaspiracid shellfish poisoning (AZSP) have been identified in association with HABs (Ferrante et al., 2012). Also, injury and death of fish, shellfishes and other marine animals following excessive respiration and or decomposition, production of exudates, reactive oxygen species (ROS) or noxious toxins during HABs have been reported (Narayana et al., 2014; Svendsen et al., 2018; Twiner et al., 2012; Walker et al., 2018). Some economic consequences of HABs already described include reduced demand for affected products (Getchis and Shumway, 2017), closure of important shellfisheries (Jin et al., 2008) and desalination plants (Richlen et al., 2010), and loss of revenue (Anderson et al., 2000; Getchis and Shumway, 2017; Hoagland et al., 2002).

Increasing occurrences and adverse effects of MMBs in marine ecosystems have continued to stir interest in the scientific community (Anantharaman et al., 2009). Coastal habitats are amongst the most affected due to their shallow nature and high susceptibility to changing environmental conditions (Anderson et al., 2012). Changes in the physicochemical (temperature, salinity, dissolved nutrients) conditions of the water are mostly brought about by varying micro-climatic conditions, which usually differ from one geographical location to another (Guinder and Molinero, 2013). Hence, studies geared towards an understanding of major environmental factor/s promoting MMBs (including HABs) are required at regional levels for better environmental health management.

The resources from India's marine environment provide a livelihood to more than 3.5 million people and an estimated income of worth \$7 billion in a year through recreation, fishing and other economic activities (Nayak, 2017; Saxena, 2012; Singh, 2003). However, the recurrent blooms of microalgae (including HABs) pose a threat to these ecosystems, as well as the economic, social, and ecological services which they provide (D'Silva et al., 2012; Padakumar et al., 2012). The environmental factors triggering such occurrences are not adequately understood. No study has been conducted that describes the specific physicochemical parameters conditions that exclusively responsible for marine microalgal bloom (MMBs) formation in and around the Indian peninsula. In this study, MMBs around the Indian peninsula coast from the first report in 1908 to 2017 were reviewed, and the various incidents, causative organisms, and relating physicochemical conditions reported were compiled. The relationship between these physicochemical conditions and

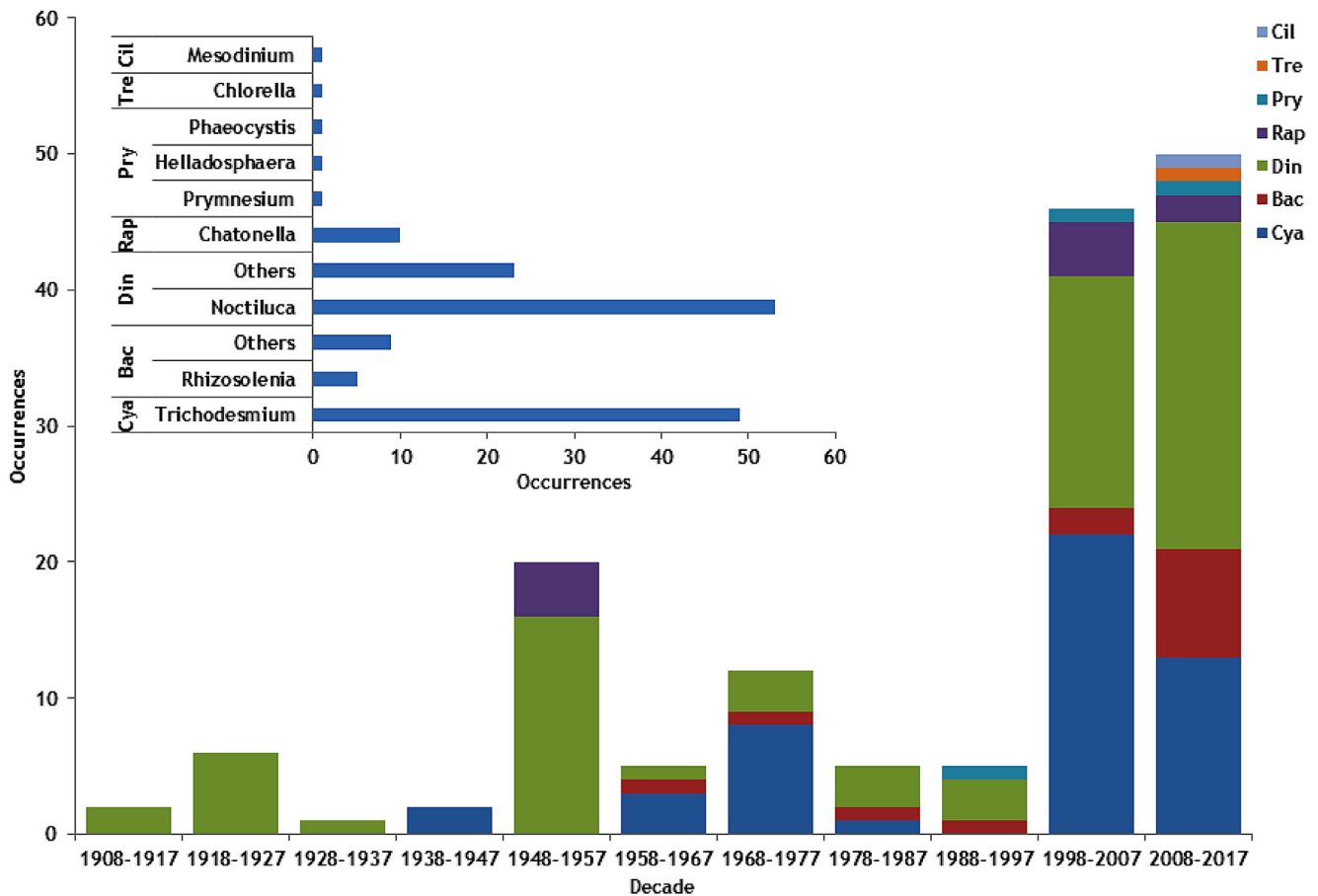


**Figure 1** Incidences of marine microalgal blooms around the Indian peninsula from 1908 to 2017. Inset: Occurrences by different bloom-forming organisms. In general, and in the inserted figure, grouping was done by classes and genera, respectively. Cya – Cyanophyceae, Bac – Bacillariophyceae, Din – Dinophyceae, Rap – Raphidophyceae, Pry – Prymnesiophyceae, Tre – Trebouxiophyceae, Cil – Ciliata.

blooms of the different taxa was also examined in order to determine the critical parameters influencing specific blooms along the coast of the Indian peninsula.

## 2. Data retrieval and analysis

A total of 106 articles published on occurrences of MMBs around the Indian peninsula coast from the first report in 1908 to 2017 (110 years) were accessed. Subsequently, information regarding period, location, causative organism, and taxonomy were retrieved (Supplementary Tables 1 and 2). Decadal and seasonal occurrences of such events were compiled concerning taxonomic class and dominant genera (Figures 1 and 2). In order to obtain the spatial distribution of blooms, latitude and longitude data obtained from the literature were inputted into Arc Map 10.5 software in decimal degrees (Figure 3). In instances where none was available in the source article, relevant values were obtained from <https://google.com/maps>.

Also, cell density and physicochemical conditions, e.g., sea surface temperature (SST), pH, salinity, dissolved oxygen (DO),  $\text{NO}_3\text{-N}$ ,  $\text{NO}_2\text{-N}$ ,  $\text{NH}_3\text{-N}$ ,  $\text{PO}_4\text{-P}$ , and  $\text{SiO}_4\text{-Si}$  reported during each bloom event were obtained, and the average, standard deviation and range values for individual species

**Table 1** Eigenvalues of the correlation matrix.

	Eigenvalue	Percentage of variance	Cumulative percentage of variance
1	2.08543	41.71	41.71
2	1.11257	22.25	63.96
3	0.98019	19.60	83.56
4	0.53595	10.72	94.28
5	0.28586	5.72	100.00

and class were determined using Microsoft Excel 10 software (Table 1). Satellite datasets available for major parameters considered, i.e., SST, salinity, nitrate, phosphate, and silicate, including wind speed and mixed layer depth (MLD), were retrieved from relevant sources (Supplementary Table 3). The datasets acquired were limited to the area covered by bloom events reported in this study (Latitude  $6.00^\circ$  to  $24.00^\circ\text{N}$  and Longitude  $64.00^\circ$  to  $93.08^\circ\text{E}$ ).

Indirect gradient analysis, like the Principal component analysis (PCA), was carried out in order to establish the correlation between blooms formed by different taxa and abi-

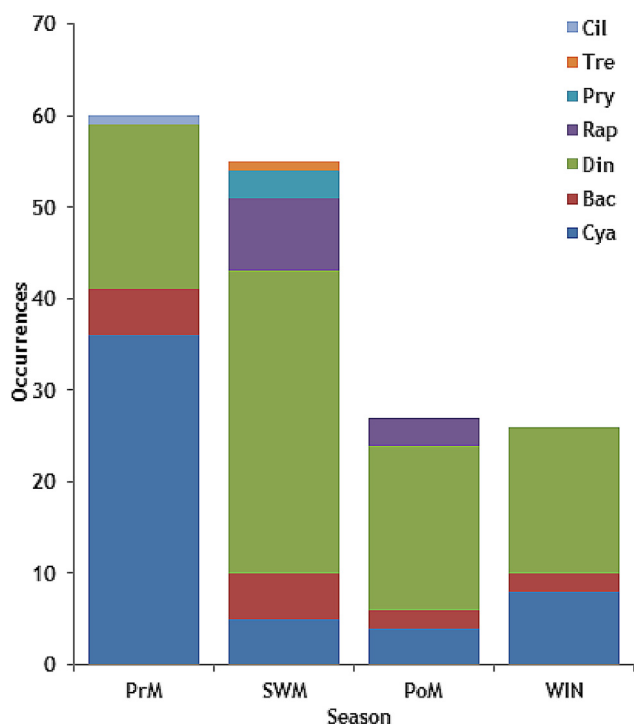


**Figure 2** Seasonal occurrences of marine microalgal blooms around the Indian peninsula from 1908 to 2017. Cya – Cyanophyceae, Bac – Bacillariophyceae, Din – Dinophyceae, Rap – Raphidophyceae, Pry – Prymnesiophyceae, Tre – Trebouxiophyceae, Cil – Ciliata, PrM – Pre-Monsoon, SWM – South-west monsoon, PoM – Post-monsoon, WIN – Winter.

otic factors by correlating the ordination scores (Figure 4).  $\text{NO}_2\text{-N}$  and  $\text{NH}_3\text{-N}$  values were not included in the PCA due to low/no availability of on the spot recorded data. In an instance where one or more physicochemical parameter(s) was not reported, the entire data for such an event was excluded from the PCA analysis. Log transformation,  $\text{Log}_{10}(X+1)$  was carried out before analyzing data using Origin software version 8.5.1. One way ANOVA was employed to evaluate the significant difference between decadal mean annual temperatures and salinities obtained from satellite database using SPSS 16.0 software (Supplementary Table 4).

Bloom events, as a result of the sudden proliferation of one or more species of microalgae, were included only in this study for doing cause and effect analysis based on the reported visible discoloration (red tide) or patches on water, injury or loss of aquatic life, and/or toxicity to humans (International Council for the Exploration of the Sea, 1984). The least cell concentrations attributed to the blooms of the various taxonomic classes in this study were  $6.2 \times 10^4$  cells/L (Qasim, 1970) for cyanophyceae,  $1.3 \times 10^4$  cells/L for bacillariophyceae (Sanilkumar et al., 2009a),  $1.0 \times 10^4$  and  $9.0 \times 10^4$  cells/L for *Noctiluca* (Padmakumar et al., 2016a) and other dinophyceae, respectively (Iyer et al., 2008),  $24.0 \times 10^4$  cells/L for raphidophyceae (Jugnu, 2006),  $186.0 \times 10^4$  cells/L for prymnesiophyceae (Ramaiah et al., 2005),  $19.4 \times 10^4$  cells/L for trebouxiophyceae (Asha et al., 2015) and  $100.0 \times 10^5$  cells/L for ciliates (Sahu et al., 2016). A HAB event was identified as an incident associated with devastating impacts such as mortality of aquatic fauna (e.g., fish, and shellfish), human injury and death (e.g., res-

piratory difficulty, hospitalization, shellfish poisoning), and or economic hardship due to grounded or reduced fishing activity (Sanseverino et al., 2016).

### 3. Results and discussion

#### 3.1. Biophysical and meteorological characteristics around the Indian peninsula coast

The Indian peninsula is bordered on the western side by the Arabian Sea (AS) and the eastern side by the Bay of Bengal (BOB). Both ecosystems form part of the North Indian Ocean and are influenced by intense, annually reversing monsoon winds and seasonally varying sea surface circulation (Chowdary et al., 2016). Strong southwesterly monsoon winds blowing from June to September induce the summer monsoon, also known as the south-west monsoon (SWM). This season is characterized by heavy precipitation, strong water mixing and upwelling of cold, saline, nutrient-rich, and oxygen-depleted waters from the subsurface to the surface along the coast. This effect is most pronounced along the south-west coast (Attri and Tyagi, 2010). Generally, low SST ( $27.7^\circ\text{C}$  in AS and  $28.5^\circ\text{C}$  in BOB), high MLD (65 m in AS and 45 m in BOB), and nutrient concentration ( $\text{NO}_3\text{-N}$  of around  $5 \mu\text{M}$ ,  $\text{PO}_4\text{-P}$  up to  $0.75 \mu\text{M}$  and  $\text{SiO}_4\text{-Si}$  up to  $20 \mu\text{M}$ ) are recorded. Surface salinity is higher in the AS remains relatively high ( $\sim 35.6$  psu) during this period as compared to the BOB ( $\sim 33.6$  psu), owing to lower precipitation of around 130 cm/month in the AS than in the BOB ( $\sim 350$  cm/month). Surface salinity in the AS remains relatively high ( $\sim 35.6$  psu) during this period, while that in the BOB is low ( $\sim 33.6$  psu), due to higher precipitation (350 cm/month) in the BOB than in the AS (130 cm/month) (Supplementary Figures 3–7).

Another major cause of low salinity in the BOB is the large amount of run-off/freshwater which it receives from major rivers which are located along its northern part, e.g., River Brahmaputra and Ganges, Mahanadi, Godavari, Krishna, and Cauvery. The freshwater flux from these rivers reaches up to  $14 \times 10^4 \text{ m}^3/\text{s}$  during SWM. About 60% of the entire freshwater received in the season (Chaitanya et al., 2014). The AS is fed by small rivers, e.g., Sabarmati, Mahi, Narmada, and Tapi. AS receives a comparatively lower input of freshwater as compared to BoB due to low precipitation. River run-off also contributes to the source of nutrient enrichment in both the AS and BOB during SWM. A southwesterly flow is known as the West Indian Coastal Current (WICC), which prevails during this season and carries colder and more saline water to the east coast (Panikkar and Jayaraman, 1966). Low saline water is observed along the west coast below  $15^\circ\text{N}$  due to the southward advection of low salinity surface water from the coastal margin up north by this current, as well as the input of run-off water from nearby areas (Behara et al., 2019).

Cold, dry northeastern monsoon winds usher in the northeast monsoon or winter (WIN) season. The winds blow in the south-west direction and result in the vertical mixing of surface water with deeper nutrient-rich water due to heat loss resulting from cooling. The lowest average SST of  $27.3^\circ\text{C}$  and  $27.9^\circ\text{C}$  in the AS and BOB, respectively, is recorded during this period along with little rainfall (Attri and Tyagi, 2010). Mean salinity of around 32.3 psu is recorded in the

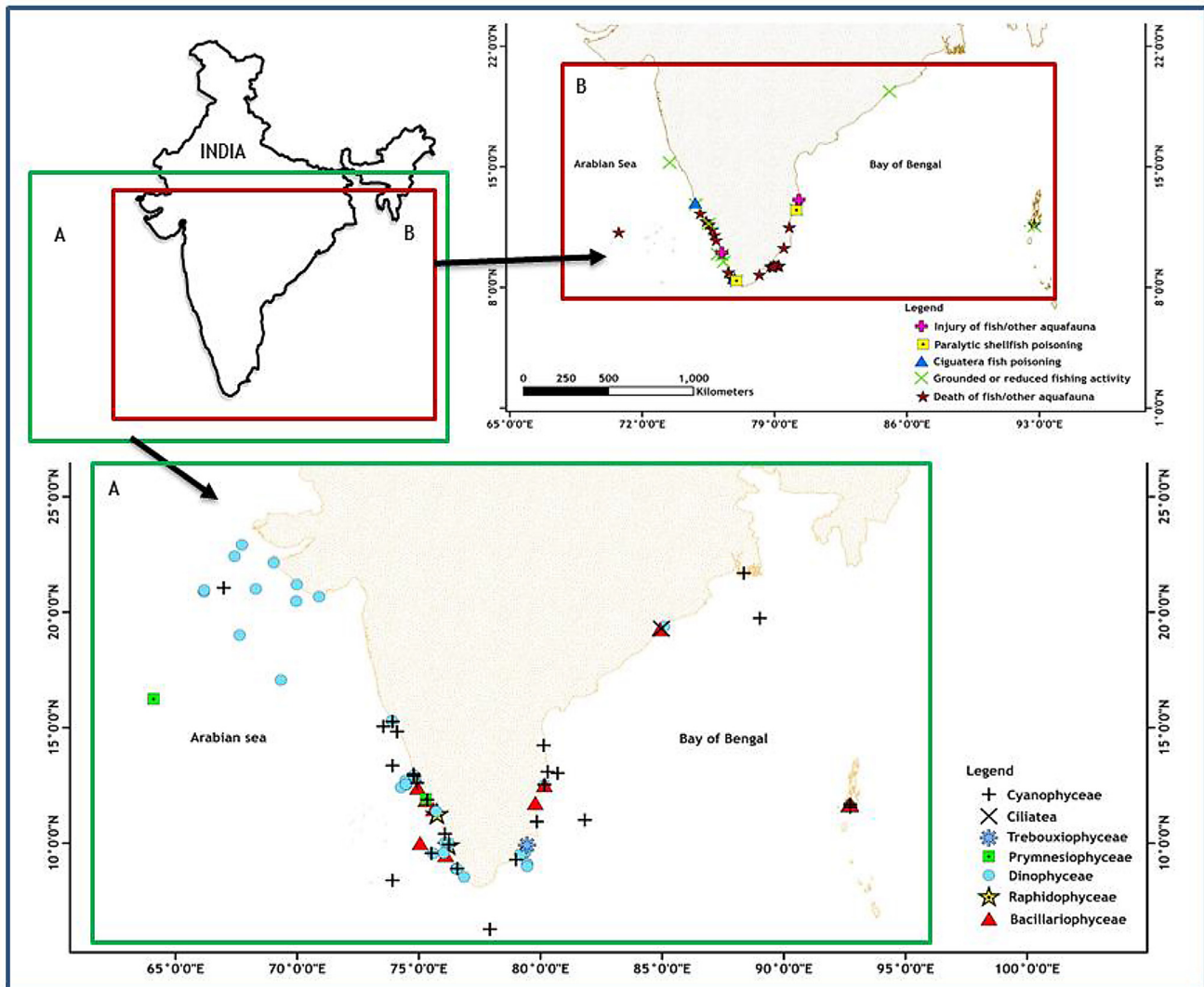


**Figure 3** Distribution of marine microalgal blooms around the Indian peninsula from 1908 to 2017. A – Non-harmful occurrences. B – Harmful algal blooms.

BOB while that in the AS is around 35.4 psu. High nutrient levels, up to  $8 \mu\text{M}$  of  $\text{NO}_3\text{-N}$ ,  $0.75 \mu\text{M}$  of  $\text{PO}_4\text{-P}$ , and  $10 \mu\text{M}$  of  $\text{SiO}_4\text{-Si}$  are observed. Also, wind speed and mixed layer depth increase reaching a maximum of  $\sim 9 \text{ m/s}$  and  $75 \text{ m}$ , respectively, around January. The utmost of these conditions generally occurs along the extreme north and south coasts of the peninsula (Supplementary Figs. 1–7). East Indian Coastal Current (EICC) flows along the eastern boundary towards the west direction and carries low salinity water from the BOB into the southern AS. The winter season runs from December to February (Akhil et al., 2014).

A period of transition known as the post-monsoon season (PoM) follows the SWM before the start of the NEM. It is generally characterized by the withdrawal of monsoon and high SST ( $28^\circ\text{C}$  in AS and  $28.5^\circ\text{C}$  in BOB) along both coasts. Surface salinity is  $\sim 36$  psu in the AS and  $\sim 33$  psu in the BOB. Cyclonic depression and heavy, widespread rainfall occur along the eastern coast (Anoopa, 2017). Hot and dry winds characterize the pre-monsoon (PrM) season. A maximum average SST of above  $29^\circ\text{C}$  is recorded also recorded in both basins. Surface salinity is also high, around 35.5 psu

in the AS and 33.5 psu in the BOB. The season is characterized by cyclonic storms which move in the north-western direction, and short durations of rainfall. Most of these occur in the Bay of Bengal (BOB) (Anoopa, 2017). According to the Asia-Pacific Data Research Centre (2018), the average salinity of the seawater increases from the northern part to the southern part in the BOB. The same increases from the southern part to the northern part in general in the AS. However, in the case of SST, both the BOB and AS exhibit a similar pattern of distribution, i.e., from north to the south gradient (Mohapatra et al., 2015).

### 3.2. Occurrences of MMBs around the Indian Peninsula

A total of 154 MMBs comprising 24 genera under the class: dinophyceae (9 genera), bacillariophyceae (8 genera), prymnesiophyceae (3 genera), cyanophyceae, raphidophyceae, trebouxiophyceae, and ciliatae (1 genus each) were reported around the Indian peninsula from 1908 to 2017 (Figure 1; Supplementary Tables 1 and 2). Among

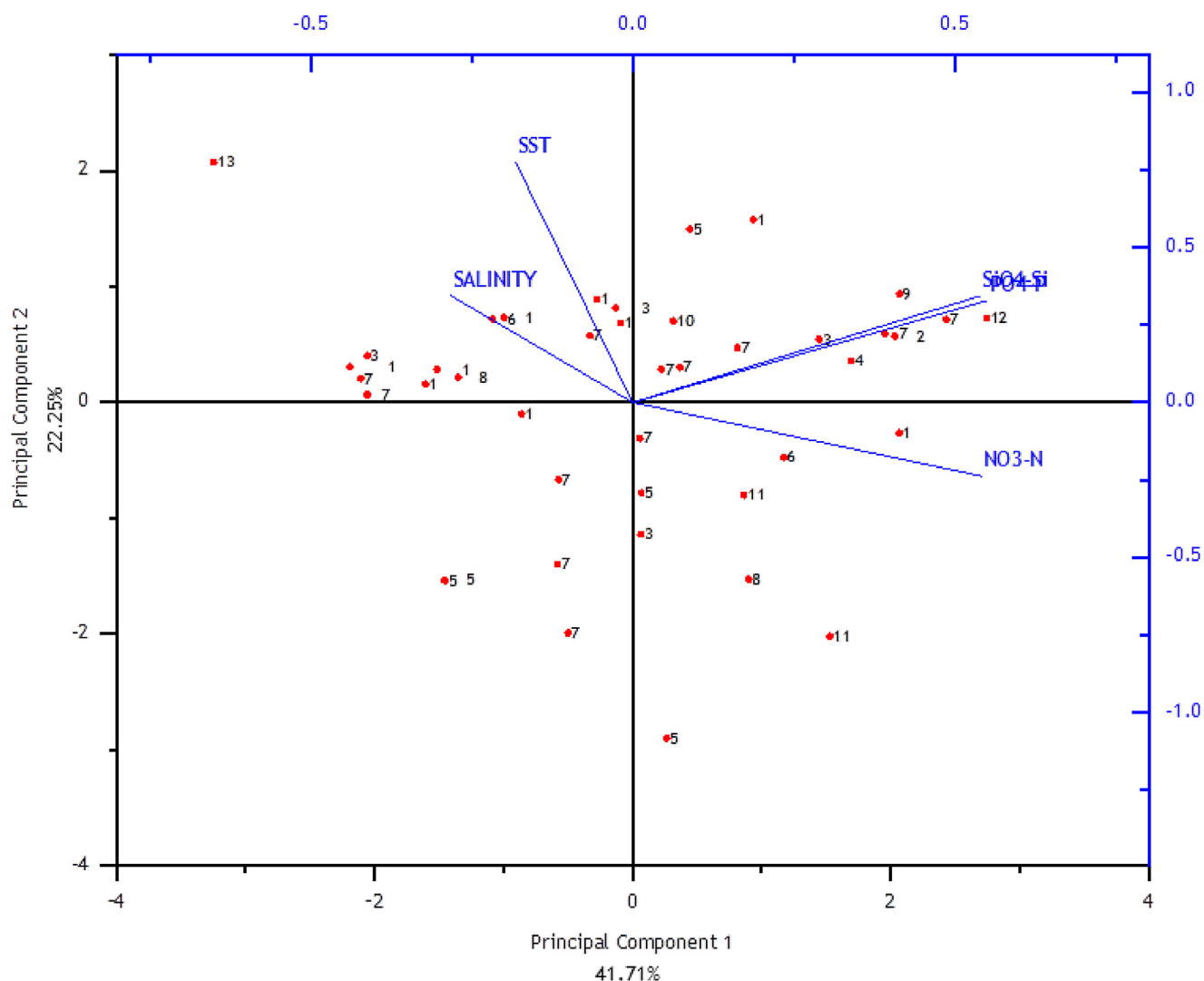


**Figure 4** PCA biplot showing the relationship between the blooms of various phytoplankton with environmental variables. 1. Cyanophyceae (1. *Trichodesmium*), 2–6 Bacillariophyceae (2. *Coscinodiscus*, 3. *Rhizosolenia*, 4. *Leptocylindrus*, 5. *Asterionella*, 6. *Chaetoceros*), 7–10. Dinophyceae (7. *Noctiluca*, 8. *Protoperidinium*, 9. *Karenia*, 10. *Gonyaulax*), 11. Raphidophyceae (11. *Chaetoceros*), 12. Prymnesiophyceae (12. *Prymnesium*), 13. Trebouxiophyceae (13. *Chlorella*).

all the MMBs recorded from this region, *Noctiluca* (dinophyceae) and *Trichodesmium* (cyanophyceae) were the dominant bloom-forming genera and accounted for 34.4% and 31.8% respectively (Figure 1).

### 3.2.1. Temporal occurrences

In the first three decades (1908 to 1937), occurrences of MMBs recorded were limited to those of the dinophyceae. However, over time, blooms of additional taxa emerged. During the last decade alone (2008–2017), blooms of two new taxa, such as the trebouxiophyceae and ciliates were recorded. A remarkable increase in the incidence of MMBs along the Indian peninsula has been recorded from 1948 to 2017. The occurrences of MMBs were increased from 1948 to 2017. Twenty incidents were recorded from 1948 to 1957, 46 incidents occurred from 1998 to 2007, and 50 incidents were also recorded from 2008 to 2017. All through 1948 to 1957, only the dinophyceae remained dominant (80%), while

in the second to the last decade, cyanophyceae was dominant (47.8%) followed by dinophyceae (37.0%). In the last decade, dinophyceae (48.0%) again replaced cyanophyceae (26.0%) and remained dominant. Appearances of dinoflagellate blooms were consistently recorded every decade except between 1938 to 1947 and 1988 to 1997. Also, those of bacillariophyceae appeared regularly from 1958 to 2017 (Figure 1).

MMBs were most pronounced during the PrM season, followed by the SWM season. Blooms of cyanophyceae dominated during the PrM season, while those of dinophyceae dominated during the SWM season. Events attributed to the raphidophyceae and prymnesiophyceae were most pronounced during the SWM season, while those associated with the bacillariophyceae were remarked during PrM and SWM. Blooms of ciliata were featured only in the PrM season, whereas those of trebouxiophyceae were recorded only in the SWM season (Figure 2).

**Table 2** Factor loading matrix of total variance explained by each vector of the principal component analysis.

	Coefficients of PC1	Coefficients of PC2
SST	−0.18153	<b>0.77412</b>
Salinity	−0.28219	<b>0.34455</b>
NO <sub>3</sub> -N	<b>0.54157</b>	−0.23703
PO <sub>4</sub> -P	<b>0.54986</b>	0.32851
SiO <sub>4</sub>	<b>0.54016</b>	0.34339

Note: factors/parameters with significant weight are in bold.

### 3.2.2. Spatial occurrences

From the 154 MMBs reported, 103 were recorded along the western coast. Also, on both the east and west coast, higher incidences were observed along with the southern parts than the northern parts. For instance, 36 out of the 38 events of HABs recorded along the Indian peninsula coast occurred in the southern part. Blooms of the raphidophyceae and prymnesiophyceae were mainly recorded along the southwestern coast. Those of ciliata and trebouxiophyceae occurred along the south-eastern coast alone, whereas, MMBs, those were dominated by the cyanophyceae and dinophyceae were featured both the west and east coast (Figure 3a).

### 3.3. Physiochemical conditions during occurrences of MMBs

#### 3.3.1. Principal component analysis

PCA identified two principal components (PC1 and PC2) with eigenvalues greater than 1. Both components cumulatively explained 63.96% of the total variance in the conditions of the various blooms recorded. Principal component 1 (PC1) accounted for 41.71% (Eigenvalue = 2.08543) of the total variance recorded and had high positive loadings of NO<sub>3</sub>-N (0.54), PO<sub>4</sub>-P (0.55), SiO<sub>4</sub>-Si (0.54). SST and salinity weight recorded were low (−0.18 and −0.28 respectively), implying that water eutrophication was the significant condition explained by this component. However, principal component 2 (PC2) represented 22.25% (Eigenvalue = 1.11257) of the total variance and had higher loading of SST (0.77) and salinity (0.35), indicating that both factors were mainly responsible for the blooms explained by it (Tables 1 and 2). As presented on the biplot, nutrients (NO<sub>3</sub>-N, PO<sub>4</sub>-P, and SiO<sub>4</sub>-Si) had higher weight than SST and salinity, revealing that on the overall, they had more influence on the occurrences of blooms (Figure 4).

#### 3.3.2. Cyanophyceae (*Trichodesmium*), Trebouxiophyceae and Ciliata blooms

Blooms of cyanophyceae (*Trichodesmium*) and trebouxiophyceae (*Chlorella marina*) were recorded under the higher condition of SST (30.26±1.38°C and 31.42±0.00°C respectively) and salinity (34.29±1.16 and 51.75±0.00 psu respectively), as well as the low condition of NO<sub>3</sub>-N (1.50±3.02 μM and 0.01±0.00 μM respectively), NO<sub>2</sub>-N (0.16±0.12 μM and 0.04±0.00 μM respectively), PO<sub>4</sub>-P (0.53±0.82 μM and 0.04±0.00 μM respectively) and SiO<sub>4</sub>-Si (4.10±4.45 μM

and 0.23±0.00 μM respectively) (Table 3). The PCA biplot further validated this, as appearances of both taxa were mainly positively correlated with SST and salinity, and negatively with the nutrients. However, some blooms of the cyanophyceae were positively correlated with PO<sub>4</sub>-P and SiO<sub>4</sub>-Si. The bloom of trebouxiophyceae was more closely associated with water salinity than SST due to the remarked salinity condition in which it was recorded (Figure 4). Hence, high water salinity was a significant driver in the occurrence of its bloom. *Chlorella* strains have been reported to be capable of active growth under high conditions of temperature and salinity up to 42.5°C (Ouyang et al., 2010) and 60 psu (Kakarla et al., 2018) respectively, as well as minimal nutrient conditions (Mata et al., 2010; Nigam and Singh, 2011).

Most of the MMBs dominated by cyanophyceae occurred during high SST and salinity, along with high PO<sub>4</sub>-P and SiO<sub>4</sub>-Si (Figure 4), which tallied with the PC2 in which SST, salinity, PO<sub>4</sub>-P, and SiO<sub>4</sub>-Si had positive loading (Table 2). Thus, the component mainly explained the principal factor responsible for the occurrence of blooms of this taxon – high SST and salinity. The dominance of cyanophyceae, during PrM when SST and salinity conditions were high (≥29°C and 33–35 psu respectively) further established the role of these parameters in driving its blooms (Supplementary Figure 1 and 2). Coincidentally, a significant increase in SST condition (at p<0.01) along the coast of India between 1938 and 1947 matched with the first record of blooms of cyanophyceae (Supplementary Table 4). Similar to this study, SST and salinity have been reported as significant parameters influencing the abundance and distribution of cyanophyceae (*Trichodesmium*) in different oceans (Agarwin et al., 2013; Jiang et al., 2017; Liu and Tang, 2012; Rodier and Borgone, 2008; Rouco et al., 2014, 2016; Walworth et al., 2015). Breitbart et al. (2007) discussed that *Trichodesmium* (cyanophyceae) was capable of growing at a wide temperature range of 20 to 34°C, while Full and Bell (2003) prescribed that a salinity range of 22–43 psu as favorable for growth. The specific range of SST (27.50–33.50°C) and salinity (32.14–35.86 psu), also support the similar observation recorded around the Indian peninsula.

The low NO<sub>3</sub>-N condition under which most blooms of the cyanophyceae (*Trichodesmium*) were recorded in this study (Figure 4) is associated with the diazotrophic nature of the organism and in agreement with available reports (Holl and Montoya, 2005; Mulholland and Capone, 1999). NO<sub>3</sub><sup>-</sup>N deficient condition promotes diazotrophy – the fixation of atmospheric nitrogen into usable forms for growth in *Trichodesmium*, thus enabling it to outgrow other organisms (D'Silva et al., 2012). High SiO<sub>4</sub>-Si level associated with some bloom of the cyanophyceae (*Trichodesmium*) could have resulted from its non-uptake. High PO<sub>4</sub>-P levels recorded during certain events might be connected with its requirement for growth and metabolism (Qu et al., 2019). Also, low wind speed (~5 m/s), water mixing and high stratification prevalent during the PrM season (Supplementary Figures 3 and 4) could have also promoted the buoyancy of the organism, and its ability to form extensive blooms (Capone et al., 1997).

The bloom of ciliata (*Mesodinium rubrum*) was rare, and no information about physicochemical conditions was recorded. However, studies published have identified high

**Table 3** Parameters recorded in association with blooming phytoplankton along the coasts of India (APDRC, 2019, Lotliker et al., 2018, Madhav and Kondalarao, 2004, Madhu et al., 2011a, Madhu et al., 2011, Madhupratap et al., 2000, Martins et al., 2010, Mathew et al., 1988, Annamalai et al., 2016, Matondkar et al., 2004, Matondkar et al., 2006, Minu et al., 2015, Mishra et al., 2005, Mohanty et al., 2007, Nagabhushanam, 1967, Nashad et al., 2017, Nayak et al., 2000, Nayar and Prabhu, 2001, Nunez et al., 2011, Padmakumar et al., 2008, Padmakumar et al., 2010a, Padmakumar et al., 2011, Padmakumar et al., 2016b, Arun et al., 2012, Peter et al., 2016, Prabhu et al., 1965, Prasad, 1958, Raghavan et al., 2010, Raji and Padmavati, 2014, Ramamurthy, 1973, Rao, 1969, Rekha et al., 2012, Sachithanandam et al., 2013, Sahu et al., 2018, Sanilkumar et al., 2009b, Baliarsingh et al., 2016, Sanilkumar et al., 2012, Sargunam et al., 1989, Sasamal et al., 2005, Satpathy et al., 2007, Shaju et al., 2018, Shetye et al., 2013, Shunmugam et al., 2017, Subrahmanyam, 1954, Sulochanan et al., 2014, Tada et al., 2016, Thomas, 2014, Thomas et al., 2014b, Berdalet et al., 2019, Turner et al., 2017, Venugopal et al., 1979, Vijayalakshmy et al., 2018, Xu et al., 2019, Brand and Compton, 2007, Capone et al., 2005, Chandrasekhararao et al., 2018, Chellam and Alagaraswami, 1978, Choudhury and Panigrahy, 1989, Cicily et al., 2013, Daniel et al., 1979, Desa et al., 2005, Devassy, 1974, Devassy et al., 1978, Dharani et al., 2004, Dwivedi et al., 2015, Dwivedi et al., 2012, Dwivedi et al., 2006, Eashwar et al., 2001, Edwards et al., 2006, Ferrante et al., 2012, Figler et al., 2019, Garcia et al., 2019a, Garcia et al., 2019b, Gobler et al., 2017, Gomes et al., 2014, Gopakumar et al., 2009, Al-azri et al., 2007, Harrison et al., 2011, Heil et al., 2014, Hemalatha et al., 2016, Hiremath and Mathad, 2010, Hornell, 1908, Hornell, 1917, Hornell and Nayudu, 1923, Indian Space Research Organization, ISRO 1999, Jabir et al., 2013, Jasmine et al., 2005, Jones et al., 2017, Joseph et al., 2008, Jyothibabu et al., 2017, Jyothibabu et al., 2003, Karthik and Padmavati, 2018, Katti et al., 1988, KNMI Climate Explorer website 2018, KNMI Climate Explorer website 2018, Kumar et al., 2015, Kumar et al., 2009).

Class	Cell density ( $\times 10^5$ cells L <sup>-1</sup> )	SST (°C)	pH	Salinity	DO (mg L <sup>-1</sup> )	NO <sub>3</sub> -N (μM)	NO <sub>2</sub> -N (μM)	NH <sub>3</sub> -N (μM)	PO <sub>4</sub> -P (μM)	SiO <sub>4</sub> (μM)	Chlorophyll <i>a</i> (μg L <sup>-1</sup> )	Reference(s)
<b>1. Bacillariophyceae</b>												
<i>Asterionella japonica</i> (n=6)	61013.07±181495.78 (0.84-545000.00)	26.86±2.83 (24.00-31.58)	7.82±0.00 (7.82-7.82)	32.29±2.45 (28.66-34.83)	5.85±1.78 (3.08-7.46)	1.62±2.06 (0.02-5.05)	0.03±0.04 (0.00-0.09)	-	0.27±0.53 (0.00-1.43)	1.47±2.19 (0.03-5.10)	53.39±51.01 (5.63-132.17)	7; 26; 59; 68; 69
<i>Chaetoceros</i> spp. (n=1)	4.90±0.00	-	-	-	-	-	-	-	-	-	7.50±0.00 (7.50-7.50)	38
<i>C. curvisetus</i> (n=1)	2.75±0.00 (2.75-2.75)	31.30±0.00 (31.30-31.30)	8.05±0.00 (8.05-8.05)	31.96±0.00 (31.96-31.96)	7.03±0.00 (7.03-7.03)	0.29±0.00 (0.29-0.29)	0.01±0.00 (0.01-0.01)	0.74±0.00 (0.74-0.74)	0.02±0.00 (0.02-0.02)	4.22±0.00 (4.22-4.22)	5.80±0.00 (5.80-5.80)	Begum et al. 2015
<i>C. tortissimum</i> (n=1)	617.86±0.00 (617.86-617.86)	29.14±0.00 (29.14-29.14)	7.93±0.00 (7.93-7.93)	28.43±0.00 (28.43-28.43)	3.40±0.00 (3.40-3.40)	4.27±0.00 (4.27-4.27)	0.33±0.00 (0.33-0.33)	-	0.28±0.00 (0.28-0.28)	10.90±0.00 (10.90-10.90)	0.19±0.00 (0.19-0.19)	Karthik and Padmavati (2014)
<i>Coscinodiscus asteromphalus</i> var. <i>centralis</i> (n=1)	35.07±0.00 (35.07-35.07)	27.50±0.00 (27.50-27.50)	8.00±0.00 (8.00-8.00)	34.33±0.00 (34.33-34.33)	7.12±0.00 (7.12-7.12)	2.70±0.00 (2.70-2.70)	0.00±0.00 (0.00-0.00)	-	1.75±0.00 (1.75-1.75)	37.90±0.00 (37.90-37.90)	104.90±0.00 (104.90-104.90)	26; 63
<i>Fragilaria oceanica</i> (n=1)	368.00±0.00 (368.00-368.00)	-	-	32.36±0.00 (32.36-32.36)	-	0.03±0.00 (0.03-0.03)	-	-	0.03±0.00 (0.03-0.03)	-	123.48±0.00 (123.48-123.48)	11
<i>Hemidiscus hardmannianus</i> (n=1)	0.32±0.00 (0.32-0.32)	-	-	-	-	-	-	-	-	-	-	71
<i>Leptocylindrus</i> sp. (n=1)	14.79 ± 0.00 (14.79-14.79)	29.30±0.00 (29.30-29.30)	-	29.30±0.00 (29.30-29.30)	8.16±0.00 (8.16-8.16)	2.62±0.00 (2.62-2.62)	-	-	1.77±0.00 (1.77-1.77)	9.83±0.00 (9.83-9.83)	-	43
<i>Pleurosigma</i> sp. (n=1)	20.00±0.00 (20.00-20.00)	-	-	-	-	-	-	-	-	-	-	11
<i>Rhizosolenia</i> sp. (n=1)	10.00±0.00 (10.00-10.00)	-	-	-	-	-	-	-	-	-	-	11
<i>R. alata</i> (n=3)	1.02±0.53 (0.41-1.36)	27.00±2.29 (24.50-29.00)	8.30±0.14 (8.20-8.40)	34.67±0.58 (34.00-35.00)	4.25±0.69 (3.46-4.76)	0.72±0.90 (0.10-1.76)	0.11±0.04 (0.08-0.14)	-	0.82±0.56 (0.40-1.45)	16.38±8.55 (11.40-26.26)	12.31±3.19 (8.64-14.30)	8; 21

(continued on next page)

Table 3 (continued)

Class	Cell density ( $\times 10^5$ cells L <sup>-1</sup> )	SST (°C)	pH	Salinity	DO (mg L <sup>-1</sup> )	NO <sub>3</sub> -N ( $\mu$ M)	NO <sub>2</sub> -N ( $\mu$ M)	NH <sub>3</sub> -N ( $\mu$ M)	PO <sub>4</sub> -P ( $\mu$ M)	SiO <sub>4</sub> ( $\mu$ M)	Chlorophyll <i>a</i> ( $\mu$ g L <sup>-1</sup> )	Reference(s)
<i>R. imbricata</i> (n=1)	240.00±0.00 (240.00-240.00)	31.14±0.00 (31.14-31.14)	8.23±0.00 (8.23-8.23)	34.21±0.00 (34.21-34.21)	6.50±0.00 (6.50-6.50)	0.27±0.00 (0.27-0.27)	0.00±0.00 (0.0-0.00)	-	0.00±0.00 (0.0-0.00)	0.00±0.00 (0.0-0.00)	-	Saravanae et al., 2016
<b>Mean ± SD (Range)</b> n = 17	<b>25019.74±116139.89</b> <b>(0.32-545000.00)</b>	<b>27.71±2.65</b> <b>(24.00-31.58)</b>	<b>8.09±0.20</b> <b>(7.82-8.40)</b>	<b>32.52±2.38</b> <b>(28.43-35.00)</b>	<b>5.73±1.74</b> <b>(3.08-8.16)</b>	<b>1.46±1.67</b> <b>(0.18-5.05)</b>	<b>0.08±0.11</b> <b>(0.00-0.33)</b>	<b>0.37±0.52</b> <b>(0.00-0.74)</b>	<b>0.51±0.68</b> <b>(0.00-1.77)</b>	<b>8.15±10.92</b> <b>(0.00-37.90)</b>	<b>44.12±49.46</b> <b>(0.19-132.17)</b>	
<b>2. Ciliatea</b>												
<i>Mesodinium rubrum</i> (n=1)	100.00±0.00 (100.00-100.00)	-	-	-	-	-	-	-	-	-	-	61
<b>3. Cyanophyceae</b>												
<i>Trichodesmium erythraeum</i> (n=21)	13064.38±38283.15 (0.62-115142.40)	30.23±1.53 (27.50-33.50)	8.13±0.18 (7.90-8.40)	33.99±1.10 (32.14-35.47)	6.03±2.00 (2.66-9.11)	1.61 ± 3.25 (0.00-10.00)	0.19 ± 0.11 (0.03-0.29)	-	0.58±0.87 (0.00-2.80)	4.28±4.64 (0.00-14.00)	19.71 ± 38.98 (0.08-127.00)	4; 10; 13; 23; 27; 28; 29; 31; 37; 41; 42; 48; 52; 57; 69; 70
<i>T. thiebautii</i> (n=2)		29.07±0.00 (29.07-29.07)	-	35.26±0.00 (35.26-35.26)	9.11±0.00 (9.11-9.11)	0.03 ± 0.00 (0.03-0.03)	-	0.84 ± 0.00 (0.84-0.84)	0.11 ± 0.00 (0.11-0.11)	1.29 ± 0.00(1.29-1.29)	-	48; 57
<i>T. hildebrandtii</i> (n=1)	3.00±0.00 (3.00-3.00)	-	-	-	-	-	-	-	-	-	-	51
<i>Trichodesmium</i> sp. (n=4)	0.04±0.00 (0.04-0.04)*	30.38±0.28 (30.00-30.61)	-	35.40±0.52 (34.67-35.86)	5.84±0.06 (5.80-5.89)	0.79±0.31 (0.58-1.01)	0.03±0.00 (0.03-0.03)	-	0.22±0.13 (0.13-0.31)	2.27±0.00 (2.27-2.27)	14.82±18.02 (2.50-35.50)	13; 23; 54
<b>Mean ± SD (Range)</b> n = 49	<b>11758.24±36329.26</b> <b>(0.73-115140.00)</b>	<b>30.26±1.38</b> <b>(27.50-33.50)</b>	<b>8.13±0.18</b> <b>(7.90-8.40)</b>	<b>34.29±1.16</b> <b>(32.14-35.86)</b>	<b>6.00±1.83</b> <b>(2.66-9.11)</b>	<b>1.50±3.02</b> <b>(0.00-10.00)</b>	<b>0.16±0.12</b> <b>(0.03-0.29)</b>	<b>26.85±42.77(0.00-2.80)</b> <b>(0.10-125.0)</b>	<b>0.53±0.82</b> <b>(0.00-14.00)</b>	<b>4.10±4.45</b> <b>(0.00-14.00)</b>	<b>18.58±34.62</b> <b>(0.08-127.00)</b>	
<b>4. Dinophyceae</b>												
<i>Noctiluca miliaris</i> (n= 38)	511.14± 1695.85 (0.01-8100.00)	28.14±1.90 (25.02-32.13)	8.05±0.24 (7.54-8.40)	34.12±2.75 (25.00-40.00)	5.42±1.51 (2.20-9.16)	2.13±2.75 (0.00-11.06)	0.51±0.86 (0.00-3.28)	5.18±6.05 (1.21-14.90)	0.91±1.28 (0.00-4.56)	6.38±9.49 (0.11-32.61)	9.01±8.08 (0.34-26.50)	2; 3; 6; 11; 12; 14; 15; 16; 17; 18; 19; 20; 24; 25; 30; 32; 35; 36; 37; 39; 40; 41; 44; 45; 46; 47; 48; 49; 53; 62; 65; 66; 69; 72; 75; 76

(continued on next page)

**Table 3** (continued)

Class	Cell density ( $\times 10^5$ cells L <sup>-1</sup> )	SST (°C)	pH	Salinity	DO (mg L <sup>-1</sup> )	NO <sub>3</sub> -N ( $\mu$ M)	NO <sub>2</sub> -N ( $\mu$ M)	NH <sub>3</sub> -N ( $\mu$ M)	PO <sub>4</sub> -P ( $\mu$ M)	SiO <sub>4</sub> ( $\mu$ M)	Chlorophyll <i>a</i> ( $\mu$ g L <sup>-1</sup> )	Reference(s)
<i>Karenia mikimotoi</i> (n=3)	38.46±64.18 (0.90-112.57)	29.25±1.52 (28.37-31.00)	7.56±0.39 (7.25-8.00)	32.04±4.78 (26.52-34.80)	2.40±0.71 (1.90-2.90)	2.26±1.62 (0.80-4.00)	0.14±0.16 (0.02-0.25)	4.85±0.00 (4.85-4.85)	5.74±3.71 (1.46-8.00)	32.30±0.00 (32.30-32.30)	56.80±0.00 (56.80-56.80)	22; 33; 59
<i>Cochlodinium</i> sp. (n=1)	1.40±0.00 (1.40-1.40)	27.00±0.00 (27.00-27.00)	7.40±0.00 (7.40-7.40)	33.00±0.00 (33.00-33.00)	-	2.40±0.00 (2.40-2.40)	24.52±0.00 (24.52- 24.52)	14.72±0.00 (14.72- 14.72)	15.95±0.00 (15.95- 15.95)	-	1.20±0.00 (1.20-1.2)	40
<i>Gonyaulax polygramma</i> (n=2)	2555.00±3457.75 (110.00-5000.00)	29.55±0.00 (29.55-29.55)	-	34.10±0.00 (34.10-34.10)	6.38±0.00 (6.38-6.38)	1.65±0.00 (1.65-1.65)	-	-	0.60±0.00 (0.60-0.60)	10.00±0.00 (10.00-10.00)	13.15±0.00 (13.15-13.15)	52; Padmakumar et al. 2018
<i>Dinophysis</i> sp. (n=1)	3.10±0.00 (3.10-3.10)	-	-	-	-	-	-	-	-	-	-	38
<i>Prorocentrum</i> sp. (n=1)	1.50±0.00 (1.50-1.50)	-	-	-	-	-	-	-	-	-	-	38
<i>Protoperidinium</i> sp. (n=1)	5000.0±0.0 (5000.0-5000.0)	29.00±0.00 (29.00-29.00)	8.34±0.00 (8.34-8.34)	34.64±0.00 (34.64-34.64)	8.65±0.00 (8.65-8.65)	0.00±0.00 (0.00-0.00)	-	-	0.25±0.00 (0.25-0.25)	1.68±0.00 (1.68-1.68)	0.90±0.00 (0.90-0.90)	63
<i>Protoperidinium divergens</i> (n=1)	350.00±0.00 (350.00-350.00)	26.00±0.00 (26.00-26.00)	7.70±0.00 (7.70-7.70)	31.00±0.00 (31.00-31.00)	2.23±0.00 (2.23-2.23)	1.12±0.00 (1.12-1.12)	1.12±0.00 (1.12-1.12)	-	0.29±0.00 (0.29-0.29)	9.33±0.00 (9.33-9.33)	10.96±0.00 (0.13-0.13)	55
<b>Mean±SD (Range)</b>	<b>644.19±1785.35</b> (0.01-8100.00)	<b>28.22±1.83</b> (25.02- 32.13)	<b>7.94±0.33</b> (7.25-8.40)	<b>33.80±2.84</b> (25.00- 40.00)	<b>5.03±1.72</b> (1.90-9.16)	<b>2.12±2.47</b> (0.00- 11.06)	<b>1.61±5.31</b> (0.00- 24.52)	<b>5.99±5.83</b> (1.21- 14.90)	<b>1.87±3.45</b> (0.00- 15.95)	<b>7.93±10.41</b> (0.11-32.61)	<b>10.36±12.27</b> (0.13-56.80)	
<b>5. Prymnesiophyceae</b>												
<i>Prymnesium parvum</i> (n=1)	800.00±00.00 (800.00-800.00)	28.00±0.00 (28.00-28.00)	8.00±0.00 (8.00-8.00)	34.00±0.00 (34.00-34.00)	1.50±0.00 (1.50-1.50)	5.60±0.00 (5.60-5.60)	-	-	1.90±0.00 (1.90-1.90)	62.00±0.00 (62.00-62.00)	13.54±0.00 (13.54-13.54)	73
<i>Helladosphaera</i> spp. (n=1)	135.23±0.00 (135.23-135.23)	-	7.72±0.00 (7.72-7.72)	36.36±0.00 (36.36-36.36)	6.51±0.00 (6.51-6.51)	6.84±0.00 (6.84-6.84)	0.97±0.00 (0.97-0.97)	9.10±0.00 (9.10-9.10)	1.22±0.00 (1.22-1.22)	8.27±0.00 (8.27-8.27)	-	56
<i>P. globosa</i> (n=1)	25800.00±0.00 (25800.00-25800.00)	-	-	-	-	0.00±0.00 (0.00-0.00)	-	-	0.30±0.00 (0.30-0.30)	-	5.06±0.00 (5.06-5.06)	33
<b>Mean ± SD (Range)</b>	<b>8911.74±14629.44</b> (135.23-25800.00)	<b>28.00±1.00</b> (26.00- 28.00)	<b>7.86±0.20</b> (7.72-8.00)	<b>32.09±3.78</b> (28.00- 36.36)	<b>6.03±3.96</b> (1.41- 11.00)	<b>5.45±3.14</b> (0.00-7.80)	<b>0.32±0.56</b> (0.00-0.97)	<b>9.10±0.00</b> (9.10-9.10)	<b>1.78±1.91</b> (0.30-5.00)	<b>19.18±28.64</b> (3.00-62.00)	<b>8.82±3.76</b> (5.06-13.54)	
<b>6. Raphidophyceae</b>												
<i>Chatonella marina</i> (n=4)	768.18±1355.44 (45.00-2800.00)	27.08±2.12 (25.56-30.20)	7.55±0.43 (7.06-7.86)	32.30±2.79 (29.33-34.87)	2.99±2.57 (0.22-6.42)	3.34±3.90 (0.14-9.02)	0.06±0.05 (0.02-0.12)	0.51±0.01 (0.50-0.51)	1.23±1.23 (0.27-2.99)	4.26±2.04 (2.81-5.70)	16.96±14.12 (8.30-37.97)	26; 39; 50; 64; 65; 70; 74
<b>7. Trebouxiophyceae</b>												
<i>Chlorella marina</i> (n=1)	2.12±0.00 (2.12-2.12)	31.42±0.00 (31.42-31.42)	7.62±0.00 (7.62-7.62)	51.75±0.00 (51.75-51.75)	5.40±0.00 (5.40-5.40)	0.01±0.00 (0.01-0.01)	0.04±0.00 (0.04-0.04)	6.75±0.00 (6.75-6.75)	0.04±0.00 (0.04-0.04)	0.23 ±0.00 (0.23-0.23)	18.41±0.00 (18.41-18.41)	5

Note: Reference number is mentioned in the reference section in []

\* implies value presented in filament/L, n = number of events

water temperature, salinity, irradiance, column stratification stability, and low nutrient conditions as factors favoring its bloom (Liu et al., 2012; van Beusekom et al., 2009). The PrM season in which its bloom occurred was characterized by similar conditions along the coast of India (Supplementary Figures 1–7). Considering the ability of the cyanophyceae (*Trichodesmium*), trebouxiophyceae (*Chlorella marina*) and ciliatea (*Mesodinium rubrum*) to grow favorably under high water temperature and salinity, the incidence of their blooms could increase along the Indian peninsula coast in the near future, as the SST and salinity conditions increase rapidly (Supplementary Figure 3).

### 3.3.3. Blooms of Bacillariophyceae, Prymnesiophyceae, and Raphidophyceae

Blooms attributed to the bacillariophyceae, prymnesiophyceae, and raphidophyceae were mainly recorded under a lower water temperature condition of  $27.71 \pm 2.65^\circ\text{C}$ ,  $28.00 \pm 1.00^\circ\text{C}$ , and  $27.08 \pm 2.12^\circ\text{C}$  respectively, and lower salinity of  $32.52 \pm 2.38$ ,  $32.09 \pm 3.78$  and  $33.30 \pm 2.79$  psu respectively as compared to those of the cyanophyceae, trebouxiophyceae, and dinophyceae. Nutrient levels in water during the incidents of prymnesiophyceae and raphidophyceae were much higher ( $5.45 \pm 3.14$  and  $3.34 \pm 3.90$   $\mu\text{M}$  for  $\text{NO}_3\text{-N}$ ,  $1.78 \pm 1.91$  and  $1.23 \pm 1.23$   $\mu\text{M}$  for  $\text{PO}_4\text{-P}$ ,  $19.18 \pm 28.6$  and  $4.26 \pm 2.04$   $\mu\text{M}$  for  $\text{SiO}_4\text{-Si}$  respectively).  $\text{SiO}_4\text{-Si}$  concentration was also high ( $8.15 \pm 10.9$   $\mu\text{M}$ ), while  $\text{NO}_3\text{-N}$ ,  $\text{NO}_2\text{-N}$ ,  $\text{NH}_3\text{-N}$  and  $\text{PO}_4\text{-P}$  ( $1.46 \pm 1.67$   $\mu\text{M}$ ,  $0.08 \pm 0.11$   $\mu\text{M}$ ,  $0.37 \pm 0.52$   $\mu\text{M}$ , and  $0.51 \pm 2.04$   $\mu\text{M}$  respectively) were low (Table 3; Figure 4). PC1 indicates that the high and positive weightage of nutrients, i.e.,  $\text{NO}_3\text{-N}$  (0.54),  $\text{PO}_4\text{-P}$  (0.55), and  $\text{SiO}_4\text{-Si}$  (0.54), might have been played a crucial role in developing the prymnesiophyceae and raphidophyceae dominated blooms around the Indian peninsula. Hence, PC1 primarily described the key physicochemical factors, i.e., nutrients, which were responsible for the blooms of both taxa. The lower factor weight recorded for SST and salinity revealed that they had minimal influence on the occurrence of their blooms (Table 2).

During the SWM season when blooms of the raphidophyceae and prymnesiophyceae were mostly recorded, eutrophication was apparent along the coast of India (Figure 2; Supplementary Figures 5–7). This high nutrient condition occurred as a result of the upwelling of nutrient-rich deep water and the input of run-offs. Blooms of bacillariophyceae may be primarily triggered by the bioavailability of high nutrients concentration (eutrophication), including silicates, and secondarily influenced by rainfall and river run-off. Therefore, bacillariophyceae blooms were reported in both the PrM and SWM period. Blooms of raphidophyceae and prymnesiophyceae appeared mainly along the southern coast (mainly the south-west), where these conditions were most prevalent (Supplementary Figures 3–7; Figure 4). The low surface salinity associated with their occurrences might be due to the input of freshwater from local rainfall and run-off, as well as the southward advection of low saline waters from the northwest coast by the West Indian coast current, WICC (Behara et al., 2019; Kumar and Mathew, 1997; Subrahmanyam et al., 2011).

Low nutrient conditions observed during the blooms of the bacillariophyceae could be as a result of the fast consumption of nutrients during bloom. Previous studies carried

out in the field as well as in the laboratory revealed that the concentration of macronutrients, e.g.,  $\text{NO}_3\text{-N}$ ,  $\text{PO}_4\text{-P}$  and  $\text{SiO}_4\text{-Si}$  (in the case of diatoms) mostly limited the growth and biomass development of the bacillariophyceae, raphidophyceae and prymnesiophyceae, wherein faster growth and higher cell density was reached under nutrient replete conditions (Gypens et al., 2007; Schoemann et al., 2005; Wang et al., 2011). The persistent appearance of their blooms in recent decades could be an indication of increasing eutrophication along the coast of India. Madeswaram et al. (2018) assessed the water quality along the coast of India from 1990 to 2015 and revealed that the annual average of  $\text{NO}_3\text{-N}$  increased from  $< 5$   $\mu\text{M}$  to  $6$   $\mu\text{M}$ ,  $\text{NH}_3\text{-N}$  from  $< 0.5$  to  $1$   $\mu\text{M}$ ,  $\text{PO}_4\text{-P}$  from  $< 1$  to  $1.7$   $\mu\text{M}$ , and  $\text{SiO}_4\text{-Si}$  from  $< 2$  to  $10$   $\mu\text{M}$  at Kerala coast, Southwest India where most bloom incidents have been reported. This observation might be attributed to increasing sewage discharge, industrial wastes, and agricultural run-off as a result of an increase in population and urbanization (Prema et al., 2017).

### 3.3.4. Dinophyceae bloom

In general, blooms of the dinophyceae were recorded under wide-ranging SST ( $25.02\text{--}32.13^\circ\text{C}$ ), pH ( $7.25\text{--}8.40$ ), salinity ( $25.00\text{--}40.00$  psu),  $\text{NO}_3\text{-N}$  ( $0.00\text{--}11.60$   $\mu\text{M}$ ),  $\text{NO}_2\text{-N}$  ( $0.00\text{--}24.52$   $\mu\text{M}$ ),  $\text{NH}_3\text{-N}$  ( $1.21\text{--}14.90$   $\mu\text{M}$ ),  $\text{PO}_4\text{-P}$  ( $0.00\text{--}15.95$   $\mu\text{M}$ ) and  $\text{SiO}_4\text{-Si}$  ( $0.11\text{--}32.61$   $\mu\text{M}$ ) conditions (Table 3; Figure 4). This observation corroborates the apparent appearance of blooms of this taxon every season along the coast of India. However, the dominance of its blooms during SWM and along the west coast (particularly south-west coast) suggested that water eutrophication had a major influence. Blooms of *Karenia* and *Cochlodinium* mostly occurred under high  $\text{NO}_3\text{-N}$  ( $2.26 \pm 1.62$  and  $2.40 \pm 0.00$   $\mu\text{M}$  respectively) and  $\text{PO}_4\text{-P}$  ( $5.74 \pm 3.71$ ,  $15.95 \pm 0.00$   $\mu\text{M}$  respectively), while those of *Noctiluca*, *Gonyaulax*, and *Protoberidinium* were recorded under low conditions ( $2.13 \pm 2.75$ ,  $1.65 \pm 0.00$  and  $1.12 \pm 0.00$   $\mu\text{M}$  respectively for  $\text{NO}_3\text{-N}$ , and  $0.91 \pm 1.28$ ,  $0.60 \pm 0.00$  and  $0.27 \pm 0.03$   $\mu\text{M}$  respectively for  $\text{PO}_4\text{-P}$ ).  $\text{SiO}_4\text{-Si}$  concentration was high during the bloom of most of the genera in this taxon (Table 3).

The low nutrient condition recorded during the bloom of *Noctiluca*, *Gonyaulax*, and *Protoberidinium* could be as a result of high nutrient uptake by bloom biomass, and their ability to exhibit mixotrophy by simultaneously taking up nutrients in the water and also feeding on other smaller ( $5$  to  $60$   $\mu\text{m}$ ) phytoplankton which is increasing in abundance in response to nutrient input (Jeong et al., 2005; Zhang et al., 2016). Both laboratory and field studies have revealed that diatoms, prymnesiophytes, cryptophytes and other small-sized phytoplankton of  $5$  to  $60$   $\mu\text{m}$  constitute important food source for these dinoflagellates (Gomes et al., 2014; Gribble, 2007; Jeong et al., 2005; Kopuz et al., 2014; Stoecker et al. 2017; Turkoglu, 2013; Zhang et al., 2016). These taxa have been reported to be dominant along the southwestern part of the Indian peninsula coast and increase in biomass during the SWM season, which is characterized by nutrient upwelling (Ahmed et al., 2016; Rai and Rajashekhar, 2014; Thomas et al., 2013). The highest incidence of blooms of *Noctiluca*, mainly red *Noctiluca* was recorded in the same location and season (Supplementary Table 1; Figures 2 and 3).

It was observed that green *Noctiluca* predominantly formed bloom in the northwest coast of India, where lower water mixing and higher water column stability and stratification are recorded. The supply of SiO<sub>4</sub>-Si in the upper mixed layer of the area is limited as compared to NO<sub>3</sub>-N and PO<sub>4</sub>-P due to mixing, which does not reach the silicline (Sarma et al., 2019). This condition is likely to have conferred a better condition for the photosynthetic green *Noctiluca* than the heterotrophic red one. It was observed that the range of SST and salinity conditions (25.02–32.13°C and 25.00–40.00 psu respectively) under which blooms of *Noctiluca* were recorded in this study exceeded the optimum of 10–30°C and 28–36 psu respectively specified in the literature (Harrison et al. 2011; Huang and Qi, 1997; Miyaguchi et al., 2006; Tada et al., 2004). This phenomenon implies that the strains which form bloom along the coast of India are adapted to high temperature and salinity. Hence the rising SST and salinity conditions along the Indian peninsula might not pose a hindrance to growth and the formation of their blooms under favorable environmental conditions of high nutrients and prey abundance. Increasing eutrophication, SST, and surface salinity (Supplementary Table 4) could be promoting blooms of the dinophyceae along the coast of India.

### 3.4. Consequences of MMBs around the Indian peninsula

#### 3.4.1. Impact on human health

Harmful blooms of marine microalgae around the Indian peninsula coast were associated with an adverse impact on human health on different occasions during the study period. Two paralytic shellfish poisoning (PSP) outbreaks were recorded. The first, which occurred in 1981 at Valayar village, Tamil Nadu, southeast coast of India, resulted in the death of 3 individuals while 85 others were hospitalized. The incident happened following the consumption of contaminated *Meretrix casta* by the affected persons (Silas et al., 1982). During the second occasion, which was recorded in September 1997 along Vizhinjam, Kerala, southwest coast of India, *Perna indica* was the vector involved, and 7 deaths, including over 500 hospitalizations were documented (Karunasagar et al., 1998). In general, the victims displayed symptoms typical of PSP, including vomiting, numbness of limbs, and tingling sensation in the facial area. The causative taxa could not be identified in both instances. Similar outbreaks in neighboring waters of Malaysia and the Philippines were recently attributed to the toxic blooms of *Alexandrium tamivayanchi* (Mohammad-Noor et al., 2018) and *Pyrodinium bahamense* (Ching et al., 2015; Suleiman et al., 2017).

Two human intoxication events linked to ciguatera fish poisoning (CFP) were also recently reported. Both events resulted from the consumption of red snapper (*Lutjanus bohar*) contaminated with ciguatoxin (CTX) from an unknown toxic dinoflagellate suspected to be *Gambierdiscus* (dinophyceae). The initial episode, which was recorded in June 2015 along with Mangalore, Karnataka, involved two individuals (Rajeish et al., 2016), while the second one recorded in January 2016 along Trivandrum, Kerala, involved 6 individuals (Rajisha et al., 2017). No human death was recorded

during both events. However, the victims presented symptoms including abdominal pain, vomiting, diarrhea, chest burning, paresthesia of the upper and lower limbs, the reversal of hold and old sensations, and tingling sensation in the throat and tip of the tongue within 4–6 hours of consuming the contaminated fish. Mice injected with extract prepared from the tissue of the fish sample displayed signs typical of ciguatera poisoning, including reduced movement activity, diarrhea, paralysis of hind limbs, gasping for air, difficulty in breathing, and finally death. Ciguatoxin-1 (CTX-1) was detected at 17 ng and 16.25 ng per 100 g of flesh during the respective events. The authors emphasized the need for the country to institute a surveillance system that will be geared towards screening seafood landed across the coast of the country as well as consumer's awareness for their safety.

On particular occasions, the strong stench emanating from the massive bloom of *Helladosphaera* sp. (prymnesiophyceae) and *Karenia brevis* (dinophyceae) along Malabar shore, southwestern coast of India was associated with respiratory difficulty in children living in nearby areas (Ramaiah et al., 2005; Robin et al., 2013). The particular event related to *Helladosphaera* sp. resulted in the hospitalization of over 200 children who developed symptoms like chest pain, nausea, and short periods of breathlessness (Ramaiah et al., 2005). In order to confirm whether the toxicity observed during *K. brevis* bloom was due to the production of the neurotoxin, Robin and colleagues subjected extract of mussel (*P. indica*) sampled from the site of bloom to mouse bioassay and observed that the symptoms recorded were not due to such (Robin et al., 2013). Generally, HAB forming species produce toxins under physiological stress conditions. The observation of Robin et al. (2013) might have occurred due to very little or no accumulation of brevetoxins within a primary consumer-like *P. indica*, as *P. indica* can sustain a long time without opening its valves, and avoiding siphoning in adverse hydrological conditions.

#### 3.4.2. Impact of HABs on the ecosystem and associated biota

Three events of harmful *Trichodesmium erythraeum* (cyanophyceae) blooms were associated with the mortality of aquatic animals (Chacko, 1942; Chidambaram and Unny, 1944; Ramamurty, 1970). In a severe case reported by Chacko (1942) at Krusaddai Island, 756 holothurians, 250 fishes belonging to 16 genera and other bottom fauna like crabs, sea urchins, and mollusks were killed along a shoreline of about 2.4 km in one day. Death of the affected animals was mainly attributed to asphyxiation, due to hypoxic conditions in water that resulted from excessive respiration and decay of bloom. Water discoloration, the emanation of noxious smell, and low fish catch were also reported during other blooms of *T. erythraeum* (Karthik and Padmavati, 2017; Krishnan et al., 2007; Mohanty et al., 2010; Verlançar, 1978).

Six incidents of *Noctiluca scintillans* (dinophyceae) bloom were associated with the death of aquatic fauna (Aiyar, 1936; Anantharaman et al., 2010; Bimachar and George, 1950; Mohammed, 2003; Mohammed et al., 2007; Shayak et al., 2005). Marked reduction in fish catch was also documented on five occasions (Bimachar and George,

1950; Devassy and Nair, 1987; Jugnu, 2006; Padmakumar et al., 2010b, 2016a) while in another event fishes caught by fishermen were more or less in exhausted condition (Aiyar, 1936). The death of aquatic biota recorded during blooms of this organism was mainly linked to the release of mucoid substances, which altered the viscosity of water and caused mechanical obstruction, low oxygen condition, and asphyxiation. On another occasion, Naqvi et al. (1998) reported that the mucoid substance released during a bloom of the same organism made smaller fishes bioluminescent at night and therefore exposed them to the predatory ones.

On two occasions, the harmful bloom of *Karenia mikimotoi* (dinophyceae) produced hypoxic conditions in water and also obstructed the gill lamellae of fish, causing asphyxiation and death (Iyer et al., 2008; Robin et al., 2013). Many economic fish species, e.g., *Sardinella longiceps*, *Arius arius*, *Seganus javus*, *Psettodes erumei*, *Monacanthus hispidus*, *Diodon hystrix*, *Anguilla* sp. and *Rastrelliger kanagurta* were killed and the livelihood of local fishermen was also adversely impacted. Iyer et al. (2008) reported that the concentration of H<sub>2</sub>S in water reached 1.6 mg L<sup>-1</sup> following the decomposition of biomass at the end of the bloom. Detrimental *Gonyaulax* (dinophyceae) blooms have also impacted marine waters around the Indian peninsula in a similar manner to those of *K. mikimotoi* (Modayil, 2004; Prakash and Sarma, 1964).

*Chatonella marina* (raphidophyceae) blooms were implicated in the mass mortality of bivalves, e.g., *Macra violacea*, demersal fishes, e.g., Eel, sciaenids, croakers, green mussels, and mole crab, and shrimp fishes, e.g., *Chanos chanos*, *Mugucephalus* sp., *Penaeus monodon*, *Penaeus indicus*, *Melapenaeus dobsoni*, and *M. affinis*, etc. (Jugnu, 2006; Sarangi and Mohammed, 2011). In a particular event, an unusually high catch of catfish in disoriented condition was reported (Jugnu, 2006). The toxicity was proposed to be due to the production of haemolytic compounds and hypoxia. A bloom of *Hemidiscus hardmannianus* (bacillariophyceae) was also associated with massive mortality of *Sardinella longiceps*, *Muraenesox cinereus*, *Arius maculatus*, *Lutjanus malabaricus*, *M. dobsoni*, etc., (Subramanian and Purushothaman, 1985), while that of *Asterionella glacialis* (bacillariophyceae) was linked with a decline in the fish catch (Satpathy and Nair, 1996).

### 3.4.3. Impact of MMBs on socio-economic status

Harmful events of MMBs around the Indian peninsula pose adverse socio-economic implications. Such effects could be linked with the cost of cleaning affected areas, purifying water for various use, loss of income and revenue associated with a reduction in yield of fish resource and demand for seafood, loss of jobs and productivity, morbidity and treatment, investigation, as well as local aesthetics (Adams et al., 2018; Hoagland et al., 2002). According to Hoagland and Scatasta (2006), economic losses from HABs could be a difficult task, owing to indirect effects that might not be readily accounted for. Financial losses regarding HABs around the Indian peninsula have not been estimated and reported to date. However, it is worthy to note that the west coast of the Indian peninsula where HABs were most pronounced contributes the majority (69.8%) of marine fish landings in the country (Sathianandan, 2017). Substantial impacts could occur in the near future amidst increas-

ing occurrences of blooms. A comprehensive evaluation of economic losses associated with the occurrences of MMBs around the Indian peninsula is highly required for the effective management of India's fisheries potential.

## 4. Conclusions

A total of 154 events of MMBs were recorded from 1908 to 2017 around the Indian peninsula. Bloom forming species of these MMBs were related to 24 genera belonging to seven taxonomic classes, including cyanophyceae, bacillariophyceae, dinophyceae, raphidophyceae, prymnesiophyceae, trebouxioophyceae, and ciliata. In the initial years of the 20<sup>th</sup> century, only dinophyceae blooms were reported. Those of cyanophyceae were reported only after 1937. After that, the bacillariophyceae became reported as bloom-forming species after 1957. The trebouxioophyceae and ciliata appeared as new bloom-forming taxa in the last decade (2008–2017). Blooms of *Noctiluca* (dinophyceae) and *Trichodesmium* (cyanophyceae) were most predominant around the Indian peninsula and accounted for 34.4% and 31.8% of all incidents, respectively. Occurrences related to the cyanophyceae (*Trichodesmium*) were mainly driven by high SST and salinity, while those of bacillariophyceae, dinophyceae, raphidophyceae and, prymnesiophyceae were promoted by eutrophication. In addition to high nutrient conditions, blooms of *Noctiluca* (dinophyceae) were related to the abundance of prey organisms. Mainly, the cyanophyceae, bacillariophyceae, dinophyceae, raphidophyceae, and prymnesiophyceae caused HABs around the Indian peninsula. The impacts these HABs included environmental perturbation, mass mortality of aquatic fauna, altered fishing activity, human intoxication, e.g., paralytic and ciguatera shellfish poisoning, and even death. The knowledge of the environmental conditions promoting blooms along the coast of India is useful for bloom management planning and decisions. Surveillance programs for phycotoxins levels in the environment and local seafood, as well as sustainable environmental practices, will help to curtail the occurrences and spread of MMBs as well as related HABs around the Indian peninsula.

## Acknowledgments

The authors would like to thank the TWAS-CSIR fellowship for providing funding for Ph.D. research and study. Climate/oceanographic data were provided by the Asia-Pacific-Data-Research Center (<http://www.apdrc.soest.hawaii.edu>), Koininklijk Nederlands Meteorologisch Instituut (<https://www.knmi.nl>) and National Oceanic and Atmospheric Sciences ([www.esrl.noaa.gov](http://www.esrl.noaa.gov)). This manuscript is assigned CSIR-CSMCRI contribution number 161/2018.

## Supplementary materials

Supplementary material associated with this article can be found, in the online version, at <https://doi.org/10.1016/j.oceano.2020.08.008>.

## References

- The numbers in square brackets refer to Table 3.
- Adams, C.M., Larkin, S.L., Hoagland, P., Sancewich, B., 2018. Assessing the economic consequences of Harmful Algal Blooms: A Summary of existing literature, research methods, data, and information Gaps. In: Shumway, S.E., Burkholder, J.M., Morton, S.L. (Eds.), *Harmful Algal Blooms: A Compendium Desk Reference*. John Wiley & Sons Ltd, UK, 243–336. <https://doi.org/10.1002/9781118994672.ch8>
- Agawin, N.S.R., Tovar-Sánchez, A., De Zarruk, K.K., Duarte, C.M., Agustí, S., 2013. Variability in the abundance of *Trichodesmium* and nitrogen fixation activities in the subtropical NE Atlantic. *J. Plankton Res.* 35 (5), 1126–1140. <https://doi.org/10.1093/plankt/fbt059>
- Ahmed, A., Kurian, S., Gauns, M., Chndrasekhararao, A.V., Mulla, A., Naik, B., Naik, H., Naqvi, S.W.A., 2016. Spatial variability in phytoplankton community structure along the eastern Arabian Sea during the onset of south-west monsoon. *Cont. Shelf Res.* 119, 30–39. <https://doi.org/10.1016/j.csr.2016.03.005>
- Aiyar, R.G., 1936. Mortality of fish of the Madras coast. *Curr. Sci.* 4 (7), 488–489. <https://doi.org/10.1093/plankt/fbt059>
- Akhil, V.P., Durand, F., Lengaigne, M., Vialard, J., Keerthi, M.G., Gopalakrishna, V.V., Deltel, C., Papa, F., Montegut, CB, 2014. A modeling study of the processes of surface salinity seasonal cycle in the Bay of Bengal. *J. Geophys. Res. Ocean.* 119 (6), 3926–3947. <https://doi.org/10.1002/2013JC009632>
- Al-azri, A., Al-hashmi, K., Goes, J., Gomes, H., Rushdi, A.I., Al-Habsi, H., Al-Khusaibi, S., Al-Kindi, R., Al-Azri, N., 2007. Seasonality of the bloom-forming heterotrophic dinoflagellate *Noctiluca scintillans* in the Gulf of Oman in relation to environmental conditions. *Int. J. Oceanogr.* 2 (1), 51–60.
- Aleynik, D., Dale, A.C., Porter, M., Davidson, K., 2016. high-resolution hydrodynamic model system suitable for novel harmful algal bloom modelling in areas of complex coastline and topography. *Harmful Algae* 53, 102–117. <https://doi.org/10.1016/j.hal.2015.11.012>
- Anantharaman, P., Thirumaran, G., Arumugam, R., Kanna, R.R.R., Hemalatha, A., Kannathasan, A., Sampathkumar, P., Balasubramanian, T., 2009. Monitoring of *Noctiluca* bloom in Mandapam and Keelakarai coastal waters, Southeast coast of India. *Recent Res. Sci. Technol.* 2 (10), 51–58, [1].
- Anantharaman, P., Thirumaran, G., Arumugam, R., Kanna, R.R.R., Hemalatha, A., Kannathasan, A., Sampathkumar, P., Balasubramanian, T., 2010. Monitoring of *Noctiluca* bloom in Mandapam and Keelakarai coastal waters, Southeast coast of India. *Recent Res. Sci. Technol.* 2 (10), 51–58.
- Anderson, D.M., Cembella, A.D., Hallegraef, G.M., 2012. Progress in understanding harmful algal blooms (HABs): Paradigm shifts and new technologies for research, monitoring, and management. *Ann. Rev. Mar. Sci.* 4, 143–176. <https://doi.org/10.1146/annurev-marine-120308-081121>
- Anderson, D.M., Hoagland, P., Kaoru, Y., White, A.W., 2000. Estimated annual economic impacts of harmful algal blooms (HABs) in the United States. Woods Hole Oceanographic Institution WHOI-2000-11. <https://doi.org/10.1575/1912/96>
- Annamalai, J., Shanmugam, J., Nallamuthu, T., 2016. Salt stress enhancing the production of phytochemicals in *Chlorella vulgaris* and *Chlamydomonas reinhardtii*. *J. Algal Biomass Util.* 7 (1), 37–44.
- Anoopa, P.C., 2017. Salinity distribution in the upper layers of the Bay of Bengal and its response to climatic events. *Cochin University of Science and Technology*, 29–32.
- APDR, 2019. dchart for public users, A PRIDE Pilot Project, 2019. <http://apdr.soest.hawaii.edu/dchart/index.html?dsetid=176b1cea22a96e6f9ab6f1846956d93> (accessed on 17/05/2019).
- Arun, K.M., Karthik, R., Sai, E.S., Padmavati, G., 2012. The occurrence of *Trichodesmium erythraeum* bloom in the coastal waters of South Andaman. *Int. J. Curr. Res.* 4 (11), 281–284, [2].
- Asha, P.S., Diwakar, K., Sivanesh, H., Kaladharan, P., 2015. Bloom of microalga *Chlorella marina* (Butcher) in the Karapad lagoon, Gulf of Mannar, southeast coast of India. *J. Mar. Biol. Assoc. India* 57 (1), 31–35. <https://doi.org/10.6024/jmbai.2015.57.1.01806-04>, [3].
- Attri, S.D., Tyagi, A., 2010. Climate profile of India. *Environ. Meteorol. India Meteorol. Dep.* 2–5. <https://doi.org/10.1007/s12524-010-0015-9>
- Baliarsingh, S.K., Lotliker, A.A., Trainer, V.L., Wells, M.L., Parida, C., Sahu, B.K., Srichandan, S., Sahoo, S., Sahu, K.C., Kumar, T.S., Blair, P., Bay, PB, Bay, P., 2016. Environmental dynamics of red *Noctiluca scintillans* bloom in tropical coastal waters. *Mar. Pollut. Bull.* 111 (1–2), 277–286. <https://doi.org/10.1016/j.marpolbul.2016.06.103>, [4].
- Begum, M., Sahu, B.K., Das, A.K., Vinithkumar, N.V., Kirubakaran, R., 2015. Extensive *Chaetoceros curvisetus* bloom in relation to water quality in Port Blair Bay, Andaman Islands. *Environ. Monit. Assess.* 187 (5), art. no. 226, <https://doi.org/10.1007/s10661-015-4461-2>, [5].
- Behara, A., Vinayachandran, P.N., 2019. Influence of rainfall over Eastern Arabian Sea on its salinity. *J. Geophys. Res.* 124 (7), 1–18. <https://doi.org/10.1029/2019JC014999>
- Berdalet, E., Fleming, L.E., Gowen, R., Davidson, K., Hess, P., Backer, L.C., Moore, S.K., Hoagland, P., Enevoldsen, H., 2019. Marine harmful algal blooms, human health, and well-being: challenges and opportunities in the 21st century. *J. Mar. Biol. Assoc. UK* 96 (1), 61–91. <https://doi.org/10.1017/S0025315415001733>
- Bhimachar, B.S., George, P.C., 1950. Abrupt set-backs in the fisheries of the Malabar and Kanara coasts and “red water” phenomenon as their probable cause. *Proc. Indian Acad. Sci. – Sect. B* 31, 339–350. <https://doi.org/10.1007/BF03050614>, [6].
- Binding, C.E., Greenberg, T.A., Mccullough, G., Watson, S.B., Page, E., 2018. An analysis of satellite-derived chlorophyll and algal bloom indices on Lake Winnipeg. *J. Great Lakes Res.* 44 (3), 436–446. <https://doi.org/10.1016/j.jglr.2018.04.001>
- Brand, L.E., Compton, A., 2007. Long-term increase in *Karenia brevis* abundance along the Southwest Florida Coast. *Harmful Algae* 6 (2), 232–252. <https://doi.org/10.1016/j.hal.2006.08.005>
- Breitbarth, E., Oschlies, A., Laroche, J., 2007. Physiological constraints on the global distribution of *Trichodesmium* – Effect of temperature on diazotrophy. *Biogeosciences. Eur. Geosci. Union* 4 (1), 53–61. <https://doi.org/10.5194/bg-4-53-2007>
- Brierley, A.S., 2017. Plankton. *Curr. Biol* 27 (11), R478–R483. <https://doi.org/10.1016/j.cub.2017.02.045>
- Capone, D.G., Burns, J.A., Montoya, J.P., Subramaniam, A., Mahaffey, C., Gunderson, T., Michaels, A.F., Carpenter, E.J., 2005. Nitrogen fixation by *Trichodesmium* spp.: An important source of new nitrogen to the tropical and subtropical North Atlantic Ocean. *Global Biogeochem. Cy.* 19 (2), 1–17. <https://doi.org/10.1029/2004GB002331>
- Capone, D.G., Zehr, J.P., Paerl, H.W., Bergman, B., Carpenter, E.J., 1997. *Trichodesmium*, a globally significant marine cyanobacterium. *Science* 276 (5316), 1221–1229. <https://doi.org/10.1126/science.276.5316.1221>
- Chacko, P.I., 1942. An usual incidence of mortality of marine fauna. *Curr. Sci.* 11 (10), 404 pp.
- Chaitanya, A.V.S., Lengaigne, M., Vialard, J., V., G., Durand, F., Kranthikumar, C., Amritash, S., Suneel, V., Papa, F., Ravichandran, M., 2014. Salinity measurements collected by fishermen reveal a “river in the sea” flowing along the eastern coast. *Bull. Am. Meteorological Soc.* 95 (12), 1897–1908. <https://doi.org/10.1175/BAMS-D-12-00243.1>
- Chandrasekhararao, A.V., Kurian, S., Vidya, P.J., Gauns, M., Shenoy, D.M., Mulla, A., Naik, H., Reddy, T.V., Naqvi, S.W.A., 2018. Phytoplankton response to the contrasting physical regimes in the eastern Arabian Sea during the northeast mon-

- soon. *J. Marine Syst.* 182, 56–66. <https://doi.org/10.1016/j.jmarsys.2018.02.002>
- Chassot, E., Bonhommeau, S., Dulvy, N.K., Mélin, F., Watson, R., Gascuel, D., Le Pape, O., 2010. Global marine primary production constrains fisheries catches. *Ecol. Lett.* 13 (4), 495–505. <https://doi.org/10.1111/j.1461-0248.2010.01443.x>
- Chellam, A., Alagarswami, K., 1978. Blooms of *Trichodesmium thiebautii* and their effect on experimental pearl culture at Vepalodai. *Indian. J. Fish.* 25, 237–239.
- Chidambaram, K., Unny, M.M., 1944. Note on the swarming of the planktonic algae *Trichodesmium erythraeum* in the Pamban area and its effect on the fauna. *Curr. Sci.* 13, 263.
- Ching, P.K., Ventura, R.J., de los Reyes, V.C., Sucaldito, M.N., Tayag, E., 2015. Lethal paralytic shellfish poisoning from consumption of green mussel broth, Western Samar, Philippines, August 2013. *West. Pacific Surveill. Response J.* 6 (2), 22–26. <https://doi.org/10.5365/wpsar.2015.6.1.004>
- Choudhury, S.B., Panigrahy, R.C., 1989. Occurrence of bloom of diatom *Asterionella glacialis* in near-shore waters of Gopalpur, Bay of Bengal (India). *Indian J. Mar. Sci.* 18 (3), 204–206, [7].
- Chowdary, J.S., Srinivas, G., Fousiya, T.S., Parekh, A., Gnanaseelan, C., Seo, H., Mackinnon, J.A., 2016. Representation of Bay of Bengal upper-ocean salinity in general circulation models. *Oceanography* 29 (2), 38–49. <https://doi.org/10.5670/oceanog.2016.37>
- Cicily, L., Padmakumar, K.B., Asha Devi, C.R., Sanjeevan, V.N., 2013. Occurrence of a multi-species diatom bloom dominated by *Proboscia alata* (Brightwell) Sandstorm along the south-west coast of India. *Oceanol. Hydrobiol. Stud.* 42, 40–45. <https://doi.org/10.2478/s13545-013-0055-1>, [8].
- D’Silva, M.S., Anil, A.C., Naik, R.K., D’Costa, P.M., 2012. Algal blooms: A perspective from the coasts of India. *Nat. Hazards* 63 (2), 1225–1253. <https://doi.org/10.1007/s11069-012-0190-9>
- Daniel, A., Nagabhushanam, A.K., Chakrapany, S., 1979. On bioluminescent *Noctiluca* swarms associated with the movement of extensive shoals of flying-fishes and schools of Dolphins in the northern Arabian Sea in February 1974. *Rec. Zool. Surv. India* 75, 237–246, [9].
- Desa, Elgar, Suresh, T., Matondkar, SGP, Desa, Ehrlich, Goes, J., Mascarenhas, A., Parab, S.G., Shaikh, N., Fernandes, C.E.G., 2005. Detection of *Trichodesmium* bloom patches along the eastern Arabian Sea by IRS-P4/OCM ocean color sensor and by in-situ measurements. *Indian J. Mar. Sci.* 34 (4), 374–386, [10].
- Devassy, V.P., 1974. Observations on the bloom of a diatom *Fragilaria oceanica* Cleve. *Mahasagar* 7 (1–2), 101–105, [11].
- Devassy, V.P., Bhattathiri, P.M.A., Qasim, S.Z., 1978. *Trichodesmium* phenomenon. *Indian J. Mar. Sci.* 7 (3), 168–186, [12].
- Devassy, V.P., Nair, S.R.S., 1987. Discolouration of water and its effect on fisheries along the Goa coast. *Mahasagar-Bulletin Natl. Inst. Oceanogr.* 20, 121–128, [13].
- Dharani, G., Abdul Nazar, A.K., Kanagu, L., Venkateswaran, P., Kumar, T.S., Ratnam, K., Venkatesan, R., Ravindran, M., 2004. On the recurrence of *Noctiluca scintillans* bloom in Minnie Bay, Port Blair: Impact on water quality and bioactivity of extracts. *Curr. Sci.* 87 (7), 990–994, [14].
- Dwivedi, R., Rafeeq, M., Smitha, B.R., Padmakumar, K.B., Thomas, L.C., Sanjeevan, V.N., Prakash, P., Raman, M., 2015. Species identification of mixed algal bloom in the Northern Arabian Sea using remote sensing techniques. *Environ. Monit. Assess.* 187, 51. <https://doi.org/10.1007/s10661-015-4291-2>, [15].
- Dwivedi, R.M., Chauhan, R., Solanki, H.U., Raman, M., Matondkar, SGP, Madhu, V.R., Meenakumari, B., 2012. Study of ecological consequence of the bloom (*Noctiluca miliaris*) in off shore waters of the Northern Arabian Sea. *Indian J. Mar. Sci.* 41 (4), 304–313, [16].
- Dwivedi, R.M., Raman, M., Parab, S., Matondkar, S.G.P., Nayak, S., 2006. Influence of northeasterly trade winds on intensity of winter bloom in the Northern Arabian Sea. *Curr. Sci.* 90 (10), 1397–1406, [17].
- Eashwar, M., Nallathambi, T., Kuberaraj, K., Govindarajan, G., 2001. *Noctiluca* blooms in Port Blair Bay, Andamans. *Curr. Sci.* 81 (2), 203–206, [18].
- Edwards, M., Johns, D.G., Leterme, S.C., Svendsen, E., Richardson, A.J., 2006. Regional climate change and harmful algal blooms in the northeast Atlantic. *Limnol. Oceanogr.* 51 (2), 820–829. <https://doi.org/10.4319/lo.2006.51.2.0820>
- Ferrante, M., Sciacca, S., Fallico, R., Fiore, M., Conti, G.O., Ledda, C., 2012. Relationship between body composition, smoking, and physical fitness of Malaysian Armed Forces Naval Trainees. *Open Access Sci. Reports Bergqvist* 1, 548. <https://doi.org/10.4172/scientificreports.548>
- Figler, A., B-Beres, V., Dobronoki, D., Marton, K., Nagy, S.A., Bacsi, I., 2019. Salt tolerance and desalination abilities of nine common green microalgae isolates. *Water* 11 (2), art. no. 2527. <https://doi.org/10.3390/w11122527>
- Fu, F.-X., Bell, P.R.F., 2003. Effect of salinity on growth, pigmentation, N<sub>2</sub> fixation, and alkaline phosphatase activity of cultured *Trichodesmium* sp. *Mar. Ecol. Prog. Ser.* 257, 69–76. <https://doi.org/10.3354/meps257069>
- Garcia, H.E., Weathers, K., Paver, C.R., Smolyar, I., Boyer, T.P., Locarnini, R.A., Zweng, M.M., Mishonov, A.V., Baranova, O.K., Reagan, J.R., 2019a. Dissolved Inorganic Nutrients (phosphate, nitrate, silicate). In: Mishonov, A. (Ed.). *World Ocean Atlas 2018*. National Centers for Environmental Information, NOAA, Vol. 4. <https://www.nodc.noaa.gov/cgi-bin/OC5/SELECT/woaselect.pl>
- Garcia, H.E., Weathers, K., Paver, C.R., Smolyar, I., Boyer, T.P., Locarnini, R.A., Zweng, M.M., Mishonov, A.V., Baranova, O.K., Reagan, J.R., 2019b. Dissolved Inorganic Nutrients (Dissolved oxygen, apparent Oxygen Utilization, and Oxygen saturation). In: Mishonov, A. (Ed.). *World Ocean Atlas 2018*. National Centers for Environmental Information, NOAA, Vol. 3. <https://www.nodc.noaa.gov/cgi-bin/OC5/SELECT/woaselect.pl?parameter=4>
- Getchiss, T., Shumway, S., 2017. Harmful Algae: An Executive Summary. Connecticut Sea Grant College Program, CTSG-17-08, 16 pp., <https://seagrant.uconn.edu/wp-content/uploads/sites/1985/2017/08/algae-summary-web.pdf> (accessed on 24/8/2020).
- Gireesh, R., Varghese, M., Thomas, V.J., 2015. Phytoplankton – collection, estimation, classification, and diversity. In: *Summer School on Recent Advances in Marine Biodiversity Conservation and Management*. Kochi.
- Gobler, C.J., Doherty, O.M., Hattenrath-Lehmann, T.K., Griffith, A.W., Kang, Y., Litaker, W., 2017. Ocean warming since 1982 has expanded the niche of toxic algal blooms in the North Atlantic and North Pacific oceans. *PNAS* 114 (19), 4975–4980. <https://doi.org/10.1073/pnas.1619575114>
- Gomes, R.H., Goes, JI, Matondkar, S.G.P., Buskey, E.J., Basu, S., Parab, S., Thoppil, P., 2014. Massive outbreaks of *Noctiluca scintillans* blooms in the Arabian Sea due to spread of hypoxia. *Nat. Commun.* 5. <https://doi.org/10.1038/ncomms5862>, [19].
- Gopakumar, G., Sulochanan, B., Venkatesan, V., 2009. Bloom of *Noctiluca scintillans* (Macartney) in Gulf of Mannar, south-east coast of India. *J. Mar. Biol. Assoc. India* 51 (1), 75–80, [20].
- Gribble, K.E., Nolan, G., Anderson, D.M., 2007. Biodiversity, biogeography, and potential trophic impact of *Protoperdinium* spp. (Dinophyceae) off the southwestern coast of Ireland. *J. Plankton Res.* 29 (11), 931–947. <https://doi.org/10.1093/plankt/fbm070>
- Gypens, N., Lacroix, G., Lancelot, C., 2007. Causes of variability in diatom and *Phaeocystis* blooms in Belgian coastal waters between 1989 and 2003: A model study. *J. Sea Res.* 57, 19–35. <https://doi.org/10.1016/j.seares.2006.07.004>

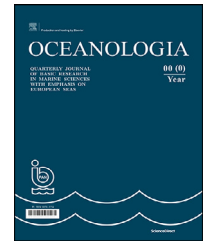
- Harrison, P.J., Furuya, K., Glibert, P.M., Xu, J., Liu, H.B., Yin, K., Lee, J.H.W., Anderson, D.M., Gowen, R., Al-Azri, A.R., Ho, A.Y.T., 2011. Geographical distribution of red and green *Noctiluca scintillans*. *Chinese J. Oceanol. Limnol.* 29, 807–831. <https://doi.org/10.1007/s00343-011-0510-z>
- Heil, C.A., Dixon, L.K., Hall, E., Garrett, M., Lenes, J.M., O'Neil, J.M., Walsh, B.M., Bronk, D.A., Killberg-Thoreson, L., Hitchcock, G.L., Meyer, K.A., Mulholland, M.R., Procise, L., Kirkpatrick, G.J., Walsh, J.J., Weisberg, R.W., 2014. Blooms of *Karenia brevis* (Davis) G. Hansen & Ø. Moestrup on the West Florida Shelf: Nutrient sources and potential management strategies based on a multi-year regional study. *Harmful Algae* 38, 127–140. <https://doi.org/10.1016/j.hal.2014.07.016>
- Hemalatha, A., Suresh, M., Giriya, K., Anantharaman, P., 2016. Observation of diatom bloom dominated by *Rhizosolenia alata* in Cuddalore coastal waters, southeast coast of India. *Seaweed Res. Util.* 38 (2), 9–12, [21].
- Hiremath, S., Mathad, P., 2010. Impact of salinity on the physiological and biochemical traits of *Chlorella vulgaris* Beijerinck. *J. Algal Biomass Util.* 1 (2), 51–59.
- Hoagland, P., Anderson, D.M., Kaoru, Y., White, A.W., 2002. The economic effects of Harmful Algal Blooms in the United States: Estimates, Assessment, Issues, and Information Needs. *Estuaries* 25, 819–837. <https://doi.org/10.1007/BF02804908>
- Hoagland, P., Scatasta, S., 2006. The Economic effects of harmful algal blooms. In: Graneli, E., Turner, J. (Eds.), *Ecology of harmful algae*. Ecological Studies (Analysis and Synthesis). Springer, Berlin, Heidelberg, 391–402.
- Holl, C.M., Montanya, J.P., 2005. Interactions between nitrate uptake and nitrogen fixation in continuous cultures of the marine diazotroph. *J. Phycol.* 41 (6), 1178–1183. <https://doi.org/10.1111/j.1529-8817.2005.00146.x>
- Hornell, J., 1908. Report of the results of a fishery cruise along the Malabar coast to the Laccadive Islands in 1908. *Madras Fish Bull.* 4, 71–126.
- Hornell, J., 1917. A new protozoan cause of widespread mortality among marine fishes. *Madras Fish Bull.* 11, 53.
- Hornell, J., Nayudu, M.R., 1923. A contribution to the life history of the Indian sardine with note on the plankton of the Malabar coast. *Madras Fish Bull.* 17, 129.
- Huang, C., Qi, Y., 1997. The abundance cycle and influence factors on red tide phenomena of *Noctiluca scintillans* (Dinophyceae) in Dapeng Bay, the south. *J. Plankton Res.* 19 (3), 303–318. <https://doi.org/10.1093/plankt/19.3.303>
- Ignatiades, L., 2016. Redefinition of cell size classification of phytoplankton - A potential tool for improving the quality and assurance of data interpretation. *Mediterr. Mar. Sci.* 171 (1), 56–64. <https://doi.org/10.12681/mms.1332>
- Indian Space Research Organization, ISRO, 1999. Ocean Colour Monitor of IRS-P4 Satellite Tested. <https://www.isro.gov.in/update/03-jun-1999/ocean-colour-monitor-of-irs-p4-satellite-tested> (accessed on 27/03/2020).
- Iyer, C.S.P., Robin, R.S., Sreekala, M.S., Kumar, S., 2008. *Karenia mikimotoi* bloom in Arabian Sea. *Harmful Algae News* 37, 9–10, [22].
- Jabir, T., Dhanya, V., Jesmi, Y., Prabhakaran, M.P., Saravanane, N., Gupta, G.V.M., Hatha, A.A.M., 2013. Occurrence and distribution of a Diatom-diazotrophic Cyanobacteria association during a *Trichodesmium* bloom in the Southeastern Arabian Sea. *Int. J. Oceanogr.* 6. Art. no. 350594, <https://doi.org/10.1155/2013/350594>, [23].
- Jasmine, P., Shaiju, P., Rejomon, G., Thresiamma, J., Nair, K.K., 2005. Red tide of *Noctiluca miliaris* off south of Thiruvananthapuram subsequent to the 'stench event' at the southern Kerala coast. *Cur. Sci.* 89 (9), 1472–1473, [24].
- Jeong, H.J., Yoo, Y.Du, Seong, K.A., Kim, J.H., 2005. Feeding by the mixotrophic red-tide dinoflagellate *Gonyaulax polygramma*: mechanisms, prey species, effects of prey concentration, and grazing impact. *Aquat. Ecol.* 38 (3), 249–257.
- Jiang, Z., Chen, J., Zhou, F., 2017. Summer distribution patterns of *Trichodesmium* spp. in the Changjiang (Yangtze River) Estuary and adjacent East China Sea shelf. *Oceanologia* 59 (3), 248–261. <https://doi.org/10.1016/j.oceano.2017.02.001>
- Jin, D., Thunberg, E., Hoagland, P., 2008. Economic impact of the 2005 red tide event on commercial shellfish fisheries in New England. *Ocean Coast. Manag.* 51 (5), 420–429. <https://doi.org/10.1016/j.ocecoaman.2008.01.004>
- Jones, T., Parrish, J.K., Punt, A.E., Trainer, V.L., Kudela, R., Lang, J., Brancato, M.S., Odell, A., Hickey, B., 2017. Mass mortality of marine birds in the Northeast Pacific caused by *Akashiwo sanguinea*. *Mar. Ecol. Prog. Ser.* 579, 111–127. <https://doi.org/10.3354/meps12253>
- Joseph, T., Shaiju, P., Laluraj, C.M., Balachandran, K.K., Nair, M., George, R., Nair, K.K.C., Sahayak, S., Prabhakaran, M.P., 2008. Nutrient environment of red tide-infested waters off southwest coast of India. *Environ. Monit. Assess.* 143 (1–3), 355–361. <https://doi.org/10.1007/s10661-007-9938-1>
- Jugnu, R., 2006. *Studies on the Prevalence of Algal Blooms Along Kerala Coast, India*. Cochin University of Science and Technology, 49–179.
- Jyothibabu, R., Karnan, C., Jagadeesan, L., Arunpandi, N., Pandiarajan, R.S., Muraliedharan, K.R., Balachandran, K.K., 2017. *Trichodesmium* blooms and warm-core ocean surface features in the Arabian Sea and the Bay of Bengal. *Mar. Pollut. Bull.* 121 (1–2), 201–215. <https://doi.org/10.1016/j.marpolbul.2017.06.002>
- Jyothibabu, R., Madhu, N.V., Murukesh, N., Haridas, P.C., Nair, K.K.C., Venugopal, P., 2003. Intense blooms of *Trichodesmium erythraeum* (Cyanophyta) in the open waters along east coast of India. *Indian J. Mar. Sci.* 32 (2), 165–167, [25].
- Kakarla, R., Choi, J., Yun, J., Kim, B., Heo, J., Lee, S., Cho, D., Ramanan, R., Kim, H., 2018. Application of high-salinity stress for enhancing the lipid productivity of *Chlorella sorokiniana* HS1 in a two-phase process. *J. Microbiol.* 56, 56–64. <https://doi.org/10.1007/s12275-018-7488-6>
- Karthik, R., Padmavati, G., 2014. Dinoflagellate bloom produced by *Protoperidinium divergens*. Response to ecological parameters and anthropogenic influences in the Junglighthat Bay of South Andaman Islands. *Appl. Environ. Res.* 36 (4), 19–27. <https://doi.org/10.14456/aer.2014.10>, [26].
- Karthik, R., Padmavati, G., 2017. Temperature and salinity are the probable causative agent for the *Trichodesmium erythraeum* (Cyanophyceae) algal bloom on the Burmanallah Coastal Waters of South Andaman Island. *World Appl. Sci. J.* 35 (8), 1271–1281. <https://doi.org/10.5829/idosi.wasj.2017.1271.1281>, [27].
- Karthik, R., Padmavati, G., 2018. Intense rare bloom of *Chaetoceros tortissimum* (Gran) in relation to water quality assessed using multivariate statistical approach at Chouldari Bay, South Andaman Island. *Cah. Biol. Mar.* 58, 423–433. <https://doi.org/10.21411/CBM.A.C3348C08>, [81].
- Karunasagar, I., Joseph, B., Philipose, K.K., Karunasagar, I., 1998. Another outbreak of PSP in India. *Harmful Algae News* 17, 1.
- Katti, R.J., Gupta, C.T.R., Shetty, H.P.C., 1988. On the occurrence of "green tide" in the Arabian Sea off Mangalore. *Curr. Sci.* 57 (7), 380–381, [28].
- Kim, H.G., Park, J.S., Lee, S.G., An, K.H., 1993. Population cell volume and carbon content in monospecific dinoflagellate blooms. *Dev. Mar. Bio.* 3, 108–144.
- KNMI Climate Explorer website, 2018. Sea surface salinity annual and monthly mean. [https://climexp.knmi.nl/get\\_index.cgi](https://climexp.knmi.nl/get_index.cgi) (accessed on 21/05/2019).
- KNMI Climate Explorer website, 2018. [https://climexp.knmi.nl/select.cgi?id=someone@somewhere&field=coads\\_sst](https://climexp.knmi.nl/select.cgi?id=someone@somewhere&field=coads_sst) (accessed on 21/05/2019).

- Kopuz, U., Feyzioglu, A.M., Valente, A., 2014. Seasonal Changes of Phytoplankton Chlorophyll a, Primary Production and their Relation in the Continental Shelf Area of the South Eastern Black Sea. *Turkish J. Fish. Aquat. Sci.* 14 (3), 261–268. <https://doi.org/10.4194/1303-2712-v14>
- Krishnan, A.A., Krishnakumar, P.K., Rajagopalan, M., 2007. *Trichodesmium erythraeum* (Ehrenberg) bloom along the south-west coast of India (Arabian Sea) and its impact on trace metal concentrations in seawater. *Estuar. Coast. Shelf Sci.* 71 (3–4), 641–646. <https://doi.org/10.1016/j.ecss.2006.09.012>, [29].
- Kumar, M.A., Padmavati, G., Pradeep, H.D., 2015. Occurrence of *Trichodesmium erythraeum* (Cyanophyte) bloom and its effects on the fish catch during April 2013 in the Andaman Sea. *Appl. Environ. Res.* 37 (2), 48–57. <https://doi.org/10.14456/aer.2015.15>, [30].
- Kumar, P.V.H., Mathew, B., 1997. Salinity distribution in the Arabian Sea. *Indian J. Mar. Sci.* 26 (3), 271–277.
- Kumar, S.P., Roshin, R.P., Narvekar, J., Kumar, P.K.D., Vivekanandan, E., 2009. Response of the Arabian Sea to global warming and associated regional climate shift. *Mar. Environ. Res.* 68 (5), 217–222. <https://doi.org/10.1016/j.marenvres.2009.06.010>
- Liu, C.L., Tang, D.L., 2012. Spatial and temporal variations in algal blooms in the coastal waters of the western South China Sea. *J. Hydro-Environ. Res.* 6 (3), 239–247. <https://doi.org/10.1016/j.jher.2012.02.002>
- Liu, H., Song, X., Huang, L., Tan, Y., Zhong, Y., Huang, J.R., 2012. Potential risk of *Mesodinium rubrum* bloom in the aquaculture area of dapeng'ao cove, China: Diurnal changes in the ciliate community structure in the surface water. *Oceanologia* 54 (1), 109–117. <https://doi.org/10.5697/oc.54-1.109>
- Lotliker, A.A., Baliarsingh, S.K., Trainer, V.L., Wells, M.L., Wilson, C., Bhaskar, T.V.S.U., Samanta, A., Shahimol, S.R., 2018. Characterization of oceanic *Noctiluca* blooms not associated with hypoxia in the Northeastern Arabian Sea. *Harmful Algae* 74, 46–57. <https://doi.org/10.1016/j.hal.2018.03.008>
- Madeswaram, P., Ramana, M. V, Rajeevan, M., Ramanathan, V., Patra, S., Sivasdas, S.K., Boopathi, T., Bharathi, M.D., Anuradha, S., Muthukumar, C., 2018. Status Report: Seawater Quality at Selected Locations along Indian Coast: Status Report Seawater Quality Monitoring (SWQM) (1990–2015). <https://www.nccr.gov.in/?q=technical-report> (accessed on 09/06/2020).
- Madhav, V.G., Kondalarao, B., 2004. Distribution of phytoplankton in the coastal waters of east coast of India. *Indian J. Mar. Sci.* 33 (3), 262–268, [32].
- Madhu, N.V., Jyothibabu, R., Maheswaran, P.A., 2011a. Enhanced chlorophyll a and primary production in the northern Arabian Sea during the spring intermonsoon due to green *Noctiluca scintillans* bloom. *Mar. Biol. Res.* 892, 182–188. <https://doi.org/10.1080/17451000.2011.605143>, [31].
- Madhu, N.V., Reny, P.D., Paul, M., Ullas, N., Resmi, P., 2011. Occurrence of red tide caused by *Karenia mikimotoi* (toxic dinoflagellate) in the Southwest Coast of India. *Indian J. Geo-Marine Sci.* 40 (6), 821–825, [32].
- Madhupratap, M., Sawant, S., Gauns, M., 2000. A first report on a bloom of the marine prymnesiophycean, *Phaeocystis globosa* from the Arabian Sea. *Oceanol. Acta* 23 (1), 83–90. [https://doi.org/10.1016/S0399-1784\(00\)00109](https://doi.org/10.1016/S0399-1784(00)00109), [33].
- Martins, A., Caetano, N.S., Mata, T.M., 2010. Microalgae for biodiesel production and other applications: A review. *Renew. Sustain. Energy Rev.* 14 (1), 217–232. <https://doi.org/10.1016/j.rser.2009.07.020>
- Mata, T.M., Martins, A.A., Caetano, N.S., 2010. Microalgae for biodiesel production and other applications: A review. *Renew. Sustain. Energy Rev.* 14 (1), 217–232. <https://doi.org/10.1016/j.rser.2009.07.020>.
- Mathew, K.J., Raj, I.D., Selvaraj, G.S.D., 1988. Phytoplankton blooms along the Indian coasts - Some highlights. Marine Fisheries Information Service, Technical, and Extension Series. Cochin, India 4, 11–13. [http://eprints.cmfri.org.in/2788/1/Article\\_06.pdf](http://eprints.cmfri.org.in/2788/1/Article_06.pdf). (accessed on 24/08/2020), [35].
- Matondkar, S.G.P., Bhat, S.R., Dwivedi, R.M., Nayak, S.R., 2004. Indian satellite IRS-P4 (OCEANSAT) monitoring algal blooms in the Arabian Sea. *Harmful Algae News* 26, 4–5, [34].
- Matondkar, S.G.P., Dwivedi, R.M., Parab, S., Pednekar, S., Desa, E.S., 2006. Satellite and ship studies of phytoplankton in the North-eastern Arabian during 2000–2006 period. In: Froulin, R.J., Agarwal, V.K., Kawamura, H., Nayak, S., Pan, D. (Eds.), *Proc. SPIE 6406, Remote Sens. Marine Environ.* 640611 (28 November 2006), Goa, 1–10, <https://doi.org/10.1117/12.693693>, [35].
- Minu, P., Shaju, S.S., Souda, V.P., Usha, B., Ashraf, P.M., Meenakumari, B., 2015. Hyperspectral variability of phytoplankton blooms in Coastal Waters off Kochi, South-eastern Arabian Sea. *Fish. Technol.* 52, 218–222, [36].
- Mishra, S., Sahu, G., Mohanty, A.K., Singh, S.K., Panigrahy, R.C., 2005. Impact of the Diatom *Asterionella glacialis* (Castracane) bloom on the water quality and phytoplankton community structure in coastal waters of Gopalpur Sea, Bay of Bengal. *Asian J. Water, Environ. Pollut.* 3, 71–77, [37].
- Miyaguchi, H., Fujiki, T., Kikuchi, T., Kuwahara, V.S., Toda, T., 2006. Relationship between the bloom of *Noctiluca scintillans* and environmental factors in the coastal waters of Sagami. *J. Plankton Res.* 28, 313–324. <https://doi.org/10.1093/plankt/fbi127>
- Modayil, M.J., 2004. Dinoflagellates taint Thiruvananthapuram coast, in Altered river flow, a threat to the lifeline of coastal waters. In: Anthony, G. (Ed.), *Central Marine Fisheries Research Institute (CMFRI) Newsletter No. 103*, 3, [38].
- Mohamed, K.S., Kripa, V., Jugnu, R., Radhakrishnan, P., Alloycious, P.S., Sharma, J., Joseph, M., Velayudhan, T.S., 2007. Mortality of farmed pearl oyster *Pinctada fucata* (Gould, 1850) due to the blooming of *Noctiluca scintillans* and *Cochlodinium* sp. at Kollam Bay, Kerala. *J. Mar. Biol. Assoc. India* 49, 213–218, [39].
- Mohammad-Noor, N., Adam, A., Lim, P.T., Leaw, C.P., Lau, W.L.S., Liow, G.R., Muhamad-bunnori, N., Hamdan, N., Md-nor, A., Kemat, N., Muniandi, D., 2018. First report of paralytic shellfish poisoning (PSP) caused by *Alexandrium tamiyavanichii* in Kuantan Port, Pahang. East Coast of Malaysia. *Phycol. Res.* 66, 37–44. <https://doi.org/10.1111/pre.12205>
- Mohammed, G., 2003. Algal bloom and mass mortality of fishes and mussels along Kozhikode coast. *Mar. Fish. Infor. Serv. T & E. Ser.* 175, 7–8, [41].
- Mohanty, A.K., Satpathy, K.K., Sahu, G., Hussain, K.J., Prasad, M.V.R., Sarkar, S.K., 2010. Bloom of *Trichodesmium erythraeum* (Ehr.) and its impact on water quality and plankton community structure in the coastal waters of southeast coast of India. *Indian J. Mar. Sci.* 39 (3), 323–333, [40].
- Mohanty, A.K., Satpathy, K.K., Sahu, G., Sasmal, S.K., Sahu, B.K., Panigrahy, R.C., 2007. Red tide of *Noctiluca scintillans* and its impact on the coastal water quality of the near-shore waters, off the Rushikulya River. Bay of Bengal. *Curr. Sci.* 93 (5), 616–618, [41].
- Mohapatra, M., Nayak, D.P., Sharma, M., Sharma, R.P., Bandyopadhyay, B.K., 2015. Evaluation of official tropical cyclone landfall forecast issued by India meteorological department. *J. Earth Syst. Sci.* 124 (4), 861–874. <https://doi.org/10.1007/s12040-015-0581-x>
- Mulholland, M.R., Capone, D.G., 1999. Nitrogen fixation, uptake, and metabolism in natural and cultured populations of *Trichodesmium* spp. *Mar. Ecol. Prog. Ser.* 188, 33–49.
- Nagabhushanam, A.K., 1967. On an unusual dense phytoplankton bloom around Minicoy Island (Arabian Sea), and its effect on the local Tuna fisheries. *Curr. Sci.* 36 (22), 611–612.
- Naqvi, S.W.A., George, M.D., Narvekar, P.V., Jayakumar, D.A., Shailaja, M.S., Sardesai, S., Sarma, V.V.S.S., Shenoy, D.M., Naik, H., Maheswaran, P.A., Kumari, K.K., Rajesh, G., Sudhir, A.K., Binu, M.S., 1998. Severe fish mortality associated with

- 'red tide' observed in the sea off Cochin. *Curr. Sci.* 75 (6), 543–544.
- Narayana, S., Chitra, J., Tapase, S.R., Thamke, V., Karthick, P., Ramesh, C., Murthy, K.N., Ramasamy, M., Kodam, K.M., Mohanraju, R., 2014. Toxicity studies of *Trichodesmium erythraeum* (Ehrenberg, 1830) bloom extracts from Phoenix Bay, Port Blair. *Andamans. Harmful Algae* 40, 34–39. <https://doi.org/10.1016/j.hal.2014.10.003>, [42].
- Nashad, M., Menon, N.N., Joseph, C.A., Pettersson, L.H., Menon, N.R., 2017. First report of *Leptocylindrus* sp. bloom in the coastal waters of Kerala (southeast Arabian Sea). *J. Mar. Biol. Assoc. India* 59 (1), 28–33. <https://doi.org/10.6024/jmbai.2017.59.1.1937-00>, [43].
- Nayak, B.B., Karunasagar, I., Karunasagar, I., 2000. Bacteriological and physico-chemical factors associated with *Noctiluca miliaris* bloom along with Mangalore, south-west coast of India. *Indian J. Mar. Sci.* 29 (2), 139–143, [44].
- Nayak, S., 2017. Geo-spatial Information Science Coastal zone management in India - present status and future needs. *Geo-spatial Inf. Sci.* 20 (2), 174–183. <https://doi.org/10.1080/10095020.2017.1333715>
- Nayar, S., Prabhu, H.V., 2001. Bloom of *Noctiluca scintillans* MacCartney in the Arabian Sea Off Mangalore Southwest India. *Asian Fish. Sci.* 14, 77–82, [45].
- Nigam, S., Prakash, M., Sharma, R., 2011. Effect of Nitrogen on Growth and Lipid Content of *Chlorella pyrenoidosa* Effect of Nitrogen on Growth and Lipid Content of *Chlorella pyrenoidosa*. *Am. J. Biochem. Biotechnol.* 7 (3), 126–131. <https://doi.org/10.3844/ajbbsp.2011.126.131>
- Nunez, V.E.J., Garate-Lizarraga, I., Band-Schmidt, C.J., Cordero-Tapia, A., Lopez-Cortes, D.J., Sandoval, F.E.H., Heredia-Tapia, A., Bustillos-Guzman, J.J., 2011. Impact of harmful algal blooms on wild and cultured animals in the Gulf of California. *J. Environ. Biol.* 32 (4), 413–423.
- Ouyang, Z.-R., Wen, X.-B., Geng, Y.-H., Mei, H., Hu, H.-J., Zhang, G.-Y., Le, Y.-G., 2010. The effects of light intensities, temperatures, pH, and salinity on photosynthesis of *Chlorella*. *J. Wuhan Botanical Res.* 28 (1), 49–55. <https://doi.org/10.3724/SP.J.1142.2010.00049>
- Padmakumar, Cicily, L., Sudhakar, M., Bijoy, N.S., 2016a. Extensive outbreaks of heterotrophic dinoflagellate *Noctiluca scintillans* blooms along coastal waters of the South Eastern Arabian Sea. *Harmful Algae News* 11–12, [46].
- Padmakumar, K.B., Menon, N.R., Sanjeevan, V.N., 2012. Is occurrence of harmful algal blooms in the Exclusive Economic Zone of India on the Rise? *Int. J. Oceanogr.* 2012, art. no. 263946, 7 pp., <https://doi.org/10.1155/2012/263946>
- Padmakumar, K.B., Sanilkumar, M.G., Saramma, A.V., Sanjeevan, V.N., Menon, N.R., 2008. Green tide of *Noctiluca miliaris* in the Northern Arabian Sea. *Harmful Algae News* 36, 12, [47].
- Padmakumar, K.B., Smitha, B.R., Thomas, L.C., Fanimol, C.L., SreeRanjima, G., Menon, N.R., Sanjeevan, V.N., 2010a. Blooms of *Trichodesmium erythraeum* in the South Eastern Arabian Sea during the onset of 2009 summer monsoon. *Ocean Sci. J.* 45, 151–157. <https://doi.org/10.1007/s12601-010-0013-4>, [48].
- Padmakumar, K.B., SreeRanjima, G., Fanimol, C.L., Menon, N.R., Sanjeevan, V.N., 2010b. Preponderance of heterotrophic *Noctiluca scintillans* during a multi-species diatom bloom along the south-west coast of India. *Int. J. Ocean. Oceanogr.* 4 (1), 55–63, [49].
- Padmakumar, K.B., Thomas, L.C., Salini, T.C., John, E., Menon, N.R., Sanjeevan, V.N., 2011. Monospecific bloom of noxious raphidophyte *Chattonella marina* in the coastal water of South West coast of India. *Int. J. Biosci* 1 (1), 57–69, [50].
- Padmakumar, K.B., Thomas, L.C., Salini, T.C., Vijayan, A., 2018. Subsurface bloom of dinoflagellate *Gonyaulax polygramma* Stein in the shelf waters off Mangalore – South Eastern Arabian Sea. *Indian J. Geo. Mar. Sci.* 47 (8), 1658–1664, [51].
- Padmakumar, K.B., Thomas, L.C., Vimalkumar, K.G., Devi, C.R.A., Maneesh, TP, Vijayan, A., Gupta, G.V.M., Sudhakar, M., 2016b. Hydrobiological responses of the North Eastern Arabian Sea during late winter and early spring inter-monsoons and the repercussions on open ocean blooms. *J. Mar. Biol. Assoc. UK* 97 (7), 1467–1478. <https://doi.org/10.1017/S0025315416000795>, [52].
- Panikkar, N.K., Jayaraman, R., 1966. Biological and oceanographic differences between the Arabian Sea and the Bay of Bengal, as observed from the Indian region. *Proc. Indian Acad. Sci.* 64 (5), 231–240. <https://doi.org/10.1007/BF03052161>
- Passow, U., Carlson, C., 2012. The biological pump in a high CO<sub>2</sub> world. *Mar. Ecol. Prog. Ser.* 470, 249–271. <https://doi.org/10.3354/meps09985>
- Peter, S., Agnes, F., Sreeparvathy, P., Pillai, D., Kumar, B.M., 2016. *Noctiluca scintillans* (Macartney) Kofoid and Swezy Bloom and its Impact on the Coastal Water Quality off Alappuzha, Arabian Sea. *Fish. Technol.* 53, 82–85, [53].
- Prabhu, M.S., Ramamurthy, S., Kuthalingham, M.D.K., Dhulkhed, M.H., 1965. On an unusual swarming of the planktonic Blue-green algae *Trichodesmium* spp., off Mangalore. *Limnol. Oceanogr.* 34 (3), 95, [54].
- Prakash, A., Sarma, A.H.V., 1964. On the occurrence of “Red water” phenomenon on the west coast of India. *Curr. Sci.* 33 (6), 168–170, [55].
- Prasad, R.R., 1958. A note on the occurrence and feeding habits of *Noctiluca* and their effects on the plankton community and fisheries. *The Proc. Indian Acad. Sci. Section B* 47 (6), 331–337, [53].
- Prema, D., Singh, V.V., Jeyabaskaran, R., Kripa, V., 2017. Reactive nitrogen in coastal and marine waters of India and its relationship with marine aquaculture. In: Abrol, Y.P., Adhya, T.K., Aneja, V.P., Raghuram, N., Pathak, H., Kulshrestha, U., Sharma, C., Singh, B. (Eds.), *The Indian Nitrogen Assessment: Sources of reactive nitrogen, environmental and climate effects, management options, and policies*. Woodhead Publ., Duxford, 305–320. <https://doi.org/10.1016/B978-0-12-811836-8.00020-3>
- Qasim, S.Z., 1970. Some characteristics of a *Trichodesmium* bloom in the Laccadives. *Deep. Res. Oceanogr. Abstr.* 17 (3), 655–660. [https://doi.org/10.1016/0011-7471\(70\)90077-X](https://doi.org/10.1016/0011-7471(70)90077-X), [56].
- Qu, P., Fu, F., Kling, J.D., Huh, M., Wang, X., Hutchins, D.A., 2019. Distinct responses of the nitrogen-fixing marine cyanobacterium *Trichodesmium* to a thermally variable environment as a function of phosphorus availability. *Front. Microbiol.* 10, art. no. 1282. <https://doi.org/10.3389/fmicb.2019.01282>
- Raghavan, B.R., Deepthi, T., Ashwini, S., Shylini, S.K., Kumar-swami, M., Kumar, S., Lotliker, A.A., 2010. Spring inter monsoon algal blooms in the Eastern Arabian Sea: Shallow marine encounter off Karwar and Kumbla Coast using a Hyperspectral radiometer. *Int. J. Earth Sci. Eng.* 3 (6), 827–832, [57].
- Rai, S.V., Rajashekhar, M., 2014. Seasonal assessment of hydrographic variables and phytoplankton community in the Arabian Sea. *Brazilian J. Oceanogr.* 62 (4), 279–293. <https://doi.org/10.1590/S1679-87592014069906204>
- Rajeish, M., Shekar, M., Madhushree, H.N., 2016. Presumptive case of ciguatera fish poisoning in Mangalore, India. *Curr. Sci.* 111 (9), 1543–1547. <https://doi.org/10.18520/cs/v111/i9/1536-1543>
- Raji, K., Padmavati, G., 2014. Dinoflagellate Bloom Produced by *Protoperidinium divergens* response to ecological parameters and anthropogenic influences in the Junglight Bay of South Andaman Islands. *App. Envi. Res.* 36 (4), 19–27. <https://doi.org/10.14456/aer.2014.10>, [55].
- Rajisha, R., Kishore, P., Panda, S.K., Harikrishnan, G., Ajitha, K.C., Suresh, M.K., Chowdhury, L.M., Ravishankar, C.N., Kumar, A., 2017. Incidence of Ciguatera fish poisoning in Trivandrum, India. *Indian J. Fish.* 64 (4), 129–133. <https://doi.org/10.21077/ijf.2017.64.4.71558-20>

- Ramaiah, N., Paul, J.T., Fernandes, V., Raveendran, T., Raveendran, O., Sundar, D., Revichandran, C., Shenoy, D.M., Mangesh, G., Kurian, S., Gerson, V.J., Shoji, D.T., Madhu, N.V., Kumar, S.S., Lokabharathi, P.A., Shetye, S.R., 2005. The September 2004 stench off the southern Malabar coast – A consequence of holococcolithophore bloom. *Curr. Sci.* 88 (4), 551–554, [58].
- Ramamurthy, V.D., 1970. Antibacterial activity of the marine blue-green alga *Trichodesmium erythraeum* in the gastro-intestinal contents of the seagull *Larus brunicephalus*. *Mar. Biol.* 6, 74–76. <https://doi.org/10.1007/BF00352610>
- Ramamurthy, V.D., 1973. Infrared spectral analysis of antibacterial substance isolated from *Trichodesmium erythraeum* (Marine Blue Green Alga). *Hydrobiologia* 41, 247–250. <https://doi.org/10.1007/BF00016449>, [59].
- Rao, D.V.S., 1969. *Asterionella japonica* bloom and discoloration off Waltair, Bay of Bengal. *Limnol. Oceanogr.* 14 (4), 632–634. <https://doi.org/10.1080/01431160500185391>, [60].
- Rekha, V., Gurusamy, R., Santhanam, P., Devi, A.S., Ananth, S., 2012. Culture and biofuel production efficiency of marine microalgae *Chlorella marina* and *Skeletonema costatum*. *Indian J. Geo-Marine Sci.* 41 (2), 152–158.
- Richlen, M.L., Morton, S.L., Jamali, E.A., Rajan, A., Anderson, D.M., 2010. The catastrophic 2008-2009 red tide in the Arabian Gulf region, with observations on the identification and phylogeny of the fish-killing dinoflagellate *Cochlodinium polykrioides*. *Harmful Algae* 9 (2), 163–172. <https://doi.org/10.1016/j.hal.2009.08.013>
- Robin, R.S., Kanuri, V.V., Muduli, P.R., Mishra, R.K., Jaikumar, M., Karthikeyan, P., Kumar, C Suresh, Kumar, C Saravana, 2013. Dinoflagellate bloom of *Karenia mikimotoi* along the South-east Arabian Sea, Bordering Western India. *J. Ecosyst.* 2013, art. no. 463720, 11 pp., <https://doi.org/10.1155/2013/463720>, [61].
- Rodier, M., Le Borgne, R., 2008. Population dynamics and environmental conditions affecting *Trichodesmium* spp. (filamentous cyanobacteria) blooms in the south–west lagoon of New Caledonia. *J. Exp. Mar. Bio. Ecol.* 358 (1), 20–32. <https://doi.org/10.1016/j.jembe.2008.01.016>
- Rouco, M., Haley, S.T., Alexander, H., Wilson, S.T., Karl, D.M., Dyhrman, S.T., 2016. Variable depth distribution of *Trichodesmium* clades in the North Pacific Ocean. *Environ. Microbiol. Rep.* 8 (6), 1058–1066. <https://doi.org/10.1111/1758-2229.12488>
- Rouco, M., Joy-Warren, H., McGillicuddy, D.J., Waterbury, J.B., Dyhrman, S.T., 2014. *Trichodesmium* sp. clade distributions in the western North Atlantic Ocean. *Limnol. Oceanogr.* 59 (6), 1899–1909. <https://doi.org/10.4319/lo.2014.59.6.1899>
- Sachithanandam, V., Mohan, P.M., Karthik, R., Sai Elangovan, S., Padmavathi, G., 2013. Climate changes influence the phytoplankton bloom (Prymnesiophyceae: *Phaeocystis* spp.) in the North Andaman coastal region. *Indian J. Mar. Sci.* 42 (1), 58–66, [60].
- Sahayak, S., Jyothibabu, R., Jayalakshmi, K.J., Habeebrehman, H., Sabu, P., Prabhakaran, M.P., Jasmine, P., Shaiju, P., Rejomon, G., Thresiamma, J., Nair, K.K., 2005. Red tide of *Noctiluca miliaris* off south of Thiruvananthapuram subsequent to the 'stench event' at the southern Kerala coast. *Curr. Sci. India* 89 (9), 1472–1473, [62].
- Sahu, B.K., Panigrahy, R.C., Baliarsingh, S.K., Parida, C., Sahu, K.C., Lotliker, A.A., 2016. Red-tide of *Mesodinium rubrum* (Lohmann, 1908) in Indian waters. *Curr. Sci. India* 110 (6), 982–983. <https://doi.org/10.18520/cs/v110/i6/982-983>, [63].
- Sahu, B.K., Pati, P., Panigrahy, R.C., 2018. Impact on climate change on marine plankton with special reference to Indian seas. *Indian J. Geo-Mar. Sci.* 47 (2), 259–268.
- Sanilkumar, M.G., Padmakumar, K.B., Menon, N.R., Joseph, K.J., Sanjeevan, V.N., Saramma, V.A., 2009b. Algal blooms along the coastal waters of south-west India during 2005-08. *J. Mar. Biol. Assoc. India* 51 (1), 69–74, [64].
- Sanilkumar, M.G., Thomas, A.M., Shyamkumar, S., Philip, R., Hatha, A.A.M., Sanjeevan, V.N., Saramma, A.V., 2009a. First report of *Protoperdinium* bloom from India waters. *Harmful Algae News* 39, 15, [65].
- Sanilkumar, M.G., Thomas, A.M., Vijayalakshmi, K.C., Hatha, A.A.M., Sarama, A., 2012. *Chattonella marina* bloom in the coastal sea off Mahe, Southwest India. *Curr. Sci.* 103 (6), 624–626, [66].
- Sanseverino, I., Conduto, D., Pozzoli, L., Dobricic, S., Lettieri, T., 2016. Algal bloom and its economic impact. *EUR* 27905 EN. <https://doi.org/10.2788/660478>
- Sarang, R.K., Mohammed, G., 2011. Seasonal algal bloom and water quality around the coastal Kerala during south-west monsoon using in situ and satellite data. *Indian J. Mar. Sci.* 40 (3), 356–369, [65].
- Saravane, N., Sachithanandam, V., Muruganandam, M., Nagaarjunan, P., Mohan, P.M., 2016. Climate change and anthropogenic influences on *Rhizosolenia imbricata* climatic changes and anthropogenic influences on *Rhizosolenia imbricata* Brightwell 1858 Bacillariophyceae Bloom in Sisostris Bay. Port Blair. *Indian J. Geo-Mar. Sci.* 45 (3), 425–430, [67].
- Sargunam, C.A., Rao, V.N.R., Nair, K.V.K., 1989. Occurrence of *Noctiluca* bloom in Kalpakkam coastal waters, East coast of India. *Indian J. Mar. Sci.* 18 (4), 289–290, [73].
- Sarma, V.V.S.S., Patil, J.S., Shankar, D., Anil, A.C., 2019. Shallow convective mixing promotes massive *Noctiluca scintillans* bloom in the northeastern Arabian Sea. *Mar. Pollut. Bull.* 138, 428–436. <https://doi.org/10.1016/j.marpolbul.2018.11.054>, [68].
- Sasamal, S.K., Panigrahy, R.C., Misra, S., 2005. *Asterionella* blooms in the north-western Bay of Bengal during 2004. *Int. J. Remote Sens.* 26 (17), 3853–3858. <https://doi.org/10.1080/01431160500185391>, [69].
- Sathianandan, T.V., 2017. Marine fish production in India – present status. [http://eprints.cmfri.org.in/14022/1/Training%20manual%20on%20Advances%20in%20Marine%20Fish%20Production%20in%20India\\_2019\\_Marine%20Fish%20Production.pdf](http://eprints.cmfri.org.in/14022/1/Training%20manual%20on%20Advances%20in%20Marine%20Fish%20Production%20in%20India_2019_Marine%20Fish%20Production.pdf) (accessed on 09/12/2019).
- Satpathy, K.K., Nair, K.V.K., 1996. Occurrence of phytoplankton bloom and its effect on coastal water quality. *Indian J. Mar. Sci.* 25 (2), 145–147, [70].
- Satpathy, K.K., Mohanty, A.K., Sahu, G., Venkatesan, R., Natesan, U., Rajan, M., Section, I.S., Group, S., Nadu, T., 2007. On the occurrence of *Trichodesmium erythraeum* (Ehr.) bloom in the coastal waters of Kalpakkam, east coast of India. *J. Sci. Technol.* 1 (2), 1–9. <https://doi.org/10.17485/ijst/2008/v1i2/7>, [71].
- Saxena, A., 2012. Marine Biodiversity in India: Status and Issues. Uttar Pradesh State Biodivers. Board, 22 May 2012. *Int. Day Mar. Biodivers.* 127–134.
- Schoemann, V., Becquevort, S., Stefels, J., Rousseau, V., Lancelot, C., 2005. *Phaeocystis* blooms in the global ocean and their controlling mechanisms: a review. *J. Sea Res.* 53 (1–2), 43–66. <https://doi.org/10.1016/j.seares.2004.01.008>
- Shaju, S.S., Akula, R.R., Jabir, T., 2018. Characterization of light absorption coefficient of red *Noctiluca scintillans* blooms in the South Eastern Arabian Sea. *Oceanologia* 60 (3), 419–425. <https://doi.org/10.1016/j.oceano.2017.12.002>, [72].
- Sharma, R., Singh, G.P., Sharma, V.K., 2012. Plant pathology & microbiology effects of culture conditions on growth and biochemical profile of *Chlorella*. *J. Plant Pathology Microbiol* 3, 1–6. <https://doi.org/10.4172/2157-7471.1000131>
- Shetye, S., Sudhakar, M., Jena, B., Mohan, R., 2013. Occurrence of nitrogen-fixing cyanobacterium *Trichodesmium* under elevated p CO<sub>2</sub> conditions in the Western Bay of Bengal. *Int. J. Oceanogr.* 2013, art. no. 350465. <https://dx.doi.org/10.1155/2013/350465>, [73].

- Shunmugam, S., Gayathri, M., Prasannabalaji, N., Thajuddin, N., Muralitharan, G., 2017. Unraveling the presence of multi-class toxins from *Trichodesmium* bloom in the Gulf of Mannar region of the Bay of Bengal. *Toxicon* 135, 43–50. <https://doi.org/10.1016/j.toxicon.2017.06.003>
- Silas, G.S., Alagarwami, K., Narasimham, K.K., Appukuttan, K.K., Muthiah, P., 1982. Country Reports: India. In: Davy, F.B., Graham, M. (Eds.), *Bivalve Culture in Asia and the Pacific*. Proc. Workshop, Singapore, 34–43.
- Singh, H.S., 2003. Marine protected areas in India. *Indian J. Mar. Sci.* 32 (3), 226–233.
- Smayda, T.J., 1997. Bloom dynamics: Physiology, behavior, trophic effects. *Limnol. Oceanogr.* 42 (5 pt. 2), 1132–1136. [https://doi.org/10.4319/lo.1997.42.5\\_part\\_2.1132](https://doi.org/10.4319/lo.1997.42.5_part_2.1132)
- Stoecker, D.K., Hansen, P.J., Caron, D.A., Mitra, A., 2017. Mixotrophy in the marine plankton. *Ann. Rev. Mar. Sci.* 9, 311–335. <https://doi.org/10.1146/annurev-marine-010816-060617>
- Subrahmanyam, B., Murty, V.S.N., Heffner, D.M., 2011. Sea surface salinity variability in the Tropical Indian Ocean. *Remote Sens. Environ.* 115 (3), 1–43. <https://doi.org/10.1016/j.rse.2010.12.004>
- Subrahmanyam, R., 1954. On the life-history and ecology of *Hornelia marina* gen. et sp. nov., (Chloromonadineae), causing green discoloration of the sea and mortality among marine organisms off the Malabar coast. *Indian J. Fish.* 1–2, 182–203, [70].
- Subramanian, A., Purushothaman, A., 1985. Mass mortality of fish and invertebrates associated with a bloom of *Hemidiscus hardmannianus* (Bacillariophyceae) in Parangipettai (southern India). *Limnol. Oceanogr.* 30 (4), 910–911. <https://doi.org/10.4319/lo.1985.30.4.0910>, [74].
- Suleiman, M., Jeep, J., Rundi, C., Chua, T.H., 2017. Case Report: Paralytic Shellfish poisoning in Sabah, Malaysia. *Am. J. Trop. Med. Hyg.* 97 (6), 1731–1736. <https://doi.org/10.4269/ajtmh.17-0589>
- Sulochanan, B., Dineshbabu, A.P., Saravanan, R., Bhat, S., Lavanya, S., 2014. Locating *Noctiluca miliaris* in the Arabian Sea: An optical proxy approach. *Limnol. Oceanogr.* 59 (6), 2042–2056. <https://doi.org/10.4319/lo.2014.59.6.2042>, [75].
- Svendsen, M.B.S., Andersen, N.R., Hansen, P.J., Steffensen, J.F., 2018. Effects of Harmful Algal Blooms on Fish: Insights from *Prymnesium parvum*. *Fishes* 3 (1), 11. <https://doi.org/10.3390/fishes3010011>
- Tada, K., Plthakpol, S., Montani, S., 2004. Seasonal variation in the abundance of *Noctiluca scintillans* in the Seto Inland Sea. *Japan. Plankt. Biol. Ecol.* 51 (1), 7–14.
- Tada, K., Plthakpol, S., Montani, S., 2016. Seasonal variation in the abundance of *Noctiluca scintillans* in the Seto Inland Sea. *Japan. Plankt. Biol. Ecol.* 51 (1), 7–14.
- Thomas, A.M., 2014. Algal blooms and Associated Bacteria along the Southwest coast of India. *Cochin University of Science and Technology, Kochi, India*, 116–138.
- Thomas, A.M., Sanilkumar, M.G., Vijayalakshmi, K.C., Hatha, A.A.M., Saramma, A.V., 2014. Dynamic changes in bacterial population and corresponding exoenzyme activity in response to a tropical phytoplankton bloom *Chattonella marina*. *J. Mar. Bio.* 2014, art. no. 918614, 6 pp., <https://dx.doi.org/10.1155/2014/918614>, [77].
- Thomas, L.C., Padmakumar, K.B., Smitha, B., Devi, C.R.A., Nandan, S.B., Sanjeevan, V.N., 2013. Spatio-temporal variation of microphytoplankton in the upwelling system of the south-eastern Arabian Sea during the summer monsoon of 2009. *Oceanologia* 55 (1), 185–204. <https://doi.org/10.5697/oc.55-1.185>
- Turkoglu, M., 2013. Red tides of the dinoflagellate *Noctiluca scintillans* associated with eutrophication in the Sea of Marmara (the Dardanelles, Turkey). *Oceanologia* 55 (3), 709–732. <https://doi.org/10.5697/oc.55-3.709>
- Turner, A.D., Dhanji-Rapkova, M., Rowland-Pilgrim, S., Turner, L.M., Rai, A., Venugopal, M.N., Karunasagar, I., Godhe, A., 2017. Assessing the presence of marine toxins in bivalve mollusks from south-west India. *Toxicon* 140, 147–156. <https://doi.org/10.1016/j.toxicon.2017.11.001>
- Twiner, M.J., Flewelling, L.J., Fire, S.E., Bowen-Stevens, S.R., Gaydos, J.K., Johnson, C.K., Landsberg, J.H., Leighfield, T.A., Mase-Guthrie, B., Schwacke, L., van Dolah, F.M., Wang, Z., Rowles, T.K., 2012. Comparative analysis of three brevetoxin-associated bottlenose dolphin (*Tursiops truncatus*) mortality events in the Florida Panhandle region (USA). *PLoS ONE*. 7 (8), art. no. e42974. <https://doi.org/10.1371/journal.pone.0042974>
- Van Beusekom, J.E.E., Mendedoht, D., Augustin, C.B., Schilling, M., Boersma, M., 2009. Phytoplankton, protozooplankton, and nutrient dynamics in the Bornholm Basin (Baltic Sea) in 2002–2003 during the German GLOBEC Project. *Int. J. Earth Sci.* 98, 251–260. <https://doi.org/10.1007/s00531-007-0231-x>
- Venugopal, P., Haridas, P., Madhuratap, M., Rao, T.S.S., 1979. Incidence of red water along the Kerala Coast. *Ind. J. Mar. Sciences* 8 (2), 94–97, [78].
- Verlancar, X.N., 1978. Some observation on the *Trichodesmium* bloom along south-west coast of India. *Mahasagar-Bull. Natl. Inst. Oceanogr.* 11 (3–4), 221–224, [79].
- Vijayalakshmy, K.C., Abhijith, M., Megha, MK, Hatha, A.A.M., Saramma, A.V., 2018. Incidence of heterotrophic red *Noctiluca scintillans* blooms along Chavakkad, south-west coast of India. *Indian J. Geo Mar. Sci.* 47 (8), 1648–1651, [80].
- Walker, J., Shaver, D., Stacy, B., Flewelling, L., Broadwater, M., Wang, Z., 2018. Brevetoxin exposure in sea turtles in south Texas (USA) during *Karenia brevis* red tide. *Dis. Aquat. Organ* 127 (2), 145–150. <https://doi.org/10.3354/dao03194>
- Walworth, N., Pfreundt, U., Nelson, W.C., Mincer, T., Heidelberg, J.F., Fu, F., 2015. *Trichodesmium* genome maintains abundant, widespread noncoding DNA in situ, despite oligotrophic lifestyle. *PNAS* 112 (14), 4251–4256. <https://doi.org/10.1073/pnas.1422332112>
- Wang, Z., Yuan, M., Liang, Y., Lu, S., 2011. Effects of temperature and organic and inorganic nutrients on the growth of *Chattonella marina* (Raphidophyceae) from the Daya Bay, South China Sea. *Acta Oceanol. Sin.* 30 (3), 124–131. <https://doi.org/10.1007/s13131-011-0127-2>
- Willis, C., Papatathanasopoulou, E., Russel, D., Artioli, Y., 2018. Harmful algal blooms: the impacts on cultural ecosystem services and human well-being in a case study setting, Cornwall, UK. *Mar. Policy* 97, 232–238. <https://doi.org/10.1016/j.marpol.2018.06.002>
- Xu, Y., Zhang, T., Zhou, J., 2019. Historical occurrence of algal blooms in the Northern Beibu Gulf of China and implications for future trends. *Front. Microbiol.* 10, art. no. 451. <https://doi.org/10.3389/fmicb.2019.00451>
- Zhang, S., Liu, H., Guo, C., Harrison, P.J., 2016. Differential feeding and growth of *Noctiluca scintillans* on monospecific and mixed diets. *Mar. Ecol. Prog. Ser.* 549, 27–40. <https://doi.org/10.3354/meps11702>



## ORIGINAL RESEARCH ARTICLE

# Comparison of methods for nocturnal sampling of predatory zooplankters in shallow waters

Tomasz B. Linkowski<sup>a,\*</sup>, Ryszard Kornijów<sup>a</sup>, Maciej Karpowicz<sup>b</sup>

<sup>a</sup>Department of Fisheries Oceanography and Marine Ecology, National Marine Fisheries Research Institute, Gdynia, Poland

<sup>b</sup>Department of Hydrobiology, Faculty of Biology, University of Białystok, Białystok, Poland

Received 9 April 2020; accepted 15 October 2020

Available online 23 October 2020

## KEYWORDS

Sampling methods;  
Shallow waters;  
Vistula Lagoon;  
Column sampler;  
Light traps,  
*Leptodora*;  
*Neomysis*;  
*Cercopagis*

**Abstract** The aim of the study was to assess the suitability of a plankton net (diameter of 60 cm, mesh size of 500  $\mu\text{m}$ ) and a column sampler (length of 200 cm, diameter of 5 cm) for estimating the density of zooplankton predatory species (*Neomysis integer*, *Leptodora kindtii*, *Cercopagis pengoi*). Nocturnal sampling was performed once a month (May–November 2018) in the Vistula Lagoon (southern Baltic) in the range depth of 1.3–3.6 m. Statistical analysis indicated no significant differences between the *N. integer* and *C. pengoi* density estimated by the two sampling gears. In the case of *L. kindtii*, the mean density obtained by the column sampler was higher when analyzing all samples together and/or deep-water samples only ( $p < 0.02$ ). However, no such differences were found at shallow stations i.e. up to ca. 2 m in depth. It was assumed that the more suitable sampling equipment for estimating zooplankton abundance in a shallow, well-mixed transitional (brackish) basin is the column sampler. This type of gear, so far used mainly for sampling of micro and mesozooplankton, allows the simultaneous nocturnal collection of the entire zooplankton size spectrum, including representatives of large predatory species. The suitability of light traps for qualitative studies of zooplankton species responding positively to light under the high turbidity of the Vistula Lagoon was also investigated. The traps proved to be most useful for *N. integer* (100% frequency), and much less for *L. kindtii* (46.2%) and *C. pengoi* (27.3%).

© 2020 Institute of Oceanology of the Polish Academy of Sciences. Production and hosting by Elsevier B.V. This is an open access article under the CC BY-NC-ND license (<http://creativecommons.org/licenses/by-nc-nd/4.0/>).

\* Corresponding author at: Department of Fisheries Oceanography and Marine Ecology, National Marine Fisheries Research Institute, Koltątaja 1, 81–332 Gdynia, Poland.

E-mail address: [t.linkowski@mir.gdynia.pl](mailto:t.linkowski@mir.gdynia.pl) (T.B. Linkowski).

Peer review under the responsibility of the Institute of Oceanology of the Polish Academy of Sciences.



<https://doi.org/10.1016/j.oceano.2020.10.001>

0078-3234/© 2020 Institute of Oceanology of the Polish Academy of Sciences. Production and hosting by Elsevier B.V. This is an open access article under the CC BY-NC-ND license (<http://creativecommons.org/licenses/by-nc-nd/4.0/>).

## 1. Introduction

Predatory species of the crustacean zooplankton play an important role in the functioning of the food web of aquatic ecosystems. They are an important food source for organisms at higher trophic levels (Hostens and Mees, 1999; Ojaveer et al., 2004; Søndergaard et al., 2000;

Vijverberg et al., 1990, 2005; Vogt et al., 2013), and regulate the abundance and species structure of mesozooplankton, thus competing for food with the early developmental stages of fish (Aaser et al., 1995; Branstrator and Lehman, 1991; Herzig, 1995; Herzig and Auer, 1990; Lehtiniemi and Gorokhova, 2008; Naumenko and Telesh, 2019; Ojaveer et al., 2004; Pichlová-Ptáčnicková and Vanderploeg, 2009; Pichlová and Brandl, 2003). Indirectly, through the trophic cascade, they also influence the alternative development of primary producers (phytoplankton vs. macrophytes) and water quality (Jeppesen et al., 1994; Moss, 1994).

In fresh and brackish waters, some predatory crustaceans are of particular importance. These are cladocerans *Leptodora kindtii*, *Cercopagis pengoi* (Branstrator and Lehman, 1991; Golubkov and Litvinchuk, 2015; Herzig and Auer, 1990; Karabin, 1974; Lesutienė et al., 2012; Naumenko, 2018; Naumenko and Telesh, 2019; Pichlová-Ptáčnicková and Vanderploeg, 2009; Pichlová and Brandl, 2003) and, optionally, planktonic (necto-benthic) Mysidae – *Neomysis integer* (Aaser et al., 1995; Arndt and Jansen, 1986; Jeppesen et al., 1994). The determination of the abundance and biomass, as well as seasonal variability of all size fractions of the zooplankton in brackish waters (estuaries, lagoons, coastal lakes), including larger predatory species, is quite a challenging task. The methods currently used for mesozooplankton sampling differ in the efficiency and selectivity, so that the results are not always comparable (Gutkowska et al., 2012; Lesutienė et al., 2012; Wojtal et al., 1999). The efficiency of samplers originally developed for sampling from different depths (e.g. Ruttner sampler and similar) is lower for larger predatory species than in case of plankton nets with a larger mesh size (Lesutienė et al., 2012; Wojtal et al., 1999). In contrast, a larger mesh size for adequate filtration prevents sampling of smaller organisms such as rotifers or early larval stages of Copepoda. As a result, for a reliable estimation of the abundance/biomass of all size fractions, it is usually impossible to avoid collecting zooplankton in parallel by different methods (Wojtal et al., 1999).

The column sampler is a simple device that is often used for water sampling, including plankton in shallow basins or mesocosms (Gyllström et al., 2005; Kornijów et al., 2005; Moss et al., 1998). Youngbluth et al. (1983) were the first to demonstrate almost double the efficiency of the column sampler than the plankton net for the collection of copepod nauplii in shallow and well-mixed lagoon waters. Also, Livings et al. (2010) comparing the efficiency of a Wisconsin-type net (inlet diameter 130 mm) and two types of column samplers in terms of the efficiency of determining zooplankton abundance in shallow, polymictic lakes, assessed the column sampler as a more precise equipment. However, this assessment was based on a study of the sampling efficiency of several mesozooplankton taxa, and therefore, did not take into account predatory species, usually of a larger size and potentially greater ability to avoid the sampling gear. The suitability of column samplers for studying the vertical distribution and daily migrations of *L. kindtii* and two predatory species of copepods was found by Chang and Hanazato (2004). They used a column sampler of a similar size to the one that we used (210 × 5 cm), but equipped

with a lower hydraulic valve allowing for sampling at different depths and not only at the surface.

In case of *L. kindtii*, difficulties in estimating the abundance/biomass are additionally linked to the active avoidance of certain sampling gears during daytime surveys (Horppila et al., 2017), and to daily vertical migrations as a way to reduce pressure from predators (Vijverberg, 1991; Vogt et al., 2013). As a consequence, sampling during the day, regardless of the type of sampling gear used, may lead to understated results. However, only in a few cases, zooplankton studies were conducted at night (Alajarvi and Horppila, 2004; Horppila et al., 2017; Vogt et al., 2013; Wojtal et al., 1999).

Daily migrations also create difficulty when estimating the abundance of *N. integer*. Sampling during the day causes that the abundance of crustaceans may be underestimated even several times (2–4 times). An additional difficulty is associated with the necto-benthic occurrence of this species during the daytime (Irvine et al., 1995; Jeppesen et al., 1994). Arndt and Jansen (1986) used various types of nets and hand dredges, as well as floating and submerged light traps for sampling *N. integer* in the Darss-Zingst Bodden chain (western Baltic). In turn, Jeppesen et al. (1994) and Irvine et al. (1995) applied vertical tows using a plankton net with an opening diameter of 50–90 cm for sampling *N. integer*.

In the literature, there is no comparison of the different methods used for plankton sampling including reliable estimation of the abundance of *N. integer* and *L. kindtii*. Therefore we have conducted such studies in the Vistula Lagoon, known for the occurrence of the above mentioned predatory crustaceans, as well as the invasive Ponto-Caspian predatory cladoceran *C. pengoi* (Fadeev and Tarasov, 2001; Kornijów, 2018; Naumenko, 2009, 2018; Polunina, 2005; Ten, 1992). Our aim was to compare two ways of sampling zooplankton under the conditions of a shallow-water transitional basin to determine the optimal gear for estimating the abundance of three predatory crustacean zooplankton representatives (*L. kindtii*, *N. integer*, *C. pengoi*). We have taken into account the two most frequently used quantitative methods of sampling plankton organisms: direct sampling with the plankton net and water collection with the column sampler. Besides, we used light traps to detect the occurrence of predatory crustaceans. The samples were collected from pelagic and littoral zones to determine the impact of the habitat on the effectiveness of sampling equipment.

## 2. Material and methods

### 2.1. Research area

Comparative research was conducted in the Polish part of the Vistula Lagoon (southern Baltic). It is a shallow-water basin (mean depth of 2.7 m) with an area of 838 km<sup>2</sup>. The exchange of waters between the lagoon and the sea takes place through the Strait of Baltiysk, located in the Russian part of the basin. As a result, the maximum salinity value of about 6 g/kg at the strait gradually decreases to <1 g/kg at the western ends of the basin (Chubarenko and

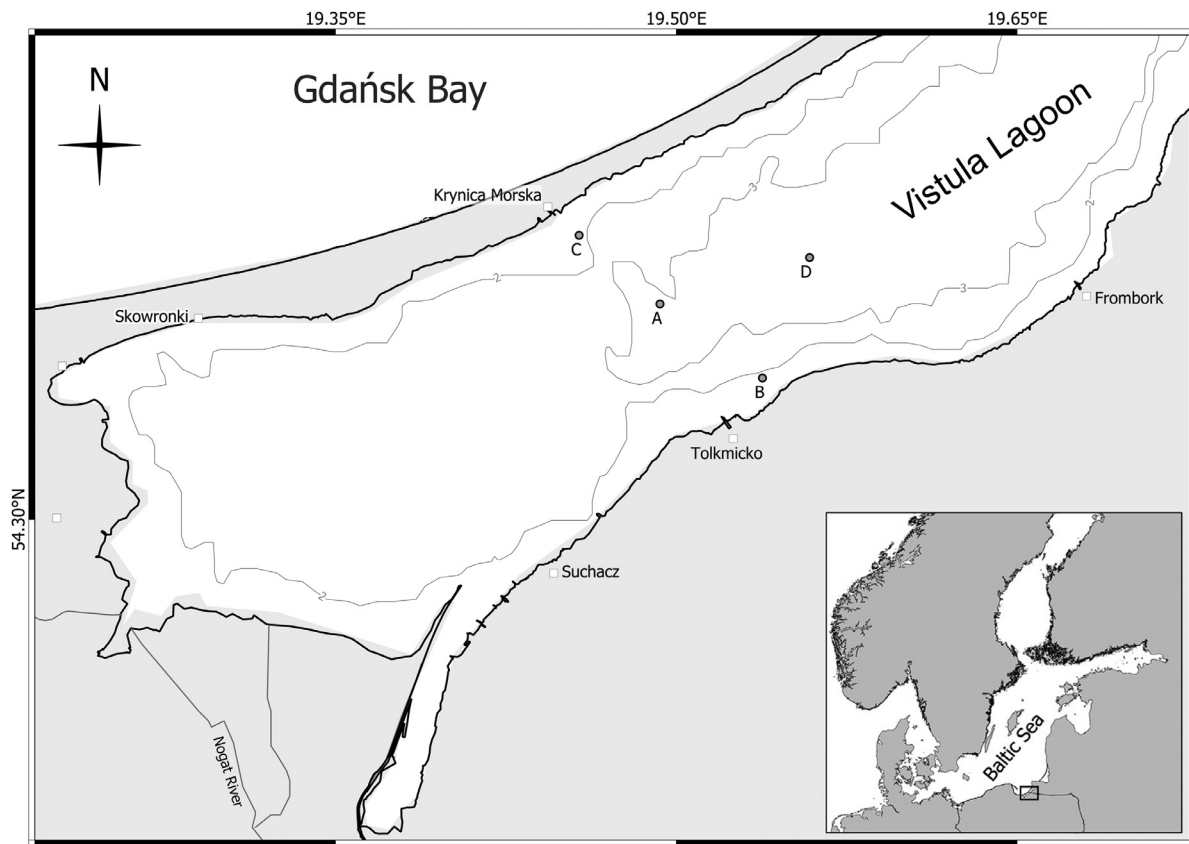


**Figure 1** The geographical location of paired samples collected with the plankton net and column sampler in the Polish part of Vistula Lagoon (southern Baltic).

Margoński, 2008). Most of the research was conducted at two stations located approximately on the fairway line between the ports of Tolkmicko and Krynica Morska. Station A: (54,35528°N, 19,49281°E) was located centrally at a depth of about 3 m in the open water zone (pelagic). Station B: (54,3363°N, 19,53793°E) was located in a line of Tolkmicko in the littoral zone at a depth of 1.16–1.88 m, where the bottom was overgrown with the vast patches of *Potamogeton perfoliatus* L. Samples were taken with three sampling gears at least once a month.

Four additional samples, occasionally taken from other locations where light traps were not exposed, were also used for the analyses: Station Ba located near station B (ca. 50 m), and once at two stations in the open water zone of varying depth: station C, depth 2.21 m (included arbitrarily in “shallow stations”); station D, depth 3.64 m. The location of the sampling sites is shown in Figure 1.

## 2.2. Sampling gear, method of collecting and analyzing zooplankton samples

The column sampler was a polycarbonate pipe 2 m long and 50 mm in internal diameter. When submersed, the upper end of the pipe was closed with a rubber cork to keep the water inside the sampler during recovering it aboard. At every station, 10 liters of water were taken, i.e. 3 to 5 sampler contents, depending on the depth of the station, and then filtered through a 50  $\mu\text{m}$  mesh netting.

For vertical tows, a conical plankton net with an opening diameter of 60 cm, a length of 1 m and a mesh size of 500  $\mu\text{m}$  was used. The circular frame of the plankton net was supported by a 10 cm width collar to prevent contamination of the zooplankton sample by bottom sediments. The net was lowered to the bottom and after approx. 30–60 seconds (depending on the depth and wind force) was lifted at a speed of about 0.5  $\text{m s}^{-1}$ . The volume of water filtered through the plankton net was calculated based on the flowmeter indications (General Oceanic) and the net opening area. Sampling performed with the column sampler and with the net were conducted after nightfall. The volume of water filtered in one tow was from 230 to 1610 liters, depending on the station depth and weather conditions. Performing vertical hauls was often not possible due to strong winds and the requirement that the net should stay on the bottom 30–60 seconds to let *Neomysis integer* return to the bottom surface disturbed by the lowered net. A small drift was observed even the boat was always anchored that led to partly oblique rather than 100% vertical hauls and resulted in a larger volume of filtered water than could be expected solely from the water depth and the net opening surface. Light traps usually are used for qualitative research of zooplankton that responds positively to the light attraction (McLeod and Costello, 2017). We used light traps to verify if the analyzed predatory species were present in the environment, as due to their low abundance and/or avoiding the sampling gear could be missing in the



**Figure 2** Light trap used in this project: a) overall look; b) light module. The arrow indicates the location of the battery compartment cap of the light module.

samples collected with the plankton net or column sampler. Our light traps were made as described by (Watson et al., 2002) with minor modifications (Figure 2).

The trap consisted of two connected black polyethylene buckets with a capacity of 20 liters each (height 33 cm, bottom diameter 27 cm, top diameter 32 cm), connected by a steel frame. A float was attached to the upper part of the frame, and a rope with an anchor to the lower part. The total height of the device with the frame and float was 138 cm. In the upper part of the trap, 9 funnel-shaped head-

lights with an area of 45 cm<sup>2</sup> made of transparent polyethylene were mounted. Their larger diameter (78 mm) was integrated with the trap wall, while the smaller (21 mm) was directed to the inside of the trap, constituting at the same time the entrance funnel. White light attracting zooplankters was emitted by light modules made of acrylic cylinders with a diameter of 15 mm and a length of 30 cm (Figure 2b). Each module was equipped with 54 diodes arranged in three rows of 18 pieces and placed in a sealed transparent acrylic sleeve mounted vertically in the center of the upper part of the trap, where there were also light-emitting headlights. Each module was equipped with an energy source in the form of two 9V alkaline cells (type: 6LR61). After a single use, the cells were replaced with new ones to avoid changing the intensity of the emitted light as a result of partial battery depletion. The lower part of the light trap was a sampling container for draining plankton when the whole device was retrieved from the water. For this purpose, six "filtering windows" measuring 5 × 19 cm each, made of a plankton net with a mesh size of 500 μm, were installed. The light traps were exposed before nightfall and were retrieved the next morning. The location of the light-emitting trap part in the water column depended on the depth at particular stations. At station A it was about 1.5–1.8 m from the surface, at the station in the area of submerged vegetation (B) about 0.7–1.0 m.

Samples were taken between May and November 2018 at approximately monthly intervals from the MIR-2 research boat (Table 1). Altogether a total of 53 zooplankton samples were collected, including 15 samples using light traps, 19 samples using vertical tows with a plankton net, and 19 samples using a column sampler. All collected zooplankton samples were immediately preserved with 40% borax-buffered formalin at a ratio of 1/9 of formalin to sample volume. When analyzing the composition of plankton from the plankton net and light traps sub-samples were taken up to 200 individuals of each species, while in case of samples collected with the column sampler, all collected material was analyzed.

Basic environmental parameters (salinity and temperature) were measured with a CastAway™ CTD probe before collecting zooplankton samples and deploying light traps. Moreover, during the retrieval of light traps, the transparency of water was measured with a Secchi disc. The number of samples collected by particular sampling gears in the

**Table 1** Number of zooplankton samples collected by different gears and environmental variables in the Polish part of the Vistula Lagoon, southern Baltic in April–November 2018. Variable values are the means of the sampling occasions.

Month	No. of samples			Environmental variables (mean values)				
	Light traps	Plankton net	Column sampler	Temperature [°C]		Salinity [g/kg]		Secchi depth [m]
				surface	bottom	surface	bottom	
May	3	3	3	17.52	17.76	1.39	1.58	0.40
June	2	2	2	21.48	21.16	1.94	1.91	0.39
July	2	3	3	25.78	25.77	2.32	2.33	0.55
August	2	5	5	21.51	21.33	2.79	2.81	0.73
September	2	2	2	19.17	18.94	3.17	3.16	1.35
October	2	2	2	13.08	12.83	3.76	4.28	1.38
November	2	2	2	8.85	8.85	3.98	3.98	1.55

subsequent months, as well as the environmental parameters are presented in Table 1.

## 2.3. Statistical methods

Dependent t-test for paired samples was used to compare the effectiveness of predatory crustacean sampling using vertical tows with a plankton net and a column sampler. Statistical calculations were performed with the data analysis software system STATISTICA v. 10 (StatSoft. Inc., 2011).

Due to the different depths at the sampled stations and the different vertical range of impact of the studied gears (column sampler – from the surface to approx. 2 m in depth, plankton net – from the bottom to the surface), the analysis was performed separately for three data sets to exclude the impact of the depth factor on the results: (i) all samples, (ii) samples from deeper stations (bottom depth range 3.08–3.64 m), (iii) samples from shallower stations (1.16–2.21 m). The comparison of sampling efficiency using two studied gears was also performed separately for each of the three predatory species.

## 3. Results

### 3.1. Environmental parameters

Basic environmental parameters (Table 1) are presented to draw attention to seasonal changes and characteristics of changes in the water column. The observed changes in water temperature were characteristic of shallow water basins in the temperate zone. In the course of the research period, a clear trend of salinity increase was noted, i.e. from about 1.4 g/kg in May to about 4.0 g/kg and even more in October and November. A seasonal trend also applies to the Secchi depth, i.e. the water transparency. It increased significantly at the end of the growing season (Table 1).

### 3.2. Comparison of the sampling gears

The comparison of results obtained with three different methods gives an overview of the effectiveness of particular sampling gears for determining the occurrence of predatory crustaceans in the environment (Table 2). The frequency of occurrence of particular species in the gears applied provides some indication of their suitability for sampling the analyzed species. *Neomysis integer* showed the highest susceptibility to light attraction and occurred in all samples (frequency of occurrence = 100%). The frequency of this species in samples from the plankton net and column sampler was significantly lower (84.2% and 36.3%, respectively). The efficiency of light attraction for *Leptodora kindtii* and *Cercopagis pengoi* was significantly lower, amounting to 42.6% and 27.3%, respectively. *L. kindtii* specimens were most often found in samples obtained with the net and sampler rather than with the light traps (Table 2), while *C. pengoi* was most often caught using the plankton net.

The results of the statistical analysis of the density of the three predatory species based on the samples taken with the plankton net and column sampler are shown in Table 3. The efficiency of the column sampler and plankton

net applied for *N. integer* and *C. pengoi* sampling, calculated based on all compared samples, as well as separately for materials collected at deep-water and shallow-water stations, did not differ significantly (Table 3). In the case of *L. kindtii*, the mean density obtained by sampling using the column sampler and plankton net differed considerably when analyzing all samples together and deep-water samples ( $p < 0.02$ ). The mean density of *L. kindtii* was significantly higher for the samples taken with the sampler than for those taken with the plankton net. However, no such differences were found at shallow stations (Table 3).

## 4. Discussion

The efficiency of sampling *Neomysis integer* and *Cercopagis pengoi* using two sampling gears for quantitative studies, i.e. the plankton net and column sampler, proved to be comparable as we found no significant differences in the density of the two species estimated by these gears (Table 2). However, the reason for the lack of significant differences may be due to the low density of these crustaceans or uneven/aggregated distribution (see: Wojtal et al., 1999).

There were no significant differences in the density of *Leptodora kindtii* obtained with the net and column sampler at shallow water stations. This was in the opposition to the deeper stations ( $> 2.2$  m) and all the stations analyzed together. It resulted from the different water column penetration depths of the gears, i.e. from the bottom to the surface (plankton net) vs. from the surface to the depth of 2 m (column sampler). Higher density in samples taken with the column sampler than with the plankton net at deep-water stations may indirectly indicate that this is the effect of uneven distribution of the *L. kindtii* in the water column, implying higher values in the surface layer of 0–2 m in depth.

The results obtained and the assessment of the effectiveness of the samplers could also be influenced by the difference in abundance of the studied crustaceans. The assessment of the density of most numerous *L. kindtii* based on sampling with the column sampler is considered more reliable than based on tows performed with the plankton net. The opposite conclusion can be drawn for *C. pengoi* which was a less abundant species. The small volume of water collected using the column sampler does not allow recommending this gear for surveying not abundant species.

The problem of differences in the volume of water filtered by various gears was also raised by Wojtal et al. (1999). Despite the lack of statistically significant differences between the vertical density of *L. kindtii* determined by using a bongo and a 5 L Bernatowicz's sampler, the authors found that the results from the sampler are not useful for determining the vertical distribution of this predatory cladocerans in a shallow dam reservoir. In their opinion, the large differences in the volume of water filtered by the bongo and taken with the sampler, combined with the aggregated distribution of zooplankton, resulted in very high variability of the results obtained by the sampler (Wojtal et al., 1999). As an additional reason for the unreliable results in a near-surface layer of 1–2 m using Bernatowicz's sampler, the authors recognized the ability of this cladoceran to avoid the sampler, despite the research was performed in the night time.

**Table 2** Total number of three predatory zooplankton species caught with a single deployment of light traps (LT), density [spec. L<sup>-1</sup>] estimated by vertical tows of a plankton net (VPN) and a column sampler (CS). The frequency (F) of occurrence [%] of species in samples collected by each gear is presented at the bottom of the table. x – the gear was not applied on this date and station

Date	Station	Depth [m]	<i>Neomysis integer</i>			<i>Leptodora kindtii</i>			<i>Cercopagis pengoi</i>		
			LT [total number]	VPN [spec. L <sup>-1</sup> ]	CS [spec. L <sup>-1</sup> ]	LT [total number]	VPN [spec. L <sup>-1</sup> ]	CS [spec. L <sup>-1</sup> ]	LT [total number]	VPN [spec. L <sup>-1</sup> ]	CS [spec. L <sup>-1</sup> ]
21/22 May	A	3.24	15	0.003	0	53	0.504	1.5	21	0.0204	0.3
21/22 May	B	1.7	45	0	0	896	0.002	1.4	0	0.0028	0
21/22 May	Ba	1.3	56	0.0024	0	9	1.296	0.7	0	0.0169	0
12/13 Jun	A	3.15	154	0.005	0	38400	22.016	29.4	41	0.0252	0
12/13 Jun	B	1.53	8	0.0041	0	49	12.928	14.5	0	0	0
25/26 Jul	A	3.47	3104	0	0	0	0.113	3.9	0	0	0.4
25/26 Jul	B	1.84	1520	0.0525	0.1	0	0.613	5.8	0	0	0
26 Jul	A	3.49	x	0.007	0.1	x	0.712	3.2	x	0	0
22/23 Aug	A	3.46	1424	0.079	0.9	0	0.388	2.3	0	0.053	0
22/23 Aug	B	1.88	276	0.0731	0	84	2.401	0	13	0.069	0.1
22 Aug	Ba	1.58	x	0.002	0	x	0.319	0.6	x	0	0
22 Aug	D	3.64	x	0.030	0.4	x	0.098	1.3	x	0.019	0
22 Aug	C	2.21	x	0.006	0	x	0.019	0.8	x	0.002	0
20/21 Sep	A	3.4	18944	0.776	0.5	0	0	0.2	0	0.004	0
20/21 Sep	B	1.87	14672	0.166	0	0	0	0	0	0.003	0
18/19 Oct	A	3.52	1576	0.083	0	0	0	0.2	0	0	0
18/19 Oct	B	1.75	11456	0	0.4	0	0	0	0	0	0
7/8 Nov	A	3.4	968	0.007	0.1	0	0	0	0	0	0
7/8 Nov	B	1.73	155082	1.111	0	0	0	0	0	0	0
F [%]			100.0	84.2	36.8	46.2 <sup>*)</sup>	76.5 <sup>*)</sup>	82.4 <sup>*)</sup>	27.3 <sup>**)</sup> 1	66.7 <sup>**)</sup>	20.0 <sup>**)</sup>

<sup>\*)</sup> For F calculations, the November results were not included, as *L. kindtii* was found in none of the sampling gears.

<sup>\*\*)</sup> For F calculations, the October and November results were not included, as *C. pengoi* was found in none of the sampling gears.

**Table 3** The quantitative effectiveness of zooplankton sampling with two different gears: the column sampler (CS) and the vertical plankton net (VPN) compared by the dependent t-test for paired samples. The calculations were made separately for all stations, shallow ( $\leq 2$  m) and deep stations ( $> 2$  m). Statistically significant differences are marked in bold.

	<i>Leptodora kindtii</i>			<i>Cercopagis pengoi</i>			<i>Neomysis integer</i>		
	All	Shallow	Deep	All	Shallow	Deep	All	Shallow	Deep
CS mean [spec. L <sup>-1</sup> ]	4.387	3.400	5.250	0.080	0.025	0.117	0.139	0.050	0.250
SD mean	7.828	5.267	9.846	0.148	0.050	0.183	0.250	0.127	0.325
VPN mean [spec. L <sup>-1</sup> ]	2.765	2.517	2.982	0.020	0.020	0.021	0.145	0.163	0.124
SD mean	6.245	4.667	7.695	0.023	0.032	0.019	0.304	0.345	0.266
df	14	6	7	9	3	5	17	9	7
t	2.630	1.002	2.682	1.243	0.544	1.221	-0.074	-0.916	0.321
p	<b>0.020</b>	0.355	<b>0.031</b>	0.245	0.624	0.277	0.942	0.384	1.067

The suitability of column samplers for studying the vertical distribution and daily migrations of *L. kindtii* was found by Chang and Hanazato (2004) while the presented results regarding the possibility of sampling *N. integer* with the column sampler as well as using light traps at the same time as active sampling devices (plankton net and column sampler) are novelties of this paper.

The light traps used in this study, based on the project of Watson et al. (2002) are classified by McLeod and Costello (2017) as cylindrical traps with reflector light emission and entrance funnels located in the center of the headlights. Only raw results of the sampling were presented and no attempt has been made to determine the effectiveness of sampling of particular species. This is due to the fact that several abiotic factors that may potentially influence the effectiveness of light traps have not been studied, e.g. the area of light exposure under different conditions of water transparency, changes in the night time duration in the research cycle, cloudiness and phase of the moon, which may affect the results (McLeod and Costello, 2017).

The light traps were used to obtain additional information on the occurrence of the predatory zooplankters in case of the lack or low effectiveness of the active gears used. *N. integer* was recorded less frequently by the column sampler and plankton net than in the light traps. This trend was particularly noticeable in relation to the results obtained with the column sampler (Table 2), which may be associated with relatively low density of *N. integer* and a small volume of water taken for analyses with this gear. The difference in the frequency of *L. kindtii* in the light traps and active gears are no longer so unambiguous, which may be the result of factors that have a potential impact on attraction by light (e.g. moon phase and cloudiness, degree of water turbidity), as well as a drastic decrease in the density of this species in the environment at the end of observations. A similar limitation on the interpretation of the efficiency of light trap sampling applies also to *C. pengoi*, which was the least abundant species and had the shortest period of occurrence.

The light traps, which are considered to be passive gears for the collection of different groups of aquatic organisms, are most often used in habitats that limit the use of active plankton sampling gears (e.g. coral reefs or mangroves). Light traps are also used to sample organisms which avoid

plankton nets (for a review see: McLeod and Costello, 2017). The suitability of light traps for zooplankton sampling in the littoral of inland lakes under dense vegetation conditions has been demonstrated by Szlauer (1971).

The information on the effectiveness of sampling using light traps of the species considered in this study is quite limited. Among others, Arndt and Jansen (1986) listed light traps as one of the sampling gears used in their research focused on *N. integer*. In their opinion, estimating the abundance of this species is difficult due to the occurrence in swarms, as well as vertical and horizontal migrations. A positive response to the light attraction of two species of Mysidacea (*N. integer* and *Mysis mixta*) was also noted in the Puck Bay (Southern Baltic) in the NMFRI project, which used among others the same light traps as in the current studies (Linkowski unpubl.). Szlauer (1971) using a light trap of his own design in freshwater basins, identified *L. kindtii* in a group of cladocerans highly susceptible to being attracted by light.

## 5. Conclusions

Our study compared the efficiency of nocturnal sampling of three species of predatory zooplankton in a shallow transitional basin with two different gears (plankton net and column sampler), against the background of their occurrence confirmed by the light traps. The obtained results offer the possibility of collecting integrated zooplankton samples (covering all size fractions of organisms occurring in the water column) with one gear, i.e. the column sampler. This conclusion is valid when accepting certain limitations. Firstly, the surveys must be performed at night and, due to the small volume of water collected, the representativeness of the data obtained for the less numerous species, e.g. *Cercopagis pengoi*, will be limited. In case of applying a longer column sampler than the one used in this study, e.g. 4 m long, the range of depths, which can be sampled representatively with this gear, can probably remarkably increase. This creates an opportunity to determine the density of all zooplankton size fractions with a single gear in numerous shallow-water transitional habitats, the depth of which does not exceed the length of the sampler.

The results obtained indicate high effectiveness of light traps as a method to determine the occurrence and possibly seasonal distribution, in particular of *Neomysis integer*, and to a lesser extent also of *Leptodora kindtii* and *C. pengoi*, in a shallow, turbid and well mixed lagoon-type transitional basin.

## Acknowledgement

The paper is a result of the project DOT 18/Lagoon (Trophic interactions and their consequences for water quality in the Vistula Lagoon under the anticipated increase of human pressure), supported by the statutory funds of the National Marine Fisheries Research Institute, Gdynia, Poland. The engagement of one author has received financial support from the Polish Ministry of Science and Higher Education under subsidy for maintaining the research potential of the Faculty of Biology, University of Białystok. We are grateful to the members of the Department of Logistics and Monitoring (NMFRI) Mr. Radostaw Zaporowski and Mr. Władysław Gawel for their help in the field sampling. We kindly acknowledge detailed comments and suggestions made by anonymous reviewers which certainly improved the final version of the paper.

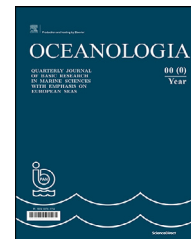
## References

- Aaser, H.F., Jeppesen, E., Sondergaard, M., 1995. Seasonal dynamics of the mysid *Neomysis integer* and its predation on the copepod *Eurytemora affinis* in a shallow hypertrophic brackish lake. *Mar. Ecol. Prog. Ser.* 127, 47–56. <https://doi.org/10.3354/meps127047>
- Alajarvi, E., Horppila, J., 2004. Diel variations in the vertical distribution of crustacean zooplankton and food selection by planktivorous fish in a shallow turbid lake. *Int. Rev. Hydrobiol.* 89, 238–249. <https://doi.org/10.1002/iroh.200310707>
- Arndt, E.A., Jansen, W., 1986. *Neomysis integer* (Leach) in the chain of Boddens South of Darss Zingst (Western Baltic). *Ecophysiology and population dynamics*. *Ophelia* 1–15.
- Branstrator, D.K., Lehman, J.T., 1991. Invertebrate predation in Lake Michigan: Regulation of *Bosmina longirostris* (O. F. Mueller) by *Leptodora kindtii* (Focke). *Limnol. Oceanogr.* 36, 483–495.
- Chang, K.H., Hanazato, T., 2004. Diel vertical migrations of invertebrate predators (*Leptodora kindtii*, *Thermocyclops taihokuensis*, and *Mesocyclops* sp.) in a shallow, eutrophic lake. *Hydrobiologia* 528, 249–259. <https://doi.org/10.1007/s10750-004-3952-x>
- Chubarenko, B., Margoński, P., 2008. The Vistula Lagoon. In: Schiewer, U. (Ed.), *Ecology of Baltic Coastal waters*. Ecological Studies Springer-Verlag, Berlin-Heidelberg, 167–195.
- Fadeev, V.I., Tarasov, V.G., 2001. Structure and production parameters of the Mysidacea from the Vistula Lagoon, Baltic Sea. *Tezisy dokladov VIII Syjezda Gidrobiologicheskogo Obschestva RAN* 3, 311–312 [in Russian].
- Golubkov, S.M., Litvinchuk, L.F., 2015. The role of the alien species *Cercopagis pengoi* in zooplankton of the Eastern Gulf of Finland of the Baltic Sea. *Doklady Biol. Sci.* 462, 121–123. <https://doi.org/10.1134/S0012496615030011>
- Gutkowska, A., Paturej, E., Kowalska, E., 2012. Qualitative and quantitative methods for sampling zooplankton in shallow coastal estuaries. *Ecohydrol. Hydrobiol.* 12, 253–263. [https://doi.org/10.1016/S1642-3593\(12\)70208-2](https://doi.org/10.1016/S1642-3593(12)70208-2)
- Gyllström, M., Hansson, L.A., Jeppesen, E., Garcia-Criado, F., Gross, E., Irvine, K., Kairesalo, T., Kornijów, R., Miracle, M.R., Nykanen, M., Nöges, T., Romo, S., Stephen, D., Van Donk, E., Moss, B., 2005. The role of climate in shaping zooplankton communities of shallow lakes. *Limnol. Oceanogr.* 50, 2008–2021. <https://doi.org/10.4319/lo.2005.50.6.2008>
- Herzig, A., 1995. *Leptodora kindtii*: efficient predator and preferred prey item in Neusiedler-See, Austria. *Hydrobiologia* 307, 273–282. <https://doi.org/10.1007/Bf00032021>
- Herzig, A., Auer, B., 1990. The feeding behavior of *Leptodora kindtii* and its Impact on the zooplankton community of Neusiedler-See (Austria). *Hydrobiologia* 198, 107–117. <https://doi.org/10.1007/Bf00048627>
- Horppila, J., Laakso, S., Niemisto, J., Nurminen, L., 2017. Size-specific net avoidance behavior leads to considerable underestimation of the biomass of *Leptodora kindtii* during day time sampling. *Int. Rev. Hydrobiol.* 102, 151–158. <https://doi.org/10.1002/iroh.201701902>
- Hostens, K., Mees, J., 1999. The mysid-feeding guild of demersal fishes in the brackish zone of the Westerschelde estuary. *J. Fish. Biol.* 55, 704–719. <https://doi.org/10.1111/j.1095-8649.1999.tb00712.x>
- Irvine, K., Snook, D., Moss, B., 1995. Life histories of *Neomysis Integer*, and its copepod prey, *Eurytemora affinis*, in a eutrophic and brackish shallow lake. *Hydrobiologia* 304, 59–76. <https://doi.org/10.1007/Bf02530704>
- Jeppesen, E., Sondergaard, M., Kanstrup, E., Petersen, B., Eriksen, R.B., Hammershoj, M., Mortensen, E., Jensen, J.P., Have, A., 1994. Does the impact of nutrients on the biological structure and function of brackish and fresh-water lakes differ? *Hydrobiologia* 275, 15–30.
- Karabin, A., 1974. Studies on the predatory role of the cladoceran *Leptodora kindtii* (Focke), in secondary production of two lakes with different trophy. *Ekol. Pol.* 22, 295–310.
- Kornijów, R., 2018. Ecosystem of the Polish part of the Vistula Lagoon from the perspective of alternative stable states concept, with implications for management issues. *Oceanologia* 60 (3), 390–404. <https://doi.org/10.1016/j.oceano.2018.02.004>
- Kornijów, R., Vakkilainen, K., Horppila, J., Luokkanen, E., Kairesalo, T., 2005. Impacts of a submerged plant (*Elodea canadensis*) on interactions between roach (*Rutilus rutilus*) and its invertebrate prey communities in a lake littoral zone. *Freshwater Biol.* 50, 262–276. <https://doi.org/10.1111/j.1365-2427.2004.01318.x>
- Lehtiniemi, M., Gorokhova, E., 2008. Predation of the introduced cladoceran *Cercopagis pengoi* on the native copepod *Eurytemora affinis* in the northern Baltic Sea. *Mar. Ecol. Prog. Ser.* 362, 193–200. <https://doi.org/10.3354/meps07441>
- Lesutienė, J., Semenova, A., Griniene, E., Gasiunaite, Z.R., Savickyte, V., Dmitrieva, O., 2012. Abundance dynamics and functional role of predaceous *Leptodora kindtii* in the Curonian Lagoon. *Cent. Eur. J. Biol.* 7, 91–100. <https://doi.org/10.2478/s11535-011-0098-5>
- Livingston, M.E., Schoenebeck, C.W., Brown, M.L., 2010. Comparison of Two Zooplankton Sampling Gears in Shallow, Homogeneous Lakes. *Prairie Naturalist* 42, 19–23.
- McLeod, L.E., Costello, M.J., 2017. Light traps for sampling marine biodiversity. *Helgol. Mar. Res.* 71, art. no. 2. <https://doi.org/10.1186/s10152-017-0483-1>
- Moss, B., 1994. Brackish and freshwater shallow lakes - different systems or variations on the same theme? *Hydrobiologia* 275, 1–14. <https://doi.org/10.1007/BF00026695>
- Moss, B., Kornijów, R., Measey, G.J., 1998. The effects of nymphaeid (*Nuphar lutea*) density and predation by perch (*Perca fluviatilis*) on the zooplankton communities in a shallow lake. *Freshwater Biol.* 39, 689–697. <https://doi.org/10.1046/j.1365-2427.1998.00322.x>

- Naumenko, E.N., 2009. Zooplankton in different types of estuaries (using Curonian and Vistula estuaries as an example). *Inland Water Biol.* 2, 72–81. <https://doi.org/10.1134/S1995082909010118>
- Naumenko, E.N., 2018. Seasonal and long-term dynamics of population abundance of the invasive species *Cercopagis pengoi* (Ostroumov, 1891) in the Vistula (Kaliningrad) Lagoon of the Baltic Sea. *Russian J. Biol. Invasions* 9, 147–154. <https://doi.org/10.1134/s207511171802008x>
- Naumenko, E.N., Telesh, I.V., 2019. Impact of the Invasive Species *Cercopagis pengoi* Ostroumov, 1891 on the Structural and Functional Organization of Zooplankton in the Vistula Lagoon of the Baltic Sea. *Russian J. Biol. Invasions* 10, 246–257. <https://doi.org/10.1134/S2075111719030081>
- Ojaveer, H., Simm, M., Lankov, A., 2004. Population dynamics and ecological impact of the non-indigenous *Cercopagis pengoi* in the Gulf of Riga (Baltic Sea). *Hydrobiologia* 522, 261–269. <https://doi.org/10.1023/B:Hydr.0000029927.91756.41>
- Pichlová-Ptáčnicková, R., Vanderploeg, H.A., 2009. The invasive cladoceran *Cercopagis pengoi* is a generalist predator capable of feeding on a variety of prey species of different sizes and escape abilities. *Fund. Appl. Limnol.* 173, 267–279. <https://doi.org/10.1127/1863-9135/2009/0173-0267>
- Pichlová, R., Brandl, Z., 2003. Predatory impact of *Leptodora kindtii* on zooplankton community in the Slapy Reservoir. *Hydrobiologia* 504, 177–184. <https://doi.org/10.1023/B:HYDR.0000008517.64246.f4>
- Polunina, J., 2005. Populations of two predatory cladocerans in the Vistula Lagoon – the native *Leptodora kindtii* and the non-indigenous *Cercopagis pengoi*. *Oceanol. Hydrobiol. St.* 34, 249–260.
- Søndergaard, M., Jeppesen, E., Aaser, H.F., 2000. *Neomysis integer* in a shallow hypertrophic brackish lake: distribution and predation by three-spined stickleback (*Gasterosteus aculeatus*). *Hydrobiologia* 428, 151–159. <https://doi.org/10.1023/A:1003923600795>
- StatSoft. Inc., 2011. STATISTICA (data analysis software system). Version 10. [www.statsoft.com](http://www.statsoft.com)
- Szlauer, L., 1971. Fishing of lake Arthropoda into light traps. *Pol. Arch. Hydrobiol.* 18, 81–91.
- Ten, V.V., 1992. Population structure, life cycle and production characteristics of mysids from the Vistula Bay, Baltic Sea, Ecological fisheries research in the Vistula Lagoon of the Baltic Sea, Trudy AtlantNIRO 64–83, 64–83 [In Russian].
- Vijverberg, J., 1991. Variability and possible adaptive significance of day-time vertical distribution of *Leptodora kindtii* (Focke) (Cladocera) in a shallow eutrophic lake. *Hydrobiol. Bull.* 25, 85–91. <https://doi.org/10.1007/BF02259594>
- Vijverberg, J., Boersma, M., Vandensen, W.L.T., Hoogenboezem, W., Lammens, E.H.R.R., Mooij, W.M., 1990. Seasonal variation in the interactions between piscivorous fish, planktivorous fish and zooplankton in a shallow eutrophic lake. *Hydrobiologia* 207, 279–286. <https://doi.org/10.1007/Bf00041466>
- Vijverberg, J., Koelewijn, H.P., van Densen, W.L.T., 2005. Effects of predation and food on the population dynamics of the raptorial cladoceran *Leptodora kindtii*. *Limnol. Oceanogr.* 50, 455–464. <https://doi.org/10.4319/lo.2005.50.2.0455>
- Vogt, R.J., Matthews, B., Cobb, T.P., Graham, M.D., Leavitt, P.R., 2013. Food web consequences of size-based predation and vertical migration of an invertebrate predator (*Leptodora kindtii*). *Limnol. Oceanogr.* 58, 1790–1801. <https://doi.org/10.4319/lo.2013.58.5.1790>
- Watson, M., Power, R., Simpson, S., Munro, J.L., 2002. Low cost light traps for coral reef fishery research and sustainable ornamental fisheries. *NAGA* 25 (2), 4–7.
- Wojtal, A., Frankiewicz, P., Zalewski, M., 1999. The role of the invertebrate predator *Leptodora kindtii* in the trophic cascade of a lowland reservoir. *Hydrobiologia* 416, 215–223. <https://doi.org/10.1023/A:1003815520751>
- Youngbluth, M.J., Gibson, R.A., Holt, J.K., 1983. Use of a simple water column sampler to monitor chemical and biological conditions in shallow waters. *Florida Scientist* 46, 15–21.

Available online at [www.sciencedirect.com](http://www.sciencedirect.com)

ScienceDirect

journal homepage: [www.journals.elsevier.com/oceanologia](http://www.journals.elsevier.com/oceanologia)

## ORIGINAL RESEARCH ARTICLE

# Do seasonal dynamics influence traits and composition of macrobenthic assemblages of Sundarbans Estuarine System, India?

Moumita Bhowmik, Sumit Mandal\*

Marine Ecology Laboratory, Department of Life Sciences, Presidency University, Kolkata, India

Received 6 May 2020; accepted 19 October 2020

Available online 5 November 2020

**KEYWORDS**

Macroinvertebrates;  
Biological Traits  
Analysis;  
RLQ;  
Succession;  
Sundarbans

**Abstract** The present study investigates the influence of seasonal dynamics on macrobenthic assemblages in four seasons of 2017–2018 from the central sector of Indian Sundarbans which is under the constant threat of climate change. Besides taxonomic analysis, a trait-based approach has also been applied to assess the change in their ecosystem functioning. The maximum species density ( $11675 \pm 11883.31 \text{ ind. m}^{-2}$ ) was observed during the spring season which declines considerably in the monsoon season ( $5875 \pm 6224.08 \text{ ind. m}^{-2}$ ). A total of 95 macrobenthic taxa were recorded from Sundarbans and they were dominated by families like Capitellidae, Donacidae, Magelonidae, Nereididae, Paraonidae and Spionidae. Overall, polychaetes have shown higher taxonomic and functional variation than other groups. Opportunistic polychaete species have shown a prominent compositional shift during post-monsoon seasons. Both the univariate and multivariate analyses have shown a significant relation between macrobenthic composition and environmental parameters. SIMPER has depicted that environmental parameters made the station 4 unique for several types of molluscs like *Acteocina estriata*, *Stenothyra deltae* and *Meretrix meretrix* during spring. Trait percentages also showed a seasonal succession pattern and among the trait categories, burrowers and deposit feeders dominated the estuary. A gradual increase in suspension feeders in spring has been noticed. RLQ

\* Corresponding author at: Marine Ecology Laboratory, Department of Life Sciences, Presidency University, 86/1 College Street, Kolkata 700073, India.

E-mail address: [sumit.dbs@presiuniv.ac.in](mailto:sumit.dbs@presiuniv.ac.in) (S. Mandal).

Peer review under the responsibility of the Institute of Oceanology of the Polish Academy of Sciences.



Production and hosting by Elsevier

<https://doi.org/10.1016/j.oceano.2020.10.002>

0078-3234/© 2020 Institute of Oceanology of the Polish Academy of Sciences. Production and hosting by Elsevier B.V. This is an open access article under the CC BY-NC-ND license (<http://creativecommons.org/licenses/by-nc-nd/4.0/>).

approach with fourth-corner analysis was used to unravel the relationship between traits and environmental parameters. Hence, the present study provided a comprehensive idea about the species composition along with their trait categories from such a dynamic habitat. That could be the first stepping stone for a long term monitoring of macrobenthic assemblages from this largest delta on earth.

© 2020 Institute of Oceanology of the Polish Academy of Sciences. Production and hosting by Elsevier B.V. This is an open access article under the CC BY-NC-ND license (<http://creativecommons.org/licenses/by-nc-nd/4.0/>).

## 1. Introduction

An estuary acts as a transitional zone between marine and freshwater domains where it plays a crucial role in controlling fluxes between ecosystems as well as in faunal distribution (Modéran et al., 2010). Being a buffer zone, estuaries share both the characteristics of the river and ocean. It has been continually exposed to various hydrological pressures, which results in a highly dynamic habitat. Moreover, due to high productivity, estuaries serve as breeding and nursery grounds for various faunal communities. However, in recent times, it has become one of the most degraded ecosystems globally (Kennish, 2002). Furthermore, due to various anthropogenic pressures and its proximity to harbours, these areas might be under the threat of bioinvasion (Taupp and Wetzel, 2019).

Macrobenthos are the dominant member of the benthic community and also act as a food source for various demersal predators inhabiting in the same ecosystem (Griffiths et al., 2017). Macrobenthic species perform invaluable ecosystem services during the process of feeding, tube construction and bioturbation which mediates the exchange of energy and matter between sediment and water column (Mestdagh et al., 2018; Rhoads and Young, 1971). Additionally, macrobenthic species can enhance sediment accumulation and thereby protect the habitat from erosion. By their physiological activities, they can also influence benthic-pelagic coupling and perform a crucial role in bioturbation which have been the focal point in major ecological studies (Zhang et al., 2019). Among the macrobenthic community, polychaetes represent as the most dominant and ecologically diverse component and due to their wide range of habitat variation and diverse feeding guild in different trophic level, they can be used as a bioindicator in environmental monitoring programmes (Fauchald and Jumars, 1979).

In general, the macrobenthic assemblages were assessed and their ecosystem functioning has been monitored using a traditional taxonomy-based approach in most of the Indian estuaries. Nevertheless, in recent years BTA (Biological Traits Analysis) approach is getting considerable attention. BTA can be applied to a series of characters like life history, feeding habit, body size, a pattern of mobility, type of development (Bremner et al., 2003) to delineate ecosystem functioning (Dolédec et al., 2006). The selected biological characteristics might be shared by different representatives of macrobenthic assemblages with different taxonomic identities; therefore this approach can portray large geographical ranges with gradients in species composition and diverse taxonomic entities. Moreover, it is

a valuable approach to measure ecosystem structure independently of its biogeography (Dolédec et al., 1999). BTA advocates the theory of environmental filters that recognize a subset of total species assemblages with distinct traits or phenotypes representing a particular environmental condition. According to this theory, more tolerant species can sustain in adverse condition by replacing sensitive species (Keddy, 1992). With recent methodological advances, another multivariate ordination method (RLQ) has been used in combination with fourth-corner analysis (Dolédec et al., 1996; Dray and Legendre, 2008; Legendre et al., 1997) in our study. This approach is contemporary to macrobenthic studies (Hu et al., 2019; Piló et al., 2016; Wouters et al., 2018) and robust in estimating functional diversity and the impact of disturbances on benthic animals. The RLQ has gained its importance in recent years due to its potential to identify the relationship among traits and environmental parameters.

Sundarbans Estuarine System (SES) is the largest monsoonal micro-tidal deltaic front comprising hundred-odd estuaries located alongside the Indian coast. It has been declared as a world heritage site by UNESCO in 1997 and recently as a Ramsar site in 2019 ([http://wiienviis.nic.in/Database/ramsar\\_wetland\\_sites\\_8224.aspx](http://wiienviis.nic.in/Database/ramsar_wetland_sites_8224.aspx)). The geographic location has made the SES vulnerable to tidal surges and cyclones. Its mangrove inhabitants absorb and reduce the impact of cyclonic storms coming from the Bay of Bengal (Chatterjee et al., 2013). Besides, climate change induced eustatic sea-level rise has altered the tropical deltas and SES is not an exception.

In the last couple of decades, a handful of studies have been conducted from the viewpoint of biogeochemistry, water quality analysis, phytoplankton, zooplankton and meiobenthos from the Indian sector of Sundarbans (Dey et al., 2012; Ghosh et al., 2018; Ghosh and Mandal, 2019; Manna et al., 2010; Mukhopadhyay et al., 2006; Nandy et al., 2018a, 2018b). Due to its strategic location inside the biosphere reserve, most of the areas are inaccessible to researchers. Though the meagre amount of studies on macrobenthos has been reported from the western part, howbeit a dearth of information is available from the central sector of Indian Sundarbans. Furthermore, only analysis of species composition is not enough to unriddle their seasonal succession pattern from such a complex ever-changing habitat like SES which needs to be supplemented by BTA approach.

Against this backdrop, the present study is a maiden endeavour to unravel the following questions: (I) how does macrobenthic community structure along with trait modalities alter spatiotemporally at the Matla River? (II)

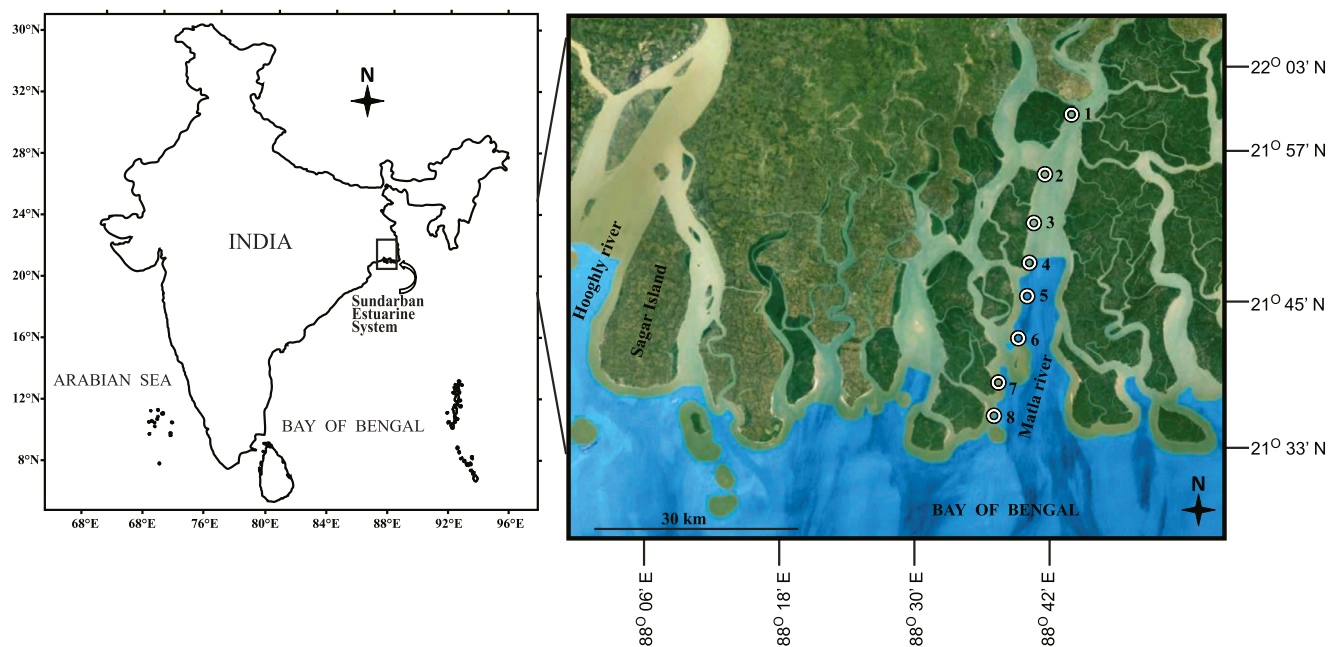


**Figure 1** The geographic location of the stations sampled in the Sundarbans estuarine system (SES). All sampling stations spread on the Matla River are marked with station number.

how do environmental alterations govern the community structure of macrobenthic assemblages?

## 2. Material and methods

### 2.1. Study area

The present investigation was carried out as a part of Ministry of Earth Sciences (MoES) funded project in Sundarbans Estuarine System (SES) during May 2017 (Summer), August 2017 (Monsoon), November 2017 (Winter) and March 2018 (Spring). The sampling period was chosen based on the IMD (Indian Meteorological Department) report. Seasons can be categorized as a dry summer with frequent storm and cyclonic events, huge precipitation during the southwest monsoon, cool and dry winter, and spring with phytoplankton bloom. However, seasonal demarcation is gradually becoming lost due to unpredictable downpour induced by low-pressure cyclonic events in recent years (Fukushima et al., 2019; Rastogi et al., 2018). The samples were collected along the estuarine gradient from north to south selecting eight stations at the Matla River. The details of the study stations have been furnished in Figure 1.

The Matla River is considered to be the largest estuary in SES. Being the longest and widest (L: 125 km, W: 26 km) river, it experiences high meandering courses with a sharp bend (Chatterjee et al., 2013). In recent times, due to high siltation, the central sector of this river has been disconnected from freshwater supply and discharge led the river primarily fed by the oceanic tide and characterized by variable sediment texture, salinity, conductivity and other environmental parameters. The estuarine condition of the Matla River is maintained by monsoonal runoff

alone (Trivedi et al., 2016) which has been reflected in the biodiversity associated with it (Rudra, 2018).

### 2.2. Sample collection and analysis

Macrobenthic samples were collected in triplicate using a Van Veen grab (0.04 m<sup>2</sup>) from each of the eight stations. The collected samples were in situ washed through a 0.5 mm mesh sieve, transferred to plastic bags and immediately fixed in 4% buffered formalin in seawater, and stained with rose Bengal aqueous solution. In the laboratory, animals were sorted, identified to the lowest practical taxonomic level following standard literature (Day, 1967; Dey, 2006; Fauvel, 1953; Misra, 1995; Southern, 1921), and counted. Numerical data was extrapolated into ind. m<sup>-2</sup>. Water and sediment samples were collected along with macrobenthic sampling for analysis of major environmental parameters. Sediment samples were taken separately for the analysis of organic content by wet oxidation method using chromic acid digestion followed by titration with 0.2 N ferrous ammonium sulfate solutions (El Wakeel and Riley, 1957). Soil texture was determined following pipette analysis (Buchanan, 1984). The temperature was measured in situ using a mercury thermometer. Microphytobenthos was estimated as chlorophyll *a* (Chl *a*) concentration. The top one cm of sediment was cut, placed in a 15 ml polyethylene bottle and preserved in liquid nitrogen onboard. Chl *a* concentration was measured with 90% acetone extraction of pigments and same for phaeopigment subsequent acidification with diluted hydrochloric acid, in the laboratory, following a standard protocol (Strickland and Parsons, 1972).

Bottom water samples were collected by Niskin water sampler (5 L) for analysis of water quality parameters including dissolved nutrients. Water temperature and

pH were recorded in situ with the help of mercury-in-glass Celsius thermometers and digital pH meters (Orion star A211), respectively. Furthermore, Secchi disc was also used to determine the transparency of water at each station. Water samples for analysis of salinity and nutrients were collected in pre-cleaned 500 ml plastic bottles and transported to the laboratory stored in iceboxes. Dissolved oxygen (DO) and salinity were analyzed following a standard protocol (Strickland and Parsons, 1972). Water samples for nutrient analysis were filtered through GF/F (mesh size 0.7  $\mu\text{m}$ ) filter papers using Millipore filtering unit and were analyzed for nitrite ( $\text{NO}_2\text{-N}$ ), nitrate ( $\text{NO}_3\text{-N}$ ), ammonium ( $\text{NH}_4\text{-N}$ ), inorganic phosphate ( $\text{PO}_4\text{-P}$ ) and silicate ( $\text{SiO}_4\text{-Si}$ ) following the standard protocol (Grasshoff et al., 1999). Suspended particulate matter (SPM) analysis was performed according to the method of Grasshoff et al. (1999). Monthly average rainfall data for the study period were collected from the Customized Rainfall Information System (CRIS), Hydromet Division, India Meteorological Department, Ministry of Earth Sciences, New Delhi IMD ([http://hydro.imd.gov.in/hydrometweb/\(Sgkp1rg45430qze451wildiil\)/DistrictRaifall.aspx](http://hydro.imd.gov.in/hydrometweb/(Sgkp1rg45430qze451wildiil)/DistrictRaifall.aspx)).

### 2.3. Data analysis

Univariate and multivariate analyses of data were performed using PRIMER v 6 software (Clarke and Gorley, 2006; Clarke et al., 2008) with PERMANOVA add-on package (Anderson et al., 2008). Non-multidimensional scaling (NMDS) and Bray–Curtis similarity index were constructed based on macrofaunal density after square root transformation. A similarity profile (SIMPROF) test was conducted to detect the significantly different station groups using the default of 1000 permutations for the mean similarity profile and 999 permutations for the simulated profile with a significance level of 0.05. Similarity percentage (SIMPER) was then used to identify the species contributing to intra-group similarity and those species responsible for the dissimilarity between groups. A global BEST permutation test (999 permutations) was performed on log (x+1) transformed and normalized environmental data, and square root transformed biological data using Spearman rank correlation between environmental variables and benthic patterns (Clarke et al., 2008). The following indices were also determined based on macrobenthic density: Shannon diversity  $H'$  ( $\log_e$ ), Margalef's species richness  $d$ , Pielou's evenness  $J'$  and Simpson index  $1-\lambda'$ . To investigate the spatiotemporal effect on total macrofaunal density, trait categories and environmental parameters were analyzed through two way Permutational Multivariate Analysis of Variance (PERMANOVA) with a station as the first factor (8 stations) and a season as the second factor (4 seasons). All PERMANOVA tests were done on Bray-Curtis similarity matrices using permutation of residuals under a reduced model, with 999 permutations. The BIOta ENVIRONMENTAL matching (BIO-ENV) analysis was performed on the similarity matrix based on density data to relate macrofaunal assemblages to environmental parameters (Clarke and Warwick, 2001). To evaluate the relationship between the polychaete community and environmental variables, Canon-

ical Correspondence Analysis (CCA) was applied using the Multivariate Statistical Package (MVSP) v3.1 (Kovach, 1998).

The selection of trait categories and their analysis followed the method described in Bremner et al. (2003, 2006), Hu et al. (2019), Pacheco et al. (2011), Piló et al. (2016). The biological traits database of total macrobenthos identified in the study was developed by extracting information from various sources like published literature (Bremner et al., 2003, 2006; Egres et al., 2019), books (Dey, 2006; Fauchald and Jumars, 1979; Giese and Pierce, 1977; Jumars et al., 2015), websites (Polytraits) (Faulwetter et al., 2014) and Biological Traits Information Catalogue (BIOTIC, MarLIN, 2006). For certain cases, traits for individual genera or species were not available, data from other species in the same family were used (Supplementary Table S1). Among three matrices, first and second were made with trait categories and density data for individual species on each study stations in four seasons. The third matrix was constructed by multiplying the trait categories with respective density value. Taxa were scored for each trait using fuzzy coding principle (Chevene, 1994) and then converted to proportions of one for each trait. In this study, the coding followed a scale ranging from 0 (no affinity) to 3 (total affinity). For any obligate trait, it has been scored as 3 and rest of the other traits as 0. The final matrix was transformed square root and analyzed with PCA for each trait separately.

### 2.4. RLQ and fourth-corner analysis

Another multivariate technique RLQ (Dolédec et al., 1996) in combination with the fourth-corner method (Dray et al., 2014; Legendre et al., 1997) was conducted to estimate the relationship between environmental factors and species trait modalities in relation to RLQ axis. Before analyzing, three separate tables L (species distribution across samples: sites in the row and species in the column), R (environmental parameters of samples: sites in rows and environmental variables in columns) and Q (species traits: species in rows and traits in the columns) were constructed. In order to perform the RLQ, each of the tables needs to be analyzed separately. Correspondence analysis (CA) and principal component analysis (PCA) were applied to table L and Q respectively (Dray et al., 2014) whereas, for table R, Hill-Smith analysis (Dray, 2013) was employed. RLQ analysis alone can give insights on the global visual summary of the relationship among these three metrics however, in combination with fourth-corner analysis; it can portray the significance of these bivariate associations. Additionally, the Monte-Carlo test was run with 49999 random permutations of model 2 (to test the null hypothesis: taxon densities with fixed traits are unrelated to environmental parameters) and model 4 (taxon densities with fixed environmental factors are not influenced by species traits), then adjusted the p-value accordingly (Benjamini and Hochberg, 1995; Dray, 2013). The RLQ/fourth-corner combined analysis was performed using “ade4” package (Dray and Dufour, 2007) available in R software (version 4.0.1).

**Table 1** Seasonal mean  $\pm$  SD of water quality parameters.

	Summer	Monsoon	Winter	Spring
Temperature ( $^{\circ}\text{C}$ )	31.95 $\pm$ 1	30.10 $\pm$ 0.69	24.73 $\pm$ 0.88	28.14 $\pm$ 1.10
Salinity (psu)	29.26 $\pm$ 5.14	17.00 $\pm$ 0.65	14.80 $\pm$ 1.59	27.21 $\pm$ 1.84
DO ( $\text{mg L}^{-1}$ )	4.77 $\pm$ 0.12	5.15 $\pm$ 0.56	7.46 $\pm$ 0.39	6.54 $\pm$ 0.32
pH	8.12 $\pm$ 0.03	7.83 $\pm$ 0.18	8.12 $\pm$ 0.04	8.11 $\pm$ 0.03
Chlorophyll <i>a</i> ( $\mu\text{g L}^{-1}$ )	4.10 $\pm$ 0.55	2.45 $\pm$ 0.65	1.13 $\pm$ 0.68	3.74 $\pm$ 2.15
Phaeopigment ( $\mu\text{g L}^{-1}$ )	0.44 $\pm$ 0.20	0.21 $\pm$ 0.12	0.17 $\pm$ 0.07	0.53 $\pm$ 0.44
Nitrate ( $\mu\text{M}$ )	13.55 $\pm$ 1.20	13.11 $\pm$ 3.89	16.41 $\pm$ 2.76	6.46 $\pm$ 0.97
Nitrite ( $\mu\text{M}$ )	0.57 $\pm$ 0.16	0.39 $\pm$ 0.20	0.73 $\pm$ 0.14	1.31 $\pm$ 0.18
Phosphate ( $\mu\text{M}$ )	1.37 $\pm$ 0.08	1.36 $\pm$ 0.22	1.03 $\pm$ 0.13	0.83 $\pm$ 0.17
Silicate ( $\mu\text{M}$ )	28.80 $\pm$ 2.83	15.17 $\pm$ 2.22	32.89 $\pm$ 4.67	14.51 $\pm$ 0.88
Ammonium ( $\mu\text{M}$ )	2.64 $\pm$ 0.57	0.45 $\pm$ 0.13	0.18 $\pm$ 0.02	0.19 $\pm$ 0.03

### 3. Results

#### 3.1. Environmental parameters

Environmental parameters were characterized by a strong temporal but meagre spatial variation. PERMANOVA result depicted all the parameters were significant ( $p \leq 0.05$ ) with seasons only, whereas dissolved silicate and nitrate had significant value at both scales. Bottom water salinity ranged from 35.04–12.13 in summer (Stn. 4) and winter (Stn. 1) respectively whereas, level of dissolved oxygen showed an increasing trend towards monsoon and post-monsoon seasons (Table 1). The essential micronutrients concentrations varied both spatially and temporally in the present study. The average nitrate concentration varied between ( $6.46 \pm 0.97 \mu\text{M}$ ) to ( $16.41 \pm 2.76 \mu\text{M}$ ) during spring and winter respectively (Table 1). However, average nitrite concentration varied from ( $0.39 \pm 0.20 \mu\text{M}$ ) to ( $1.31 \pm 0.18 \mu\text{M}$ ) during monsoon and spring correspondingly (Table 1). Dissolved inorganic nutrients like ammonium or phosphate were recorded in negligible amount except in upper stretch stations where anthropogenic activities are evident (Table 1). The sediment contained the highest amount of Chl *a* in winter compared to other seasons (Table 2). Organic enrichment was moderate, being lowest during winter (Table 2). The sediment texture was mostly silty with a variable amount of clay and sand (Figure 2). Silt percentage ranged from 59.35 to 66.92 in spring and summer respectively. Likewise, the clay percentage also showed a similar seasonal trend. Overall, the BIOENV revealed a weak correlation ( $p = 0.498$ ) between environmental parameters and benthic data. Among all, organic matter, chlorophyll *a*, nitrite and phosphate showed the best correlation.

#### 3.2. Taxonomic composition of macrobenthic community

Total macrobenthic density revealed a significant differences (PERMANOVA) among seasons ( $F = 7.7355$ ,  $p = 0.001$ ) and stations ( $F = 4.6651$ ,  $p = 0.001$ ). The macrofaunal community of 95 taxa, belonging to 6 phyla was recorded during the faunistic surveillance. Among these, 56 species belong to Annelida, 1 to Sipuncula, 24 to Mollusca, 11 to Arthropoda, 2 from Cnidaria and 1 from Echinodermata. Overall,

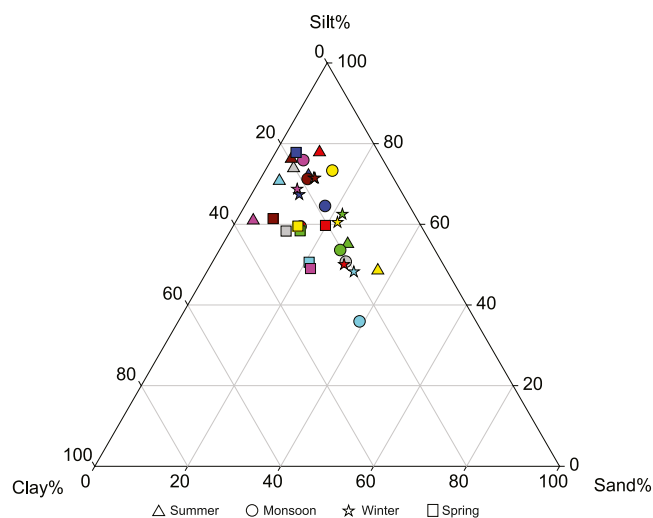


**Figure 2** Ternary plot showing the sediment texture pattern of eight stations in four distinct seasons. Red: stn. 1, Dark blue: stn. 2, Green: stn. 3, Yellow: stn. 4, Grey: stn. 5, Brown: stn. 6, Light blue: stn. 7, Purple: stn. 8

Annelida were numerically dominant (76.25% of the total macrobenthos), followed by Mollusca (10.5%), Arthropoda (9.2%), Cnidaria (2%), Sipuncula (1.6%) and Echinodermata (0.3%). The maximum species count ( $11675 \pm 11883.31 \text{ ind. m}^{-2}$ ) was observed during spring that declines considerably ( $5875 \pm 6224.08 \text{ ind. m}^{-2}$ ) during monsoon. Effects of environmental perturbation on macrobenthic density varied accordingly in spatial scale throughout the study period. Among all, the macrobenthic density at station 1 in summer was mostly affected during monsoon and drastically reduced from  $3758 \pm 3916 \text{ ind. m}^{-2}$  to  $233 \pm 270 \text{ ind. m}^{-2}$  (Figure 3a). Density in stations 1, 4, 6 and 7 comparatively declined in spring compared to the previous season (Figure 3a).

Polychaete density was found to be highest ( $8117 \pm 5235.67 \text{ ind. m}^{-2}$ ) in winter and lowest ( $4300 \pm 3716.99 \text{ ind. m}^{-2}$ ) in monsoon (Figure 3b). A total of 56 species from 26 families have constructed the entire polychaete community during the study period (Table 3). Few species like *Cossura coasta*, *Dendronereis aestuarina*,

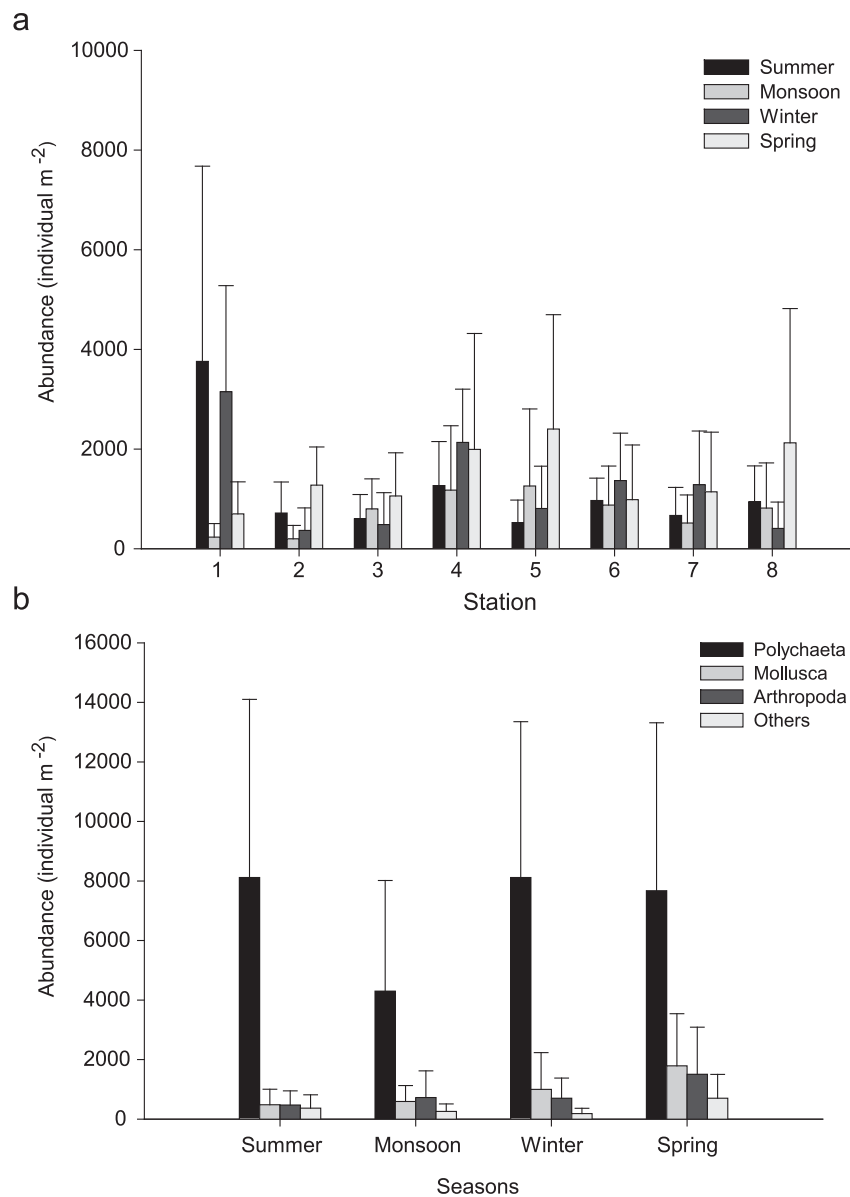


**Figure 3** a) Spatiotemporal variation of macrobenthic density during the study period, b) seasonal variation of macrofaunal groups during the study period.

*Heteromastus similis*, *Magelona cincta*, *Micronephthys oligobranchia*, *Prionospio cirrifera* and *Sternaspis scutata* prevailed the estuary throughout the study period. *Paraprionospio pinnata*, *H. similis* and *M. cincta* dominated during summer and monsoon albeit in winter *H. similis* was replaced by another cognate capitellid (*Parheteromastus tenuis*) (Supplementary Table S2). However, in spring the composition was completely different, represented by species from Spionidae (*Prionospio cirrifera*) and Nereididae families (*Neanthes meggitti*) which recorded highest densities among four seasons. Individuals of genus *Prionospio* showed a marked variation in appearance as well in density. In summer and winter, *P. pinnata* dominated the estuary, mostly towards down stretch stations, however in winter they were abundant in innermost station. Moreover, *P. pinnata* and *P. cirrifera* showed interspecific replacement in spring (Supplementary Table S2). Overall,

capitellids and spionids prevailed the estuary throughout seasons. The innermost stations were mostly composed of opportunistic species due to organic enrichment and anthropogenic input. The average molluscan density varied from  $1792 \pm 1751.04$  ind. m<sup>-2</sup> to  $483 \pm 518.60$  ind. m<sup>-2</sup> in spring and summer respectively. Molluscs were composed of 8 species (5 families) of bivalve and 16 species (15 families) of gastropod. Among bivalves, *Donax incarnatus* and *Meretrix meretrix* were most dominant, whereas on the other hand, *Pirenella cingulata* and *Acteocina estriata* were dominant among gastropods. Molluscs were abundant mostly in middle stretch (stations 4 and 5) of the estuary.

### 3.3. Statistical analysis

Bray–Curtis similarity based on the macrofaunal density categorized the estuarine zone into several groups with

**Table 2** Spatio-temporal variation in sediment parameters.

Stations	Temperature (°C)				Chlorophyll <i>a</i> ( $\mu\text{g g}^{-1}$ )				Phaeopigment ( $\mu\text{g g}^{-1}$ )				Organic carbon %				Organic matter %			
	Summer	Monsoon	Winter	Spring	Summer	Monsoon	Winter	Spring	Summer	Monsoon	Winter	Spring	Summer	Monsoon	Winter	Spring	Summer	Monsoon	Winter	Spring
1	32.50	29.50	25.50	30.00	2.37	3.76	1.53	0.71	0.33	0.35	0.27	0.21	1.15	1.14	0.53	1.95	1.99	1.96	0.91	3.37
2	31.50	30.00	25.50	29.00	1.48	1.02	0.51	0.97	0.23	0.14	0.09	0.18	0.89	0.81	0.02	0.88	1.53	1.39	0.03	1.52
3	31.00	30.50	24.75	30.00	0.64	0.51	2.85	0.97	0.12	0.00	0.29	0.27	0.76	0.96	0.06	0.83	1.31	1.66	0.10	1.44
4	31.00	31.00	25.50	30.00	0.33	2.06	0.36	0.45	0.06	0.20	0.06	0.51	0.75	0.70	0.73	1.03	1.28	1.21	1.26	1.77
5	31.50	31.50	26.50	31.00	1.45	1.04	3.08	1.68	0.23	0.14	0.46	0.30	0.86	0.96	0.15	0.82	1.48	1.66	0.26	1.41
6	32.00	30.50	26.00	26.00	0.95	0.51	0.69	1.07	0.15	0.14	0.21	0.18	0.96	1.14	0.23	0.81	1.65	1.96	0.39	1.39
7	31.50	31.50	25.50	28.00	0.97	1.35	1.53	0.45	0.18	0.29	0.32	0.33	0.90	0.28	0.24	0.49	1.55	0.48	0.42	0.85
8	32.00	30.50	26.00	29.50	1.66	0.84	1.35	0.10	0.27	0.15	0.24	0.27	1.20	0.78	0.11	0.63	2.06	1.34	0.19	1.08

**Table 3** CCA code and RLQ code for the list of taxa are tabulated.

Species name	CCA code	RLQ code
<b>Annelida</b>		
<i>Ancistrosyllis matlaensis</i>	1	Anma
<i>Ancistrosyllis</i> sp.	2	AnS
<i>Aphelochaeta multifilis</i>	3	Apmu
<i>Aricidea</i> sp.	4	ArS
<i>Axiothella obockensis</i>	5	Axob
<i>Barantolla sculpta</i>	6	Basc
<i>Capitella capitata</i>	7	Caca
<i>Chloeia parva</i>	8	Chpa
<i>Cossura coasta</i>	9	Coco
<i>Dendronereis aestuarina</i>	10	Deae
<i>Diopatra cuprea</i>	11	Dicu
<i>Dipolydora normalis</i>	12	Dino
<i>Mysta ornata</i>	13	Myor
<i>Euclymene annandalei</i>	14	Euan
<i>Gattyana fauveli</i>	15	Gafa
<i>Glycera alba</i>	16	Glal
<i>Glycera longipinnis</i>	17	Gllo
<i>Glycera tessellata</i>	18	Glte
<i>Glycinde oligodon</i>	19	Glol
<i>Goniada emerita</i>	20	Goem
<i>Hermudura annandalei</i>	21	Hean
<i>Hesione splendida</i>	22	Hesp
<i>Heteromastus similis</i>	23	Hesi
<i>Kuwaita heteropoda</i>	24	Kuhe
<i>Levinsenia</i> sp.	25	LeS
<i>Lumbrineris latreilli</i>	26	Lula
<i>Lumbrineris polydesma</i>	27	Lupo
<i>Lumbrineris</i> sp.	28	LuS
<i>Magelona cincta</i>	29	Maci
<i>Micronephthys oligobranchia</i>	30	Miol
<i>Namalycastis fauveli</i>	31	Nafa
<i>Namalycastis indica</i>	32	Nain
<i>Neanthes glandicincta</i>	33	Negl
<i>Neanthes meggitti</i>	34	Neme
<i>Nephtys polybranchia</i>	35	Nepo
<i>Notomastus giganteus</i>	36	Nogi
<i>Owenia fusiformis</i>	37	Owfu
<i>Paraprionospio pinnata</i>	38	Papi
<i>Parheteromastus tenuis</i>	39	Pate
<i>Perinereis cultrifera</i>	40	Pecu
<i>Perinereis nigropunctata</i>	41	Peni
<i>Polydora ciliata</i>	42	Poci
<i>Polydora</i> sp.	43	PoS
<i>Potamilla leptochaeta</i>	44	Pole
<i>Prionospio cirrifera</i>	45	Prci
<i>Prionospio saldanha</i>	46	Prsa
<i>Sabellaria pectinata</i>	47	Sape
<i>Scoloplos sagarensis</i>	48	Scsa
<i>Scyphoproctus armatus</i>	49	Scar
<i>Sigambra constricta</i>	50	Sicn
<i>Sigatargis commensalis</i>	51	Sico
<i>Spio bengalensis</i>	52	Spbe
<i>Sternaspis scutata</i>	53	Stsc

(continued on next page)

Table 3 (continued)

Species name	CCA code	RLQ code
<i>Syllis cornuta</i>	54	Syco
<i>Terebellides stroemii</i>	55	Test
<i>Anelassorhynchus microrhynchus</i>	56	Anmi
<b>Sipuncula</b>		
<i>Phascolosoma (Phascolosoma) arcuatum</i>		Phar
<b>Mollusca</b>		
<i>Donax incarnatus</i>		Doin
<i>Macoma</i> sp.		MaS
<i>Meretrix meretrix</i>		Meme
<i>Modiolus</i> sp.		MoS
<i>Protapes</i> sp.		PrS
<i>Solen vagina</i>		Sova
<i>Strigilla splendida</i>		Stsp
<i>Tegillarca granosa</i>		Tegr
<i>Acrilla acuminata</i>		Acac
<i>Acteocina estriata</i>		Aces
<i>Austropilula beddomeana</i>		Aube
<i>Ellobium gangeticum</i>		Elga
<i>Haloa crocata</i>		Hacr
<i>Littorina obtusata</i>		Liob
<i>Nassarius foveolatus</i>		Nafo
<i>Notocochlis</i> sp.		NoS
<i>Phalium</i> sp.		PhS
<i>Pirenella alata</i>		Pial
<i>Pirenella cingulata</i>		Pici
<i>Stenothyra deltae</i>		Stde
<i>Telescopium telescopium</i>		Tete
<i>Thais</i> sp.		ThaS
<i>Thiara</i> sp.		ThiS
<i>Turritella</i> sp.		TuS
<b>Arthropoda</b>		
<i>Ampelisca pusilla</i>		Ampu
<i>Balanus</i> sp.		BaS
<i>Gammarus</i> sp.1		GaS1
<i>Gammarus</i> sp.2		GaS2
Harpacticoid Copepod		Hac
<i>Ingolfiella</i> sp.		InS
<i>Paradiastylis</i> sp.		PaS
<i>Penaeus monodon</i>		Pemo
<i>Metaplax intermedia</i>		Mein
<i>Scylla serrata</i>		Scse
<i>Sphaeroma annandalei annandalei</i>		Span
<b>Cnidaria</b>		
<i>Actiniaria</i> sp.1		AcS I
<i>Actiniaria</i> sp.2		AcS II
<b>Echinodermata</b>		
<i>Amphioplus (Lymanella) depressus</i>		Amde

marked variation between the sampling seasons and stations. It has delineated two groups and one separate station (SIMPROF test  $p < 0.05$ ) during summer (Figure 4a). According to SIMPER analysis, *Heteromastus similis* contributed 15.91% and 21.63% in group 1 (66.91% similarity) and group 2 (58.22%) formation respectively (Supplementary Table S3). Moreover, station 1 has been separated from these two groups due to its different species composition like

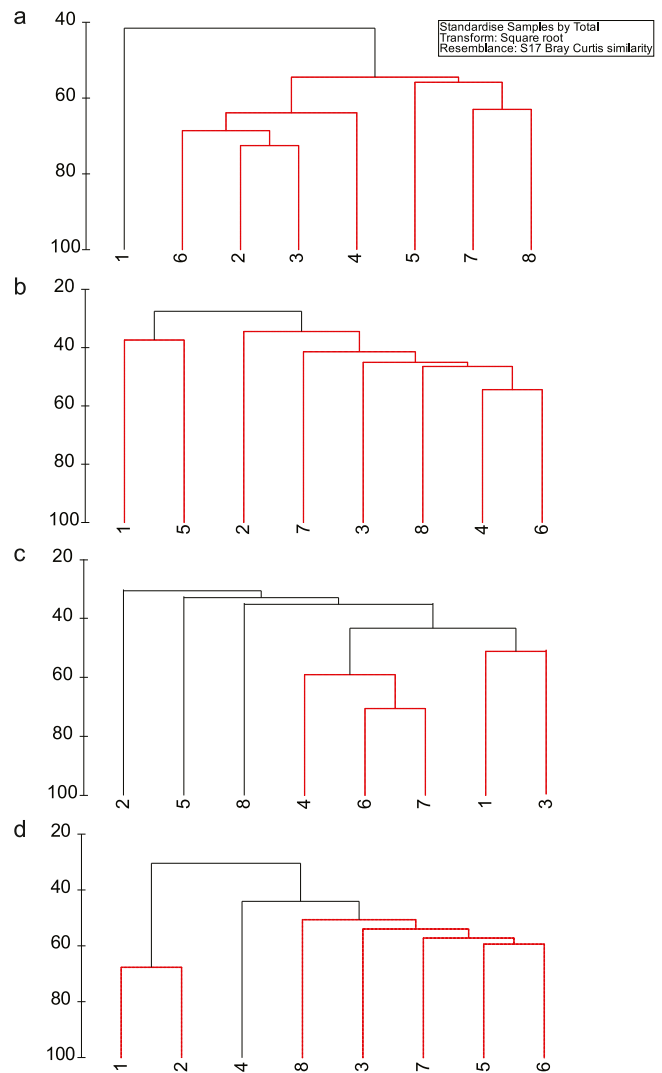


**Figure 4** Cluster plot based on Bray–Curtis similarity coefficient of macrobenthic species in four distinct seasons; a) summer, b) monsoon, c) winter, d) spring.

*Magelona cincta*, *Micronephthys oligobranchia* and *Perinereis nigropunctata*. In monsoon, two major groups have been identified, mirrored by *H. similis* a major contributor (23.88%) behind the formation of group 2 (41.40% similarity) and separation of group 1 and 2 (Figure 4b). *Terebellides stroemii* played an overriding role in shaping the station 8 distinguished from the rest of the stations in winter that has made station 8 completely separated from rest of the other stations might be due to the location of this particular station was at the mouth of the estuary (Figure 4c). In spring, upstream and downstream stations have diverged into two prominent groups except station 4 having unique species composition like *Acteocina estriata*, *Stenothyra deltae* and *Meretrix meretrix* (Figure 4d).

Ordination resulting from CCA biplot for 56 polychaete community showed five axes representing 82.42% cumulative constrain percentage where axis 1 and 2 showed 0.93% and 0.86% species environmental correlation, respectively. A total of ten variables significantly explained in the biplot (Figure 5a). Axis 1 was influenced by clay percentage, sand

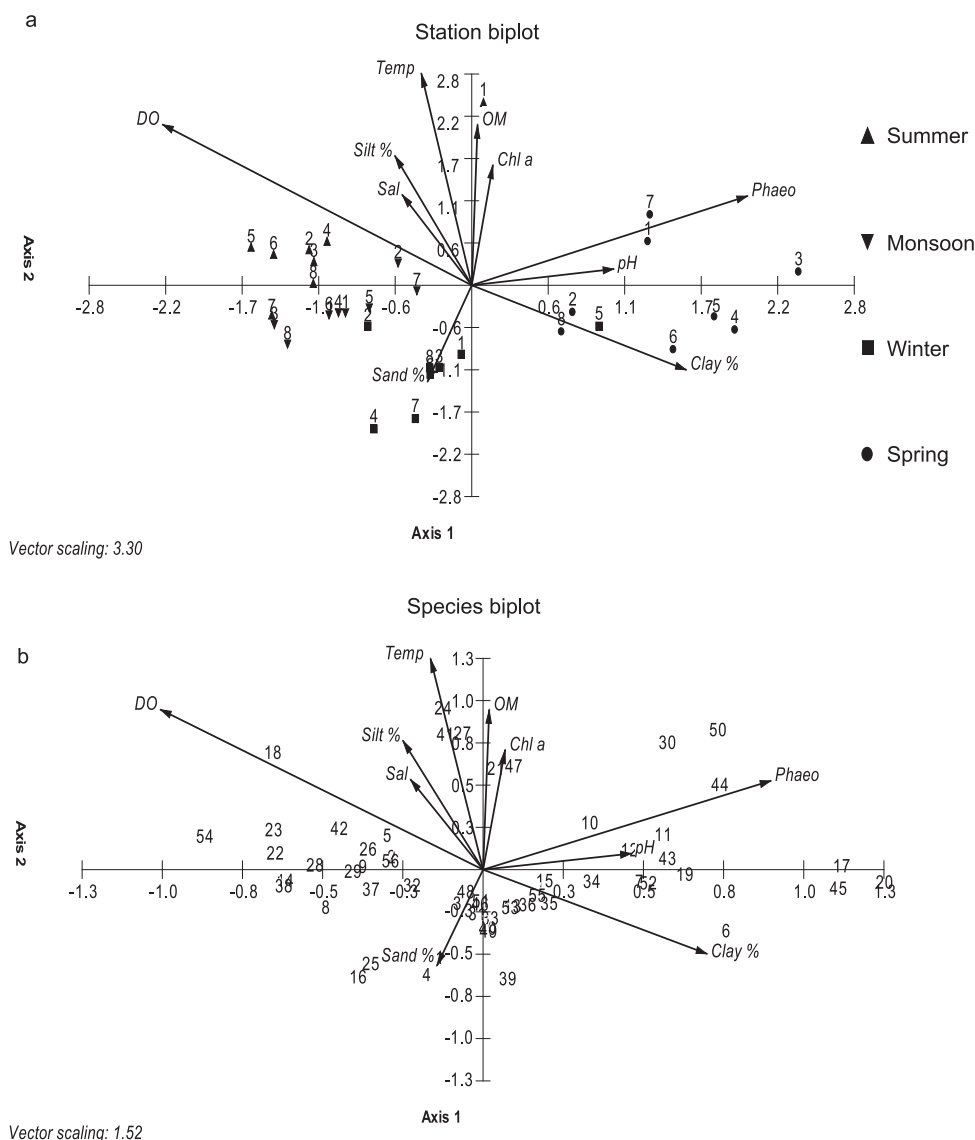


**Figure 5** Canonical correspondence analysis (CCA) ordination for polychaete species and environmental variables. The environmental variables (temperature, salinity, pH, Dissolved Oxygen, sand %, silt %, clay %, chlorophyll *a*, phaeopigment, Organic Matter) are indicated by arrows. Station codes and species codes are given in Figure 1 and Table 3 respectively.

percentage whereas; axis 2 was driven by remaining parameters. Being influenced by DO vector, most of the stations in summer occupied the upper left quadrant but station 1 was exceptionally profited by organic content. Most of the stations in monsoon and winter clustered together in lower left quadrant and majority were favoured by sand % vector. During winter, all the stations were positioned towards sand percentage vector except station 5 which showed affinity towards clay percentage. In spring, all the stations were positioned in the right quadrant profiting mostly by clay percentage. In species biplot (Figure 5b), *Ancistrosyllis matlaensis*, *Namalycastis fauveli*, *Prionospio saldanha*, *Scoloplos sagarensis*, *Sigatargis commensalis*, *Levinsenia* sp. have shown a positive correlation with sand % whereas, *Nephtys polybranchia*, *Notomastus giganteus*, *Sternaspis scutata*, *Terebellides stroemii* showed affinity to the percentage of clay present in the sediment.

### 3.4. Biotic indices

All the diversity indices showed significant (PERMANOVA,  $p \leq 0.05$ ) variation with seasons. Shannon diversity  $H'(\log_e)$  followed a seasonal trend of winter > spring > monsoon > summer, where the maximum and minimum values were recorded at station 1 in winter (3.55) and station 2 in monsoon (2.02), respectively. The similar seasonal pattern was also observed in case of total population density (N) and Simpson index ( $1-\lambda$ ). Margalef's species richness recorded highest (10.27) during winter at station 1 and lowest (2.13) during monsoon at station 2 (Table 4).

### 3.5. Biological Trait Analysis

In the present study, BTA on total macrobenthos has depicted a distinct variation influenced by seasonal

**Table 4** Seasonal variation in macrobenthic community indices for all stations. S = Total number of species, N = Total population density, d = Species richness (Margalef's), J' = Pielou's evenness, H' (log<sub>e</sub>) = Shannon index, 1-λ = Simpson index.

Stations	S	N	d	J'	H' (log <sub>e</sub> )	1-λ
<b>Summer</b>						
1	24	43	6.13	0.95	3.03	0.97
2	15	34	3.97	0.95	2.57	0.94
3	16	37	4.17	0.97	2.68	0.95
4	18	37	4.70	0.95	2.75	0.95
5	11	27	3.04	0.91	2.19	0.89
6	13	29	3.55	0.92	2.36	0.92
7	10	27	2.73	0.92	2.13	0.90
8	18	36	4.73	0.95	2.74	0.95
<b>Monsoon</b>						
1	12	33	3.15	0.98	2.44	0.94
2	8	27	2.13	0.97	2.02	0.89
3	13	31	3.49	0.94	2.41	0.93
4	28	49	6.92	0.98	3.26	0.98
5	23	41	5.91	0.95	2.99	0.96
6	23	44	5.82	0.97	3.04	0.97
7	15	35	3.92	0.97	2.62	0.95
8	22	42	5.62	0.96	2.98	0.97
<b>Winter</b>						
1	42	54	10.27	0.95	3.55	0.98
2	16	38	4.13	0.98	2.71	0.96
3	19	41	4.83	0.98	2.89	0.97
4	27	42	6.96	0.93	3.08	0.97
5	23	40	5.95	0.95	2.98	0.96
6	23	41	5.91	0.95	2.97	0.97
7	22	43	5.58	0.97	3.00	0.97
8	15	35	3.94	0.96	2.61	0.95
<b>Spring</b>						
1	17	38	4.41	0.97	2.74	0.96
2	13	27	3.66	0.89	2.27	0.89
3	22	37	5.80	0.93	2.87	0.95
4	28	46	7.04	0.96	3.18	0.97
5	33	48	8.26	0.95	3.31	0.98
6	22	42	5.62	0.96	2.97	0.97
7	22	41	5.66	0.95	2.95	0.96
8	32	47	8.06	0.94	3.27	0.98

perturbation. Among 19 trait categories (Table 5), 17 were most prominent at both the spatiotemporal scale. Trait categories like motile, burrower and surface deposit feeder dominated the estuary whereas, discretely motile, tube dweller, carnivores or scavengers and sexual reproduction (brooder and spawner) were also widespread (Figure 6). In case of body size trait, large animals were found in upper stretch being maximum at station 2 during spring (Figure 6a). Motile species showed significant variation among seasons ( $p < 0.05$ ). Maximum contribution (61.33%) of discretely motile species was gradually replaced by motile species in the following seasons. Sessile animals could not significantly persist in this entire estuarine stretch (Figure 6b). Burrowers were most prevalent in all four seasons. Moreover, the contribution of other categories

**Table 5** List of biological traits, abbreviations and categories used to describe macrobenthic assemblages.

Trait (Abbreviations)	Categories
Body size (BS)	1. Small (SM) (<3 cm) 2. Medium (ME) (3–6 cm) 3. Large (LA) (>6 cm)
Motility (M)	1. Motile (MO) 2. Discretely motile (DM) 3. Sessile (SE)
Living habitat (LH)	1. Tube dweller (TU) 2. Burrower (BU) 3. Free swimmer (FS) 4. Crawler (CR) 5. Attached (AT)
Feeding strategy (F)	1. Sub surface deposit feeder (SSDF) 2. Surface deposit feeder (SDF) 3. Suspension feeder (SF) 4. Carnivore (CAR) 5. Herbivore (HER)
Reproductive strategy (RS)	1. Asexual (A) 2. Sexual – Brooder (SB) 3. Sexual – Spawner (SS)

of this trait showed a significant difference in the temporal scale (Figure 6c). Deposit feeding was the most dominant feeding strategy in this estuary, though a gradual appearance of suspension-feeding groups in spring has also been noticed. Sub-surface deposit feeders (SSDF) contributed maximum in summer which declined in spring (Figure 6d). In most of the stations, spawners were the dominant trait modality, howbeit in few stations like 1, 2 (spring), a gradual succession of brooders has been noticed compared to previous seasons (Figure 6e).

In the PCA, four seasons have distinctly clustered where monsoon and winter were clustered alongside. For body size trait, PC1 and PC2 showed 79.9% and 98.9% cumulative variation where the small size (SM) was positively correlated with PC 2 (0.509) and negatively with PC 1 (−0.666) (Figure 7a). For mobility trait, MO was negative towards PC1 (−0.667) howbeit, DM was positive towards that axis (0.737) (Figure 7b). Burrowers were positively aligned to both PC1 and PC2 where stations 6 in summer and spring were positioned (Figure 7c). In Figure 7d, among feeding strategy trait categories, PC1 and PC 2 explained 56.8% and 77.3% cumulative variation where, SDF and SF both were negatively explained by PC2 (−0.306 and −0.749, respectively), CAR and HER were negative towards PC1 (−0.659 and −0.140 respectively); conversely, SSDF was positive towards both the axes. Except stations 1 and 2, the rest of the stations showed the maximum percentage of SF during spring (Figure 6d) as illustrated in the PCA plot (Figure 7d). In Figure 7e, SB positively explained PC2 (0.011), whereas SS was positive towards PC1 (0.534).

The RLQ analysis has depicted some correlation between the metrics (Table 6). Subsequently, fourth corner analysis was performed, among the 323 possible associations at a significance level of ( $\alpha = 0.05$ ), only 11 significant associations (3 negative and 8 positive) were found following Dray and

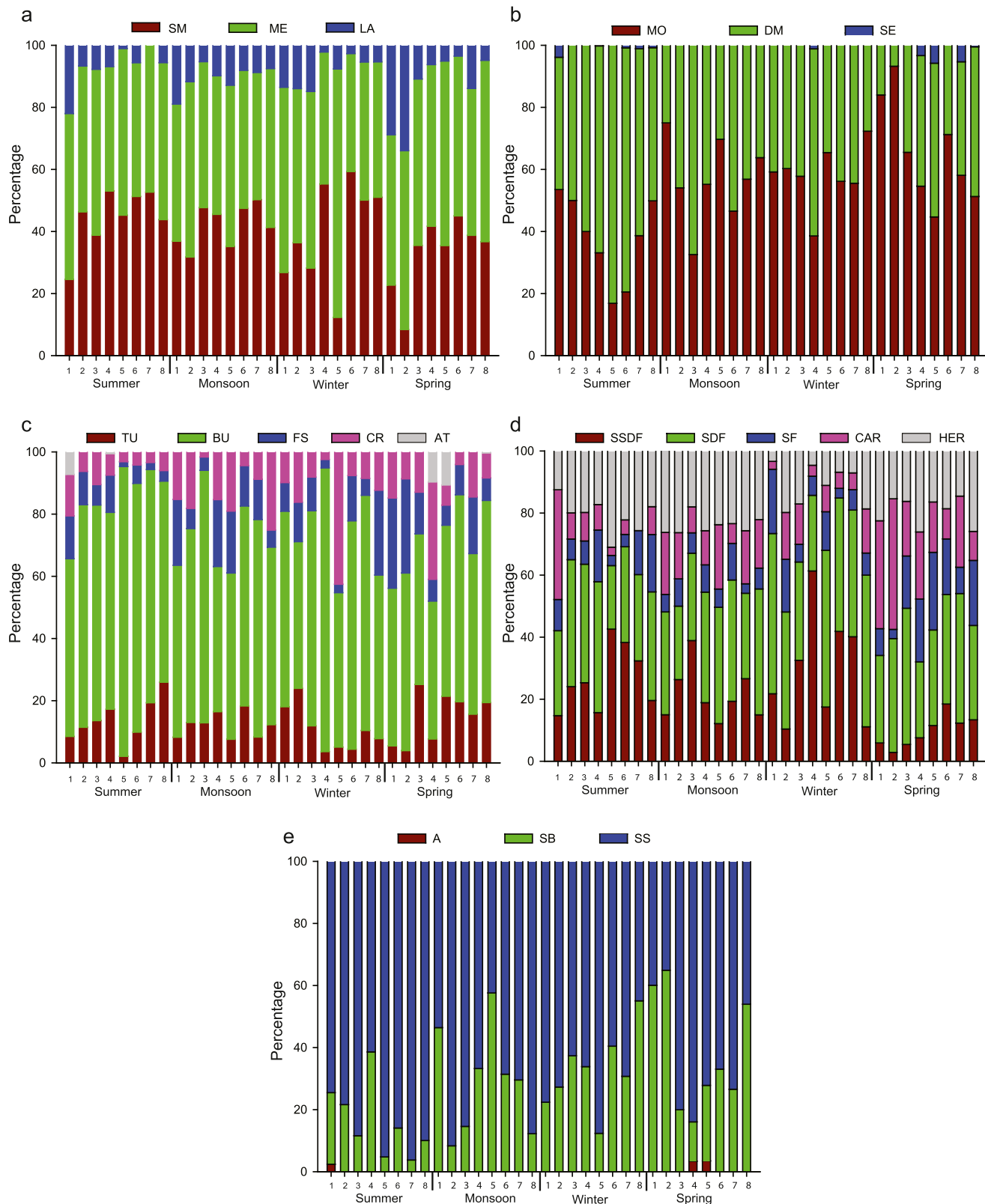


**Figure 6** Percentage of trait categories for macrobenthic assemblages at eight different stations for four different seasons. a) Body size, b) mobility, c) living habitat, d) feeding strategy, e) reproductive strategy. The abbreviations are available in Table 5.

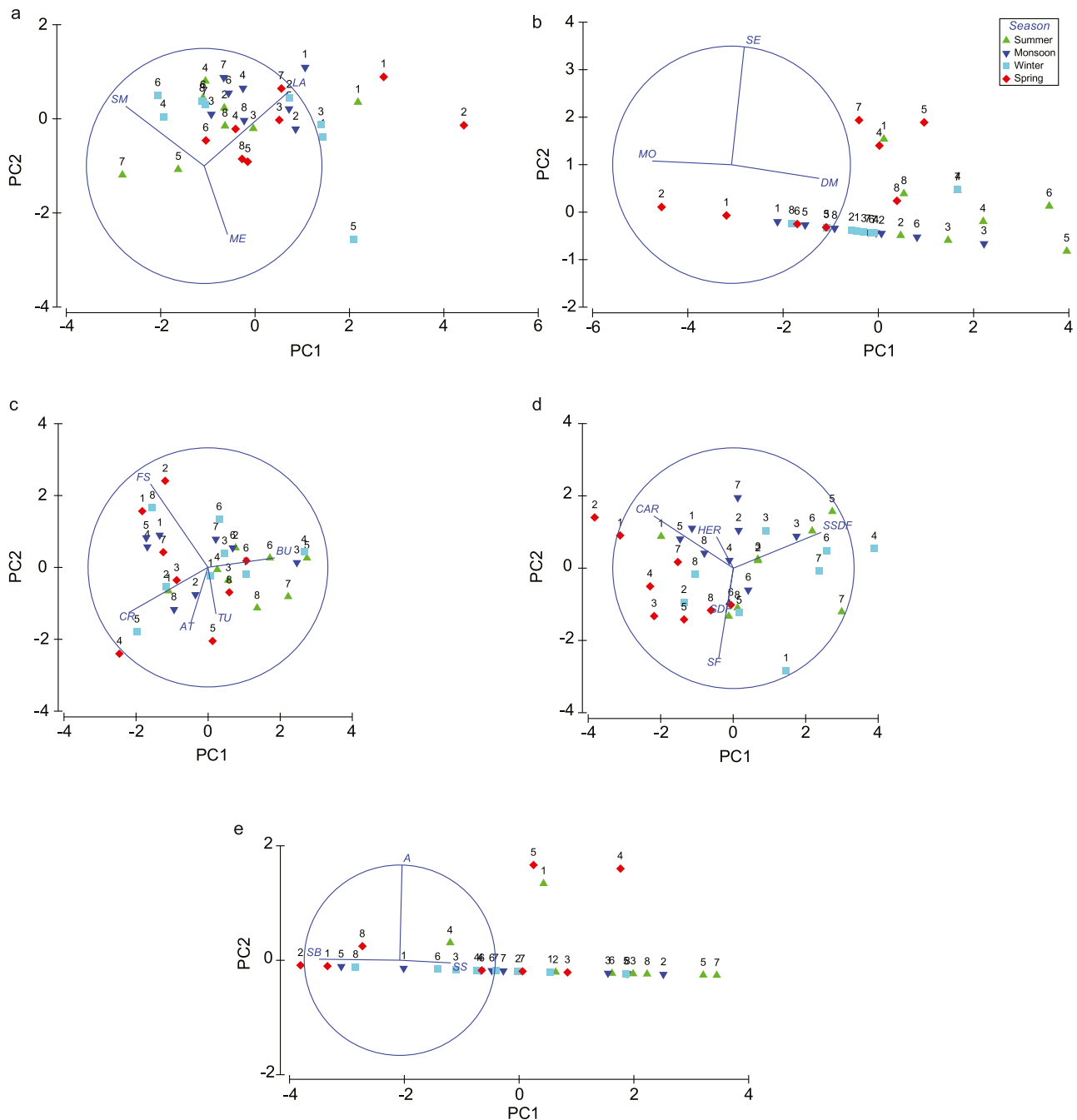


**Figure 7** PCA ordinations depicting the variability in assemblage trait composition across stations and seasons. a) Body size, b) mobility, c) living habitat, d) feeding strategy, e) reproductive strategy. The abbreviations are available in Table 5.

Legendre (2008) approach. When  $p$  values were adjusted for multiple testing, there was no significant association. Subsequently, combining both RLQ and the fourth corner analysis, the global test did not reveal any significant relationships between species distribution and environmental parameters (model 2,  $p$  value = 0.08100) as well as between species distribution and species traits (model 4,  $p$  value = 0.40174). The first RLQ axis represents the 58.09% of the total variation while the second RLQ axis represents 23.97% (Table 6), encompassing the most important associations between traits, environment parameters and responsible species

composition (Supplementary Table S4a,b). The positive part of axis 1 and negative part of axis 2 have revealed that suspension feeders and free swimmers are negatively associated with the level of suspended particulate matter (SPM) in water (Figure 8a,b). The negative part of axis 1 and positive part of axis 2 clearly highlight the presence of small-sized burrowers represented by polychaete genus *Ancistrosyllis* and *Sigambra* (Fig. 8b). Traits like carnivores and large or medium body size are mostly occupied at the positive part of axis 1 and the negative part of axis 2 (Figure 8b). Discretely motile animals such as glycerids are

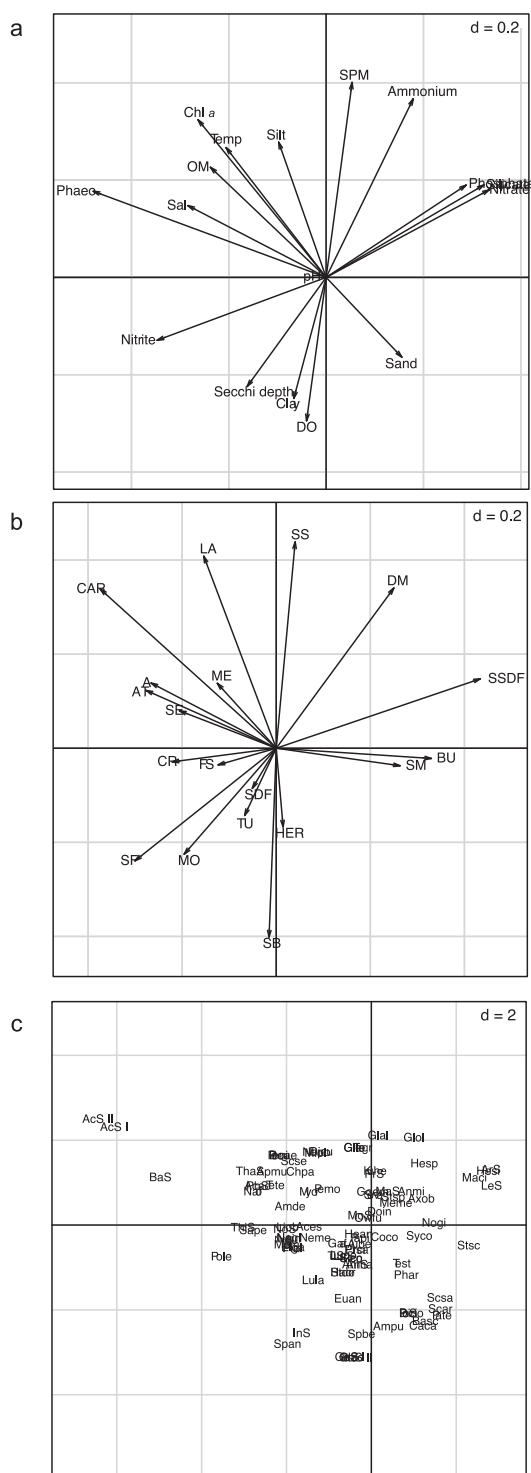


**Figure 8** a) RLQ diagram as defined by the 1st and 2nd axes with the projection of environmental variables (SPM – suspended particulate matter, DO – dissolved oxygen, Sal – salinity, OM – organic matter, Chl *a* – Chlorophyll *a*, Temp – sediment temperature, b) RLQ diagram as defined by the 1st and 2nd axes with the projection of trait categories (see Table 5 for the abbreviations of trait categories), c) RLQ diagram as defined by the 1st and 2nd axes with the projection of species (see Table 3 for respective RLQ codes of species). The *d* value in the upper right corner is the scale of the graph given by a grid.

**Table 6** RLQ results. Individual R-L-Q separate analysis and RLQ analysis.

Separated analysis	Axis 1 eigenvalue (Variance %)	Axis2 eigenvalue (Variance %)
R/Hill-Smith	5.78 (40.06)	3.91 (27.12)
L/CA	0.58 (28.66)	0.43 (21.41)
Q/PCA	4.37 (32.16)	3.22 (23.71)
RLQ Analysis	Axis 1	Axis 2
Eigenvalues	1.22	0.50
Variance %	58.09	23.97
R/RLQ		
Variance	1.80	2.21
Variance %	28.75	43.27
Q/RLQ		
Variance	1.81	1.47
Variance %	28.88	28.72
L/RLQ		
Variance	0.34	0.22
Variance %	5.37	4.28

positioned at the positive part of both the axis (Figure 8b,c).

## 4. Discussion

### 4.1. Environmental parameters

As estuaries are expressions of communication among land, river and ocean processes, therefore climate change mediated any environmental perturbation has a potential to affect estuarine ecosystem (Rybczyk and Day, 2013). In the present study, most of the environmental parameters were significantly influenced by seasons. Bottom water salinity showed a marked seasonal variation but spatially it was almost homogeneous throughout the entire estuarine stretch. Seasonal dynamics of Sundarbans delta is mostly controlled by monsoon induced hydrological changes. Unusual rainfall and a monsoon break are common phenomena in this system. SES experienced an unusual downpour (in October) at the beginning of the post-monsoon season (Supplementary Figure S1) and that might have exerted effects on hydrological parameters as reflected in our study. Bottom water salinity showed a marked seasonal variation being lowest during winter. A similar observation was recorded from the northern part of Bay of Bengal (Pant et al., 2015) as well as from Sundarbans (Saha et al., 2001), where authors explained that apart from rainfall mediated freshwater flux, high horizontal advection and lower tidal amplitude are crucial factors of anomalous salinity during winter. However, homogeneity in salinity can be explained as the Matla River has lost its freshwater connection due to high siltation and neotectonic activity mediated tilting of Eastern Bengal basin in recent years (Manna et al., 2010; Raha et al., 2012; Stanley and Hait, 2000). This phenomenon has been also reported from different estuaries around the globe, as

in Kromme estuary (Wortmann et al., 1998) and Nile River (Aleem, 1972). As the central sector of Sundarbans has been isolated from the western part, and no freshwater connection of this part exists, so estuarine nature of the Matla River is exclusively maintained by monsoonal runoff and tidal action. According to Raha et al. (2012), the salinity of this central part (in the year 2001–2002) ranged from 5–6, but in recent years it has gradually increased up to 35.4 as reflected in our study. Besides that, the lowest DO value was recorded during summer which can be attributed to increased water temperature during this period (Vega et al., 1998). However, rests of the other seasons have higher values of DO, showing no sign of hypoxia in the bottom water. Generally, seasonal pattern in mangrove litterfall and decomposition influences the temporal dynamics of dissolved inorganic nutrients in mangrove dominated estuaries (Lara and Dittmar, 1999) was also emulated in our study. Sundarbans estuarine system is comparatively a pristine zone and there is no record of sewage discharge or groundwater seepage, hence litterfall and excretory and/or decomposition product of aquatic organisms might be the only source of ammonia throughout the estuarine stretch. Except few upper stretch stations, rest of our study stations fall under the Sundarbans biosphere reserve and have restricted anthropogenic activities. From the viewpoint of granulometry, the area is mostly silty with a variable amount of finer and coarser sediment particles. The slow tectonic activity of the entire Bengal basin has a profound effect on the sedimentation pattern of Sundarbans delta. In contrast to the western part, islands of the central region (study site) are expanding owing to accretion (Raha et al., 2012). Due to this continuous sediment reworking process, the granulometry of our study sites has not followed any pattern. Besides this, monsoonal runoff has a substantial influence on the sediment granulometry. Furthermore, monsoonal rainfall leads to sediment agitation that scours the finer particles and therefore, coarser element like sand predominate the sediment texture (Ghosh et al., 2018). Conclusively, change in the grain size was influenced by high sedimentation as well as rainfall during the study period.

#### 4.2. Macrobenthic assemblages

Estuarine macrobenthos are always under the influence of disharmonic environment with fluctuating salinity and variable sediment composition (Elliott and Whitfield, 2011). Generally, they have higher physiological capabilities to tolerate fluctuating saltwater incursion mediated ionic imbalance, which is common phenomenon in estuaries (Little et al., 2017). Likewise, a natural or abrupt change in salinity is among the major constraints that estuarine fauna must challenge. Moreover, these anomalies in salinity can affect their recruitment pattern and acts as the migrational cue that ultimately module their population dynamics (Wilson and Fleeger, 2013). Nonetheless, the rate and scale of salinity change is important as it can diminish the diversity of a biota (Attrill, 2002). The total macrobenthic density was highest at station 1 during summer, mostly composed of some opportunistic species from families like Capitellidae, Glyceridae, Nephtyidae, Nereidae. Organic enrichment in sediment tends to decrease the penetration of oxygen, creating an anoxic condition which can be

favoured by opportunists. In estuaries, monsoonal runoff causes drastic fall in macrobenthic density which starts to replenish by the colonization of juveniles as well as the reestablishment of adult fauna in post-monsoon and continues afterwards (Gaonkar et al., 2013). Nevertheless, few stations like 1, 4, 6 and 7 showed deviation from that conventional pattern where macrobenthic density in winter starts to decline in the subsequent season. This might be attributed to the post-settlement mortality driven by salinity and bioturbation mediated sediment disturbances (Hunt and Scheibling, 1997).

Polychaetes contributed 74% of macrofaunal density and considered as a numerically dominant class which is the common for intertidal sheltered mudflats. It has been also stated that estuaries and coasts that have a high saline zone, preferably contain polychaetes more often than any other macrobenthic taxa (Alongi, 1989). Few dominating families were Capitellidae, Spionidae, Cossuridae constituted the polychaete assemblages. Being the most dominant family, capitellids receive much attention for their capacity to tolerate the environmental fluctuations as well as, their cosmopolitan distribution (Bissoli and Bernardino, 2018; Fernández-Rodríguez et al., 2019; Rao, 1980). A cycle of high density among capitellids was clearly noticed, alternately dominated by *Heteromastus similis* and *Parheteromastus tenuis* where each species can partially exclude the other in different seasons. This type of interaction can be explained by species succession model where intra-specific competition for resource availability took place between two species of the same guild and one outcompete the other and/or habitat modification by earlier species has encouraged the settlement of the next species (Harkantra and Rodrigues, 2003; Peterson, 1977; Rhoads and Germano, 1982; Thistle, 1981). According to Harkantra and Rodrigues (2003) species succession can be brought about by south western monsoon mediated biotic and abiotic changes. Similar to their study, in the present study also species succession became prominent after a downpour in the monsoon season. According to Medeiros et al. (2016), tropical estuaries those are least affected by anthropogenic activities are governed by constant modification or replacement rather than nestedness which has been clearly depicted in the present study by species succession. This type of succession along the spatiotemporal gradient can cause habitat mosaicism in the estuary (Chen et al., 2015; Thistle, 1981). Besides this, both the families like Capitellidae and Spionidae prevailed in the estuary throughout the study period. This can be explained as persistence in family level accomplished by losing and gaining of the species (Hylleberg and Natewathana, 1984). Among molluscs, *Donax incarnatus* was the most dominant taxa as they are well adapted to tropical intertidal life (Alongi, 1989) and similarly, in our study a seasonal pattern has been portrayed through their population dynamics. During monsoon, their population drastically reduced to 70% of the density found in summer but they were gradually established by new recruiters with their bimodal reproduction in October–January and April–June (Alongi, 1989; Ansell and Trueman, 1973; Harkantra and Parulekar, 1985).

According to SIMPER analysis, upper stretch stations have always been separated from others due to the contribution of *H. similis* in both summer and monsoon. It can

be explained as sediment of this area is comparatively rich in organic content due to anthropogenic input or mangrove litter which provides a better habitat for capitellids. However, in winter, the contribution of *T. stroemii* has separated station 8 from other stations. During spring, the environmental parameters made station 4 a favourable habitat for molluscs like *Acteocina estriata*, *Stenothyra deltae* and *Meretrix meretrix* and thus separated from rest of the stations. In Canonical Correspondence Analysis (CCA), station biplot has shown that stations in summer were influenced by DO which can be attributed to elevated temperature during summer that inversely declined DO (Vega et al., 1998). In monsoon and winter seasons, stations were mostly dominated by sand as heavy rainfall during July as well as in October causing the wash off of uppermost finer particles. Species biplot clearly depicts that environmental parameters like sand %, clay %, sediment phaeopigment, temperature, organic carbon (OC) were the most important factors in structuring the polychaete community. According to the finding of Penry and Jumars (1990), the gut of *S. scutata* has been found to be filled with muds and their preference towards finer particles is in agreement with the present study. *Micronephthys oligobranchia* is a muscular shallow-water burrower and prefer the clayey substratum; as Ronan (1977) has found one of the species from this genus that are mostly found in muddy sediment at Bodega Harbour. Carnivores like pilargids have shown an affinity with sand % (Jumars et al., 2015). Overall, a higher level of biodiversity was indicated by Shannon, Margalef's and Pielou's evenness indices. The substrate heterogeneity of this estuary plays a pivotal role in structuring this ecologically diverse community and allows coexistence of several species with different successional stages.

### 4.3. Biological Traits Analysis (BTA)

Approaches to BTA from transitional zones like estuaries is often challenging in terms of finding detailed and accurate trait information (Tyler et al., 2012). Biological trait analysis furnishes information on species distribution based on their biological characteristics providing a trait profile of benthic assemblages and complements their bioassessment measures (Munari, 2013). In this study, changes in functional characters are broadly concurrent with the seasonal succession of species assemblages. The most important environmental factor that regulates the body size trait is sediment grain size (Bremner et al., 2006). As depicted in our study, large animals were prevalent in station 2 when the percentage of silt was comparatively higher than any other stations in spring. The small size allows animals to become more specialized in diversified elements of the environmental mosaics (Hutchinson and MacArthur, 1959). Overall, small animals dominated the estuary which imparts an indication of a continuously perturbed environment. Not only body size, but also the rate of mobility is remarkably regulated by the granulometry of the habitat. Mobility is a crucial trait that affects food capture method and also defines the trophic relationship in the benthic community (Sigala et al., 2012). In the present study, the arrival of spring brings the changes in the sedimentology and concurrently all the motile species of the previous season were gradually replaced by discretely motile species. According

to Hunt and Scheibling (1997), an increase in macrofaunal predators can hamper the recruitment of sessile organism. In connection with this hypothesis, it can be inferred that the predator effect might have played a crucial role in suppression of sessile animal population throughout the estuary. The same authors have postulated that a gradual increase in motile species over the evolutionary time scale has a strong influence in constructing modern marine benthos by gaining fitness against predation. The living habitat (LH) trait was mostly represented by burrowers who requires soft and penetrable substratum to make successful burrow habitat. As the entire study stretch is mostly silty clay, so the prevalence of burrowers like Paraonidae, Sternaspidae is justified. Burrowers can act as sediment reworker through the suspension of fine particle into overlying water. By acting as a molecular sieve, it allows the increase of the oxygen content at the sediment-water interface (Aller, 1983; Bremner et al., 2006; Constable, 1999). Moreover, burrows provide a microenvironment that leads to nutrient cycling and increased organic matter decomposition. According to RLQ analysis, the prevalence of burrowers is generally correlated with the sand percentage in the sediment. Presence of various feeding type trait indicates diverse food sources available in the estuary and it may also accentuate more diverse pathway of energy recycling (Sigala et al., 2012). Deposit feeders are mostly affected by sediment particle size whereas, suspension feeders are mostly regulated by hydrodynamics and physical processes in the water column and they generally do not prefer to live in areas where fine sediments can disrupt their feeding apparatus (Constable, 1999). In the present study, a gradual appearance of suspension feeders was observed in spring contributed by some spionids like *Paraprionospio pinnata* and *Spio bengalensis* as they have the ability to switch their feeding mode from deposit to suspension feeding in presence of adequate horizontal flux of sediment particles (Jumars et al., 2015). It may also be noticed in bivalves depending on predator pressure and other local environmental factors. The behaviour and the rate of suspension feeders are also regulated by the particulate organic matter content whereas, deposit feeders increase when particles are deposited in the sediment or suspended in the water column (Bock and Miller, 1996; Peterson and Skilleter, 1994). Suspension feeder bivalves are the crucial driver in benthic-pelagic coupling. They capture suspended organic matter and phytoplankton, thus contribute significantly in whole ecosystem productivity (Newell, 2004; Tillin et al., 2006; Rosenberg 2001). Nevertheless, the dominance of deposit feeders was due to their broader range of food materials acceptance (Sigala et al., 2012). Commonly, diet type is highly regulated by grain size of the sediment. As described by Wu and Shin (1997), particle size and organic content are the major drivers that affect colonization of soft-bottom benthos. In carnivory trait category, species like *Micronephthys oligobranchia*, *Dendroneis aestuarina*, *Kuwaita heteropoda* contributed the most. Oug et al. (2012) have documented that carnivory is related to coarser and low porosity sediment. The prevalence of carnivores is also an indication of improved sediment quality that allows species with various feeding modes to flourish concurrently (Hu et al., 2019).

In the future climate change scenario, the seasonal dynamics of Sundarbans is going to alter (IPCC, 2013). Fur-

thermore, it has also been conjectured that summers are projected to be dried and warmer with reduced freshwater flow-mediated salinity incursion and Sundarbans is not an exception. This might also be associated with an unusual shift in monsoonal activity with late onset and late withdrawal (IMD, 2010; Little et al., 2017) which would have profound repercussion on benthic biota. According to a time series analysis, the central part of Indian Sundarbans has been predicted to be under the threat of hypersalinisation with an increment of around 13.05 psu/decade, howbeit both western and eastern part have shown a decreasing trend of salinisation (Trivedi et al., 2016). Furthermore, studies have also revealed a gradual disappearance of freshwater preferring mangrove species as well as a compositional shift in phytoplankton community due to rapid salinity incursion in the central sector (Chaudhuri and Choudhury, 1994; Raha et al., 2012). It would be difficult to ascertain the changes in macrobenthic community in comparison with previous studies due to the unavailability of data from this sector of Sundarbans.

Seasonal succession in any community can be better apprehended by tracking trait modalities using BTA. Being dynamic, the estuarine macrobenthos is always facing a continuous seasonal perturbation, where BTA is a new approach to unravel the functionality of every species in a community. However, due to the lack of precise information on traits, sometimes BTA may fail to portray the species level changes on the trait analysis. As depicted in the present study, interspecific replacement between two of the spionid species due to seasonal fluxes cannot be properly pointed out through BTA as these two congener species share almost similar trait modalities. Some of these species have similar traits which may lead to functional redundancy in a community and can be substituted with very little or no effect on ecosystem processes (Rosenfeld, 2002). In Piló 2016, authors have stated that functional redundancy is very much relevant to naturally disturbed estuaries where long term intrinsic adaptations of local species are evident. Furthermore, it is hard to determine the specific environmental factors that are regulating trait categories in a complex estuarine ecosystem like Sundarbans. Hence, the underlined mechanism in gaining evolutionary fitness against climate change mediated habitat modification in the Sundarbans ecosystem would be an interesting area to explore for future researchers.

## 5. Conclusion

The present study has been the first attempt (1) to document 95 macrobenthic taxa with comprehensive information of their community pattern, distribution and spatiotemporal variation along the Matla River of Sundarbans over four distinct seasons of 2017–2018, (2) to document multiple biological traits of the macrobenthic community for better understanding of their seasonal succession pattern. A prominent succession pattern has been noticed in species of several families like Capitellidae, Spionidae as well as in trait composition like type of a mobility, body size, living habitat and feeding strategy. Trait categories like discretely motile animals gradually replaced by motile animals in monsoon and post-monsoon seasons. The gradual

increase in suspension feeder was contributed by certain species like *Paraprionospio pinnata* and *Spio bengalensis* that have the adaptive ability to switch their feeding mode. It has also been explained how environmental perturbations act as a crucial driver for changes in the macrobenthic community structure. Moreover, the changing trend of annual temperature, rainfall pattern and frequencies of tropical cyclones have continually acted as a stressor for the biota which affects the species composition and regular succession pattern as mirrored in our study. Hence, long term monitoring with additional trait categories is needed to understand the benthic ecosystem functioning more precisely and their changes due to perturbed environmental factors from the world's largest deltaic ecosystem.

## Acknowledgement

The authors wish to express their gratitude to The Vice Chancellor, Presidency University for providing facilities and encouragement to carry out the above research work. The authors thank the Editor and anonymous reviewers for their constructive comments. The authors are grateful to Mr. Subham Mridha, University of Zürich, Switzerland for his kind help in RLQ analysis and generating the R plots. We also thank Dr. Meenakshi Chatterjee of Basanti Devi College, Kolkata for her ever willing help and co-operation during the study. This work is supported by a grant awarded to S. M. from Ministry of Earth Sciences (MoES/36/OOIS/Extra/24/2013 dated 11.04.2016). Thanks are also due to the Directorate of Forest and the Sundarban Biosphere Reserve, Government of West Bengal for permission to work in some of the Reserve Forest areas (permission letters memo no. 3837/WL/4R-6/2017 dated 11.08.2017 and 3100/WL/4R-6/2018 dated 05.09.2018). The authors would also like to express their appreciation to the members of the Marine Ecology Laboratory for excellent teamwork.

## Supplementary materials

Supplementary material associated with this article can be found, in the online version, at <https://doi.org/10.1016/j.oceano.2020.10.002>.

## References

- Aleem, A.A., 1972. Effect of river outflow management on marine life. *Mar. Biol.* 15, 200–208. <https://doi.org/10.1007/BF00383550>
- Aller, R.C., 1983. The importance of the diffusive permeability of animal burrow linings in determining marine sediment chemistry. *J. Mar. Res.* 41 (2), 299–322. <https://doi.org/10.1357/002224083788520225>
- Alongi, D.M., 1989. Ecology of tropical soft-bottom benthos: a review with emphasis on emerging concepts. *Rev. Biol. Trop.* 37, 85–100.
- Anderson, M.J., Gorley, R.N., Clarke, K.R., 2008. PERMANOVA A+ for PRIMER: Guide to Software and Statistical Methods. PRIMER-E, Plymouth, UK.
- Ansell, A.D., Trueman, E.R., 1973. The energy cost of migration of the bivalve *Donax* on tropical sandy beaches. *Mar. Behav. Physiol.* 2, 21–32. <https://doi.org/10.1080/10236247309386914>

- Attrill, M.J., 2002. A testable linear model for diversity trends in estuaries. *J. Anim. Ecol.* 71 (2), 262–269. <https://doi.org/10.1046/j.1365-2656.2002.00593.x>
- Benjamini, Y., Hochberg, Y., 1995. Controlling the False Discovery Rate: A Practical and Powerful Approach to Multiple Testing. *J. R. Stat. Soc. Ser. B Methodol.* 57, 289–300.
- Bissoli, L.B., Bernardino, A.F., 2018. Benthic macrofaunal structure and secondary production in tropical estuaries on the eastern marine ecoregion of Brazil. *Peer J.* 6, e4441. <https://doi.org/10.7717/peerj.4441>
- Bock, M.J., Miller, D.C., 1996. Fluid flow and suspended particulates as determinants polychaete feeding behavior. *J. Mar. Res.* 54 (3), 565–588. <https://doi.org/10.1357/0022240963213547>
- Bremner, J., Rogers, S., Frid, C., 2003. Assessing functional diversity in marine benthic ecosystems: a comparison of approaches. *Mar. Ecol. Prog. Ser.* 254, 11–25. <https://doi.org/10.3354/meps254011>
- Bremner, J., Rogers, S.I., Frid, C.L.J., 2006. Methods for describing ecological functioning of marine benthic assemblages using biological traits analysis (BTA). *Ecol. Indic.* 6 (3), 609–622. <https://doi.org/10.1016/j.ecolind.2005.08.026>
- Buchanan, J.B., 1984. Sediment analysis. In: Holme, N.A., McIntyre, A.D. (Eds.), *Methods for the Study of Marine Benthos*. Blackwell Scientific Publications, Oxford, 41–65.
- Chatterjee, M., Shankar, D., Sen, G.K., Sanyal, P., Sundar, D., Michael, G.S., Chatterjee, A., Amol, P., Mukherjee, D., Suprit, K., Mukherjee, A., Vijith, V., Chatterjee, S., Basu, A., Das, M., Chakraborti, S., Kalla, A., Misra, S.K., Mukhopadhyay, S., Mandal, G., Sankar, K., 2013. Tidal variations in the Sundarbans Estuarine System, India. *J. Earth Syst. Sci.* 122 (4), 899–933. <https://doi.org/10.1007/s12040-013-0314-y>
- Chaudhuri, A.B., Choudhury, A., 1994. *Mangroves of the Sundarbans. Volume One: India*. IUCN Wetland Programme, Bangkok, Thailand, 2479 pp.
- Chen, Q., Li, J., Zhang, L., Lu, H., Ren, H., Jian, S., 2015. Changes in the macrobenthic faunal community during succession of a mangrove forest at Zhanjiang, South China. *J. Coast. Res.* 31 (2), 315–325. <https://doi.org/10.2112/JCOASTRES-D-13-00019>
- Chevone, F., Dolédec, S., Chessel, D., 1994. A fuzzy coding approach for the analysis of long-term ecological data. *Freshw. Biol.* 31, 295–309. <https://doi.org/10.1111/j.1365-2427.1994.tb01742.x>
- Clarke, K.R., Warwick, R.M., 2001. *Change in Marine Communities: An Approach to Statistical Analysis and Interpretation*, 2nd edn., PRIMER-E, Plymouth, UK.
- Clarke, K.R., Gorley, R.N., 2006. *PRIMER v6: User Manual/Tutorial*. PRIMER-E, Plymouth.
- Clarke, K.R., Somersfield, P.J., Gorley, R.N., 2008. Testing of null hypotheses in explanatory community analyses: Similarity profiles and biota-environment linkage. *J. Exp. Mar. Biol. Ecol.* 366 (1–2), 56–69. <https://doi.org/10.1016/j.jembe.2008.07.009>
- Constable, A.J., 1999. Ecology of benthic macro-invertebrates in soft-sediment environments: A review of progress towards quantitative models and predictions. *Aust. J. Ecol.* 24, 452–476. <https://doi.org/10.1046/j.1442-9993.1999.00977.x>
- Day, J.H., 1967. *A monograph on the polychaeta of southern Africa. Part I (Errantia) & II (Sedentaria)*. Trustees of the British Museum (Natural History), London, 656 pp.
- Dey, A., 2006. *Handbook on mangrove associate molluscs of Sundarbans XI. Zoological Survey of India*, 96 pp.
- Dey, M., Ganguly, D., Chowdhury, C., Majumder, N., Jana, T.K., 2012. Intra-annual variation of modern foraminiferal assemblage in a tropical mangrove ecosystem in India. *Wetlands*. 32, 813–826. <https://doi.org/10.1007/s13157-012-0312-x>
- Dolédec, S., Chessel, D., ter Braak, C.J.F., Champely, S., 1996. Matching species traits to environmental variables: a new three-table ordination method. *Environ. Ecol. Stat.* 3 (2), 143–166. <https://doi.org/10.1007/BF02427859>
- Dolédec, S., Statzner, B., Bournard, M., 1999. Species traits for future biomonitoring across ecoregions: patterns along a human-impacted river. *Freshw. Biol.* 42 (4), 737–758. <https://doi.org/10.1046/j.1365-2427.1999.00509.x>
- Dolédec, S., Phillips, N., Scarsbrook, M., Riley, R.H., Townsend, C.R., 2006. Comparison of structural and functional approaches to determining land use effects on grassland stream invertebrate communities. *J. N. Am. Benthol. Soc.* 25 (1), 44–60. [http://dx.doi.org/10.1899/0887-3593\(2006\)25\[44: COSAJA\]2.0.CO;2](http://dx.doi.org/10.1899/0887-3593(2006)25[44: COSAJA]2.0.CO;2)
- Dray, S., Dufour, A.B., 2007. The ade4 package: implementing the duality diagram for ecologists. *J. Stat. Softw.* 22, 1–20.
- Dray, S., Legendre, P., 2008. Testing the species traits–environment relationships: the fourth-corner problem revisited. *Ecology*. 89, 3400–3412.
- Dray, S., 2013. *A Tutorial to Perform Fourth-Corner and RLQ Analyses in R*.
- Dray, S., Choler, P., Dolédec, S., Peres-Neto, P.R., Thuiller, W., Pavoine, S., ter Braak, C.J.F., 2014. Combining the fourth-corner and the RLQ methods for assessing trait responses to environmental variation. *Ecology*. 95 (1), 14–21. <https://doi.org/10.1890/13-0196.1>
- Egres, A.G., Hatje, V., Miranda, D.A., Gallucci, F., Barros, F., 2019. Functional response of tropical estuarine benthic assemblages to perturbation by Polycyclic Aromatic Hydrocarbons. *Ecol. Indic.* 96, 229–240. <https://doi.org/10.1016/j.ecolind.2018.08.062>
- El Wakeel, S.K., Riley, J.P., 1957. The Determination of Organic Carbon in Marine Muds. *ICES J. Mar. Sci.* 22, 180–183. <https://doi.org/10.1093/icesjms/22.2.180>
- Elliott, M., Whitfield, A.K., 2011. Challenging paradigms in estuarine ecology and management. *Estuar. Coast. Shelf Sci.* 94 (4), 306–314. <https://doi.org/10.1016/j.ecss.2011.06.016>
- Fauchald, K., Jumars, P.A., 1979. *The Diet of Worms: a Study of Polychaete Feeding Guilds*. *Mar. Biol. Ann. Rev.* 17, 193–284.
- Faulwetter, S., Markantonatou, V., Pavlouidi, C., Papageorgiou, N., Keklikoglou, K., Chatziniolaou, E., Pafilis, E., Chatzigeorgiou, G., Vasileiadou, K., Dailianis, T., Fanini, L., Koulouri, P., Arvanitidis, C., 2014. Polytraits: A database on biological traits of marine polychaetes. *Biodiversity Data J.* 2, e1024. <https://doi.org/10.3897/BDJ.2.e1024>
- Fauvel, P., 1953. *The fauna of India including Pakistan, Ceylon, Burma and Malaya: Annelida, Polychaeta*. The Indian Press, Allahabad, 507 pp.
- Fernández-Rodríguez, V., Santos, C.S.G., Pires, A.P.F., 2019. Meta-analysis of the effects of organic matter on polychaetes of the east coast of South America. *Mar. Environ. Res.* 149, 148–156. <https://doi.org/10.1016/j.marenvres.2019.06.001>
- Fukushima, A., Kanamori, H., Matsumoto, J., 2019. Regionality of long-term trends and interannual variation of seasonal precipitation over India. *Prog. Earth Planet. Sci.* 6, 1–20. <https://doi.org/10.1186/s40645-019-0255-4>
- Gaonkar, U.V., Sivadas, S.K., Ingole, B.S., 2013. Effect of tropical rainfall in structuring the macrobenthic community of Mandovi estuary, west coast of India. *J. Mar. Biol. Assoc. U.K.* 93 (7), 1727–1738. <https://doi.org/10.1017/S002531541300026X>
- Ghosh, M., Mandal, S., Chatterjee, M., 2018. Impact of unusual monsoonal rainfall in structuring meiobenthic assemblages at Sundarban estuarine system, India. *Ecol. Indic.* 94, 139–150. <https://doi.org/10.1016/j.ecolind.2018.06.067>
- Ghosh, M., Mandal, S., 2019. Does vertical distribution of meiobenthic community structure differ among various mangrove habitats of Sundarban Estuarine System? *Reg. Stud. Mar. Sci.* 31, 1–11. <https://doi.org/10.1016/j.rsma.2019.100778>
- Giese, A., Pierser, J., 1977. In: *Reproduction of Marine Invertebrates Volume IV Molluscs: Gastropods and Cephalopods*, 4. Acad. Press, 369 pp.

- Grasshoff, K., Kremling, K., Ehrhardt, M., 1999. *Methods of seawater analysis*, 3rd edn. Verlag Chemie, Weinheim, Germany, 634 pp.
- Griffiths, J.R., Kadin, M., Nascimento, F.J.A., Tاملander, T., Törnroos, A., Bonaglia, S., Bonsdorff, E., Brüchert, V., Gårdmark, A., Järnström, M., Kotta, J., Lindegren, M., Nordström, M.C., Norkko, A., Olsson, J., Weigel, B., Žydelis, R., Blenckner, T., Niiranen, S., Winder, M., 2017. The importance of benthic-pelagic coupling for marine ecosystem functioning in a changing world. *Glob. Chang. Biol.* 23 (6), 2179–2196. <https://doi.org/10.1111/gcb.13642>
- Harkantra, S.N., Parulekar, A.H., 1985. Community structure of sand-dwelling macrofauna of an estuarine beach in Goa, India. *Mar. Ecol. Prog. Ser.* 30, 291–294.
- Harkantra, S.N., Rodrigues, N.R., 2003. Pattern of species succession of soft-bottom macrofauna in the estuaries of Goa, west coast of India. *Curr. Sci.* 85 (10), 1458–1474. <https://doi.org/10.2307/24108829>
- Hunt, H.L., Scheibling, R.E., 1997. Role of early post-settlement mortality in recruitment of benthic marine invertebrates. *Mar. Ecol. Prog. Ser.* 155, 269–301. <https://doi.org/10.3354/meps155269>
- Hutchinson, G.E., MacArthur, R.H., 1959. A theoretical ecological model of size distributions among species of animals. *Am. Nat.* 93, 117–125.
- Hyllberg, J., Natewathana, A., 1984. Responses of polychaete families to monsoon and offshore mining associated sediment disturbance. In: Hutchings, P.A. (Ed.), *Proceedings of the First International Polychaete Conference*, Sydney. The Linnean Society of New South Wales, 279–291.
- Hu, C., Dong, J., Gao, L., Yang, X., Wang, Z., Zhang, X., 2019. Macrobenthos functional trait responses to heavy metal pollution gradients in a temperate lagoon. *Environ. Pollut.* 253, 1107–1116. <https://doi.org/10.1016/j.envpol.2019.06.117>
- IMD, 2010. 348 Climate Profile of India. *Environ. Monit. Res. Centre, India Meteorol. Dep.* 122.
- IPCC, 2013. *Climate Change 2013. The Physical Science Basis, Contribution of Working Group I to the Fifth Assessment Report of the Intergovernmental Panel on Climate Change*. Cambridge University Press, Cambridge, United Kingdom and New York, NY, USA.
- Jumars, P.A., Dorgan, K.M., Lindsay, S.M., 2015. Diet of Worms Emended: An Update of Polychaete Feeding Guilds. *Ann. Rev. Mar. Sci.* 7, 497–520. <https://doi.org/10.1146/annurev-marine-010814-020007>
- Keddy, P., 1992. Assembly and response rules: two goals for predictive community ecology. *J. Veg. Sci.* 3 (2), 157–164. <https://doi.org/10.2307/3235676>
- Kennish, M.J., 2002. Environmental threats and environmental future of estuaries. *Environ. Conserv.* 29 (1), 78–107. <https://doi.org/10.1017/S0376892902000061>
- Kovach, W.L., 1998. *MVSP—multi-variate statistical package for windows*, Ver 3.0. Kovach computing services, Pentraeth.
- Lara, R.J., Dittmar, T., 1999. Nutrient dynamics in a mangrove creek (North Brazil) during the dry season. *Mangroves and Salt Marshes.* 3, 185–195.
- Legendre, P., Galzin, R., Harmelin-Vivien, M.L., 1997. Relating behavior to habitat: solutions to the fourth corner problem. *Ecology.* 78 (2), 547–562. [https://doi.org/10.1890/0012-9658\(1997\)078\[0547:RBTHST\]2.0.CO;2](https://doi.org/10.1890/0012-9658(1997)078[0547:RBTHST]2.0.CO;2)
- Little, S., Wood, P.J., Elliott, M., 2017. Quantifying salinity-induced changes on estuarine benthic fauna: The potential implications of climate change. *Estuar. Coast. Shelf Sci.* 198 (B), 610–625. <https://doi.org/10.1016/j.ecss.2016.07.020>
- Manna, S., Chaudhuri, K., Bhattacharyya, S., Bhattacharyya, M., 2010. Dynamics of Sundarban estuarine ecosystem: eutrophication induced threat to mangroves. *Sal. Sys.* 6 (8), 1–16. <https://doi.org/10.1186/1746-1448-6-8>
- MarLIN, 2006. BIOTIC — Biological Traits Information Catalogue. Marine Life Information Network Marine Biological Association of the United Kingdom, Plymouth, available at: [www.marlin.ac.uk/biotic](http://www.marlin.ac.uk/biotic) (accessed at: 03/01/2016).
- Medeiros, C.R., Hepp, L.U., Patrício, J., Molozzi, J., 2016. Tropical estuarine macrobenthic communities are structured by turnover rather than nestedness. *PLoS One.* 11 (9), 1–14. <https://doi.org/10.1371/journal.pone.0161082>
- Mestdagh, S., Bagaço, L., Braeckman, U., Ysebaert, T., De Smet, B., Moens, T., Van Colen, C., 2018. Functional trait responses to sediment deposition reduce macrofauna-mediated ecosystem functioning in an estuarine mudflat. *Biogeosciences.* 15, 2587–2599. <https://doi.org/10.5194/bg-15-2587-2018>
- Misra, A., 1995. *Polychaetes*. In: *Hugli Matla Estuary. Estuarine Ecosystem Series 2. Zoological Survey of India, Calcutta*, 93–155.
- Modéran, J., Bouvais, P., David, V., Le Noc, S., Simon-Bouhet, B., Niquil, N., Miramand, P., Fichet, D., 2010. Zooplankton community structure in a highly turbid environment (Charente estuary, France): spatio-temporal patterns and environmental control. *Estuar. Coast. Shelf Sci.* 88 (2), 219–232. <https://doi.org/10.1016/j.ecss.2010.04.002>
- Mukhopadhyay, S.K., Biswas, H., De, T.K., Jana, T.K., 2006. Fluxes of nutrients from the tropical River Hooghly at the land-ocean boundary of Sundarbans, NE Coast of Bay of Bengal, India. *J. Mar. Syst.* 62 (1–2), 9–21. <https://doi.org/10.1016/j.jmarsys.2006.03.004>
- Munari, C., 2013. Benthic community and biological trait composition in respect to artificial coastal defence structures: A study case in the northern Adriatic Sea. *Mar. Environ. Res.* 90, 47–54. <https://doi.org/10.1016/j.marenvres.2013.05.011>
- Nandy, T., Mandal, S., Chatterjee, M., 2018a. Intra-monsoonal variation of zooplankton population in the Sundarbans Estuarine System, India. *Environ. Monit. Assess.* 190 (10), 1–20. <https://doi.org/10.1007/s10661-018-6969-8>
- Nandy, T., Mandal, S., Deb, S., Ghosh, M., Nath, T., Chatterjee, M., 2018b. Short-term variations in surface water properties in the Sundarban Estuarine System, India. *Sustain. Water Resour. Manag.* 4, 559–566. <https://doi.org/10.1007/s40899-017-0139-y>
- Newell, R.I.E., 2004. Ecosystem influences of natural and cultivated populations of suspension-feeding bivalve molluscs: a review. *J. Shellfish Res.* 23 (1), 51–61.
- Oug, E., Fleddum, A., Rygg, B., Olsford, F., 2012. Biological traits analyses in the study of pollution gradients and ecological functioning of marine soft bottom species assemblages in a fjord ecosystem. *J. Exp. Mar. Biol. Ecol.* 432–433, 94–105. <https://doi.org/10.1016/j.jembe.2012.07.019>
- Pacheco, A.S., González, M.T., Bremner, J., Oliva, M., Heilmayer, O., Laudien, J., Riascos, J.M., 2011. Functional diversity of marine macrobenthic communities from sublittoral soft-sediment habitats off northern Chile. *Helgol. Mar. Res.* 65 (3), 413–424. <https://doi.org/10.1007/s10152-010-0238-8>
- Pant, V., Girishkumar, M.S., Bhaskar, T.V.S.U., Ravichandran, M., Papa, F., Thangaprakash, V.P., 2015. Observed interannual variability of near surface salinity in the Bay of Bengal. *J. Geophys. Res.* 120 (5), 3315–3329. <https://doi.org/10.1002/2014JC010340>
- Penry, D.L., Jumars, P.A., 1990. Gut architecture, digestive constraints and feeding ecology of deposit-feeding and carnivorous polychaetes. *Oecologia.* 82, 1–11.
- Peterson, C.H., 1977. Competitive organization of the soft-bottom macrobenthic communities of southern California lagoons. *Mar. Biol.* 43, 343–359. <https://doi.org/10.1007/BF00396928>
- Peterson, C.H., Skilleter, G.A., 1994. Control of foraging behaviour of individuals within an ecosystem context: the clam *Macoma balthica*, flow environment, and siphoncropping fishes. *Oecologia.* 100 (3), 256–267. <https://doi.org/10.1007/BF00316953>

- Piló, D., Ben-Hamadou, R., Pereira, F., Carriço, A., Pereira, P., Corzo, A., Gaspar, M.B., Carvalho, S., 2016. How functional traits of estuarine macrobenthic assemblages respond to metal contamination? *Ecol. Indicat.* 71, 645–659.
- Raha, A., Das, S., Banerjee, K., Mitra, A., 2012. Climate change impacts on Indian Sunderbans: A time series analysis (1924–2008). *Biodivers. Conserv.* 21, 1289–1307. <https://doi.org/10.1007/s10531-012-0260-z>
- Rao, D.S., 1980. Ecology of *Heteromastus similis* Southern 1921 (Polychaeta: Capitellidae) in the Vasishta Godavari estuary. *Proc. Anim. Sci.* 89, 407–414. <https://doi.org/10.1007/BF03179126>
- Rastogi, D., Ashfaq, M., Leung, L.R., Ghosh, S., Saha, A., Hodges, K.I., Evans, K., 2018. Characteristics of Bay of Bengal monsoon depressions in the 21st century. *Geophys. Res. Lett.* 45 (13), 6637–6645. <https://doi.org/10.1029/2018GL078756>
- Rhoads, D.C., Young, D.K., 1971. Animal-sediment relations in Cape Cod Bay, Massachusetts II. Reworking by *Molpadia oolitica* (Holothuroidea). *Mar. Biol.* 11, 255–261. <https://doi.org/10.1007/BF00401273>
- Rhoads, D.C., Germano, J.D., 1982. Characterization of organic-sediment relations using sediment profile imaging: an efficient method of remote ecological monitoring of the seafloor (Remots™ systems). *Mar. Ecol. Prog. Ser.* 8 (2), 115–128.
- Ronan Jr, T.E., 1977. Formation and paleontologic recognition of structures caused by marine annelids. *Paleobiology.* 3 (4), 389–403.
- Rosenberg, R., 2001. Marine benthic faunal successional stages and related sedimentary activity. *Sci. Mar.* 65, 107–119.
- Rosenfeld, J.S., 2002. Functional redundancy in ecology and conservation. *Oikos.* 98 (1), 156–162. <https://doi.org/10.1034/j.1600-0706.2002.980116.x>
- Rudra, K., 2018. The Sundarban. In: Rudra, K. (Ed.), *Rivers of the Ganga-Brahmaputra-Meghna delta. Geography of the physical environment.* Springer, Cham, 107–124. [https://doi.org/10.1007/978-3-319-76544-0\\_8](https://doi.org/10.1007/978-3-319-76544-0_8)
- Rybczyk, J.M., Day Jr., J.W., 2013. Global climate change and estuarine systems. In: Day, Jr., J.W., Crump, B.C., Kemp, W.M., Yáñez-Arancibia, A. (Eds.), *Estuarine Ecology*, 501–518.
- Saha, S.B., Bhattacharyya, S.B., Mitra, A., Pandey, B.K., Choudhury, A., 2001. Physicochemical characteristics in relation to pollution and phytoplankton production potential of a brackish water ecosystem of Sundarbans in West Bengal. *Trop. Ecol.* 42 (2), 199–205.
- Sigala, K., Reizopoulou, S., Basset, A., Nicolaidou, A., 2012. Functional diversity in three Mediterranean transitional water ecosystems. *Estuar. Coast. Shelf Sci.* 110, 202–209. <https://doi.org/10.1016/j.ecss.2012.06.002>
- Southern, R., 1921. Polychaeta of the Chilka Lake and also of fresh and brackish waters in other parts of India. *Mem. Indian Mus.* 5, 563–659.
- Stanley, D.J., Hait, A.K., 2000. Holocene depositional patterns, neotectonics and Sundarban mangroves in the western Ganges-Brahmaputra delta. *J. Coast. Res.* 16 (1), 26–39. <https://doi.org/10.2307/4300009>
- Strickland, J.D.H., Parsons, T.R., 1972. *A practical handbook of seawater analysis.* Fisheries Research Board of Canada, Ottawa, 328 pp.
- Taupp, T., Wetzel, M.A., 2019. Functionally similar but taxonomically different: Benthic communities in 1889 and 2006 in an industrialized estuary. *Estuar. Coast. Shelf Sci.* 217, 292–300. <https://doi.org/10.1016/j.ecss.2018.11.012>
- Thistle, D., 1981. Natural physical disturbances and communities of marine soft bottoms. *Mar. Ecol. Prog. Ser.* 6 (2), 223–228.
- Tillin, H.M., Hiddink, J.G., Jennings, S., Kaiser, M.J., 2006. Chronic bottom trawling alters the functional composition of benthic invertebrate communities on a sea-basin scale. *Mar. Ecol. Prog. Ser.* 318, 31–45. <https://doi.org/10.3354/meps318031>
- Trivedi, S., Zaman, S., Chaudhuri, T.R., Pramanick, P., Fazli, P., Amin, G., Mitra, A., 2016. Inter-annual variation of salinity in Indian Sundarbans. *Indian J. Geo-Mar. Sci.* 45 (3), 410–415.
- Tyler, E.H., Somerfield, P.J., Berghe, E.V., Bremner, J., Jackson, E., Langmead, O., Palomares, M.L.D., Webb, T.J., 2012. Extensive gaps and biases in our knowledge of a well-known fauna: implications for integrating biological traits into macroecology. *Glob. Ecol. Biogeogr.* 21 (9), 922–934. <https://doi.org/10.1111/j.1466-8238.2011.00726.x>
- Vega, M., Pardo, R., Barrado, E., Debán, L., 1998. Assessment of seasonal and polluting effects on the quality of river water by exploratory data analysis. *Water Res.* 32 (12), 3581–3592. [https://doi.org/10.1016/S0043-1354\(98\)00138-9](https://doi.org/10.1016/S0043-1354(98)00138-9)
- Wilson, J.G., Fleeger, J.W., 2013. *Estuarine benthos.* In: Day, Jr., J.W., Crump, B.C., Kemp, W.M., Yáñez-Arancibia, A. (Eds.), *Estuarine Ecology*, 303–326.
- Wortmann, J., Hearne, J.W., Adams, J.B., 1998. Evaluating the effects of freshwater inflow on the distribution of estuarine macrophytes. *Ecol. Modell.* 106 (2–3), 213–232. [https://doi.org/10.1016/S0304-3800\(97\)00197-X](https://doi.org/10.1016/S0304-3800(97)00197-X)
- Wouters, J.M., Gusmao, J.B., Mattos, G., Lana, P., 2018. Polychaete functional diversity in shallow habitats: Shelter from the storm. *J. Sea Res.* 135, 18–30. <https://doi.org/10.1016/j.seares.2018.02.005>
- Wu, R.S.S., Shin, P.K.S., 1997. Sediment characteristics and colonization of soft-bottom benthos: A field manipulation experiment. *Mar. Biol.* 128, 475–487. <https://doi.org/10.1007/s002270050114>
- Zhang, Q., Li, J., Hu, G., Zhang, Z., 2019. Bioturbation potential of a macrofaunal community in Bohai Bay, northern China. *Mar. Pollut. Bull.* 140, 281–286. <https://doi.org/10.1016/J.MARPOLBUL.2019.01.063>

Available online at [www.sciencedirect.com](http://www.sciencedirect.com)

ScienceDirect

journal homepage: [www.journals.elsevier.com/oceanologia](http://www.journals.elsevier.com/oceanologia)

## ORIGINAL RESEARCH ARTICLE

# Spatiotemporal pattern of degradation in arid mangrove forests of the Northern Persian Gulf

Hana Etemadi<sup>a</sup>, Joseph M. Smoak<sup>b,\*</sup>, Esmail Abbasi<sup>a</sup>

<sup>a</sup>Environmental Science, Persian Gulf Research Institute, Persian Gulf University, Bushehr, Iran

<sup>b</sup>School of Geosciences, University of South Florida, Florida, USA

Received 1 May 2020; accepted 22 October 2020

Available online 4 November 2020

## KEYWORDS

Sea-level rise;  
Climate change;  
Arid mangrove;  
Wetland expansion;  
Persian Gulf  
mangroves

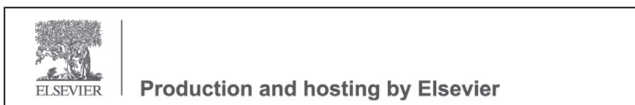
**Abstract** Climate change is a major threat to mangrove ecosystems worldwide but particularly those in arid regions that exist near the limit of tolerance to extremes in temperature, precipitation, and salinity. Here we examine Persian Gulf arid mangrove ecosystems from the Nayband and Mond Protected Area in the south-west region of Iran to determine the ability of tidal mangrove forests to respond to rapid urban and industrial development, sea-level rise (SLR), and temperature and precipitation changes. Sea level has been rising by approximately 4 mm yr<sup>-1</sup> in this region and might be intensified by subsidence on the order of 1–2 mm yr<sup>-1</sup> due to natural phenomena as well as anthropogenic activities associated with fluid extraction. We use remote sensing along with statistical analysis to effectively monitor mangrove area changes over 60 years and infer responses to past environmental trends. Our spatiotemporal analysis demonstrates expansion in some areas and reduction in others. NDVI (Normalized Difference Vegetation Index) results indicate that Nayband mangroves are healthy and expanded between the years of 1990 and 2002 which could be in response to rising temperatures and above-average precipitation. However, NDVI changes after 2002 demonstrate the mangrove health and area have decreased which could be in response to industrial and urban development that occurred immediately after 1997. The natural stresses in this extreme system are being exacerbated by climate change and anthropogenic pressures as such it is essential to develop ways to reduce vulnerability through strategic management planning.

© 2020 Institute of Oceanology of the Polish Academy of Sciences. Production and hosting by Elsevier B.V. This is an open access article under the CC BY-NC-ND license (<http://creativecommons.org/licenses/by-nc-nd/4.0/>).

\* Corresponding author at: School of Geosciences, University of South Florida, Florida 33701, USA.

E-mail address: [smoak@usf.edu](mailto:smoak@usf.edu) (J.M. Smoak).

Peer review under the responsibility of the Institute of Oceanology of the Polish Academy of Sciences.



<https://doi.org/10.1016/j.oceano.2020.10.003>

0078-3234/© 2020 Institute of Oceanology of the Polish Academy of Sciences. Production and hosting by Elsevier B.V. This is an open access article under the CC BY-NC-ND license (<http://creativecommons.org/licenses/by-nc-nd/4.0/>).

## 1. Introduction

Spatial patterns and community structure of mangroves are influenced by complex and cumulative interactions of many natural factors such as sea level, precipitation, hydrology, landscape position, sediment dynamics, storm-driven processes, and human-induced factors such as urbanization land-use change, aquaculture, and agriculture (Alongi, 2018; Sippo et al., 2018). Climate change will impact the mangrove forest health and expansion by rising sea level, cyclone activity, temperature, and precipitation changes (Breithaupt et al., 2019; Sanders et al., 2016; Smoak et al., 2013). There is uncertainty in how mangrove ecosystems will respond to these climate-related impacts (Alongi, 2008), and these responses have not been fully addressed experimentally. Both fluctuating sea levels and temperature regimes have had a vast influence on mangrove distributions globally (Lovelock et al., 2017; Spencer et al., 2016). But, rising sea level might be the most important factor which affects the spatial distribution of mangrove tidal forest in the long term (Gilman et al., 2006). Rapid twenty-first-century sea-level rise (SLR) as a climate-change consequence has been cited as a serious threat to mangroves, which have responded to past sea-level changes by migrating landward, only if space for mangrove transgression is available, and/or upward if there is sufficient material available for accretion (Etemadi et al., 2018; Schuerch et al., 2018).

Over the last century, global sea-level rise rates are estimated at  $1.7 \text{ mm yr}^{-1}$  while many areas as a consequence of regional factors including subsidence have experienced higher rates (IPCC, 2007). Saintilan et al. (2020) indicated the rate of global SLR increased twofold over the 20th century and demonstrated mangroves will be unable to keep pace with SLR by accretion after 2050. Based on NOAA data, sea level in the Persian Gulf has risen at a rate of  $3.8 \text{ mm yr}^{-1}$  from 1992 until recently ([www.star.nesdis.noaa.gov](http://www.star.nesdis.noaa.gov)). Goharnejad et al. (2013) projected mean sea-level rise to the year 2100 in Bushehr province (our study site) to be  $3.6$  and  $7.2 \text{ mm yr}^{-1}$  for A1B and A2 IPCC scenarios (IPCC scenarios; <https://www.ipcc.ch/site/assets/uploads/2018/03/sres-en.pdf>) as the best and worst-case, respectively. Irani et al. (2017) recently indicated sea-level changes in the Persian Gulf and Oman Sea under RCP 2.6, RCP 4.5, RCP 6.0, and RCP 8.5 are predicted to be  $6.1$ ,  $7.1$ ,  $7.3$ , and  $9.8 \text{ mm yr}^{-1}$ , respectively, by 2100. These projected rates in the Persian Gulf are higher than the global projected rates while the accretion rates in these arid zones are typically low (Adame et al., 2020).

Temperature and precipitation patterns as fundamental meteorological variables have the potential to change mangrove function such as leaf formation, photosynthesis rates, and seedling establishment (Feher et al., 2017; Osland et al., 2016). The globally averaged surface air temperature data as calculated by a linear trend, showed a warming of  $0.85$  [ $0.65$  to  $1.06$ ] $^{\circ}\text{C}$ , over the period from 1880 to 2001 (IPCC, 2013). Furthermore, minimum temperatures globally are increasing at twice the rate of maximum temperatures (Walther et al., 2002). Etemadi et al. (2016) reported that the minimum temperature in the south of Iran increased ( $+3.14^{\circ}\text{C}$ ) over the past 42 years. Osland et al. (2013) found that a  $2$ – $4^{\circ}\text{C}$  increase in annual mean minimum tempera-

ture can result in relatively dramatic mangrove range expansion into the more temperate salt marshes, and would cause the elimination of salt marshes in Texas, 95% reduction in Louisiana, and 60% reduction in Florida. In addition, mangrove vegetation productivity is expected to increase where the temperature does not exceed an upper threshold of  $38$ – $40^{\circ}\text{C}$  (Field, 1995). Mean annual precipitation on the northern coast of the Persian Gulf and Oman Sea was reduced by 43% from the year 2000 (FAO, 2007). In arid regions where freshwater supply is further reduced and salinity increases, mangrove expansion under a new climate regime is uncertain (Adame et al., 2020; Alongi, 2015; Sanders et al., 2016).

Anthropogenic impact, particularly land-use change and deforestation, also coastal development, pollution and oil spills, timber, and charcoal production will have a major influence on mangrove loss (Hamilton and Casey, 2016; Mafihgohami et al., 2020). The effluent from the petroleum industry exacerbates impacts on biota and causes environmental degradation (Sam et al., 2017). These toxicological and physical adverse impacts might be severe, like defoliation or mangrove death, and/or long-lasting, like reduction in seed survival, plant reproduction, and faunal population (Burns et al., 1999; Hoff and Michel, 2014). Moreover, oil products may coat aerial and submerged roots, and disturb direct absorption causing mangrove degradation (Proffitt et al., 1995). Human impact coupled with oil and petroleum pollution have already damaged a large area of Nigerian mangrove forests (Lindén and Pålsson, 2013). Oil production has degraded at least 126,000 ha of mangrove vegetation since 1958 (Duke, 2016). Pollution and nutrient enrichment, as well as changes that alter the hydrologic flow, caused the mangrove area to be reduced by 44% in Tampa Bay, (Florida, USA) (Sharitz and Pennings, 2006). Wibowo and Supriatna (2010) estimated that population growth, land-use change, and land-based pollution are likely to degrade mangroves of each Indonesia's coastal cities between 20% and 60% in the next 20 years. Deterioration in the health of mangroves especially in these arid regions has been documented (Almahasheer et al., 2013). The main cause is uncertain, however, accelerating SLR, severe anthropogenic activities and harsh climatic conditions are all potential contributors.

Due to the vast spectral and spatial resolution of conventional imagery and the cost-effective, time-efficient, Remote Sensing techniques have a synoptic capability in mangrove mapping and monitoring (Kuenzer et al., 2011). Multispectral satellite sensors like Landsat TM, ETM+ and SPOT are valuable sources of remotely-sensed data in mangrove studies over several decades (Giri et al., 2015). Red [R] and near-infrared [NIR] wavelengths have been used to identify mangrove vegetation based on spectral reflectance and spectral difference measurements such as the normalized difference vegetation index (NDVI) (Green et al., 1997). NDVI is one of the most common methods for mangrove health monitoring (Binh et al., 2005). Numerous investigations on mangroves have used NDVI to represent mangrove canopy closure, productivity, condition, health, and above-ground biomass (AGB) (Almahasheer, 2018; Arshad et al., 2020; Bartholy and Pongracz, 2005; Giri et al., 2007; Kovacs et al., 2004; Walters et al., 2008; Zomer et al. 2009). Other studies have applied satellite imagery to evaluate

the relationship between coastal change and mangrove distribution (Feng et al., 2020; Hu et al., 2018; Jayanthi et al., 2018). In detailed satellite imagery analysis, Lee and Yeh (2009) demonstrated landward encroachment of mangroves which doubled in extent over 10 years.

Mangroves along the Persian Gulf live in extreme temperature, radiation, and salinity but extremely low precipitation which causes a low diversity of mangroves in this arid region (Mafi-gholami et al., 2020). Mangroves in arid zones have low primary productivity, low sediment deposition, and consequently a low rate of vertical accretion (Adame et al., 2020). Therefore, the growth and survival of these mangroves are under threat because they already exist at their tolerance threshold. These conditions makes them highly vulnerable to any additional stressors like anthropogenic activity and/or climatic changes. Moreover, mangroves in arid regions are investigated with insufficient representation in global assessments. Ward et al. (2016) highlight the vast knowledge gaps of climate change impacts on mangroves located in the Middle East region.

We examine Nayband Bay and Mond Protected Areas, along the northern coast of the Persian Gulf in Iran using Landsat imagery products and aerial photography. The goal is to examine the spatiotemporal pattern of degradation as well as the areal gain and loss in these arid mangrove forests to determine how they have responded to environmental changes. Also, we examine the ability of tidal mangrove forests to respond to rapid development, sea-level rise, temperature, and precipitation changes. We hypothesize that many of these environmental changes will cause degradation as these systems already exist near their stress threshold. Few studies have involved a comparative analysis of the impacts of climate-related factors and anthropogenic activities on mangroves in this arid zone. Furthermore, ecological health and migrational patterns are required to improve our understanding of the resilience of mangrove ecosystems to harsh environmental conditions as well as aid in conservation planning.

## 2. Site description

The Nayband Marine-Coastal National Park and Mond Marine-Coastal area are protected areas located in southwest Iran along the northern coast of the Persian Gulf (Figure 1). This area has been described as the most rapidly developing area in the world with an endangered and fragile ecosystem (Bryant, 1981). The Mond protected area (46500 ha) extends between latitudes 27°48'–28°9'N and longitudes 51°15'–51°36'E. The Mond River empties into the Persian Gulf in the northern part of this basin. Nayband National Park (49815 ha) with several large marine estuaries is one of the most important habitats in the northern Persian Gulf. Nayband is located near the city of Assaluyeh which is in a major petrochemical region with numerous gas and oil production factories and refineries (Zare-Zadeh Mehrizi et al., 2011).

Bidkoon and Basatin are mangrove areas within Nayband Marine-Coastal National Park. The Malgonze mangroves are found along the southern section of the Mond protected area. Both areas are dominated by *Avicenna marina*. The

mangrove population structures in the study sites are presented in Table 1 (Kouhgard et al., 2015). These mangroves exist in an extreme environment under an arid climate with hypersaline conditions (37.9–41.3 ppt) (Hassanzadeh et al., 2011; Ibrahim et al., 2020; Moaddab et al., 2017), and without direct riverine input. The vegetation occupies alluvial and Solenchak soils in the area (Mostafavi et al., 2004). The mean annual air temperature is 27°C and ranges between 11 to 41°C. The mean annual minimum and maximum temperatures are 20.5 and 32.8°C, respectively. The mean relative humidity is 43%. Dominant wind direction is north-west to south-east. Rainfall is less than 250 mm yr<sup>-1</sup> and 60% of this rainfall occurs between December and February. Rainfall is nearly absent during the summer season from June to September. The tidal cycles are semi-diurnal and varying in amplitude between approximately 50 to 150 cm, reaching maximum during monsoon and post-monsoon and the minimum occurs during the summer (<http://www.irimo.ir>). Tides are characterized as upper microtidal (1.5–2 m tidal range).

The Nayband coastal area was considered nearly undisturbed until 1990 when rapid development in the oil and gas industry began. Following this rapid development, Asaloyeh's population grew rapidly along with the development increasing from 893 in 1995 to 65584 in 2011 (Didari, 2017). Due to the presence of the largest natural gas field in the world and the associated activities near the study area, the health of these marine ecosystems are threatened, and coastal habitats have been severely degraded already (Kalhori and Kokya, 2012).

## 3. Method

### 3.1. Past climatic analysis

We applied the non-parametric Mann-Whitney two-sample test (Pettitt, 1979) to identify the change point in the pattern of annual precipitation between 1969 and 2015 acquired from the Iran Meteorological Organisation (2016) (<http://www.irimo.ir>). Using t-test, we compared the mean of each rainfall variable during the period of pre- and post-change point, once the change point had been identified. Focusing on the non-parametric Mann-Whitney two-sample test, two data samples (pre and post-changes datasets) are independent if they come from distinct populations and the samples do not affect each other. By using the Mann-Whitney-Wilcoxon test, population distributions can be identified as being identical without assuming them to follow a normal distribution. In other words, the null hypothesis is that mangrove datasets in pre- and post-changes have identical populations (Etemadi et al., 2016). Statistical software, SPSS was used to perform the statistical analysis.

Time-series trends are examined with Mann-Kendall non-parametric statistical test (Kendall, 1975). This test examines if a time-series dataset shows a significant increase or decrease over time. The Mann-Kendall statistical test has been widely applied to determine the significance of trends in meteorological time series (Silva et al., 2013; Tabari and Marofi, 2011). The linear regression models are most valid at weekly or monthly scales than on a daily scale (Caissie, 2006). Linear and second-order polynomial regres-

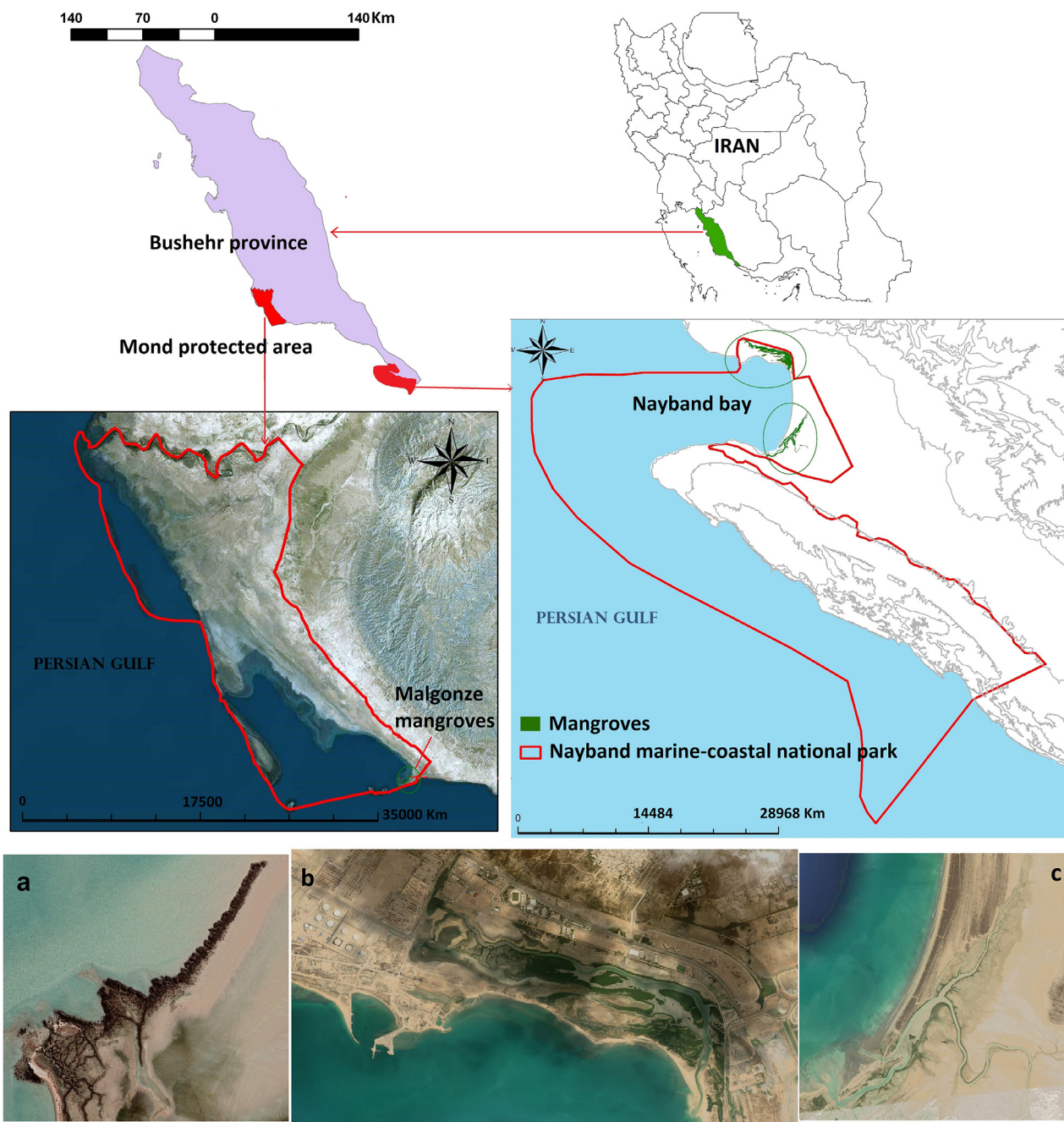


**Figure 1** Location of Mond Protected Area and Nayband Marine National Park in Bushehr province in Iran, Malgonze Mangroves (a), Bidkhood Mangroves (b), Basatin Mangroves (c).

**Table 1** Mangrove population structures in Bidkhood and Basatin site.

	Density (tree per hectare)	Total height (cm)	Crown diameter (cm)	Diameter at breast height (DBH) (cm)	Aerial roots per tree	Mangrove species
Bidkhood site	3136 ± 177.8	276.1 ± 31.1	245 ± 41.5	13 ± 1.9	21.7 ± 11.3	<i>Avicenna marina</i>
Basatin site	1875 ± 335.3	228 ± 61.4	230 ± 61.2	13.5 ± 3.6	19.8 ± 11.5	<i>Avicenna marina</i>

sion models were fit to the average of mean temperature in winter and summer from 1696 to 2015.

### 3.2. Geodetic leveling

Geodetic leveling produces a higher order of accuracy normally expanded over wide areas, to provide accurate vertical control for surveying and mapping operations. The object of using the geodetic leveling data is to find the elevation of a given point with respect to mean sea level at tide gauge stations as a reference datum. Data were obtained from the Geodetic and Surveying Department in Iran National Cartographic Center (<http://www.ncc.org.ir>). The location of geodetic leveling spread from Choghadak (28.986°N, 51.036°E) to Kangan (28.206°N, 51.308°E) during the period from 1990 to 2007. Stations from Kangan to Asaloyeh were destroyed as a result of the construction of oil and gas refineries and petroleum industry-related infrastructure.

### 3.3. Sea level rise trend

Data from the closest tide gauge stations to Mond and Nayband were analyzed to characterize sea-level changes as well as to distinguish any relationships between sea-level and areal extent of mangrove. These tide gauge stations included: (a) Kangan station (27.83°N, 52.55°E), (b) Emamhasan station (29.83°N, 50.25°E). Monthly sea-level time series runs from 1995–2009 at Kangan and Emamhasan station. Data were obtained from the Coastal Area Hydrography Management in National Cartographic Center (<http://www.ncc.org.ir>). Linear and second-order polynomial regression models were fit to the mean monthly sea-level data.

### 3.4. Remote sensing analysis

The remote sensing sources used in this study included digital aerial imagery and time series of Landsat TM, ETM+ and OLI images from one scene (path 162, row 41) covering the study area from February of the years 1990, 2002 and 2015. Landsat satellite data used in the studies were acquired through the U.S. Geological Survey (USGS), Center for Earth Resources Observation and Science (EROS) (<http://eros.usgs.gov>). By using L1T Landsat images with high geometric accuracies (RMSE less than 30 meters) (Zhu and Woodcock, 2014), a geometric correction was unnecessary. Radiometric correction was applied using the dark pixel subtraction algorithm (Hadjimitsis et al., 2010) on Landsat images at the initial stage of pre-processing. Landsat images were calibrated to radiance and reflectance values. The 2015 Digital Orthographic was acquired from the Pars Special Economic Energy Zone in Bushehr province. All the remote sensed data was collected from a single scene in February. Digital image processing software ENVI 5.1 and ArcGIS 10.1 were used to process and analyze the spatial data.

Medium-scale (1:25,000) black and white panchromatic aerial photographs procured by the Iranian National Geographical Organization in 1956 were also scanned and imported into ArcGIS (ESRI Inc. version 10.1). These images

were imported as geospatial digital images at a resolution of 1000 dots per inch. In addition, we used tonality (contrast), crown texture, structure, tree height, and relative position on the ground attributes to distinguish mangroves.

GPS was used in the field to determine the position of 40 ground control points located at distinctive positions selected from the imagery. All images and aerial photographs were geometrically corrected using ground control points for the second time.

The near-infrared (NIR) (760–900 nm) and red (RED) (630–690 nm) bands are strongly reflected and absorbed by plants. Therefore, they are often applied to represent the amount of greenness or biomass of mangroves, which in turn can reflect their health or photosynthetic activity (Kovacs et al. 2005). NDVI (Normalized Difference Vegetation Index) was calculated using Eq. (1).

$$NDVI = (NIR - RED) / (NIR + RED), \quad (1)$$

where Red and NIR stand for the spectral reflectance measurements acquired in the red (visible) and near-infrared regions, respectively. NDVI values range from  $-1$  to  $1$ , representing a reaction to photosynthetic activity, that is the higher the NDVI value the greater the health and vegetation cover (Green et al., 1997; Meneses-Tovar, 2011). NDVI values close to  $0$  were classified as sparse vegetation or bare land, and values below zero were depicted as wet soils and water. We considered 5 classes for the NDVI value for each image. Class 0 is non-mangrove area, classes 1, 2, 3 and 4 are sparse, low, medium, and thick mangrove cover, respectively. A maximum likelihood classification (MLC) program was used to classify three land cover types consisting of mangrove (class 2), water (class 3), and others (barren land, agriculture, habitation) (class 1). Imagery analysis techniques were integrated with geographic information systems (GIS) to perform spatial differentiation of vegetation changes. The displayed image with the above classes was enhanced spectrally by histogram equalization. We identified Nayband mangrove forest cover change (gain and loss) from 1990 to 2015 using Landsat satellite data and GIS software.

## 4. Result and discussion

### 4.1. Climatic variables

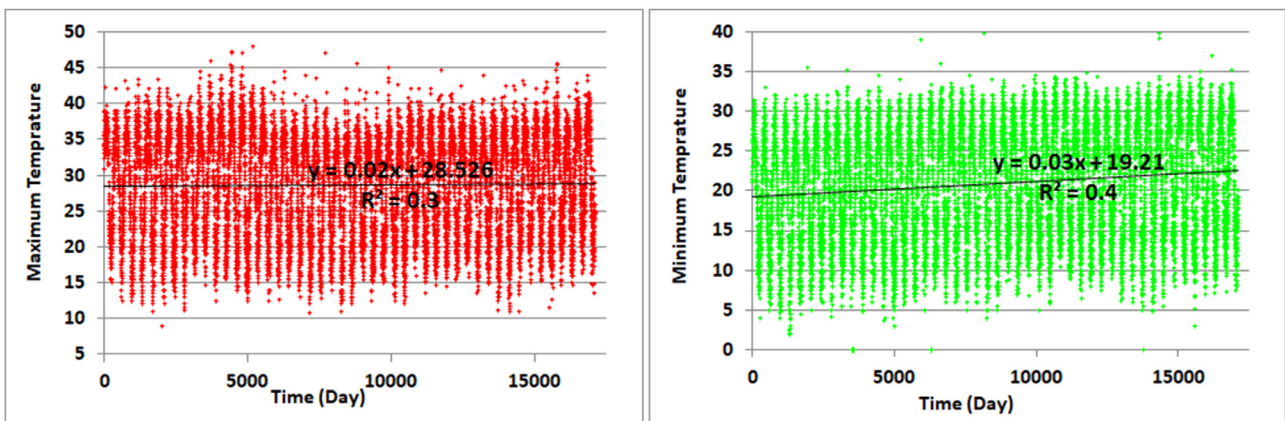
The Mann-Kendall (MK) test was used to detect the increasing or decreasing trends of climatic variables, and whether the trend was statistically significant. Table 2 presents the MK statistics for Min, Max, mean temperature and precipitation as the most important climatic variables for the period of 1969 to 2015 in Bushehr station. A positive or negative value indicates an increasing or decreasing trend, respectively. Table 3 shows a significant trend (0 shows no significant trend; 1 depicts significant trend) in climatic variables in a period from 1969 to 2015 at Bushehr station. Results showed that the Min and mean temperature trends were significant for most months of the year at 95% confidence while Max temperature did not show a significant trend. Asfaw et al. (2018) found the same result which revealed an increasing trend for mean and Min temperatures overtime

**Table 2** Statistics of Mann-Kendall test for climatic variables in a period of 1969 to 2015 in Bushehr station.

	Jan	Feb	Mar	Apr	May	Jun	July	Aug	Sep	Oct	Nov	Dec	Annual
Tmin	1.25	1.83	2.43	4.40	5.21	5.19	5.27	4.95	5.53	4.75	3.48	2.22	6.67
Tmax	-0.44	-0.29	-0.86	0.34	1.85	0.57	0.12	1.08	0.98	-0.66	0.45	-0.87	0.55
Tmean	0.47	0.62	1.07	1.97	3.23	2.85	1.98	0.99	2.63	3.74	1.99	1.49	3.95
Rain	1.68	0.67	0.51	-0.12	-3.87	-9.65	-9.74	-10.2	-10.4	-4.98	-0.09	0.55	1.57

**Table 3** Significant trends in climatic variables in a period of 1969 to 2015 in Bushehr station.

	Jan	Feb	Mar	Apr	May	Jun	July	Aug	Sep	Oct	Nov	Dec	Annual
Tmin	0	0	1	1	1	1	1	1	1	1	1	1	1
Tmax	0	0	0	0	0	0	0	0	0	0	0	0	0
Tmean	0	0	1	1	1	1	1	0	1	1	1	0	1
Rain	0	0	0	0	1	1	1	1	1	1	0	0	0

**Figure 2** Linear regression of minimum and maximum temperature in Bushehr station.

significantly while the trend for Max temperature showed a non-significant increasing trend.

Based on the regression equation of minimum temperature (Tmin) and maximum temperature (Tmax) in Bushehr station (Figure 2), we calculated that minimum, maximum and mean temperature has increased 0.075, 0.011, and 0.037°C per year, respectively. Furthermore, the total increase in minimum temperature during the 47 year period was 3.53°C. The analysis also revealed an increase in mean (+1.74°C) and maximum (+0.51°C) temperatures during the 47 years (Figure 2). This increase is considerably high in comparison with the global mean temperature which has risen by 0.8°C from 1880 to 2012 (IPCC, 2013). The regression results on seasonal mean temperatures also showed increases in the period from 1969 to 2015 during winter (December, January, and February) and summer (June, July, and August) in a range of +1.8 and +1.7, respectively (Figure 3). Previous meteorological studies in Iran also demonstrated that warming tendencies are primarily a result of Tmin increases (Etemadi et al., 2014; Kharin et al. 2007; Rahimzadeh et al., 2009; Soltani et al., 2016). It has also been observed that annual mean Max and Min temperatures increased by 0.31 and 0.59°C per decade across Iran, respectively (Soltani et al., 2016). Etemadi

et al. (2016) reported that the minimum temperatures in the south of Iran increase by +3.14°C over the past 42 years and predicted an increase to temperatures above 38°C during warm seasons by 2080–2099. By extrapolation of the temperature linear regression to 2100, the results depict that Max and Min temperature will rise above 33°C (photosynthesis rate declines above 33°C) from May to November and from June to October, respectively. Rising temperatures in the sub-tropical region like the northern coast of the Persian Gulf where mangroves exist near their thermal tolerance limits will cause a reduction in photosynthesis rates and growth by the end of the century. On the contrary, increasing air temperature in cooler regions may allow mangroves to expand to poleward. This might occur because of a reduction in the frequency of extreme cold events (Cavanaugh et al., 2014). Etemadi et al. (2016) found that increasing air temperatures due to climate change are likely to influence mangrove development such as causing the mangroves flowering and fruiting period to shift to earlier in the year.

The Mann-Kendall test results (Table 2 and 3) showed that there was a significant reduction in summer and fall precipitation from May to October and no significant trend from November to April. Based on the sum of annual

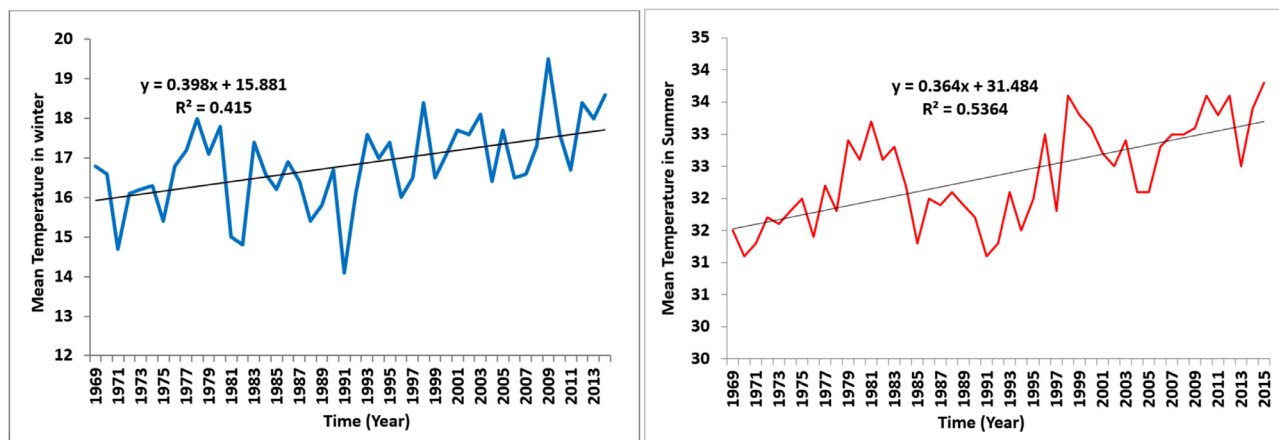


Figure 3 Linear regression of winter and summer mean temperature in Bushehr station.

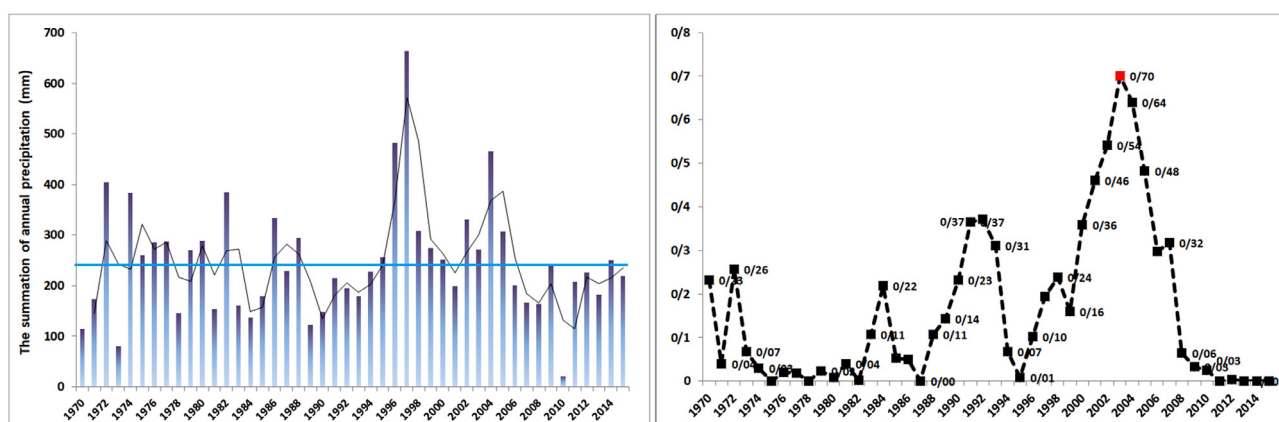


Figure 4 Sum of annual precipitation (left) – result of the Pettitt-Mann-Whitney test (right).

precipitation during the 47 years (1969–2015), long-term mean annual precipitation was 246.5 mm and years with precipitation lower than 246.5 are considered dry years (Figure 3). Based on this information, several consecutive dry years (i.e., drought period) occurred between 1989–1994 and 2006–2013 in our study area.

Abnormal distribution of precipitation, especially in arid areas with fewer and sparse rainfall events, has been emphasized in the literature as a non-normal variable because of mostly uneven distribution (Samadi et al., 2013). Change-point analysis using the Pettitt-Mann-Whitney test (Figure 4) indicated that 2003 was the change point. Rainfall variability comparison in pre and post-2003, as well as t-test, indicated that the rainfall variables (proportion of consecutive rainy days  $\geq 2$ ,  $\geq 5$ ,  $\geq 10$ , and  $\geq 25$  days) are significantly (P-value < 0.05) different in pre- and post-2003 with a significant reduction in post-2003. Persian Gulf mangroves are adapted to exist near the limit of tolerance for extremes in temperature, rainfall, and salinity (Schile et al., 2016). Precipitation changes have been shown to have a major effect on mangrove growth and mangrove area changes in Qeshm, Iran, during the period of 1975–2005 (Salehipour-Milani and Jafari-Beglu, 2012). In addition, increased salinity can convert the landward zone to hypersaline flats. Decreasing biodiversity, reducing net primary productivity and growth causing a notable reduction in mangrove area as a

consequence of rainfall reduction, increased evaporation and salinity (Gilman et al., 2008). While increased precipitation will likely increase riverine discharge along with the delivery of allochthonous sediments which may allow surface elevation to keep up with sea-level rise (Ranasinghe et al., 2013). Allochthonous inputs into systems without direct river discharge (e.g., our study site) are limited to marine and eolian sources, and therefore a change in precipitation is unlikely to affect them. Rainfall reduction and temperature increasing trend in warm seasons in our study site may also result in a higher degree of dryness which causes more evaporation and increases salinity in the region. However, more evaporation causes a greater concentration of pollutants discharged into the Persian Gulf which has little ability to flush itself clean (Bryant, 1981).

#### 4.2. Geodetic leveling

Lowering surface elevation as a consequence of human activities such as fossil fuel and groundwater extraction, and industrial development might enhance relative SLR impact in this region. Geodetic leveling was used to determine the contribution of deep subsidence to relative SLR. Based on the elevation changes and the mean elevation change data in Bushehr Province geodetic leveling stations from 1990 through 2007 (Figure 6), we determined that the highest

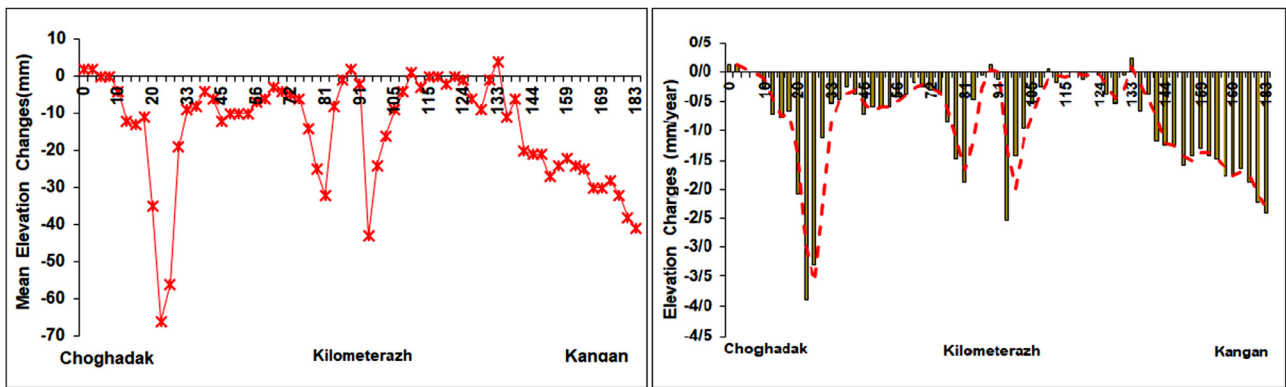


Figure 5 Elevation changes (left), mean elevation changes (right) in geodetic leveling station during 1990 to 2007.

subsidence occurred near Ahram (28.881°N, 51.274°E) exceeding 4 mm yr<sup>-1</sup>. Abdan (28.079°N, 51.766°E) and Kangan (28.206°N, 51.308°E) had approximately 2.5 mm yr<sup>-1</sup> subsidence. Therefore subsidence contributes to substantial elevation change in this region. A rate of 1.5 mm yr<sup>-1</sup> was established as the mean subsidence in Bushehr province by averaging all mean elevation change data. Mapping based on the industry seismic profiles and well log data indicates rates of 1–2 mm yr<sup>-1</sup> subsidence along the Iranian coast of the Gulf (Swift et al., 1988). There is no available data on shallow subsidence (surface accretion change exceeds surface elevation change) of these mangroves therefore we apply the land surface subsidence data. The subsidence as a deep land movement will add to the rate of mangrove inundation. Also, the presence of extensive oil and natural gas extraction in this region is likely to enhance the subsidence rate which will exacerbate mangrove elevation losses compared to sea level. Land surface subsidence due to fluid withdrawal are well documented (Fielding et al., 1998; Ketelaar, 2009; Schoonbeek, 1976).

### 4.3. Sea-level rise

Global mean SLR from tide gauges and altimetry observations increased to 3.6 mm yr<sup>-1</sup> over the period 2005–2015 (Oppenheimer et al., 2019). Ecstatic SLR rates are projected to be between 8 and 16 mm yr<sup>-1</sup> equivalent to a 0.8 to 1.6 m sea-level increase over the next 100 years (IPCC, 2013; Pachauri et al., 2014). Under RCP 8.5, the rate of sea-level rise will be 15 mm yr<sup>-1</sup> (10–20 mm yr<sup>-1</sup>, likely range) in 2100 (Oppenheimer et al., 2019). Figure 5 represents the sea-level rise at the Kangan and Emamhasan tide gauge stations. Mean monthly sea-level data was calculated by averaging hourly sea level in each month which adequately removes sub-annual cyclical tidal constituents. A linear regression model fit to the mean monthly sea-levels indicates a mean sea-level rise trend of 4 mm yr<sup>-1</sup> at Kangan and 10 mm yr<sup>-1</sup> over the observed 14 years at Emamhasan. Regional factors (e.g., tectonic processes, ocean circulation, elevation changes of the wetland sediment surface, coastal subsidence, and sediment budgets) (Lovelock et al., 2015) account for the differences. Extrapolation suggests sea level will rise by 33 and 82 cm at Kangan and Emamhasan, respectively, by the end of the century. The Kangan tide gauge data is expected to be more reliable for our purposes

due to closer proximity to our study sites. The Laboratory for Satellite Altimetry in NOAA estimated  $3.8 \pm 0.4$  mm yr<sup>-1</sup> sea-level rise in the Persian Gulf based on measurements from satellite radar altimeters between 1992–2016 (<https://www.star.nesdis.noaa.gov>). Based on the IPCC report the rate of sea-level rise in the Middle East is 2.2–3.3 mm yr<sup>-1</sup> (IPCC, 2013, 2014). Thus, Kangan SLR (4 mm yr<sup>-1</sup>) slightly exceeds the maximum range limit in the Middle East.

Since the sea-level rise is the predominant factor influencing mangrove position, numerous studies have investigated mangrove systems' response to sea-level rise (Alongi, 2015; Elison, 2015; Saintilan, 2020; Schuerch et al. 2018). A study found many mangrove sites in Brazil with accretion rates between 2.2 and 10.2 mm yr<sup>-1</sup> are currently keeping pace with SLR (Ward et al., 2016). Overall, less subsidence than accretion rate creates positive surface elevation for mangrove to keep pace with SLR (Lovelock et al., 2015; Ward et al., 2016). However, mangrove landward migration into previously freshwater systems is likely to occur if sediment accretion is unable to keep pace with SLR and suitable migration space exists. Alongi (2015) examined accretion and sea-level rise in many different regions of the world and found that mangrove systems may respond in complex ways to sea-level rise, but there was a significant relationship between these two factors (i.e., accretion and SLR).

The tidal range is known as a controlling factor in mangrove relocation and movement. Furthermore, mangroves in areas with a high tidal range (macro-tidal and meso-tidal coast) might be able to keep pace with accelerating SLR (Alongi, 2008), therefore they are more resilient to SLR influences because of enhanced sediment concentrations and flood dominance (Friedrichs and Perry, 2001). Mangroves in micro-tidal (e.g., tidal range less than 1 m) to meso-tidal (e.g., tidal range between 1.0 and 3.5 m) are more likely to migrate to keep up with relative SLR. But, mangroves in macro-tidal coasts (tidal range more than 5 m) have expanded more than mangroves in micro-tidal areas (Elison, 2015). The low tidal range (1.5–2 m) in our study area makes these mangroves particularly vulnerable to SLR impacts and likely will necessitate migration or loss. Lovelock et al. (2015) suggested that Indo-pacific mangrove forests with low tidal range and low sediment supply could be submerged as soon as 2070.

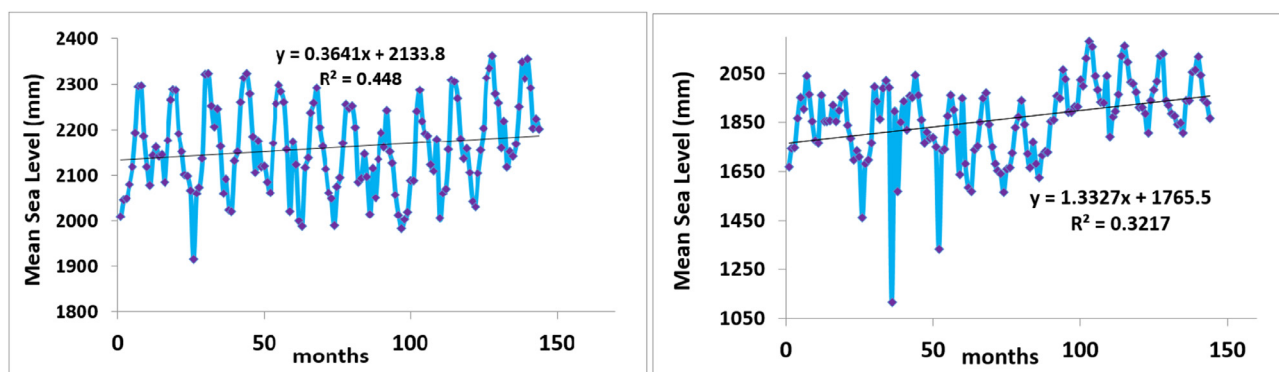


**Figure 6** Relative sea level rise in Kangan Tide Gauge Station (left) = 4 (mm/year), in Emamhasan Tide Gauge Station (right) = 10 (mm/year).

In addition, since Mond and Nayband mangroves do not have a riverine source of sediment these systems are much more vulnerable to the impact of sea-level rise than riverine systems. The most vulnerable mangroves to climate change impact are located where rivers are lacking and/or where the landform is subsiding (Alongi, 2008). Based on SLR data in the Persian Gulf as well as the study site (Figure 5), land surface subsidence (Figure 6), no riverine supply of sediment, and low vertical accretion rates of arid zone mangroves, especially in Persian Gulf coastal area (Adame et al., 2020), these mangroves are unlikely to keep pace with SLR, and mangrove landward migration is much likely to occur if anthropogenic factors do not limit mangrove expansion. Schuerch et al. (2018) recently highlighted projected coastal wetlands gains of up to 60% in the landward direction. The 60% increase assumes space will exist for migration, however, anthropogenic activities in many parts of the world have created impediments to migration, like in semi-arid north Brazil where Godoy and de Lacerda (2015) documented the loss of suitable migration space by a housing development. Consequently, SLR is likely to cause mangrove losses at the seaward edge.

Therefore, our study sites in an arid region with no riverine discharge, landform subsidence, micro-tidal regime, growth limitation from low rainfall, and hypersaline conditions are some of the most vulnerable mangroves in the world. However, there are no records of accretion rate in mangrove systems therefore we survey these mangrove expansion patterns by satellite imagery during the study time-frame.

#### 4.4. Remote sensing analysis

Bidkhood mangrove area has significantly decreased (Figure 7) during the 60 year period from 1956 to 2015. Mangrove vegetation cover has been reduced from 130 ha in 1956 to only 96 ha remaining in 2015. The spatial changes indicate that most of the loss has occurred on the landward side. In addition, Basatin mangrove cover has been reduced (Figure 7) from 46 to 41 during the same 60 years. Basatin mangrove area loss was particularly evident in the more landward mangroves. The results show that Bidkhood and Basatin mangroves (Figure 7) expanded between the years of 1990 to 2002, but decreased between 1956 and 1990 and again after 2002. While it was expected that the

sea level rise of 4 mm yr<sup>-1</sup> would lead to landward migration, these systems might be limited in their ability to colonize in the landward direction due to unfavorable conditions produced via the discharge of industrial effluents and municipal wastewaters into the area. There are large natural gas fields, refineries, petrochemical companies as well as abundant manufacturing facilities and ancillary industries near the Bidkhood and Basatin mangrove sites which developed mostly after 1995 and are the source of many pollutants (Shojaei-Gori et al., 2013). The most important external threats for Bushehr mangrove sites are the construction of petroleum sites and large investments for oil extraction as well as failure to establish integrated coastal zone management (Padash et al., 2016). This environmental stress may increase mangrove vulnerability to the already harsh climate condition such as hyper-salinity.

The Malgonze mangrove area was selected as a control site because it is located far from polluted areas where oil and gas companies are prevalent. The Malgonze mangrove area increased from 9.3 ha in 1956 to 11 ha in 2015 (Figure 8). These mangroves have expanded in the landward direction, while seaward mangroves have been lost likely due to rising sea level. Sea-level rise increases tidal inundation depth and frequency which can decrease mangrove seedling growth and the rate of photosynthesis on the seaward side (Kemp et al., 2011), but by migrating landward mangrove seedling have a greater chance to establish, mature, and reproduce (Abel et al., 2011). Mangrove landward migration has been documented as a response to SLR in the Ten Thousand Island region of Florida (Krauss et al., 2011), Louisiana (Mckee et al., 2004; Perry and Mendelsohn, 2009), Trinidad (Ramcharan, 2004), Hawaii (Chimner et al., 2006) and Mexico (López-Medellín et al., 2011) and Iran (Etemadi et al., 2018).

The assumption that mangroves in Basatin and Bidkhood were diminished due to harmful effects related to pollution is based on the relatively high concentrations of contaminants in this area and the known harm these contaminants cause to the mangrove function. Davari et al (2013) reported that heavy metal concentrations in mangrove soil in Bidkhood and Basatin were higher than in the Malgonze mangrove site, which were also higher than the permissible limits for soil based on US EPA standard. They concluded that oil and gas production at the South Pars field was the main reason for this contamination because of the proximity of

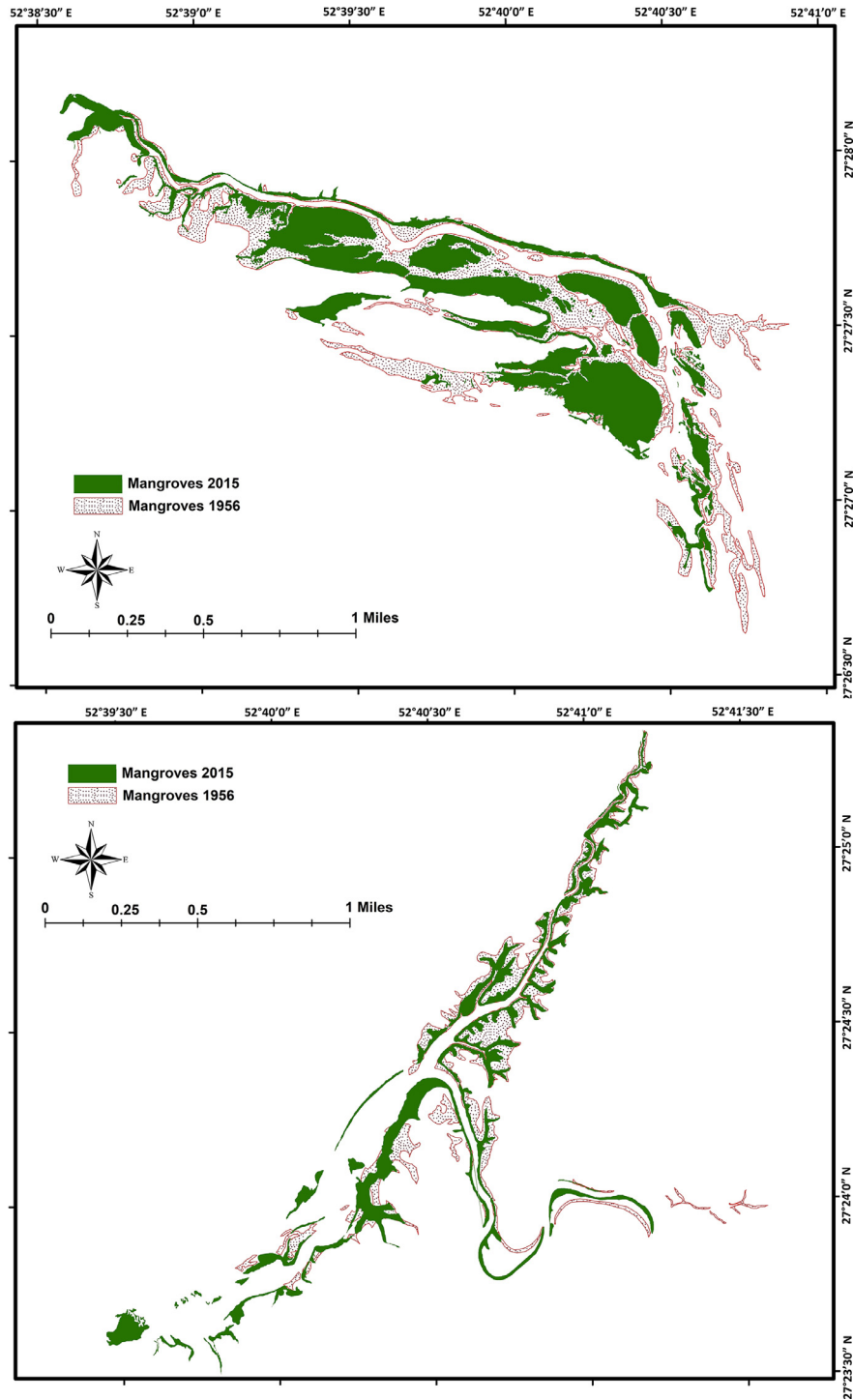
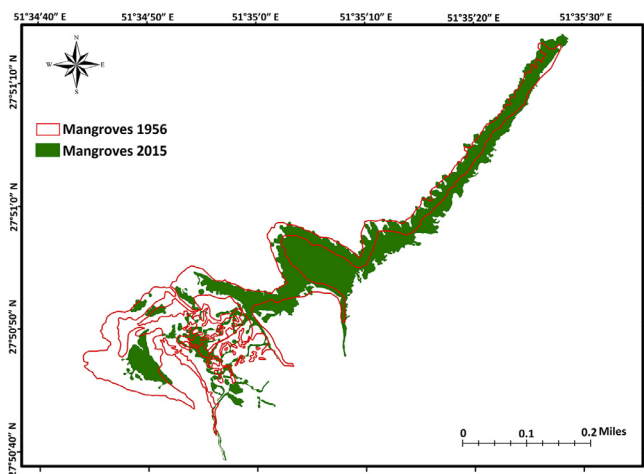


Figure 7 Bidkhoneh (above) and Basatin (below) mangrove area changes in Nayband Marine National Park from 1956 to 2015.

the Bidkhoneh and Basatin site to the discharging of industrial effluents to Nayband Bay. Zare-marivan (2010) found there was the contamination of petroleum-related heavy metals (Ni, V and S) in Nayband bay sediment. Also, the concentrations of Pb and Cd in Nayband bay sediment were higher than the Persian Gulf standards (Dehghani et al., 2014). The presence of toxic substrates such as petroleum waste, anoxia, and hydrogen sulfide in the mud of mangroves lim-

ited the pneumatophore functions and consequently jeopardizes mangrove survival (Snedaker et al., 1981). The influence of pollution is tested indirectly by investigating mangrove health changes through vegetation index which evaluates green density and physiological properties of mangrove canopies. Many studies applied the NDVI model to monitor mangrove health and density (Almahasheer, 2018; Arshad et al., 2020; Samant and



**Figure 8** Malgonze mangroves area changes in Mond Protected Area from 1956 to 2015.

Hazra, 2017; Sari and Rosalina, 2016). Landsat imageries have been used to generate NDVI to monitor vegetation health changes in the years 1990, 2002, and 2015. Figure 9 represents NDVI index in Bidkhood and Basatin mangroves in February which is the main growth month in the south of Iran. Results showed that the quality and quantity of mangrove vegetation cover changes have been noticeable. Mangroves with NDVI class 1 decreased from 1990 to 2002, but class 2 and 3 increased in this same time period. Between 2002 and 2015, mangroves with NDVI class 1 declined and vast mangrove cover converted mostly to mangroves with NDVI class 3 and 4. The northern portion of mangroves in Basatin was lost but in the southern parts,

new mangrove cover with NDVI class 4 was generated. It is inferred that the mangrove losses after 2002 are mostly attributed to the pollution from industrial and urban development that occurred post-1997. Maleki-Zade (2014) studied land-use change and temperature anomalies in Nayband National Marine Park. The results showed that 34 ha of mangrove vegetation was lost from 1998 to 2013. Furthermore, releasing industrial wastewater from the South Pars gas field (phase 9 and 10) was the most important cause of this degradation. Maleki-Zade (2014) also demonstrated a noticeable temperature increasing in the mangrove forest and grassland in this district. Kouhgardi and Shakerdargah (2015) revealed that pollution caused by rapid urban and industrial development in Nayband National Marine Park may lead to the mortality of mangrove forests due to effects on root, leaf, and soil.

Land-cover change detection has been widely applied in coastal environmental monitoring (Ghosh et al., 2015) and forest monitoring (Kennedy et al., 2007). Specifically, supervised land classifications are the most widely used land class detection method. Variations in land cover categories of the three major classes (bare land, open water, and mangrove) were considered for the change detection study. Classified maps from the years 1990, 2002, and 2016 are presented in Figure 10. Overall classification accuracy ranged from 80% to 86%. The Kappa coefficient is a level of agreement of the pixels based clustering on image classification and field observations (Lillesand et al., 2007). The overall kappa statistics of those images range from 0.80 to 0.85. Land cover gain and loss change based on percent change for each land-cover class in Bidkhood and Basatin regions are shown in Figure 11. During the period 1990–2002, the mangrove area expanded from 66 to 100 ha, the soil area decreased by 55 ha from 703 to 648 ha while 35 ha switched to mangrove

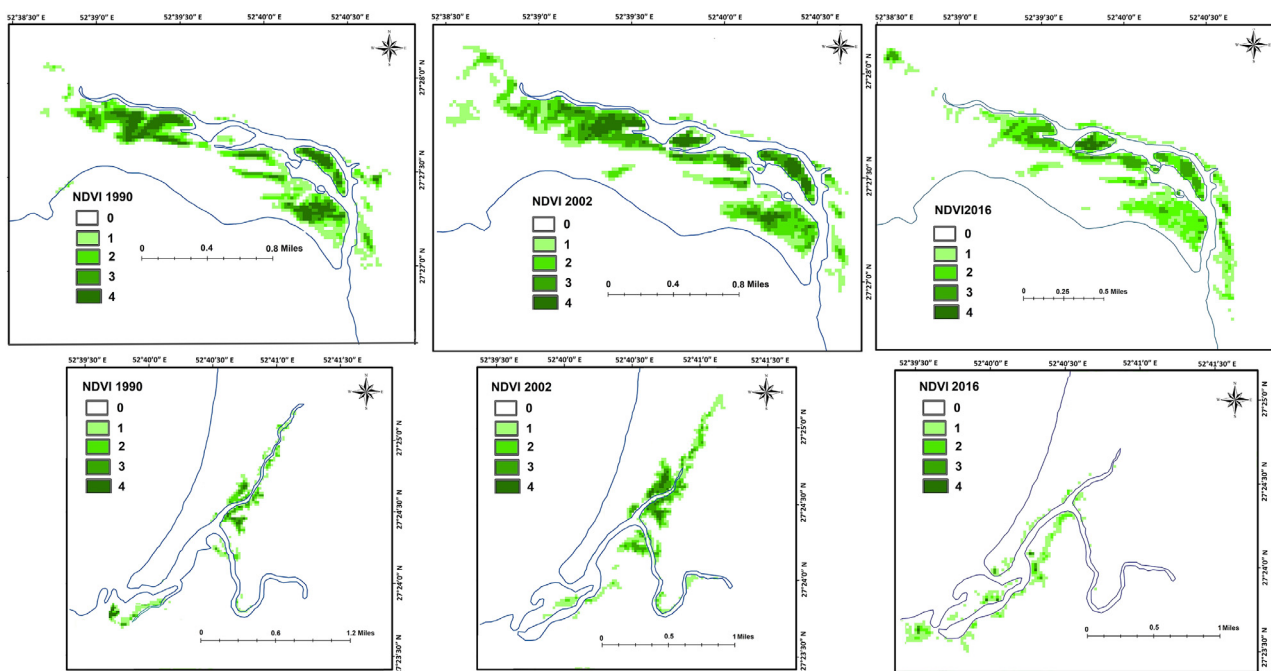


**Figure 9** NDVI Bidkhood (above) Basatin (below) mangrove forest in the years of 1990, 2002 and 2015. Class 0 is non-mangrove area, class 1, 2, 3 and 4 are sparse, low, medium and thick mangrove cover, respectively.

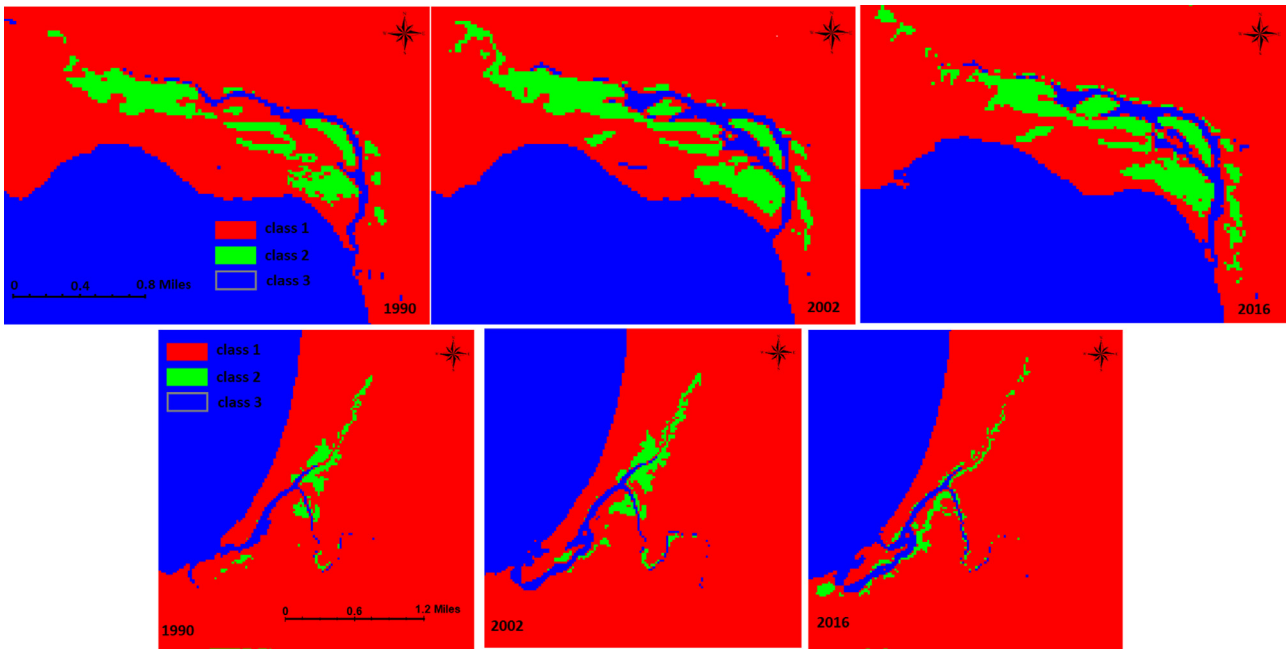


**Figure 10** Bidkhoon (above) Basatin (below) area classification images in the years of 1990, 2002 and 2015. Land (barren land, agriculture, habitation) (class 1), mangrove (class 2), and water (class 3).

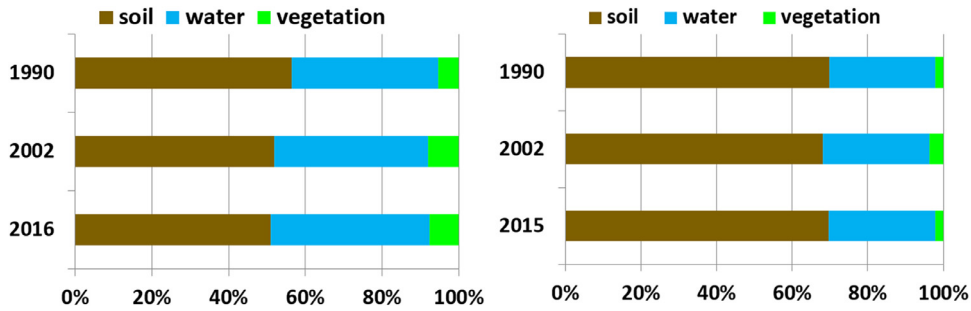


**Figure 11** Percentage change of land cover categories, Bidkhoon (left), Basatin (right) from 1990 to 2015.

**Table 4** Changes in land cover categories area (ha) and percent (%) in the years 1990, 2002 and 2015.

Area (ha) Bastamin				Area (ha) Bidkhoon			
	2015	2002	1990		2015	2002	1990
soil	1326.8	1298.3	1334	soil	636.84	648.7	703.2
water	537	535.5	533	water	514.98	499.5	478.8
vegetation	40.5	70.7	37.6	vegetation	96.6	100.2	66.3
% change Bastamin				% change Bidkhoon			
	2015	2002	1990		2015	2002	1990
soil	69.6	68.14	69.96	soil	51	51.96	56.32
water	28.23	28.1	27.9	water	41.24	40	38.35
vegetation	2.12	3.71	2.23	vegetation	7.74	8.03	5.31

and 15 ha became open water. In the years between 2002 and 2015, the mangrove area decreased by 4 ha (i.e., from 100.2 to 96.6 ha) and became open water. Soil area decreased from 648 to 636 ha. Similar results were found in the Basatin region. Table 4 represents changes in land cover categories area in the years 1990, 2002, and 2014. Results indicated that the open water area has increased while the

soil and mangrove area in Bidkhoon and Bastain sites decreased over this 26-year period demonstrating that in the Nayband region SLR causes more land to convert to open water. Etemadi et al. (2018) reported that Jask mangroves forest in Iran are not keeping pacing with SLR as there was a significant correlation between relative SLR and mangroves area migration in the landward direction.

## 5. Conclusion

Minimum temperature (3.53°C), increased significantly during the 47 years examined. Moreover, drought elongation and precipitation reduction occurred after 2003. These conditions lead to more evaporation and elevated salinity which increases stress on Persian Gulf mangroves which already exist near the limit of tolerance in terms of temperature and salinity. We also found rising sea level rates (4 mm yr<sup>-1</sup>) are partially due to deep subsidence (1–2 mm yr<sup>-1</sup>). Furthermore, studied mangroves with no riverine discharge, subsidence, and the micro-tidal regime are extremely vulnerable to the impact of SLR. Based on the result of land-use change analysis and the expansion of open water to the land over 26 years, it is likely that relative SLR including subsidence is the main driving factor.

Our spatiotemporal analysis demonstrates that the Malgonze mangrove site has been expanding to landward while the seaward area has been converted to open water. However, the Nayband mangrove area dramatically decreased in the past 60 years. NDVI results show that the Nayband mangroves maintained a healthy condition and expanded between the years of 1990 and 2002 which could be the result of rising temperatures and above-average precipitation. However, NDVI changes after 2002 demonstrate the mangrove health and area have decreased. The control site at Malgonze showed landward migration compared to the decreasing mangrove health and area at the Nayband site after 2002. This lead to the conclusion that the proximity to the large natural gas fields and industrial effluent which was discharged directly into the estuaries, and began immediately after 1997, caused a reduction in the mangrove vegetated area.

We concluded that the mangroves in this region of the world have numerous threats including pollution, rising sea level, increasing temperature, and decreasing rainfall. The combination of these factors is likely to exacerbate mangrove degradation in the near future. A broad range of management and conservation planning would be necessary to reduce the impact.

## Acknowledgments

This research was sponsored by Persian Gulf University (PGU) Department of Environment at Persian Gulf Research Institute.

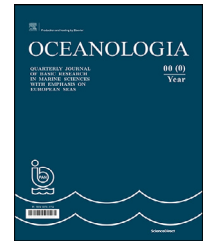
## References

- Abel, N., Gorrdard, R., Harman, B., Leitch, A., Langridge, J., Ryan, A., Heyenga, S., 2011. Sea level rise, coastal development and planned retreat: analytical framework, governance principles and an Australian case study. *Environ. Sci. Policy* 14 (3), 279–288. <https://doi.org/10.1016/j.envsci.2010.12.002>
- Adame, M.F., Reef, R., Santini, N.S., Najera, E., Turschwell, M.P., Hayes, M.A., Masque, P., Lovelock, C.E., 2020. Mangroves in arid regions: Ecology, threats, and opportunities. *Estuar. Coast. Shelf Sci.* art no. 106796. <https://doi.org/10.1016/j.ecss.2020.106796>
- Almhasheer, H., 2018. Spatial coverage of mangrove communities in the Arabian Gulf. *Environ. Monit. Assess.* 190 (2), art. no. 85. <https://doi.org/10.1007/s10661-018-6472-2>
- Almhasheer, H., Al-Taisan, W., Mohamed, M.K., 2013. Mangrove deterioration in Tarut Bay on the eastern province of the Kingdom of Saudi Arabia. *Pakhtunkhwa. J. Life Sci.* 1 (02), 49–59.
- Alongi, D.M., 2008. Mangrove forests: resilience, protection from tsunamis, and responses to global climate change. *Estuar. Coast. Shelf Sci.* 76 (1), 1–13. <https://doi.org/10.1016/j.ecss.2007.08.024>
- Alongi, D.M., 2015. The impact of climate change on mangrove forests. *Curr. Clim. Chang. Rep.* 1 (1), 30–39. <https://doi.org/10.1007/s40641-015-0002-x>
- Alongi, D.M., 2018. Mangrove forests. In: *Blue Carbon: Coastal Sequestration for Climate Change Mitigation*. Springer International Publ, Cham, 23–36. <https://doi.org/10.1007/978-3-319-91698-9>
- Arshad, M., Eid, E.M., Hasan, M., 2020. Mangrove health along the hyper-arid southern Red Sea coast of Saudi Arabia. *Environ. Monit. Assess.* 192 (3), 1–15. <https://doi.org/10.1007/s10661-020-8140-6>
- Asfaw, A., Simane, B., Hassen, A., Bantider, A., 2018. Variability and time series trend analysis of rainfall and temperature in northcentral Ethiopia: A case study in Woleka sub-basin. *Weather. Clim. Extremes.* 19, 29–41. <https://doi.org/10.1016/j.wace.2017.12.002>
- Bartholy, J., Pongracz, R., 2005. Extremes of ground-based and satellite measurements in the vegetation period for the Carpathian Basin. *Phys. Chem. Earth Pt. A/B/C* 30 (1–3), 81–89. <https://doi.org/10.1016/j.pce.2004.08.012>
- Binh, T.N.K.D., Vromant, N., Hung, N.T., Hens, L., Boon, E.K., 2005. Land cover changes between 1968 and 2003 in Cai Nuoc, Ca Mau peninsula, Vietnam. *Environ. Dev. Sustain.* 7 (4), 519–536. <https://doi.org/10.1007/s10668-004-6001-z>
- Breithaupt, J.L., Hurst, N., Steinmuller, H.E., Duga, E., Smoak, J.M., Kominoski, J.S., Chambers, L.G., 2019. Biogeochemical impacts of storm surge sediments in coastal wetlands: Hurricane Irma and the Florida Everglades. *Estuaries Coast.* 43 (5), 1090–1103. <https://doi.org/10.1007/s12237-019-00607-0>
- Bryant, M., 1981. The Persian Gulf: Pollution and Development. *Environ. Conserv* 8 (1), 44. <https://doi.org/10.1017/S0376892900026692>
- Burns, K.A., Codi, S., Swannell, R.J.P., Duke, N.C., 1999. Assessing the oil degradation potential of endogenous micro-organisms in tropical marine wetlands. *Mangroves and Salt Marshes* 3 (2), 67–84. <https://doi.org/10.1023/A:1009968101790>
- Caissie, D., 2006. The thermal regime of rivers: a review. *Freshw. Biol.* 51 (8), 1389–1406. <https://doi.org/10.1111/j.1365-2427.2006.01597.x>
- Cavanaugh, K.C., Kellner, J.R., Forde, A.J., Gruner, D.S., Parker, J.D., Rodriguez, W., Feller, I.C., 2014. Poleward expansion of mangroves is a threshold response to decreased frequency of extreme cold events. *PNAS USA* 111 (2), 723–727. <https://doi.org/10.1073/pnas.1315800111>
- Chimner, R.A., Fry, B., Kaneshiro, M.Y., Cormier, N., 2006. Current Extent and Historical Expansion of Introduced Mangroves on O'ahu, Hawai'i. *Pac. Sci.* 60 (3), 377–383. <https://doi.org/10.1353/psc.2006.0013>
- Davari, A., Khorasani, N., Daneshkar, A., 2013. Comparison of Heavy Metal Concentration in Bidekhun, Basatin and Melgonze Mangrove Forests. *Iran. J. Appl. Ecol.* 1 (2), 15–26 (in Persian).
- Dehghani, M., Nabipour, I., Dobaradaran, S., Godarzi, H., 2014. Cd and Pb concentrations in the surface sediments of the Asaluyeh Bay, Iran. *JCHR* 3 (1), 22–30. <http://jhr.ssu.ac.ir/article-1-156-fa.html>
- Duke, N.C., 2016. Oil spill impacts on mangroves: recommendations for operational planning and action based on a global review. *Mar. Pollut. Bull.* 109 (2), 700–715. <https://doi.org/10.1016/j.marpolbul.2016.06.082>
- Ellison, J.C., 2015. Vulnerability assessment of mangroves to climate change and sea-level rise impacts. *Wetl. Ecol.*

- Manag. 23 (2), 115–137. <https://doi.org/10.1007/s11273-014-9397-8>
- Etemadi, H., Samadi, S., Sharifikia, M., 2014. Uncertainty analysis of statistical downscaling models using general circulation model over an international wetland. *Clim. Dyn.* 42 (11–12), 2899–2920. <https://doi.org/10.1007/s00382-013-1855-0>
- Etemadi, H., Samadi, S.Z., Sharifikia, M., Smoak, J.M., 2016. Assessment of climate change downscaling and non-stationarity on the spatial pattern of a mangrove ecosystem in an arid coastal region of southern Iran. *Theor. Appl. Climatol.* 126 (1–2), 35–49. <https://doi.org/10.1007/s00704-015-1552-5>
- Etemadi, H., Smoak, J.M., Karami, J., 2018. Land use change assessment in coastal mangrove forests of Iran utilizing satellite imagery and CA–Markov algorithms to monitor and predict future change. *Environ. Earth. Sci* 77 (5), art. no. 208. <https://doi.org/10.1007/s12665-018-7392-8>
- FAO, 2007. *The world's mangroves 1980–2005*. FAO Forestry Paper, Forest Resources Division. FAO, Rome, 77.
- Feher, L.C., Osland, M.J., Griffith, K.T., Grace, J.B., Howard, R.J., Stagg, C.L., Enwright, N.M., Krauss, K.W., Gabler, C.A., Day, R.H., Rogers, K., 2017. Linear and nonlinear effects of temperature and precipitation on ecosystem properties in tidal saline wetlands. *Ecosphere*. 8 (10), art. no. e01956. <https://doi.org/10.1002/ecs2.1956>
- Feng, Z., Tan, G., Xia, J., Shu, C., Chen, P., Wu, M., Wu, X., 2020. Dynamics of mangrove forests in Shenzhen Bay in response to natural and anthropogenic factors from 1988 to 2017. *J. Hydrol.* 591, art. no. 125271. <https://doi.org/10.1016/j.jhydrol.2020.125271>
- Field, C.D., 1995. Impact of expected climate change on mangroves. In: Wong, Y.S., Tam, N.F.Y. (Eds.), *Asia-Pacific Symposium on Mangrove Ecosystems*. Springer, Dordrecht, 75–81. [https://doi.org/10.1007/978-94-011-0289-6\\_10](https://doi.org/10.1007/978-94-011-0289-6_10)
- Fielding, E.J., Blom, R.G., Goldstein, R.M., 1998. Rapid subsidence over oil fields measured by SAR interferometry. *Geophys. Res. Lett.* 25 (17), 3215–3218. <https://doi.org/10.1029/98GL52260>
- Friedrichs, C.T., Perry, J.E., 2001. Tidal salt marsh morphodynamics: a synthesis. *J. Coast. Res.* 27, 7–37.
- Ghosh, M.K., Kumar, L., Roy, C., 2015. Monitoring the coastline change of Hatiya Island in Bangladesh using remote sensing techniques. *ISPRS J. Photogramm. Remote Sens.* 101, 137–144. <https://doi.org/10.1016/j.isprsjprs.2014.12.009>
- Gilman, E.L., Ellison, J., Duke, N.C., Field, C., 2008. Threats to mangroves from climate change and adaptation options: a review. *Aquat. Bot.* 89 (2), 237–250. <https://doi.org/10.1016/j.aquabot.2007.12.009>
- Gilman, E.L., Ellison, J., Jungblut, V., Van Lavieren, H., Wilson, L., Areki, F., Brighthouse, G., Bungitak, J., Dus, E., Henry, M., Kilman, M., 2006. Adapting to Pacific Island mangrove responses to sea level rise and climate change. *Clim. Res.* 32 (3), 161–176. <https://doi.org/10.3354/cr032161>
- Giri, C., Long, J., Abbas, S., Murali, R.M., Qamer, F.M., Pengra, B., Thau, D., 2015. Distribution and dynamics of mangrove forests of South Asia. *J. Environ. Manag.* 148, 101–111. <https://doi.org/10.1016/j.jenvman.2014.01.020>
- Giri, C., Pengra, B., Zhu, Z., Singh, A., Tieszen, L.L., 2007. Monitoring mangrove forest dynamics of the Sundarbans in Bangladesh and India using multi-temporal satellite data from 1973 to 2000. *Estuar. Coast. Shelf Sci.* 73 (1–2), 91–100. <https://doi.org/10.1016/j.ecss.2006.12.019>
- Godoy, M., Lacerda, L., 2015. Mangroves response to climate change: a review of recent findings on mangrove extension and distribution. *Ana. Acad. Bras. Cienc.* 87, 651–667. <https://doi.org/10.1590/0001-3765201520150055>
- Goharnejad, H., Shamsai, A., Hosseini, S.A., 2013. Vulnerability assessment of southern coastal areas of Iran to sea level rise: evaluation of climate change impact. *Oceanologia* 55 (3), 611–637. <https://doi.org/10.5697/oc.55-3.611>
- Green, E.P., Mumby, P.J., Edwards, A.J., Clark, C.D., Ellis, A.C., 1997. Estimating leaf area index of mangroves from satellite data. *Aquat. Bot.* 58 (1), 11–19. [https://doi.org/10.1016/S0304-3770\(97\)00013-2](https://doi.org/10.1016/S0304-3770(97)00013-2)
- Hadjimitsis, D.G., Papadavid, G., Agapiou, A., Themistocleous, K., Hadjimitsis, M.G., Retalis, A., Michaelides, S., Chrysoulakis, N., Toullos, L., Clayton, C.R.I., 2010. Atmospheric correction for satellite remotely sensed data intended for agricultural applications: impact on vegetation indices. *Nat. Hazards Earth Syst. Sci.* 10 (1), 89–95. <https://doi.org/10.5194/nhess-10-89-2010>
- Hamilton, S.E., Casey, D., 2016. Creation of a high spatio-temporal resolution global database of continuous mangrove forest cover for the 21st century (CGMFC-21). *Glob. Ecol. Biogeogr.* 25 (6), 729–738. <https://doi.org/10.1111/geb.12449>
- Hassanzadeh, S., Hosseinibalam, F., Rezaei-Latifi, A., 2011. Numerical modelling of salinity variations due to wind and thermal forcing in the Persian Gulf. *Appl. Math. Model.* 35 (3), 1512–1537. <https://doi.org/10.1016/j.apm.2010.09.029>
- Hoff, R.Z., Michel, J., 2014. *Oil Spills in Mangroves: Planning and response considerations United States*. NOAA Ocean Service, Office of Response and Restoration. Ntnl. Gov. Publ., USA, 96 pp.
- Hu, L., Li, W., Xu, B., 2018. Monitoring mangrove forest change in China from 1990 to 2015 using Landsat-derived spectral-temporal variability metrics. *Int. J. Appl. Earth Obs. Geoinf.* 73, 88–98. <https://doi.org/10.1016/j.jag.2018.04.001>
- Ibrahim, H.D., Xue, P., Eltahir, E.A., 2020. Multiple Salinity Equilibria and Resilience of Persian/Arabian Gulf Basin Salinity to Brine Discharge. *Front. Mar. Sci.* 7, art. no. 573. <https://doi.org/10.3389/fmars.2020.00573>
- IPCC, 2007. *Contribution of Working Group I to the Fourth Assessment Report of the Intergovernmental Panel on Climate Change*. Cambridge University Press, 1056 pp.
- IPCC, 2013. *Climate Change 2013. The physical Science Basis. Summary for policymakers*. Contribution of Working Group I to the Fifth Assessment Report of the Intergovernmental Panel on Climate Change. Cambridge Univ. Press, New York, 1535 pp.
- IPCC, 2014. *Climate change 2014: impacts, adaptation, and vulnerability*. Cambridge Univ. Press, New York, 1132 pp.
- Irani, M., Massah Bavani, A., Bohluly, A., Alizadeh Katak Lahijani, H., 2017. Sea Level Rise in Persian Gulf and Oman Sea Due to Climate Change in the Future Periods. *JPHGR* 49 (4), 603–614. <https://doi.org/10.22059/jphgr.2018.221101.1006966>
- Jayanthi, M., Thirumurthy, S., Nagaraj, G., Muralidhar, M., Ravichandran, P., 2018. Spatial and temporal changes in mangrove cover across the protected and unprotected forests of India. *Estuar. Coast. Shelf Sci.* 213, 81–91. <https://doi.org/10.1016/j.ecss.2018.08.016>
- Kalthori, A., Kokya, A., 2012. Evaluation of Anthropogenic Impacts on Soiland Regolith Materials Based on BCR Sequential Extraction Analysis. *Int. J. Environ. Res.* 6 (1), 185–194. <https://doi.org/10.22059/ijer.2011.485>
- Kemp, A.C., Horton, B.P., Donnelly, J.P., Mann, M.E., Vermeer, M., Rahmstorf, S., 2011. Climate related sea-level variations over the past two millennia. *PNAS USA* 108 (27), 11017–11022. <https://doi.org/10.1073/pnas.1015619108>
- Kendall, M.G., 1975. *Rank correlation methods*. Charles Griffin, London, 202 pp.
- Kennedy, R.E., Cohen, W.B., Schroeder, T.A., 2007. Trajectory-based change detection for automated characterization of forest disturbance dynamics. *Remote Sens. Environ.* 110 (3), 370–386. <https://doi.org/10.1016/j.rse.2007.03.010>
- Ketelaar, V.B.H., 2009. Subsidence due to hydrocarbon production in the Netherlands. In: *Satellite radar interferometry: Subsidence monitoring techniques*. Springer, Dordrecht, 7–26. [https://doi.org/10.1007/978-1-4020-9428-6\\_2](https://doi.org/10.1007/978-1-4020-9428-6_2)
- Kharin, V.V., Zwiers, F.W., Zhang, X., Hegerl, G.C., 2007. Changes in temperature and precipitation extremes in the IPCC ensemble

- of global coupled model simulations. *J. Clim.* 20 (8), 1419–1444. <https://doi.org/10.1175/JCLI4066.1>
- Kouhgard, E., Shakerdargah, E., 2015. Effect of Pollutions on Mangrove Forests of Nayband National Marine Park. *World Academy of Science, Engineering and Technology. Int. J. Environ. Ecol. Eng.* 9 (4), 1.
- Kovacs, J.M., Flores-Verdugo, F., Wang, J., Aspden, L.P., 2004. Estimating leaf area index of a degraded mangrove forest using high spatial resolution satellite data. *Aquat. Bot.* 80 (1), 13–22. <https://doi.org/10.1016/j.aquabot.2004.06.001>
- Krauss, K.W., From, A.S., Doyle, T.W., Doyle, T.J., Barry, M.J., 2011. Sea-level rise and landscape change influence mangrove encroachment onto marsh in the Ten Thousand Islands region of Florida, USA. *J. Coast. Conserv.* 15 (4), 629–638. <https://doi.org/10.1007/s11852-011-0153-4>
- Kuenzer, C., Bluemel, A., Gebhardt, S., Quoc, T.V., Dech, S., 2011. Remote sensing of mangrove ecosystems: A review. *Remote Sens.* 3 (5), 878–928. <https://doi.org/10.3390/rs3050878>
- Lee, T.M., Yeh, H.C., 2009. Applying remote sensing techniques to monitor shifting wetland vegetation: A case study of Danshui River estuary mangrove communities, Taiwan. *Ecol. Eng.* 35 (4), 487–496. <https://doi.org/10.1016/j.ecoleng.2008.01.007>
- Lillesand, T.M., Keifer, R.W., Chipman, J.W., 2007. *Remote Sensing and Image Interpretation*. John Wiley & Sons, Inc., New York, 724 pp.
- Lindén, O., Pålsson, J., 2013. Oil contamination in Ogoniland, Niger delta. *Ambio* 42 (6), 685–701. <https://doi.org/10.1007/s13280-013-0412-8>
- López-Medellín, X., Ezcurra, E., González-Abraham, C., Hak, J., Santiago, L.S., Sickman, J.O., 2011. Oceanographic anomalies and sea-level rise drive mangroves inland in the Pacific coast of Mexico. *J. Veg. Sci.* 22 (1), 143–151. <https://doi.org/10.1111/j.1654-1103.2010.01232.x>
- Lovelock, C.E., Cahoon, D.R., Friess, D.A., Guntenspergen, G.R., Krauss, K.W., Reef, R., Rogers, K., Saunders, M.L., Sidik, F., Swales, A., Saintilan, N., 2015. The vulnerability of Indo-Pacific mangrove forests to sea-level rise. *Nature* 526 (7574), 559–563. <https://doi.org/10.1038/nature15538>
- Lovelock, C.E., Feller, I.C., Reef, R., Hickey, S., Ball, M.C., 2017. Mangrove dieback during fluctuating sea levels. *Sci. Rep.* 7 (1), 1–8. <https://doi.org/10.1038/s41598-017-01927-6>
- Mafi-Gholami, D., Zenner, E.K., Jaafari, A., Bui, D.T., 2020. Spatially explicit predictions of changes in the extent of mangroves of Iran at the end of the 21st century. *Estuar. Coast. Shelf Sci.* 237, art. no. 106644. <https://doi.org/10.1016/j.ecss.2020.106644>
- Maleki-Zade, A., 2014. *Monitoring thermal land use and cover change due to Pars Special Economic Energy Zone by use of satellite imageries*. M. Sc. thesis. Natural Resource College, Isfahan Industrial Univ.
- McKee, K.L., Mendelssohn, I.A., Materne, M., 2004. Acute salt marsh dieback in the Mississippi River deltaic plain: a drought-induced phenomenon? *Glob. Ecol. Biogeogr.* 13 (1), 65–73. <https://doi.org/10.1111/j.1466-882X.2004.00075.x>
- Meneses-Tovar, C.L., 2011. NDVI as indicator of degradation. *Unasylva* 238 (62), 39–46.
- Moaddab, A.R., Khabazi, M., Roosta, H., 2017. Determining the rate of salinity of Persian Gulf waters with the aid of satellite images and least squares method. *Open J. Mar. Sci.* 7 (01), art. no. 155. <https://doi.org/10.4236/ojms.2017.71012>
- Mostafavi, H., Kiabi, B., Mahini, E., Mehrabian, A., Naghinejad, E., 2004. *Ecological Evaluation of Mond Protected Area. Corporate scientific project between Department of the Environment of Bushehr Province and Shahid Beheshti University, Bushehr, 133 pp.*
- Oppenheimer, M., Glavovic, B.C., Hinkel, J., van de Wal, R., Magnan, A.K., Abd-Elgawad, A., Cai, R., Cifuentes-Jara, M., DeConto, R.M., Ghosh, T., Hay, J., Isla, F., Marzeion, B., Meyssignac, B., Sebesvari, Z., 2019. Chapter 4: Sea Level Rise and Implications for Low Lying Islands, Coasts and Communities. In: Pörtner, H.-O., Roberts, D.C., Masson-Delmotte, V., Zhai, P., Tignor, M., Poloczanska, E., Mintenbeck, K., Alegría, A., Nicolai, M., Okem, A., Petzold, J., Rama, B., Weyer, N.M. (Eds.), *IPCC Special Report on the Ocean and Cryosphere in a Changing Climate*. Cambridge Univ. Press, Cambridge, UK, 321–445.
- Osland, M.J., Enwright, N., Day, R.H., Doyle, T.W., 2013. Winter climate change and coastal wetland foundation species: salt marshes vs. mangrove forests in the southeastern United States. *Glob. Change Biol.* 19 (5), 1482–1494. <https://doi.org/10.1111/gcb.12126>
- Osland, M.J., Enwright, N.M., Day, R.H., Gabler, C.A., Stagg, C.L., Grace, J.B., 2016. Beyond just sea-level rise: Considering macroclimatic drivers within coastal wetland vulnerability assessments to climate change. *Glob. Change Biol.* 22 (1), 1–11. <https://doi.org/10.1111/gcb.13084>
- Pachauri, R.K., Allen, M.R., Barros, V.R., Broome, J., Cramer, W., Christ, R., Church, J.A., Clarke, L., Dahe, Q., Dasgupta, P., Dubash, N.K., 2014. *Climate change 2014: synthesis report. Contribution of Working Groups I, II and III to the fifth assessment report of the Intergovernmental Panel on Climate Change*, 151 pp.
- Padash, A., Jozi, S.A., Nabavi, S.M.B., Dehzad, B., 2016. Stepwise strategic environmental management in marine protected area. *GJESM* 2 (1), 49–60. <https://doi.org/10.7508/gjesm.2016.01.006>
- Perry, C.L., Mendelssohn, I.A., 2009. Ecosystem effects of expanding populations of *Avicennia germinans* in a Louisiana salt marsh. *Wetlands* 29 (1), 396–406. <https://doi.org/10.1672/08-100.1>
- Pettitt, A.N., 1979. A non-parametric approach to the change-point problem. *J. Roy. Stat. Soc. C - App.* 28 (2), 126–135. <https://doi.org/10.2307/2346729>
- Proffitt, C.E., Devlin, D.J., Lindsey, M., 1995. Effects of oil on mangrove seedlings grown under different environmental conditions. *Mar. Pollut. Bull.* 30 (12), 788–793. [https://doi.org/10.1016/0025-326X\(95\)00070-4](https://doi.org/10.1016/0025-326X(95)00070-4)
- Rahimzadeh, F., Asgari, A., an Fattahi, E., 2009. Variability of extreme temperature and precipitation in Iran during recent decades. *Int. J. Climatol.* 29 (3), 329–343. <https://doi.org/10.1002/joc.1739>
- Ramcharan, E.K., 2004. Mid-to-late Holocene sea level influence on coastal wetland development in Trinidad. *Quat. Int.* 120 (1), 145–151. <https://doi.org/10.1016/j.quaint.2004.01.013>
- Ranasinghe, R., Duong, T.M., Uhlenbrook, S., Roelvink, D., Stive, M., 2013. Climate-change impact assessment for inlet-interrupted coastlines. *Nat. Clim. Change* 3 (1), 83–87. <https://doi.org/10.1038/nclimate1664>
- Saintilan, N., Khan, N.S., Ashe, E., Kelleway, J.J., Rogers, K., Woodroffe, C.D., Horton, B.P., 2020. Thresholds of mangrove survival under rapid sea level rise. *Science*. *Science* 368 (6495), 1118–1121. <https://doi.org/10.1126/science.aba2656>
- Salehipour-Milani, A., Jafari-Beglu, M., 2012. Satellite-based assessment of the area and changes in the mangrove ecosystem of the Qeshm island, Iran. *J. Environ. Res. Dev.* 7, 1052–1060.
- Sam, K., Coulon, F., Prpich, G., 2017. Management of petroleum hydrocarbon contaminated sites in Nigeria: Current challenges and future direction. *Land Use Policy* 64, 133–144. <https://doi.org/10.1016/j.landusepol.2017.01.051>
- Samadi, S., Wilson, C.A., Moradkhani, H., 2013. Uncertainty analysis of statistical downscaling models using Hadley Centre Coupled Model. *Theor. Appl. Climatol.* 114 (3–4), 673–690. <https://doi.org/10.1007/s00704-013-0844-x>
- Samanta, K., Hazra, S., 2017. Mangrove Forest Cover Changes in Indian Sundarban (1986–2012) Using Remote Sensing and GIS. In: Hazra, S., Mukhopadhyay, A., Ghosh, A.R., Mitra, D., Dadhwal, V.K. (Eds.), *Environment and Earth Observation: Case*

- Studies in India. Springer Int. Publ., Cham, 97–108. <https://doi.org/10.1007/978-3-319-46010-9>
- Sanders, C.J., Maher, D.T., Tait, D.R., Williams, D., Holloway, C., Sippo, J.Z., Santos, I.R., 2016. Are global mangrove carbon stocks driven by rainfall? *J. Geophys. Res. Biogeosci.* 121 (10), 2600–2609. <https://doi.org/10.1002/2016JG003510>
- Sari, S.P., Rosalina, D., 2016. Mapping and monitoring of mangrove density changes on tin mining area. *Procedia Environ. Sci.* 33, 436–442. <https://doi.org/10.1016/j.proenv.2016.03.094>
- Sharitz, R.R., Pennings, S.C., 2006. Development of wetland plant communities in Ecology of freshwater and estuarine wetlands. In: Batzer, D.P. (Ed.), *Ecology of Freshwater and Estuarine Wetlands*. Univ. California Press, Berkley, 133–150. <https://doi.org/10.1525/california/9780520247772.003.0006>
- Schile, L.M., Kauffman, J.B., Crooks, S., Fourqurean, J.W., Glavan, J., Megonigal, J.P., 2016. Limits on Carbon Sequestration in Arid Blue Carbon Ecosystems. *Ecol. Appl.* 27 (3), 859–874. <https://doi.org/10.1002/eap.1489>
- Schoonbeek, J.B., 1976. Land subsidence as a result of natural gas extraction in the province of Groningen. SPE European Spring Meeting, 8–9 April. Soc. Petrol. Eng. Publ., Amsterdam, The Netherlands. <https://doi.org/10.2118/5751-MS>
- Schuerch, M., Spencer, T., Temmerman, S., Kirwan, M.L., Wolff, C., Lincke, D., McOwen, C.J., Pickering, M.D., Reef, R., Vafeidis, A.T., Hinkel, J., 2018. Future response of global coastal wetlands to sea-level rise. *Nature* 561 (7722), 231–234. <https://doi.org/10.1038/s41586-018-0476-5>
- Shojaei-Gori, J., Jafari, A., Soltani, A., Ghasemi, A., Sirghani, M., 2013. The investigation of Nyband and Basatin Mangrove degradation in Boshehr province. *Environ. Res.* 17 (9), 187–196 (in Persian).
- Silva, R.M., Santos, C.A.G., Macêdo, M.L.A., Silva, L.P., Freire, P.K.M.M., 2013. Space-time variability of rainfall and hydrological trends in the Alto São Francisco River basin. *IAHS-AISH Publ.*, 359 pp.
- Sippo, J.Z., Lovelock, C.E., Santos, I.R., Sanders, C.J., Maher, D.T., 2018. Mangrove mortality in a changing climate: An overview. *Estuar. Coast. Shelf Sci.* 215, 241–249. <https://doi.org/10.1016/j.ecss.2018.10.011>
- Smoak, J.M., Breithaupt, J.L., Smith, T.J., Sanders, C.J., 2013. Sediment accretion and organic carbon burial relative to sea-level rise and storm events in two mangrove forests in Everglades National Park. *Catena* 104, 58–66.
- Snedaker, S.C., Jimenez, J.A., Brown, M.S., 1981. Anomalous aerial roots in *Avicennia germinans* L., in Florida and Costa Rica. *Bull. Mar. Sci.* 31, 467–470.
- Soltani, M., Laux, P., Kunstmann, H., Stan, K., Sohrabi, M.M., Molanejad, M., Sabziparvar, A.A., SaadatAbadi, A.R., Ranjbar, F., Roustaei, I., Zawar-Reza, P., 2016. Assessment of climate variations in temperature and precipitation extreme events over Iran. *Theor. Appl. Climatol.* 126 (3–4), 775–795. <https://doi.org/10.1007/s00704-015-1609-5>
- Spencer, T., Schuerch, M., Nicholls, R.J., Hinkel, J., Lincke, D., Vafeidis, A.T., Reef, R., McFadden, L., Brown, S., 2016. Global coastal wetland changes under sea-level rise and related stresses: The DIVA Wetland Change Model. *Glob. Planet. Change* 139, 15–30. <https://doi.org/10.1016/j.gloplacha.2015.12.018>
- Swift, S.A., Uchupi, E., Ross, D.A., 1988. Late Cenozoic geology of the central Persian Gulf from industry well data and seismic profiles. *Tech. Mem. WHOI* 01-98, 76. <https://doi.org/10.1575/1912/1926>
- Tabari, H., Marofi, S., 2011. Changes of pan evaporation in the west of Iran. *Water Resour. Manag.* 25 (1), 97–111. <https://doi.org/10.1007/s11269-010-9689-6>
- Walters, B.B., Rönnbäck, P., Kovacs, J.M., Crona, B., Hussain, S.A., Badola, R., Primavera, J.H., Barbier, E., Dahdouh-Guebas, F., 2008. Ethnobiology, socio-economics and management of mangrove forests: A review. *Aquat. Bot.* 89 (2), 220–236. <https://doi.org/10.1038/416389a>
- Walther, G.R., Post, E., Convey, P., Menzel, A., Parmesan, C., Beebee, T.J., Fromentin, J.M., Hoegh-Guldberg, O., Bairlein, F., 2002. Ecological responses to recent climate change. *Nature* 416 (6879), 389–395. <https://doi.org/10.1038/416389a>
- Ward, R., Friess, D., Day, R., Mackenzie, R., 2016. Impacts of climate change on global mangrove ecosystems: a regional comparison. *EHS* 2 (4), 1–25. <https://doi.org/10.1002/ehs2.1211>
- Wibowo, A., Supriatna, S., 2010. Coastal Environmental Vulnerability on Coastal Cities in Indonesia. *Jurnal Ilmu dan Teknologi Kelautan Tropis* 3, 20. <https://doi.org/10.29244/jitkt.v3i2.7818>
- Zare-marivan, H., 2010. Distribution of heavy metals associated with petroleum in the northern Persian Gulf: Bushehr and Nayband Bay area. *J. Persian Gulf* 1 (1), 1–6 (in Persian).
- Zare-Zadeh Mehrizi, T., Khoshbakht, K., Mahdavi Damghani, A., Kambouzia, J., 2011. Studying effects of reduction in tidal flooding on the structure of mangrove forests; a case study from Nayband Coastal National Park. *Environ. Sci.* 8 (4), 43–58 (in Persian).
- Zhu, Z., Woodcock, C.E., 2014. Continuous change detection and classification of land cover using all available Landsat data. *Remote Sens. Environ.* 144, 152–171. <https://doi.org/10.1016/j.rse.2014.01.011>
- Zomer, R.J., Trabucco, A., Ustin, S.L., 2009. Building spectral libraries for wetlands land cover classification and hyperspectral remote sensing. *J. Environ. Manag.* 90 (7), 2170–2177. <https://doi.org/10.1016/j.jenvman.2007.06.028>



ORIGINAL RESEARCH ARTICLE

# Impact of human-altered hydrographical setting on the Copepod community structure in an extensive tropical estuary along the southwest coast of India

Arunpandi Nagarathinam<sup>a</sup>, Jyothibabu Retnamma<sup>a,\*</sup>,  
Jagadeesan Loganathan<sup>a,b</sup>, Parthasarathi Singaram<sup>a</sup>, Anjusha Arayillath<sup>a</sup>,  
Albin Konnakamannil Jose<sup>a</sup>

<sup>a</sup> CSIR – National Institute of Oceanography, Regional Centre, Kochi, India

<sup>b</sup> CSIR – National Institute of Oceanography, Regional Centre, Visakhapatnam, India

Received 31 August 2020; accepted 23 October 2020

Available online 5 November 2020

## KEYWORDS

Mesozooplankton;  
Copepods;  
Barrage;  
Multivariate analysis;  
Kochi backwaters

**Abstract** This study presents how human-altered hydrographical settings (flow restrictions) impacts the natural distribution and community structure of copepods in the Kochi Backwaters (KBW), the largest monsoonal estuary along the southwest coast of India. This study is primarily based on an extensive seasonal sampling in the KBW and their comparison with a historical data set. Thannermukkom Barrage (TB) was built in the southern section of the KBW in the 1970s to prevent saline water intrusion to the upstream during the non-monsoon periods. Thirteen locations (1–4 in the downstream, 5–9 in the midstream, and 10–13 in the upstream) were sampled in this study over the entire stretch of the KBW during the Pre-Southwest Monsoon (PRM), Southwest Monsoon (SWM), and Post-Southwest Monsoon (PSWM). The overall effect of TB in the KBW is a seaward push of mesohaline conditions during all seasons with varying intensities. In response to the seaward push of mesohaline conditions, copepods *Acartiella keralensis*, *Acartia plumosa*, *Acartia* sp., *Pseudodiaptomus annandalei*, *Pseudodiaptomus serricaudatus*, *Euterpina acutifrons* and *Oithona brevicornis* showed a corresponding spatial shift for their highest abundance and diversity from midstream during PRM to the downstream during the SWM/PSWM. Multivariate and IndVal analysis demarcated many indicator species of cope-

\* Corresponding author at: CSIR – National Institute of Oceanography, Regional Centre, Kochi, India. Phone +91 (0) 484 2390814, Fax +91 (0) 484 2390618.

E-mail address: [rjyothibabu@nio.org](mailto:rjyothibabu@nio.org) (J. Retnamma).

Peer review under the responsibility of the Institute of Oceanology of the Polish Academy of Sciences.



Production and hosting by Elsevier

<https://doi.org/10.1016/j.oceano.2020.10.004>

0078-3234/© 2020 Institute of Oceanology of the Polish Academy of Sciences. Production and hosting by Elsevier B.V. This is an open access article under the CC BY-NC-ND license (<http://creativecommons.org/licenses/by-nc-nd/4.0/>).

pods of different hydrographical settings in the KBW. A comparison with the historical data set showed that there is an apparent long-term change in hydrography, copepod composition and community structure in the upstream of the KBW due to TB.

© 2020 Institute of Oceanology of the Polish Academy of Sciences. Production and hosting by Elsevier B.V. This is an open access article under the CC BY-NC-ND license (<http://creativecommons.org/licenses/by-nc-nd/4.0/>).

## 1. Introduction

Mesozooplankton (>200  $\mu\text{m}$ ) play a vital role in the aquatic environment in transferring energy in the lower level (plankton) food web to higher trophic levels. The distribution of copepods, the most abundant component of the mesozooplankton (>60% in abundance), is mainly influenced by the salinity of the estuarine and coastal waters (Chen et al., 2011; Roman et al., 2000). During the Southwest Monsoon (SWM; June–September), the high precipitation and land runoff lead to freshwater dominance in Indian (monsoonal) estuaries (Arunpandi et al., 2020; Haridevan et al., 2015; Vijith et al., 2009). Soon after the SWM, the river flow decreases, and seawater intrusion becomes prominent in these estuaries. Kochi (Cochin) backwaters (KBW) is the largest estuary along the southwest coast of India (Kurup et al., 1990) sustaining estuarine, brackish and freshwater conditions extending from Azhikode in the north to Alleppey in the south (Figure 1a).

The KBW receives the seasonal highest amount of freshwater influx during the southwest monsoon (SWM – June to September) every year (Arunpandi et al., 2020; Jyothibabu et al., 2006; Kurup, 1990; Srinivas et al., 2003). Thannermukkom barrage (TB), is a saltwater regulator constructed in the south side of KBW in 1976 (Figure 1b–d). Four rivers (Manimala, Meenachil, Pamba and Achenkovil) enter the KBW from the south of TB and make a combined discharge of  $\sim 20000 \times 10^6 \text{ m}^3$  per year (Qasim, 2003; Srinivas et al., 2003). TB was constructed in 1976 mainly to prevent saltwater intrusion to the Southern part (upstream) of the KBW during non-monsoon (Pre-Southwest Monsoon – SWM; Post-Southwest Monsoon – PSWM) period. The closing (PSWM to PRM) and opening (SWM) of the shutters of TB usually takes 3–4 days. TB has a length of 1250 m with 63 shutters (93 Vents  $12.5 \times 5.47 \text{ m}$ ). TB has also facilitated (Report on visit to Vembanad Kol, 2008) many of the livelihood activities of people involved in agriculture, fishing, tourism, inland navigation, coir retting, and lime shell collection. But over the years, the flow restrictions in the KBW by TB caused severe ecological deterioration, which leads to the eutrophication, massive distribution of exotic water weeds (*Eichornia*, *Monochoria* etc.) and dwindling of many endemic faunal resources (Gopalan, 1991).

The changing flow regime of KBW due to the closing of TB shutters causes several environmental issues (Qasim, 2003; Revichandran et al., 2011), which includes increased siltation (Gopalan, 1991), spread of aquatic weeds, eutrophication and oxygen depletion. Earlier studies have shown the disruption of the natural ecological balance, thereby imposing adverse effects on the migrating fauna of prawn, fish and clam (Kannan, 1979; Padmakumar et al., 2002). Some general aspects of TB impacts on the hydrogra-

phy and the living resources in the KBW were investigated in the past (Achari, 1988; Arun, 2009; Buyukates and Roelke, 2005; Froneman, 2004; Haridevan et al., 2015; Kibirige and Perissinotto, 2003; Menon et al., 2000). However, still, there is no comprehensive data available on the extent to which TB influences the distribution of plankton in KBW, which is particularly crucial because plankton is globally considered as an excellent indicator of environmental change (Mackey et al., 1996; Millie et al., 1993; Pinckney et al., 2001). Therefore, in this seasonal study, we focused on the copepod composition and their community structure in different sections (downstream, midstream and upstream) of the KBW mainly to know what alteration TB has caused to the plankton composition and distribution. The following objectives were covered in this study (a) to understand the seasonal ecological differences in the KBW on a spatial scale and (b) assess the impact of TB on the copepods composition and community structure in the KBW and (c) to identify the indicator species of copepods to the different hydrographical settings in the KBW.

## 2. Material and methods

### 2.1. Sampling

The KBW (area  $256 \text{ km}^2$  and volume  $0.55 \text{ km}^3$ ) is situated between  $09^\circ 00' \text{N}$ – $10^\circ 40' \text{N}$  and  $76^\circ 00' \text{E}$ – $77^\circ 30' \text{E}$ . In general, TB is fully opened from June to September (Southwest Monsoon) and remains closed from March to May (Premonsoon/Pre-Southwest Monsoon). The present sampling was done during three seasons; August 2013 (Southwest Monsoon; SWM), December 2013 (Post-Southwest Monsoon; PSWM) and March 2015 (Pre-Southwest Monsoon; PRM). Samples were collected from 13 locations from the downstream (Kochi inlet) to the upstream (Alapuzha in the south of TB). A speed boat was used for sampling to cover the entire stretch of KBW almost at the same tidal phase. Nine stations were to the north of TB (1–9) and four stations to the south (10–13). Among these stations, 1–4 represent the downstream, 5–9 the middle stream and 10–13 the upstream. According to the salinity ranges suggested by McLusky (1993), KBW has several salinity levels such as euhaline (> 30), polyhaline (18–30), (c) mesohaline (5–18), oligohaline (0.5–5) and (e) limnetic (< 0.5).

### 2.2. Physico-chemical parameters

Vertical distribution of salinity was measured using a CTD (Sea CAT SBE 19 plusV2). Water samples were collected using Niskin sampler for measuring the chemical and biological parameters such as dissolved oxygen, nutrients, total

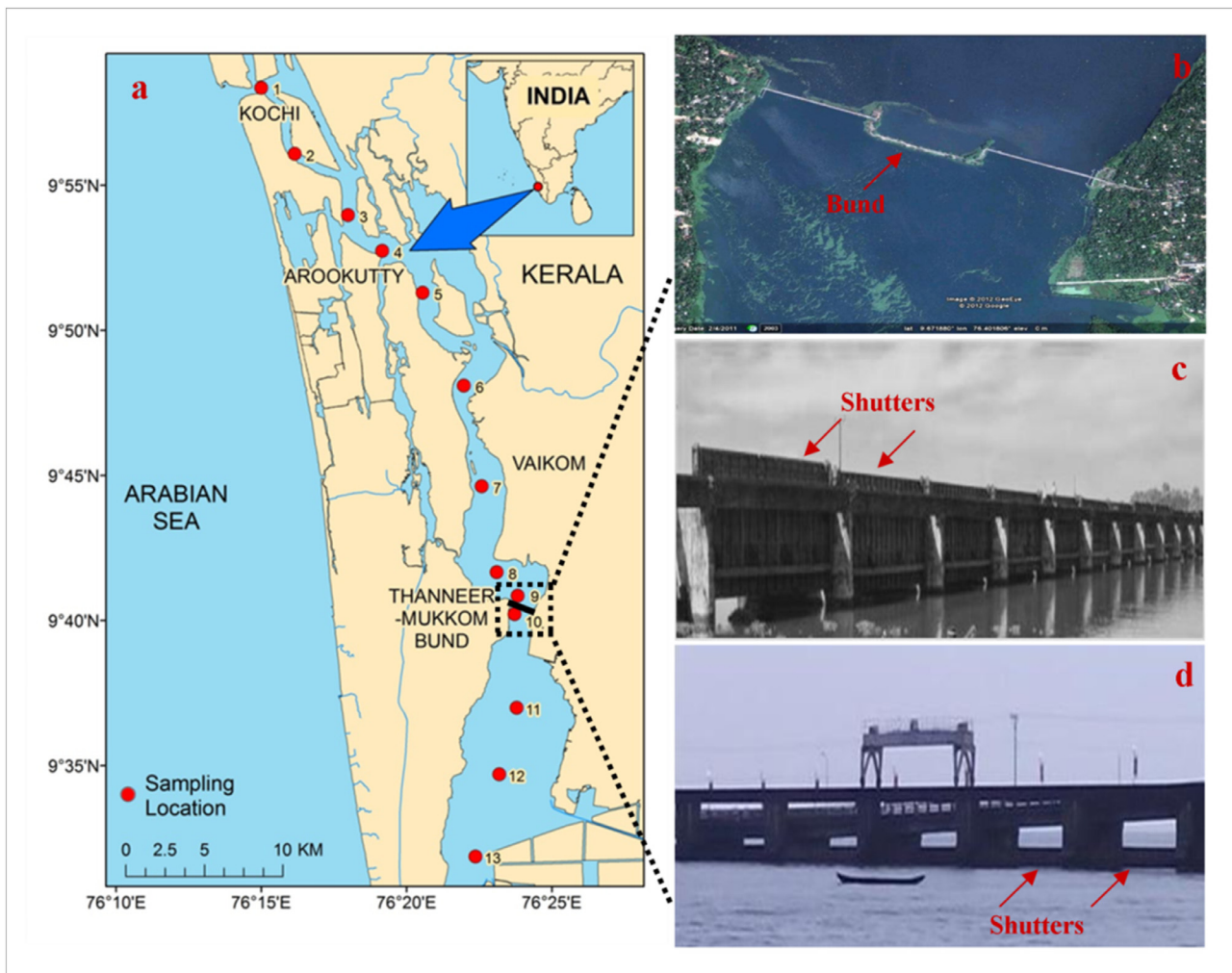


**Figure 1** (a) Sampling locations in the Kochi backwaters (KBW), (b) Google Earth image of Thanneermukkom barrage (TB), (c) open TB and (d) closed TB. Red arrows in (c) and (d) show the state of shutters (open/closed).

Chlorophyll *a* (Chl *a*) and mesozooplankton. Dissolved oxygen was measured using the modified Winkler method. For nutrient analysis, collected samples were kept in an icebox and transported to the laboratory where they were stored under  $-20^{\circ}\text{C}$  till analysis. They were measured based on the standard procedure (Grasshoff et al., 1983). For turbidity, samples were measured by a calibrated turbidity meter (EU-TECH TN-100) as per the nephelometric principles.

### 2.3. Biological components

Chlorophyll *a* (Chl *a*) was measured from 2 L water samples. For total Chl *a* analysis, 500 ml of water subsamples were filtered through  $0.2\ \mu\text{m}$  (Whatman GF/F filters). Phytoplankton concentrated on filter paper was extracted for Chl *a* using 10 ml of 90% acetone (in amber tubes) overnight (UNESCO, 1994) and measured through a calibrated Turner Fluorometer (Turner designs – 7200). Mesozooplankton was sampled using a WP net (mesh size  $200\ \mu\text{m}$ ) with a mouth area of  $0.25\ \text{m}^2$ . The plankton net was towed horizontally at slow speed (2 knots), just below the water surface ( $\sim 1\ \text{m}$  depth). A flow meter (Hydro-bios) was

attached across the mouth to calculate the volume of the water filtered. The samples collected were preserved in 4% formaldehyde for later enumeration and identification. Zooplankton group abundance was measured using the standard procedure of Postal et al. (2000). Among the sorted samples, cladocerans were identified up to genus level, whereas copepods were identified up to species levels using standard literature (Conway et al., 2003; Gardner and Szabo, 1982; Kasturirangan, 1963; Sewell, 1999; Tanaka, 1956).

### 2.4. Statistical analysis

#### 2.4.1. Grouping of locations

A euclidian distance matrix type of cluster/NMDS analysis was performed for the grouping of locations based on their similarity for hydrographical parameters. Cluster/NMDS analysis was performed separately for three seasons. The locations within the cluster have more similarity, whereas the groups are dissimilar. Hydrographical parameters were normalised before the analysis of the cluster. SIMPROF permutation analysis was performed to test the significance of the clustering pattern.

#### 2.4.2. Indicator species (IndVal) analysis

The representative species in each assemblage of copepods are identified based on indicator value (IndVal) index (Dufrêne and Legendre, 1997). IndVal primarily reflects whether the species assemblages are symmetric or asymmetric between different groups of observations. IndVal index reaches the maximum (100%) when all the individuals of a species occur in a single group of observations (centre of distribution), which essentially represents the asymmetric distribution of that species between the groups. On the other hand, the IndVal index reaches the lowest when the species are symmetrically distributed between the groups (Hunt and Hosie, 2006). According to Dufrêne and Legendre (1997), a minimum of 25% IndVal can be considered as the threshold level to determine IndVal species in a group of observations. In the present study,  $\geq 40\%$  IndVal value was used as the threshold to demarcate the IndVal species.

#### 2.4.3. Univariate and multivariate analysis

Differences in hydrographical and biological components were tested through ANOVA. Initially, datasets were tested for their distribution. The datasets in normal distribution parametric ANOVA with Tukey's HSD posthoc test was performed to compare the difference between the clusters, whereas the heterogeneity sample distribution non-parametric ANOVA (Kruskal-Wallis) with Dunns post hoc test was performed for comparing the differences between the clusters. The tests of normality, parametric and non-parametric ANOVA were carried out in XL stat pro-software pack up. The interrelationships within and between the environmental parameters and the biological parameters (Chlorophyll *a* and copepod species) were analysed using RDA (CANOCO 4.5). Primarily, the data was tested with Detrended Correspondence Analysis for finding a suitable ordination technique. The Detrended Correspondence Analysis results showed axis gradient length  $< 2$ , suggesting the use of a linear multivariate RDA as the most appropriate method (Leps and Smilauer, 2003). The biological variables were log-transformed before the analysis. The ordination significance was tested with Monte Carlo permutation tests (499 unrestricted permutations) ( $p < 0.05$ ). RDA was represented in the form of Triplots in which points display sampling stations (black circles), and biological (dotted green lines) and arrows showed environmental variables (blue lines); salinity was denoted with dotted pink colour.

### 3. Results

#### 3.1. Physico-chemical parameters

##### 3.1.1. Salinity

The distribution of salinity showed the dominance of salinity during the PRM period (Figure 2) wherein, polyhaline/euhaline (26.4 salinity) levels were found in the downstream, mesohaline (11–13.5 salinity) levels in the midstream, and oligohaline (0.9–4.9 salinity) in the upstream. Salinity gradients were evident from the downstream to the upstream with a marked difference ( $\sim 5$  salinity) caused by TB. During the SWM, the surface waters were limnohaline (0.06 and 1.60 salinity) (Table 1), which extended over the entire stretch of the KBW except for the

bar mouth. During the PSWM period, the mesohaline (16.4 salinity) condition prevailed over the downstream and in the midstream reaches oligohaline to mesohaline levels, whereas oligohaline (0.64 salinity) levels in the upstream of KBW.  $\sim 1.4$  unit salinity difference was noticed between the downstream and upstream of KBW (Table 1).

##### 3.1.2. Nutrients

Spatially, the distribution of nutrients showed varies pattern. In the present study, nitrate ( $\text{NO}_3$ ) concentration ranged between 0.63 and 18.53  $\mu\text{M}$  and did not show any clear trend in the distribution. However, during SWM, nitrate was relatively high (from 10.8 to 18.53  $\mu\text{M}$ ) and uniform over the entire KBW compared to PSWM (from 3.1 to 15.2  $\mu\text{M}$ ) and PRM (from 0.63 to 10.9  $\mu\text{M}$ ) (Table 1 and Figure 3c, 4c and 5c). Phosphate ( $\text{PO}_4$ ) concentrations varied from 0.15 to 2.05  $\mu\text{M}$  during the PRM period (Table 1 and Figure 3d); 0.13 to 0.37  $\mu\text{M}$  during the SWM (Figure 4d) and from 0.28 to 1.02  $\mu\text{M}$  during the PSWM (Figure 5d). The concentration was generally high in the downstream locations, which was lower during the SWM compared to the PRM and the PSWM period. Significantly high silicate concentration found in the KBW throughout the year. Silicate concentration varied from 13 to 49.1  $\mu\text{M}$  during the PRM (Table 1 and Figure 3e); 92.77 to 126.29  $\mu\text{M}$  during the SWM (Figure 4e) and 15.33 to 25.47  $\mu\text{M}$  during the PSWM (Figure 5e). Silicate was five times higher in the downstream during the SWM compared to PRM (Table 1). Spatially, silicate concentration was higher in the upstream locations compared to downstream and midstream of the KBW (Table 1).

##### 3.1.3. Dissolved oxygen, turbidity

Dissolved oxygen ranged between 3.98 and 5.92 mg/L during the PRM; 5.78 to 7.06 mg/L during the SWM, and 4.05 to 5.09 mg/L during the PSWM period. Spatially, DO was high in upstream locations. Seasonally, DO was high during the SWM period and found saturated levels in the entire study area (Table 1). Turbidity ranged between 1.1 and 4.3 NTU during the PRM (Table 1 and Figure 3f), 1.83 to 17.37 NTU during the SWM (Table 1 and Figure 4f) and 1.9 to 7.97 NTU during the PSWM (Table 1 and Figure 5f). Irrespective of the seasons, turbidity was found to be high in the downstream. In the entire stretch of the study area, turbidity was high during the SWM, followed by PSWM and the least during the PRM (Table 1). Phosphate concentration was relatively high in the downstream compared to the upstream during PRM and PSWM while silicate showed a reverse trend. During the SWM period, a variation in nutrients was low between the downstream, midstream and upstream of KBW (Table 1).

#### 3.2. Clustering of locations based on the hydrographical features

Based on the distribution of the hydrographical parameters, the sampling locations grouped into four different groups during the PRM period viz., locations 1 and 2 in cluster I, locations 3 to 6 in cluster II, 7–9 in cluster III and 10–14 in cluster IV. The spatial distribution of hydrographical parameters and their mean values are presented in Figure 3. During the PRM, cluster I was formed in the extreme downstream locations, which was characterised as polyhaline

**Table 1** Spatial and seasonal distribution of environmental and biological parameters.

Parameters		Stations												
		1	2	3	4	5	6	7	8	9	10	11	12	13
<b>PRM</b>	Salinity	26.4	21.01	15.05	14.27	13.5	12.15	10.49	10.99	9.92	4.9	1.07	1.01	0.89
	DO (mg/L)	3.98	4.47	4.95	4.76	4.92	5.31	5.63	5.13	5.74	5.24	5.06	6.00	5.92
	NO <sub>3</sub> (μM)	2.81	1.95	0.63	0.81	1.37	3.46	5.68	9.06	9.73	10.93	11.21	9.55	7.43
	PO <sub>4</sub> (μM)	1.85	2.05	1.45	1.12	0.80	0.82	0.35	0.32	0.24	0.24	0.16	0.15	0.19
	SiO <sub>4</sub> (μM)	13.00	20.00	24.00	14.40	16.0	22.00	28.65	28.15	32.30	38.65	37.00	41.25	49.10
	Turbidity (NTU)	4.30	3.90	3.27	3.37	3.40	3.31	3.69	2.21	2.13	1.43	1.48	1.10	1.26
	Chl <i>a</i> (mg m <sup>-3</sup> )	2.3	4.62	4.28	3.64	3.86	6.42	1.95	2.89	1.55	2.1	9.22	2.35	3.05
	MSP (No. m <sup>-3</sup> )	394.9	340.51	654.01	596.1	501.1	318.7	285.1	192.4	99.53	96.8	73.34	67.97	100.7
<b>SWM</b>	Salinity	1.60	0.11	0.15	0.10	0.09	0.34	0.11	0.25	0.08	0.08	0.09	0.08	0.06
	DO (mg/L)	5.78	5.91	5.95	6.01	6.09	6.17	6.2	6.2	6.26	6.7	6.98	7.01	7.06
	NO <sub>3</sub> (μM)	16.96	11.73	12.36	10.80	14.61	12.77	13.32	15.10	18.53	12.20	13.14	10.45	10.36
	PO <sub>4</sub> (μM)	0.37	0.26	0.21	0.29	0.26	0.24	0.24	0.16	0.13	0.17	0.17	0.17	0.19
	SiO <sub>4</sub> (μM)	101.9	92.7	102.7	110.6	113.5	118.5	118.1	114.3	113.3	124.1	124.7	126.2	121.3
	Turbidity (NTU)	10.92	17.37	11.52	4.94	5.28	4.99	4.99	4.98	3.02	2.73	4.15	2.45	1.83
	Chl <i>a</i> (mg m <sup>-3</sup> )	2.9	3	3.17	1.68	2.6	3.5	3.47	2.39	3.41	4.2	2.66	1.63	1.11
	MSP (No. m <sup>-3</sup> )	85.85	73.69	143.17	74.86	76.72	47.82	72.19	91.19	63.42	55.63	16.07	13.22	36.56
<b>PSWM</b>	Salinity	16.4	14.4	12.2	7.58	6.80	6.35	5.65	4.63	2.02	0.64	0.16	0.12	0.12
	DO (mg/L)	4.05	5.09	5.08	4.8	4.09	4.05	4.16	4.85	4.47	4.87	4.92	4.72	4.36
	NO <sub>3</sub> (μM)	4.57	3.1	3.26	8.71	11.99	13.05	12.75	12.06	12.51	13.71	14.46	15.22	12.96
	PO <sub>4</sub> (μM)	1.02	0.99	0.86	0.68	0.64	0.46	0.46	0.43	0.38	0.37	0.28	0.28	0.30
	SiO <sub>4</sub> (μM)	17.80	16.31	16.03	16.56	17.26	19.43	18.88	15.33	16.79	21.04	25.47	21.65	25.41
	Turbidity (NTU)	7.97	7.80	4.79	2.75	2.90	2.72	2.38	2.10	1.90	2.50	2.99	2.06	2.23
	Chl <i>a</i> (mg m <sup>-3</sup> )	2.88	2.69	3.02	2	2.35	2.68	3.8	2.53	1.48	1.96	3.17	6.61	4.2
	MSP (No. m <sup>-3</sup> )	803.3	1866.7	1460.6	483.46	306.86	219.27	288.77	324.76	253.7	222.53	144.30	132.86	146.23

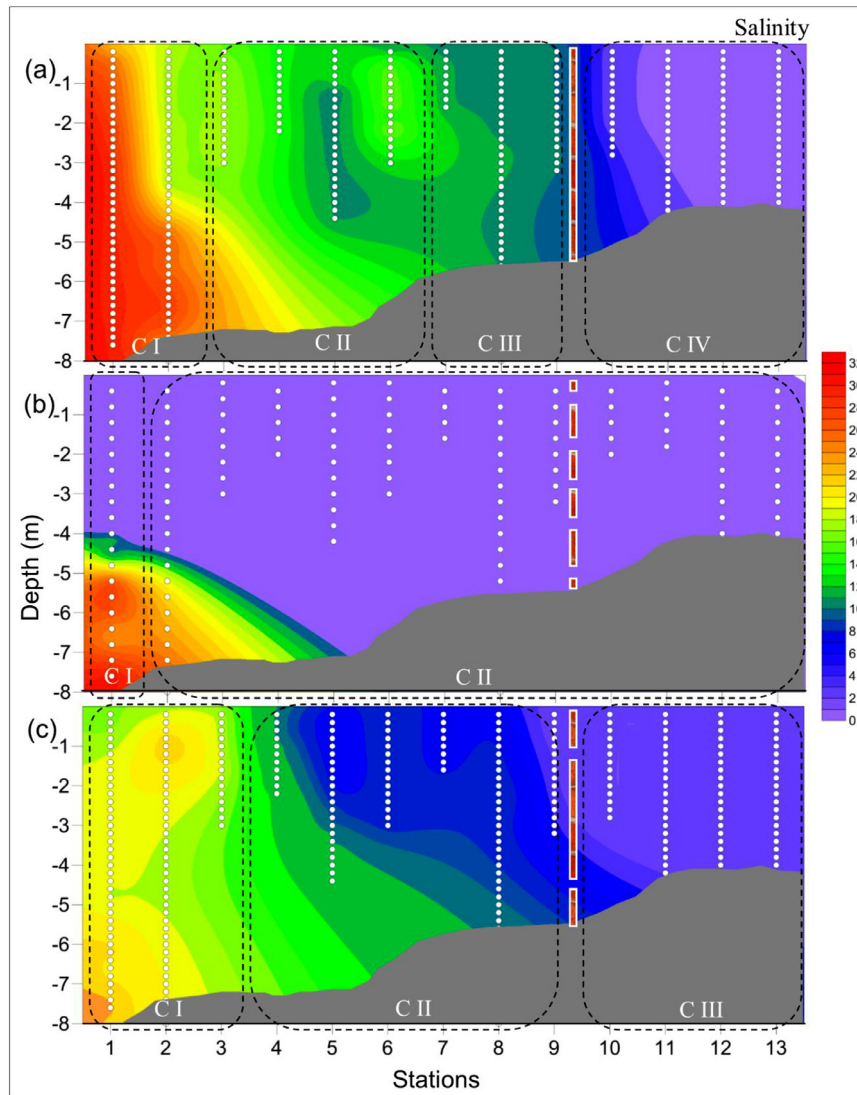


**Figure 2** The distribution of salinity in the Kochi backwaters. Red coloured bricks indicate TB across the Kochi backwaters. (a) Pre-southwest monsoon (PRM): cluster I (C I) indicates downstream polyhaline locations, cluster II (C II) and cluster III (C III) midstream mesohaline locations, and cluster IV (C IV) upstream oligohaline locations. (b) Southwest Monsoon (SWM): cluster I (C I) extreme downstream and cluster II (C II) oligohaline/limnetic condition in the midstream and upstream. (c) Post-southwest monsoon (PSWM): cluster I (C I) was mesohaline downstream locations, cluster II (C II) was mesohaline to oligohaline midstream locations, and cluster III (C III) was limnetic upstream locations.

salinity (av.  $23.7 \pm 3.8$ ), turbidity (av.  $4.1 \pm 0.28$  NTU), rich in phosphate (av.  $1.95 \pm 0.14 \mu\text{M}$ ) and low-silicate (av.  $16.5 \pm 4.9 \mu\text{M}$ ). Cluster II represents the midstream locations with mesohaline salinity (av.  $14.5 \pm 2.1$ ), moderate phosphate (av.  $1.04 \pm 0.3 \mu\text{M}$ ) and turbidity (av.  $3.3 \pm 0.6$  NTU). Cluster III represents the upstream region near to TB (locations 7–9) characterised by mesohaline salinity (av.  $10.46 \pm 0.53$ ), rich in silicate (av.  $29.7 \pm 2.26$ ) and low phosphate (av.  $0.3 \pm 0.05$ ). Cluster IV was in the upstream of KBW (locations 10–14) with oligohaline salinity (av.  $2 \pm 1.9$ ), high silicate (av.  $41.5 \pm 5.3$ ) and low turbidity (av.  $1.3 \pm 0.17$ ). Pairwise comparison test showed that the downstream and midstream clusters varied significantly from the upstream cluster. A comparison of the upstream and downstream regions with salinity, phosphate and turbidity showed a clear

difference during the PRM. In contrast, they were not significant in the case of silicate and nitrate.

During the SWM period, the KBW was entirely freshwater dominated (oligohaline), and spatial variation in salinity was minimum, due to which, no apparent clustering of locations was evident (Figure 4). During the PSWM, three clusters of locations were formed. Cluster I with locations 1 to 3 represented the downstream, cluster II with locations 4 to 9 in the midstream and cluster III with locations 10–13 in the upstream (Figure 5). Cluster I was characterised by mesohaline salinity (av.  $14.3 \pm 2.1$  salinity), moderate turbidity (av.  $6.9 \pm 1.8$  NTU) and phosphate (av.  $0.95 \pm 0.08 \mu\text{M}$ ). Cluster II was characterised by mesohaline to oligohaline levels of salinity (7.58 to 2.02) and low turbidity (av.  $2.4 \pm 0.39$  NTU). Cluster III in the upstream (locations 10–13) was

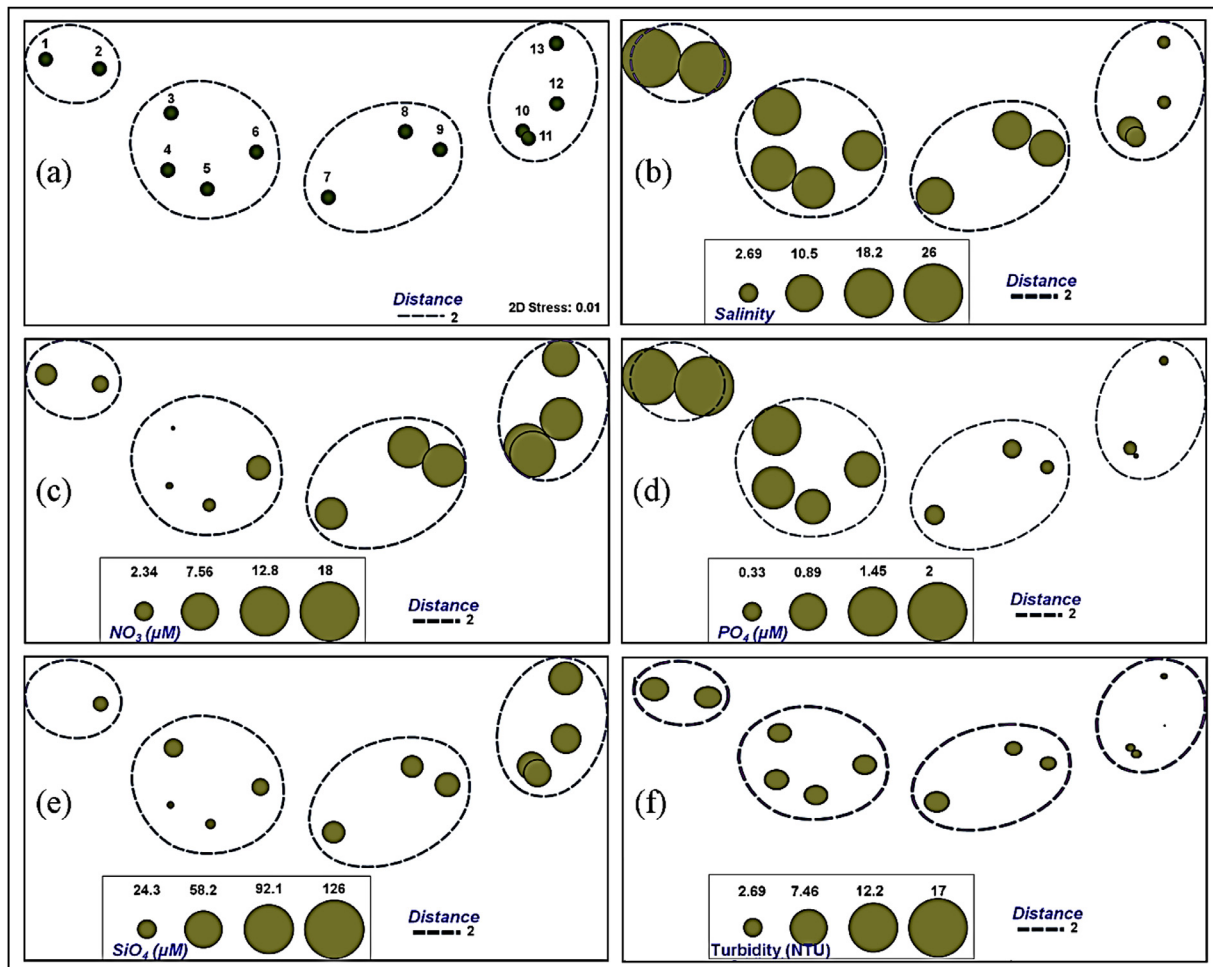


**Figure 3** Grouping of (a) locations based on physicochemical variables in the KBW during the Pre-Southwest Monsoon (PRM). In subsequent panels, the proportionate concentration of (b) salinity, (c) nitrate ( $\text{NO}_3$ ), (d) phosphate ( $\text{PO}_4$ ), (e) silicate ( $\text{SiO}_4$ ) and (f) turbidity have been presented.

limnohaline (av.  $0.26 \pm 0.25$  salinity), less turbid (av.  $2.4 \pm 0.4$  NTU) and low phosphate (av.  $0.3 \pm 0.04 \mu\text{M}$ ).

### 3.3. Biological parameters

#### 3.3.1. Chlorophyll *a* (Chl *a*)

Chl *a* was always in the high concentration range in the KBW. The total Chl *a* distribution in the study area is presented in Table 1. During PRM season total Chl *a* ranged from 1.95 to  $9.22 \text{ mg m}^{-3}$ , during SWM season Chl *a* ranged from 1.11 to  $4.2 \text{ mg m}^{-3}$  and 1.48 to  $6.61 \text{ mg m}^{-3}$  in PSWM. Chl *a* was the lowest in the upstream region during SWM as compared to the other periods. The maximum Chl *a* was noticed ( $9.22 \text{ mg m}^{-3}$ ) during PRM at the upstream region.

#### 3.3.2. Mesozooplankton (MSP) abundance

The total MSP abundance ranged from 13.22 to  $1866 \text{ No m}^{-3}$  (Table 1). During the PRM period, MSP abundances varied from 67.97 to  $654 \text{ No. m}^{-3}$  (Table 1). The mean MSP abundance differed between the cluster locations (Figure 6a) with a maximum in the midstream (cluster II) compared to the downstream (cluster I) or upstream regions (cluster III and IV). During the SWM, the MSP abundance decreased in

the downstream and midstream compared to the PRM period (Figure 6b). During the PSWM period, MSP abundance was high in the downstream (cluster I) compared to midstream (cluster II) and upstream (cluster III) (Figure 6c). During PRM high abundance of MSP was observed in the midstream and during SWM and PSWM it was in the downstream region. Overall, the mesozooplankton abundance was found high in the mesohaline condition, specifically, in salinity levels 10–18 (Figure 6).

#### 3.3.3. Mesozooplankton (MSP) groups

The MSP community was composed of nine groups; Copepods, Cladocera, Decapods larvae, Molluscan larvae, Ostracods, Lucifer's, Chaetognatha, fish eggs and Hydromedusae. The contribution of various groups to the total mesozooplankton abundance differed between space and seasons. During the PRM, copepods were high in the midstream (cluster II) and downstream (cluster I) compared to the upstream locations (Figure 6a). Copepods contributed 49–73% to the total MSP abundance during the PRM. Cladoceran contributed 24–40% and their presence was spatially high in the upstream locations (cluster III and IV) compared to midstream and downstream locations (cluster II and I).

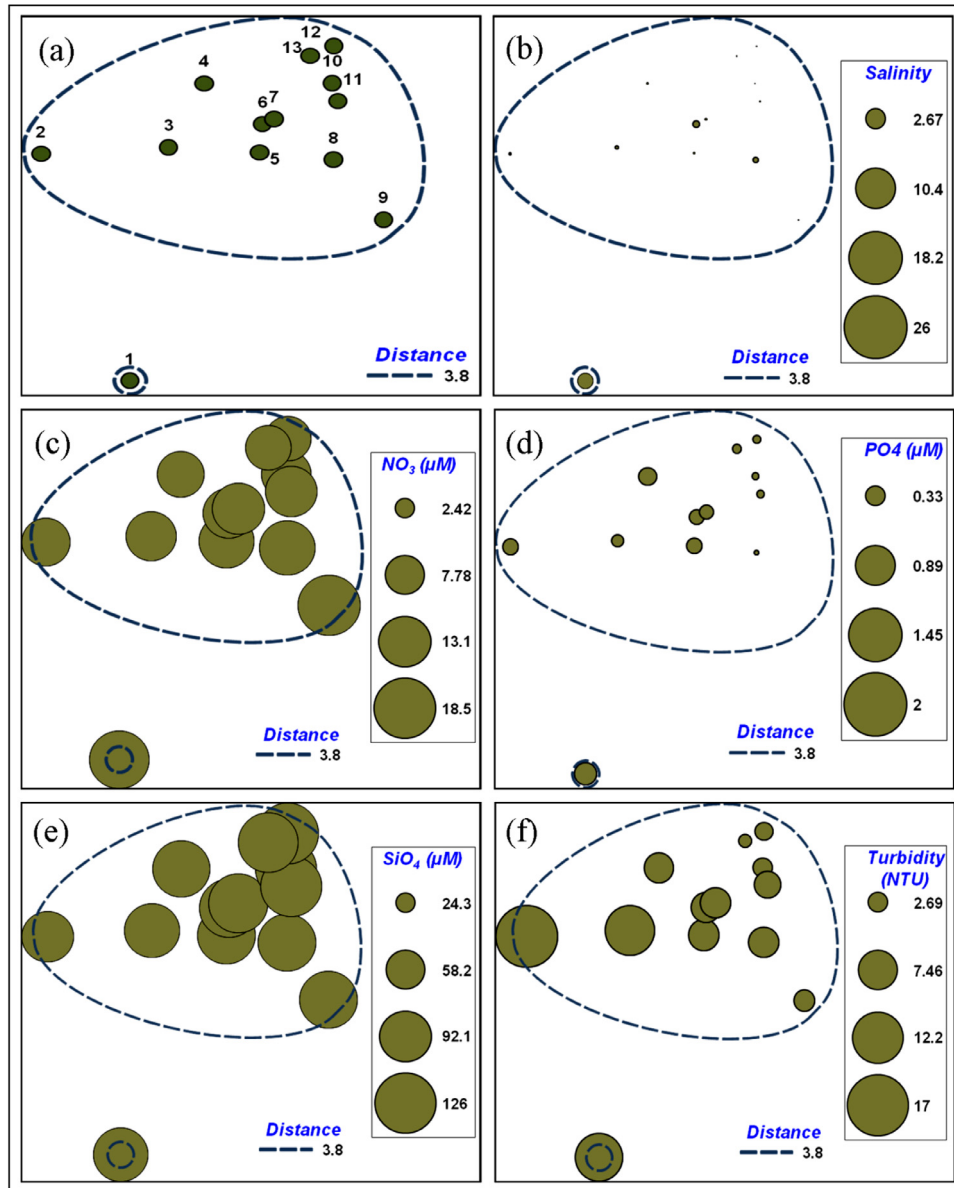


**Figure 4** Grouping of (a) locations based on physicochemical variables in the KBW during the Southwest Monsoon (SWM). In subsequent panels, the proportionate concentration of (b) salinity, (c) nitrate (NO<sub>3</sub>), (d) phosphate (PO<sub>4</sub>), (e) silicate (SiO<sub>4</sub>) and (f) turbidity have been presented.

During the SWM, six groups of MSP were recorded, where copepods varied from 6 to 85 No. m<sup>-3</sup> and contributing 54–58% in total abundance (Figure 6b). During this time, cladocerans contributed 32–37% of the total abundance and were high in upstream locations (cluster II). During the PSWM period, nine MSP groups were recorded. In general, Chaetognatha, hydromedusae and Lucifers were found in the downstream locations during PRM, and PSWM periods, whereas their abundance was completely absent in the KBW during SWM. Chaetognatha, hydromedusae and Lucifers collectively contributed <8% of the total abundance.

#### 3.3.4. Copepod community structure

Out of the 28 copepods species identified during the present study (Table 2), 20 belongs to the order calanoid, 6 to cyclopoid and two species to harpacticoid. Calanoids were

the predominant form in the downstream and midstream regions during the PRM and PSWM; wherein cyclopoids were found dominant in the upstream locations. Some of the species like *Pseudodiaptomus annandalei* and *Acartia plumosa* were found throughout the KBW irrespective of seasons. During PSWM *A. plumosa* was dominated (>50%) and at the same time, there was an incidence of *Acartia* sp., swarm in the downstream (mesohaline) region especially in station 2 and 3.

During PRM, IndVal analysis of copepods showed a significant difference between the cluster assemblages (Table 3). In cluster I copepods, *Acartia centrura*, *Acartia danae*, *Acartia erythraea*, *Acartia southwelli*, *Labidocera acuta*, *Centropages* sp., *Corycaeus* (>80 IndVal) were dominant and appeared as the indicator species of polyhaline downstream region. Similarly, in cluster II, such as *Acartia*

**Table 2** Copepod species abundance during the Pre-Southwest Monsoon (PRM), Southwest Monsoon (SWM) and Post Southwest Monsoon (PSWM) periods in the Kochi back waters. Symbols: + indicates <1%, ++ indicates >1–5%, +++ indicates >5–10%, # indicates >10–20%, ## indicates >20–30%, ### indicates >30–40%, \* indicates >40–50%, \*\* indicates >50–60% and (-) indicates absence.

	Species name	PRM				SWM		PSWM		
		Cluster I	Cluster II	Cluster III	Cluster IV	Cluster I	Cluster II	Cluster I	Cluster II	Cluster III
<b>Copepods</b>	<i>Acartia centrura</i>	++	+	-	-	-	-	+	-	-
	<i>Acartia danae</i>	+++	+	-	-	-	-	+	-	-
	<i>Acartia erythraea</i>	++	-	-	-	-	-	-	-	-
	<i>Acartia plumosa</i>	+++	###	##	+	+++	++	**	###	++
	<i>Acartia southwelli</i>	++	-	-	-	-	-	-	-	-
	<i>Acartia</i> sp.	++	#	++	+	-	-	+++	+++	+
	<i>Acartiella gravelyi</i>	-	-	++	#	#	#	-	++	#
	<i>Acartiella keralensis</i>	-	++	+	++	+++	#	+	++	++
	<i>Acrocalanus gracilis</i>	##	++	-	-	-	-	+++	+	-
	<i>Allodiaptomus mirabilipes</i>	-	-	++	#	+++	+++	-	+++	#
	<i>Allodiaptomus</i> sp.	-	-	+	++	+++	#	-	++	++
	<i>Labidocera acuta</i>	++	+	-	-	-	-	+	-	-
	<i>Centropages</i> sp.	++	+	-	-	-	-	+	-	-
	<i>Heliodiaptomus cinctus</i>	-	-	*	+++	+++	+++	-	++	+++
	<i>Limnocalanus macrurus</i>	-	-	-	+++	+++	#	-	+	+++
	<i>Paracalanus</i> sp.	+++	+	-	-	-	-	++	+	-
	<i>Paracalanus parvus</i>	+++	++	-	-	-	-	++	+	-
	<i>Pseudodiaptomus annandalei</i>	+++	###	#	++	++	++	#	##	++
	<i>Pseudodiaptomus serricaudatus</i>	++	+++	-	-	++	+	++	+	-
	<i>Pseudodiaptomus bingami malayalus</i>	-	-	++	++	++	++	-	++	++
	<i>Corycaeus</i> sp.	#	+	-	-	-	-	++	-	-
	<i>Nitocra</i> sp.	-	++	++	-	++	-	+	++	-
	<i>Euterpina acutifrons</i>	++	++	-	-	++	-	++	+	-
	<i>Oithona rigida</i>	+++	++	-	-	-	-	++	+	-
	<i>Oithona brevicornis</i>	++	++	-	-	-	-	++	+	-
	<i>Thermocyclops</i> sp.	-	-	-	++	#	#	-	+	++
<i>Mesocyclops</i> sp.	-	-	++	#	#	#	-	++	#	
<i>Microcyclops</i> sp.	-	-	++	##	+++	#	-	++	##	

**Table 3** Copepods Indicator species (IndVal analysis) in each cluster assemblages during the Pre-Monsoon (PRM) and Post-Southwest Monsoon (PSWM) periods.

	Cluster 1		Cluster II		Cluster III		Cluster IV	
	Species name	IndVal	Species name	IndVal	Species name	IndVal	Species name	IndVal
<b>PRM</b>	<i>Acartia centrura</i>	90.5	<i>Acartia plumosa</i>	72.5	<i>Heliodiaptomus cinctus</i>	51.2	<i>Acartiella gravely</i>	83.7
	<i>Acartia danae</i>	83.6	<i>Acartia</i> sp.	86.9			<i>Allodiaptomus mirabilipes</i>	83.1
	<i>Acartia erythraea</i>	100	<i>Acartiella keralensis</i>	61.6			<i>Allodiaptomus</i> sp.	95.5
	<i>Acartia southwelli</i>	100	<i>Pseudodiaptomus annandalei</i>	64.9			<i>Limnocalanus macrurus</i>	100
	<i>Acrocalanus gracilis</i>	69.0	<i>Pseudodiaptomus serricaudatus</i>	88.0			<i>Thermocyclops</i> sp.	100
	<i>Labidocera acuta</i>	81.4	<i>Nitocra</i> sp.	58.1			<i>Mesocyclops</i> sp.	90.4
	<i>Centropages</i> sp.	95.6	<i>Euterpina acutifrons</i>	72.8			<i>Microcyclops</i> sp.	93.8
	<i>Paracalanus</i> sp.	70.0	<i>Oithona brevicornis</i>	65.9				
	<i>Paracalanus parvus</i>	53.9						
	<i>Corycaeus</i>	90.3						
	<i>Oithona rigida</i>	51.4						
	<b>PSWM</b>	<i>A. centrura</i>	50	<i>Allodiaptomus mirabilipes</i>	63.0	<i>Acartiella gravely</i>	65.7	
<i>Acartia plumosa</i>		84.4	<i>Heliodiaptomus cinctus</i>	63.2	<i>Allodiaptomus</i> sp.	52.1		
<i>Acartia</i> sp.		77.9			<i>Limnocalanus macrurus</i>	78.5		
<i>Acrocalanus gracilis</i>		100			<i>Thermocyclops</i> sp.	54.7		
<i>Labidocera acuta</i>		50			<i>Mesocyclops</i> sp.	79.2		
<i>Centropages</i> sp.		50			<i>Microcyclops</i> sp.	87.4		
<i>Paracalanus</i> sp.		100						
<i>Paracalanus parvus</i>		100						
<i>Pseudodiaptomus annandalei</i>		59.7						
<i>Pseudodiaptomus serricaudatus</i>		100						
<i>Corycaeus</i>		50						
<i>Euterpina acutifrons</i>		94.3						
<i>Oithona rigida</i>		96.0						
<i>Oithona brevicornis</i>		96.8						

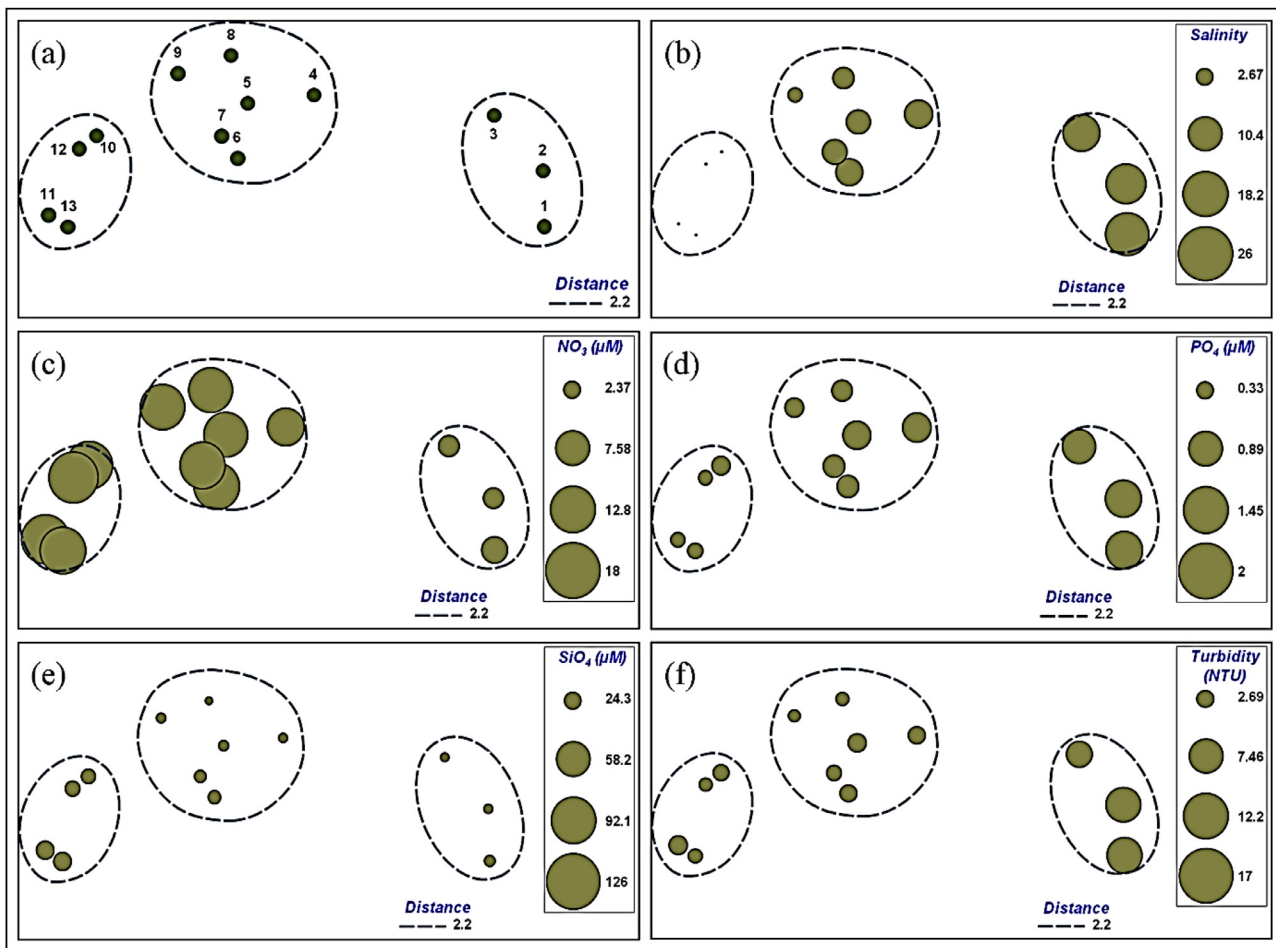


**Figure 5** Grouping of (a) locations based on physicochemical variables in the KBW during the Post-Southwest Monsoon (PSWM). In subsequent panels, the proportionate concentration of (b) salinity, (c) nitrate ( $\text{NO}_3$ ), (d) phosphate ( $\text{PO}_4$ ), (e) silicate ( $\text{SiO}_4$ ) and (f) turbidity have been presented.

sp., *Pseudodiaptomus serricaudatus* represents the indicators of mesohaline midstream region. In the other hand, *Heliodyptomus cinctus* was predominated in the cluster III mesohaline (locations 7–9) region. And in cluster IV, *Acartiella gravelyi*, *Allodiaptomus mirabilipes*, *Allodiaptomus* sp., *Limnocalanus macrurus*, *Thermocyclops* sp., *Mesocyclops* sp., *Microcyclops* sp., (>80 IndVal) represented the oligohaline indicator species in the upstream region. During the SWM period, copepod species composition and abundance were almost the same over the entire stretch of the KBW, and therefore no specific indicator species was not evident in IndVal analyses. During the PSWM, In cluster I, *A. plumosa*, *Acrocalanus gracilis*, *Paracalanus* sp., *Paracalanus parvus*, *Pseudodiaptomus serricaudatus*, *Euterpina acutifrons*, *Oithona rigida* and *Oithona brevicornis* were indicative copepod species and represents the mesohaline downstream region; in cluster II *A. mirabilipes* and *H. cinctus* represented as intermediate species, which characterised as mesohaline to oligohaline levels of salinity in the midstream locations; and in cluster III, species such as *Mesocyclops* sp., *Microcyclops* sp., were dominated and represented in the limn haline upstream region (Table 3).

### 3.4. Regions of high MSP/copepod abundance and diversity

Multivariate RDA was performed to identify the hydrographical conditions, which was the most favouring environment to the mesozooplankton abundance and copepods community structure in the KBW. Salinity, nutrients (nitrate, silicate, phosphate) and turbidity were found to influence the copepods community structure, even though salinity as the significant factor which is explaining 38% variance during PRM and PSWM periods. And Monte Carlo significance test showed that the ordination pattern was substantial during the PRM and PSWM periods (Figure 7). During the PRM period, the downstream locations showed (cluster I) high saline and turbidity, which is declined towards the upstream locations that evident in the RDA triplot. The mesohaline region can be identified in the cluster II midstream locations, which shows in the lower right side of RDA, nitrate and silicate axes were oriented just opposed to salinity and phosphate that indicating their inverse relationship. The salinity values overlaid in the RDA plot shows the cluster I downstream locations had polyhaline salinity levels while

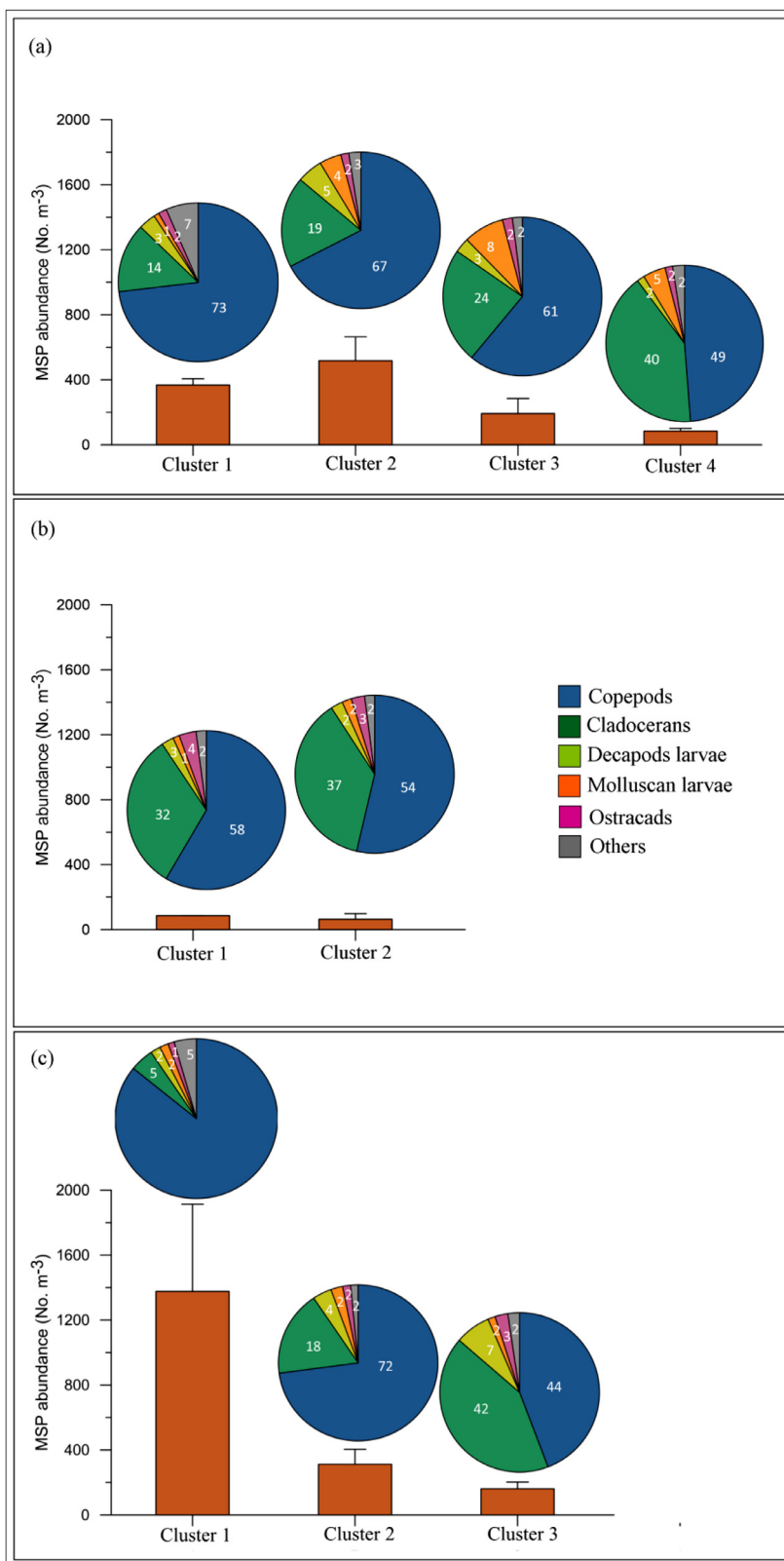


**Figure 6** The total MSP abundance (bars) and their group composition (pie chart) in various clusters during (a) Pre-Southwest Monsoon (PRM), (b) Southwest Monsoon (SWM) and (c) Post-Southwest Monsoon (PSWM). Cluster locations are in accordance with Figure 2. Mean – bar chart; error bars – standard deviation.

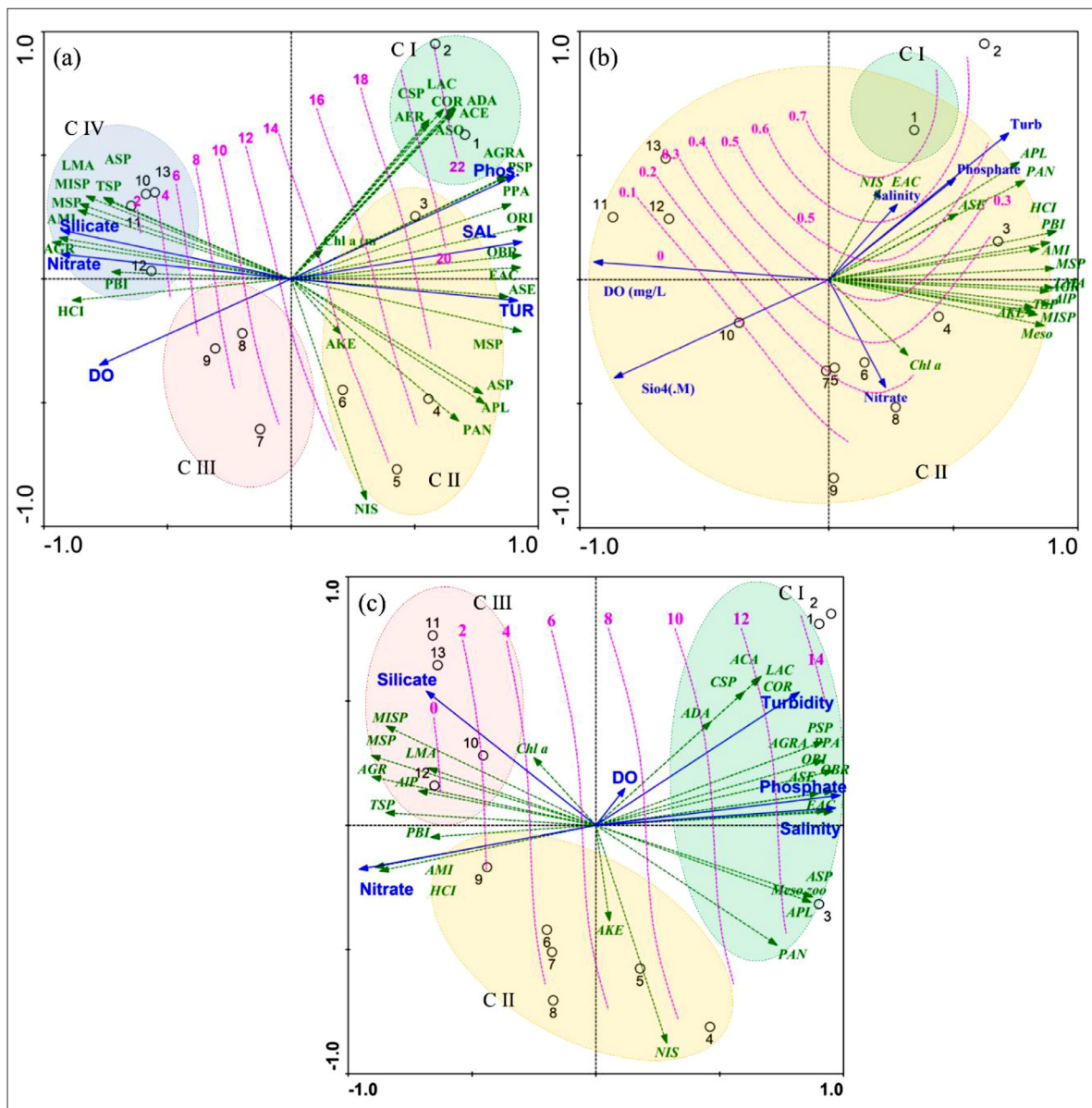


**Figure 7** RDA triplot showing the distribution and interrelationships of environmental and biological parameters during (a) Pre-Southwest Monsoon (PRM), (b) Southwest Monsoon (SWM) and (c) Post-Southwest Monsoon (PSWM). The overlaid attribution contours (pink dotted line and values) represent the spatial distribution of salinity and its relationship with other environmental and biological components. Biological and environmental parameters are displayed by arrows; the blue-dotted arrows indicate the former, and the green arrows the latter. Abbreviations: SAL – Salinity; Tur – Turbidity; Chl a – Chlorophyll a; DO – Dissolved Oxygen; MSP – Mesozooplankton. *Acartia centrura* (ACA), *Acartia danae* (ADA), *Acartia erythraea* (AER), *Acartia plumosa* (APL), *Acartia southwelli* (ASO), *Acartia* sp. (ASP), *Acartiella graveleyi* (AGR), *Acartiella keralensis* (AKE), *Acrocalanus gracilis* (AGRA), *Allodiaptomus mirabilipes* (AMI), *Allodiaptomus* sp. (AIP), *Labidocera acuta* (LAC), *Centropages* sp. (CSP), *Heliodiaptomus cinctus* (HCI), *Limnocalanus macrurus* (LMA), *Paracalanus* sp. (PSP), *Paracalanus parvus* (PPA), *Pseudodiaptomus annandalei* (PAN), *Pseudodiaptomus serricaudatus* (ASE), *Pseudodiaptomus bingami malayalus* (PBI), *Corycaeus* (COR), *Nitochara* sp. (NIS), *Euterpina acutifrons* (EAC), *Oithona rigida* (ORI), *Oithona brevicornis* (OBR), *Thermocyclops* sp. (TSP), *Mesocyclops* sp. (MSP), *Microcyclops* sp. (MISP). C I indicates cluster I, C II cluster II, C III cluster III and C IV cluster IV.

the cluster II, midstream locations are mesohaline. In the upstream, salinity variations were evident nearby TB locations. Upstream locations (7–9) near to TB was mesohaline salinity levels (Av.  $10.5 \pm 0.5$  salinity), whereas the upstream locations (10–13) was oligohaline levels of salinity (4.9–0.9). The high salinity and phosphate in the downstream could be due to tidal activity and wa-

ter circulation. The prevalence of oligohaline salinity conditions in the locations 10–13 and mesohaline conditions in the locations (7–9) of KBW is the clear evidence of the hydraulic barrage (TB) in preventing salinity incursion towards upstream.

During PRM, MSP was oriented to the right side in RDA plot overlaid on salinity indicating their preference to the

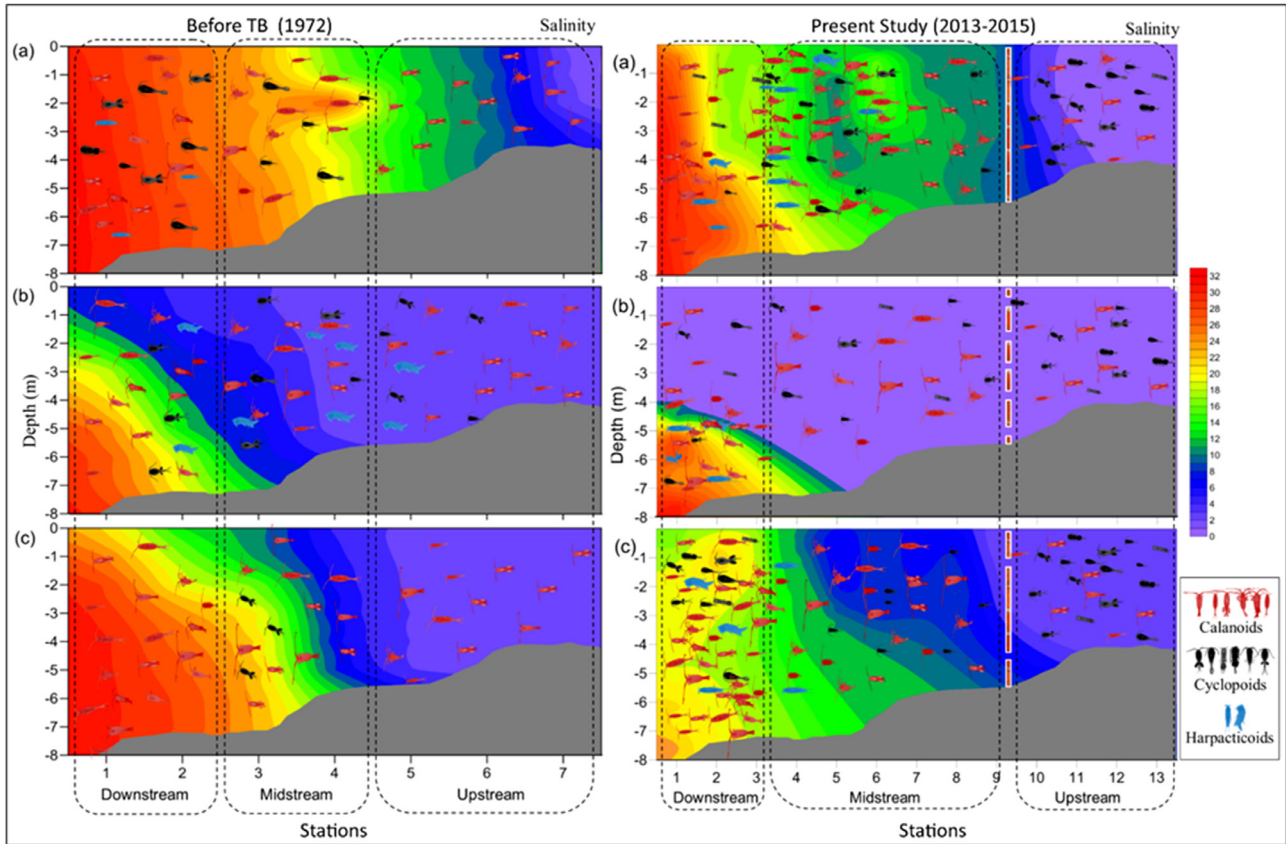


**Figure 8** Comparison of salinity levels and copepods distribution in 1972 (before TB) and in the present study in the KBW. (a) Pre-Southwest Monsoon (PRM), (b) Southwest Monsoon (SWM) and (c) Post-Southwest Monsoon (PSWM) season. Salinity distribution before TB is based on Haridas et al. (1973).

mesohaline region. RDA triplot clearly shows that copepods species composition varied spatially with the variation of salinity in the KBW. In the cluster I, the copepod species such as *A. centrura*, *A. danae*, *L. acuta*, *Centropages* sp., *Corycaeus*, *A. erythraea*, *A. southwelli*, *A. gracilis*, *Paracalanus* sp., *P. parvus*, and *O. rigida*, species are oriented top right side of the plot represents their high abundance in polyhaline salinity, which prevails in the extreme downstream locations (1 and 2). And the other copepod species in the cluster II, *Acartiella keralensis*, *A. plumosa*, *Acartia* sp., *P. annandalei*, *P. serricaudatus*, *Nitocra* sp., *O. brevicornis* and *E. acutifrons* oriented to the right side of the plot indicates their preference to the mesohaline condition in the midstream. Similarly in cluster IV, upstream locations species such as *Thermocyclops* sp., *Microcyclops* sp., *Mesocyclops* sp., *A. gravelyi*, *A. mirabilipes*, *L. macrurus* and *Allodiaptomus* sp., oriented to the left side of the plot and opposite the salinity that indicates oligohaline is their favourable condition (Figure 7). Cluster III oriented to the lower left side of the plot and separated from cluster IV shows the marked difference in their copepods composition. However, cluster III (locations 7–9) has a close affinity with cluster II (locations 3–6) indicating both of them in mesohaline conditions.

During the SWM, the entire study area was dominated by freshwater when limnohaline condition prevailed everywhere except in the extreme downstream. Therefore, there

was no clear pattern in the distribution of copepods during the SWM. Salinity was less discernible during the SWM due to the predominance of freshwater in the entire KBW. During the PSWM, the RDA plot demarcated clear spatial difference in the hydrographical parameters and copepod community structure. Salinity and turbidity were spatially high in the downstream, and their increasing gradients were oriented to the right side of the plot. Salinity overlay showed that the downstream locations had mesohaline, which decreased towards the upstream locations. Copepods total abundance was found to be in higher abundance in the downstream region, and these parameters were oriented in the right side of the plot with mesohaline. Copepods species composition varied widely during PSWM relation to salinity as evident in the triplot. The copepods species *A. centrura*, *Acartia* sp., *A. plumosa*, *A. kerlelensis*, *L. acuta*, *Centropages* sp., *Corycaeus*, *Paracalanus* sp., *A. gracilis*, *P. parvus*, *O. rigida*, *O. brevicornis*, *P. serricaudatus*, *E. acutifrons* and *P. annandalei* species were oriented to the right side of the plot that representing the cluster I locations in the mesohaline condition. On the other hand, in cluster II of midstream locations, copepods *Microcyclops* sp., *Mesocyclops* sp., *L. macrurus*, *A. gravelyi*, *Allodiaptomus* sp., *Thermocyclops* sp., *A. mirabilipes* and *H. cinctus* were oriented to the left side of the plot showing their affinity to oligohaline to limnohaline conditions (Figure 7). It is noteworthy that during PRM and PSWM seasons, the downstream, midstream and

upstream regions of the KBW has a significant difference in copepod species composition. RDA triplot clearly showed that copepods composition was always high in the mesohaline level of salinity, especially in salinity ranges 10–15, during the PRM and PSWM period. This mesohaline condition in the KBW persisted in the midstream during the PRM and downstream during the PSWM period.

#### 4. Discussion

The prevalence of polyhaline conditions in the downstream and oligohaline/limnohaline conditions in the upstream of KBW due to TB seems to have a substantial impact on the MSP and copepod community structure. Salinity distribution in the KBW was spatially distinct during PRM and PSWM (Figure 2a) due to the progressive increase in the tidal activity (Jyothibabu et al., 2006; Qasim, 2003). Mesohaline condition prevailed in the downstream during the PSWM, which changed to polyhaline during the PRM. During the PSWM period, the midstream, was oligohaline to mesohaline, whereas the upstream remained limnohaline, which turned to oligohaline during PRM (Figure 2). Previous studies have established that KBW is highly influenced by seawater intrusion during the PRM and PSWM and massive freshwater incursion during the SWM (Madhupratap, 1987; Menon et al., 2000; Qasim, 2003). For clear understand the current situation the present study surface salinity values were compared with the salinity values of Haridas et al., (1973) whom was reported in 1972 before the construction of TB (Figure 8). In his study during PRM salinity values varied from 8 to 31 and the maximum value was reported in downstream euhaline region and low in the upstream mesohaline region; during SWM ranged from 0.2 to 6.5 and during PSWM salinity was ranged from 0.3 to 23.5. The present salinity levels in the upstream region of the KBW show around 11 units drop during the PRM and 1 unit drop during PSWM compared to the historical times. Such a drop in salinity caused by TB altered the plankton functional groups in the KBW (Anjusha et al., 2018; Arunpandi et al., 2020; Haridevan et al., 2015).

Dissolved oxygen (DO) levels were high in the upstream with a minimum variation on either side of TB. DO was seasonally high during SWM (Table 1) and decreased lightly after that, following the pattern presented in Sooria et al., (2015). Turbidity is an indicator of estuarine conditions like flooding or re-suspension (Anon, 2001). Turbidity was always maximum in the downstream compared to midstream and upstream (Table 1). During the PRM period, turbidity was high in the downstream compared to midstream and upstream, which coincided with the estuarine turbidity maximum (Menon et al., 2000; Sooria et al., 2015). The KBW turbidity was generally high during the SWM period followed by PSWM and PRM. During the SWM season, turbidity in the KBW increased by 2–3 folds compared to the PRM, due to increased land runoff (Nasir, 2010).

Nitrate concentration did not show a definitive distribution pattern though it was relatively high in the upstream locations than the downstream. During the SWM, nitrate concentration was high in the entire stretch of KBW compared to PSWM and PRM (Figure 3c, 4c and 5c). In the downstream, silicate concentration was five-folds higher during the SWM

compared to PRM period, especially towards the upstream locations compared to the downstream and middle estuary. The four rivers emptying into the upstream are sources of high nutrient levels in the KBW system irrespective of the seasons (Jyothibabu et al., 2006; Mohan et al., 2016; Qasim, 2003). There seem to be some non-point sources of nitrogen input (Arunpandi et al., 2017; Jagadeesan et al., 2016; Jyothibabu et al., 2006; Saraladevi et al., 1983; Sooria et al., 2015). The phosphate concentration was high in the downstream but decreased towards the upstream region. Compared to PRM, phosphate concentration decreased during the SWM in the entire stretch of KBW. The phosphate level in the KBW was the seasonal highest during the PRM due to high salinity and desorption of phosphate from the suspended particles (Martin et al., 2008; Sooria et al., 2015). Seasonal variations in the biological components of KBW closely followed the salinity variations (Madhupratap, 1987) with enhanced Chl *a* in regions of high nutrients (Arunpandi et al., 2020; Jyothibabu et al., 2006; Madhu et al., 2007a,b).

During the PRM, MSP abundance was high in the midstream compared to downstream and upstream. MSP abundance was minimum in the upstream compared to the downstream. However, during the SWM, MSP abundance decreased in the downstream and midstream compared to PRM period (Figure 6a), which was in accordance to earlier studies (Madhupratap, 1987; Wellershaus, 1974). It is likely that during SWM, the high freshwater flow physically pushes MSP to the downstream region (Sooria et al., 2015). During the PSWM, MSP abundance was higher in the upstream compared to the midstream and upstream (Figure 6c). It also clear that calanoid was the dominant copepod in the midstream and downstream, whereas cyclopoid dominated in the upstream.

Madhupratap and Haridas (1975) had presented the mesozooplankton composition in the KBW based on a study carried out in 1972 when there was no TB. The MSP total abundance in the KBW in the upstream during PRM, south of the presents TB, was from 246.6 to 505.2 No m<sup>-3</sup> and during PSWM was from 1 to 227.7 No m<sup>-3</sup>. In the present study, it is found significantly low, i.e., from 67.9 to 100.7 No m<sup>-3</sup> during PRM and from 144.3 to 222 No m<sup>-3</sup> during PSWM. Moreover, a significant variation in the composition of various MSP groups is evident in these studies. Overall, the seasonal copepod percentage contribution in the present study (PRM – 62%, SWM – 56% and PSWM – 67%), was remarkably higher than those presented in Madhupratap and Haridas (1975) which was 26%, 17% and 36%, respectively. Besides, cyclopoid copepods were found less in the upstream region, and calanoids are found dominant during PRM and PSWM before TB was functional (Madhupratap and Haridas, 1975). But cyclopoids were found dominant in the upstream region in the present study (Figure 8). In short, the MSP distribution shows that TB has a profound influence on the MSP composition and copepods species distribution, since the barrage imposes restrictions on natural flow pattern and significantly alters the salinity levels in the KBW.

There are some past studies available on the salinity tolerance of copepods in the KBW (Madhupratap and Haridas, 1975; Madhupratap, 1979; Martin Thompson, 1991; Tranter and Abraham, 1971; Vineetha et al., 2015). Tranter and Abraham (1971) observed *Acartia bilobata*, *A. centrura*,

*Acartia spinicauda*, *A. gravelyi* in saline conditions and *A. erythraea*, and *A. southwelli* in the high saline downstream region of KBW. Similarly, species such as *A. keralensis* and *Acartia negligens* were recorded in low saline regions during SWM, while *Acartia plumosa* was present throughout the year. Madhupratap (1979) reported that *P. annandalei* has a salinity tolerance up to 35 units, while other species such as *Accrocalanus similis*, *Acartia bowmani*, *A. centrura* and *A. bilobata* have less tolerance to salinity and they prefer the midstream of the KBW during the high saline period. During the SWM, copepods *H. cinctus*, *A. mirabilipes*, *A. gravelyi*, *Pseudodiaptomus binghami malayalus*, *O. brevicornis*, *O. hebes* and *O. nana* were found in the low salinity (limnohaline) upstream region. And also *Acartia* spp., *Paracalanus aculeatus*, *P. crassirostris*, *P. serricaudatus* and *P. jonesi* were found in high saline condition while *Acartia pacifica* and *A. southwelli* in extreme downstream of KBW. When compared the present study with Martin Thompson (1991), it was observed that both the studies have recorded almost similar copepods composition in different parts of the KBW.

However, the present study is the first attempt to scientifically assess the changes in the distribution and composition of MSP/ copepods community in the KBW due to the hydrographical changes imparted by TB during non-monsoon periods. The results show that copepods species showed significant zonal variations in the KBW due to the closure of TB. Statistical results also revealed salinity as the primary factor controlling the distribution and abundance of copepods in the KBW. It was also found that copepod *A. centrura*, *A. danae*, *L. acuta*, *Centropages* sp., *Corycaeus*, *A. erythraea*, *A. southwelli*, *Acrocalanus gracilis*, *Paracalanus* sp., *P. parvus*, *E. acutifrons*, *O. rigida* and *O. brevicornis* have preferred the polyhaline regions of KBW (downstream), whereas *A. keralensis*, *A. plumosa*, *Mesocyclops* sp., *Acartia* sp., *P. annandalei*, *P. pseudodiaptomus serricaudatus* and *Nitocra* sp.) have preferred the mesohaline (5–18 salinity) regions. On the other hand, copepods *Acartia* sp., *L. macrurus*, *Thermocyclops* sp., *Microcyclops* sp., *Mesocyclops* sp., *Acartiella gravelyi* and *A. mirabilipes* preferred the oligohaline (0.5–5 salinity) conditions. Since the TB remains open during the SWM, the entire KBW was freshwater dominated exhibiting less spatial variations in copepod composition and abundance.

Even during the PSWM period onwards, the copepod population thriving in the upstream was found to relocate towards the downstream for the mesohaline salinity. For eg.: *A. centrura*, *A. danae*, *Acartia* sp., *A. plumosa*, *A. keralensis*, *L. acuta*, *Centropages* sp., *Corycaeus*, *Paracalanus* sp., *A. gracilis*, *P. parvus*, *O. rigida*, *O. brevicornis*, *P. serricaudatus*, *E. acutifrons* and *P. annandalei* were found to relocate towards downstream, resulting in the retention of limnohaline and oligohaline tolerant species (*Microcyclops* sp., *Mesocyclops* sp., *L. macrurus*, *A. gravelyi*, *Allodiaptomus* sp., *Thermocyclops* sp., *Pseudodiaptomus binghami malayalus*, *A. mirabilipes* and *H. cinctus*) in the upstream. The shift in the niche of copepods to downstream of KBW has an impact on the biological productivity pattern and its conversion to higher trophic levels. The entire KBW was reported to be biologically productive, especially during the non-monsoon periods, due to the increase in the salinity. However, the natural seawater intrusion was prevented by the construction of TB. The closure of the barrage has cre-

ated a stagnant freshwater body (of ~80 km<sup>2</sup>) in the upstream region, where it disconnected from the hydrodynamic processes in the KBW. The significant spatial shift in the copepods species (IndVal analysis) is clear evidence showing how artificial barrages can alter the natural biological assemblages in an ecosystem.

## 5. Conclusion

This study presented the seasonal hydrographical settings and the MSP/copepod assemblages in the KBW. It shows that Thanneremukam barrage (TB) has a measurable impact on the distribution of mesozooplankton/copepods during the non-monsoon period. TB restricts the water flow and prevents the incursion of saline water into the upstream region, and alters the copepod community in different sections of the KBW. Copepods community in the KBW as a whole favoured mesohaline salinity levels (especially ~10–18 salinity). This study showed that several copepods performed a spatial shift in their preferred habitat due to the flow restrictions in the KBW caused by TB. The statistical results revealed salinity as the most significant environmental variable that controls the composition, distribution and abundance of copepods in the KBW. The flow inhibition of TB in the upstream of the KBW was reflected in a remarkable change in the copepod composition. Hence, this study proposes copepods as an effective bioindicator to monitor changes in hydrographical settings in the natural aquatic ecosystem by artificial barrages.

## Acknowledgements

The authors thank the Director, CSIR – National Institute of Oceanography (CSIR-NIO), India, for facilities and support. We thankfully acknowledge all of our colleges in National Institute of Oceanography, India who helped in carrying out the fieldwork. The first author acknowledges the Department of Science and Technology (DST) for providing him DST-INSPIRE Fellowship (IF120804). This is NIO contribution 6613.

## References

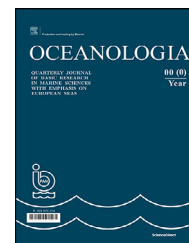
- Achari, G.P., 1988. Induced breeding and early development of *Villorita cyprinoides* Var *cochinensis* with comments on hatchery system. CMFRI Bull. 42, 344–348.
- Anjusha, A., Jyothibabu, R., Jagadeesan, L., Arunpandi, N., 2018. Role of rotifers in microzooplankton community in a large monsoonal estuary (Cochin backwaters) along the west coast of India. Environ. Monit. Assess. 190, art. no. 295.
- Anon, 2001. Ecology and fisheries investigation in Vembanad Lake. CIFRI Bull 07, 38 pp.
- Arun, A.U., 2009. An assessment on the influence of salinity in the growth of black clam (*Villorita cyprinoides*) in cage in Cochin Estuary with a special emphasis on the impact of Thanneermukkom salinity barrier. Aquacult. Aquarium Conserv. Legis. 2, 319–330.
- Arunpandi, N., Jyothibabu, R., Jagadeesan, L., Gireeshkumar, T.R., Karnan, C., Naqvi, S.A., 2017. *Noctiluca* and copepods grazing on the phytoplankton community in a nutrient-enriched coastal

- environment along the southwest coast of India. *Environ. Monit. Assess.* 189, art. no. 351.
- Arunpandi, N., Jyothibabu, R., Jagadeesan, L., Albin, K.J., Savitha, K.M., Parthasarathi, S., 2020. Impact of salinity on the grazing rate of a cladocera (*Latonopsis australis*) in a large tropical estuarine system. *Environ. Monit. Assess.* 192 (2), 1–3.
- Buyukates, Y., Roelke, D., 2005. Influence of pulsed inflows and nutrient loading on zooplankton and phytoplankton community structure and biomass in microcosm experiments using estuarine assemblages. *Hydrobiologia* 548, 233–249.
- Chen, M., Chen, B., Harrison, P.J., Liu, H., 2011. Dynamics of meso-zooplankton assemblages in subtropical coastal waters of Hong Kong: a comparative study between a eutrophic estuarine and a mesotrophic coastal site. *Cont. Shelf Res.* 31, 1075–1086. <https://doi.org/10.1016/j.csr.2011.03.011>
- Conway, D.V.P., White, R.G., Hugues-Dit-Ciles, J., Gallienne, C.P., Robins, D.B., 2003. Guide to the coastal and surface zooplankton of the South-Western Indian Ocean. *Occas. Publ. Mar. Biol. Assoc.* 15, 356 pp.
- Dufrene, M., Legendre, P., 1997. Species assemblages and indicator species: the need for a flexible asymmetrical approach. *Ecol. Monogr.* 67 (3), 345–366.
- Froneman, P.W., 2004. Zooplankton community structure and biomass in a southern African temporarily open/closed estuary. *Estuar. Coast. Shelf Sci.* 60, 125–132.
- Gardner, G.A., Szabo, I., 1982. British Columbia pelagic marine copepoda. *Dept. Fisher. Ocean., Ottawa* 313–334.
- Gopalan, U.K., 1991. *Kayal Nammude Sampath*. Kerala Shashtra Sahitya Parishad, Kozhikode.
- Grasshoff, K., Ehrhardt, M., Kremling, K., 1983. *Methods of seawater analysis*. Verlag Chemie GmbH, Weinheim, 600 pp.
- Haridas, P., Pratap, M.M., Rao, T.S.S., 1973. Salinity, temperature, oxygen and zooplankton biomass of the backwaters from Cochin to Alleppey. *Indian J. Geo-Mar. Sci.* 2, 94–102.
- Haridevan, G., Jyothibabu, R., Arunpandi, N., Jagadeesan, L., Biju, A., 2015. Influence of salinity on the life table demography of a rare Cladocera *Latonopsis australis*. *Environ. Monit. Assess.* 187, art. no. 643.
- Hunt, B.P.V., Hosie, G.W., 2006. The seasonal succession of zooplankton in the Southern Ocean south of Australia. part I: the seasonal ice zone. *Deep Sea Res. PT I: Oceanogr. Res. Pap.* 53, 1182–1202.
- Jagadeesan, L., Jyothibabu, R., 2016. Tumour-like anomaly of copepods-an evaluation of the possible causes in Indian marine waters. *Environ. Monit. Assess.* 188, art. no. 244.
- Jyothibabu, R., Madhu, N.V., Jayalakshmi, K.V., Balachandran, K.K., Shiyas, C.A., Martin, G.D., Nair, K.K.C., 2006. Impact of freshwater influx on microzooplankton mediated food web in a tropical estuary (Cochin backwaters India). *Estuar. Coast. Shelf Sci.* 69, 505–518.
- Kannan, K.P., 1979. Ecological and socio-economic consequences of water-control projects in the Kuttanad region of Kerala. *Proc. Indian Acad. Sci. C: Eng. Sci.* 2, 417–433.
- Kasturirangan, L.R., 1963. In: *A Key for the Identification of the More Common Planktonic Copepoda: Of Indian Coastal Waters: Indian National Committee on Oceanic Research, Publ. No. 2. Pubs. Counc. Scient. Indust. Res. (C.S.I.R.), New Delhi, India*, 1–87.
- Kibirige, I., Perissinotto, R., 2003. The zooplankton community of the Mpenjati Estuary, a South African temporarily open/closed system. *Estuar. Coast. Shelf Sci.* 58, 727–741.
- Kurup, B.M., Sebastian, M.J., Sankaran, T.M., Rabindranath, P., 1990. Exploited fishery resources of the Vembanad Lake. Part III. Clam fisheries. *Mahasagar* 23, 127–137.
- Leps, J., Smilauer, P., 2003. *Multivariate analysis of ecological data using CANOCO*. Cambridge Univ. Press.
- Mackey, M.D., Mackey, D.J., Higgins, H.W., Wright, S.W., 1996. CHEMTAX-a program for estimating class abundances from chemical markers: application to HPLC measurements of phytoplankton. *Mar. Ecol. Prog. Ser.* 144, 265–283.
- Madhu, N.V., Balachandran, K.K., Martin, G.D., Jyothibabu, R., Thottathil, S.D., Nair, M., Joseph, T., Kusum, K.K., 2007a. Short-term variability of water quality and its implications on phytoplankton production in a tropical estuary (Cochin backwaters India). *Environ. Monit. Assess.* 170, 287–300.
- Madhu, N.V., Jyothibabu, R., Balachandran, K.K., Honey, U.K., Martin, G.D., Vijay, J.G., Shiyas, C.A., Gupta, G.V.M., Achuthankutty, C.T., 2007b. Monsoonal impact on planktonic standing stock and abundance in a tropical estuary (Cochin backwaters-India). *Estuar. Coast. Shelf Sci.* 73, 54–64.
- Madhupratap, M., Haridas, P., 1975. Composition and variations in the abundance of zooplankton of backwaters from Cochin to Alleppey. *Indian J. Mar. Sci.* 4, 77–85.
- Madhupratap, M., 1979. Distribution, community structure and species succession of copepods from Cochin backwaters. *Indian J. Mar. Sci.* 8, 1–8.
- Madhupratap, M., 1987. Status and strategy of zooplankton of tropical Indian estuaries. A review. *Bull. Plankton Soc. Japan* 34, 65–81.
- Martin, G.D., Vijay, J.G., Laluraj, C.M., Madhu, N.V., Joseph, T., Nair, M., Gupta, G.V.M., Balachandran, K.K., 2008. Fresh water influence on nutrient stoichiometry in a tropical estuary, southwest coast of India. *Appl. Ecol. Environ. Res.* 6, 57–64.
- Martin Thompson, P.K., 1991. Ecology of the cyclopoid from the Cochin backwater. *J. Mar. Biol. Ass. India.* 33 (1&2), 350–365.
- McLusky, D.S., 1993. Marine and estuarine gradients an overview. *Neth. J. Aquat. Ecol.* 27, 489–493.
- Menon, N.N., Balchand, A.N., Menon, N.R., 2000. Hydrobiology of the Cochin backwater system- a review. *Hydrobiologia* 430, 149–183.
- Millie, D.F., Paerl, H.W., Hurlley, J.P., 1993. Microalgal pigment assessments using high-performance liquid chromatography: a synopsis of organismal and ecological applications. *Can. J. Fish. Aquat. Sci.* 50 (11), 2513–2527.
- Mohan, A.P., Jyothibabu, R., Jagadeesan, L., Lallu, K.R., Karan, C., 2016. Summer monsoon onset-induced changes of autotrophic pico-and nanoplankton in the largest monsoonal estuary along the west coast of India. *Environ. Monit. Assess.* 188, art. no. 93.
- Nasir, U.P., 2010. *Water quality assessment and isotope studies of Vembanad Wetland System* Ph.D. thesis. Centre for Water Resources Development and Management, University of Calicut.
- Padmakumar, K.G., Krishnan, A., Radhika, R., Manu, P.S., Shiny, C.K., 2002. Open water fishery interventions in Kuttanad, Kerala, with reference to fishery decline and ecosystem changes. In: Boopendranath, M.R., Meenakumari, B., Joseph, J., Sankar, T.V., Pravin, P., Edwin, L. (Eds.), *Riverine and Reservoir Fisheries of India*. Soc. Fish. Technol., Cochin, 15–24.
- Pinckney, J.L., Richardson, T.L., Millie, D.F., Paerl, H.W., 2001. Application of photopigment biomarkers for quantifying microalgal community composition and in situ growth rates. *Org. Geochem.* 32 (4), 585–595.
- Postel, L., Fock, H., Hagen, W., 2000. Biomass and abundance. In: *ICES Zooplankton Methodology Manual*. Acad. Press, London, 83–170.
- Qasim, S.Z., 2003. *Indian estuaries*. Pvt. Ltd. Heredia Marg, Ballard Estate, Mumbai, 259 pp.
- Report on Visit to Vembanad Kol, 2008. Report on Visit to Vembanad Kol, Kerala, a wetland included under the National Wetland Conservation and Management Programme of the Ministry of Environment and Forests, 1–22.
- Revichandran, C., Srinivas, K., Muraleedharan, K.R., Rafeeq, M., Amaravayal, S., Vijayakumar, K., Jayalakshmy, K.V., 2011. Environmental set-up and tidal propagation in a tropical estuary

- with dual connection to the sea (SW Coast of India). *Environ. Earth Sci.* 66, 1031–1042.
- Roman, M.R., Smith, S., Wishner, K., Zhang, X., Gowing, M., 2000. Mesozooplankton production and grazing in the Arabian Sea. *Deep-Sea Res.* 47, 1423–1450. [https://doi.org/10.1016/S0967-0645\(99\)00149-6](https://doi.org/10.1016/S0967-0645(99)00149-6)
- Saraladevi, K., Venugopal, P., Remani, K.N., Zacharias, D., Unnithan, R.V., 1983. Nutrients in some estuaries of Kerala. *Ma-hasagar* 16, 161–173.
- Sewell, R.B.S., 1999. In: *The copepoda of Indian seas*, 10. Daya Books, 407 pp.
- Sooria, P.M., Jyothibabu, R., Anjusha, A., Vineetha, G., Vinita, J., Lallu, K.R., Paul, M., Jagadeesan, L., 2015. Plankton food web and its seasonal dynamics in a large monsoonal estuary (Cochin backwaters, India) – significance of mesohaline region. *Environ. Monit. Assess.* 187, art. no. 427.
- Srinivas, K., Revichandran, C., Thottam, T.J., Maheswaran, P.A., Asharaf, T.T., Murukesh, N., 2003. Currents in the Cochin estuarine system [southwest coast of India] during March 2000. *Indian J. Mar. Sci.* 32, 123–132.
- Tanaka, O., 1956. The pelagic copepods of the izu region, middle Japan systematic account II.- Families Paracalanidae and Pseudocalanidae. *Publ. Seto Mar. Biol. Lab.* 3, 367–406.
- Tranter, D.J., Abraham, S., 1971. Coexistence of species of Acartiidae (Copepoda) in the Cochin Backwater, a monsoonal estuarine lagoon. *Mar. Biol.* 11 (3), 222–241.
- UNESCO, 1994. *Protocols for the Joint Global Ocean Flux Study. Manual and Guides no. 29.* UNESCO, Paris, 170 pp.
- Vijith, V., Sundar, D., Shetye, S.R., 2009. Time-dependence of salinity in monsoonal estuaries. *Estuar. Coast. Shelf Sci.* 85, 601–608.
- Vineetha, G., Madhu, N.V., Kusum, K.K., Sooria, P.M., 2015. Seasonal dynamics of the copepod community in a tropical monsoonal estuary and the role of sex ratio in their abundance pattern. *Zool. stud.* 54 (1), 54.
- Wellershaus, S., 1974. Seasonal changes in the zooplankton population in the Cochin Backwater (a South Indian estuary). *Aquat. Ecol.* 8, 213–223.

Available online at [www.sciencedirect.com](http://www.sciencedirect.com)

ScienceDirect

journal homepage: [www.journals.elsevier.com/oceanologia](http://www.journals.elsevier.com/oceanologia)

ORIGINAL RESEARCH ARTICLE

# Statistical analysis of Mediterranean coastal storms

Nikolas T. Martzikos<sup>a,\*</sup>, Panayotis E. Prinos<sup>b</sup>, Constantine D. Memos<sup>a</sup>,  
Vasiliki K. Tsoukala<sup>a</sup>

<sup>a</sup>Laboratory of Harbour Works, School of Civil Engineering, National Technical University of Athens 5, Zografou, Greece

<sup>b</sup>Hydraulics Laboratory, Department of Civil Engineering, Aristotle University of Thessaloniki, Thessaloniki, Greece

Received 25 March 2020; accepted 6 November 2020

Available online 18 November 2020

## KEYWORDS

Mediterranean Sea;  
Coastal storms;  
Extreme events;  
Coastal engineering

**Abstract** Coastal storms as extreme hydrometeorological events have severe impacts on the coasts and consequently affect the coastal communities, attracting considerable research interest nowadays. Attempting to understand the risk of these extreme events, a coastal storm analysis is accomplished by studying the parameters which define a coastal storm and their properties, such as the wave height, the wave period, the duration, the calm period, and the storm energy. The frequency of occurrence of coastal storms, the thresholds of storm parameters and the way they are interrelating with each other draw a rough outline of wave climate during coastal storm events for a specific location. This information is valuable afterwards for the design of coastal structures and the coastal zone management. In this work, buoy datasets from 30 locations in the Mediterranean Sea are analysed for describing coastal storm activity. A sample of 4008 coastal storms is identified. Each location faces around 10–14 coastal storms per year, with most of them to occur in winter months and their characteristics to be site-dependent. Their average duration is lower than 30 hours, and 25% of them are consecutive events which hit the same location in less than a day. Furthermore, the wave period and the main direction present no remarkable fluctuations during a coastal storm. With this analysis, a

\* Corresponding author at: Laboratory of Harbour Works, School of Civil Engineering, National Technical University of Athens 5, Heron Polytechniou Str. 15780, Zografou, Greece.

E-mail addresses: [nmartzikos@central.ntua.gr](mailto:nmartzikos@central.ntua.gr), [nmarz83@hotmail.com](mailto:nmarz83@hotmail.com) (N.T. Martzikos), [prinosp@civil.auth.gr](mailto:prinosp@civil.auth.gr) (P.E. Prinos), [cmemos@mail.ntua.gr](mailto:cmemos@mail.ntua.gr) (C.D. Memos), [vsoukala@hydro.civil.ntua.gr](mailto:vsoukala@hydro.civil.ntua.gr) (V.K. Tsoukala).

Peer review under the responsibility of the Institute of Oceanology of the Polish Academy of Sciences.



Production and hosting by Elsevier

<https://doi.org/10.1016/j.oceano.2020.11.001>

0078-3234/© 2020 Institute of Oceanology of the Polish Academy of Sciences. Production and hosting by Elsevier B.V. This is an open access article under the CC BY-NC-ND license (<http://creativecommons.org/licenses/by-nc-nd/4.0/>).

deeper understanding of coastal storm severity is pursued, gaining knowledge about their past activity, in order to be prepared in the future and to protect the coastal areas.  
 © 2020 Institute of Oceanology of the Polish Academy of Sciences. Production and hosting by Elsevier B.V. This is an open access article under the CC BY-NC-ND license (<http://creativecommons.org/licenses/by-nc-nd/4.0/>).

## 1. Introduction

Researchers all over the world are focused on coastal storms to study their impacts and learn more about their severity. Considering the coastal storms as storm events with impacts on coastal areas, they can cause serious problems such as coastal flooding, beach erosion, and damages on ports. The management of such events, the preparedness, and an informed coastal community are of great importance and more urgent, especially nowadays in a changing climate.

Climate change and related extreme events causing infrastructure damages and resulting in human losses, have turned coastal communities and consequently coastal storms into the centre of attention over the past decades. In this context, the latest reports of the Intergovernmental Panel on Climate Change (IPCC, 2018, 2019), the United Nations Framework Convention on Climate Change (UNFCCC) meetings, such as the well known Paris Agreement (UNFCCC, 2016) and the Fourth National Climate Assessment of U.S. Global Change Research Program (2018), give an incredible boost to the field of science communication regarding the climate change. On the other hand, many extreme events hit coastal communities causing losses of billions of euros in the last two decades. The hurricane Sandy (22 October–2 November 2012) (Binder et al., 2015; Rosenzweig and Solecki, 2014), the cyclone Xynthia (27–28 February 2010) (Bertin et al., 2012; Ferreira et al., 2017), the hurricane Katrina (23–31 August 2005) (Irish et al., 2008; Kates et al., 2006) are some of the most recent and among the costliest and deadliest storms in human history, which have changed the way the humans act, protect and prepare themselves within an everchanging environment.

Many research projects have also focused on the hazards and the risk management of extreme events for coastal

communities. PEARL (Karavokiros et al., 2016), RISC-KIT (Van Dongeren et al., 2014), MICORE (Ciavola et al., 2011b), and THESEUS (Zanuttigh, 2011) are typical examples of this progress for European seas, while their deliverables stand as a significant source of information for any researcher.

Storm identification can be carried out by using the important storm parameters and their thresholds, such as the significant wave height ( $H$ ), the duration of a storm event ( $D$ ), and the calm period ( $I$ ). The significant wave height should exceed a certain threshold and remain over this for a time period (De Michele et al., 2007; Li et al., 2014). The clusters of these exceedances are considered as storm events and the storm duration is defined as the time period in which the significant wave height remains over the threshold (Boccotti, 2000). The minimum duration is also defined, discarding all the events that last a shorter time. The calm period, or the inter-arrival time according to Corbella and Stretch (2013) and De Michele et al. (2007), is the time period between the start of the upcoming event and the end of the previous event. If the calm period is too short, then the neighbouring storm events could be considered as one, prolonging in this way the storm event and consequently extending the duration. For example according to Figure 1, which is based on previous work of Wahl et al. (2016) and Li et al. (2014), the consecutive events over the threshold have duration  $D_1$ ,  $D_3$  and  $D_5$ . The first two of them could be considered as one storm event, due to their short calm period ( $D_2$ ), with final storm duration  $D=t_4-t_1$ . The next event with duration  $D_5$  is independent from the previous, due to the long calm period ( $D_4$ ), but it is not considered as a storm event because of its short duration ( $D_5$ ). The calm period threshold is essential for the identification of consecutive coastal storms. A sequence of storm events, cause extensive damages on coastal zones, affecting the coastal morphology and could be more destruc-

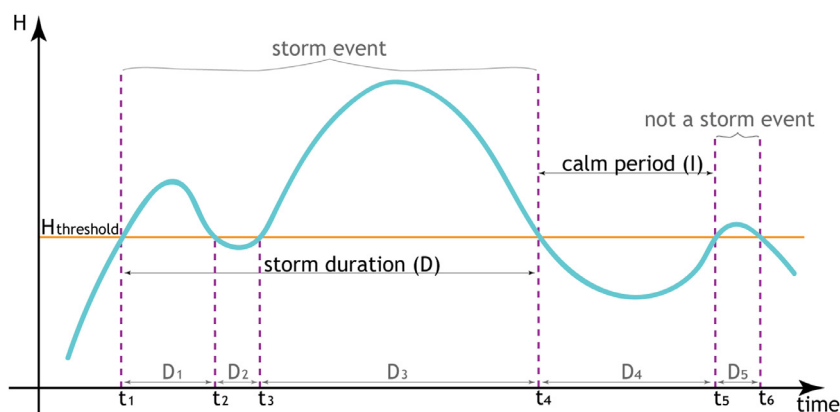


Figure 1 Definition of the storm event and the description of important parameters.

tive than isolated events in many cases (Dissanayake et al., 2015; Ferreira, 2005; Sénéchal et al., 2017).

The coastal storm thresholds are site-specific and they depend on the synoptic systems, the bathymetry, the local characteristics, and the exposure of a location to the winds and the big waves (Harley, 2017). Other parameters which are taken into account in such analyses are the main direction of coastal storms and their energy. Moreover, the mean, the maximum or the peak value of the important parameters (Dissanayake et al., 2015; Lin-Ye et al., 2016) are also used in coastal storm analysis.

Trying to understand the storminess, which denotes the frequency of occurrence of coastal storms and their severity, a large dataset of wave climate is required. However, the time series of storm characteristics, acquired from buoys measurements, are rarely used, mainly due to their spatial availability and their limitation about temporal data coverage. The majority of the data are not available before 1978 (Caires and Sterl, 2005). Data are not available everywhere, even nowadays, but only for specific locations. For instance, in the Mediterranean Sea, Spain and France have a dense network of buoys to record the wave climate of their seas, in contrast with the other European countries, which have very few (i.e. Greece, Italy, Bulgaria and Romania) and other countries that have none at all. However, the buoys are frequently out of order, or they are moving over the years, changing their position. The available datasets are usually non-continuous and with many gaps. Hence, a lot of research is based on model and satellite data before or after a reanalysis (Dee et al., 2011; Kistler et al., 2001; Sartini et al., 2017), which are operationally more efficient and cost-effective.

Up to now, significant research has been conducted for the wave climate and storm events along European coasts. Usually, it is not limited in the Mediterranean Sea (Almeida et al., 2011; Ciavola et al., 2011a), it is based on model data (Androulidakis et al., 2015; Lionello et al., 2012, 2008; Vousdoukas et al., 2016) and often examines storms from the climatology viewpoint, investigating the characteristics and the frequency of occurrence for cyclones or medicanes in the Mediterranean region (Cavicchia et al.,

2014; Emanuel, 2005; González-Alemán et al., 2019; Lionello et al., 2006; 2016).

This work is based on buoy wave measurements, presents a coastal storm activity over the Mediterranean Sea, through the frequency of storm occurrence and the statistical analysis of their parameters. The purpose is to gain a deeper understanding of coastal storm severity, their past activity, and their seasonal variation over the years in a changing climate.

Based on many works cited above which are usually focused at a specific area, an extensive database of wave measurements at 30 coastal locations is analysed. The data consist of buoys measurements and not of model simulations. As a follow-up of previous works, a general methodology for coastal storm identification is described here and a coastal storm analysis is presented.

In the following sections, the data and the study area are described, the methodology for the identification of coastal storm events and the estimation of storm characteristics are presented. Information about the coastal storm thresholds, the descriptive statistics of important parameters, the coastal storm duration and the calm period, the variance of the wave period and the direction, are also included. Finally, the results draw conclusions about the different locations and the variation of storm parameters in the Mediterranean Sea.

## 2. Data and study area

A dataset from wave recordings from buoys at 30 locations over the Mediterranean Sea, in Greece, Italy, France and Spain, is analysed. The data were obtained by the databases of Puertos del Estado ([www.puertos.es](http://www.puertos.es)), Copernicus ([www.copernicus.eu](http://www.copernicus.eu)) and EMODnet ([www.emodnet.eu](http://www.emodnet.eu)), covering in general, a time period since the 1980s. The 30 locations are selected because the buoys are close to the coast (Figure 2), in order to analyse coastal storms. A brief description of these stations is presented in Table 1, including sampling and regional details. The temporal data coverage – or the period for which data are available – de-



**Figure 2** Regional description of the buoys' location over the Mediterranean Sea. The squares indicate buoys which are out of order (last check October 13, 2020).

**Table 1** Coordinates and sampling details of buoys stations for 30 locations in the Mediterranean Sea.

Location	Coordinates [Longitude, Latitude]	Depth [m]	Distance from coast [km]	Covering Period	Duration of record [months]	Sampling Interval [hr]
Greece						
1	Athos [24.73°E, 39.97°N]	215	27.7	25/05/2000–31/05/2017	181	3.0
2	Lesvos [25.80°E, 39.15°N]	120	4.5	29/05/1999–28/07/2012	133	3.0
3	Skyros [24.46°E, 39.11°N]	83	14.4	28/08/2007–18/07/2012	57	3.0
4	Mykonos [25.46°E, 37.51°N]	80	5.3	27/05/1999–30/04/2017	132	3.0
5	Santorini [25.50°E, 36.26°N]	286	9.2	28/05/1999–27/07/2012	141	3.0
6	Heraklion [25.07°E, 35.43°N]	170	5.1	15/07/2016–31/05/2017	8	3.0
7	Kalamata [22.09°E, 36.97°N]	290	4.2	17/10/1999–17/05/2011	57	3.0
8	Pylos [21.60°E, 36.83°N]	3016	7.2	09/11/2007–30/06/2016	92	3.0
9	Zakynthos [20.60°E, 37.96°N]	297	7.5	08/11/2007–23/01/2012	47	3.0
Italy						
10	Venice [12.66°E, 44.97°N]	33	7.3	01/06/2013–01/01/2015	18	0.5
11	Crotone [17.22°E, 39.02°N]	37	1.3	04/06/2013–10/12/2014	17	0.5
12	Catania [15.15°E, 37.43°N]	45	5.3	06/01/2013–01/01/2015	14	0.5
13	Palermo [13.33°E, 38.26°N]	135	6.9	01/06/2013–30/10/2014	8	0.5
France						
14	Alistro [9.64°E, 42.26°N]	116	6.7	29/10/2013–01/06/2017	16	0.5
15	La Revellata [8.65°E, 42.57°N]	194	5.6	30/10/2013–30/06/2017	8	0.5
16	Nice [7.23°E, 43.64°N]	45	1.7	22/06/2010–07/03/2016	38	0.5
17	Porquerolles [6.21°E, 42.93°N]	347	5.4	24/04/2008–24/08/2012	44	0.5
18	Marseille [5.23°E, 43.21°N]	30	8.9	17/04/2011–30/06/2017	61	0.5
19	Sete [3.78°E, 43.37°N]	34	6.2	06/10/2009–30/06/2017	88	0.5
20	Leucate [3.12°E, 42.92°N]	43	4.8	06/10/2009–30/06/2017	82	0.5
21	Banyuls [3.17°E, 42.49°N]	15	3.2	06/10/2009–19/05/2017	83	0.5
Spain						
22	Cabo Begur [3.65°E, 41.92°N]	1200	34.6	27/03/2001–31/03/2019	170	1.0
23	Barcelona [2.20°E, 41.32°N]	68	2.5	08/03/2004–31/03/2019	152	1.0
24	Tarragona [1.19°E, 41.07°N]	15	0.8	12/11/1992–22/12/2017	283	1.0
25	Valencia [0.20°W, 39.51°N]	50	9.1	08/06/2005–30/10/2013	97	1.0
26	Cabo De Gata [2.32°W, 36.57°N]	536	20.1	28/04/2003–23/03/2018	137	1.0
27	Malaga [4.42°W, 36.69°N]	15	1.5	19/11/1985–31/03/2019	382	1.0–3.0
28	Dragonera [2.10°E, 39.56°N]	135	17.5	29/11/2006–31/03/2017	136	1.0
29	Capdepera [3.49°E, 39.65°N]	48	3.1	01/01/2000–01/04/2014	163	1.0
30	Son Bou [4.06°E, 39.90°N]	5	0.5	5/10/2011–31/01/2016	52	1.0

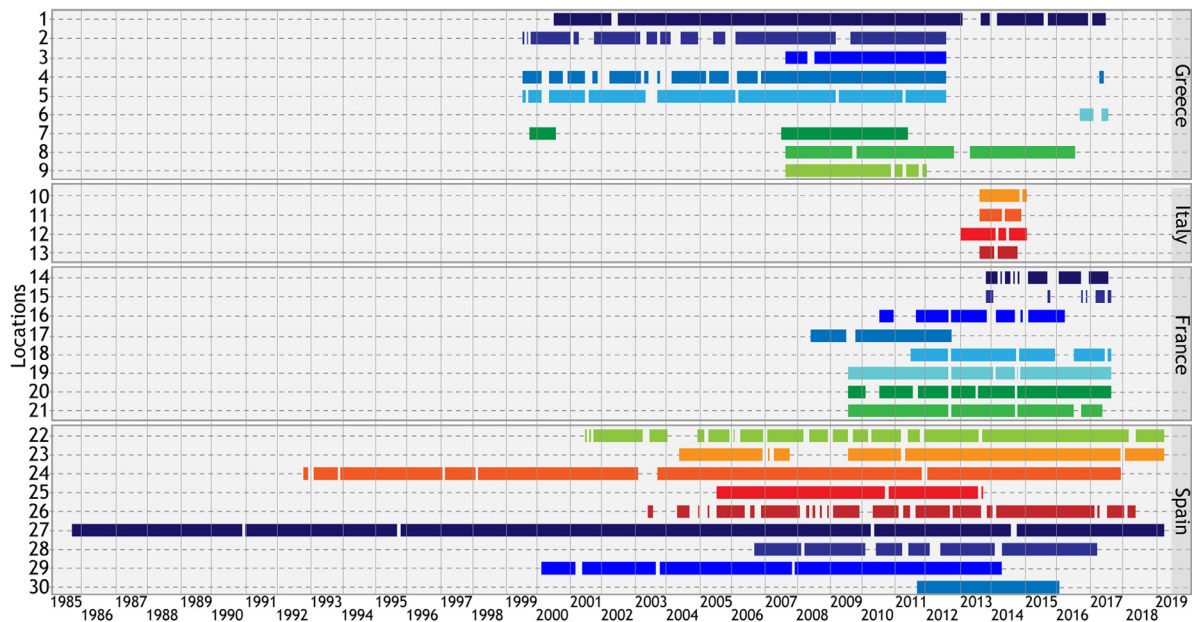


Figure 3 Temporal availability and coverage of historical data.

depends on the operation period of buoys, with most of them to be examined until 30/6/2017. Wherever more data were available, the examined period is extended up to 31/3/2019 (Figure 3). According to the database of EMODnet, in Italy, only a few buoys are nowadays in operation, and most of the Greek buoys are out of order at this moment (see also Figure 2).

This analysis is mainly based on the wave height and the wave period. These critical parameters have been estimated by the operational centres of data providers, following a spectral analysis or zero-crossing method (Copernicus Marine In Situ Tac Data Management Team, 2018; OceanSITES, 2015). However, the spectral significant wave height ( $H_{m0}$ ) and the wave period at the spectral peak, also known as peak period ( $T_p$ ), are preferred, and hereinafter referred to as  $H$  and  $T$  for brevity.

All the errors and the missing values which can often happen are rejected, through a data cleaning process. The events with a measurement gap greater than 18 hours are also excluded, considering that the specific buoy might be out of operation for a while. The elapsed time between consecutive measurements, also known as the sampling interval, mostly varies from 0.5 to 3 hours (Table 1).

### 3. Methodology

Considering coastal storms as extreme hydrometeorological or meteo-oceanic phenomena, the Extreme Value Theory (EVT) is applied for the analysis and the description of such events. The EVT is widespread in the last decades and becoming increasingly popular by work of Coles (2001) which described thoroughly the theoretical background of this field. Since then, numerous works and applications in EVT had a high impact on coastal engineering (Caires and Sterl, 2005; Mazas and Hamm, 2011; Menéndez et al., 2009; Méndez et al., 2006; Ruggiero et al., 2010; Vinoth and Young, 2011). The Block Maxima (BM)

and the Peak Over Threshold (POT) methods are both the fundamental approaches in EVT, which are quite different in their application (Arns et al., 2013; Bezak et al., 2014; Jarušková and Hanek, 2006). In brief, the BM method is based on the analysis of maximum values of a dataset or within a specific block. However, it is also very common, as an alternative method, to take the  $r$ -largest order statistics (Coles, 2001; Dey et al., 2015). Therefore, the BM is not recommended when the reference period is only a few years or decades (Caires and Sterl, 2005). On the other hand, the POT method analyses time-series that extracted from the initial dataset when they exceed a specific threshold (Coles, 2001; Ferreira and Guedes Soares, 1998).

Following the definitions of Harley (2017) and Ciavola et al. (2014), the coastal storm is defined as “any meteorologically-induced disturbed sea state that causes changes and damages to the coastal zones, impinging the coastal morphology and the infrastructure”. For the definition of coastal storms, the closest buoys from the coast are considered and the events with a measurement gap greater than 18 hours are discarded (at the phase of data cleaning). The coastal storms are identified by applying the EVT for the definition of  $H$  threshold and using the thresholds of duration and calm period. Finally, the storm characteristics and storm activity are investigated. The methodology which is adopted here is presented in Figure 4. All the estimations are performed in R language (R Core Team, 2020).

#### 3.1. Coastal storm identification

The identification is conducted at each location, through the thresholds of the significant wave height, the duration, and the calm period. In literature, storm thresholds are defined in different ways and mostly depend on the available data. The threshold of significant wave height is the primary threshold in this procedure and is used to extract the most

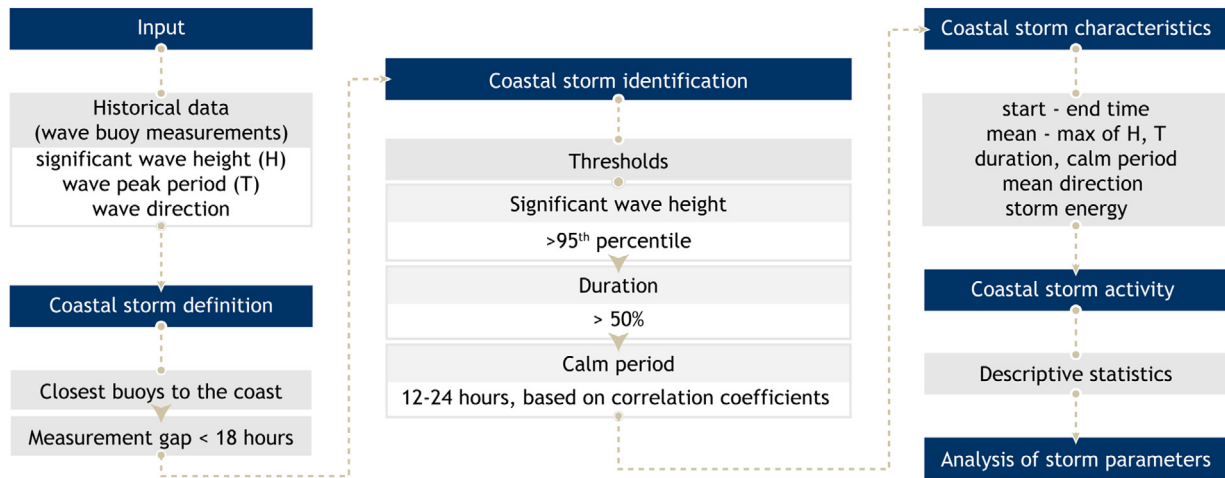


Figure 4 Description of the methodology.

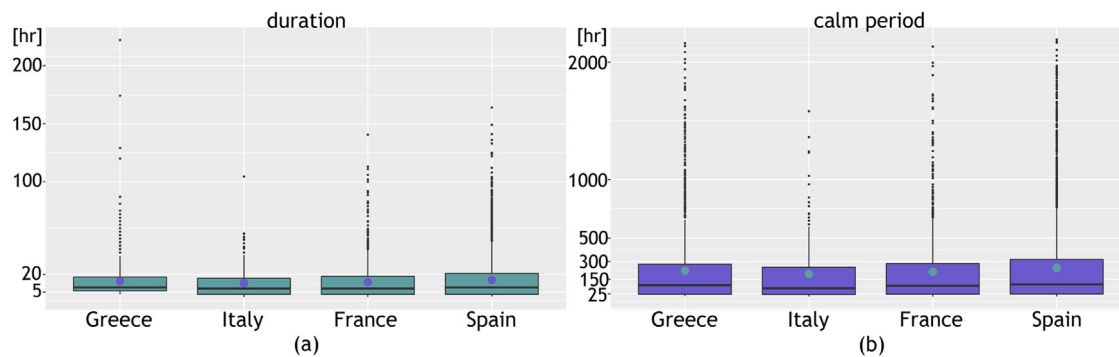


Figure 5 Boxplots for the range of the duration of storm events (a) and the calm period between two consecutive storm events (b), when it does not exceed three months (in approximately 2190 hours).

extreme values. Consequently, the data are filtered by the thresholds of duration and calm period.

### 3.1.1. Significant wave height threshold

The threshold of significant wave height  $H_{thr}$  could be selected inter alia by a) defining a specific value as representative for a specific location (Corbella and Stretch, 2012b), b) following the stability check for the parameters of extreme value distribution as it was proposed by Coles (2001) and also used by Bernardara et al. (2014) and Martzikos et al. (2018), c) using a high percentile of the data set, usually over 90 or 95%, to describe and analyse only the most extreme events (Davies et al., 2017; Masselink et al., 2014; Rangel-Buitrago, 2011; Tsoukala et al., 2016), or d) taking a linear equation between the mean value and the standard deviation of an important parameter. The last methodology was proposed by Yevjevich (1967) for the drought analysis but is also used similarly by Almeida et al., (2011) for the storms.

Given the short reference period of data, the POT method is used in this analysis. Hence, the  $H_{thr}$  is taken as the 95<sup>th</sup> percentile of the significant wave height at each location. Starting with this threshold, exceedances over this are extracted and are grouped, representing the coastal storm events.

### 3.1.2. Duration and calm period thresholds

Taking for each country a sample of storm duration and calm period, both thresholds of the minimum duration and the calm period ( $I_{thr}$ ) of consecutive coastal storms are decided based on the range of these parameters. The boxplots of Figure 5 illustrate the full range and the distribution of these parameters, without significant divergences between countries. The rectangles of boxplots correspond to the interquartile range (75<sup>th</sup>–25<sup>th</sup> percentile), while everything out of this range is considered an outlier. Inside the rectangle, the dot represents the mean value, and the horizontal line shows the median.

Regarding duration (Figure 5a), the upper side of the rectangles is almost 20 hours, which means that 75% of events last less than 20 hours. So, the minimum storm duration has no meaning to be set higher than this value. The average duration (internal dot) is almost 10 hours, for all the countries, while the median and thus 50% (horizontal line) of events last less than 7.5 hours. Trying to analyse the most severe events, the minimum duration is considered appropriate to be higher than the median, investigating the upper 50% of events, but without exceeding the mean value. The minimum coastal storm duration is set at 9 hours for all the examined locations, which is also multiple of 3 hours based on the longest sampling interval.

Hence, the events with a duration of less than 9 hours are ignored.

The calm period is essential for the separation of coastal storm events and their independence. Coastal storms with a long calm period might occur in different seasons and they are certainly not related to each other. The short calm period means more dependent events that usually could be unified. For the investigation of the calm period, we focus only on the closest consecutive events which have a calm period of less than three months (approximately 2190 hours). Following the boxplots of Figure 5b, the examined events have an average calm period around 200 hours (internal dots), and 50% of them usually occur in less than 87.5 hours from the previous event. The lower side of rectangles shows that 25% of storms are consecutive events which hit the same location in a row in less than 24 hours.

From a meteorological perspective, two coastal storm events are independent if they are developed in different synoptic systems. On the other hand, the consecutive coastal storms which belong to the same synoptic system, could have similar characteristics and be dependent. It is quite rational to have dependent events into the same weather system, but it is conceivable that this may happen in different systems also. The threshold of calm period  $I_{thr}$  can be determined better in a physical way, as the mean calm period between consecutive synoptic systems (tropical or extratropical cyclones). The concurrent weather satellite images and the weather maps could be very useful, but up to now, all this information is difficult to get. Corbella et al. (2015) link the atmospheric circulation patterns with the spectral characteristics of ocean waves trying to improve the identification of statistically independent storm events. In extreme value analysis of rainfall and flooding events, the independence of consecutive events is ensured by using the minimum inter-event period (Freitas et al., 2020; Jean et al., 2018). Similarly, the independence of coastal storms is usually approached by taking a fixed value of calm period (e.g. 12, 24, 36 hours) between coastal storms.

Here, based on wave measurements, the independence of coastal storms and the definition of the calm period threshold is approached by the estimation of correlation coefficients. More specifically, the coefficients of Spearman's rho ( $\rho$ ), Kendall's tau ( $\tau$ ), and Pearson's  $r$  are estimated, trying to understand the behaviour of  $H$  and  $T$  within consecutive coastal storms.

The Spearman's rho ( $\rho$ ), Kendall's tau ( $\tau$ ), and Pearson's  $r$  coefficients measure the association strength between two numeric variables. The three coefficients are usually used for the independence of different variables (Kereszturi et al., 2016; Williams et al., 2016) or the correlation between different samples of the same variable. Two samples are strongly associated when  $\rho$ ,  $\tau$ , and  $r$  values are close to 1 or  $-1$ . On the contrary, both samples are considered independent when the coefficients are close to zero. The correlation coefficients vary in their effectiveness and usually one of them is more appropriate than the other (Ferguson et al., 2000), thus all of them are estimated to get a better overview.

The Spearman's rho ( $\rho$ ), when the samples have no ties, is estimated based on Eq. (1) (Hollander et al., 2015). The

$R_i$  and  $S_i$  are the ranks of  $X_i$  and  $Y_i$  variables (when both samples are on ascending order). Here,  $X_i$  and  $Y_i$  represent the  $H$  or  $T$  of consecutive coastal storm events.

$$\rho = 1 - \frac{6 \sum_{i=1}^n (S_i - R_i)^2}{n(n^2 - 1)} \tag{1}$$

The Kendall's tau ( $\tau$ ) statistic, or the Kendall rank correlation coefficient, is used primarily when the data do not necessarily come from a bivariate normal distribution. The estimation is done according to Eqs. (2) and (3) (Hollander et al., 2015) for two different samples, with the same length  $n$  and without ties.

$$\tau = \frac{2 \sum_{i=1}^{n-1} \sum_{j=i+1}^n Q((X_i, Y_i), (X_j, Y_j))}{n(n-1)} \tag{2}$$

$$Q((X_i, Y_i), (X_j, Y_j)) = \begin{cases} 1, & \text{if } (Y_j - Y_i)(X_j - X_i) > 0 \\ -1, & \text{if } (Y_j - Y_i)(X_j - X_i) < 0 \end{cases} \text{ for } 1 \leq i < j \leq n \tag{3}$$

The Pearson's ( $r$ ) statistic is given by the Eq. (4) for two samples or variables  $X=(X_1, \dots, X_n)$ ,  $Y=(Y_1, \dots, Y_n)$ , with mean values  $\bar{X}$ ,  $\bar{Y}$ .

$$r = \frac{\sum_{i=1}^n (X_i - \bar{X})(Y_i - \bar{Y})}{\sqrt{\sum_{i=1}^n (X_i - \bar{X})^2 \sum_{i=1}^n (Y_i - \bar{Y})^2}} \tag{4}$$

The above coefficients are estimated for  $H$  and  $T$  for all the consecutive events at each location. The correlation coefficients  $\rho$ ,  $\tau$ , and  $r$  which are close to zero, are only taken into consideration. It is optimum to analyse the longest coastal storms, working with a lot of data, but quite often coastal storms consist of short length time-series. Hence, for the best performance, a small extension is accomplished whenever an event consists of less than 10 values, by taking some additional values of  $H$  or  $T$ , before the first event and after the end of the second event.

Given that the calm period threshold usually ranges around 24 hours in literature, the above analysis provides more information for selecting the optimum threshold. The calm period threshold is set as the minimum calm period, which ensures a weak correlation of  $H$  samples, based on  $\rho$ ,  $\tau$ , and  $r$ , for the most consecutive coastal storms (and similarly for  $T$ ).

The results are classified by the calm period into 15 classes, from 12 to 96 hours. The representative of each class is the upper boundary and is set as multiple of 6, dividing a day into quartiles. However, the first class is 12 hours, and all the previous cases are merged into one, setting a half-day milestone for the calm period. For instance, all the above statistics are estimated for Barcelona and are presented in Figure 6. Based on significant wave height (Figure 6), the calm period of 12 and 42 hours are the most dominant, for all the correlation coefficients. In Figure 6b 12 and 30 hours are the prevailing calm periods, especially for Pearson's  $r$  coefficient. This finding means that the most independent consecutive events in Barcelona have a calm period of 12 or 42 hours. Hence, the twelve-hourly calm period is considered as the calm period threshold for Barcelona.

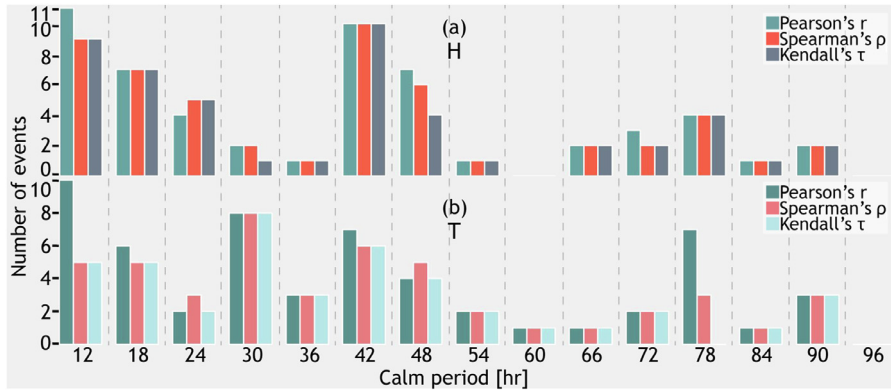


**Figure 6** The number of coastal storm events in Barcelona, which are not correlated with the next event, having the Spearman's  $\rho$ , Kendall's  $\tau$ , and Pearson's  $r$  coefficients close to zero, for  $H$  (a) and  $T$  (b).

### 3.2. Coastal storm characteristics

After the storm identification, the important storm characteristics are estimated to describe each coastal storm, namely the start and the end date, the duration, the mean and the max value of  $H$  and  $T$ , the direction, the energy, and the calm period.

The wave period and the wave direction have slight variation during a coastal storm. For this investigation, the coefficient of variation ( $CV$ ) is estimated (Eq. (5)) at each coastal storm, dividing the standard deviation ( $s$ ) with the mean value ( $\bar{x}$ ) of each parameter. The coefficient of variation shows the homogeneity of wave period and the direction and how normally are spread around the mean during a storm. It should be noted that the circular mean and standard deviation have been used in the case of direction, (Jammalamadaka and SenGupta, 2001).

$$CV = \frac{s}{\bar{x}} \tag{5}$$

The coastal storm energy ( $E$ ) is estimated for each event by using Eq. (6), as it was proposed by Dolan and Davis (1992), where  $t_1$  and  $t_2$  denote the beginning and the end of an event respectively.

$$E = \int_{t_1}^{t_2} H_s^2 dt \tag{6}$$

For the energy estimation, the coastal storm duration and the sampling interval may need to be corrected. When-

ever the first value of  $H$  during a coastal storm is not equal to the threshold, a correction is applied for the estimation of the duration. More specifically, the properties of similar triangles from Geometry are used to approximate better the storm duration, considering a more linear shape of a storm. Following the above assumption, the  $H$  threshold is set at the first and the last value for each storm event and the duration is extended by adding a short time period  $s_4$ , following Figure 7), before and after the initially estimated duration. Consequently, the corrected duration is considered as the storm duration ( $D$ ). Also, when the sampling interval ( $dt$ ) is non-constant during a coastal storm, the  $H$  values are distributed uniformly according to the duration (Figure 7b), and hence the storm energy is estimated based on a new average time step ( $dt$ ).

The wave energy flux ( $P$ ) (Boccotti, 2014) is also estimated using Eq. (7). The wave energy ( $E$ ), per unit surface area, is estimated by the Eq. (8) where  $g$  is the gravitational acceleration and  $\rho$  denotes the density of salt water. The  $C_g$  denotes the group velocity that depends on many wave parameters (e.g. wave period, wave length) and it is different for the shallow, intermediate, and deep waters. The energy flux is estimated at each hour of storm duration and then the sum of these values gives the energy flux for the coastal storm.

$$P = E \cdot C_g \tag{7}$$

$$E = \frac{1}{8} \rho \cdot g \cdot H^2 \tag{8}$$

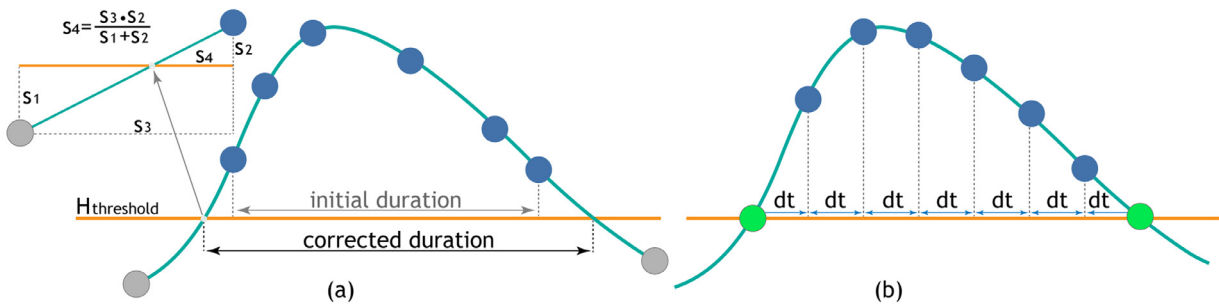


**Figure 7** (a) The correction of storm duration when the first and the last value of  $H$  are not equal to the threshold, extending by  $s_4$  the storm duration, according to properties of similar triangles. (b) The values of  $H$  are distributed uniformly by  $dt$  when the sampling interval ( $dt$ ) is not constant during a coastal storm.

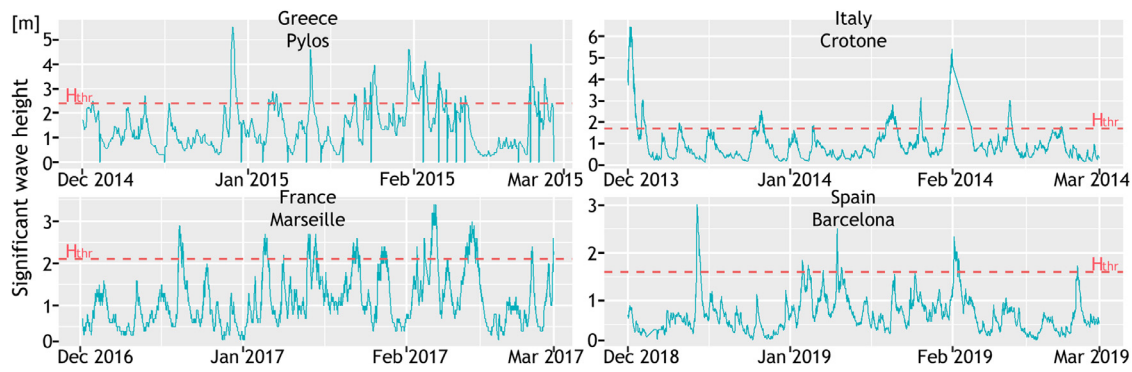


Figure 8 Illustration of significant wave height variation and their thresholds for 4 typical locations.

### 4. Analysis of results

The analysis of 30 different locations and their datasets, provides valuable information about the variation of important parameters (Figure 8) and the storm activity over the Mediterranean Sea during the last decades. Following the above methodology, the coastal storms thresholds are defined and subsequently, the coastal storm events are identified and analysed.

#### 4.1. Coastal storm thresholds

For the coastal storm identification, three thresholds are considered regarding a) the significant wave height, b) the duration, and c) the calm period. As indicated previously, the threshold of minimum duration is generally set at 9 hours for all the examined locations. The  $H_{thr}$  is defined as the 95% of the sample of significant wave height per location and the  $I_{thr}$  is established according to the correlation coefficients Spearman’s  $\rho$ , Kendall’s  $\tau$ , and Pearson’s  $r$ . The general framework of this methodology is very common in literature but differs in the way the thresholds are set (Bernardara et al., 2014; Corbella and Stretch, 2013; Lira-Loarca et al., 2020; Lin-Ye et al. 2016) while sometimes they are defined based on previous studies (De Michele et al., 2007; Li et al., 2018, 2014) or without describing the following procedure. The thresholds of the significant wave height ( $H_{thr}$ ) and the calm period ( $I_{thr}$ ) between two consecutive events are estimated for each location (Table 2).

Similar findings are also presented in other studies. For instance, the calm period threshold of 12 hours is in agreement with the results of Lin-Ye et al. (2016) for Barcelona and the north-western Mediterranean Sea. For Marseille, Bernardara et al. (2014) identify the independence threshold at 24 hours while our results show 12 hours. For Sete in the Gulf of Lions, Gervais et al. (2012) indicate that storms with  $H=2.7$  m or higher can cause specific impacts in beach morphology or overtopping. Here, for Sete the  $H_{thr}$  is 1.7 m, the average  $H$  of all events is 2.36 m and the average of the most extreme events is at 3.33 m, which means that concur. For all the cases, any divergences might be rational and the comparison is not indicative owing to the different reference periods and the model data that use which usually overestimate the mean value of important parameters.

Table 2 The estimated thresholds of the significant wave height ( $H_{thr}$ ) and the calm period of consecutive storm events ( $I_{thr}$ ), for the 30 examined locations.

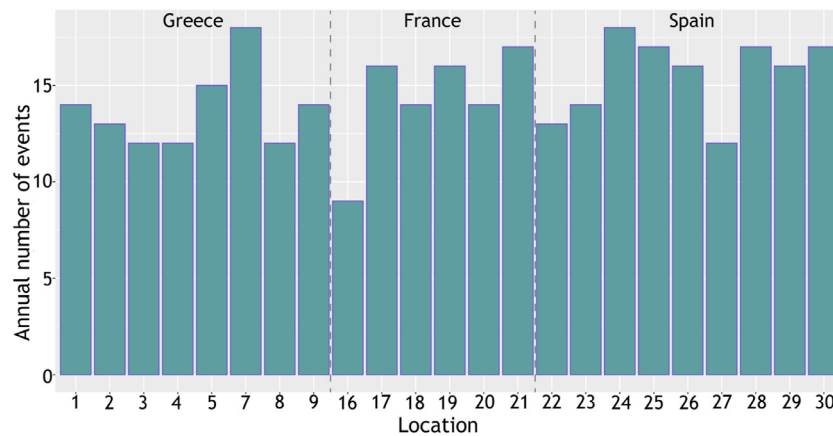
Location	$H_{thr}$ [m]	$I_{thr}$ [hr]
Greece		
1 Athos	2.3	12
2 Lesbos	1.9	12
3 Skyros	2.3	12
4 Mykonos	2.4	12
5 Santorini	2.0	18
6 Heraklion	1.8	18
7 Kalamata	0.9	18
8 Pylos	2.4	12
9 Zakynthos	2.0	18
Italy		
10 Venice	1.3	18
11 Crotone	1.7	24
12 Catania	1.5	12
13 Palermo	2.2	24
France		
14 Alistro	1.6	18
15 La Revellata	3.1	24
16 Nice	1.3	12
17 Porquerolles	2.6	12
18 Marseille	2.1	12
19 Sete	1.7	12
20 Leucate	1.7	12
21 Banyuls	1.7	12
Spain		
22 Cabo Begur	3.4	18
23 Barcelona	1.6	12
24 Tarragona	1.1	12
25 Valencia	1.4	24
26 Cabo De Gata	2.4	12
27 Malaga	1.2	12
28 Dragonera	2.7	12
29 Capdepera	2.5	18
30 Son Bou	1.4	24

#### 4.2. Descriptive statistics

In this work, 4008 coastal storms are analysed, corresponding to 41–127 storm events per year. Most of them (77–

**Table 3** The total number of examined coastal storm events at each country and their characteristics.

	Overall	Oct.–Mar.	Apr.–Sep.	Annual average				Average temporal coverage [years]
				Overall	Oct.–Mar. %	Apr.–Sep. %	Per location	
Greece	1103	950	153	98	86	14	12	8.8
Italy	87	69	18	41	78	22	10	1.2
France	633	509	124	87	80	20	13	5.5
Spain	2185	1668	517	127	77	23	14	14.6

**Figure 9** The annual average number of coastal storms for each location, (the locations with a short temporal coverage are not included).

86%) occur in winter months, especially from October to March (Table 3). The average temporal coverage of datasets is shorter than 15 years. Trying to understand better the frequency of storm occurrence, the annual average of coastal storms per location is also estimated, excluding the short-length datasets to avoid the underestimation (i.e. Heraklion, Allistro and La Revellata). Subsequently, 10–14 coastal storms, on average, hit the examined coastal areas annually. More specifically, the frequency of occurrence is taking into account for each location, and the annual average is presented in Figure 9. Once again, the locations with a short dataset, regarding the duration of the record, are not included in Figure 9 (i.e. Heraklion, Venice, Crotona, Catania, Palermo, Alistro and La Revellata). The percentage frequency of coastal storm occurrence at a monthly level, as presented in Figure 10, confirms that coastal storms are more frequent in the winter semester for each location. During a summer month (July, June, August) the coastal storm activity is usually less than 5% of the annual coastal storm activity, while the percentage for a winter month varies between 10% to 30%. Furthermore, it is worth mentioning that storm activity is more intense during the summer for most of the Spanish locations.

The present findings could be used in the future by any researcher who wants to pursue a coastal storm analysis at the examined locations. The annual or the monthly frequency of occurrence of coastal storms, according to Figures 9 and 10, is useful for applying extreme value analysis based on the Block Maxima or the r-largest order statistics (Coles, 2001; Dey et al., 2015). Comparatively,

Bernardara et al. (2014), working with a more extended dataset, detect in Marseille 10 events per year, while the above analysis identifies 14 events. Lionello et al., (2016) describing the climatology of cyclones in the Mediterranean, present the variation of cyclones per month, with average 18 events, but this value corresponds to all the Mediterranean region; thus it is not directly comparable. Previous studies have indicated that the most active areas in cyclones in the Mediterranean Sea are the Aegean, the Adriatic, the Gulf of Genoa, the Gulf of Lion, and the Catalan Sea (Cavicchia et al., 2014; González-Alemán et al., 2019; Lionello et al., 2006). This information ties well with the findings of the present study, where the highest frequency of coastal storms as well as the highest values of  $H$  and  $T$  were identified in representative coastal locations of the aforementioned seas; namely in Athos, Pylos, La Revellata, Porquerolles, Cabo Begur.

The overview of Mediterranean coastal storms analysis is completed with the description of the different descriptive coefficients (Table 4). The mean ( $m_H$  and  $m_T$ ) and the maximum ( $max_H$  and  $max_T$ ) values of all significant wave heights and wave periods ( $m_T$ ) are estimated at each location for all storm events. The storm energy, the wave energy flux and the storm duration of events are presented by their mean values and described respectively by  $m_E$ ,  $m_p$ , and  $m_D$ . Finally, the most extreme events are examined by taking the average of the highest 5% of all the wave heights ( $m_{H5\%}$ ) and the wave periods ( $m_{T5\%}$ ) that occur at a given location.

The highest significant wave heights occur at exposed locations, where the fetches are long, such as Cabo Begur in

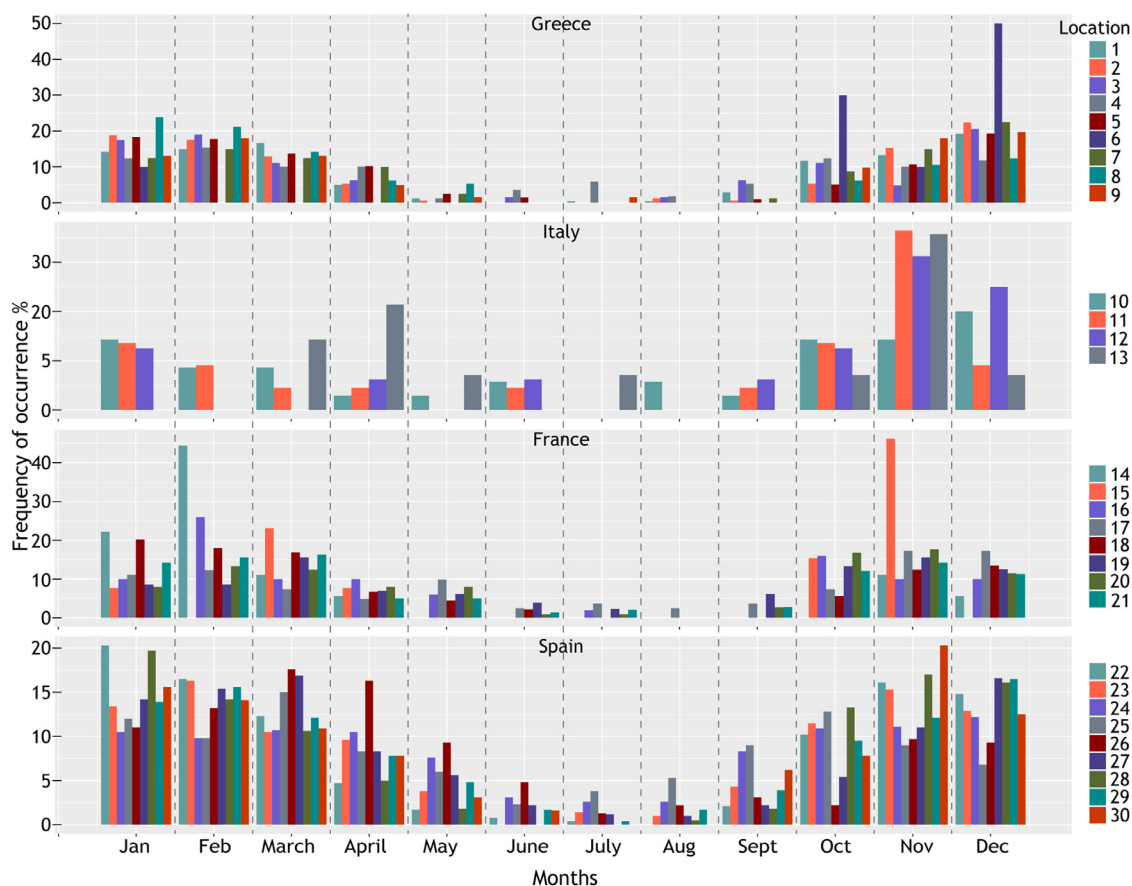


**Figure 10** The percentage monthly frequency of coastal storm occurrence for each location.

Spain, La Revellata in France, Palermo in Italy and Pylos in Greece. On the other hand, the lowest wave heights appear in shallow waters and sheltered locations, such as Kalamata (Greece), Venice (Italy), Nice (France) and Tarragona (Spain). This analysis is of essential importance for buoys very close to the coasts (i.e. Tarragona, Malaga and Son Bou in Spain) and furthermore when the depth is increasing (i.e. Crotone and Nice). For the above cases, the waves travel to the coasts preserving their characteristics, contrary to the buoys in deep waters where many processes (e.g. refraction, shoaling or breaking) induce significant changes to incident waves.

The highest values of  $T$  and  $E$  also appear to the most exposed locations, as previously. For the most extreme events, the analysis reveals that  $m_{H5\%}$  and  $m_{T5\%}$  are approximately 12% higher than  $m_H$ ,  $m_T$  respectively, giving valuable information for each location. The coastal storm energy varies between 38 and 447  $m^2$  hr and given its dependence on the  $H$  and the  $D$ , is high when these parameters have also high values. Coastal storms with the highest energy occur in Pylos, Palermo, La Revellata and Cabo Begur, locations in deep waters. Moreover, it could be stated that coastal storms in Greece have higher energy than those of the other countries, followed by Spain, France and Italy. The wave energy flux at each location varies between 1014.57 and 37867.01 Whr/m having similar trends with the coastal storm energy. Given that the coastal storm impacts are not clearly associated with the storm energy and the energy flux, the infor-

mation about energy could be used for the determination of storm severity.

### 4.3. Duration and calm period

The examined coastal storm events have a mean duration between 18 to 31 hours, while the shortest events occur in Palermo, Italy and the longest in Malaga, Spain (Table 4). Additional analysis for the duration is accomplished by taking the events which exceed the significant wave height threshold, before rejecting some of them due to the threshold of minimum duration of 9 hours as described in 3.1.2. The boxplots of Figure 11a show the full range of the storm duration. The average duration is lower than 30 hours, and according to the median, 50% of coastal storms last less than a day.

Moreover, it is shown that the variation of the median is very small for Greek and Spanish locations. The upper quartile (75%) is almost the same for Greek locations which are not in the centre of Aegean Sea, as well as for Leucate, Sete and Banyuls in France. The highest upper quartiles and the most outliers of duration occur in Spain. In the same context, Lionello et al. (2006) state that the shortest cyclones in Mediterranean last lower than 12 hours and the most severe cyclones have an average duration 18–24 hours. It could be said that the coastal storm duration has the same characteristics, according to Figure 11, and it is a rational

**Table 4** Basic statistics of the most important parameters during a coastal storm event for the examined locations.

Location	$m_H$ [m]	$max_H$ [m]	$m_T$ [s]	$max_T$ [s]	$m_E$ [m <sup>2</sup> hr]	$m_p$ [Whr/m]	$m_D$ [hr]	$m_{H5\%}$ [m]	$m_{T5\%}$ [s]
Greece									
1 Athos	3.01	5.99	7.57	19.99	243.84	19850.37	27.06	4.01	9.05
2 Lesvos	2.52	14.71	7.30	19.32	169.71	14645.21	24.13	4.33	10.58
3 Skyros	3.01	5.45	7.82	10.04	248.04	20495.81	28.10	3.75	8.81
4 Mykonos	3.10	5.76	7.87	11.36	234.35	20860.71	27.38	5.13	9.47
5 Santorini	2.46	4.92	7.37	13.82	143.32	10966.83	24.51	3.08	9.16
6 Heraklion	2.47	4.25	7.33	10.04	191.64	16720.21	31.13	2.77	7.61
7 Kalamata	1.28	3.28	7.37	11.13	38.93	3049.20	24.31	1.76	9.13
8 Pylos	3.10	7.57	8.95	13.71	273.69	25949.15	28.64	4.05	10.21
9 Zakynthos	2.68	9.37	9.49	24.37	219.77	13874.17	28.82	4.62	18.37
Italy									
10 Venice	1.67	3.77	6.39	10.53	57.91	3956.21	20.23	2.34	8.34
11 Crotone	2.34	6.46	8.26	13.33	178.60	12565.84	29.09	3.41	9.67
12 Catania	2.21	4.96	8.57	12.50	131.63	10365.29	24.03	3.92	10.33
13 Palermo	2.85	5.49	8.99	13.33	152.46	15581.80	18.50	3.73	11.90
France									
14 Alistro	2.25	5.80	7.45	11.80	128.61	11851.22	23.31	3.45	9.12
15 La Revellata	3.94	7.70	9.65	13.30	374.49	33189.66	22.57	5.32	10.88
16 Nice	1.73	4.00	7.23	13.30	69.23	5042.72	22.45	2.24	10.82
17 Porquerolles	3.06	6.20	8.52	12.10	175.94	14482.73	19.09	3.85	10.07
18 Marseille	2.47	8.60	7.45	25.00	123.21	7947.60	20.57	3.10	8.94
19 Sete	2.36	5.90	7.41	11.80	162.38	10889.63	27.70	3.33	9.34
20 Leucate	2.33	9.10	7.40	28.60	164.50	11851.71	27.74	3.57	9.56
21 Banyuls	2.15	12.80	7.27	25.00	127.29	3901.43	25.77	3.17	9.80
Spain									
22 Cabo Begur	4.05	7.40	8.06	12.70	446.36	37867.01	26.98	5.11	9.91
23 Barcelona	2.03	5.20	7.56	12.30	118.88	10077.18	27.49	2.83	9.46
24 Tarragona	1.39	3.90	6.97	12.20	52.57	2024.92	25.02	1.81	7.09
25 Valencia	1.80	4.50	7.35	12.50	101.38	7684.43	29.51	2.42	9.57
26 Cabo De Gata	2.94	6.60	7.42	10.60	205.07	16190.26	23.47	3.76	8.77
27 Malaga	1.69	4.70	6.94	15.60	98.79	3720.91	30.37	2.47	6.83
28 Dragonera	3.27	6.30	8.24	12.80	269.30	26876.39	24.97	4.03	9.93
29 Capdepera	3.16	7.00	8.88	12.80	264.94	21296.32	25.88	4.16	10.09
30 Son Bou	1.73	4.98	5.33	8.52	89.94	1014.57	28.98	2.25	6.30

outcome since coastal storms originate from cyclones and synoptic systems.

The average calm period of coastal storms is shorter than 625 hours, or less than one month, according to Figure 11b. Most events (75%) have calm period less than 750 hours, while 25% of events have calm period almost 150 hours, hitting consecutively the same location in less than a week. In general, the variation of the calm period is higher than the duration. The median is around 190 hours for most Greek locations and around 250 hours for Spain. The highest upper quartiles belong, again, in Spain and the average calm period of 500 hours is the most common in Spanish locations. The results about the mean storm duration and the calm period are also important for the coastal erosion (Callaghan et al., 2008; Corbella and Stretch, 2012a; Dissanayake et al., 2015), the vulnerability of coastal structures and their design (Lira-Loarca et al., 2020; Salvadori et al., 2014). Consecutive storm events and events with long duration are responsible for significant loads in the coastal structures as a well as for the short time for beach recovery.

#### 4.4. The variance of the wave period and the direction

Another issue that emerged from the data analysis is that the wave period ( $T$ ) and the main direction ( $D_{ir}$ ) are usually quite stable during a coastal storm. To understand the level of dispersion around the mean (or the circular mean), the coefficient of variation (CV) of these parameters is estimated for each coastal storm (Figure 12). Regarding the wave period, no significant patterns are detected between locations, but it can generally be stated that 75% of storm events have the CV usually less than 0.15 and for 25% of them the CV is even less than 0.05 (Figure 12a).

Similarly, Figure 12b shows the range of CV for the coastal storm direction (wherever is available), which is shorter than the wave period. The upper boundary of boxplots shows that 75% of coastal storms have the CV less than 0.08. Following the boxplots, it is shown that there is no high dispersion for  $T$  and  $D_{ir}$  during a coastal storm. The values of  $T$  and  $D_{ir}$  are normally spread around the mean during

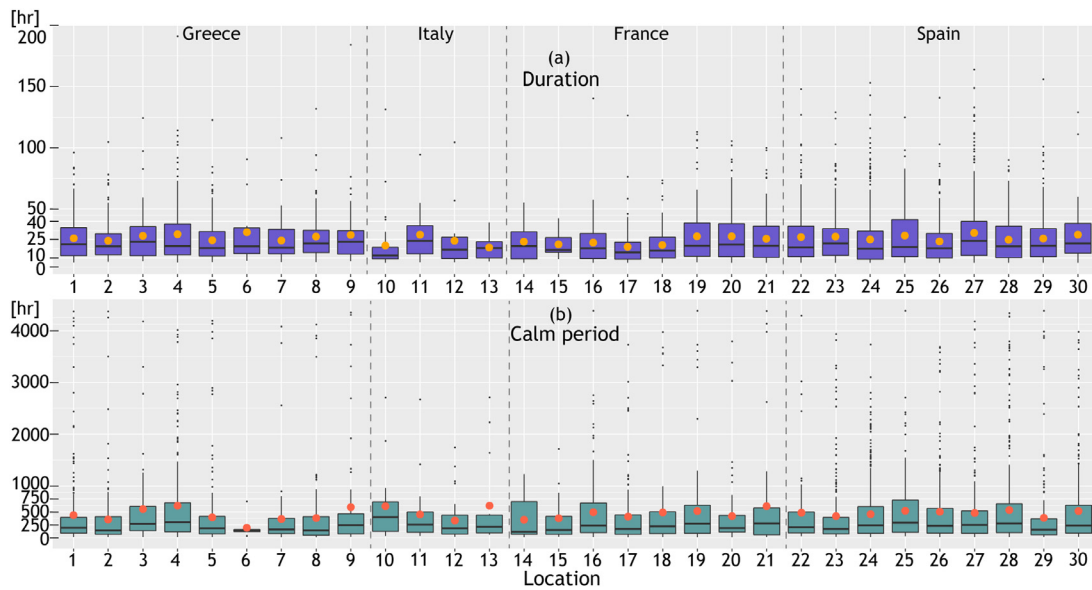


**Figure 11** Boxplots for the full range of variation of coastal storm duration (a) and the calm period between two consecutive events (b).

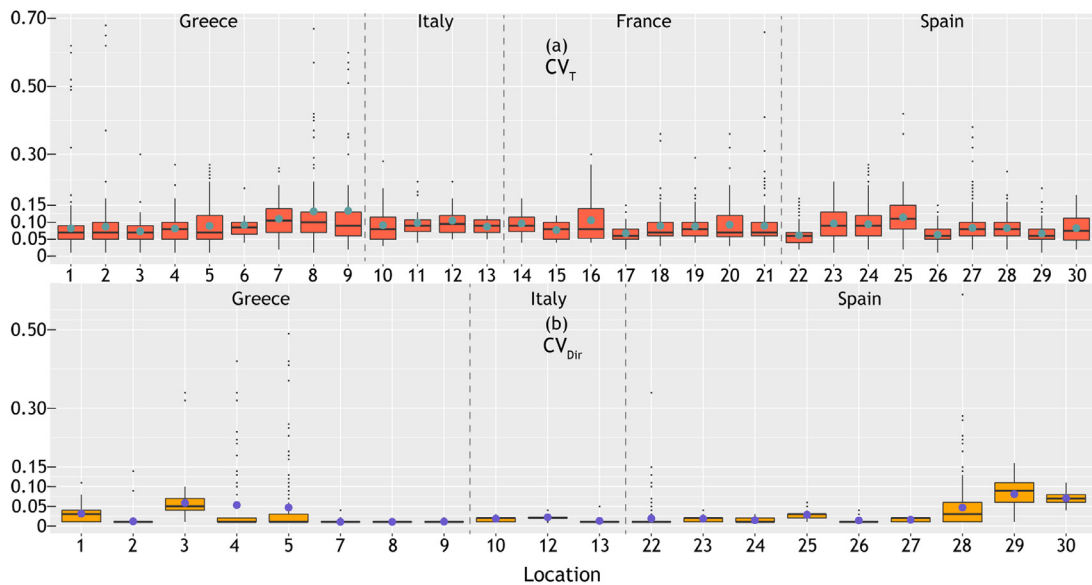


**Figure 12** Boxplots for the full range of the coefficient of variation for (a) the wave period and (b) the wave direction.

a coastal storm for the majority of storm events and thus the mean value can represent efficiently the coastal storm wave period and the direction.

### 5. Conclusions

In the context of this work, a deeper understanding of coastal storms is pursued, providing knowledge on the coastal storms in the Mediterranean Sea, as well as on the variation of their parameters, and their characteristics. The novelty lies on the analysis of big datasets from buoys measurements at various coastal locations in the Mediterranean. A general methodology for coastal storm identification is described thoroughly. All this information could be useful

to researchers, engineers, organisations, or stakeholders on their effort to understand better the coastal storms, to protect and inform the coastal communities from coastal storm impacts in a changing climate.

The coastal storm events are studied and analysed based on their characteristics and not on their impacts on coastal morphology and infrastructure. To achieve this, the coastal storm is defined by taking the closest buoys from the coast and by applying the 95<sup>th</sup> percentile of H as the primary threshold for storms identification. Furthermore, two more thresholds are used for the storm identification (minimum duration and calm period).

A dataset of wave buoys measurements from 30 different locations over the Mediterranean is analysed, and a total amount of 4008 storm events are identified, covering

coastal areas in Greece, Italy, France, and Spain for the period 1985–2019. A detailed descriptive analysis is provided, which includes the mean and the maximum value of storm parameters. The range of storm parameters is site-specific since storm characteristics depend on the water depth and the bathymetry. Their extreme values and the intense coastal storm activity occur in areas that have also significant cyclonic activity. The exposure of coastal areas is inherently linked to the wave height and wave period. Indeed, the most exposed locations are associated with the most extreme values of wave height and wave period, whereas the most sheltered ones are identified where the lowest values of  $H$  and  $T$  occur. According to the results, 10–14 storm events occur per year in a Mediterranean coastal area, and most of them span from October to March. The examined events have an average duration lower than 30 hours, and 25% of them are consecutive events which hit the same location in less than a day.

Another concluding remark of this work is that the wave period and the wave direction present no remarkable fluctuation during a coastal storm event, according to their coefficient of variation. Therefore, the mean values of  $T$  and  $D_{ir}$  describe sufficiently the wave period and the direction of a coastal storm.

The limitations are mainly related to the sampling interval of buoys measurements (0.5–3 hours). In addition, the temporal data coverage is also very short and different for few locations. The latter is restrictive on providing a more general overview of coastal storm activity. Such technical barriers, including the collection of the respective data and the encoding of different data (i.e. file formats, variables' names) make this work more demanding and time-consuming, especially during the process of data mining. In this context, all Italian and some French locations with short coverage are excluded from the annual frequency of occurrence (Figure 9). For these reasons, it is quite difficult to conclude about climate change and how it affects the frequency of coastal storms over the years.

For future research, a more extensive database, with the shortest possible sampling interval, is essential to avoid the use of general thresholds. The thresholds for the significant wave height, storm duration and calm period could be redefined for each location, through the consideration of smaller values compared to ones used here. The satellite data, the information about synoptic systems, and other parameters such as atmospheric pressure should be included for a more detailed coastal storm analysis. For such analyses, a denser network of buoys and increased data availability are also needed to identify the storm activity for more locations and assess their relationship. At a next level, this analysis and its findings could be used, as the basis for the development of synthetic storms and the storm modelling at the examined locations.

## Acknowledgements

The authors thank Puertos del Estado, the Copernicus and the EMODnet for providing the wave climate data from their database. We also gratefully acknowledge the important feedback of the anonymous reviewers, which was valuable for improving our work. This work is part of Mr

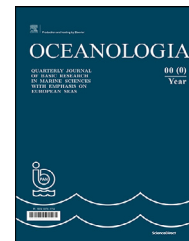
Martzikos' PhD thesis and it was co-financed by Greece and the European Union (European Social Fund-ESF) through the Operational Programme 'Human Resources Development, Education and Lifelong Learning' in the context of the project 'Strengthening Human Resources Research Potential via Doctorate Research' (MIS-5000432), implemented by the State Scholarships Foundation (IKY).

## References

- Almeida, L.P., Ferreira, Ó., Vousdoukas, M.I., Dodet, G., 2011. Historical variation and trends in storminess along the Portuguese South Coast. *Nat. Hazards Earth Syst. Sci.* 11, 2407–2417. <https://doi.org/10.5194/nhess-11-2407-2011>
- Androulidakis, Y.S., Kombiadou, K.D., Makris, C.V., Baltikas, V.N., Krestenitis, Y.N., 2015. Storm surges in the Mediterranean Sea: Variability and trends under future climatic conditions. *Dyn. Atmos. Ocean.* 71, 56–82. <https://doi.org/10.1016/j.dynatmoce.2015.06.001>
- Arns, A., Wahl, T., Haigh, I.D., Jensen, J., Pattiaratchi, C., 2013. Estimating extreme water level probabilities: A comparison of the direct methods and recommendations for best practise. *Coast. Eng.* 81, 51–66. <https://doi.org/10.1016/j.coastaleng.2013.07.003>
- Bernardara, P., Mazas, F., Kergadallan, X., Hamm, L., 2014. A two-step framework for over-threshold modelling of environmental extremes. *Nat. Hazards Earth Syst. Sci.* 14, 635–647. <https://doi.org/10.5194/nhess-14-635-2014>
- Bertin, X., Bruneau, N., Breilh, J.-F., Fortunato, A.B., Karpytchev, M., 2012. Importance of wave age and resonance in storm surges: The case Xynthia, Bay of Biscay. *Ocean Model* 42, 16–30. <https://doi.org/10.1016/j.ocemod.2011.11.001>
- Bezak, N., Brilly, M., Šraj, M., 2014. Comparison between the peaks-over-threshold method and the annual maximum method for flood frequency analysis. *Hydrol. Sci. J.* 59, 959–977. <https://doi.org/10.1080/02626667.2013.831174>
- Binder, S.B., Baker, C.K., Barile, J.P., 2015. Rebuild or Relocate? Resilience and Postdisaster Decision-Making After Hurricane Sandy. *Am. J. Community Psychol.* 56, 180–196. <https://doi.org/10.1007/s10464-015-9727-x>
- Boccotti, P., 2014. *Wave Mechanics and Wave Loads on Marine Structures*, 1st edn., Butterworth-Heinemann.
- Boccotti, P., 2000. Chapter 6 The Wave Climate. In: Elsevier Oceanography Series. Elsevier Science, 183–206. [https://doi.org/10.1016/S0422-9894\(00\)80032-X](https://doi.org/10.1016/S0422-9894(00)80032-X)
- Caires, S., Sterl, A., 2005. 100-Year Return Value Estimates for Ocean Wind Speed and Significant Wave Height from the ERA-40 Data. *J. Clim.* 18, 1032–1048. <https://doi.org/10.1175/JCLI-3312.1>
- Callaghan, D.P., Nielsen, P., Short, A., Ranasinghe, R., 2008. Statistical simulation of wave climate and extreme beach erosion. *Coast. Eng.* 55, 375–390. <https://doi.org/10.1016/j.coastaleng.2007.12.003>
- Cavicchia, L., von Storch, H., Gualdi, S., 2014. Mediterranean Tropical-Like Cyclones in Present and Future Climate. *J. Clim.* 27, 7493–7501. <https://doi.org/10.1175/JCLI-D-14-00339.1>
- Ciavola, P., Ferreira, O., Dongeren, A., Van, Vries, J.V.T.de, Armaroli, C., Harley, M., 2014. Prediction of Storm Impacts on Beach and Dune Systems. In: *Hydrometeorological Hazards*. John Wiley & Sons, Ltd., Chichester, UK, 227–252. <https://doi.org/10.1002/9781118629567.ch3d>
- Ciavola, P., Ferreira, O., Haerens, P., Van Koningsveld, M., Armaroli, C., 2011a. Storm impacts along European coastlines. Part 2: lessons learned from the MICORE project. *Environ. Sci. Policy* 14, 924–933. <https://doi.org/10.1016/j.envsci.2011.05.009>

- Ciavola, P., Ferreira, O., Haerens, P., Van Koningsveld, M., Armaroli, C., Lequeux, Q., 2011b. Storm impacts along European coastlines. Part 1: The joint effort of the MICORE and ConHaz Projects. *Environ. Sci. Policy* 14, 912–923. <https://doi.org/10.1016/j.envsci.2011.05.011>
- Coles, S., 2001. An Introduction to Statistical Modeling of Extreme Values, Springer Series in Statistics. Springer, London, London. <https://doi.org/10.1007/978-1-4471-3675-0>
- Copernicus Marine In Situ Tac Data Management Team, 2018. Copernicus Marine in situ TAC – physical parameters list. <https://doi.org/10.13155/53381>
- Corbella, S., Pringle, J., Stretch, D.D., 2015. Assimilation of ocean wave spectra and atmospheric circulation patterns to improve wave modelling. *Coast. Eng.* 100, 1–10. <https://doi.org/10.1016/j.coastaleng.2015.03.003>
- Corbella, S., Stretch, D., 2012a. Multivariate return periods of sea storms for coastal erosion risk assessment. *Nat. Hazards Earth Syst. Sci.* 12, 2699–2708. <https://doi.org/10.5194/nhess-12-2699-2012>
- Corbella, S., Stretch, D.D., 2013. Simulating a multivariate sea storm using Archimedean copulas. *Coast. Eng.* 76, 68–78. <https://doi.org/10.1016/j.coastaleng.2013.01.011>
- Corbella, S., Stretch, D.D., 2012b. Predicting coastal erosion trends using non-stationary statistics and process-based models. *Coast. Eng.* <https://doi.org/10.1016/j.coastaleng.2012.06.004>
- Davies, G., Callaghan, D.P., Gravois, U., Jiang, W., Hanslow, D., Nichol, S., Baldock, T., 2017. Improved treatment of non-stationary conditions and uncertainties in probabilistic models of storm wave climate. *Coast. Eng.* 127, 1–19. <https://doi.org/10.1016/j.coastaleng.2017.06.005>
- De Michele, C., Salvadori, G., Passoni, G., Vezzoli, R., 2007. A multivariate model of sea storms using copulas. *Coast. Eng.* 54, 734–751. <https://doi.org/10.1016/j.coastaleng.2007.05.007>
- Dee, D.P., Uppala, S.M., Simmons, A.J., Berrisford, P., Poli, P., Kobayashi, S., Andrae, U., Balmaseda, M.A., Balsamo, G., Bauer, P., Bechtold, P., Beljaars, A.C.M., van de Berg, L., Bidlot, J., Bormann, N., Delsol, C., Dragani, R., Fuentes, M., Geer, A.J., Haimberger, L., Healy, S.B., Hersbach, H., Hólm, E.V., Isaksen, L., Kållberg, P., Köhler, M., Matricardi, M., McNally, A.P., Monge-Sanz, B.M., Morcrette, J.-J., Park, B.-K., Peubey, C., de Rosnay, P., Tavolato, C., Thépaut, J.-N., Vitart, F., 2011. The ERA-Interim reanalysis: configuration and performance of the data assimilation system. *Q. J. R. Meteorol. Soc.* 137, 553–597. <https://doi.org/10.1002/qj.828>
- Dey, D., Roy, D., Yan, J., 2015. Univariate Extreme Value Analysis. In: *Extreme Value Modeling and Risk Analysis*. Chapman and Hall/CRC, 1–22. <https://doi.org/10.1201/b19721-2>
- Dissanayake, P., Brown, J., Wisse, P., Karunarathna, H., 2015. Effects of storm clustering on beach/dune evolution. *Mar. Geol.* 370, 63–75. <https://doi.org/10.1016/j.margeo.2015.10.010>
- Dolan, R., Davis, R., 1992. An Intensity Scale for Atlantic Coast Northeast Storms. *J. Coast. Res.* 8, 840–853.
- Emanuel, K., 2005. Genesis and maintenance of “Mediterranean hurricanes”. *Adv. Geosci.* 2, 217–220. <https://doi.org/10.5194/adgeo-2-217-2005>
- Ferguson, T.S., Genest, C., Hallin, M., 2000. Kendall’s tau for serial dependence. *Can. J. Stat.* 28, 587–604. <https://doi.org/10.2307/3315967>
- Ferreira, J.A., Guedes Soares, C., 1998. An Application of the Peaks Over Threshold Method to Predict Extremes of Significant Wave Height. *J. Offshore Mech. Arct. Eng.* 120, 165–176. <https://doi.org/10.1115/1.2829537>
- Ferreira, Ó., 2005. Storm Groups versus Extreme Single Storms: Predicted Erosion and Management Consequences. *J. Coast. Res.* 21, 221–227.
- Ferreira, Ó., Plomaritis, T.A., Costas, S., 2017. Process-based indicators to assess storm induced coastal hazards. *Earth-Science Rev.* 173, 159–167. <https://doi.org/10.1016/j.earscirev.2017.07.010>
- Freitas, E., da, S., Coelho, V.H.R., Xuan, Y., Melo, D., de, C.D., Gadelha, A.N., Santos, E.A., Galvão, C., de, O., Ramos Filho, G.M., Barbosa, L.R., Huffman, G.J., Petersen, W.A., Almeida, C., das, N., 2020. The performance of the IMERG satellite-based product in identifying sub-daily rainfall events and their properties. *J. Hydrol.* 589, 125–128. <https://doi.org/10.1016/j.jhydrol.2020.125128>
- Gervais, M., Balouin, Y., Belon, R., 2012. Morphological response and coastal dynamics associated with major storm events along the Gulf of Lions Coastline, France. *Geomorphology* 143–144, 69–80. <https://doi.org/10.1016/j.geomorph.2011.07.035>
- González-Alemán, J.J., Pascale, S., Gutierrez-Fernandez, J., Murakami, H., Gaertner, M.A., Vecchi, G.A., 2019. Potential Increase in Hazard From Mediterranean Hurricane Activity With Global Warming. *Geophys. Res. Lett.* 46, 1754–1764. <https://doi.org/10.1029/2018GL081253>
- Harley, M., 2017. Coastal Storm Definition. In: *Coastal Storms*. John Wiley & Sons, Ltd, Chichester, UK, 1–21. <https://doi.org/10.1002/9781118937099.ch1>
- Hollander, M., Wolfe, D., Chicken, E., 2015. Nonparametric Statistical Methods, Wiley Series in Probability and Statistics. Wiley, New York. <https://doi.org/10.1002/9781119196037>
- IPCC, 2019. Special Report on the Ocean and Cryosphere in a Changing Climate [WWW Document]. URL <https://www.ipcc.ch/srocc/>
- IPCC, 2018. Global Warming of 1.5°C [WWW Document]. URL <https://www.ipcc.ch/sr15/>
- Irish, J.L., Resio, D.T., Ratcliff, J.J., 2008. The Influence of Storm Size on Hurricane Surge. *J. Phys. Oceanogr.* 38, 2003–2013. <https://doi.org/10.1175/2008JPO3727.1>
- Jammalamadaka, S.R., SenGupta, A., 2001. Topics in Circular Statistics, Series on Multivariate Analysis. WORLD SCIENTIFIC. <https://doi.org/10.1142/4031>
- Jarušková, D., Hanek, M., 2006. Peaks over threshold method in comparison with block-maxima method for estimating return levels of several northern Moravia precipitation and discharges series. *J. Hydrol. Hydromech.* 54, 309–319.
- Jean, M.-È., Duchesne, S., Pelletier, G., Pleau, M., 2018. Selection of rainfall information as input data for the design of combined sewer overflow solutions. *J. Hydrol.* 565, 559–569. <https://doi.org/10.1016/j.jhydrol.2018.08.064>
- Karavokiros, G., Lykou, A., Koutiva, I., Batica, J., Kostaridis, A., Alves, A., Makropoulos, C., 2016. Providing Evidence-Based, Intelligent Support for Flood Resilient Planning and Policy: The PEARL Knowledge Base. *Water* 8, 392. <https://doi.org/10.3390/w8090392>
- Kates, R.W., Colten, C.E., Laska, S., Leatherman, S.P., 2006. Reconstruction of New Orleans after Hurricane Katrina: A research perspective. *Proc. Natl. Acad. Sci.* 103, 14653–14660. <https://doi.org/10.1073/pnas.0605726103>
- Kereszturi, M., Tawn, J., Jonathan, P., 2016. Assessing extremal dependence of North Sea storm severity. *Ocean Eng.* 118, 242–259. <https://doi.org/10.1016/j.oceaneng.2016.04.013>
- Kistler, R., Collins, W., Saha, S., White, G., Woollen, J., Kalnay, E., Chelliah, M., Ebisuzaki, W., Kanamitsu, M., Kousky, V., van den Dool, H., Jenne, R., Fiorino, M., 2001. The NCEP–NCAR 50–Year Reanalysis: Monthly Means CD–ROM and Documentation. *Bull. Am. Meteorol. Soc.* 82, 247–267. [https://doi.org/10.1175/1520-0477\(2001\)082<0247:TNNYRM>2.3.CO;2](https://doi.org/10.1175/1520-0477(2001)082<0247:TNNYRM>2.3.CO;2)
- Li, F., van Gelder, P.H.A.J.M., Ranasinghe, R., Callaghan, D.P., Jongejan, R.B., 2014. Probabilistic modelling of extreme storms along the Dutch coast. *Coast. Eng.* 86, 1–13. <https://doi.org/10.1016/j.coastaleng.2013.12.009>
- Li, F., Zhou, J., Liu, C., 2018. Statistical modelling of extreme storms using copulas: A comparison study. *Coast. Eng.* 142, 52–61. <https://doi.org/10.1016/j.coastaleng.2018.09.007>

- Lin-Ye, J., Garcia-Leon, M., Gracia, V., Sanchez-Arcilla, A., 2016. A multivariate statistical model of extreme events: An application to the Catalan coast. *Coast. Eng.* 117, 138–156. <https://doi.org/10.1016/j.coastaleng.2016.08.002>
- Lionello, P., Bhend, J., Buzzi, A., Della-Marta, P.M., Krichak, S.O., Jansà, A., Maheras, P., Sanna, A., Trigo, I.F., Trigo, R., 2006. Chapter 6 Cyclones in the Mediterranean region: Climatology and effects on the environment. 325–372. [https://doi.org/10.1016/S1571-9197\(06\)80009-1](https://doi.org/10.1016/S1571-9197(06)80009-1)
- Lionello, P., Cogo, S., Galati, M.B., Sanna, A., 2008. The Mediterranean surface wave climate inferred from future scenario simulations. *Glob. Planet. Change* 63, 152–162. <https://doi.org/10.1016/j.gloplacha.2008.03.004>
- Lionello, P., Galati, M.B., Elvini, E., 2012. Extreme storm surge and wind wave climate scenario simulations at the Venetian littoral. *Phys. Chem. Earth, Parts A/B/C* 40–41, 86–92. <https://doi.org/10.1016/j.pce.2010.04.001>
- Lionello, P., Trigo, I.F., Gil, V., Liberato, M.L.R., Nissen, K.M., Pinto, J.G., Raible, C.C., Reale, M., Tanzarella, A., Trigo, R.M., Ulbrich, S., Ulbrich, U., 2016. Objective climatology of cyclones in the Mediterranean region: a consensus view among methods with different system identification and tracking criteria. *Tellus A Dyn. Meteorol. Oceanogr.* 68, art. no. 29391. <https://doi.org/10.3402/tellusa.v68.29391>
- Lira-Loarca, A., Cobos, M., Losada, M.Á., Baquerizo, A., 2020. Storm characterization and simulation for damage evolution models of maritime structures. *Coast. Eng.* 156, art. no. 103620. <https://doi.org/10.1016/j.coastaleng.2019.103620>
- Martzikos, N., Afentoulis, V., Tsoukala, V., 2018. Storm clustering and classification for the port of Rethymno in Greece. *Water Util. J.* 67–69.
- Masselink, G., Austin, M., Scott, T., Poate, T., Russell, P., 2014. Role of wave forcing, storms and NAO in outer bar dynamics on a high-energy, macro-tidal beach. *Geomorphology* 226, 76–93. <https://doi.org/10.1016/j.geomorph.2014.07.025>
- Mazas, F., Hamm, L., 2011. A multi-distribution approach to POT methods for determining extreme wave heights. *Coast. Eng.* 58, 385–394. <https://doi.org/10.1016/j.coastaleng.2010.12.003>
- Méndez, F.J., Menéndez, M., Luceño, A., Losada, I.J., 2006. Estimation of the long-term variability of extreme significant wave height using a time-dependent Peak Over Threshold (POT) model. *J. Geophys. Res.* 111, art. no. C07024. <https://doi.org/10.1029/2005JC003344>
- Menéndez, M., Méndez, F.J., Izaguirre, C., Luceño, A., Losada, I.J., 2009. The influence of seasonality on estimating return values of significant wave height. *Coast. Eng.* 56, 211–219. <https://doi.org/10.1016/j.coastaleng.2008.07.004>
- OceanSITES, 2015. OceanSITES Data Format Reference Manual.
- R Core Team, 2020. R: A language and environment for statistical computing.
- Rangel-Buitrago, N., 2011. An application of Dolan and Davis (1992) classification to coastal storms in SW Spanish littoral. *ics2011.pl*.
- Rosenzweig, C., Solecki, W., 2014. Hurricane Sandy and adaptation pathways in New York: Lessons from a first-responder city. *Glob. Environ. Chang.* 28, 395–408. <https://doi.org/10.1016/j.gloenvcha.2014.05.003>
- Ruggiero, P., Komar, P.D., Allan, J.C., 2010. Increasing wave heights and extreme value projections: The wave climate of the U.S. Pacific Northwest. *Coast. Eng.* 57, 539–552. <https://doi.org/10.1016/j.coastaleng.2009.12.005>
- Salvadori, G., Tomasicchio, G.R., D'Alessandro, F., 2014. Practical guidelines for multivariate analysis and design in coastal and off-shore engineering. *Coast. Eng.* 88, 1–14. <https://doi.org/10.1016/j.coastaleng.2014.01.011>
- Sartini, L., Besio, G., Cassola, F., 2017. Spatio-temporal modelling of extreme wave heights in the Mediterranean Sea. *Ocean Model* 117, 52–69. <https://doi.org/10.1016/j.ocemod.2017.07.001>
- Sénéchal, N., Castelle, B., Bryan, K.R., 2017. Storm Clustering and Beach Response. In: *Coastal Storms*. John Wiley & Sons, Ltd., Chichester, UK, 151–174. <https://doi.org/10.1002/9781118937099.ch8>
- Tsoukala, V.K., Chondros, M., Kapelonis, Z.G., Martzikos, N., Lykou, A., Belibassakis, K., Makropoulos, C., 2016. An integrated wave modelling framework for extreme and rare events for climate change in coastal areas – The case of Rethymno, Crete. *Oceanologia* 58 (2), 71–89. <https://doi.org/10.1016/j.oceano.2016.01.002>
- UNFCCC, 2016. Report of the Conference of the Parties on its twenty-first session, held in Paris from 30 November to 13 December 2015 Conf. CoP 21, FCCC/CP/2015/10, United Nations Framework Convention on Climate Change, 16 pp.
- USGCRP, 2018. Impacts, Risks, and Adaptation in the United States: The Fourth National Climate Assessment, II Vol., Washington, DC. <https://doi.org/10.7930/NCA4.2018>
- Van Dongeren, A., Ciavola, P., Viavattene, C., de Kleermaeker, S., Martinez, G., Ferreira, O., Costa, C., McCall, R., 2014. RISC-KIT: Resilience-Increasing Strategies for Coasts – toolKIT. *J. Coast. Res.* 70, 366–371. <https://doi.org/10.2112/SI70-062.1>
- Vinoth, J., Young, I.R., 2011. Global Estimates of Extreme Wind Speed and Wave Height. *J. Clim.* 24, 1647–1665. <https://doi.org/10.1175/2010JCLI3680.1>
- Vousdoukas, M.I., Voukouvalas, E., Annunziato, A., Giardino, A., Feyen, L., 2016. Projections of extreme storm surge levels along Europe. *Clim. Dyn.* 47, 3171–3190. <https://doi.org/10.1007/s00382-016-3019-5>
- Wahl, T., Plant, N.G., Long, J.W., 2016. Probabilistic assessment of erosion and flooding risk in the northern Gulf of Mexico. *J. Geophys. Res. Ocean.* 121, 3029–3043. <https://doi.org/10.1002/2015JC011482>
- Williams, J., Horsburgh, K.J., Williams, J.A., Proctor, R.N.F., 2016. Tide and skew surge independence: New insights for flood risk. *Geophys. Res. Lett.* 43, 6410–6417. <https://doi.org/10.1002/2016GL069522>
- Yevjevich, V.M., 1967. An objective approach to definitions and investigations of continental hydrologic droughts. *J. Hydrol.* 23.
- Zanuttigh, B., 2011. Coastal flood protection: What perspective in a changing climate? The THESEUS approach. *Environ. Sci. Policy* 14, 845–863. <https://doi.org/10.1016/j.envsci.2011.03.015>



ORIGINAL RESEARCH ARTICLE

# Species-level associations of phytoplankton with environmental variability in the Neva Estuary (Baltic Sea)

Mikhail Golubkov\*, Vera Nikulina, Sergey Golubkov

Zoological Institute of Russian Academy of Sciences, St. Petersburg, Russian Federation

Received 26 May 2020; accepted 13 November 2020

Available online 27 November 2020

## KEYWORDS

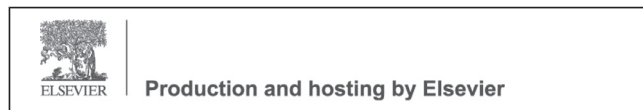
Gulf of Finland;  
Species composition;  
Eutrophication;  
Harmful algae;  
Long-term  
observations;  
Climate change

**Abstract** Changes in phytoplankton communities due to anthropogenic nutrient load and climate change often lead to eutrophication and harmful algal blooms that can affect biogeochemical cycling. However, little is known about the specific responses of various species to environmental variables. 17-year long data on the midsummer phytoplankton biomass in the Neva Estuary were analyzed to show the changes in the composition of phytoplankton in relation to water depth, transparency, salinity, temperature, concentrations of total phosphorus and chlorophyll *a*, and plankton primary production. One hundred seventy-four species and forms from eight taxonomic classes were found in phytoplankton. Fifteen species were potentially harmful. The most diverse and abundant groups were cyanobacteria, green algae and diatoms. Canonical Correspondence Analysis showed that the biomass of various species from each phytoplankton group correlated differently with environmental factors. However, within each group, there were some predominant trends in the correlative response to changes in environmental variables. The biomass of cyanobacteria was high in the middle and lower reaches of the estuary and, in general, positively correlated with water salinity. The biomass of most species of green algae and diatoms correlated negatively with it. These algae showed a positive trend in biomass in the upper and middle reaches of the estuary during the last decades that may be

\* Corresponding author at: Zoological Institute of Russian Academy of Sciences, 199034, Universitetskaya emb. 1, St. Petersburg, Russian Federation.

*E-mail address:* [golubkov\\_ms@mail.ru](mailto:golubkov_ms@mail.ru) (M. Golubkov).

Peer review under the responsibility of the Institute of Oceanology of the Polish Academy of Sciences.



explained by changes in weather conditions. Taking into account that climate models predict future increases in precipitation and temperature in the northern Baltic, the future expansion of freshwater phytoplankton species in estuaries of the northern Baltic Sea is very likely.

© 2020 Institute of Oceanology of the Polish Academy of Sciences. Production and hosting by Elsevier B.V. This is an open access article under the CC BY-NC-ND license (<http://creativecommons.org/licenses/by-nc-nd/4.0/>).

## 1. Introduction

Eutrophication and harmful algal blooms have been recognized as one of the major environmental problems of coastal areas around the world (Damar et al., 2020; Heisler et al., 2008; Holt et al., 2016; Kahru et al., 2020). This problem has been especially acute in recent years due to anthropogenic nutrient load and climate change, which may exacerbate the negative consequences of human activities (Behrenfeld et al., 2006; Doney et al., 2012; Golubkov and Alimov, 2010; Golubkov and Golubkov, 2020; Teutschbein et al., 2017). Improving our understanding of the factors that determine the development of algae in general and toxic species in particular requires determination and quantification of the physico-chemical environmental factors that create conditions for the accelerated growth and dominance of various groups and species of algae in the phytoplankton community (Stauffer et al., 2020). Such studies are important for understanding the patterns of formation of species diversity in plankton communities (Huisman and Weissing, 1999), for forecasting the direction of biogeochemical cycles and fish productivity (Boyce et al., 2010; Golubkov et al., 2020), and for predicting possible negative phenomena for humans, both on a regional and global scale (Dzierzbicka-Głowacka et al., 2011).

The Baltic Sea is highly susceptible to eutrophication caused by the influx of nutrients from densely populated and intensively cultivated catchment areas (Wasmund et al., 2011). The Neva Estuary, situated at the top of the Gulf of Finland, is one of the most eutrophic areas of the Baltic Sea (Golubkov and Alimov, 2010). The primary productivity and biomasses of autotrophic organisms in the estuary are high, mainly due to eutrophic effects of the large nutrient inflow from the Neva River, which is the major contributor of freshwater to the Baltic Sea (Golubkov, 2009; Golubkov et al., 2017). The Neva Estuary is characterized by a number of features that make it a convenient site for studying the relationships between physico-chemical factors and species composition and productivity of phytoplankton, which is important not only regionally, but also globally. It is a brackish-water, non-tidal and shallow water area, with vertical and horizontal gradients of salinity and temperature, concentrations of nutrients, and indicators of phytoplankton productivity. Plankton communities of the estuary include freshwater and marine species; eurytopic species also make up a significant proportion (Telesh et al., 2008).

Long-term data on seasonal dynamics of phytoplankton in the middle reach of the Neva Estuary show that since the late 1990s – early 2000s mean seasonal biomass of phytoplankton increased approximately twofold as compared with the 1980s (Nikulina, 2003). In addition, a significant increase in plankton primary production was observed in

the 2010s (Golubkov et al., 2017), and apparently this was due not only to the anthropogenic nutrient load, but also to changes in weather conditions in recent years because of the global warming, which manifests regionally in warm winters and cool rainy summer seasons (Golubkov and Golubkov, 2020).

Most regional climate models predict future increases in winter and summer air temperatures and precipitation in the northern Baltic regions (Meier et al., 2012; Teutschbein et al., 2017). Changes in weather conditions affect water temperatures and salinity, nutrient concentrations and plankton primary production (Friedland et al., 2012; Golubkov and Golubkov, 2020; Holt et al., 2016; Myakisheva, 1996). As a result, in addition to an increase in phytoplankton productivity, this leads to a change in the dominant groups in the phytoplankton community in various regions of the Baltic Sea (Jaanus et al., 2011; Klais et al., 2011; Nikulina, 2003; Wasmund et al., 2011), which affects biogeochemical cycling (Golubkov et al., 2020; Neumann and Schernewski, 2008; Spilling et al., 2018). In the Neva Estuary, diatoms (Bacillariophyceae) were the dominant group of phytoplankton until the late 1990s (Nikulina, 2003). Cyanobacteria were an important group only in late July and August. However, since the early 2000s, cyanobacteria biomass and the period of their predominance in plankton have increased significantly, which was accompanied by an increase in the total biomass of phytoplankton, as well as in its primary production and chlorophyll concentration (Golubkov et al., 2017; Nikulina, 2003). Later in the 2010s, the biomass of dinoflagellates also increased (Golubkov et al., 2019a). The same changes in the dominance of dinoflagellates and diatoms were observed in the Baltic Proper in the late 1980s and could be attributed to warming rather than to eutrophication (Wasmund, 2017). This leads to a regime shift because differences in the sinking of these two classes of phytoplankton affect ecosystem functioning and eutrophication feedback loops (Spilling et al., 2018; Wasmund et al., 2017). If diatoms are dominant, their rapid sinking reduces the food stock for zooplankton but delivers plenty of food to the zoobenthos. On the contrary, dinoflagellates sink slowly, mainly providing organic matter to pelagic consumers. To assess the environmental status of the Baltic Sea a pre-core indicator diatom/dinoflagellate index (Dia/Dino index) was developed (Wasmund et al., 2017).

The purpose of this study was to find statistical relationships between physical and chemical factors of the environment and indicators of phytoplankton productivity and biomass of various groups and species of phytoplankton in the Neva Estuary. Although statistical relationships do not reflect causality, they provide clues for finding the environmental conditions that regulate the development of

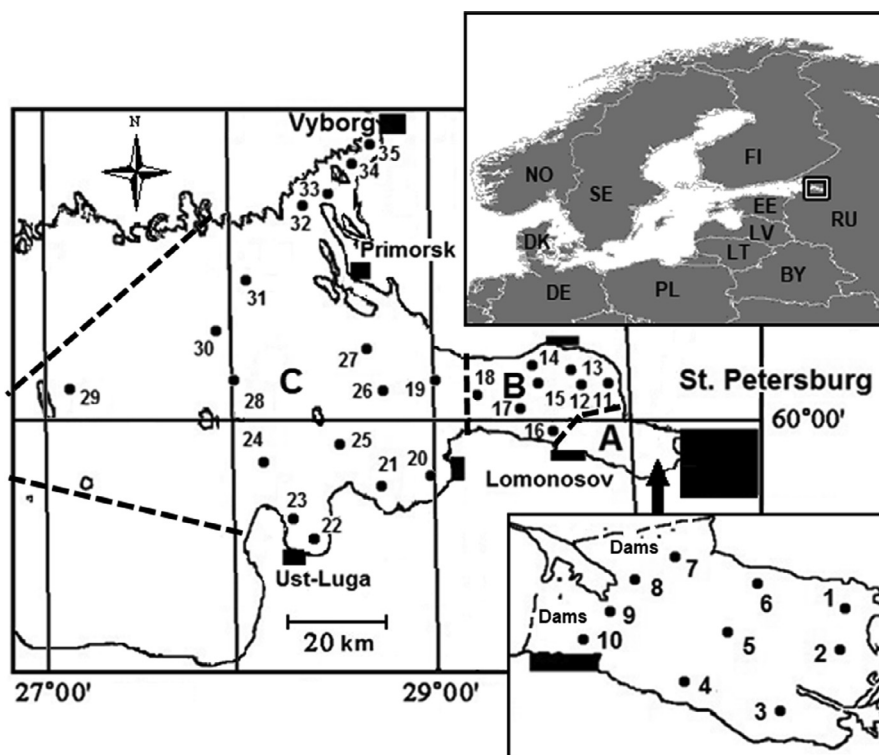


**Figure 1** The Neva Estuary with an indication of sampling stations (A – the upper reach; B – the middle reach; C – the lower reach). The dotted line shows the boundaries between reaches. Two-letter country codes are given according to ISO 3166-1 alpha-2 (International Organization for Standardization (ISO) 2020).

algae and the dominance of certain groups and species in the phytoplankton community. This can help simulate conditions to predict the likelihood of abundant algal blooms in the future and forecast which groups of phytoplankton will dominate non-toxic green and diatoms, or potentially toxic cyanobacteria and dinoflagellates.

## 2. Material and methods

### 2.1. Study area

The Neva Estuary receives water from the Neva River, a relatively short canal (74 km) between Lake Ladoga and the Gulf of Finland, whose catchment area exceeds 280,000 km<sup>2</sup>, and the water discharge averages 2,490 m<sup>3</sup> s<sup>-1</sup> (78.6 km<sup>3</sup> yr<sup>-1</sup>), which is about a fifth of the total river discharge into the Baltic Sea.

Flood Protective Facility (Dams) separated the upper reach of the estuary from its lower reaches (Figure 1). It consists of eleven dams separated by broad water passages and ship gates in its southern and northern parts. The surface area of the upper reach (UR), is about 400 km<sup>2</sup>, the salinity – 0.07–0.2 PSU. The depth of the UR is 1.6–5 m, the water residence time is 5.5 days. There is no temperature stratification in this reach of the estuary. High water turbidity (Secchi depth does not exceed 1.8 m) constrains the distribution of bottom vegetation in the UR. The middle reach (MR) of the Neva Estuary is brackish-water and located between Dams and a longitude of ca. 29°10'E (Figure 1). The salinity of surface waters in this part of the

estuary ranges from 0.5 to 3 PSU, and the depth – from 7 to 14 m in the eastern MR and up to 25 m in its western part. The water residence time is approximately 45 days. There is temperature stratification in the western part of the MR in summer: a warm water upper layer (UL) and a cold water deep layer (DL). The lower reach (LR) of the Neva Estuary located to the west of the ca. 29°10'E and to the east of the border of territorial waters of Russia (Figure 1). It has a depth up to 60 m, temperature stratification in summer and the salinity of UL up to 5.5 PSU. The water residence time is about 1500 days. The Neva Estuary is the recipient of discharges of treated and untreated wastewaters from St. Petersburg City, which is the largest megalopolis in the Baltic region with a population of more than 5 million citizens (Golubkov et al., 2019). A more detailed description of the estuary was given in previous publications (Golubkov et al., 2017; Golubkov and Golubkov, 2020; Telesh et al., 2008).

### 2.2. Sampling

Ten stations in the UR, eight stations in the MR and seventeen stations in the LR were sampled from 20th of July – to 5th of August 2003–2019. The number of stations varied in different years (Supplementary Table 1). Secchi depth (Sec), salinity (S) and temperature (T) were measured at each station. T and S were measured by the CTD90m probe (Sea&Sun Tech., Germany) every 20 cm from the surface to the bottom in the whole water column. Taking into account that according to these measurements the whole water column in the shallow UR was mixed, we collected five water samples (2 l each): from the surface, half a meter from the bottom

and from three equal depths between them. Samples from different depths were taken in order to avoid errors associated with the vertical distribution of different phytoplankton species in the water column. These samples were composited and mixed to make up a pooled sample (10 l). Samples of total phosphorus and chlorophyll *a* (three replicates of water collection) were taken from these pooled samples.

In the LR of the estuary (Figure 1), integrated water samples were taken from the UL. Five water samples (2 l each) were taken from the UL: from the surface, the thermocline and from three equal depths between them. These samples were mixed to create a pooled sample (10 l). The samples for chlorophyll *a* and total phosphorus (three replicates of water collection) were taken from these pooled samples.

### 2.3. Sample analysis

Three hundred millilitres of water were filtered through 0.85  $\mu\text{m}$  membrane filters (Millipore AAWP) to determine the chlorophyll *a* (C) concentration, which was followed by 90% acetone extraction and spectrophotometric determination (Grasshoff et al., 1999). Total phosphorus (TP) was determined after acid hydrolysis with the molybdate blue method (Grasshoff et al., 1999).

The primary production of plankton (PP) in the water column were measured by the oxygen method of light and dark bottles (Hall et al., 2007; Vernet and Smith, 2007). Since the depth of the UL practically coincided with the depth of euphotic zone in mid-summer 900 ml of water from the UL pooled samples from the MR, the LR and from the whole water column in the UR were used to determine PP. Three 100 ml light and three dark bottles were filled with the water from each sampling station and exposed in an aquarium on the ship's deck in shadow during 6 h at a surface water temperature to estimate PP. Three 100 ml bottles (control bottles) were filled with the water from each sampling station to determine the oxygen contents in water at the beginning of the experiment. The Winkler method was used to determine the oxygen contents in the control, the light and the dark bottles (Hall et al. 2007). The gross primary production under 1 m<sup>2</sup> of water surface was calculated according to Vollenweider (1969). The rate of plankton production was recalculated to organic carbon as recommended by Wetzel and Likens (2000) using a factor 0.43 mgC mlO<sup>-1</sup> (Håkanson and Boulion, 2002). A more detailed description of the method and experimental design is given in Golubkov et al. (2017).

### 2.4. Phytoplankton assemblages

Phytoplankton (volume 0.3 l) was taken in one replicate of water collection from pooled samples and fixed with acid Lugol's solution. The phytoplankton taxa were identified and counted in sedimentation chambers (10–25 ml) with an inverted Hydro-Bios microscope. Phytoplankton biomass was calculated in the total volume of algal cells according to Olenina et al. (2006) and expressed in wet weight (WW) mg l<sup>-1</sup>. Identification of phytoplankton taxa was conducted according to Kiselev (1954), Pankov (1976) and Tikkanen (1986). Phytoplankton species have been listed in the modern nomenclature according to Guiry and Guiry (2020).

### 2.5. Statistical analysis

The biomass for each of taxonomic classes was averaged for each station and was visualized using SURFER 8.0. Annual trends were estimated by averaging the biomass of each taxonomic class and were visualized using Microsoft Excell.

Canonical Correspondence Analysis (CCA) was used to assess the effect of environmental variables on phytoplankton groups and species in the Neva Estuary. S, T, Sec, TP, C and PP were used as environmental data sources. CCA was performed using R software (version 3.6.0; R Development Core Team, 2020; [www.r-project.org/](http://www.r-project.org/)), R package 'vegan' (Oksanen et al., 2020) and visualised by R package 'ggplot2' (Wickham et al., 2020). We used only species that were found at least five times over the entire period of observation. The biomass of various species from the phytoplankton community was used as a biological data source. Prior to the CCA, each environmental variable was tested using the variance inflation factor (VIF). Function 'vif.cca' was used to give the variance inflation factors for each constraint and contrast in the constraints of the environmental variables. Variance inflation was a diagnostic tool to identify useless constraints. A common rule is that values over 10 indicate redundant constraints. If later constraints were complete linear combinations of conditions or previous constraints, they were completely removed from the estimation, and no biplot scores were calculated for these aliased constraints. A constrained model based on the length of the gradient calculated by CCA was built by function 'vare.cca'. It is based on Chi-squared distances and performs weighted linear mapping. Monte Carlo replacement tests (999 permutations) were carried out to determine the environmental factors that significantly explained the spatial distribution characteristics of the phytoplankton communities. R package 'ggplot2' was used to build CCA biplots. For better understanding the results of CCA we provided ordination diagram separately for eight taxonomical classes of algae.

In a CCA biplot, the arrows for environmental variables point in the general direction of maximum environmental change across the diagram with statistical significance ( $p < 0.05$ ), and their lengths are approximately proportional to the rate of change in that direction. The correlation between biomasses of phytoplankton and environmental factors was examined based on the angle between arrows; an angle smaller than 90° indicates a positive correlation between the variables; the smaller the angle, the closer the positive correlation of the two variables. An angle between 90° and 180° suggests a negative correlation. Finally, there is no correlation between two variables when their angle is 90°. The projection of phytoplankton species biomass on the environmental variable vector is an approximation of the "optima" regarding that particular variable (ter Braak and Verdonschot, 1995).

## 3. Results

### 3.1. Environmental parameters

The environmental variables in the Neva Estuary during the study period are shown in Table 1. The shallowest sampling station 3 with a depth of 1.6 m was located in

**Table 1** Environmental variables in the Neva Estuary during the study period.

Parameter	minimum	maximum	median	mean	SD
Water depth [m]	1.6	61.0	12.7	23.5	11.5
Depth of water layer above thermocline [m]	1.6	21.5	7.5	9.3	3.5
Salinity of water layer above thermocline [PSU]	0.05	5.55	1.80	2.73	1.04
Temperature of water layer above thermocline [°C]	16.2	26.2	19.8	20.0	2.12
Secchi depth [m]	0.3	4.3	1.6	2.0	0.7
Total phosphorus concentration in water layer above the thermocline [mg m <sup>-3</sup> ]	5.4	230.3	37.4	50.6	39.1
Chlorophyll <i>a</i> [mg m <sup>-3</sup> ]	0.88	127.65	14.5	17.50	17.25
Plankton primary production [gC m <sup>-2</sup> d <sup>-1</sup> ]	0.05	4.14	1.06	1.21	0.78

the upper reach of the estuary, and the deepest station 29 with a depth of 61 m was in the lower reach of the estuary (Table 1). The mean depth of UL was 9.3 m, but maximum depth was 21.5 m. The water temperature of UL varied within 10 degrees, from 16 to 26°C, averaging 20°C. The salinity of the water in this layer reached 5.5 PSU, averaging 2.7 PSU. Secchi depth varied from 0.2 m in the eastern part to more than 4 meters in the westernmost part of the estuary, with an average of 2 meters. The concentration of phosphorus averaged 50 mg m<sup>-3</sup>, the maximum TP (230 mg m<sup>-3</sup>) was at station 6 in 2017. The concentration of chlorophyll *a* varied from 0.8 to 127 mg m<sup>-3</sup>, and the primary production of plankton varied from 0.05 to 4.14 gC m<sup>-2</sup> d<sup>-1</sup> (Table 1). A detailed description of spatial and temporal pattern of environmental variables is given in Golubkov et al. (2017) and Golubkov and Golubkov (2020).

### 3.2. Phytoplankton assemblages: composition, trends and correlations with environmental variables

A total of 174 species and forms identified to genus from eight taxonomic classes were found in summer phytoplankton during the study period (Supplementary Table 2). The largest number of species (64) belonged to Chlorophyceae (Table 2), which accounted for 37% of the total species richness of phytoplankton. However, the biomass of green algae has been distributed across numerous species. It included many rare species (approximately 55%) that were found no more than 4 times at all stations during the study period. The most common species with the highest biomass in this class were *Monorahidium contortum* ((Thuret) Komárková-Legnerová 1969), *Mougeotia* sp. and *Mucidosphaerium pulchellum* ((H.C.Wood) C.Bock, Proschold & Krienitz 2011), which were observed 173, 119 and 81 times, respectively (Table 2). Green algae ranked second in the total phytoplankton biomass in the estuary. The highest biomasses were observed in its upper reach (Figure 2).

Cyanobacteria ranked second in species richness, but first in phytoplankton biomass (Table 2). Their biomass was particularly high in the middle and lower reaches of the estuary (Figure 2). The most common species with the highest biomass were *Dolichospermum flos-aquae* ((Brébisson ex Bornet & Flahault) P.Wacklin, L.Hoffmann & J.Komárek 2009), *Aphanizomenon flos-aquae* (Ralfs ex Bornet & Flahault 1886), *Limnithrix planctonica* ((Woloszynska) Meffert

1988) and *Planktothrix agardhii* ((Gomont) Anagnostidis & Komárek 1988) (Table 2).

Diatoms ranked third in species richness and biomass of phytoplankton (Table 2, Figure 2). As in green algae, their biomass was higher in the upper and middle reaches of the estuary (Figure 2). The most common species from this class were *Aulacoseira islandica* ((O.Müller) Simonsen 1979), *Skeletonema subsalsum* ((Cleve-Euler) Bethge 1928), *Tabellaria fenestrata* ((Lyngbye) Kützing 1844), *Skeletonema costatum* ((Greville) Cleve 1873) and *Pantocsekiella kuetzingiana* ((Thwaites) K.T.Kiss and E.Ács 2016) had the highest biomasses among these algae (Table 2).

These above-mentioned three classes together accounted for 76% of the total species richness and 74% of the total biomass of phytoplankton. Therefore, they can be considered dominant in the midsummer phytoplankton community in the Neva Estuary. The remaining five phytoplankton groups were not abundant, and their proportion in the total biomass was usually small. However, some species from these groups had a high biomass and frequency of occurrence. Chrysophyceae and Dinophyceae species accounted for 7% of the total species richness of phytoplankton (Table 2). The proportion of Dinophyceae in the total biomass of phytoplankton was about 5%, and the proportion of Chrysophyceae – only about 2%. Species from the Cryptophyceae and Euglenophyceae groups accounted for 4% each of the total species richness of phytoplankton (Table 2). However, despite the small number of species (Table 2), Cryptophyceae species accounted for 13% of the total phytoplankton biomass. Their biomass was rather high in the upper and middle reaches of the estuary (Figure 2). *Komma caudate* ((L.Geitler) D.R.A.Hill 1991) dominated this group. It occurred 174 times and was the most common species in the phytoplankton in the Neva Estuary (Table 2). Other abundant species of this group, *Cryptomonas erosa* (Ehrenberg 1832) and *Cryptomonas marssonii* (Skuja 1948), were also encountered often: 136 and 81 times, respectively (Table 2). Euglenophyceae comprised a much smaller fraction, only 2%, in the total biomass of phytoplankton. *Trachelomonas volvocina* ((Ehrenberg) Ehrenberg 1834) was most common in this group, and dominated in its biomass (Table 2). Xantophyceae had the least importance in the total species richness and biomass of the summer phytoplankton of the estuary. This group included only one species, *Tribonema affine* ((Kützing) G.S.West 1904), which was not common and had the highest biomass in the UR of the estuary (Table 2, Figure 2). In general, except

**Table 2** The number of species, and the most common and dominant species in the biomass of phytoplankton in the Neva Estuary in 2003–2019.

Groups of phytoplankton	Number of species	Most common species (the number of occurrence)	Species predominant in biomass (min–average–median–max biomass per water area [WW g m <sup>-3</sup> ])
Cyanophyceae	37	<i>Dolichospermum flos-aquae</i> (128)	<i>Microcystis wesenbergii</i> (46.8–1335–230.2–11519)
		<i>Aphanizomenon flos-aquae</i> (117)	<i>Dolichospermum scheremetieviae</i> (70.1–902.9–410–3526)
		<i>Limnithrix planctonica</i> (111)	<i>Planktothrix agardhii</i> (0.7–784.2–237.0–8800)
Chlorophyceae	64	<i>Monorahidium contortum</i> (173)	<i>Mucidosphaerium pulchellum</i> (1.2–317.3–57.6–7833)
		<i>Mougeotia</i> sp. (119)	<i>Chlamidomonas</i> sp. (2.1–283.2–184.7–1319)
		<i>Mucidosphaerium pulchellum</i> (81)	<i>Sphaerocystis planctonica</i> (2.4–224.7–61.7–1393)
Bacillariophyceae	31	<i>Aulacoseira islandica</i> (112)	<i>Skeletonema costatum</i> (7.5–1465–146.4–6405)
		<i>Skeletonema subsalsum</i> (96)	<i>Pantocsekiella kuetzingiana</i> (0.8–546.4–67.2–16127)
		<i>Tabellaria fenestrata</i> (90)	<i>Lindavia glomerata</i> (0.5–313.6–145.1–3315.7)
Cryptophyceae	8	<i>Komma caudata</i> (174)	<i>Cryptomonas erosa</i> (0.5–498.8–180.8–4384)
		<i>Cryptomonas erosa</i> (136)	<i>Cryptomonas ovata</i> (1.3–426.9–126.2–7056)
		<i>Cryptomonas marssonii</i> (81)	<i>Cryptomonas marssonii</i> (1.0–410.6–213.1–2491)
Dinophyceae	13	<i>Apocalathium aciculiferum</i> (62)	<i>Peridinium cinctum</i> (18.7–610.9–304.8–2664)
		<i>Ceratium hirundinella</i> (56)	<i>Gymnodinium</i> sp. (5.2–352.6–47.6–2304)
		<i>Glenodinium</i> sp. (48)	<i>Ceratium hirundinella</i> (8.8–311.5–168.0–3200)
Euglenophyceae	7	<i>Trachelomonas volvocina</i> (46)	<i>Trachelomonas</i> sp. (16.5–395.8–139.4–2356)
		<i>Lepocinclis acus</i> (17)	<i>Trachelomonas volvocina</i> (4.0–293.4–198.3–2059.2)
Chrysophyceae	13	<i>Trachelomonas</i> sp. (11)	<i>Lepocinclis acus</i> (3.7–103.9–15.8–825)
		<i>Dinobryon divergens</i> (62)	<i>Uroglena</i> sp. (18.0–662.7–85.5–1749)
		<i>Mallomonas charkoviensis</i> (15)	<i>Dinobryon divergens</i> (1.2–111.1–38.6–1680)
Xanthophyceae	1	<i>Uroglena</i> sp. (13)	<i>Synura uvella</i> (2.1–113.2–64.3–514.6)
		<i>Tribonema affine</i> (32)	<i>Tribonema affine</i> (14.8)

Cyanobacteria, which had the highest biomass in the middle and low reaches of the Neva Estuary, other groups of phytoplankton had the highest biomass in its upper parts (Figure 2).

The biomasses of Chlorophyceae, Bacillariophyceae, Cryptophyceae and Dinophyceae showed statistically significant linear trends in the estuary in 2003–2019 (Figure 3B, C, D, E). Cyanophyceae did not show any trend at the same time (Figure 3A)

The CCA showed that the three dominant phytoplankton groups correlated differently with environmental factors. The eigenvalues of the first and second axes were 0.384 and 0.265 (Table 3). The correlations between the species biomass and the values of the environmental variables were high (0.897 and 0.859, respectively for the first and second axes). The first two axes explained 38% of species-environmental relation. Furthermore, the all axes explained 24% of the total species variance. Finally, the results of the Monte-Carlo permutation test (using the 999

permutations) showed that the analysis was statistically significant (Table 3).

The biomass of various species from each phytoplankton group correlated differently with environmental factors. However, within each group, there were some predominant trends in the correlative response to changes in environmental variables. As can be seen from the CCA biplots (Figure 4), species of diatoms and green algae are grouped in one part of the diagrams, and most of the cyanobacteria species are compactly grouped in the opposite part, separately from most species from the first two dominant phytoplankton classes. This means that the biomass of cyanobacteria was positively correlated with other one environmental factors than the biomasses of green algae and diatoms.

The biomass of most species of cyanobacteria, including dominant species, was positively correlated with salinity, depth and Secchi depth (Figure 4A). Only two species, *Coelosphaerium kuetzingianum* (Nägeli 1849) and *Oscillatoria* sp. negatively correlated with these environmental

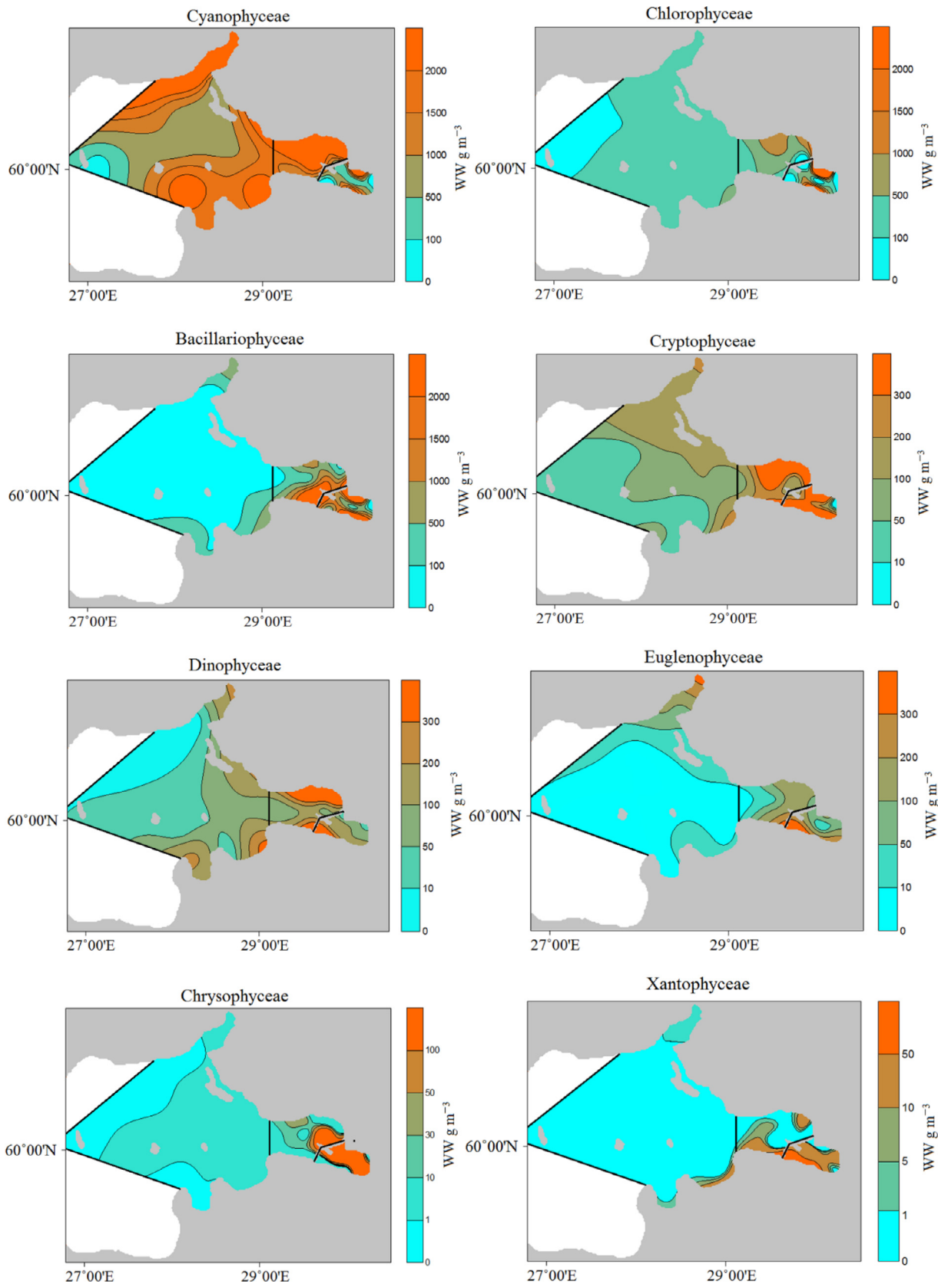


**Figure 2** Distribution of the mean values of the biomass of phytoplankton taxonomic classes in the Neva Estuary in midsummer 2003–2019. The black line shows the boundaries between reaches.

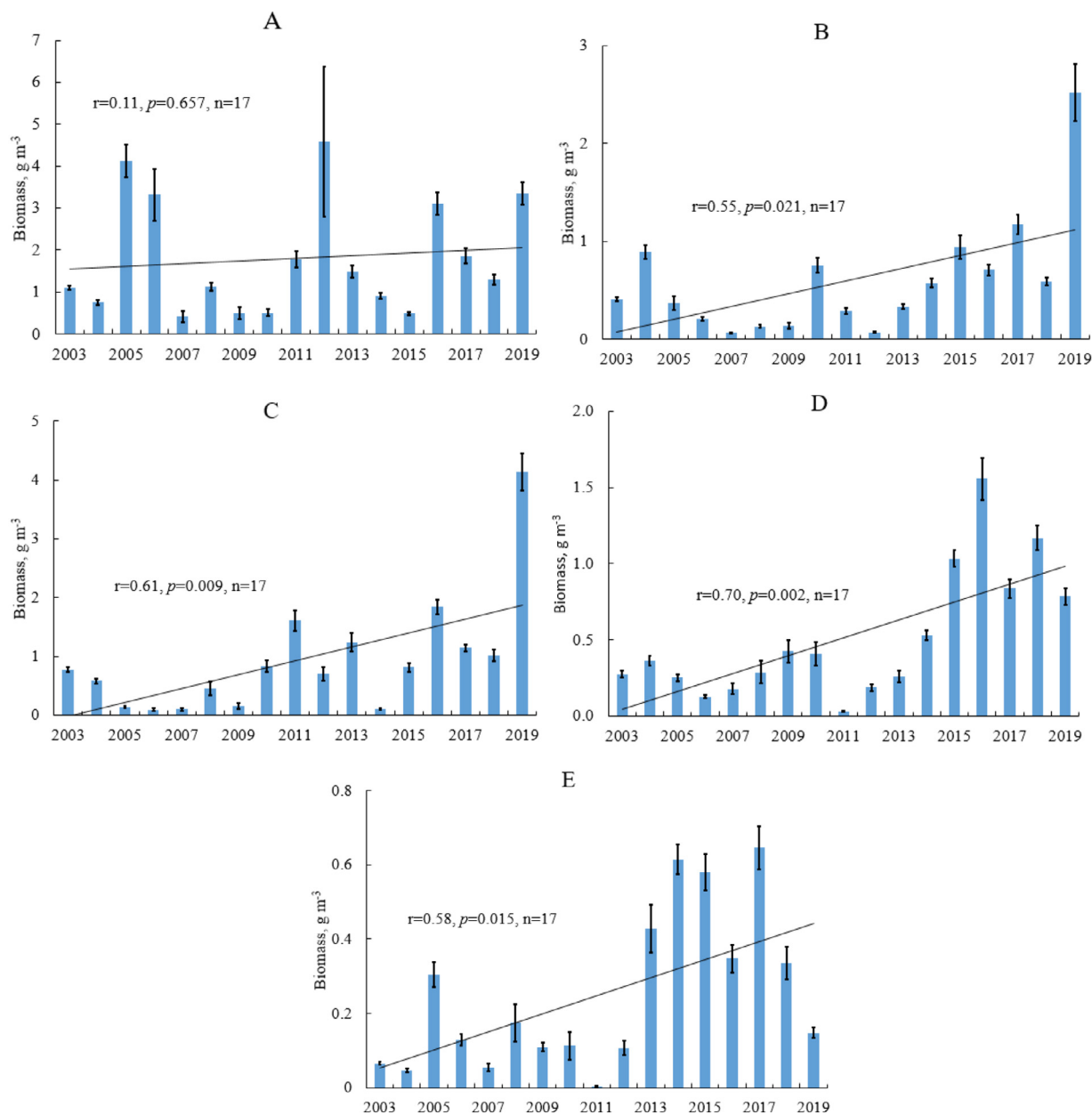


**Figure 3** Mean biomass of Cyanophyceae (A), Chlorophyceae (B), Bacillariophyceae (C), Cryptophyceae (D), Dinophyceae (E) in the Neva Estuary in midsummer 2003–2019.

**Table 3** Results of Canonical Correspondence Analysis.

Axes	1	2	3	4	Total
Eigenvalues	0.38	0.35	0.31	0.24	7.10
Canonical eigenvalues	0.38	0.26	0.19	0.15	1.70
F-ratio	9.41	6.48	2.61	2.47	
p-value	<0.001	<0.001	<0.001	0.019	
Species-environment correlations	0.90	0.86	0.77	0.70	
Cumulative % of explained variance of species data	5.4	9.1	11.8	13.9	24.0
Cumulative % of explained of species-environment relation	22.5	38.0	49.1	57.9	

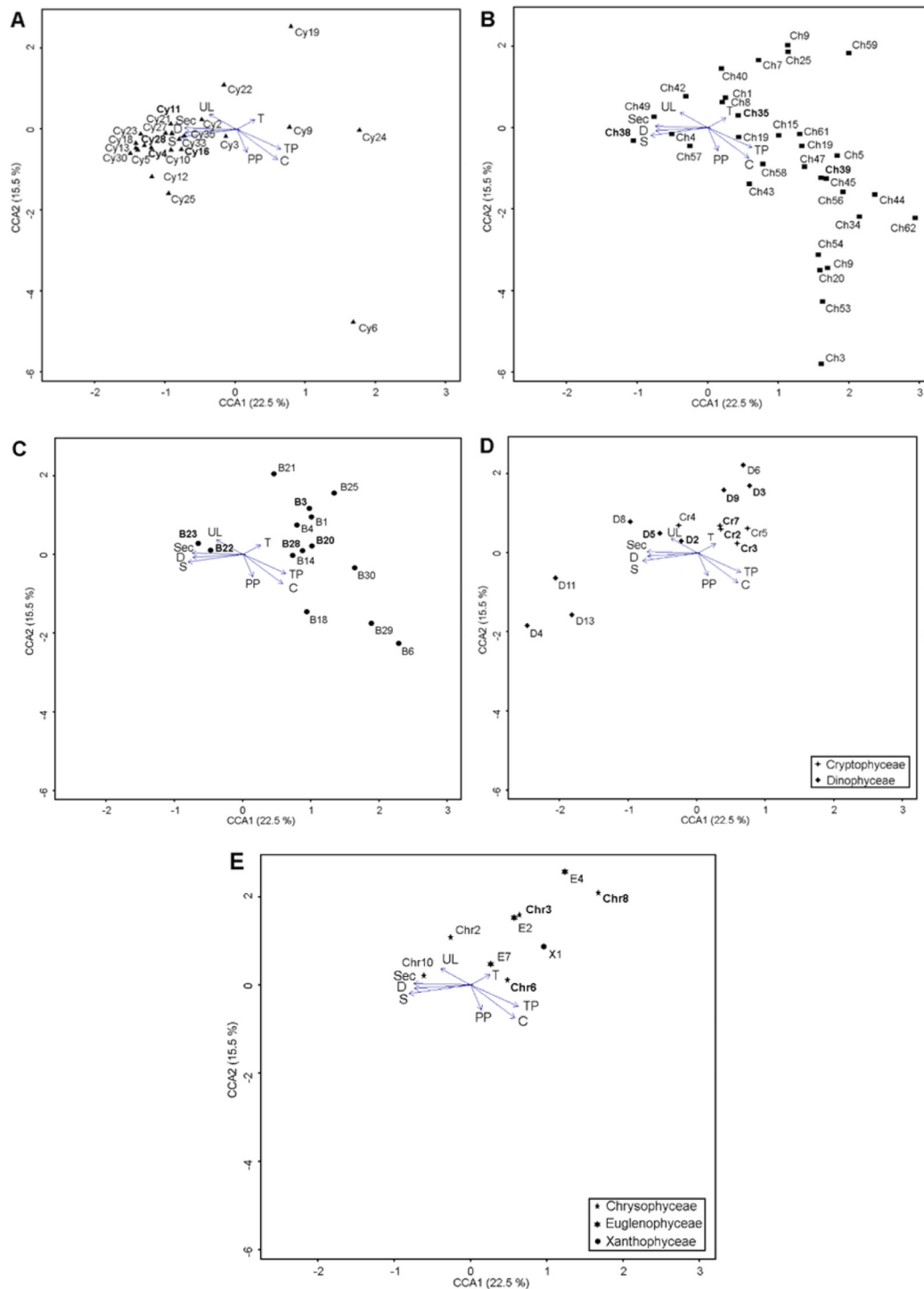


**Figure 4** Canonical Correspondence Analysis biplots with Cyanophyceae (A); Chlorophyceae (B); Bacillariophyceae (C); Dinophyceae and Cryptophyceae (D); Chrysophyceae, Euglenophyceae and Xanthophyceae (E) species and environmental variables. Dominant species are highlighted in bold. Arrows represent statistical significance ( $p < 0.05$ ) environmental variables (S – salinity [PSU]; T – temperature [ $^{\circ}\text{C}$ ]; D – water depth [m]; UL – depth of layer above thermocline [m]; Sec – Secchi depth [m]; TP – concentration of total phosphorus [ $\text{mg m}^{-3}$ ]; C – concentration of chlorophyll *a* [ $\text{mg m}^{-3}$ ]; PP – plankton primary production [ $\text{gC m}^{-2}\text{d}^{-1}$ ]). Codes of the phytoplankton taxa are given in Supplementary Table 2. The arrows for environmental variables point in the general direction of maximum environmental change across the diagram with statistical significance ( $p < 0.05$ ), and their lengths are approximately proportional to the rate of change in that direction. The correlation between biomasses of phytoplankton and environmental factors was examined based on the angle between arrows; an angle smaller than  $90^{\circ}$  indicates a positive correlation between the variables; the smaller the angle, the closer the positive correlation of the two variables. An angle between  $90^{\circ}$  and  $180^{\circ}$  suggests a negative correlation. Finally, there is no correlation between two variables when their angle is  $90^{\circ}$ . The projection of phytoplankton species biomass on the environmental variable vector is an approximation of the “optima” regarding that particular variable (ter Braak and Verdonschot, 1995).

factors. Taking into account that *C. kutzingianum* was found 54 times (Table 2), this species can be considered common for freshwater and shallow parts of the estuary. One species of cyanobacteria, *Aphanocapsa reinboldii* ((Richter) Komárek & Anagnostidis 1995), was positively correlated with TP, C, and PP (Figure 4A). In addition, *Merismopedia tranquilla* ((Ehrenberg) Trevisan 1845) was the only species that positively correlated with water temperature.

In contrast to cyanobacteria, diatoms and green algae mostly negatively correlated with water salinity and Secchi depth, and dominated in the shallower parts of the estuary with less transparent waters (Figure 4B,C). However, although in many respects the distribution of biomass of the species from these two groups was similar, there were some differences. For instance, the biomass of most species of green algae, including the dominant *M. pulchellum*, negatively correlated with the depth of UL, and positively correlated with concentrations of TP and C, and PP (Figure 4A). The biomasses of only five species, one of which was the dominant *Mougeotia* sp., positively correlated with depth, salinity and Secchi depth. Another group of seven species, with a third dominant species, *M. contortum*, was also correlated with water temperature. In other words, most species of green algae preferred those parts of the estuary where salinity was low, but the concentration of chlorophyll and primary production were high.

As green algae, biomasses of most diatom species negatively correlated with water salinity, Secchi depth and water depth (Figure 4C). Only two species of Bacillariophyceae, *S. subsalsum* and *S. costatum*, positively correlated with D, S, Sec and UL. In contrast to green algae, only three species of diatoms, *Lindavia glomerata* ((H.Bachmann) Adesalu & Julius 2017), *Belonastrum beroliensis* ((Lemmermann) Round & Maidana 2001) and *Tabellaria flocculosa* ((Roth) Kützing 1844), positively correlated with concentration of TP and C (Figure 4C). The remaining diatoms did not show significant correlations with eutrophication indicators, but positively correlated with water temperature (Figure 4C).

Almost all species from the less abundant phytoplankton groups, with the exception of dinoflagellates, mainly had the same correlations with the studied environmental factors. For instance, biomasses of all dominant Cryptophyceae species positively correlated with temperature and negatively correlated with water salinity, water depth, and Secchi depth. At the same time, their biomasses were not correlated with the concentrations of total phosphorus and chlorophyll *a*, and the primary production of plankton (Figure 4D). Only *Komma caudate* negatively correlated with TP, C and PP and positively correlated with the UL depth (Figure 4D).

Biomass of autotrophic dinoflagellates showed more complex relationships with environmental variables compared to Cryptophyceae. Part of dinoflagellates negatively correlated with water salinity, depth and Secchi depth, but positively with water temperature (Figure 4D). For example, the biomasses of *Ceratium hirundinella* ((O.F.Müller) Dujardin 1841), *Peridinium cinctum* ((O.F.Müller) Ehrenberg 1832), and *Gymnodinium* sp. positively correlated with water temperature, and negatively with water salinity, the highest biomass of these species was found in the UR and the MR of the estuary. The biomass of the dominant *Apocalathium aciculiferum* ((Lemmermann) Craveiro,

Daugbjerg, Moestrup & Calado 2016) was positively related to the UL depth. However, the biomasses of some dinoflagellate species like cyanobacteria positively correlated with salinity, depth and Secchi depth of water, but negatively correlated with water temperature (Figure 4D). In more detail, the relationship of various dinoflagellates with environmental factors in the Neva Estuary is published in Golubkov et al. (2019a).

Species from Euglenophyceae, Xanthophyceae, and most Chrysophyceae have similar correlations with the studied environmental factors and did not show significant correlations with the concentration of total phosphorus and chlorophyll *a*, and the primary production of plankton (Figure 4E). *T. affine* (Xanthophyceae), *Lepocinclis acus* ((O.F.Müller) B.Marin & Melkonian 2003), *T. volvocina* and *Trachelomonas* sp. (Euglenophyceae) and three dominant species from Chrysophyceae (*D. divergens*, *M. charkoviensis* and *Mallomonas* sp.) positively correlated with water temperature and negatively with salinity, depth and Secchi depth (Figure 4E). Among other Chrysophyceae, *Chrysooccus rufescens* (Klebs 1892) was negatively correlated to phytoplankton productivity indicators, and *Mallomonas elegans* (Lemmermann 1904), unlike previous species, was positively correlated to salinity and other physical variables (Figure 4E).

#### 4. Discussion

This study has explored and enhanced the knowledge on phytoplankton diversity and its correlation with environmental variables in the coastal waters of the easternmost Baltic Sea. In contrast to this region, the composition and biomass of phytoplankton in coastal and open waters in other parts of the Baltic are better studied (e.g., Gasiūnaitė et al., 2005; Jaanus et al., 2011; Olenina et al., 2006; Piwosza et al., 2018; Suikkanen et al., 2007; Wasmund et al., 2011, 2017). In the central Baltic, diatoms and autotrophic dinoflagellates dominate in spring and autumn phytoplankton whereas cyanobacteria dominate in the summer (Gasiūnaitė et al., 2005; Suikkanen et al., 2007; Wasmund et al., 2011). In Curonian Lagoon situated in the south-eastern part of the Baltic Sea, where salinity varies from 0 to 8 PSU, Cyanophyceae, Chlorophyceae and Bacillariophyceae are the main dominant classes in summer phytoplankton (Kreves et al., 2007). According to our results, cyanobacteria dominated the midsummer phytoplankton in the MR and LR of the Neva Estuary, whereas green algae dominated in the UR. Green algae is also common for summer phytoplankton of freshwater lakes at the watershed of the Neva Estuary (Golubkov et al., 2019b; Holopainen et al., 1996; Sharov et al., 2014), and in the coastal lakes of the southern Baltic Sea, where green algae preferred freshwaters (Obolewski et al., 2018). An analysis of our data showed that, overall, green algae dominated in more freshwaters and shallow coastal areas in the UR and the MR of the Neva Estuary (Figure 2), but some species, including the dominant *Mougeotia* sp., were abundant in the brackish parts of the estuary and showed a positive correlation with water salinity (Figure 4B). Similarly, green algae were most diverse in freshwaters and mixing zone of the Vistula River estuary (Gulf of Gdańsk). However,

species from Mamiellophyceae were characteristic groups for the brackish zone of this estuary and were found at salinities around 7 PSU (Piwożsa et al., 2018). In the Baltic Sea, periodic changes in the species composition of summer phytoplankton occur due to fluctuations in environmental factors. Analysis of long-term data showed a decrease in the proportion of green algae in the western, southern and central regions of the Baltic Sea in all seasons at the end of the 20th century (Wasmund et al., 2011). In the northern Baltic and the Gulf of Finland, on the contrary, the proportion of this group in the total biomass of phytoplankton increased from 1979 to 2003, which is apparently associated with a decrease in water salinity (Suikkanen et al., 2007). In the Neva Estuary, the biomass of green algae had statistically significant positive trend (Figure 3B).

In the Neva Estuary, many Chlorophyceae species correlated positively with total phosphorus concentration. In the most eutrophic waters, there were high biomass of *Tetrademus* sp., *Desmodesmus* sp. and *Ankistrodesmus* sp. (Figure 4 B). The same patterns were observed in Lake Ladoga, in which these species were found in its most eutrophic parts (Holopainen et al., 1996), and in the Bothnia Sea, the low saline part of the Baltic Sea (Kuosa et al., 2017).

Cyanobacteria were the dominant phytoplankton group in the MR and the LR of the Neva Estuary in 2003–2019 (Figure 2). They began to dominate phytoplankton in these parts of the estuary since the late 1990s (Nikulina, 2003). A similar increase in the significance of cyanobacteria in the summer phytoplankton was observed in the late 1990s and early 2000s in the western part of the Gulf of Finland and in different parts of the Gulf of Bothnian (Jaanus et al., 2011; Suikkanen et al., 2007). However, we did not find a continuation of this trend in the Neva Estuary in 2003–2019 (Figure 3A). Wasmund et al. (2011) showed that after the peak of 1979/1980, the proportion of cyanobacteria in the total biomass of phytoplankton in the southern Baltic even decreased, especially the proportion of *Aphanizomenon* sp. and *Nodularia spumigena* (Mertens ex Bornet & Flahault 1888).

The problem of summer cyanobacteria blooms that secrete toxins, which are dangerous to humans, is acute in the Central Baltic. Monitoring of this phenomenon by photographing the water surface from space showed that the concentration of chlorophyll in such places could be very high (Kahru et al., 2020). In the Neva Estuary, cyanobacteria blooms were also occasionally observed at some stations (Golubkov et al., 2017). According to information on species toxicity from Hallegraeff et al. (2003), thirteen species found in the estuary are harmful (Supplementary Table 2). *N. spumigena*, which produces a hepatotoxin, is the most toxic among them. Blooms of this species observed in the central Baltic Sea (Kahru et al., 2020). It was also found in the Neva Estuary, but was rare (Supplementary Table 2).

Some cyanobacteria species seem to enter the Neva Estuary from its catchment. For instance, the harmful *Microcystis wesenbergi* (Komárek) Komárek ex Komárek 2006, dominated among summer phytoplankton in the reservoir located on the northern coast of the estuary (Golubkov et al., 2019b). This species had highest biomass in the UR of the Neva Estuary. Other species, *A. flos-aqua* and *P. agardhii*, which are dominant in the Neva Estuary, are also

common in summer phytoplankton in the shallow mostly freshwater estuary, the Curonian Lagoon (Pilkaitytė, 2007) and in brackish-water Gulf of Riga (Purina et al., 2018).

Many authors believe that the development of cyanobacteria is mainly controlled by temperature, and the intensity of their development increases with increasing temperature (Gasiūnaitė et al., 2005; Obolewski et al., 2018). On the other hand, a recent study analyzing the influence of environmental factors on cyanobacteria blooms in the central part of the Baltic Sea showed that water temperature does not significantly affect the intensity of blooms in this area (Kahru et al., 2020). In our study, we also did not find such a positive correlation; on the contrary, the biomass of most species, including dominant ones, negatively correlated with water temperature (Figure 4A).

In the Neva Estuary, most species of cyanobacteria did not show correlations with phosphorus concentration and phytoplankton productivity. This suggests that the concentration of phosphorus for this group is not very important, which is also known from the literature. Kahru et al. (2020) concluded that the main factor affecting the intensity of cyanobacteria blooms is the ratio of nitrogen to phosphorus concentrations, which is consistent with earlier studies (Pliński and Jozwiak, 1999). In the Neva Estuary, phosphorus limits the development of phytoplankton in the UR, and further towards the western part of the Gulf of Finland, the role of nitrogen as a limiting element increases, and the role of phosphorus decreases (Ylöstalo et al., 2016). Thus, one of the reasons for the dominance of cyanobacteria in the MR and LR of the Neva Estuary may be the ability of many species to uptake atmospheric nitrogen, which gives them an advantage over other autotrophs under nitrogen-limited conditions.

Bacillariophyceae was also an important group of phytoplankton in the Neva Estuary in midsummer 2003–2019. Many species of diatoms, which were found in the estuary, were also common and predominated in freshwater bodies located in the estuary catchment. For example, the diatom *Aulacoseira muzzanensis* (F.Meister) Krammer 1991 dominated the summer phytoplankton in a reservoir located on the estuary coast (Golubkov et al., 2019b). *Aulacoseira* spp. and *Fragilaria crotonensis* (Kitton 1869), which negatively correlated with water salinity in the Neva Estuary (Figure 4C), were a common species for summer phytoplankton from Lake Ladoga and Lake Saimaa (Holopainen et al., 1996; Simola et al., 1993). Diatoms are also the main group of summer phytoplankton in Lake Onega, which is located in the northern part of the estuary catchment basin (Sharov et al., 2014). Only two species from the genus *Skeletonema* had a positive correlation with water salinity (Figure 4C), and had a high biomass in the MR and LR of the estuary. These species are common in phytoplankton in the central parts of the Baltic Sea (Wasmund et al., 2011) and in the Gulf of Finland (Suikkanen et al., 2007). Studies conducted in the western part of the Baltic Sea from 1997 to 2006, in the Gulf of Bothnia from 1988 to 2012, and in the Vistula lagoon at the end of 1980s and beginning of 2000s showed a general decrease in the biomass of diatoms (Henriksen, 2009; Kasperovičienė and Vaikutienė, 2007; Kuosa et al., 2017). A similar decrease in the role of diatoms in summer phytoplankton was observed in the Neva Estuary in the late 1990s (Nikulina, 2003). However, at present, we

have found a positive annual trend in biomass of Bacillariophyceae in the Neva Estuary (Figure 3C), due to an increase in biomass of freshwater species.

In recent years, intensification of harmful dinoflagellate blooms has been observed in regions across significant portions of the North Atlantic and in some regions within the North Pacific (Gobler et al., 2017). In the Baltic Sea, the role of autotrophic dinoflagellates in the spring season also has increased in last years, which in turn has affected the bacterioplankton community (Camarena-Gómez et al., 2018) and has led to a change in biogeochemical cycling (Spilling et al., 2018). In the summer seasons in 1970–2000 on the contrary, a decrease in the biomass of autotrophic dinoflagellates was observed in the southern part of the Baltic Sea, especially for the species *Gymnodinium* spp. and *Peridinium* spp. (Wasmund et al., 2011). Intensive development of *Gymnodinium* spp. was observed only in the summer of 1994, when the biomass of these species exceeded 1400 mg m<sup>-3</sup>. Low water temperatures in summer contribute to the development of dinoflagellates (Wasmund et al., 2011), so they often concentrate at a considerable depth (Gisselson et al., 2002). Our analysis showed similar results, as several marine species of dinoflagellates in the Neva Estuary had negative correlation with water temperature (Figure 4D). According to Hallegraeff et al. (2003), two species found in the estuary, *Phalacroma rotundatum* ((Claparède & Lachmann) Kofoid & J.R. Michener 1911) and *Prorocentrum lima* ((Ehrenberg) F. Stein 1878), are harmful. However, we did not record high biomass of these species in the Neva Estuary in midsummer 2003–2019 (Supplementary Table 2).

Cryptophyceae had a significant proportion in the phytoplankton biomass in the Neva Estuary. Although these algae were common throughout the estuary (Table 2), they had high biomasses in its freshwater part (Figure 2). This group of algae is an important component for the summer phytoplankton in Lake Ladoga, from which the Neva River flows. In the southern part of this lake, Cryptophyceae accounted for 30% of the total biomass of phytoplankton in July 2003 (Holopainen et al., 2006). A significant increase in the summer biomass of these algae in Baltic Proper in the summer of 1997 was associated with a decrease in salinity (Wasmund et al., 2011). This is consistent with our data.

Algae belonging to Chrysophyceae were also common in the Neva Estuary. In the Gulf of Finland and the northern Baltic Proper, an increase in the biomass of these algae was observed at the end of the 20th century (Suikkanen et al., 2007). In the Neva Estuary, all dominant species from this group positively correlated to water temperature (Figure 4E). Species of Euglenophyceae also positively correlated with water temperature and negatively with salinity in the Neva Estuary; the same correlations were observed in the central Baltic (Wasmund et al., 2011).

Most of the phytoplankton groups dominating in freshwater and slightly saline waters in the Neva Estuary showed a statistically significant trend towards an increase in their biomasses in the MR in 2003–2019, which may be associated with an increase in the amount of atmospheric precipitation in summer observed in the region in recent years. The amount of precipitation in July in the Saint Petersburg region increased from 53 mm in 2011 to 151 mm in 2016 (Golubkov and Golubkov, 2020). As a result, the

Neva River's run-off increased (Knuuttila et al., 2017); high concentrations of TP were measured in the UR of the Neva Estuary due to leaching of nutrients from the river catchment (Golubkov and Golubkov, 2020). This phenomenon is consistent with the results of model simulations, according to which an increase in the flow volume caused by an increase in net precipitation in the Baltic catchment area will stimulate nutrient loads from the land during the 21st century, especially in the northern regions (Meier et al., 2012). As was early shown, with an increase in the flow of the Neva River during rainy summers, the salinity of water in the MR of the Neva Estuary decreases (Myakisheva, 1996). Such environmental conditions should favor the development of freshwater species from various groups of phytoplankton. Taking into account that most regional climate models predict future increases in precipitation and temperature in the northern Baltic regions, the future expansion of the areas occupied by these freshwater phytoplankton species in the Neva Estuary and other estuaries of the Northern Baltic is very likely.

## Acknowledgements

The authors thank the two anonymous reviewers for their constructive comments that significantly improved the early version of the manuscript. This work was supported by the Russian Ministry of Science and Higher Education, project no. AAAA-A19-119020690091-0.

## Supplementary material

Supplementary material associated with this article can be found, in the online version, at doi:10.1016/j.oceano.2020.11.002.

## References

- Behrenfeld, M.J., O'Malley, R.T., Siegel, D.A., McClain, C.R., Sarmiento, J.L., Feldman, G.C., Milligan, A.J., Falkowski, P.G., Letelier, R.M., Boss, E.S., 2006. Climate-driven trends in contemporary ocean productivity. *Nature* 444, 752–755. <https://doi.org/10.1038/nature05317>
- Boyce, D.G., Lewis, M.R., Worm, B., 2010. Global phytoplankton decline over the past century. *Nature* 466, 591–596. <https://doi.org/10.1038/nature09268>
- Camarena-Gómez, M.T., Lipsewers, T., Piiparinen, J., Eronen-Rasimus, E., Perez-Quemaliños, D., Hoikkala, L., Sobrino, C., Spilling, K., 2018. Shifts in phytoplankton community structure modify bacterial production, abundance and community composition. *Aquat. Microb. Ecol.* 81, 149–170. <https://doi.org/10.3354/ame01868>
- Damar, A., Colijn, F., Hesse, K.J., Adrianto, L., Yonvith, Fahrudin, A., Kurniawan, F., Prismayanti, A.D., Rahayu, S.M., Rudianto, B.Y., Ramli, A., 2020. Phytoplankton Biomass Dynamics in Tropical Coastal Waters of Jakarta Bay, Indonesia in the Period between 2001 and 2019. *J. Mar. Sci. Eng.* 8 (9), 674. <https://doi.org/10.3390/jmse8090674>
- Doney, S.C., Ruckelshaus, M., Duffy, J.E., Barry, J.P., Chan, F., English, C.A., Galindo, H.M., Grebmeier, J.M., Hollowed, A.B., Knowlton, N., Polovina, J., Rabalais, N.N., Sydeman, W.J., Talley, L.D., 2012. Climate change impacts on marine ecosystems

- tems. *Annu. Rev. Mar. Sci.* 4, 11–37. <https://doi.org/10.1146/annurev-marine-041911-111611>
- Dzierzbicka-Głowacka, L., Jakacki, J., Janecki, M., Nowicki, A., 2011. Variability in the distribution of phytoplankton as affected by changes to the main physical parameters in the Baltic Sea. *Oceanologia* 53 (Suppl. 1), 449–470. <https://doi.org/10.5697/oc.53-1-TI.449>
- Friedland, R., Neumann, T., Schernewski, G., 2012. Climate change and the Baltic Sea action plan: model simulations on the future of the western Baltic Sea. *J. Marine Syst.* 105–108, 175–186. <https://doi.org/10.1016/j.jmarsys.2012.08.002>
- Gasiūnaitė, Z.R., Cardoso, A.C., Heiskanen, A.-S., Henriksen, P., Kauppila, P., Olenina, I., Pilkaityt, R., Purina, I., Razinkovas, A., Sagert, S., Schubert, H., Wasmund, N., 2005. Seasonality of coastal phytoplankton in the Baltic Sea: Influence of salinity and eutrophication. *Estuar. Coast. Shelf Sci.* 65 (1–2), 239–252. <https://doi.org/10.1016/j.ecss.2005.05.018>
- Gisselson, L.-E., Carlsson, P., Graneli, E., Pallon, J., 2002. Dinophysis blooms in the deep euphotic zone of the Baltic Sea: do they grow in the dark? *Harmful Algae* 1 (4), 401–418. [https://doi.org/10.1016/S1568-9883\(02\)00050-1](https://doi.org/10.1016/S1568-9883(02)00050-1)
- Gobler, C.J., Doherty, O.M., Hattenrath-Lehmann, T.K., Griffith, A.W., Kang, Y., Litaker, R.W., 2017. Ocean warming since 1982 has expanded the niche of toxic algal blooms in the North Atlantic and North Pacific oceans. *PNAS* 114 (19), 4975–4980. <https://doi.org/10.1073/pnas.1619575114>
- Golubkov, M., Golubkov, S., 2020. Eutrophication in the Neva Estuary (Baltic Sea): response to temperature and precipitation patterns. *Mar. Freshw. Res.* 71 (6), 583–595. <https://doi.org/10.1071/MF18422>
- Golubkov, M., Nikulina, V., Golubkov, S., 2019a. Effects of environmental variables on midsummer dinoflagellate community in the Neva Estuary (Baltic Sea). *Oceanologia* 61 (2), 197–207. <https://doi.org/10.1016/J.OCEANO.2018.09.001>
- Golubkov, S.M., 2009. Changes of biological communities in the eastern Gulf of Finland during the last century. *Proceedings of the Zoological Institute RAS* 313, 406–418
- Golubkov, S., Alimov, A., 2010. Ecosystem changes in the Neva Estuary (Baltic Sea): natural dynamics or response to anthropogenic impacts? *Mar. Pollut. Bull.* 61 (4–6), 198–204. <https://doi.org/10.1016/j.marpolbul.2010.02.014>
- Golubkov, S.M., Belyakov, V.P., Golubkov, M.S., Litvichuk, L.F., Petukhov, V.A., Gubelit, Yu.I., 2019b. Energy flows and phosphorus turnover in the system of shallow reservoir under anthropogenic stress. *Russ. J. Ecol.* 50, 560–566. <https://doi.org/10.1134/S1067413619060055>
- Golubkov, S., Golubkov, M., Tiunov, A., Nikulina, L., 2017. Long-term changes in primary production and mineralization of organic matter in the Neva Estuary (Baltic Sea). *J. Mar. Syst.* 171, 73–80. <https://doi.org/10.1016/j.jmarsys.2016.12.009>
- Golubkov, S.M., Golubkov, M.S., Tiunov, A.V., 2019. Anthropogenic carbon as a basal resource in the benthic food webs in the Neva Estuary (Baltic Sea). *Mar. Pollut. Bull.* 146, 190–200. <https://doi.org/10.1016/j.marpolbul.2019.06.037>
- Golubkov, M.S., Nikulina, V.N., Tiunov, A.V., Golubkov, S.M., 2020. Stable C and N Isotope Composition of Suspended Particulate Organic Matter in the Neva Estuary: The Role of Abiotic Factors, Productivity, and Phytoplankton Taxonomic Composition. *J. Mar. Sci. Eng.* 8 (12), 959. <https://doi.org/10.3390/jmse8120959>
- Grasshoff, K., Ehrhardt, M., Kremling, K., 1999. *Methods of Seawater Analysis*. Wiley-VCH, New York, 600 pp. (completely rev. and extended edn.).
- Guiry, M.D., Guiry, G.M., 2020. *AlgaeBase*. World-wide electronic publication. National University of Ireland, Galway <http://www.algaebase.org>.
- Hall Jr., R.O., Thomas, S., Gaiser, E.E., 2007. *Measuring freshwater primary production and respiration*. In: Fahey, T.J., Knapp, A.K. (Eds.), *Principles and Standards for Measuring Primary Production*. Oxford University Press, Oxford, 175–203.
- Hallegraeff, G.M., Anderson, D.M., Cembella, A.D., Enevoldsen, H.O., (Eds), 2003. *Manual on harmful marine microalgae*, 2nd ed. UNESCO, Paris, 793 pp.
- Heisler, J., Glibert, P.M., Burkholder, J.M., Anderson, D.M., Cochlan, W., Dennison, W.C., Dortch, Q., Gobler, C.J., Heil, C.A., Humphries, E., Lewitus, A., Magnien, R., Marshall, H.G., Sellner, K., Stockwell, D.A., Stoecker, D.K., Suddleson, M., 2008. Eutrophication and harmful algal blooms: a scientific consensus. *Harmful Algae* 8 (1), 3–13. <https://doi.org/10.1016/j.hal.2008.08.006>
- Henriksen, P., 2009. Long-term changes in phytoplankton in the Kattegat, the Belt Sea, the Sound and the western Baltic Sea. *J. Sea Res.* 61 (1–2), 114–123. <https://doi.org/10.1016/j.seares.2008.10.003>
- Holt, J., Schrum, C., Cannaby, H., Daewel, U., Allen, I., Artioli, Y., Bopp, L., Butenschon, M., Fach, B.A., Harle, J., Pushpadas, D., Salihoglu, B., Wakelin, S., 2016. Potential impacts of climate change on the primary production of regional seas: A comparative analysis of five European seas. *Prog. Oceanogr.* 140, 91–115. <https://doi.org/10.1016/j.poccean.2015.11.004>
- Holopainen, A.-L., Huttunen, P., Letanskaya, G.I., Protopopova, E.V., 1996. The trophic state of Lake Ladoga as indicated by late summer phytoplankton. *Hydrobiologia* 322, 9–16. <https://doi.org/10.1007/BF00031799>
- Holopainen, A.-L., Avinsky, V., Niinjoja, R., 2006. Seasonal succession of phytoplankton in Lake Ladoga. *Verh. Internat. Verein. Limnol.* 29 (3), 1139–1142. <https://doi.org/10.1080/03680770.2005.11902863>
- Huisman, J., Weissing, F.J., 1999. Biodiversity of plankton by species oscillations and chaos. *Nature* 402, 407–410. <https://doi.org/10.1038/46540>
- Håkanson, L., Boulion, V.V., 2002. *The Lake Foodweb – Modeling Predation and Abiotic/Biotic Interactions*. Backhuys Publishers, Leiden, 344.
- International Organization for Standardization (ISO), 2020. *Country Codes – ISO 3166*. Retrieved from <https://www.iso.org/iso-3166-country-codes.html>
- Jaanus, A., Andersson, A., Olenina, I., Toming, K., Kaljurand, K., 2011. Changes in phytoplankton communities along a north–south gradient in the Baltic Sea between 1990 and 2008. *Boreal Env. Res.* 16 (Suppl. A), 191–208
- Kahru, M., Elmgren, R., Kaiser, J., Wasmund, N., Savchuk, O., 2020. Cyanobacterial blooms in the Baltic Sea: Correlations with environmental factors. *Harmful Algae* 92, 101739. <https://doi.org/10.1016/j.hal.2019.101739>
- Kasperovičienė, J., Vaikutienė, G., 2007. Long-term changes in diatom communities of phytoplankton and the surface sediments in the Curonian Lagoon (Lithuanian part). *Transit. Water. Bull.* 1 (1), 27. <https://doi.org/10.1285/i1825229Xv1n1p27>
- Kiselev, I.A., 1954. The determinant of freshwater algae of the USSR. *Soviet Science, Moscow* 212 pp. (in Russian).
- Klais, R., Tamminen, T., Kremp, A., Spilling, K., Olli, K., 2011. Decadal-scale changes of dinoflagellates and diatoms in the anomalous Baltic Sea spring bloom. *PLoS ONE* 6, e21567. <https://doi.org/10.1371/journal.pone.0021567>
- Knuuttila, S., Räike, A., Ekholm, P., Kondratyev, S., 2017. Nutrient inputs into the Gulf of Finland: Trends and water protection targets. *J. Mar. Syst.* 171, 54–64. <https://doi.org/10.1016/j.jmarsys.2016.09.008>
- Kreus, A., Koreiviene, J., Paskauskas, R., Sulijene, R., 2007. Phytoplankton production and community respiration in different zones of the Curonian lagoon during the midsummer vegetation period. *Transit. Water. Bull.* 1 (1), 17–26. <https://doi.org/10.1285/i1825229Xv1n1p17>
- Kuosa, H., Fleming-Lehtinen, V., Lehtinen, S., Lehtiniemi, M., Nygård, H., Raateoja, M., Raitaniemi, J., Tuimala, J., Uusitalo, L., Suikkanen, S., 2017. A retrospective of the development of the Gulf of Bothnia ecosystem. *J. Mar. Syst.* 167, 78–92. <https://doi.org/10.1016/j.jmarsys.2016.11.020>

- Meier, H.E.M., Hordoir, R., Andersson, H.C., Dieterich, C., Eilola, K., Gustafsson, B.G., Höglund, A., Schimanke, S., 2012. Modeling the combined impact of changing climate and changing nutrient loads on the Baltic Sea environment in an ensemble of transient simulations for 1961–2099. *Clim. Dynam.* 39, 2421–2441. <https://doi.org/10.1007/s00382-012-1339-7>
- Myakisheva, N.V., 1996. The influence of seasonal and year-to-year variability of water discharge from the Ladoga-Neva River system on the salinity regime of the Baltic Sea. *Hydrobiologia* 322, 99–102. <https://doi.org/10.1007/BF00031812>
- Neumann, T., Schernewski, G., 2008. Eutrophication in the Baltic Sea and shifts in nitrogen fixation analyzed with a 3D ecosystem model. *J. Marine Syst.* 74 (1–2), 592–602. <https://doi.org/10.1016/j.jmarsys.2008.05.003>
- Nikulina, V.N., 2003. Seasonal dynamics of phytoplankton in the inner Neva Estuary in the 1980s and 1990s. *Oceanologia* 45 (1), 25–39
- Obolewski, K., Glińska-Lewczuk, K., Bąkowska, M., Szymańska, M., Mrozińska, N., 2018. Patterns of phytoplankton composition in coastal lakes differed by connectivity with the Baltic Sea. *Sci. Total Environ.* 631–632, 951–961. <https://doi.org/10.1016/j.scitotenv.2018.03.112>
- Oksanen, J., Blanchet, F.G., Friendly, M., Kindt, R., Legendre, P., McGlenn, D., Minchin, P.R., O'Hara, R.B., Simpson, G.L., Solyomos, P., Stevens, M.H.H., Szoecs, E., Wagner, H., 2020. *Vegan: Community Ecology Package (Version 2.5-6)* [Software]. Retrieved from <https://CRAN.R-project.org/package=vegan>.
- Olenina, I., Hajdu, S., Edler, L., Andersson, A., Wasmund, N., Busch, S., Göbel, J., Gromisz, S., Huseby, S., Huttunen, M., Jaanus, A., Kokkonen, P., Ledaine, I., Niemkiewicz, E., 2006. *Biovolumes and size-classes of phytoplankton in the Baltic Sea. BSEP* 106, 1–144
- Pankov, H., 1976. *Algenflora der Ostsee 1. Plankton.* Fischer-Verlag, Stuttgart, 493 pp.
- Pilkaitytė, R., 2007. Spring–summer transition in the Curonian lagoon (SE Baltic Sea) phytoplankton community. *Transit. Water. Bull.* 1 (1), 39–47. <https://doi.org/10.1285/i1825229Xv1n1p39>
- Piwosza, K., Catkiewicz, J., Gołębiewski, M., Creer, S., 2018. Diversity and community composition of pico- and nanoplanktonic protists in the Vistula River estuary (Gulf of Gdańsk, Baltic Sea). *Estuar. Coast. Shelf Sci.* 207, 242–249. <https://doi.org/10.1016/j.ecss.2018.04.013>
- Pliński, M., Jozwiak, T., 1999. Temperature and N:P ratio as factors causing blooms of blue-green algae in the Gulf of Gdansk (Poland). *Oceanologia* 41 (1), 73–80
- Purina, I., Labucis, A., Barda, I., Jurgensone, I., Aigars, J., 2018. Primary productivity in the Gulf of Riga (Baltic Sea) in relation to phytoplankton species and nutrient variability. *Oceanologia* 60 (4), 544–552. <https://doi.org/10.1016/j.oceano.2018.04.005>
- R Development Core Team. 2020. *The R Project for Statistical Computing (Version 4.0.0)* [Software]. Retrieved from <http://www.r-project.org>.
- Sharov, A.N., Berezina, N.A., Nazarova, L.E., Poliakova, T.N., Chekryzheva, T.A., 2014. Links between biota and climate-related variables in the Baltic region using Lake Onega as an example. *Oceanologia* 56 (2), 291–306. <https://doi.org/10.5697/OC.56-2.291>
- Simola, H., Ollikainen, M., Sandman, O., 1993. Short-core palaeolimnology of three contrasting basins of Saimaa lake complex. *Verh. Int. Ver. Limnol.* 25 (2), 1082–1085. <https://doi.org/10.1080/03680770.1992.11900328>
- Spilling, K., Olli, K., Lehtoranta, J., Kremp, A., Tedesco, L., Tamelander, T., Klais, R., Peltonen, H., Tamminen, T., 2018. Shifting diatom–dinoflagellate dominance during spring bloom in the Baltic Sea and its potential effects on biogeochemical cycling. *Front. Mar. Sci.* 5, 327. <https://doi.org/10.3389/fmars.2018.00327>
- Stauffer, B.A., Sukhatme, G.S., Caron, D.A., 2020. Physical and Biogeochemical Factors Driving Spatially Heterogeneous Phytoplankton Blooms in Nearshore Waters of Santa Monica Bay, USA. *Estuar. Coast* 43, 909–926. <https://doi.org/10.1007/s12237-020-00704-5>
- Suikkanen, S., Laamanen, M., Huttunen, M., 2007. Long-term changes in summer phytoplankton communities of the open northern Baltic Sea. *Estuar. Coast. Shelf Sci.* 71 (3–4), 580–592. <https://doi.org/10.1016/j.ecss.2006.09.004>
- Ter Braak, C.J.F., Verdonschot, P.F.M., 1995. Canonical correspondence analysis and related multivariate methods in aquatic ecology. *Aquat. Sci.* 57, 255–289. <https://doi.org/10.1007/BF00877430>
- Telesh, I.V., Golubkov, S.M., Alimov, A.F., 2008. The Neva Estuary ecosystem. In: Schiewer, U. (Ed.), *Ecology of Baltic Coastal Waters.* Springer–Verlag, Berlin, 259–284. [https://doi.org/10.1007/978-3-540-73524-3\\_12](https://doi.org/10.1007/978-3-540-73524-3_12)
- Teutschbein, C., Sponseller, R.A., Grabs, T., Blackburn, M., Boyer, E.W., Hytteborn, J.K., Bishop, K., 2017. Future riverine inorganic nitrogen load to the Baltic Sea from Sweden: An ensemble approach to assessing climate change effects. *Global Biogeochem. Cy.* 31 (11), 1674–1701. <https://doi.org/10.1002/2016GB005598>
- Tikkanen, T., 1986. *Kasviplanktonpas. Suomen Luonnosujelun. Tuki Oy, Helsinki, 278 pp.*
- Ylöstalo, P., Seppälä, J., Kaitala, S., Maunula, P., Simis, S., 2016. Loadings of dissolved organic matter and nutrients from the Neva River into the Gulf of Finland – biogeochemical composition and spatial distribution within the salinity gradient. *Mar. Chem.* 186, 58–71. <https://doi.org/10.1016/j.marchem.2016.07.004>
- Vernet, M., Smith, R.C., 2007. Measuring and modeling primary production in marine pelagic ecosystems. In: Fahey, T.J., Knapp, A.K. (Eds.), *Principles and Standards for Measuring Primary Production.* Oxford University Press, Oxford, 142–174.
- Vollenweider, R.A., 1969. *A Manual on Methods for Measuring Primary Production in Aquatic Environments.* Blackwell Scientific, Oxford, 213 pp.
- Wasmund, N., 2017. The Diatom/Dinoflagellate Index as an Indicator of Ecosystem Changes in the Baltic Sea. 2. Historical Data for Use in Determination of Good Environmental Status. *Front. Mar. Sci.* 4 (153). <https://doi.org/10.3389/fmars.2017.00153>
- Wasmund, N., Tuimala, J., Suikkanen, S., Vandepitte, L., Kraberg, A., 2011. Long-term trends in phytoplankton composition in the western and central Baltic Sea. *J. Marine Syst.* 87 (2), 145–159. <https://doi.org/10.1016/j.jmarsys.2011.03.010>
- Wasmund, N., Kownacka, J., Göbel, J., Jaanus, A., Johansen, M., Jurgensone, I., Lehtinen, S., Powilleit, M., 2017. The Diatom/Dinoflagellate Index as an Indicator of Ecosystem Changes in the Baltic Sea 1. Principle and Handling Instruction. *Front. Mar. Sci.* 4, 22. <https://doi.org/10.3389/fmars.2017.00022>
- Wetzel, R.G., Likens, G.E., 2000. *Limnological Analyses.* Springer, New York, 429 pp.
- Wickham, H., Chang, W., Henry, L., Pedersen, Th.L., Takahashi, K., Wilke, C., Woo, K., Yutani, H., Dunnington, D., RStudio, 2020. *ggplot2: Create Elegant Data Visualisations Using the Grammar of Graphics (Version 3.3.0)* [Software]. Retrieved from <https://cran.r-project.org/web/packages/ggplot2/index.html>.



Available online at [www.sciencedirect.com](http://www.sciencedirect.com)

ScienceDirect

journal homepage: [www.journals.elsevier.com/oceanologia](http://www.journals.elsevier.com/oceanologia)



## CORRIGENDUM

# Corrigendum to “Some probabilistic properties of surf parameter” [Oceanologia 62 (2020) 395–401]

Dag Myrhaug\*

*Department of Marine Technology, Norwegian University of Science and Technology (NTNU), Trondheim, Norway*

Received 15 September 2020; accepted 17 September 2020

Available online 16 October 2020

The author regrets that an error appeared in Eq. (4). of the paper:

The correct equation should read as

$$\int_{\hat{\xi}_1}^{\infty} \hat{\xi}^n p_2(\hat{\xi}) d\hat{\xi} = e^{n\mu + \frac{1}{2}n^2\sigma^2} \left( 1 - \Phi \left[ \frac{\ln \hat{\xi}_1 - (\mu + n\sigma^2)}{\sigma} \right] \right) \quad (4)$$

The author would like to apologize for any inconvenience caused.

DOI of original article: [10.1016/j.oceano.2020.02.003](https://doi.org/10.1016/j.oceano.2020.02.003)

\* Corresponding author at: Department of Marine Technology, Norwegian University of Science and Technology (NTNU), Otto Nilsens vei 10, NO-7491 Trondheim, Norway.

E-mail address: [dag.myrhaug@ntnu.no](mailto:dag.myrhaug@ntnu.no)

Peer review under the responsibility of the Institute of Oceanology of the Polish Academy of Sciences.

<https://doi.org/10.1016/j.oceano.2020.09.005>

0078-3234/© 2020 Institute of Oceanology of the Polish Academy of Sciences. Production and hosting by Elsevier B.V. This is an open access article under the CC BY-NC-ND license (<http://creativecommons.org/licenses/by-nc-nd/4.0/>).